



LAWRENCE
LIVERMORE
NATIONAL
LABORATORY

Program Pu Futures 2006

M.J. Fluss

June 22, 2006

Program for Pu Futures 2006
Pacific Grove, CA, United States
July 9, 2006 through July 13, 2006

Disclaimer

This document was prepared as an account of work sponsored by an agency of the United States Government. Neither the United States Government nor the University of California nor any of their employees, makes any warranty, express or implied, or assumes any legal liability or responsibility for the accuracy, completeness, or usefulness of any information, apparatus, product, or process disclosed, or represents that its use would not infringe privately owned rights. Reference herein to any specific commercial product, process, or service by trade name, trademark, manufacturer, or otherwise, does not necessarily constitute or imply its endorsement, recommendation, or favoring by the United States Government or the University of California. The views and opinions of authors expressed herein do not necessarily state or reflect those of the United States Government or the University of California, and shall not be used for advertising or product endorsement purposes.

This work was performed under the auspices of the U. S. Department of Energy by the University of California, Lawrence Livermore National Laboratory under Contract No. W-7405-Eng-48.

Plutonium Encaged: Pu(IV) and Model Ce(IV) Maltol Complexes

G. Szigethy^{†*}, J. Xu^{*}, D. K. Shuh[†], K. N. Raymond^{†*}

^{*}University of California at Berkeley, Berkeley CA 94720-1460

[†]Lawrence Berkeley National Laboratory, Berkeley CA 94720-1150

The coordination chemistry of plutonium remains relatively unexplored. Thus, the fundamental coordination chemistry of plutonium is being studied using simple multi-dentate ligands with the intention that the information gleaned from these studies may be used in the future to develop plutonium-specific sequestering agents. Towards this goal, hard Lewis-base donors are used as model ligands. Maltol, an inexpensive natural product used in the commercial food industry, is an ideal ligand because it is an all-oxygen bidentate donor, has a rigid structure, and is of small enough size to impose little steric strain, allowing the coordination preferences of plutonium to be the deciding geometric factor. Additionally, maltol is the synthetic precursor of 3,4-HOPO, a siderophore-inspired bidentate moiety tested by us previously as a possible sequestering agent for plutonium under acidic conditions. As comparisons to the plutonium structure, Ce(IV) complexes of the same and related ligands were examined as well. Cerium(IV) complexes serve as good models for plutonium(IV) structures because Ce(IV) has the same ionic radius as Pu(IV) (0.94 Å).^{1,2}

Plutonium(IV) maltol crystals were grown out of a methanol/water solution by slow evaporation to afford red crystals that were evaluated at the Advanced Light Source at Lawrence Berkeley National Laboratory using single crystal X-ray diffraction. Cerium(IV) complexes with maltol and bromomaltol³ were crystallized via slow evaporation of the mother liquor to afford tetragonal, black crystals. All three complexes crystallize in space group $I4_1/a$. The Ce(IV) complex is isostructural with the Pu(IV) complex, in which donating oxygens adopt a trigonal dodecahedral geometry around the metal with the maltol rings parallel to the crystallographic S_4 axis and lying in a non-crystallographic mirror plane of D_{2d} molecular symmetry (Fig 1). The metal-oxygen bonds in both maltol complexes are equal to within 0.04 Å for each oxygen type. In contrast to the maltol structures, the cerium(IV)

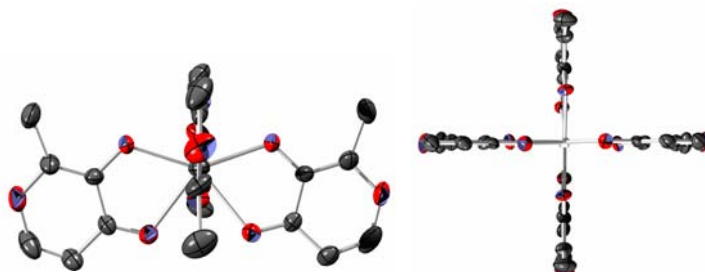


Fig 1: Crystal structures of Pu(IV)(maltol)₄ viewed from the side (left) and down the S_4 axis (right).

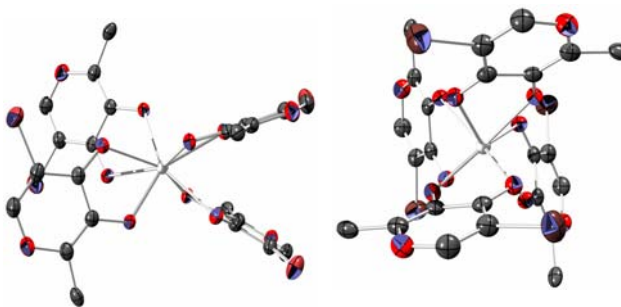


Fig 2: Crystal structures of Ce(IV)(bromomaltol)₄ views from the side (left) and down the S_4 axis (right).

bromomaltol complex arranges the maltol rings in a drastically different manner while maintaining the S_4 crystallographic symmetry (Fig 2). The coordination geometry around the cerium remains a trigonal dodecahedron, but the chelating ligands span a different set of edges as in the maltol structures; the two-fold related bromomaltol ligands twist away from planarity, breaking the D_{2d} molecular symmetry. It is unlikely that steric interaction with a bromine on the same molecule would have caused the observed rearrangement, as there would be sufficient separation between them to accommodate their bulk in the geometry of the plutonium and cerium maltol complexes. The extended packing in the unit cell of both the plutonium and cerium maltol crystals indicates that pi stacking occurs throughout the lattice via the maltol rings with close contacts between rings of approximately 3.6 Å. Introduction of the bromine to this structure would disrupt the packing that would allow these interactions, causing the molecule to adopt the geometry present in the bromomaltol structure. In this unexpected arrangement the complex is still able to maintain some pi stacking with the maltol rings of adjacent molecules with a close contact of approximately 3.3 Å. Additionally, the bromine on each ligand is arranged such that its next closest contact is with a bromine 3.64 Å away on another molecule. Despite the different ligand geometry, the bromomaltol structure exhibits metal-oxygen bond distances that are within 0.06 Å of those in the maltol complexes.

This research is supported by the Director, Office of Energy Research, Office of Basic Energy Sciences, Chemical Sciences Division, United States Department of Energy under contract number DE-AC02-05CH11231. We thank Dr. Allen Oliver for help with crystallography at the ALS of LBNL.

1. A. E. Gordon, J. Xu, K. N. Raymond, Chem. Rev. **103**, 4207 (2003)
2. K. N. Raymond, Solid State Inorg. Chem. **28**, 225 (1991)
3. J. H. Hooker, R. J. Prokop, W. E. Serbousek, M. D. Clifton, J. Org. Chem., **44**, 3408 (1979)

Plutonium Metallurgy: The materials science challenges bridging condensed-matter physics and chemistry

A.J. Schwartz

Lawrence Livermore National Laboratory, Livermore CA 94550 USA

The origins of physical metallurgy have been traced back to the highlands of western Asia northwest of the Persian Gulf as early as the year 4300 BC.¹ By 2000 BC, smelting, melting, casting, annealing, and forming of metals such as gold, silver, copper, lead, and iron had been practiced. Between 2000 BC and 1800 AD, advances in metallurgy impacted society in the areas of the arts, agriculture, industry, and military applications. By the nineteenth century, the industrial need for steel drove metallurgy to become an important discipline connecting chemistry, physics, and mechanics. Matthiessen's rule, based on an 1867 electrical conductivity investigation, is credited as the beginning of "physics of metals", solid-state physics, and now condensed-matter physics. Phase diagram investigations, the development of the constitution of alloys, and the principles of heterogeneous equilibria by Willard Gibbs were first published in 1876. Around the same time, physical chemistry was laying the basis for the study of phase transformation kinetics. Thus, by the end of the 19th century, metallurgy had established its role in the interspace between condensed-matter physics, chemistry, and crystallography.

In the 20th century, tremendous advances in metallurgy were made possible by von Laue's 1912 discovery of diffraction of x-rays and the subsequent developments by Bragg and others. This technology opened the door to crystallographic and microstructural studies of metals and alloys and the discovery of superlattice structures, Hume-Rothery alloys, Laves compounds, and the importance of point defects. Furthermore, significant developments in the understanding of solidification, nucleation and growth theory, plasticity, texture, failure, martensitic phase transformations, diffusion, and many other physical and mechanical properties of metals and alloys were made. Scientific advances in metallurgy clarified the understanding that processing of metals was responsible for setting the microstructure, and the microstructure was closely related to the performance of metals. Thus, microstructure-properties-processing relationships became the central component of 21st century metallurgy.

The understanding of metallurgy gained over the previous four millennia was vital for learning how to process and characterize the new element plutonium when it was fabricated by Seaborg, Kennedy, and Wahl in 1942.² The earliest stages in Pu metallurgy were motivated by the need to produce a product; at that time, quantity took precedence over quality. Problems with consistent density and phase transformations led C.S. Smith to suggest intentionally alloying Pu and ultimately, an alloy of 3.0 to 3.5 atomic percent Ga was used in the Trinity test.³ From 1945 onward, a tremendous amount of effort was placed on phase diagrams and phase stability. Bochvar *et al.*,⁴ Ellinger *et al.*,⁵ Zachariasen and Ellinger,⁶ Chebotarev *et al.*,⁷ Ward *et al.*,⁸ Hecker and Timofeeva,⁹ and many others contributed significantly to the understanding of crystal structures, phase diagrams, and phase stability. In the last two decades, the motivation for Pu science has shifted. No longer is the sole purpose to produce a product. Today, Pu science is more focused on understanding the fundamental relationships between electronic structure, crystallographic phase stability, and the roles of microstructure, impurities, and defects. In the

last few years, the need to understand the aging of Pu has dictated much of the science. The continuous radioactive decay of Pu produces an array of impurity daughter products that accumulate with age. How the damage introduced by radioactive decay and the resulting impurities affect metallurgical aspects of Pu, such as phase transformations and magnetic properties are areas of intense research.

Today, the boundaries between metallurgy, condensed matter physics, and physical chemistry in the study of Pu are blurred. Recent advances in our understanding of this intriguing material are being made in all areas of physical science. This presentation will highlight these exciting advances and focus on the significant challenges in the field of Pu metallurgy. Among the topics to be discussed are phase transformations and phase stability. Although there have been significant advances in our understanding of the phase diagram, even after 40+ years, the nature of the double-C curve in the time-temperature-transformation (TTT) diagram remains unresolved. Advances have been made in our knowledge of the $\delta \rightarrow \alpha'$ transformation,¹⁰⁻¹³ but less is known about the mechanism and kinetics of the α to β and reverse transformation during temperature or pressure excursions. Natural aging of Pu has been the focus of significant recent efforts,¹⁴ but we still do not fully know the mechanism(s) of delta phase stability,¹⁵ the vacancy migration energy, and the mechanism that appears to limit the size of the helium bubbles that form from the alpha decay of Pu into U and He.

With thousands of years of accumulated metallurgical knowledge of most every element in the periodic table, we substantially understand most metals. However, the 21st century finds us still perplexed by the deeply complex structure-properties-processing relations in Pu. This is a very exciting time to be engaged in Pu metallurgy. With ever-improving computational capabilities and significant focus on electronic structure calculations and experiments, there are now collaborative worldwide contributions to our understanding.

This work was performed under the auspices of U.S. Department of Energy by the University of California, Lawrence Livermore National Laboratory under contract No. W-7405-Eng-48.

¹R.F. Mehl, in *Physical Metallurgy*, ed. by R.W. Cahn and P. Haasen (North-Holland Publishing, Amsterdam 1983).

²A.F. Michaudon and I.G. Buican in *Los Alamos Science*, edited by N.G. Cooper, **26**, 4 (2000).

³E.F. Hammel in *Los Alamos Science*, edited by N.G. Cooper, **26**, 48 (2000).

⁴A.A. Bochvar, et al. in *Proceedings of the Second United Nations International Conference on the Peaceful Uses of Atomic Energy*, **6**, Geneva, (United Nations, New York, 1958) 184.

⁵F.H. Ellinger, C.C. Land, and V.O. Struebing, *J. Nuc. Mat.* **12** (2), 226 (1964).

⁶W.H. Zachariasen and F.H. Ellinger, *Acta Crystallogr.* **16**, 777 (1963).

⁷N.T. Chebotarev, E. S. Smotriskaya, M. A. Andrianov, and O. E. Kostyuk, in *Plutonium 1975 and Other Actinides*, edited by H. Blank and R. Lindner (North Holland Publishing Co., Amsterdam, 1975), 37.

⁸J.T. Orme, M.E. Faiers, and B.J. Ward in *Plutonium 1975 and Other Actinides*, edited by H. Blank and R. Lindner (North Holland Publishing Co., Amsterdam, 1975), 761.

⁹S.S. Hecker and L.F. Timofeeva in *Los Alamos Science*, edited by N.G. Cooper, **26**, 244 (2000).

¹⁰J.N. Mitchell, M. Stan, D.S. Schwartz, and C.J. Boehlert, *Met. and Mat. Trans. A*, **35A**, 2267 (2004).

¹¹K.J.M. Blobaum, et al. *Met. and Mat. Trans. A*, **37A**, 567 (2006).

¹²J.P. Hirth, J.N. Mitchell, D.S. Schwartz, and T.E. Mitchell, *Acta Mat.* **54**, 1917 (2006).

¹³K.T. Moore, et al. in *Solid-to-Solid Phase Transformations in Inorganic Materials 2005*, edited by J.M. Howe, D.E. Laughlin, J.K. Lee, U. Dahmen, and W.A. Soffa (TMS, Warrendale, 2005) 47.

¹⁴M.J. Fluss, et al. *J. Alloys and Compounds*, **368**, 62 (2004).

¹⁵M. Dormeival, N. Baclet, C. Valot, P. Rofidal, and J.M. Fournier, *J. Alloys and Compounds*, **350**, 86 (2003).

Scientific Understanding Aids Plutonium Remediation at Rocky Flats.

G. R. Choppin†, D. L. Clark*, D. R. Janecky*, L. J. Lane*

*Los Alamos National Laboratory, Los Alamos, NM 87545

†Florida State University, Tallahassee, FL 32314

BACKGROUND

The Rocky Flats Environmental Technology Site (RFETS) was a U.S. Department of Energy (DOE) environmental cleanup site located about 15 miles northwest of downtown Denver. More than 2.5 million people live within a 50-mile radius of the site, and 300,000 of those live in the Rocky Flats watershed. From 1952 - 1989, the Rocky Flats Plant made components for nuclear weapons using various radioactive and hazardous materials, including plutonium and uranium; toxic metals such as beryllium; and hazardous chemicals, such as cleaning solvents and degreasers. In 1989, Rocky Flats was raided by the FBI/EPA for alleged environmental violations, and all nuclear operations were suspended. Nearly 40 years of nuclear weapons production left behind a legacy of contaminated facilities, soils, surface and ground water. RFETS was designated as an EPA Superfund cleanup site, and in March of 1995, DOE's Baseline Environmental Management Report called for the site to be closed by the year 2060 at a cost in excess of \$37 billion.

In May of 1995, wet spring conditions and intense rainfall events at the site caused Site personnel and stakeholder groups to raise concerns about the potential for increased plutonium mobility in the RFETS environment, and the potential for increased plutonium transport offsite onto public lands. These events placed increased emphasis on the potential for soluble forms of plutonium in surface and ground waters in order to account for the appearance of plutonium at monitoring stations at the Site boundary. The accepted DOE model for risk assessment (RESRAD) assumed transport of soluble forms of contaminants, and required input of distribution coefficients (K_d) between aqueous and soluble phases. When plutonium K_d 's were input into the model, it predicted no plutonium transport, in disagreement with the observed plutonium behavior. This situation led to public mistrust and lack of confidence. When coupled with other questions regarding the mobility of different actinide elements (U, Pu, Am) at different Site locations, this situation prompted DOE and Kaiser-Hill to establish the Actinide Migration Evaluation (AME) advisory group in 1996. The group was formed to provide guidance on issues of actinide behavior and mobility in the air, surface water, groundwater, and soil.

Through a combination of expert judgement and state-of-the-art scientific measurements, it was shown that under environmental conditions at Rocky Flats, plutonium and americium form insoluble oxides. These insoluble materials are attached to natural soil organic and mineral particles that can migrate in the Rocky Flats environment by wind and surface water sedimentation/resuspension processes. This scientific understanding demonstrated that soluble transport models were not appropriate, and led to the development and application of large-scale erosion/sediment transport models. The scientific understanding developed through these integrated studies

contributed directly to the basis for plutonium and americium cleanup levels in soils and concretes. It helped all parties focus remediation efforts on surficial contamination and transport pathways (wind and surface water erosion) that posed the greatest risk to human health and the environment. It helped guide selection of surface-specific removal technologies and future land configuration strategies. Thus scientific understanding through advanced measurement techniques was developed into science-based communication and decision-making for Kaiser-Hill and DOE that helped focus Site-directed efforts in the correct areas, and aided the DOE in its effort to close the RFETS. On October 13, 2005, Kaiser-Hill Company declared to DOE the physical completion of the Rocky Flats Closure Project, culminating a 10-year, \$7 billion project – ultimately delivering nearly \$30 billion in taxpayer savings.

An overview of the Rocky Flats Site, the technical issues, the scientific experiments, the transport models, the environmental cleanup, and the final land configuration will be presented.

Supported by Kaiser-Hill, LLC, and the Division of Chemical Sciences, Geosciences, and Biosciences, Office of Basic Energy Research, U.S. Department of Energy.

PuCoGa₅ and Related Materials

J. D. Thompson, N. J. Curro, Tuson Park, E.D. Bauer, J. L. Sarrao

Los Alamos National Laboratory, Los Alamos, NM 87545 USA

Superconductivity in actinide-bearing compounds has served as a tool for guiding an interpretation of the role that 5f-electrons play in determining physical properties. Likewise, an interpretation of the mechanism of superconductivity must be consistent with what is known about the normal-state properties of these compounds. PuCoGa₅, the first Pu-based superconductor¹, exemplifies these complementary approaches to revealing the nature of plutonium's 5f-electrons in this compound. Its superconducting transition temperature T_c of 18.5K is nearly an order of magnitude higher than that of any previously known 5f-electron material but comparable to T_c 's found in some transition-metal intermetallic compounds. Unlike these other intermetallics whose superconductivity is conventional, i.e., mediated by an attractive electron-phonon interaction, the uniform magnetic susceptibility of PuCoGa₅ is Curie-Weiss-like, with an effective moment expected for a nearly localized 5f⁵ configuration. Because the presence of a local moment is detrimental to conventional superconductivity, this suggests the possibility that superconductivity of PuCoGa₅ is unconventional, e.g. mediated by a magnetic interaction, which is the case in strongly correlated electron materials, such as the high- T_c cuprates and heavy-fermion systems based on Ce or U. This possibility is borne out by NMR measurements^{2,3} that find a power-law dependence of the nuclear-spin relaxation rate $1/T_1$ in the superconducting state of PuCoGa₅ as well as in the isostructural superconductor⁴ PuRhGa₅ with $T_c=8.5$ K. Further, $1/T_1$ in the normal states of these materials also is unconventional and consistent with nuclear-spin relaxation being dominated above T_c by the presence of 5f-electron spin fluctuations. Together, these experiments lead to a picture of superconductivity mediated by magnetic fluctuations associated with Pu's 5f electrons whose characteristic spin fluctuation rate is set by hybridization with ligand electrons. This interpretation also is consistent with the suppression of T_c with self-radiation damage, the temperature dependence of electrical resistivity, the large value of a magnetic field required to suppress superconductivity, and an enhanced Sommerfeld coefficient of specific heat that are found in these Pu superconductors.

Hybridization of 5f and ligand electrons not only sets the characteristic energy scale for spin fluctuations but also the bandwidth of electronic states at the Fermi energy E_F . In a simple approximation, the inverse of the bandwidth is proportional to the density of electronic states at E_F measured by the Sommerfeld specific heat coefficient. The superconducting transition temperatures of Ce- and U-based heavy-fermion compounds, the high- T_c cuprates and these Pu superconductors appear to have a common linear dependence on the energy scale set by hybridization.² The T_c 's of PuCoGa₅ and PuRhGa₅ are intermediate to those of these two other families of superconductors, implying that the 5f electrons of the Pu superconductors are not as localized as the f-electrons in heavy-fermion systems but more localized than the d-electrons of the cuprates. This is the same correlation expected on the basis of the spatial extent of the relevant f- or d-electrons and equivalently of their effective bandwidth or Sommerfeld coefficient. Extending this picture to elemental Pu suggests that its 5f electrons are strongly hybridized with band electrons, preventing it from being either superconducting or magnetic.

Besides superconductivity, are there other surprises waiting to be found in PuCoGa₅ or PuRhGa₅? The answer is almost certainly yes. One possibility comes from a comparison with the isostructural heavy-fermion compounds CeCoIn₅ and CeRhIn₅ in which hybridization can be tuned by readily accessible pressures and magnetic fields. Though CeCoIn₅ is superconducting at atmospheric pressure, CeRhIn₅ is antiferromagnetic but becomes superconducting with applied pressure. Imposing a magnetic field on CeRhIn₅ in its superconducting state induces magnetic order that is hidden by superconductivity in the absence of a field.⁵ Various theoretical models have been proposed for how this can happen, but the observation of field-induced magnetic order coexisting with superconductivity remains unresolved. The unusual temperature dependence of the nuclear-spin relaxation rate in PuRhGa₅ is strikingly similar to that of CeRhIn₅ under pressure, suggesting that the relative f-electron hybridization is comparable in both materials which also is true for PuCoGa₅ and CeCoIn₅. From this comparison, it seems worthwhile to search for field-induced magnetism in PuRhGa₅, which, if found, would allow a new approach to probing the nature of plutonium's 5f-electrons and its the evolution with field tuning.

Work at Los Alamos was performed under the auspices of the U.S. Department of Energy, Office of Science.

- 1 J. L. Sarrao et al., Nature **420**, 297 (2002).
- 2 N. J. Curro et al., Nature **434**, 622 (2005).
- 3 H. Sakai et al., J. Phys. Soc. Jpn. **74**, 1710 (2005).
- 4 F. Wastin et al., J. Phys. Condens. Mat. **15**, s2279 (2003).
- 5 Tuson Park et al., Nature (in press).

Futuristic back-end of the nuclear fuel cycle with the partitioning of minor actinides

by

C. Madic¹, B. Boullis¹, P. Baron¹, F. Testard², M. J. Hudson³, J.-O. Liljezin⁴,
B. Christiansen⁵, M. Ferrando⁶, A. Facchini⁷, A. Geist⁸, G. Modolo⁹, A. G. Espartero¹⁰
and J. De Mendoza¹¹

1/ CEA-DEN, Marcoule and Saclay (France), 2/ CEA-DSM, Saclay (France), 3/ Univ. of Reading (U.K.), 4/ Chalmers Univ. of Technol., Göteborg (Sweden), 5/ JRC-ITU, Karlsruhe (Germany), 6/ ENEA, Saluggia (Italy), 7/ PoliMi, Milano (Italy), 8/ INE, FZ-Karlsruhe (Germany), 9/ ISR, FZ-Jülich (Germany), 10/ CIEMAT, Madrid (Spain), 11/ Univ. Auto. de Madrid, Madrid (Spain).

The reprocessing of nuclear spent fuels is industrially carried out in several countries in the world. The most important reprocessing facility is situated in France at La Hague (Aréva-Cogéma Company). Today, the aims of the reprocessing are: i) to recover the elements U and Pu which have large potentiality to produce more energy and which can be recycled as new fuels (MOX fuel for the recycled Pu), ii) to condition the nuclear wastes into solid matrices. Most of the radionuclides from the wastes are conditioned in glass. The glasses contain most of the Fission Products (FPs) and the minor actinides (MAs): Np, Am and Cm. These glass wastes will be in the future disposed of into deep geological repositories. But, the most difficult problem to define such deep geological repositories is related to the very important radiotoxicity of these glass wastes which stay very important for about 100,000 years. This is mainly due to the presence of the MAs in these glass wastes. So, a new strategy is under consideration in numerous nuclear countries: if the MAs are eliminated from the glass wastes, the definition of a deep geological repository will be more simpler. After their partitioning, the MAs can be considered as destructible by nuclear facility, such as the ADS. So, in France and in Europe, important research for MAs partitioning are done. Most of the work done was in the domain of hydrometallurgy. The most important results obtained in Europe will be presented here.

Separation of neptunium (Np)

In the spent fuel aqueous nitric acid dissolution liquor, Np exist on Np(V) (NpO_2^+) and Np(VI) (NpO_2^{2+}) forms. In order to co-extract Np with U(VI) and Pu(IV) by the TBP within the PUREX process, it is necessary to convert all the Np into its Np(VI) form which possesses a high affinity for the TBP. In order to do so, at the CEA-Marcoule, it was shown that if the $[\text{HNO}_3]$ of the dissolution liquor is higher than that used in the industrial plant at La Hague (3 M HNO_3), Np can be totally converted to Np(VI) in presence of the TBP solvent, and then Np can be co-extracted with U(VI) and Pu(IV). Such a demonstration was successfully demonstrated at CEA-Marcoule in 2005, during the treatment by the PUREX process of 14 kg of spent UOX fuel.

Separation of americium (Am) and curium (Cm)

As Am and Cm exist in the spent fuel aqueous dissolution liquor as trivalent actinide ions (An): Am(III) and Cm(III), it was necessary to design new extractant able to co-extract An(III) from the nitric acid raffinate issuing the PUREX process. Moreover, as about a third

of the FPs is composed of trivalent lanthanides ions (Ln(III)), the co-extraction of An(III) + Ln(III) is obtained. So, after the co-extraction of An(III) + Ln(III) a separation An(III)/Ln(III) should be done.

DIAMEX process. For the co-extraction of An(III)+ Ln(III) nitrates from High Active Wastes, a lot of work has been done to select a new extracting agent. The family of malonamide molecules was chosen and among more than 100 ligands tested, the DMDOHEMA was selected for the so-called DIAMEX process. The DIAMEX process was successfully tested on High Active Raffinate (HAR) both at CEA-Marcoule and at the ITU (Karlsruhe, Germany). Moreover, at the ITU, the DIAMEX process was also successfully tested using High Active Concentrate (concentration factor vs HAR of 10).

SANEX process(es). For the separation of An(III) vs Ln(III) issuing the DIAMEX process, it was necessary to define very specific extractants able to selectively extract the An(III). In this very difficult domain, several processes were designed including: i) SANEX process based on the tridentate N-ligand *iPr*-BTP, and ii) synergistic mixture of *bis*-chlorophenyl-*di*-thiophosphinic acid ((CIPh)₂PSSH) + TOPO. Hot tests of the SANEX process using BTP ligands was done at CEA-Marcoule and at the ITU. If good results were obtained, unfortunately, it was demonstrated that the BTP extractants are not sufficiently resistant vs radiolysis to be chosen as industrial extractant. The SANEX process based on (CIPh)₂PSSH + TOPO mixture was successfully tested on synthetic spiked solutions at FZ-Jülich (Germany). It should be mentioned that recently a new SANEX system has been defined by CEA and successfully tested in 2005 with real HAR.

Cm/Am separation.

As it will be difficult to destroy Cm nuclides, it was considered necessary to define an Am(III)/Cm(III) separation process. As the malonamide DMDOHEMA possesses a slight higher affinity for Am(III) vs Cm(III) ($SF_{Am/Cm} = 1.6$), a DIAMEX-2 process was defined and successfully tested at CEA-Marcoule with real hot feed.

Most of the work described herein was done within the PARTNEW European Integrated Project (IP) of FP-5. Now, since 2004, the research continues in Europe within the IP EUROPART (FP-6), which incorporates not only MAs partitioning work in hydrometallurgy, but also in pyrometallurgy.

Acknowledgements

The European Commission is acknowledged for the financial support during PARTNEW (FP-5) and EUROPART (FP-6).

Thermostatics and Kinetics of Transformations in Pu-based Alloys

P. E. A. Turchi^{*}, L. Kaufman[†], and Zi-Kui Liu^{††}

^{*}Lawrence Livermore National Laboratory (L-372), P. O. Box 808, Livermore, CA 94551 USA

[†]140 Clark Road, Brookline, MA 02445-5848 USA

^{††}The Pennsylvania State University, MS&E Department, College Park, PA 16803 USA

INTRODUCTION

Despite the recent progress made in predicting the impact of electron localization on the stability of the δ (or fcc) phase of Pu, an accurate determination of the energetics for pure Pu and its alloys still offers paramount challenges. As a viable alternative, the CALPHAD (CALCulation of Phase Diagrams) methodology¹ has been extremely successful since the 70's in describing the thermodynamics of complex multi-component alloys. Hence, before input from *ab initio* calculations to the thermodynamic database becomes a reality, statics and kinetics of phase transformations in a series of Pu-based alloys have been investigated² with CALPHAD with reference to experimental data only. Here we summarize some of the most salient conclusions of this study for the Pu-Ga alloy system.

STATICS OF PHASE TRANSFORMATIONS

In the 80's attempts have been made to assess the phase stability properties of Pu-Ga alloys by focussing on the Pu-rich part of the phase diagram³. However, since stability is a global property that requires an accurate knowledge of alloy behaviour in the whole range of composition, a new assessment was performed. The input data consisted of the phase diagram and the heats of formation of the compounds measured experimentally. Since the emphasis was put mostly on the high-temperature phase diagram data, the low temperature alloy behaviour comes out as a prediction from this assessment. As shown in Fig. 1, besides the overall agreement with the known experimental phase diagram, an eutectoid-phase decomposition is predicted at about 57 °C in the Pu-rich portion of the phase diagram in agreement with the Russian experimental results⁴. It is worth noting that the CALPHAD boundary of the two-phase region (δ +Pu₃Ga) lies on the left (*i.e.*, at lower Ga composition) of the experimental results. This finding was expected since the slow kinetics of formation of Pu₃Ga precipitates in the fcc matrix at low temperatures precludes the observation of small phase fraction of Pu₃Ga.

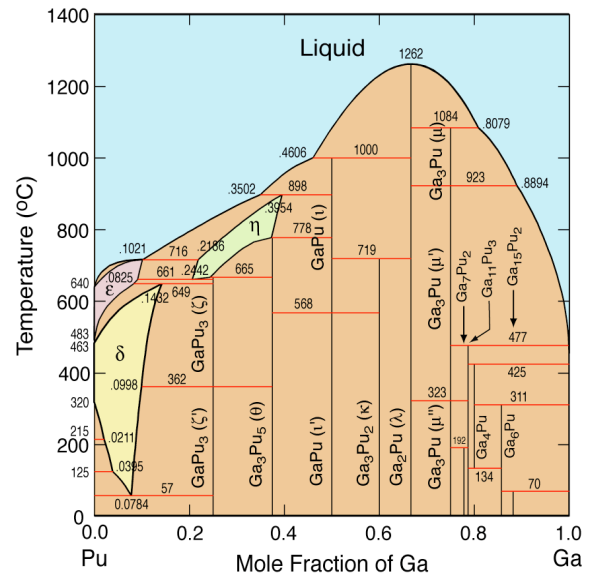


Figure 1. CALPHAD assessment of the Pu-Ga phase diagram.

KINETICS OF PHASE TRANSFORMATIONS

Kinetic modeling was applied to the study of diffusion-controlled transformation in the case of the eutectoid reaction $\delta \rightarrow \alpha + \text{Pu}_3\text{Ga}$ with the thermodynamic driving force obtained from the previous results and a mobility database built upon available experimental data. The temperature-time-transformation (TTT) curves are shown for the two separate reactions in Fig. 2. Close to the temperature of eutectoid decomposition, the time for transformation is about $1.5 \cdot 10^6$ years. Hence, although the “American” version of the phase diagram describes metastable equilibrium, the actual equilibrium eutectoid transformation is definitely inhibited by diffusion alone.

To study the early stage of the $\delta \rightarrow \alpha$ isothermal martensitic transformation, the model of martensite nucleation proposed by Cohen and Kaufman (CK)⁵, and successfully applied to Fe-Ni alloys, was adopted. In this model, the main idea is that a heterogeneity must pre-exists beyond a critical size, and to rapidly transforms in a martensite this embryo must go through a number of growth steps that are thermally activated. In the present case, a rate control reaction at the highest Ga contents was proposed to explain the transition from single to double C-shape of the TTT curves with an increase in Ga content. The results shown in Fig. 3 account for the change in time scale of the early stage of martensite nucleation with alloy composition, in agreement with those from Orme *et al.*⁶

This work was performed under the auspices of the U. S. Department of Energy by the University of California Lawrence Livermore National Laboratory under Contract W-7405-ENG-48.

1. N. Saunders and A. P. Miodownik, “CALPHAD, Calculation of Phase Diagrams: A Comprehensive Guide”, Pergamon Materials Series, vol. 1, ed. by R W. Cahn (Pergamon Press, Oxford, 1998).
2. P. E. A. Turchi, L. Kaufman, Z.-K. Liu, and S. Zhou, “Thermodynamics and Kinetics of Phase Transformations in Plutonium Alloys: Part F”, 107 pages, September 20, 2004 (LLNL UCRL-TR-206658).
3. P. H. Adler, Metall. Trans. **22A**, 2237 (1991).
4. S. S. Hecker and L. F. Timofeeva, Los Alamos Science (LANL, Los Alamos, NM) **1** (26), 244 (2000); L. F. Timofeeva, in Proceedings of the International Conference on “Aging studies and lifetime extension of Materials”, ed. by L. G. Mallison (Kluwer Academic/Plenum, New York, 2001), pp. 191-198.
5. L. Kaufman and M. Cohen, Progress in Metal Physics **7**, 165 (1958).
6. J. T. Orme, M. E. Faiers, and B. J. Ward, in “Plutonium 1975 and Other Actinides”, ed. by H. Blank and R. Lindner (North-Holland, Amsterdam, 1976), pp. 761-773.

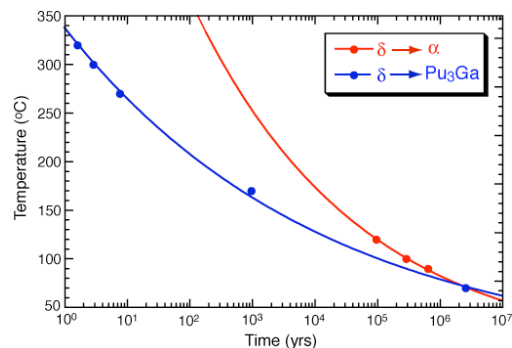


Figure 2. Calculated TTT curves for a δ matrix of $\text{Pu}_{1-x}\text{Ga}_x$ alloys transforming into the α phase, with a transformation rate of 5%.

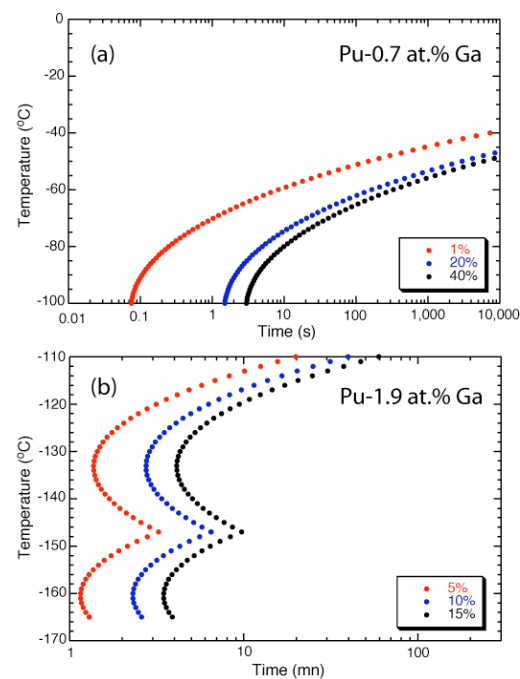


Figure 3. TTT curves associated with various rates of transformation for Pu-Ga alloys with (a) 0.7 and (b) 1.9 at.% Ga.

Zirconia inert matrix for plutonium utilisation and minor actinides disposition in reactors.

Claude Degueldre.

NES, Paul Scherrer Institute, 5232-Villigen-PSI, Switzerland.

The toxicity of the UOX spent fuel is dominated by plutonium and minor actinides (MA): Np, Am and Cm, after decay of the short live fission products. Zirconia ceramics containing Pu and MA in the form of an Inert Matrix Fuel (IMF) could be used to burn these actinides in Light Water Reactors and in High Temperature Reactors. Optimisation of the fuel designs dictated by properties such as thermal, mechanical, chemical and physical must be performed with attention for their behaviour under irradiation. Zirconia must be stabilised by yttria to form a solid solution such as $An_zY_yPu_xZr_{1-y}O_{2-y}$ where minor actinide oxides are also soluble. Burnable poison such as Gd, Ho, Er, Eu or Np, Am them-self may be added if necessary. These cubic solid solutions are stable under heavy ion irradiation. The retention of fission products in zirconia, under similar thermodynamic conditions, is a priori stronger, compared to UO_2 , the lattice parameter being larger for UO_2 than for $(Y,Zr)O_{2-x}$. $(Er,Y,Pu,Zr)O_{2-x}$ in which Pu contains 5% Am was successfully irradiated in the Proteus reactor at PSI, in the HFR facility, Petten as well as in the Halden Reactor. These irradiations make the Swiss scientists confident to irradiate such IMF in a commercial reactor that would allow later a commercial deployment of such a fuel for Pu and MA utilisation in a last cycle. The fuel forms namely pellet-fuel, cermet, cermet and coated particle fuel are discussed considering the once through strategy. For this strategy, low solubility of the inert matrix is required for geological disposal. As spent fuels these IMFs are demanding materials from the solubility point of view, this parameter was studied in detail for a range of solutions corresponding to groundwater under near field conditions. Under these conditions the IMF solubility is 10^6 times smaller than glass, which makes the zirconia material very attractive for deep geological disposal. The desired objective would be to use IMF to produce energy in reactors, opting for an economical and ecological solution. The Swiss IMF results are reported in the proceedings of the IMF workshops published in J. Nucl. Mater. (1999, 2003 & 2006) and Prog. Nucl. Energy (2001).

The theory of electronic structure and magnetic properties of Pu and Pu alloys

V.I. Anisimov

Institute of Metal Physics, 620041 Ekaterinburg GSP-170, Russia

The key question in understanding plutonium properties is a problem of $5f$ -electrons localization. For the actinides on the right side of Pu in periodic table starting from americium $5f$ -electrons are fully localized while for the left side elements they are itinerant and contribute to the chemical bonding resulting in a much smaller atomic volume. Pu itself can be as in small volume state (α phase) as well as in large volume state (δ phase). Density functional theory calculations describe well small volume phase but in order to reproduce large volume phase a strong spin-polarization of $5f$ -electrons is needed. That is in contradiction with experimental data showing that there are no local magnetic moments of Pu ions. There are two ways to explain the absence of magnetic moments on localized $5f$ electrons. One is Kondo type screening due to the hybridization of $5f$ electrons with s -, p - and d -electrons. This effect can be described in Dynamical mean-field theory calculations. Another explanation come from the taking into account very strong spin-orbit coupling in this material that can lead to the f^6 configuration with a zero value of total magnetic moment. In the talk a review will be given of various attempts to describe electronic structure and magnetic properties of Pu and Pu alloys in *ab-initio* calculations.

Solubility and Redox Equilibria of Plutonium

Th. Fanghänel^{*†}, M. Altmaier^{*}, H.R. Cho^{*}, C.M. Marquardt^{*}, V. Neck^{*}, A. Seibert[#], C. Walther^{*}, J.-I. Yun^{*}

^{*}Institut für Nukleare Entsorgung, Forschungszentrum Karlsruhe, D-76021 Karlsruhe, Germany

[†]Physikalisch-Chemisches Institut, Universität Heidelberg, D-69120 Heidelberg, Germany

[#]European Commission, JRC, Inst. for Transuranium Elements, D-76125 Karlsruhe, Germany

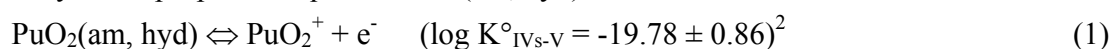
The redox behavior of Pu, the hydrolysis of Pu(IV), and the solubility of Pu(IV) hydrous oxide in the presence of oxygen are discussed controversially in the literature. Experimental results are often ascribed to radiolysis or kinetic effects, disproportionation reactions, etc. We have studied the redox behavior of Pu(IV) solutions at pH 0 – 2 as function of time and the solubility of Pu(IV) hydrous oxide at pH 2 – 13 (under Ar + traces O₂) using Pu-242. The redox potential, in many literature studies not measured or considered as not reliable, is found to be a key parameter for the understanding of the aqueous Pu chemistry. With the known equilibrium constants for the system Pu/e⁻/H⁺/OH⁻/NaCl or NaClO₄/H₂O (25°C)^{1,2} and additional data determined for PuO_{2+x}(s,hyd) and small Pu(IV) colloids/polymers (1.5 – 2 nm), which are part of the thermodynamic system, the total Pu solubility and oxidation state distribution is explained consistently in terms of equilibrium thermodynamics.

REDOX BEHAVIOR AND HYDROLYSIS OF Pu(IV) IN ACIDIC SOLUTIONS

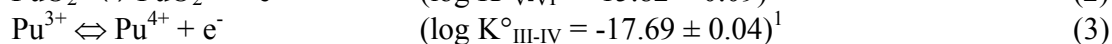
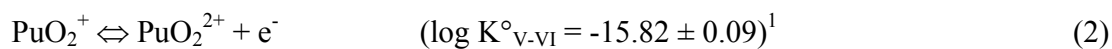
Electrochemically prepared Pu(IV) stock solutions were diluted to 10⁻⁵ to 5·10⁻⁴ M Pu(IV) solutions at pH_c = 0.3 - 2.1 in 0.5 M HCl/NaCl. The concentrations of Pu(IV)_{aq}, Pu³⁺, PuO₂⁺ and PuO₂²⁺ were determined by UV/Vis/NIR absorption spectroscopy, using a 1m-capillary cell for low concentrations. The presence or absence of Pu(IV) colloids > 5 nm was confirmed by LIBD³. The oxidation state balance determined by spectroscopy and LSC in solutions free of colloidal Pu(IV) demonstrates that the Pu(IV) absorption band at 470 nm remains unaffected by mononuclear hydrolysis reactions in the pH range 0 – 2. The decrease in the molar absorbance is only caused by the formation of polymeric/colloidal species Pu(IV)_{coll}.

The redox behavior of acidic Pu(IV) solutions is usually ascribed to the disproportionation of 2 Pu(IV) into Pu(III) and Pu(V) and/or of 3 Pu(IV) into 2 Pu(III) and Pu(VI). Accordingly, at any time the following balance must be valid: [Pu(III)] = [Pu(V)] + 2 [Pu(VI)].⁵ However, doubts on this reaction path^{3,4} are confirmed: None of the investigated solutions fulfills this balance at reaction times < 10 days. Instead, the formation of Pu(III) is equal to the simultaneous decrease of Pu(IV)_{aq}, (d[Pu(III)]/dt = - d[Pu(IV)_{aq}]/dt), i.e., {[Pu(IV)_{aq}] + [Pu(III)]} = constant and, as a consequence: d{[Pu(V)] + [Pu(VI)]}/dt = - d[Pu(IV)_{coll}]/dt.

These results indicate that the so-called ‘disproportionation of Pu(IV)’ is a two-step process. The initial step is the formation of PuO₂⁺, either by the oxidation of colloidal or polynuclear Pu(IV) species by O₂ or due to the redox equilibrium with Pu(IV) colloids > 5 nm which have thermodynamic properties equal to PuO₂(am, hyd)⁶:



The second step is the simultaneous equilibration of the redox couples Pu(V)/Pu(VI) and Pu(IV)/Pu(III) which are related by pe (and pH because of Pu(IV) hydrolysis equilibria):



The oxidation state distributions and redox potentials ($pe = 16.9 \text{ Eh(V)}$ at 25°C) measured after more than 20 days are consistent with known ‘disproportionation’ equilibria⁴⁻⁶ which correctly describe the equilibrium state, but not the underlying reaction mechanism.

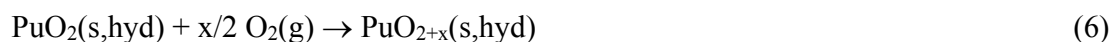
Combining reactions (3) and (4) allows to determine $\log \beta_n^{\circ}(\text{Pu}(\text{OH})_n^{4-n})$ from the relation:

$$pe + \log ([\text{Pu}^{3+}]/[\text{Pu}(\text{IV})_{\text{aq}}]) = -\log K_{\text{III-IV}} - \log (1 + \sum \beta_n^{\circ} [\text{OH}^-]^n) \quad (5)$$

The spectroscopically determined concentrations of Pu^{3+} and $\text{Pu}(\text{IV})_{\text{aq}}$ and the measured redox potentials (consistent with pe values calculated from $\log K^{\circ}_{\text{V-VI}}$ and the spectroscopically determined Pu(V) and Pu(VI) concentrations) yield the following hydrolysis constants, corrected to $I = 0$ with the SIT: $\log \beta_1^{\circ} = 14.0 \pm 0.2$, $\log \beta_2^{\circ} = 26.8 \pm 0.6$, $\log \beta_3^{\circ} = 38.9 \pm 0.9$). These values are lower than those selected in the recent NEA-TDB review².

SOLUBILITY OF Pu(IV) HYDROUS OXIDE IN THE PRESENCE OF OXYGEN

The total Pu concentrations, oxidation state distributions and redox potentials measured in solubility studies with Pu(IV) hydrous oxide under air (Rai et al.⁷) and under Ar containing only traces of O_2 (present work) indicate that O_2 is scavenged by solid $\text{PuO}_2(\text{s,hyd})$ yielding mixed valent $\text{PuO}_{2+x}(\text{s,hyd}) = (\text{Pu}^{\text{V}})_{2x}(\text{Pu}^{\text{IV}})_{1-2x}\text{O}_{2+x}(\text{s,hyd})$ as proposed by Haschke et al.⁸:



The oxidized fractions of $\text{PuO}_{2+x}(\text{s,hyd})$ (ca. 10 % in the studies of Rai et al.⁷ under air and 0.5 % in the present experiment) are correlated to the amount of oxygen in the system and/or the amount of oxidized Pu in the original Pu(IV) stock solution. At low pH they are completely soluble but at $\text{pH} > 3$, the aqueous Pu(V) concentration is limited to the solubility of $\text{PuO}_{2+x}(\text{s,hyd})$ which may be considered as solid solution $(\text{PuO}_{2.5})_{2x}(\text{PuO}_2)_{1-2x}(\text{s,hyd})$:

$$\log K_{\text{sp}}(\text{PuO}_{2.5} \text{ in } \text{PuO}_{2+x}(\text{s,hyd})) = \log ([\text{PuO}_2^+][\text{OH}^-]) = -14.0 \pm 0.8. \quad (7)$$

The low redox potentials at $\text{pH} 4 - 13$ are reproducible and independent of the initial O_2 in the system. They can be explained by equilibria between $\text{PuO}_{2+x}(\text{s,hyd})$, $\text{PuO}_2^+(\text{aq})$ and small Pu(IV) colloids/polymers (1.5 - 2 nm) which are part of the thermodynamic system and predominant at $\text{pH} > 7$. The molar standard Gibbs energy $\Delta_f G_m^{\circ}(\text{PuO}_{2+x}(\text{s,hyd}))$ derived from the solubility data is considerably less negative than calculated by Haschke et al.⁸ who assumed the oxidation of $\text{PuO}_2(\text{s})$ by reaction with water.

- 1 R.J. Lemire *et al.* (OECD-NEA TDB). Chemical thermodyn. of neptunium and plutonium, Elsevier (2001).
- 2 R. Guillaumont, *et al.* (OECD-NEA TDB). Update on the chemical thermodynamics of uranium, neptunium, plutonium, americium and technetium, Elsevier (2003).
- 3 C. Walther, Th. Fanghanel *et al.*, Actinides Research Quarterly, Los Alamos Natl. Lab., **11**, 12 (2003).
- 4 D.A. Costanzo, R.E. Biggers and J.T. Bell, J. Inorg. Nucl. Chem., **35**, 609 (1973).
- 5 H. Capdevila, P. Vitorge and E. Giffaut, Radiochim. Acta, **58/59**, 45 (1992).
- 6 H. Capdevila and P. Vitorge, Radiochim. Acta, **82**, 11 (1998).
- 7 D. Rai *et al.*, Soil Sci. Am. J. **44**, 490 (1980), Radiochim. Acta **35**, 97 (1984) and **89**, 491 (2001).
- 8 J.M. Haschke *et al.*, Science **287**, 285 (2000), J. Alloys Comp. **314**, 78 (2001) and **336**, 124 (2002).

Nuclear forensics investigations with a focus on plutonium

M. Wallenius, K. Lützenkirchen, K. Mayer, I. Ray

European Commission, Joint Research Centre, Institute for Transuranium Elements, P.O.Box 2340, 76125 Karlsruhe, Germany

ABSTRACT

Since the beginning of the 1990's when the first seizures of nuclear material were reported, IAEA has recorded over 200 cases of illicit trafficking of nuclear materials. The number of nuclear material seizures has decreased drastically from the "record" year of 1994 when 45 seizures were recorded to about 10 seizures per year at the present. However, the issue continues to attract public attention and is a reason for concern due to the hazard associated with such a materials. The radiological hazard arises from inappropriate handling, transport or storage, and even more serious concerns arise if considered in a terrorist context. Nuclear material can either be used in a radiological dispersal device, so-called "dirty bomb" or - if available in sufficient quantity and quality - in nuclear explosive devices.

Once illicitly trafficked nuclear material has been intercepted, the following questions are to be addressed: What was its intended use? Where is its origin and who was its last legal owner? Especially the origin is of prime importance in order to close the gaps and improve the physical protection at the sites where the theft or diversion occurred. The analytical strategy is following a step-by-step approach, where based on actual findings the next step is defined and performed.

Analytical methods adapted from nuclear safeguards serve as a basis in nuclear forensic analysis. However, it was soon noticed that they were not sufficient to provide answers to all the questions. Therefore, dedicated nuclear forensic methodology has been developed. This approach combines methods used in nuclear fuel cycle, materials research and environmental studies, including radiometric and mass spectrometric techniques as well as electron microscopy. The conclusions from such investigations need to be supported by reference data whenever possible.

The Institute for Transuranium Elements (ITU) has been involved nuclear forensics research since the beginning. During the last ten years, methods for the age determination of U and Pu, the geolocation of natural U, and the determination of the reactor type from the Pu isotopic composition have been developed. In addition to that some 30 samples originating from real seizures of nuclear material have been analyzed. In this paper, an overview is given on the methodologies used, on the past and on-going developments and on the experience gathered. Some selected examples shall illustrate the challenges and the complexity associated with this work.

How the *f* electrons hide

J. L. Smith, J. C. Lashley, M. E. Manley, B. Mihaila, C. P. Opeil, and R. K. Schulze

Los Alamos National Laboratory

When the *f* electrons seem to come and go in cerium, at least a magnetic moment comes and goes; so things look simple. In plutonium the magnetism that should be there, never shows up. These questions will be reviewed. Recent results will be shown that tie together neutron scattering, photoemission, and thermodynamic measurements. Along with other work, we can put some limits on models of *f*-electron behavior. It does seem as if we have made some progress after years of drought.

Insights into the bonding and electronic nature of heavy element materials

R. G. Haire

Chemical Sciences Division, Oak Ridge National Laboratory, P. O. 2008,
Oak Ridge, TN 37831-6375, USA

ABSTRACT

A long standing issue in heavy element science is what role electrons, especially the f electrons, play in chemical and physical behaviors. This interest prevails not only for differences between the two different f-electron series and but also for comparing a particular element's behavior in its elemental and combined states.

Different types of experimental results over the years have been employed to probe and evaluate the nature of bonding and electronic configurations in these materials. In some instances the conclusions arrived at from experiment and theory has differed, but recently both theory and experimental techniques have become more encompassing and sophisticated.

Interpretations about the electronic interactions and bonding at ambient or elevated temperatures in the f-elements have been employed for many years and have generated information under these conditions. More recently, structural behaviors under pressure and the associated correlations with bonding via experimental methods have become especially enlightening, and have resulted in surprising results. These experimental findings also generated increased theoretical efforts to probe and understand these changes, as well as offer new insights. Modern experimental and theoretical approaches in this arena alone have improved dramatically and now offer improved accuracies and detailed insights.

The changes in bonding and the electronic behavior of metals and alloys from the application of pressure provide different insights into the materials than examined by other techniques and under different conditions. The decreasing interatomic distances occurring under pressure alter energy levels and may provide a different potential for the overlap or hybridization of electronic orbitals. In contrast, changes observed in compounds under pressure may or may not reflect the involvement or a participating role for the f electrons. This difference with compounds probably reflects the presence and different bonding roles of the non-f element atoms, which affect not only the interatomic f-element distances but also the type of electronic orbitals encountered that can potentially interact.

Experimental results obtained from applying pressure are known for Th, Pa, U, Np, Pu, Am, Cm, Bk, and Cf, and attempts have been made to study Es. Several aspects of these elements' behaviors under pressure have also been considered theoretically, and in several instances theory and experiment have now become in accord. The recent findings with curium under pressure are exceptionally interesting, as it displays a unique

phase stabilized due to the magnetic influence of its 5f electrons¹. Yet, there remain some interesting differences between experimental and theoretical interpretations of the changes observed with americium²⁻⁷, which arises from aspects of the “fine tuning” used in the interpretations.

Different aspects of results obtained to date for f-electron materials using different experimental approaches and conditions will be examined and discussed here with regard to electronic configurations and potential changes in bonding. In addition, prospects for future efforts, the potential findings envisioned for these f-electron metals and compounds, and the effects on their fundamental and technological science offer intriguing science for the future. The different prospects presented here will also serve as introductory comments for presentations in the following sessions.

ACKNOWLEDGEMENT

Supported by the Division of Chemical Sciences, Geosciences and Bioscience, Office of Basic Energy Sciences, under DOE contract DE-ACOR-00OR22725 with ORNL, managed by UT-Battelle, LLC.

REFERENCES

1. S. Heathman, R. G. Haire, T. Le Bihan, A. Lindbaum, M. Idiri, P. Normile, S. Li, R. Ahuja, B. Johansson and G. H. Lander, *Science*, (July 1, 2005), **309**,110-113.
2. S. Heathman, R. G. Haire, T. Le Bihan, A. Lindbuam, K. Litfin, Y. Meresse and H. Libotte, *Phys. Rev. Lett.* **85** (2000) 2961.
3. A. Lindbaum, S. Heathman, K. Litfin, Y. Meresse, R. G. Haire, T. Le Bihan and H. Libotte, *Phys. Rev. B*, **67** (2001) 214101
4. P. Söderlind and A. Landa, *Phys. Rev. B*, **72**, 024109 (2005).
5. M. Pénicaud, *J. Phys.: Condens. Matter* **17**, 257 (2005); *Mat. Res. Soc. Symp. Proc.* **893** (2006) 27.
6. P. Söderlind, *Mat. Res. Soc. Symp. Proc.* **893** (2006) 15.
7. S. Y. Savrasov, K. Haule and G. Kotliar, *Phys. Rev. Lett.* **96** (2006) 036404.

Density changes of δ - plutonium with alloying elements and with aging.

W.G. Wolfer

Lawrence Livermore National Laboratory, Livermore, CA 94552, USA

Experiments are conducted at several laboratories to monitor the dimensional changes of Pu-Ga alloys with time, with temperature, and with the alloy composition. Measurements are performed by x-ray diffraction, by EXAFS, by dilatometry, and by immersion density. The dimensional changes attributed to the radioactive decay of plutonium are divided into four processes:

- 1) An initial transient expansion that manifest itself as an increase in both the lattice parameter and the length of a specimen. This expansion is reversible as it can be annealed by heating the material to a temperature above about 450 K.
- 2) A gradual long-term expansion that is attributed to the in-growth of helium bubbles and to the accumulation of actinide daughter products.
- 3) Radiation-induced void swelling is a possible process but has so far not been observed.
- 4) Transformation of the metastable Pu-Ga δ -phase.

We review the experimental data and evidence for each of these four processes and discuss recent theoretical and computational work to explain the data or to predict what might be observed in future experiments.

The transient expansion of plutonium-gallium alloys observed both in the lattice parameter as well as in the dimension of a sample held at ambient temperature is explained by assuming incipient precipitation of Pu₃Ga. However, this ordered ζ' -phase is also subject to radiation-induced disordering. As a result, the gallium-stabilized δ -phase, being metastable at ambient temperature, is both driven towards thermodynamic equilibrium by radiation-enhanced diffusion of gallium and at the same time pushed back to its metastable state by radiation-induced disordering. A steady state is reached in which only a modest fraction of the gallium present is tied up in the ζ' -phase.

Next, we discuss the analysis of irreversible volume changes due to the accumulation of helium and daughter products generated in the radioactive decay of plutonium. It is shown that the lattice parameter changes in δ -phase plutonium caused by Am, U, and Np are significant and compensate to some degree the swelling from helium bubble formation and growth. Comparison with experimental results obtained so far suggests that the decay products dominate the rate of volumetric change in the long run.

The absence of voids or any other observable radiation-induced defects (other than helium bubbles) is discussed in terms of dose rate effects, vacancy migration, nature of the self-interstitial, and dislocation bias. Several of these factors indicate that void swelling is unlikely to occur in Ga-stabilized δ -plutonium.

Plutonium Science Futures

G. H. Lander

*European Commission, Joint Research Center, Institute of Transuranium Elements,
Karlsruhe, D-76125 Germany*

Much was anticipated at the discovery of plutonium in 1941 in Berkeley, but initially the chemical and metallurgical properties were completely mystifying. By the mid 1960s the physical properties, even at low temperature were reasonably well characterized. With a few notable exceptions, e.g. photoemission, *most* properties of Pu were known by the 1970 Conference in Sante Fe. However, these properties of Pu continue to test our basic understanding even today. Actinide science has flourished in the last 50 years, and very often Pu is at the heart of it – take, for example, the recent discovery of superconductivity at 18 K in a Pu-containing compound.

This overall activity, crucial for the underpinning of nuclear technology, is at risk due to the ever-tightening regulations and difficulty of access. Of course, we cannot have Pu in every University Laboratory, but we must find a way to keep research on plutonium chemistry and physics alive and diversified, and more people interested in the basic properties, chemical and physical, of the transuranium materials. The political consequences of the actinides will not “go away” by pretending Pu does not exist.

For presentation at the “Plutonium Futures – The Science 2006”
Asilomar, CA, July 12, 2006

“Plutonium World Futures”

Siegfried S. Hecker

Center for International Security and Cooperation

Stanford University

For presentation at “Plutonium Futures – The Science 2006

Asilomar, CA

July 12, 2006

In addition to being the most complex element in the periodic table, plutonium also has great societal impact. It has become to symbolize everything we associate with the nuclear age. It evokes the entire gamut of emotions from good to evil, from hope to despair, and from the salvation of humanity to its utter destruction. No other element bears such a burden. Its discovery in 1941, following the discovery of nuclear fission in 1938, unlocked the potential and fear of the nuclear age. During the Cold War, plutonium was of interest primarily for nuclear weapons and deterrence. Beginning in the 1950s, it also became an integral part of the quest for almost limitless electrical power. Today, concerns over energy availability and global climate change have rekindled interest in nuclear power. However, to benefit from the factor of millions that splitting the atom provides, we must tackle the challenges posed by concerns about the proliferation of nuclear weapons, the disposal of nuclear waste, and the cleanup of nuclear contamination at the world's weapons sites. We can't just make plutonium go away – so we must learn to manage it, and this has to be a cooperative international venture.

Theoretical Studies of the Structure and Bonding of Actinide Complexes

B. E. Bursten^{*,†}, J. Li[#], T. Yang[†], J. L. Sonnenberg[†], and M. Mrozi[†]

^{*}Department of Chemistry, University of Tennessee, Knoxville TN 37902 USA

[†]Department of Chemistry, The Ohio State University, Columbus OH 43210 USA

[#]William R. Wiley Environmental Molecular Sciences Laboratory, Pacific Northwest National Laboratory, Richland WA 99352 USA

We have used density functional theory with relativistic corrections and higher level electronic structural methodologies to address the structure and bonding of a number of interesting actinide coordination complexes. Results will be presented on a variety of systems, including the products of laser-ablated actinide atoms with small substrate molecules, coordination complexes of actinide and actinyl ions with unusual ligands, and the multi-shell coordination chemistry of actinide ion in aqueous solution.

Among the specific systems to be discussed will be the CUO molecule, which is formed experimentally upon the reaction of U atoms with CO and which shows significant interactions with noble-gas atoms. We will recap the history of the discovery of this unusual bonding interaction, which has ultimately led to unusually extensive noble-gas coordination chemistry at a uranium center. These results will be extended to a discussion of molecular UO₂, which has received a great deal of recent experimental and theoretical study and has proven to be a vexing molecule with respect to electronic structure.

We will also present recent results on using density functional theory to describe the static structures of the first two hydration shells of the hydrated Cm³⁺ ion (Figure 1). We have used molecular dynamics calculations to determine the lifetime of the second shell, which we predict to be stable enough to be observed.

Finally, we will present our recent studies of unusual structural motifs, including bent uranyl complexes and organouranium complexes that contain “linear” Cp*-U-Cp* (Cp* = η⁵-C₅Me₅) linkages.

We gratefully acknowledge support from the Division of Chemical Sciences, Geosciences, and Biosciences, Office of Basic Energy Sciences, U.S. Department of Energy, the Ohio Supercomputer Center, and the Molecular Science Computing Facility at the Environmental Molecular Sciences Laboratory at Pacific Northwest National Laboratory.

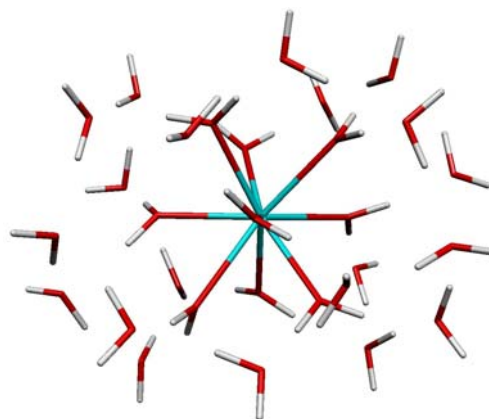


Fig 1: Depiction of the optimized structure of a Cm³⁺ ion with nine and 20 water molecules in the first and second coordination spheres: [Cm(H₂O)₉(H₂O)₂₀]³⁺

Fun at the Bottom of the Periodic Table: Novel Reactivity Patterns in Actinide Molecular Systems

Jaqueline L. Kiplinger

Los Alamos National Laboratory, Los Alamos NM 87545 USA

Although transition-metal complexes possessing terminal Schrock-type alkylidene ($M=CR_1R_2$) functionalities are well known, related actinide complexes have remained elusive.¹ Traditional routes employed for the preparation of transition-metal alkylidene complexes include α -hydrogen abstraction and carbene transfer from diazoalkanes.¹

We have investigated the reaction chemistry of low-valent organouranium complexes with diazoalkanes. Reaction of the known complex $(C_5Me_5)_2UCl_2$ with two reducing equivalents (provided by KC_8), followed by reaction with excess diphenyldiazomethane generates the bis(diphenyldiazomethane) uranium complex $(C_5Me_5)_2U(=N-N=CPh_2)(\eta^2-(N_2)-N=N=CPh_2)$ (Figure 1).

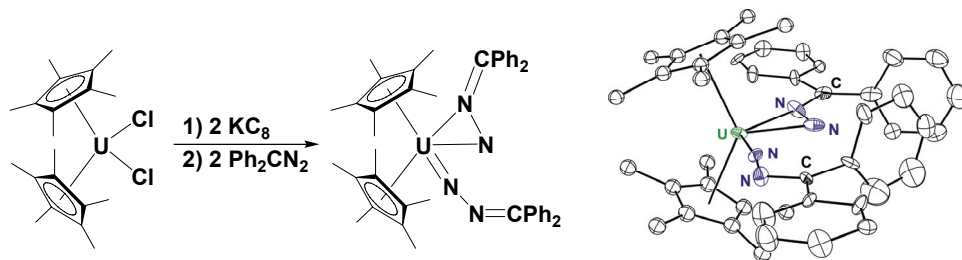


Fig 1: Synthetic scheme for the preparation of a uranium diazoalkane complex and its molecular structure.

This is the first example of a diazoalkane actinide complex and is unlike existing transition metal diazoalkane complexes in that it possesses two diazoalkane molecules bound to a single uranium metal center: one diazoalkane is coordinated to the uranium metal center in an η^1 -fashion and forms a uranium imido ($U=N$) bond with a short $U-N$ bond distance of 1.921 Å and a $U-N-N$ bond angle of 172.8°. The second diazoalkane is coordinated to the uranium in an η^2 -manner, possibly through the $N=N$ π -system ($U-N = 2.452, 2.325$ Å). The exceedingly long $N-N$ bond distance (1.411 Å) compared with that of uncomplexed diazoalkanes (1.12–1.13 Å) indicates that substantial π -backbonding from the $(C_5Me_5)_2U$ fragment (orbitals of the appropriate symmetry exist) to the diazoalkane lowest unoccupied molecular orbital (LUMO), which is $N-N$ antibonding. Interestingly, theoretical (DFT) calculations reveal an $f^1\pi^*$ electronic configuration and suggest delocalization of a 5f electron throughout the $N=N=C$ framework of the η^2 -coordinated diazoalkane. Spectroscopic data support the hypothesis of donation of electron density from the uranium metal center onto the diazoalkane molecule.

Recent reports have shown that oxidatively induced α -hydrogen abstraction may be used to prepare early transition metal alkylidene complexes.² The propensity of uranium to exist in the

hexavalent oxidation state coupled with the known oxophilicity of tetravalent uranium, suggested to us that uranium(VI) alkylidene complexes of the type, $(C_5Me_5)_2U(=O)(=CHR)$, might be prepared by oxidatively-induced α -hydrogen abstraction chemistry between uranium(IV) bis(alkyl) complexes such as $(C_5Me_5)_2U(CH_2R)_2$ and an appropriate oxygen atom transfer agent.

Pyridine N-oxide is a prototypical oxygen atom transfer reagent that has been routinely used in the synthesis of high-valent transition metal and actinide oxo complexes.³ We have found that uranium(IV) and thorium(IV) bis(alkyl) complexes of the type $(C_5Me_5)_2AnR_2$ ($An = U, Th$; $R = CH_3, CH_2Ph$) instead activate the sp^2 and sp^3 hybridized C-H bonds in pyridine N-oxide and lutidine N-oxide to produce the corresponding cyclometallated complexes, $(C_5Me_5)_2An(R)[\eta^2-(O,C)-ONC_5H_4]$ and $(C_5Me_5)_2An(R)[\eta^2-(O,C)-ON-2-CH_2-5-CH_3-C_5H_3]$ (Figure 2).⁴

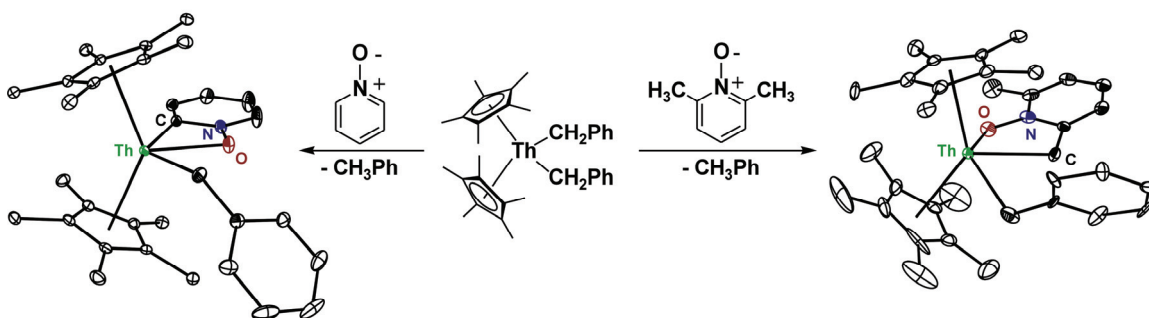


Fig 2: Scheme illustrating the reactivity of $(C_5Me_5)_2Th(CH_2Ph)_2$ towards sp^2 and sp^3 hybridized C-H bonds in pyridine N-oxides.

Interestingly, the thorium(IV) bis(alkyl) and bis(aryl) complexes $(C_5Me_5)_2ThR_2$ ($Me = CH_3, R = CH_2C_6H_5$ or C_6H_5) have been found to mediate ring-opening and dearomatization of the pyridine ring in pyridine N-oxide under ambient conditions to afford the first thorium $\eta^2-(O,N)$ oximate complexes.⁵ These reactions provide rare examples of C-H and C=N activation chemistry mediated by actinide metal ions with accessible 5f orbitals, and such transformations represent new types of reactivity available to pyridine N-oxide. Recent developments in this exciting area of chemistry will be presented.

For financial support, we acknowledge the Division of Chemical Sciences, Office of Basic Energy Sciences, and the Los Alamos National Laboratory's Laboratory Directed Research & Development (LDRD) Program.

- 1 R. R. Schrock, Chem. Rev. **102**, 145-179 (2002), and references therein.
- 2 F. Basuli, B. C. Bailey, J. Tomaszewski, J. C. Huffman, and D. J. Mindiola, J. Am. Chem. Soc. **125**, 6052-6053 (2003).
- 3 For example, see: (a) C. C. Cummins, R. R. Schrock, and W. M. Davis, Inorg. Chem. **33**, 1448-1457 (1994). (b) S. M. Mullins, A. P. Duncan, R. G. Bergman, and J. Arnold, Inorg. Chem. **40**, 6952-6963 (2001). (c) K. M. Sung, and R. H. Holm, J. Am. Chem. Soc. **123**, 1931-1943 (2001).
- 4 J. A. Pool, B. L. Scott, and J. L. Kiplinger, J. Am. Chem. Soc. **127**, 1338-1339 (2005).
- 5 J. A. Pool, B. L. Scott, and J. L. Kiplinger, Chem. Commun. 2591-2593 (2005).

Covalency in the *f*-element–chalcogen bond. Computational studies of $[M(N(EPR_2)_2)_3]$ ($M = \text{Pu, U, Ce, La}$; $E = \text{O, S, Se, Te}$; $R = \text{H, Me}$)

K. I. M. Ingram^{*}, N. Kaltsoyannis^{*}, A. J. Gaunt[†], M. P. Neu[†]

^{*} University College London, London, WC1H 0AJ, UK.

[†] Los Alamos National Laboratory, Los Alamos, NM 87545, USA.

INTRODUCTION

Current understanding of chemical bonding involving *5f*-elements still trails behind that of the transition metals and lanthanides. This is partly due to a paucity of well characterized molecular complexes featuring donor atoms spanning the range from hard to soft, as actinide chemistry has traditionally been dominated by hard donor ligands, especially oxygen. Recently, however, there has been increased research into the chemistry of the actinides with softer donor ligands such as nitrogen and sulfur. This interest is partly fundamental, but also stems from the anticipation that subtle differences between lanthanide *5d4f*- and actinide *6d5f*-orbital bonding with soft donor ligands will find application in the separation of lanthanides from actinides in, for example, nuclear wastes.¹ A thorough understanding of the changes in *f*-element–ligand bonding as the donors progress from hard to soft, especially the extent to which covalent interactions influence chemical structure and reactivity, is therefore extremely important for both fundamental and applied reasons.

At the *Actinides 2005* conference in Manchester, UK, and in reference 2, two of us reported the synthesis and characterisation of a range of homoleptic, trivalent lanthanum and uranium complexes with imidodiphosphinochalcogenide ligands $[N(EPPh_2)_2]^-$ and $[N(EP^iPr_2)_2]^-$ ($E = \text{S, Se}$). The X-ray crystal structure of $[U(N(SP^iPr_2)_2)_3]$ is shown in Figure 1.

The comparison between analogous La(III) and U(III) imidodiphosphinochalcogenide compounds is very interesting for, as shown in Table 1 below, the metal–chalcogen distances show significant differences. Clearly, the U–chalcogen distance in both types of system is significantly shorter than the corresponding La–chalcogen bond, and this difference increases as the chalcogen becomes softer. Given that the six-coordinate ionic radii of La^{3+} and U^{3+} are essentially the same, 1.045 and 1.040 Å respectively, the logical conclusion is that there is some additional bonding interaction present in the uranium compounds, presumably covalent in nature.

Building on the La(III)/U(III) results, very recent work at Los Alamos has furnished analogous Pu(III) and Ce(III) imidodiphosphinochalcogenide complexes (the six co-ordinate

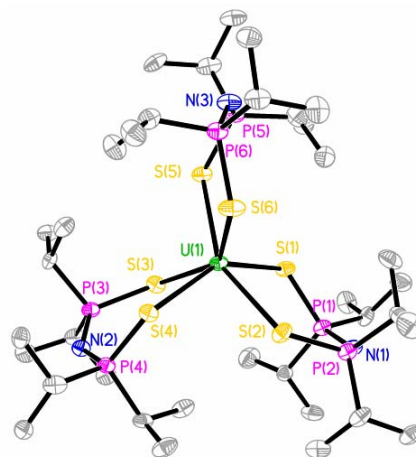


Fig 1: The X-ray crystal structure of $[U(N(SP^iPr_2)_2)_3]$.

ionic radii of Pu³⁺ and Ce³⁺ are essentially the same as one another). These results allow further An(III)/Ln(III) comparisons to be made, and also comparisons within the actinide and lanthanide series. These new compounds, and the La(III) and U(III) systems discussed above, are the focus of the present computational study, together with complexes containing oxygen- and tellurium-donor imidodiphosphinochalcogenide ligands. The extension to the O- and Te-based ligands allows us to probe the *f*-element–chalcogen bond for all of the first four group 16 elements, with the aim of establishing the extent of covalency, and its dependence upon the metal and chalcogen.

Compound	Bond	Distance/Å	Difference (La-U/Å)
[La(N(SPPh ₂) ₂) ₃]	La(III)–S	3.0214(11)	
[U(N(SPPh ₂) ₂) ₃]	U(III)–S	2.9956(5)	0.0258
[La(N(SePPh ₂) ₂) ₃]	La(III)–Se	3.1229(3)	
[U(N(SePPh ₂) ₂) ₃]	U(III)–Se	3.0869(4)	0.0360
[La(N(SP ⁱ Pr ₂) ₂) ₃]	La(III)–S	2.892(1)	
[U(N(SP ⁱ Pr ₂) ₂) ₃]	U(III)–S	2.854(7)	0.038
[La(N(SeP ⁱ Pr ₂) ₂) ₃]	La(III)–Se	3.019(3)	
[U(N(SeP ⁱ Pr ₂) ₂) ₃]	U(III)–Se	2.964(7)	0.055

Table 1: Metal–ligand bond distances in [M(N(EPR₂)₂)₃] (M = La, U; E = S, Se; R = Ph, ⁱPr).

COMPUTATIONAL STUDIES

Relativistic, gradient-corrected density functional theory has been used to probe the geometric and electronic structures of the title compounds (models for the experimentally reported systems). Excellent agreement has been found between the computed geometries and those of the experimentally characterised compounds. The bonding between the metals and the chalcogens has been investigated using a variety of analysis tools, including the Mulliken and NBO population and charge schemes, and the Ziegler-Rauk energy decomposition scheme. It will be shown that the computational data clearly indicate that there are greater covalent interactions between a given metal and the chalcogen donor atoms of the ligands as the chalcogen is altered from O to Te, and also as the metal is changed from Ln to An for a given chalcogen. The relative role of the *d* and *f* valence atomic orbitals in these covalent interactions will be discussed, as will the effects of the actinide contraction, *i.e.* the differences between analogous Pu(III) and Ce(III) complexes will be compared with the corresponding U(III) and La(III) systems.

We are grateful to the UK's EPSRC for computational resources under grant GR/S06233/01.

- 1 M. P. Jensen and A. H. Bond, *J. Am. Chem. Soc.* **124**(33), 9870 (2002).
- 2 A. J. Gaunt, B. L. Scott and M. P. Neu, *Chem. Commun.*, 3215 (2005).

Soft X-ray Emission and Absorption Spectroscopy for Curium-Nitrogen Donor Ligand Complex System

T. Yaita* and D.K. Shuh**

* Actinide Coordination Chemistry Group, Quantum Beam Science Directorate, Japan Atomic Energy Agency (JAEA), 1-1-1 Koto, Sayo-cho, Sayo-gun, Hyogo 679-5148, Japan.

** Actinide Chemistry Group, Chemical Sciences Division, Lawrence Berkeley National Laboratory (LBNL), Berkeley CA 94720-8175, USA.

INTRODUCTION

Soft donor aromatic nitrogen ligands (N-donor) often show unique properties, which are not observed in the oxygen (O)-donor type ligand complexes, in their chemical bonding with trivalent actinides. This unique feature is not observed strongly in lanthanide complexes. Therefore, the application of N-donor ligands have great promise for the partitioning of trivalent actinides from lanthanides for the transmutation of poisonous nuclides such as Am-241 by burning up with an ADS (Accelerator Driven System) or FBR (Fast Breeder Reactor system). This essential mechanism is considered to originate from a covalent interaction between the actinide and ligand, however, no detailed studies on their chemical bond from the viewpoint of electronic structure have been performed to date. In this study, we investigate the valence electronic structure for a Cm-N donor ligand utilizing soft x-ray emission and x-ray absorption spectroscopies. The x-ray emission and absorption spectra experimentally give us an approximate partial density of state (PDOS). The soft donor ligands in this study are *1,10*-Phenanthroline (Phen) and the derivatives, and show high separation factor between trivalent actinide and lanthanide ($SF=D_{Am}/D_{Eu}$, D: Distribution ratio), as shown in Fig. 1. The base Phen ligand shows an interesting substituent effect on the SF (Fig. 1) and series of studies on the electronic structure with varying SF would be of particular interest.

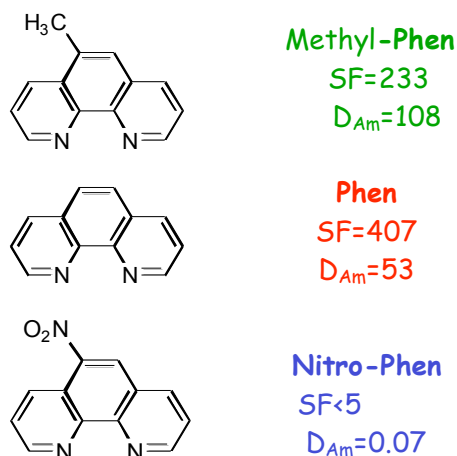


Fig. 1: *1,10*-Phenanthroline (Phen) and the derivatives.

*D_M: Distribution ratio of a metal, M;
SF= D_{Am}/D_{Eu}.

**These extractions were performed by CHCl₃ with NH₄SCN under pH=4.

EXPERIMENTAL

Complex samples were synthesized by mixing M^{3+} and ligand with a 1:2 ratio in methanol solutions. In methanol solutions, we have previously confirmed that the trivalent metal ion forms a 1:2 complex with the ligands based on UV-VIS spectrophotometric titration spectra. The x-ray emission and absorption spectra of Cm, Eu and the other lanthanides-ligand complexes were measured at the BLs 7.0.1 and 8.0.1 of the Advanced Light Source. EXAFS structural studies of the lanthanide complexes by were also performed at the BL11 of Super Photon Ring 8 GeV (SPring8).

RESULTS AND DISCUSSION

Figure 2 shows the N-K XAS and XES spectra of the Phen, Cm-Phen, and Eu-Phen complexes. All of the spectra corresponding to the ligand 2p PDOS are observed, in which both Fermi levels are located at ~ 395 eV, measured from N 1s core level. The sharp peaks in the XAS spectra arise from the $1s \rightarrow \pi^*$ transition and are observed within ~ 1.5 eV of $E - E_F$. The lineshapes of Cm-Phen complex have quite different profiles which exhibit broadening and decreased intensities compared to the Phen ligand when normalized to the peaks for the $1s \rightarrow \sigma^*$ transition at 7~12 eV. The lineshapes of the Eu-Phen spectra do not show appreciable differences compared to the spectra from base ligand. Furthermore, a significant difference in the XES (PDOS of the occupied states) of Cm-Phen spectrum appears around -6 eV (arrow in Fig. 2). It is a noteworthy result from the viewpoint of evidence for a covalent interaction between Cm and Phen ligand. Namely, it suggests that some interaction like back-donation from Cm increases the N-2p PDOS of the Phen. In this presentation, we will discuss the substituent effect in the Phen system and the molecular design of N-donor ligands for 4f/5f separations based on the results of this study.

Acknowledgements

Authors thank to the Dr. Ikeda, Mrs. Numakura and Kobayashi for the sample preparation.

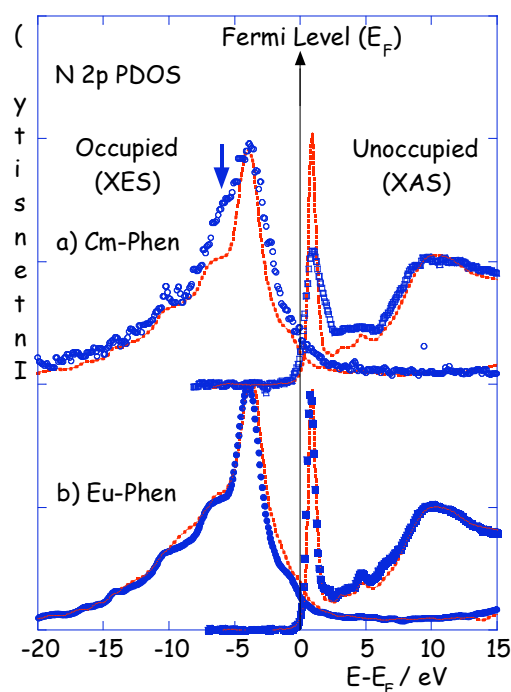


Fig.2:

The experimental N-2p PDOS for the Phen, Cm-Phen, and Eu-Phen derived from XES and XAS spectroscopies.

*The samples are: a) $\text{Cm}(\text{Phen})_2\text{Cl}_3(\text{H}_2\text{O})_x$ (○:XES, □:XAS); b)

$\text{Eu}(\text{Phen})_2\text{Cl}_3(\text{H}_2\text{O})_x$ (●:XES, ■:XAS).

** The Phen spectra are overlapped as the dashed line (---).

*** The XES spectra are obtained by x-ray irradiation at greater than 425 eV.

Muon Spin Relaxation (μ SR) Studies of α -Pu, δ -Pu and PuCoGa₅

R. H. Heffner^{a,b}, G. D. Morris^c, M. J. Fluss^d, E. D. Bauer^b, B. Chung^d, W. Higemoto^a, T. U. Ito^f, D. E. MacLaughlin^e, S. McCall^d, K. Ohishi^a, J. L. Sarrao^b and L. Shu^e

^a Japan Atomic Energy Agency, Tokai-Mura, Ibaraki-Ken, 319-1195 Japan

^b Los Alamos National Laboratory, MS K764, Los Alamos, New Mexico 87545 USA

^c TRIUMF, 4004 Wesbrook Mall, Vancouver, B.C., Canada V6T 2A3

^d Lawrence Livermore National Laboratory, Livermore, California 94552 USA

^e Department of Physics, University of California, Riverside, California 92521 USA

^f Department of Physics, Tokyo Institute of Technology, Meguro-ku, Tokyo 152-8551 Japan

During the past decade there has been a resurgence of interest in the electronic properties of Pu metal and Pu compounds, principally because the f-electrons in Pu sit at the boundary between localization and itinerancy,¹ thus presenting a challenge for modern theories of correlated electron physics.

In Pu metal interest has centered on whether or not magnetic order exists in the high temperature fcc δ phase, which occurs in pure Pu near 700 K, but can be stabilized at room temperature by alloying with a few percent Al or Ga, for example. Neutron scattering experiments² have set a limit of 0.04-0.4 μ_B for the ordered moment in δ -Pu, but only recently have theories been able to predict such a small value.³

Adding to the interest in Pu-based materials, superconductivity was recently discovered^{4,5} in PuCoGa₅ and PuRhGa₅. These compounds are structurally the same as their more studied Ce analogs CeCoIn₅ and CeIrIn₅ in which superconductivity is found to exist in close proximity to magnetic phases near a quantum critical point. A key question has been whether these structurally similar materials also possess similar superconducting order parameters, pairing mechanisms and associated magnetic and superconducting phase diagrams. Also relevant to the Pu superconductors is the effect of self-induced radiation damage on their intrinsic properties.

In this paper we summarize the results of muon spin relaxation (μ SR) measurements carried out in α - and δ -Pu (Pu alloyed with 4.3 at. % Ga) and in the superconducting state of PuCoGa₅. The Pu metal studies were designed to search for evidence of magnetic ordering, and have set the most stringent limits to date for the ordered moment: $\mu_{\text{ord}} < 10^{-3} \mu_B$, about 40 times smaller than obtained with neutron scattering. In PuCoGa₅ the temperature dependence of the magnetic penetration depth $\lambda(T)$ was investigated in a fresh sample and again in the same sample after 400 days of aging. We find $\lambda(T) \propto T$ for $T \leq T_c/2$, indicating a line of nodes in the superconducting order parameter. Remarkably, the temperature dependence of $\lambda(T)$ is little changed even after significant radiation damage.

Our results are compared to NMR experiments^{6,7} in nominally the same materials (δ -Pu, PuCoGa₅ and PuRhGa₅) to illustrate the complementarities of the techniques.

Acknowledgements: Work at LANL and LLNL (contract W-7405-Eng-48) performed under the U.S. D.O.E. Work at Riverside supported by the U.S. NSF, Grant DMR-0422674. We thank the

staff at TRIUMF and acknowledge helpful discussions with F. Jutier, G. Lander, P. M. Oppeneer, J. D. Thompson and F. Wastin.

¹ J. M. Wills *et al.*, J. of Electron Spectroscopy and Related Phenomena **135**, 163 (2004).

² J. C. Lashley *et al.* Phys. Rev. **B71**, 054416 (2005).

³ A. B. Schick *et al.* Europhys. Lett. **69** 588 (2005); A. O. Shorikov *et al.*, Phys. Rev. **B72**, 024458 (2005).

⁴ J. L. Sarrao *et al.*, Nature **420**, 297 (2002).

⁵ F. Wastin *et al.*, J. Phys.: Condens. Matter **15**, S2279 (2003).

⁶ N. J. Curro and L. Morales, MRS Society Symp. Proc. **802**, 53 (2003).

⁷ Yu. Piskunov *et al.*, Phys. Rev. **B71**, 174410 (2005); S. V. Verkhovskii *et al.*, JETP Lett. **82**, 139 (2005).

Americium under pressure

J.-C. Griveau^{*}, J. Rebizant^{*}, R.G. Haire[§], G. Kotliar[†], G.H. Lander^{*}.

^{*} European Commission, Joint Research Centre, Institute for Transuranium Elements Postfach 2340, 76125 Karlsruhe, Germany

[§] Oak Ridge National Laboratory (ORNL), Chemical Sciences Division, Office Box 2008, MS-6375, Oak Ridge, TN 37831, USA

[†] Center for Materials Theory, Department of Physics and Astronomy, Rutgers University, Piscataway, New Jersey 08854, USA

High-pressure measurements of the resistivity of americium metal (dhcp structure at ambient pressure) are reported to 27 GPa and down to temperatures of 0.4 K [1] under magnetic field. Americium is the first actinide element in which, at ambient pressures, the $5f$ electrons may be described as localized (as in most of the $4f$ rare-earth series) and thus do not participate in the bonding. Am^{3+} has an electronic ground state with a $J = 0$ singlet, so that (in Russell-Saunders coupling) $L = -S = 3$ and no magnetic moment exists. This simple picture of Am metal (6 f electrons forming an inert core decoupled from the spd electrons) led to the prediction [2] in 1975 of superconductivity in Am, a prediction soon verified [3] showing $T_c = 0.79$ K. Resistivity under pressure [4] showed that T_c rapidly increased with pressures in the GPa range. The question is when the $5f$ electrons begin to affect the low-energy properties of Am. How do they affect the superconductivity when $5f$ spectral weight is present at Fermi Energy, taking part in the formation of Cooper pairs? Previous studies [5] indicate that Am at ambient pressure is a type-I superconductor with a small zero-temperature critical field $H_c(0) = 53$ mT. The pressure dependence of the upper critical fields is surprising, with $H_c(0)$ increasing rapidly with pressure (~ 1 T at the maximum of T_c). The study of superconductivity in Am metal reveals that, contrary to expectations, the $5f$ electrons play an important role in this material even at low pressures. Furthermore, the localization-delocalization (Mott) transition in Am is a gradual phenomenon rather than the abrupt change predicted by theory. There is no sign of any transition to ordered magnetism, as judged by an anomaly in the resistivity, in contrast to the predictions [6].

This work was supported by “Training and Mobility of Researchers” program of European Union (project number EU 2000/30/02). GK is supported by DOE-DE-FG02-99ER45761..

- 1 J.-C. Griveau, Phys. Rev. Lett. **94**, 097002 (2005)
- 2 B. Johansson and A. Rosengren, Phys. Rev. B **11**, 2836 (1975)
- 3 J. L. Smith and R. G. Haire, *Science* **200**, 535 (1978)
- 4 P. Link *et al.*, J. Phys.: Con-dens. Matter **4**, 5585 (1992).
- 5 J. L. Smith *et al.*, J. Physique **40**, C4-138 (1979)
- 6 P. Söderlind *et al.*, Phys. Rev. B **61**, 8119 (2000)

Many-body Electronic Structure of Americium Metal

S. Savrasov^{*}, K. Haule[†], G. Kotliar[†]

^{*}University of California, Davis CA 95616 USA

[†]Rutgers University, Piscataway, NJ 08854 USA

INTRODUCTION

Artificially produced from Plutonium-239 in 1944, and widely used in smoke detectors Americium is the first transuranic actinide where 5f6 electrons become localized and form a closed relativistic subshell. Its recent high-pressure studies[1] have drawn much attention as understanding volume behavior in actinides systems has important consequences on their storage and disposal. They have revealed that Am undergoes a series of structural phase transitions (denoted hereafter as I, II, III, and IV) and reproduces at least two of the structures of another mysterious element, Plutonium, which links the physical behavior of all actinides materials to our fundamental understanding of bonding between their 5f- electrons. At ambient pressure Am I behaves as an ordinary metal with slightly enhanced electrical resistivity $\rho(T=300K)=68 \mu \times \text{cm}$ and no sign of ordered or disordered magnetism. This is standardly understood as a manifestation of 7F0 ground state singlet of 5f6 atomic configuration. However, the resistivity of Am raises almost an order of magnitude and reaches its value of $500 \mu \times \text{cm}$ at the orthorhombic structure of Am IV which is realized at pressures P above 16 GPa. The most prominent feature of the pressure P vs. volume V behavior is the existence of two distinct phases: the “soft” one which occurs in Am I through III as well as another “hard” phase realized in Am IV. On top of that a superconductivity in Am was first predicted[2] and then discovered[3] with Tc raising from 0.5K in Am I to 2.2K in Am II, falling slightly in Am III and then exhibiting a sharp maximum in phase IV[4].

METHOD

In this work we introduce a novel many-body electronic structure method which allows us to uncover the physics of Am. It is based on dynamical mean field theory (DMFT), a modern many body technique for treating strongly correlated electronic systems in a non-perturbative manner[5, 6] and at the same time has computational efficiency comparable with ordinary electronic structure calculations thus allowing us to deal with complicated crystal structures of real solids by self-consistent many-body calculations. Our new method considers the local Green function as a variable in the total energy functional and can be viewed as spectral density functional theory[7, 8, 9]. The advantage of such formulation as compared to original density functional theory[10] is a simultaneous access to energetics and local excitation spectra of materials with arbitrary strength of the local Coulomb interaction U.

RESULTS

The computational speed gained by our new algorithm allows us to study complicated crystal structures of Am. In particular, the existence of soft and hard phases in its equation of state can

be predicted via our self-consistent total energy calculations. Our calculation reproduces the well known fact that the f electrons in Am at zero pressure exists in a $f_6 7F_0$ configuration.

To gain theoretical insight and understand the origin of localization-delocalization transition we discuss the behavior of the electronic structure under pressure. Upon compression, the remarkable effect is observed as peak near the Fermi level gets pushed down while a resonance (small shoulder) starts forming at E_f and becomes more pronounced with increasing pressure.

The f_6 ground state of the atom starts admixing an f_7 configuration with a very large total spin of $J=7/2$. Due to hybridization with the spd bands, this large spin gets screened thus lowering the energy of the system. This is the famous Kondo mechanism, and the energy gain increases as the hybridization increases by applying pressure.

We also estimate the superconducting critical temperature by computing from first principles [11] the electron-phonon coupling of the electrons in the presence of correlations. For this purpose we have extended a newly developed dynamical mean field based linear response method, which has previously proven to provide accurate phonon spectra in correlated systems [12,13]. We estimate the coupling constant which comes out to be sufficiently high (~ 0.5) to predict superconductivity of the order of 1 K. The occurrence of the first maximum in experimental T_c vs pressure dependence, can then be understood as the result of the variation of the spd density of states which first increases as a result of a band structure effect but then eventually decreases as the hybridization with the f electron grows with the increase of mixed valence.

The content of this work is currently in press [14].

Support by the DOE grant DE-FG02 99ER45761, the NSF grants 0238188, 0312478, 0342290 and US DOE Computational Material Science Network is gratefully acknowledged.

- 1 S. Heathman, R. G. Haire, T. Le Bihan, A. Lindbaum, K. Litfin, Y. Méresse, and H. Libotte, Phys. Rev. Lett. 85, 2961 (2000).
- 2 B. Johansson and A. Rosengren, Phys. Rev. B 11, 2836 (1975).
- 3 J.L. Smith and R.G. Haire, Science 200, 535(1978).
- 4 J.-C. Griveau, J. Rebizant, and G. H. Lander, G. Kotliar, Phys. Rev. Lett. 94, 097002 (2005).
- 5 Gabriel Kotliar and Dieter Vollhardt, Physics Today 57, 53 (2004).
- 6 A. Georges, G. Kotliar, W. Krauth and M. J. Rozenberg, Rev. Mod. Phys. 68, 13 (1996).
- 7 R. Chitra, and G. Kotliar, Phys. Rev. B 63, 115110 (2001).
- 8 S. Savrasov, G. Kotliar, and E. Abrahams, Nature 410, 793 (2001).
- 9 S. Y. Savrasov, G. Kotliar, Phys. Rev. B 69, 245101 (2004).
- 10 For a review, see, e.g., Theory of the Inhomogeneous Electron Gas, edited by S. Lundqvist and S. H. March (Plenum, New York, 1983).
- 11 S. Y. Savrasov, D. Y. Savrasov and O. K. Andersen, Phys. Rev. Lett. 72, 372 (1994).
- 12 X. Dai, S. Y. Savrasov, G. Kotliar, A. Migliori, H. Ledbetter, E. Abrahams, Science 300, 953 (2003).
- 13 S. Y. Savrasov, G. Kotliar, Phys. Rev. Lett. 90, 056401 (2003).
- 14 S. Y. Savrasov, K. Haule, G. Kotliar, Phys. Rev. Lett., in press (2006); cond-mat/0507552.

Conditions for Magnetism in Pu systems

L. Havela^{*}, P. Javorsky^{*}, F. Wastin[†], E. Colineau[†], T. Gouder[†], A.B. Shick^{††}, V. Drchal^{††}

^{*}Charles University, Faculty of Mathematics and Physics, department of Electronic Structures, Ke Karlovu 5, 121 16 Prague 2, The Czech Republic

[†]European Commission, Joint Research Centre, Institute for Transuranium Elements, Postfach 2340, 76 125 Karlsruhe, Germany

^{††}Institute of Physics, Academy of Sciences of the Czech Republic, Na Slovance 2, 182 21 Prague 8, The Czech Republic

ELECTRONIC STRUCTURE OF d-Pu

While light actinide elements are Pauli paramagnets with the itinerant $5f$ states at the Fermi level, the localization for actinides behind Am leads to magnetic ordering analogous to lanthanides. The specific position of Pu just before the localization threshold should make it very sensitive to external variables, but various Pu allotropic phases have surprisingly nearly identical weak magnetic susceptibility, despite a large volume expansion exceeding 20% for the *fcc* δ -Pu comparing to monoclinic α -Pu. This situation poses a problem for theoretical description, because LDA or GGA calculations indicate the formation of magnetic moments for the expanded phases¹. Our recent LDA+U calculations² (*around mean field* version), which yield a non-magnetic ground state ($S = 0, L = 0$) and correct cohesion properties, suggest that the key, at least for δ -Pu, can be the $5f$ -count approaching the non-magnetic $5f^6$ state, i.e. much higher than the originally expected value close to 5.0. The calculations also indicate³ that the magnetic order is not established, when the lattice is expanded by Am doping, or if the dimensionality is reduced. For the terminal concentration of pure Am the LDA+U calculations³ correctly reproduce the non-magnetic $5f^6$ state.

The main characteristics of the Pu- $5f$ states is the density of one-electron states concentrated around 1 eV binding energy, while the empty states of the $5f_{7/2}$ character are about 4 eV above E_F . Variations with increasing Am concentration in the *fcc* Pu-Am solid solution were found negligible. If this picture is credible, the high value of the g -coefficient of low-temperature electronic specific heat, as well as high-intensity f -emission observed close to E_F by PES, should have been due to many-body states, as suggested in Refs.4,5. One way to test the adequacy of our LDA+U calculations is to study experimentally the behaviour of expanded Pu. For this purpose, the doping by Am is the most efficient tool. Unlike the common δ -phase stabilizing dopings by Al or Ga, the doping by Am expands the lattice, and the expansion is larger than e.g. for the Ce doping.

Considering the alternative scenario, at which a narrow $5f$ band at E_F is the key ingredient bringing δ -Pu to the verge of magnetism, such expansion should lead to increase of g , presumably to onset on magnetic order, and all properties would undergo a dramatic development due to the changing density of one-electron states at E_F , increasing up until it is suddenly forced to leave the Fermi level due to incipient localization.

PROPERTIES OF Pu-Am SYSTEM

Am doping to Pu corresponds to a dilution by a non-magnetic element. Magnetic susceptibility of Am is rather high (the value approaching $1 \cdot 10^{-8} \text{ m}^3/\text{mol}^6$) due to the Van Vleck susceptibility of the $5f^6$ state with $J = 0$. The behaviour of Am under pressure^{7,8} suggests that the localized character is not affected even if the volume is compressed to the volume of δ -Pu. We can therefore assume that the non-magnetic character of Am stays throughout the Pu-Am system at ambient pressure. This is corroborated by rather invariable character of Am electronic states obtained from calculations mentioned above. In fact, Pu and Am are not completely miscible, but the *fcc* structure extends at least to 75% Am, while remaining as a high-temperature phase of pure Am. Here we review recent results on Pu-Am system using photoelectron spectroscopy (PES) and specific heat. Although PES does not bring any direct information on a possible magnetic order, the invariable character of the Pu- $5f$ states, evidenced for concentration to about 30% Am, excludes any noticeable change of the ground state. Moreover, the g -values weakly decrease with increasing Am concentration, even if they are normalized per mole of Pu (assuming a negligible contribution from Am, as $g_{\text{Am}} = 2 \text{ mJ/mol K}^2$), from 60 mJ/mol Pu K² for Pu-8%Am to 48 mJ/mol Pu K²

for Pu-15% Am. These findings, together with the observed insensitivity of electrical resistivity and magnetic susceptibility⁹ to the volume expansion (3.5% for Pu-20% Am comparing to pure δ -Pu), indicate that the alternative $5f$ narrow-band scenario is not tenable for δ -Pu.

WHICH Pu SYSTEMS CAN BE MAGNETIC?

The non-magnetic character of δ -Pu is well established^{10,11}. We have been showing that the important feature of the non-magnetic ground state could be the proximity of the $5f$ count obtained to the non-magnetic $5f^6$ singlet. The LDA+U calculations indicate that even if such state is hybridized with conduction electrons and part of the $5f$ charge is lost, the hole in the $5f_{5/2}$ states can remain isotropic, i.e. without any spin or orbital polarization. Such state can be then robust with respect to lattice expansion or reducing the dimensionality. A hint how to reach a magnetic state for Pu would be to allow for a higher depletion of the $5f$ states by hybridization in a compound, while keeping the $5f$ band narrow enough in the sense of Hill limit arguments. Inspecting the occurrence of Pu magnetism, we can understand why the Pu chalcogenides PuS, PuSe, PuTe are weakly magnetic, while the pnictides as PuSb, with one less electron and assumed $5f^5$ state, are magnetically ordered¹². Another instructive example is the behaviour of Pu in diluted alloys. For example, Pu has magnetic moment as diluted in Pd,¹³ which contrasts with non-magnetic U diluted in Pd.¹³ A certain charge transfer towards the Pd- $4d$ states, induced by the large difference in electronegativity of Pd and the actinides, which probably eliminates the U moments, can give rise to the Pu moments. As a conclusion, we suggest that a reduction of the $5f$ count due to bonding is a necessary pre-requisite for Pu magnetism, which is indeed observed in many compounds.

The present work was undertaken within the "Actinide User Laboratory" programme conducted at the ITU-Karlsruhe. The financial support to users from the European Commission, DG-JRC is acknowledged. The work of P.J. and L.H. was also supported by the Grant Agency of the Czech Republic under the grant No. 202/04/1103.

- 1 P. Söderlind, A. Landa, B. Sadigh, Phys.Rev.B **66**, 205 109 (2002).
- 2 A.B. Shick, V. Drchal, L. Havela, Europhys.Lett. **69**, 588 (2005).
- 3 A.B. Shick, L. Havela, J. Kolorenc, V. Drchal, T. Gouder, P.M. Oppeneer, Phys.Rev.B, in press.
- 4 S.Y. Savrasov, G. Kotliar, E. Abrahams, Nature **410**, 793 (2001).
- 5 L.V. Pourovskii, M.I. Katsnelson, A.I. Lichtenstein, L. Havela, T. Gouder, F. Wastin, A.B. Shick, V. Drchal, G.H. Lander, Europhys. Lett., in press
- 6 B. Kanellakopoulos, A. Blaise, J.M. Fournier, Solid State Commun. **17**, 713 (1975).
- 7 A. Lindbaum, S. Heathman, K. Litfin, Y. Meresse, R.G. Haire, T. Le Bihan, H. Libotte, Phys.Rev.B **63**, 214101 (2001).
- 8 J.-C. Griveau, J. Rebizant, G.H. Lander, G. Kotliar, Phys.Rev.Lett. **94**, 097002 (2005).
- 9 N. Baclet et al., to be published.
- 10 J.C. Lashley, A. Lawson, R.J.McQueeney, G.H. Lander, Phys.Rev.B **72**, 054416 (2005).
- 11 R.H. Heffner et al., arXiv:cond-mat/0508694, (2005)
- 12 see various chapters in Handbook on the Physics and Chemistry of the Actinides, edited by A.J. Freeman and G.H. Lander, vols. 1 and 2, North Holland, Amsterdam, 1985
- 13 W.J. Nellis and M.B. Brodsky, Phys.Rev.B **4**, 1594 (1971).

Subsurface Bio-mediated Reduction of Higher-Valent Uranium and Plutonium

D. T. Reed^{*}, G. Smith[#], R. Deo⁺, B. Rittmann⁺, J. F. Lucchini^{*},
M. Borkowski^{*}, M. K. Richmann^{*}

^{*} Earth and Environmental Sciences Division, Los Alamos National Laboratory, Carlsbad NM 88220 USA

[#]Department of Biology, New Mexico State University, Las Cruces NM 88003 USA

⁺Center for Environmental Biotechnology, Arizona State University, Tempe AZ 85282 USA

INTRODUCTION

The role and importance of redox reactions in determining actinide subsurface mobility are beyond question. In the subsurface, redox control is often established by the iron mineralogy and associated aqueous chemistry^{1, 2}. There is also a growing recognition of the important role microbiological processes have in defining the redox chemistry of multivalent actinide species^{3, 4} by both direct and indirect means. The mechanisms by which redox control is established is a key aspect of remediation and immobilization strategies for actinides when they are present as subsurface contaminants.

The important effects of redox-active minerals (e.g. iron and iron oxides) and microbial processes on subsurface redox processes are not mutually exclusive⁵. Metal reducing bacteria often modulate the oxidation state of aqueous iron species and can solubilize iron to increase its bioavailability. It is this coupling of biological and geochemical processes, and correspondingly its effect on actinide speciation, that is the focus of our current studies. Progress made in the study of bio-mediated reduction pathways towards the reduction of Pu (VI) and U (VI) species by *S. algae BrY* under anoxic conditions is reported.

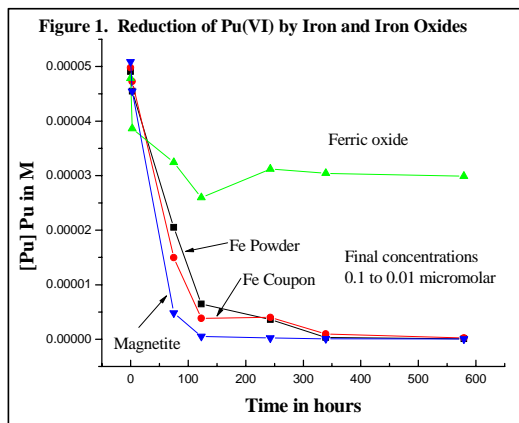
EXPERIMENTAL APPROACH

Shewanella Algae strain *BrY* is a dissimilatory gram negative iron reducing bacteria that was isolated from the Great Bay estuary, New Hampshire⁶. It is a facultative anaerobe that was grown aerobically on tryptic soy broth prior to use. Cells were harvested, rinsed in PIPES media, concentrated by centrifugation, and then re-suspended to prepare an inoculum stock prior to addition into the various growth media in an anoxic glovebox, where the experiments were conducted.

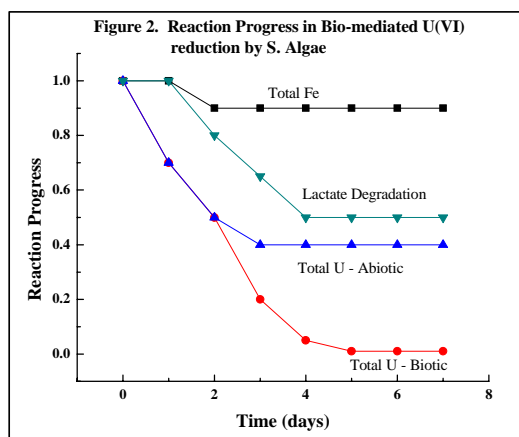
Uranium (as UO_2^{2+}) and plutonium (as PuO_2^{2+} or PuO_2^+) were the initial species added to the various growth media or groundwater simulants (~pH 7-8). Iron, when present, was added as a stabilized Fe^{3+} - NTA complex. Lactate was used as the electron donor. Total uranium, iron, and plutonium concentrations were determined by ICP-MS (Agilent) specially configured for iron analysis. Lactate was analyzed using a lactate analysis kit based on a colorimetric technique. NTA and other organics were analyzed by ion chromatography (Dionex DX 500). Absorption spectrometry (CARY 500) was used to establish and confirm the actinide and iron oxidation states.

RESULTS AND DISCUSSION

Abiotic and biotic experiments were performed. In the abiotic experiments, Pu(VI) and U(VI) were added to pH ~ 7-8 groundwater in the presence of iron and iron oxides to establish the redox trends. Example results for Pu(VI) and iron oxides are shown in Figure 1. Here it was observed that on a timeframe of less than 100 hours almost all the Pu(VI) was reduced when reduced iron was present. The most rapid reduction rate was observed with magnetite and attributed to the presence of Fe(II) in the oxide. The corresponding decrease in total plutonium concentration to sub-micromolar concentrations is indicative of a redox process where Pu(IV/III) species are being generated. When only Fe(III) was present, as was the case with hematite, the plutonium concentration did not decrease substantially but essentially all the Pu(VI) was reduced to Pu(V). U(VI), under similar conditions, was stable towards reduction for over a year although eventually reduction was noted.



In the biotic experiments performed, the goal was to establish the conditions and key mechanisms leading to actinide reduction. Direct and indirect (co-metabolic) pathways for reduction exist. In the presence of *S. algae*, and 10 mM of Fe^{3+} as an NTA complex, no reduction of iron or uranium was noted under aerobic conditions. When anaerobic conditions were established both iron (III) and uranium (VI) were reduced (see Figure 2). Although uranium precipitated, iron remained solubilized as an Fe^{2+} complex. Analogous results were obtained with plutonium but there is a much greater effect of abiotic processes and reactions. Establishing the mechanistic details of these abiotic and direct/indirect biotic processes is the subject of ongoing research.



This work is performed in part under the Actinide Chemistry and Repository Science Program supported by the Waste Isolation Pilot Plant (DOE-CBFO) and the Natural and Accelerated Bioremediation Research program (DOE-OBER/OS).

1. D.T. Reed, J.F. Lucchini, S.B. Aase, and A.J. Kropf, accepted in *Radiochim Acta*, (2006)
2. J. Farrell, W.D. Bostick, R.J. Jarabeck, and J.N. Fiedor, *Ground Water* 37(4), 618 (1999).
3. J.E. Banaszak, B.E. Rittmann, and D.T. Reed, *J. Radioanal. Nuc. Ch.* 241, 385 (1999).
4. B.E. Rittmann, J.E. Banaszak, and D.T. Reed, *Biodegradation*, 13(5) 329-42 (2002).
5. D. Fortin and S. Langley, *Earth-Sciences Reviews* 72, 1-19 (2005).
6. F. Caccavo, R.P. Blakemore, D.R. Lovley, *Appl. Environ. Microbiol.* 58, 3211-3216 (1992).

Disproportionation of Pu(IV) or a two step mechanism? Redox behavior of Pu(IV) in acidic solutions

C. Walther*, H.R. Cho*, C.M. Marquardt*, V. Neck*, A. Seibert†, J.I. Yun* and Th. Fanghänel*‡

*Forschungszentrum Karlsruhe, Institut für Nukleare Entsorgung, D-76021 Karlsruhe, Germany

†European Commission, JRC, Inst. For Transuranium Elements, D-76125 Karlsruhe, Germany

‡Physikalisch-Chemisches Institut, Ruprecht-Karls Universität,
Im Neuenheimer Feld 253, D-69120 Heidelberg, Germany

The redox behavior of plutonium in acidic solutions has been studied for many decades. The formation of Pu(III), Pu(V) and Pu(VI) in Pu(IV) solutions exposed to air is usually ascribed to the disproportionation of Pu(IV) into Pu(III) and Pu(V), followed by the reaction of Pu(V) with Pu(IV) or the disproportionation of Pu(V) into Pu(III) and Pu(VI).¹⁻⁴ As the measured oxidation state distributions led to doubts on this reaction path,^{3,5} we have revisited this topic and studied 10^{-5} to $5 \cdot 10^{-4}$ M Pu(IV) solutions ($\text{pH}_c = 0.3 - 2.1$ in 0.5 M HCl/NaCl, 22°C) as a function of time. The solutions were obtained by dilution of electrochemically prepared Pu(IV) stock solutions. The concentrations of $\text{Pu}^{\text{IV}}(\text{aq})$, Pu^{3+} , PuO_2^+ and PuO_2^{2+} were determined by UV/Vis/NIR absorption spectroscopy, using a 1m-capillary cell for low concentrations. Partly the solutions were colloid-free, partly they included Pu(IV) colloids, in particular at Pu(IV) and H^+ concentrations above the reported solubility of $\text{PuO}_2(\text{am,hyd})$.⁶ The presence or absence of Pu(IV) oxyhydroxide colloids > 5 nm was confirmed by laser-induced breakdown detection (LIBD)^{5,6}. As the fraction of polymeric or colloidal Pu(IV) cannot be quantified by spectroscopy it was calculated from the difference $[\text{Pu}]_{\text{tot}} - \{[\text{Pu}^{\text{IV}}_{\text{aq}}] + [\text{Pu}^{3+}] + [\text{PuO}_2^+] + [\text{PuO}_2^{2+}]\}$.

The disproportionation of Pu(IV) solutions at pH 0 - 2 leads to Pu(III) and, depending on pH, to Pu(V), Pu(VI) or both¹⁻⁴: $3 \text{Pu}^{4+} + 2 \text{H}_2\text{O} \Leftrightarrow 2 \text{Pu}^{3+} + \text{PuO}_2^{2+} + 4 \text{H}^+$

Accordingly and independent of whether an equilibrium state is reached or not, the following balance must be valid for Pu(III), Pu(V) and Pu(VI) formed from Pu(IV):³

$$[\text{Pu(III)}] = [\text{Pu(V)}] + 2 [\text{Pu(VI)}] \quad (1)$$

However, none of the solutions investigated in the present study (two examples are shown in Fig.1) fulfils this balance at reaction times < 10 days. Instead, the formation of Pu(III) is always approximately equal to the simultaneous decrease of $\text{Pu(IV)}_{\text{aq}}$ (Fig.1, left):

$$d[\text{Pu(III)}]/dt = - d[\text{Pu(IV)}_{\text{aq}}]/dt \quad (2)$$

i.e., $\{[\text{Pu(IV)}_{\text{aq}}] + [\text{Pu(III)}]\} = \text{constant}$ and, as a consequence:

$$d\{[\text{Pu(V)}] + [\text{Pu(VI)}]\}/dt = - d[\text{Pu(IV)}_{\text{coll}}]/dt. \quad (3)$$

At concentrations above the solubility of $\text{PuO}_2(\text{am,hyd})$ (Fig.1, right) it is directly observed, that $[\text{Pu(IV)}_{\text{coll}}] + [\text{Pu(V)}]$ remains constant.

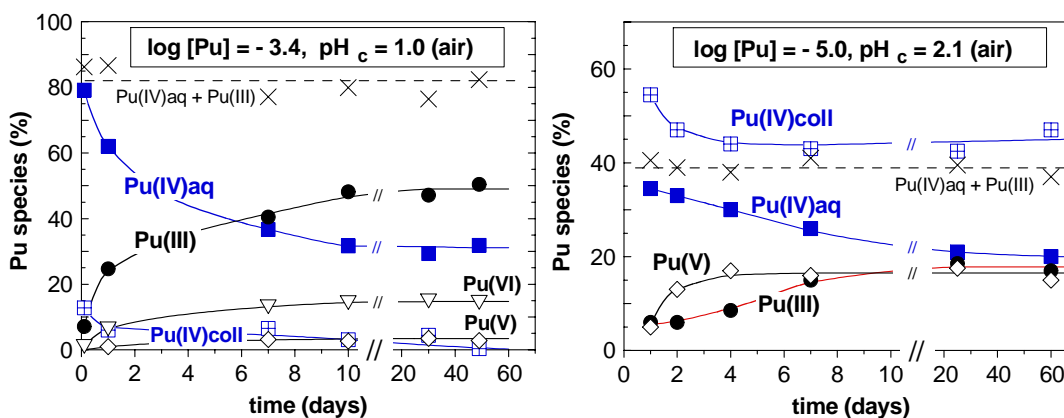
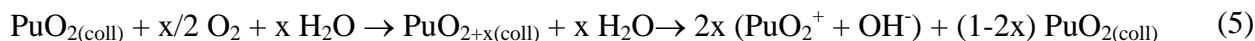


Fig 1: Oxidation state distributions of initially Pu(IV) solutions as a function of time

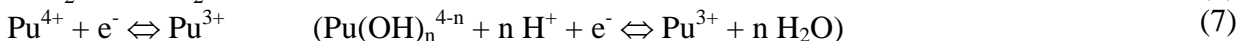
The present results indicate that the so-called ‘disproportionation of Pu(IV)’ is a two-step process. The initial step is the formation of PuO_2^+ , either by the redox equilibrium with $\text{PuO}_{2(\text{am, hyd})}$ ^{7,8} which is equal to $\text{PuO}_n(\text{OH})_{4-2n} \cdot x\text{H}_2\text{O}$ colloids > 5 nm:



or by the oxidation of colloidal or smaller polynuclear Pu(IV) species by O_2 , analogous to the water-catalyzed oxidation of solid $\text{PuO}_{2(\text{s, hyd})}$ to $\text{PuO}_{2+x(\text{s, hyd})}$ ⁹, followed by the dissolution of the oxidized Pu(V) fractions:



The second step is the simultaneous equilibration of the redox couples Pu(V)/Pu(VI) and Pu(IV)/Pu(III) which are related by pe (and pH because of Pu(IV) hydrolysis equilibria):



This mechanism explains that the sum $\{[\text{Pu(III)}] + [\text{Pu(IV)}_{\text{aq}}]\}$ always remains constant. It also explains that colloid-free Pu(IV) solutions at very low pH (e.g. pH 0.3), *i.e.*, far below the solubility of $\text{PuO}_{2(\text{am, hyd})}$,⁶ reacts much more slowly and to a lesser extent than at pH = 1.0 where polynuclear and colloidal Pu(IV) is formed immediately. In the experiment at $[\text{Pu}]_{\text{tot}} = 1.0 \cdot 10^{-5} \text{ M}$ and $\text{pH}_c = 2.1$ (Fig. 1, right), considerably above the solubility of $\text{PuO}_{2(\text{am, hyd})}$,⁶ Pu(V) is evidently formed faster than Pu(III), not simultaneously as required by the disproportionation reaction.

The oxidation state distributions and pe values measured after equilibration times of more than 20 days are consistent with the known redox equilibria (4), (6) and (7).^{7,8,10} The ‘disproportionation’ reactions also describe correctly equilibrium state thermodynamics, but not the underlying reaction mechanism.

- 1 R.E. Connick and W.H. McVey, J. Am. Chem. Soc., **75**, 474,(1953)
- 2 S.W. Rabideau, J. Am. Chem. Soc., **75**, 798 (1953) and **79**, 6350 (1957)
- 3 D.A. Costanzo, R.E. Biggers and J.T. Bell, J. Inorg. Nucl. Chem., **35**, 609 (1973)
- 4 H. Capdevila, P. Vitorge and E. Giffaut, Radiochim. Acta, **58/59**, 45 (1992)
- 5 C. Walther, C. Bitea, J.I. Yun, J.I. Kim, Th. Fanghanel, C.M. Marquardt, V. Neck and A. Seibert, Actinides Research Quarterly, Los Alamos Natl. Lab., **11**, 12 (2003)
- 6 R. Knopp, V. Neck and J.I. Kim, Radiochim. Acta, **86**, 101 (1999)
- 7 D. Rai, Radiochim. Acta, **35**, 97 (1984)
- 8 H. Capdevila and P. Vitorge, Radiochim. Acta, **82**, 11 (1998)
- 9 J.M. Haschke and V.M. Oversby, J. Nucl. Mat., **305**, 187 (2002)
- 10 R.J. Lemire, J. Fuger, H. Nitsche, P. Potter, M.H. Rand, J. Rydberg, K. Spahiu, J.C. Sullivan, W.J. Ullman, P. Vitorge, H. Wanner (OECD,NEA-TDB). *Chem. Thermodyn. Neptunium & Plutonium*. Elsevier, Holland, (2001)

Plutonium Speciation in Environmental Systems, From Hydrolysis to Aerobic and Anaerobic Biogeochemistry

M. P. Neu^{*}, S. D. Reilly^{*}, W. Runde, S. A. Stout^{*} and H. Boukhalfa^{*}

^{*}Los Alamos National Laboratory, Los Alamos CA 87545 USA

Plutonium is present in the environment as a result of nuclear energy and weapons production. Surficial contamination can be removed. Given the impressive sensitivity of radioanalytical methods and mass spectroscopy, the transport of residual contamination can be detected and tracked. However the form of Pu can rarely be determined from direct characterization. Generally, the concentration of plutonium is too low or the conditions of the measurement(s) are different from the conditions at the sample site. Thus, the plutonium migration can be observed, but not predicted since the mechanism of transport can not be discerned.

In order to develop an ability to forecast the stability and long-term fate of plutonium we must understand fundamental plutonium redox, complexation reactions, surface reactions, and coupled biogeochemical processes that can be individually parameterized and systematically combined. Together with site-specific properties, such as the chemical composition and Eh of the water, the microscopic and macroscopic mineralogy, the amount and viability of microorganisms present, and the underlying hydrology and geomorphology of the region, these thermodynamic and kinetic values can be used in fate and transport codes. This presentation will review the mechanisms and reactions that have been reported and the research that remains to realize a predictive model of plutonium speciation and resultant mobility in aqueous environmental systems.

U(VI) Silicate Solid Phases as Sinks for Sequestration of Non-U f-element Cations in the Environment

S. B. Clark*

*Washington State University, Department of Chemistry, Pullman, WA, 99164-4630

INTRODUCTION

If used nuclear fuel is disposed of in a high-level waste repository without reprocessing, the uranium fuel will oxidize on a geologic time scale to form U(VI) solids. The 1:1 uranyl silicate minerals such as uranophane ($\text{Ca}[(\text{UO}_2)_2(\text{SiO}_3\text{OH})_2] \cdot 5(\text{H}_2\text{O})$) and boltwoodite ($(\text{Na}, \text{K})[(\text{UO}_2)(\text{SiO}_3\text{OH})](\text{H}_2\text{O})_{1.5}$) may be important solids for controlling the environmental availability of other f-elements that are produced during neutron irradiation. These solids provide surfaces to which the non-U f-elements may sorb or solids into which they may be incorporated. Often, very finely divided nano-materials are present, and appear to play an important role in sequestration. Defining mechanisms of sorption and/or incorporation of these f-elements along with thermodynamic descriptions of these processes are needed for performance assessment activities in high level waste disposal. In this presentation, the chemistry of these U(VI)-silicate solids will be explored, along with the partitioning of non-U f-elements to them.

EUROPIUM PARTITIONING INTO URANOPHANE¹

Uranophane was synthesized with various mole ratios of $\text{Eu}^{3+}:\text{Ca}^{2+}$ present. In all solids prepared, the Eu^{3+} was sequestered to the U(VI) silicate solid formed. Powder x-ray diffractograms of the resulting solids indicated that on the bulk-level, the uranophane structure was preserved when the mole ratio of $\text{Eu}^{3+}:\text{Ca}^{2+}$ remained below 10%. At higher levels of Eu^{3+} , a crystalline solid was formed that was not consistent with the uranophane structure. For those solids with 10% or less Eu^{3+} present, transmission electron microscopy analysis of the solid indicates that the bulk material is actually a mixture of needle-like materials as expected for uranophane, and additional finely divided materials with diffraction patterns that are not consistent with uranophane. Microscale elemental analysis of these materials indicates that the polycrystalline solids are largely responsible for sequestration of most of the Eu^{3+} . The uranophane needles do incorporate small quantities of Eu^{3+} , but never more than 5 mole %.

NEPTUNIUM PARTITIONING TO URANOPHANE²

In this case, both uranophane and sodium boltwoodite were prepared in the presence of trace quantities of neptunium (V) as the NpO_2^+ cation (0.5 – 2.0 mole %, relative to U). In all cases, the Np is quantitatively sequestered into the U(VI) silicate solid. The presence of the Np did not alter the powder diffraction patterns of the resulting solids. Individual crystallites of the solids were analyzed with transmission electron microscopy and electron energy loss

spectroscopy to demonstrate that Np is associated with isolated solids. No evidence for discrete Np phases such as Np oxides was observed.

SUMMARY

These results will be described for Eu^{3+} and NpO_2^+ partitioning into the 1:1 U(VI) silicate solids. The structures of uranophane and boltwoodite will be described along with the possibilities for Eu^{3+} and NpO_2^+ substitution into the solids. Where possible, incorporation will be distinguished from sorption. In both cases, thermodynamic approaches for treating these processes during modelling will be described.

Project funding was provided by DOE's Office of Science, Heavy Elements program. Former graduate student, Dr. Matthew Douglas of PNNL, is acknowledged for much of the experimental work described. WSU College of Sciences Microscopy facility was used for scanning electron microscopy. Prof. Rod Ewing and Dr. Satoshi Utsunomiya of University of Michigan are acknowledged for the transmission electron microscopy work on the Eu^{3+} solids. Dr. Edgar Buck and staff of PNNL's Radiochemical Sciences and Engineering group are acknowledged for the transmission electron microscopy of the NpO_2^+ -containing solids.

- 1 Matthew Douglas, Washington State University PhD Thesis; "Uranium(VI) solid phases formed in the presence of Np and other metal cations", 2005.
- 2 M. Douglas, S. B. Clark, J. I. Friese, B. W. Arey, E. C. Buck, B. D. Hanson, S. Utsunomiya, and R. C. Ewing, "Microscale characterization of U(VI) silicate solids and associated Np", *Radiochimica Acta*, **93**, 265-272 (2005).

Radionuclide Distribution in Debris from Underground Nuclear Tests Detonated in Silicate and Carbonate Rocks

M. Zavarin, P. Zhao, Q. Hu, T. P. Rose, and A. B. Kersting

Chemical Biology and Nuclear Science Division, Lawrence Livermore National Laboratory, Livermore, CA, USA 94551

Underground nuclear detonations produce a diverse suite of radionuclides that includes tritium, fission products, activation products, and residual actinide fuel¹. The initial distribution of these species within a test cavity and chimney is determined by the temperature and pressure history immediately following the explosion.² Refractory species that condense at high temperatures tend to be partitioned into the ‘melt glass’, while volatile species that condense at lower temperatures tend to be more widely dispersed throughout the rubblized cavity-chimney environment. Recommendations for radionuclide partitioning have been published³, but for many species there is still a significant margin of uncertainty in these estimates. Furthermore, radionuclide partitioning has been developed only for tests conducted in rock or alluvium dominated by aluminosilicate minerals. No such partitioning information is available for tests conducted in carbonate rock (Figure 1).

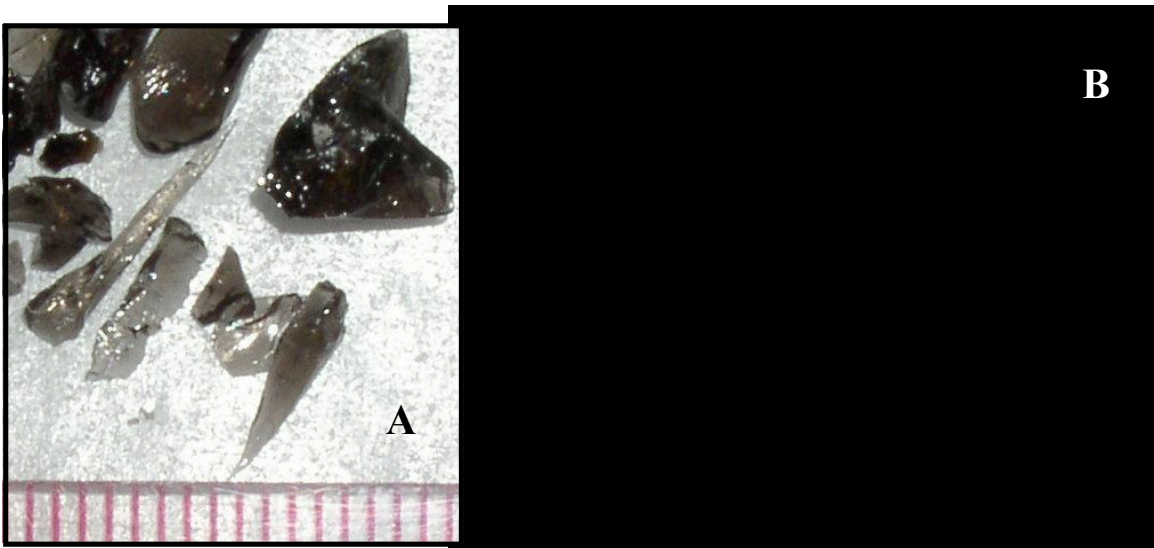


Fig 1: Photographs illustrating the textural characteristics of nuclear test debris. (A) Dark-colored aluminosilicate melt glass exhibiting typical ‘obsidian-like’ textures and (B) Friable, chalk-like carbonate test debris exhibiting only minor glassy and iron-oxide stained fragments.

We will describe the results of two separate investigations into the physical and chemical distribution of radionuclides in underground nuclear test cavities at the Nevada Test Site (NTS). In 2005, we investigated radionuclide redistribution from the Chancellor test. The Chancellor test was detonated in the U-19ad emplacement hole on 1 September 1983 at a vertical depth of 2,047 ft (624 m) below the surface of Pahute Mesa, NTS. It has an announced yield of 143 kt.⁴

The test was conducted in the Tertiary rhyolite of Echo Peak⁵, a devitrified lava of the Paintbrush Group that erupted from the Claim Canyon Caldera approximately 12.8 million years ago⁶. For plutonium, 1.5% of the inventory is contained in the rubble fraction and 98.5% is present in the melt glass. These results are in agreement with estimates reported by the IAEA³ (2% rubble, 98% glass). However, they differ from the 0% rubble fractionation (100% in glass) reported by the French³ and are less conservative than the 5% rubble fractionation (95% in glass) used in recent radionuclide contaminant transport models at the NTS. For uranium, approximately 94% of the test-derived uranium is contained in the melt glass, and 6% is in the rubble. The uranium fraction in the rubble is somewhat lower than the IAEA estimate of 10%. However, compared to plutonium, it is apparent that uranium is more volatile and is redistributed more widely in the nuclear test cavity.

Presently, we are investigating the radionuclide distribution in tests conducted in carbonate rock. Only four tests were conducted in the carbonate rock in Yucca Flat, NTS. However, two tests are located close enough to saturated water table to provide a direct path for radiologic contamination of the regional carbonate aquifer. We expect the partitioning of Pu and U in the debris from carbonate tests to differ significantly from that of tests conducted in aluminosilicate rock due to their widely differing early time pressure, temperature, and rock condensation histories. We will describe the partitioning of various classes of radionuclides between the “melt glass” and rubble in carbonate tests and compare these results to the partitioning behaviour observed in the Chancellor test. Furthermore, we will describe how the Underground Test Area (UGTA) project utilizes this partitioning information to develop radionuclide reactive transport models and predict the extent of groundwater contamination at the NTS.

This work was funded by the Underground Test Area Project, National Nuclear Security Administration, Nevada Site Office and was performed under the auspices of the U.S. Department of Energy by Lawrence Livermore National Laboratory under contract W-7405-Eng-48.

- 1 S.M. Bowen, *et al.*, Nevada Test Site Radionuclide Inventory, 1951-1992. Los Alamos National Laboratory, LA-13859-MS (2001).
- 2 I.Y. Borg, R. Stone, H.B. Levy, and L.D. Ramspott, Information Pertinent to the Migration of Radionuclides in Ground Water at the Nevada Test Site. Part 1: Review and Analysis of Existing Information. Lawrence Livermore National Laboratory, UCRL-52078 Pt. 1 (1976).
- 3 IAEA, The Radiological Situation at the Atolls of Mururoa and Fangataufa, Technical Report, Volume 3: Inventory of Radionuclides Underground at the Atolls. International Atomic Energy Agency, Vienna, Austria, IAEA-MFTR-3 (1998).
- 4 DOE/NV, United States Nuclear Tests, July 1945 through September 1992. U.S. Department of Energy, Nevada Operations Office, Las Vegas. DOE/NV-209 (Rev. 15) (2000).
- 5 Pawloski, G.A., *et al.*, Categorization of Underground Nuclear Tests on Pahute Mesa, Nevada Test Site, for Use in Radionuclide Transport Models. Lawrence Livermore National Laboratory, UCRL-TR-208347 (2002).
- 6 Sawyer, D.A., *et al.*, Episodic caldera volcanism in the Miocene southwestern Nevada volcanic field: revised stratigraphic framework, ⁴⁰Ar/³⁹Ar geochronology, and implications for magmatism and extension. *Geol. Soc. Am. Bull.*, **106**: 1304 (1994).

Microbial Transformations of Plutonium

A. J. Francis, C.J. Dodge and J.B. Gillow

Environmental Sciences Department, Brookhaven National Laboratory, Upton, NY 11973, USA

The presence of Pu in transuranic (TRU)- and mixed-wastes together with organic compounds, is a major concern because of the potential for migration from the waste repositories and contamination of the environment¹⁻⁴. Pu exists in several oxidation states (III, IV, V, VI) and as various chemical species (salts, organic complexes, colloids) having a very complex chemistry and environmental behavior. Soil pH, the presence of organics, redox conditions, mineralogy, and microbial activity affect the chemical speciation of Pu¹⁻⁵. Chelating agents, such as citric acid, are present in Waste Isolation Pilot Plant (WIPP) TRU and mixed wastes. Citric acid forms a strong complex with Pu(IV) and has been used in extracting ²³⁹Pu from contaminated soil.

Microorganisms have been detected in low-level radioactive wastes, TRU wastes, Pu-contaminated soils, and in current and planned waste-repository sites for disposal of nuclear waste. Leachates collected from the low-level radioactive-waste sites contained ²³⁸, ²³⁹, ²⁴⁰Pu (gross alpha activity of 1.7×10^5 pCi/L), aerobic- and anaerobic- bacteria (*Bacillus* sp., *Pseudomonas* sp., *Citrobacter* sp., and *Clostridium* sp.) and organic compounds^{1,2,4}. The radioactive- and organic-chemicals in the leachate were not toxic to the bacteria. Metabolically active microbes were identified at the LANL's TRU waste burial site containing ²³⁹Pu-contaminated soil. Microorganisms present in the radioactive wastes can affect the long-term stability of radionuclides. We investigated the biotransformation of Pu-citrate and Pu-nitrate by aerobic and anaerobic bacteria, respectively.

Reductive dissolution of Pu(IV) by the anaerobic bacterium *Clostridium* sp. Addition

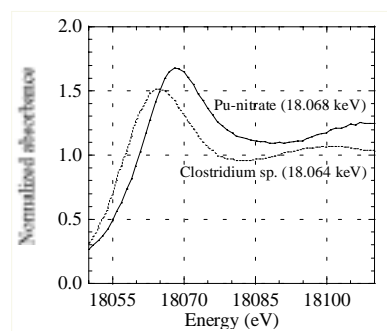


Fig 1. XANES analyses of Pu before and after bacterial action.

of 1×10^{-7} M ²⁴²Pu (IV)-nitrate had no effect upon the growth and metabolism of glucose of *Clostridium* sp. Plutonium added to the bacterial growth medium (uninoculated control) resulted in its precipitation and was removed by 0.4 μ m filtration. Speciation calculations showed that Pu most likely existed as Pu(OH)₄ at pH 6.2 due to hydrolysis and polymerization. The growth of the bacterium lowered the Eh of the medium from +50 mV to -180 mV, and the pH from 6.2 to 2.8, concomitant with the production of acetic and butyric, acids and carbon dioxide (225 μ mol). After 14h of growth, 70% of the Pu passed through a 0.4 μ m filter and 55% passed through a 0.03 μ m filter suggesting a significant portion of Pu was solubilized. Solvent extraction by thenoyltrifluoroacetone (TTA) confirmed a decrease in the polymeric form of Pu and an increase in the soluble fraction, suggesting the presence of Pu³⁺. XANES analysis of the culture at the Pu L_{III} edge (18.057 keV) confirmed that the oxidation state was Pu³⁺ (Figure 1). The Eh of the medium was low and the CO₂ concentration high, thus favouring the reduction of Pu from the tetravalent to the trivalent state. These results suggest that under appropriate conditions Pu can be reduced to Pu(III) by anaerobic bacteria.

Biotransformation of Pu(IV)-citrate complex by *Pseudomonas fluorescens*.

Electrospray ionization-mass spectrometry (ESI-MS) analysis of ^{242}Pu -citrate in the presence of

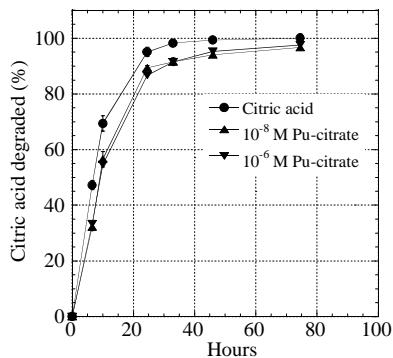


Fig 2. Effect of adding ^{242}Pu on citrate metabolism. Citric-acid concentration is 10^{-4} M.

excess citric acid indicated the presence of a biligand Pu-cit₂ complex. XANES and EXAFS analyses showed that Pu was in the +4 oxidation state and associated with citric acid as a mononuclear complex. The metabolism of citric acid by *P. fluorescens* was not affected by the presence of 10^{-5} M Pu. The Pu-citrate complex is relatively stable in the absence of bacterial activity. However, in the presence of bacteria and after complete metabolism of citrate, solvent extraction by TTA and microfiltration (0.03 μm) of the medium showed that the Pu was present in the polymeric form. High ionic strength (0.9M) of the medium affected citrate metabolism, and Pu remained in solution complexed with citric acid. The extent of formation of the Pu polymer depended on the Pu:citrate ratio, the extent of citrate metabolism, and the ionic strength of the medium.

Mobilization of Pu from contaminated Soils. Chemical characterization of Pu at contaminated sites shows that its environmental form varies according to the site and the waste stream. For example, at Rocky Flats, CO, the predominant form appears to be as $\text{PuO}_2(\text{s})$; at the Nevada Test Site Pu was associated with mineral colloids; while, at Oak Ridge, TN it is associated with organic matter. Pu is generally considered to be relatively immobile; however, its transport, albeit at very low concentrations, has been observed at several DOE sites including Rocky Flats (RF), Los Alamos National Laboratory (LANL), and Nevada Test Site (NTS)⁶. Plutonium in surface waters at the RF site was shown to be associated with organic macromolecules⁷. Studies with Pu contaminated soils show that Pu and other radionuclides can be remobilized due to enhanced aerobic or anaerobic microbial activity. Studies are under way to determine the mechanisms of dissolution of Pu from contaminated soils.

Acknowledgments

This research was supported by the Environmental Remediation Sciences Division, Office of Biological and Environmental Research, Office of Science, U.S. Department of Energy, under Contract No. DE-AC02-98CH10886.

References

- 1 A.J. Francis. 1990 *Experientia* 46: 840.
- 2 A.J. Francis, *In Plutonium in the Environment* A. Kudo, (Ed) Elsevier Science Ltd., Co., UK. 2001, pp 201-219.
- 3 R. E. Wildung, and T. R. Garland. 1982. *Appl. Environ. Microbiol.* 43: 418.
- 4 M.P. Neu, C.E. Ruggiero, and A.J. Francis. Bioinorganic Chemistry of Plutonium and Interactions of Plutonium with microorganisms and Plants. In "Advances in Plutonium Chemistry 1967-2000" D. Hoffman (Ed), 2002 pp 169-211. ANS, La Grange Park Illinois and University Research Alliance, Amarillo, Texas.
- 5 P.A. Rusin, L. Quintana, J.R. Brainard, B.A. Strietelmeier, C.D. Tait, S.A. Ekberg, P.D. Palmer, T.W. Newton, and D.L. Clark. 1994. *Environ. Sci. Technol.* 28: 1686.
- 6 A.B. Kersting, D.W. Efurud, D.L. Finnegan, D.K. Rokop, D.K. Smith, and J.L. Thomson. *Nature*. 1999, 397: 56.
- 7 P.H. Santschi, K. Roberts, and L. Guo. 2002. The organic nature of colloidal actinides transported in surface water environments. *Environ. Sci. Technol.* 36: 3711-3719.

Actinide Sorption by Well-Characterized Colloid Particles. Redox Speciation and Surface Complexation Modelling.

S.N. Kalmykov*, A.P. Novikov[†], A.B. Khasanova*, Yu.A. Teterin^{††}, B.F. Myasoedov[†], S.B. Clark^{†††}

*Lomonosov Moscow State University, Chemistry department, Moscow 119992, Russia

[†]Vernadsky Institute of Geochemistry and Analytical Chemistry, Moscow 119991, Russia

^{††}Research Centre "Kurchatov Institute", Moscow 123182, Russia

^{†††}Washington State University, Pullman WA 99164, USA

INTRODUCTION

Colloids are submicron particles ubiquitous in the subsurface environment. Due to high surface to mass ratio and small size they may be responsible for facilitated transport of contaminants including actinides. For facilitated transport in subsurface environment they should be sorbed onto colloids. The molecular level understanding of sorption is required to predict the role of colloids on actinide behaviour in the environment. This includes study of possible redox reactions, reversibility of sorption and surface complexation modelling (SCM). The aim of this work is to study neptunium and plutonium sorption and speciation on different colloid particles both synthesized in the laboratory and separated from contaminated aquifers.

EXPERIMENTAL

The SCM exercises were done with synthesized well characterized colloidal phases including goethite (α -FeOOH), hematite (α -Fe₂O₃), maghemite (γ -Fe₂O₃) and amorphous MnO₂. Most of experiments were done with actinides taken initially in pentavalent form at various concentrations, i.e. about 10^{-10} – $5 \cdot 10^{-5}$ M. Several sorption studies were performed with Pu(IV) at tracer concentrations (i.e. 10^{-11} – 10^{-10} M). For SCM the dependence of actinide sorption on pH, ionic strength and total metal concentration were obtained. For actinide redox speciation at tracer concentrations the solvent extraction technique with HDEHP and TTA were used. For macroconcentrations (i.e. $5 \cdot 10^{-6}$ M) of actinides the An4f XPS and XANES at LIII edges were used. The local environment of the actinide atom was studied by EXAFS LIII edges in fluorescent mode. The colloid particles from contaminated aquifer of oxidizing conditions (PA "Mayak", Russia) were collected anaerobically and separated by sequential micro- and ultrafiltrations (3 kD – 450 nm). The colloids were characterized by SEM, TEM-EDX and SAED. Preferential sorption of actinides was studied by nano-SIMS.

RESULTS

It was established that Pu(V) and Np(V) sorption by α -Fe₂O₃ and γ -Fe₂O₃ was not accompanied by actinide redox transformations in the studied concentration range. The sorption of actinides was defined by formation of inner-sphere surface complexes. In case of MnO₂ slow oxidation of Pu(IV) to Pu(V) and Pu(VI) was established with no redox reactions in case of Np(V). For all studied systems actinides remain in their initial redox forms in solution at least during the time of the equilibration (up to 100 days). In case of Pu(V) sorption by α -FeOOH rather fast reduction to Pu(IV) is observed. The steady state equilibrium is reached in about one day with complete reduction of Pu(V). The reduction took place in broad concentration range of

Pu (i.e. $10^{-10} - 10^{-5}$ M) that was supported by both solvent extraction, XPS and XANES. According to EXAFS two oxygen atoms are found in the first coordination sphere (possibly from surface hydroxyl groups), four oxygen atoms in the second sphere and one Fe atom in the third sphere at the distance of 3.32 Å.

The Gibbs energy minimization software (FITEQL) was used for SCM. For systems where no redox reactions take place the values of stability constants of surface complexes were obtained. In case of Np(V) sorption they change in the following sequence: $K(\text{MnO}_2) > K(\alpha\text{-FeOOH}) > K(\gamma\text{-Fe}_2\text{O}_3) \sim K(\alpha\text{-Fe}_2\text{O}_3)$ that is demonstrated in the Fig. 1.

In order to support the SCM data the groundwater sample from radionuclide contaminated aquifer was analyzed. The colloid particle composition for these sample changed in the following sequence: amorphous hydrous ferric oxide (HFO) \gg clays \approx calcite $>$ rutile \approx hematite \approx barite \approx $\text{MnO}_2 >$ monazite. According to SIMS measurements the strength of actinide binding change in the following sequence: $\text{HFO} \approx \text{MnO}_2 \gg \text{Fe}_2\text{O}_3$, while other phases did not sorb actinides. The typical elemental maps are presented in Fig. 2.

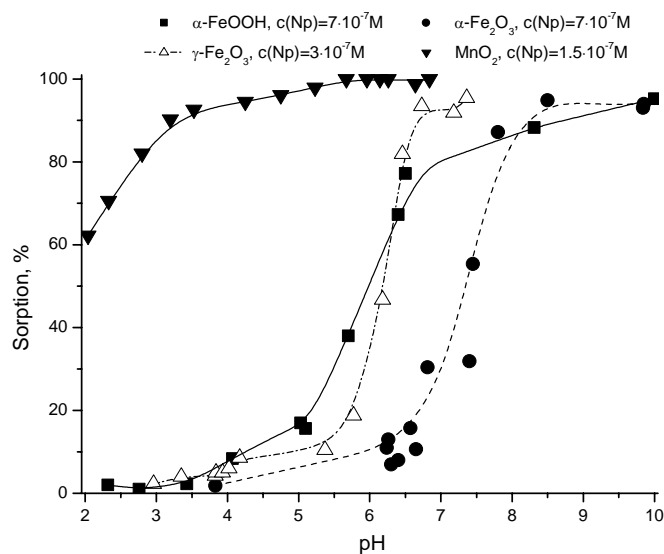


Fig 1: Sorption of Np(V) by different colloid particles

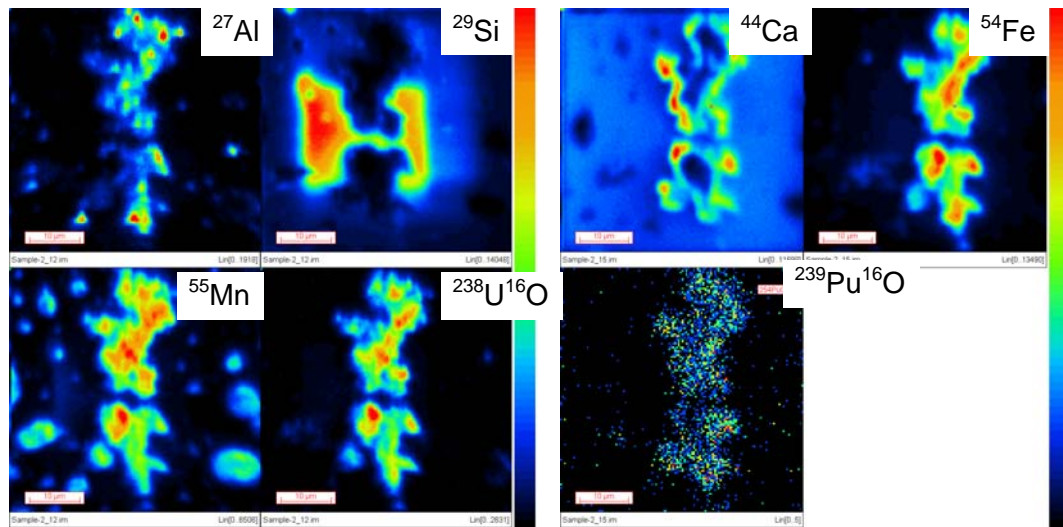


Fig 2: The ion nano-probe mapping of major elements, U and Pu for colloidal matter

The work was supported by US DOE program (RUC2-20008-MO-04) and RFBR (05-03-33028)

Cancellation of spin and orbital magnetic moments in α -Pu: theory

Per Söderlind

Lawrence Livermore National Laboratory, Livermore CA 94550, USA

INTRODUCTION

The last few years have seen an increased focus in trying to understand the actinide metals in general and plutonium in particular. One of the more fundamental issues with plutonium is the existence of a highly complex ambient-pressure phase diagram with as many as six well-defined phases (α , β , γ , δ , δ' , and ϵ).

Recently¹, calculations founded on the density-functional theory (DFT) were able to describe total energies, atomic densities, and bulk moduli remarkably well for all the Pu phases. The effects of localization (weakening metallic bond strength) of the 5f electrons proceeding from α to β and so on were apparently accurately modelled by formation of magnetic moments¹ which were smallest for the α phase and largest for the β phase. Although details of the theoretical electronic structure seem appropriate² when compared to photoemission spectra, the validity of the large magnetic moments in Pu has been questioned for some time and a summary can be found in Ref. 3. The lack of convincing experimental evidence of magnetic moments, contrasted by the firm DFT prediction of magnetism, pose an interesting problem in Pu. The literature offers several plausible explanation for this, for instance: (i) The magnetic moments in the theory have no physical meaning but provide additional degrees of freedom and variational flexibility such that other electron-correlation effects are mimicked. (ii) Fluctuations wash out the net magnetic moments on a time scale shorter than experiments. (iii) Local magnetic moments are subject to Kondo screening. (iv) The spin moments are exactly cancelled by anti-parallel orbital moments on each atomic site. The explanations (i) - (iii) cannot be investigated by a DFT approach because they rely upon deficiencies within the DFT itself. The (iv) explanation was proposed theoretically¹, but has not been investigated in detail.

The present paper discuss the possibility of a cancellation of the spin and orbital moments as a plausible reason for the lack of credible experimental evidence of sizeable net magnetic moments in Pu. This is done by means of constrained DFT calculations utilizing the so-called fixed-spin-moment method (FSM). The focus will be on the α phase because of the simplicity of the cubic crystal structure and the greater magnitude of the theoretically predicted magnetic moments.

COMPUTATIONAL DETAILS AND RESULTS

The electronic-structure calculations are performed within the framework of DFT. Since the magnetic moment is the fundamental property of interest here, we have employed the linear muffin-tin orbitals method, within the atomic sphere approximation (ASA). This technique has the advantage that both spin and orbital moments can be computed throughout the entire crystal, whereas in calculations not relying on the ASA this is typically not possible. The ASA has well-

known challenges with accuracy of structural energies, especially for open phases. Here, however, we only consider the close-packed face-centered cubic δ phase, and are less concerned with an accurate structural energy.

Every DFT calculation is associated with errors arising from necessary approximations applied in the theory. The atomic equilibrium volume for a wide range of transition and actinide metals generally has an error of about 2-3%, the bulk modulus \sim 10-20%, and the spin moment \sim 10-20%. The earlier studies¹ suggested that for δ -Pu the total magnetic moment on each site was of the order of \sim 1 μ_B , with the spin being larger than the orbital moment. Because of the non-negligible inherent inaccuracy of the DFT spin moments, it is of interest to investigate the dependence of the total magnetic moment on the spin moment. I.e., an error in the DFT

spin moment may have an important role for the sensitive cancellation of the spin and orbital components. We therefore employ the FSM method, which has been described in detail⁴ that we will not repeat here other than to say that it is a way of constraining the total spin moment in a metal to any preferred magnitude. This enables us to calculate the total magnetic moment on each site as a function of spin moment. In Fig. 1 we show the total energy and total magnetic moment as a function of spin moment. Within the expected DFT error of the spin moment (\pm 20%, vertical dashed red lines) the total moment crosses the zero axis, suggesting a possibility for a complete cancellation and a zero total moment. The total-energy shift associated with the zero moment is \sim 1 mRy which is close to the accepted DFT energy error.

To conclude, we have shown that a zero total magnetic moment is possible in δ -Pu due to the *exact* cancellation of spin and orbital components when a small correction, to compensate for an expected DFT error of the spin moment, is allowed.

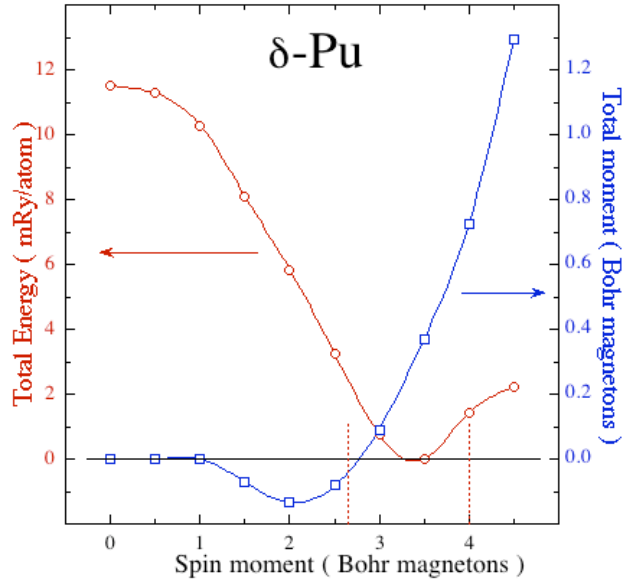


Fig 1: Total energy and moment vs. spin moment.

This work was performed under the auspices of the US DOE by the UC LLNL under contract No. W-7405-Eng-48.

- 1 P. Söderlind and B. Sadigh, Phys. Rev. Lett. **92**, 185702 (2004); P. Söderlind, EuroPhys. Lett. **55**, 525 (2001).
- 2 P. Söderlind, A. Landa, and B. Sadigh, Phys. Rev. B **66**, 205109 (2002).
- 3 J.C. Lashley *et al.*, Phys. Rev. B **72**, 054416 (2005).
- 4 K. Schwarz and P. Mohn, J. Phys. F **14**, L129 (1984).

Mechanical Behavior of Delta-Phase Plutonium-Gallium Alloys

George C. Kaschner, Michael G. Stout, Siegfried S. Hecker

Los Alamos National Laboratory, Los Alamos NM 87545

In this report, we present a constitutive model that predicts the yield strength and ultimate tensile strength (UTS) of delta-stabilized plutonium-gallium alloys (Pu-Ga). The model accounts for the effects of temperature, strain rate, grain size, and gallium (Ga) concentration. The coefficients in the model are based on ambient-pressure quasi-static data that were published in the open literature¹⁻⁶. These data include a range of gallium concentrations and purities, tested over a large range of temperatures and strain rates as shown in the table below.

Experimental Condition	Range of the Variable
Temperature, °C	- 60 to 558
Strain Rates, s ⁻¹	1.4 x 10 ⁻⁵ to 75
Stress State	tension and torsion
Microstructure	
Grain Size, μm	1 to 30 x 90
Composition	
Gallium Content, wt. %	0.29 to 1.63
Iron and Nickel Content, wt. ppm	<30 to 900
Carbon Concentration, wt. ppm	30 to 310
Experimental Results	
Yield Stress (tension), MPa	48 to 125
Ultimate Tensile Strength, MPa	66 to 174

We constructed and fitted the mechanical threshold stress (MTS) model reported by Follansbee and Kocks⁷ to predict the yield and flow stress behavior for single-phase δ-stabilized Pu-Ga alloys as a function of strain rate and temperature. Our extended model also accounts for variations in gallium content and grain size. This model has been validated against approximately 50 different experiments for both yield and ultimate strength. The predicted yield strengths agreed with the experimental data to within a ±1 standard deviation of 15%.

The key material variables potentially affecting plutonium-gallium alloys are gallium concentration, grain size, iron and nickel content, and carbon concentration. We predicted the yield strength of the alloys based on the temperature and strain rate of the experiment and the grain size and substitutional element concentration (Ga+Al+Si+Am). The model allowed us to plot yield strength against individual microstructural parameters to look for correlations. Grain size and gallium concentration appear explicitly in our MTS model. In these two cases, we took the input to the model as a reference value—20 μm for grain size and 1 wt. %, or 3.35 at. %, for gallium concentration.

We found that gallium concentration had the most significant effect on yield strength. We examined data for materials with a gallium content from approximately 1 at. % to 6 at. %, covering almost two-thirds of the entire δ-phase field retained by gallium additions. This

variation in gallium content changed the yield strength by 50%. The concentrations of impurities Al, Si, and Am, which like Ga substitute in the fcc δ -phase Pu lattice, was small in the data sets we examined and, hence, they had negligible effects on strength.

We also found that grain size had a measurable, but modest, effect on yield strength. The experimental data we examined represented samples with average grain sizes from 10 μm to about 50 μm . Our analysis of the data confirmed the observation of Wheeler, Thayer, and Robbins⁵ that the yield strength follows an inverse square-root Hall-Petch relation to grain size. The decrease of grain size from 50 μm to 10 μm produced a 15% increase in yield strength.

Lastly, we looked for a correlation between room-temperature, quasi-static yield strength and the impurity levels of iron and nickel, and carbon. We did not observe a correlation or trend in either case. The iron and nickel each form an intermetallic phase with the plutonium. Optical metallography shows that these intermetallics typically have a length scale of microns, far too large to interact effectively with dislocations and to increase the yield strength. Carbon is nearly insoluble in plutonium and forms carbide inclusions, which are also on the length scale of microns. Thus, like the iron and nickel intermetallics, the carbides are too large to affect the yield strength.

The MTS model, with the parameters defined in Stout, *et al*⁸⁻¹⁰, can now be used to isolate the influence of test conditions and some microstructural features such as composition, grain size and inclusions content. The model will predict results beyond the current literature data so long as deformation mechanisms appropriate for the MTS model apply.

- 1 S. Beitscher, J. Nucl. Mater. **24** (1967) 113.
- 2 S.S. Hecker and J.R. Morgan, in: H. Blank and R. Lindner (Ed.), Plutonium 1975 and other Actinides, North-Holland, Amsterdam, 1976, p. 697.
- 3 D.C. Miller and J.S. White, J. Nucl. Mater. **17** (1965) 54.
- 4 A.D. Wheeler and J.L. Robbins, J. Nucl. Mater. **32** (1969) 57.
- 5 A.D. Wheeler, W.L. Thayer, and J.L. Robbins, in: W.A. Miner (Ed.), Plutonium 1970 and other Actinides, Metallurgical Society of AIME, New York, 1971, p. 437.
- 6 S.S. Hecker, private communication, LANL, 1999.
- 7 P.S. Follansbee and U.F. Kocks, Acta Metall. **36** (1988) 81.
- 8 M.G. Stout, G.C. Kaschner, and S.S. Hecker, LA-994458 (2002).
- 9 M.G. Stout, G.C. Kaschner, and S.S. Hecker, *submitted to*: J. Nucl. Mater. (2006).
- 10 G.C. Kaschner, M.G. Stout, and S.S. Hecker, *submitted to*: J. Nucl. Mater. (2006).

The phase diagram Pu-Ga in the Pu-rich region

Thaddeus B. Massalski* and Adam J. Schwartz**

*Carnegie Mellon University, Pittsburgh, PA 15213, USA

**Lawrence Livermore National Laboratory, Livermore, CA, 94550, USA

ABSTRACT

The present status of the phase equilibria and phase boundaries in the Pu-rich region of the Pu-Ga phase diagram will be briefly reviewed, covering both the reported experimental work and the phase diagram calculations. We shall try to assess the overall information now available regarding the equilibrium and metastable phase boundaries, the trend of the T_0 temperature for the $\delta \rightarrow \alpha'$ transition, and the corresponding trends of the martensite-start (M_B) and martensite-revert (R_S) temperatures.

This work was performed under the auspices of U.S. Department of Energy by the University of California, Lawrence Livermore National Laboratory under contract No. W-7405-Eng-48.

Evidence for Formation of Alpha Embryos in a Pu-2.0 at% Ga Alloy at Ambient Temperature

K.J.M. Blobaum^{*}, C.R. Krenn^{*}, M.A. Wall^{*}, T.B. Massalski[†], and A.J. Schwartz^{*}

^{*}Lawrence Livermore National Laboratory, Livermore, CA 94550 USA

[†]Carnegie Mellon University, Pittsburgh, PA 15213 USA

INTRODUCTION

For a Pu-2.0 at% Ga alloy, α and Pu₃Ga are the expected stable phases at ambient conditions¹. However, the complete eutectoid decomposition to α + Pu₃Ga from the fcc δ phase is expected to take about 10,000 years², and the phase typically observed at ambient conditions is δ , which is retained in a metastable state. When the metastable δ is cooled to subambient temperatures, it partially transforms via a burst martensite mode to the monoclinic α' phase³.

It is reported that successive thermal cycles to form and revert α' in Pu-Ga alloys result in less α' formation in each cycle^{4,5}. Here, we show that certain annealing and ambient-temperature conditioning sequences result in reproducible amounts of α' formation in successive cycles.

RESULTS AND DISCUSSION

Differential scanning calorimetry (DSC) was used to investigate the amount of α' formed and reverted in thermal cycles following various conditioning treatments. The area of the $\delta \rightarrow \alpha'$ and $\alpha' \rightarrow \delta$ DSC peaks are directly proportional to the amount of α' formed. Prior to each thermal cycle, the sample was annealed at 375°C for 8 hours and then it was conditioned for 2 to 16 hours at a temperature in the range -50°C to 370°C. The amount of α' formed upon cooling a Pu-2.0 at% Ga alloy is a function of the time and temperature of this conditioning treatment.

Figure 1 shows the $\alpha' \rightarrow \delta$ reversion peaks for conditioning treatments at 25°C. Some α' is formed even when no conditioning treatment is employed (0 hours), but the amount of α' formation increases with conditioning time up to approximately 6 hours. Longer times, up to 70 hours (not shown), do not result in additional α' formation. Figure 2 shows the effect of conditioning temperature on the amount of α' formed. Conditioning at -50°C and 370°C results in approximately the same amount of α' formation as when no conditioning treatment is employed. A moderate amount of α' forms when the sample is conditioned for 13 hours at 150°C, but the largest amount is observed to form after conditioning for 12 hours at 25°C.

We hypothesize that embryos of the equilibrium α phase begin to form in the metastable δ matrix during ambient temperature conditioning treatments. These embryos may be dynamic fluctuations or static distortions that may have structural and crystallographic attributes of the α' martensite, and self-irradiation by the Pu may assist diffusional formation of the α embryos. Upon cooling, these embryos become sites for α' formation.

Formation of α' is enhanced by conditioning at 150°C, although to a lesser extent than conditioning at 25°C. At 150°C, the equilibrium phases of the Pu-2.0 at% Ga alloy are expected to be β (body-centered monoclinic) + δ . We propose that at 150°C, embryos of the β phase form.

However, they either form more slowly than α embryos, or they are not as effective at nucleating α' . Both of these hypotheses could explain the smaller amount of α' formed following the 150°C conditioning treatments compared to those at 25°C, but the latter option seems more likely since α embryos have the same crystal structure as α' , while β embryos do not.

Even the least effective conditioning treatments result in a small amount of α' formation. In these cases, it is likely that α' nucleates on intrinsic sites such as grain boundaries, impurities, etc. At 370°C, δ is the only stable phase expected, so no additional embryos would form during a conditioning treatment. At -50°C, diffusion is effectively quenched and thus α embryos are not expected to form during conditioning. Thus, the α' observed to form following conditioning treatments at 370°C and -50°C is expected to utilize only intrinsic sites for nucleation.

We propose a classical nucleation and growth model for the initial stages of α' formation⁶. When the sample is conditioned at temperatures near T_0 , diffusion is fast, but the driving force for nucleation is low. At low temperatures, diffusion is slow, but the driving force is high. Therefore, the highest nucleation rate is observed at some intermediate undercooling. In this case, 25°C appears to be near this optimal nucleation temperature.

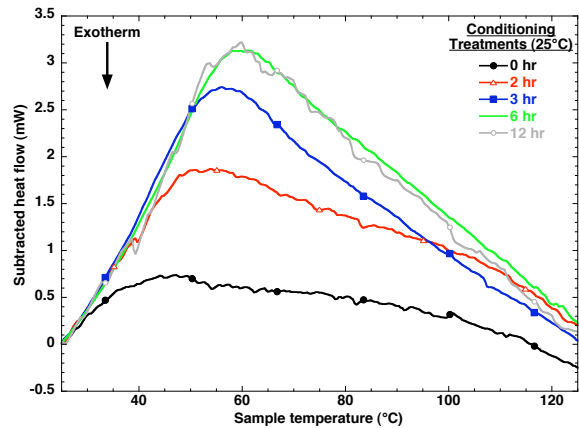


Figure 1: DSC plots showing the increase in the $\alpha' \rightarrow \delta$ reversion peak as the conditioning treatment at 25°C is increased from 0 to 12 hours.

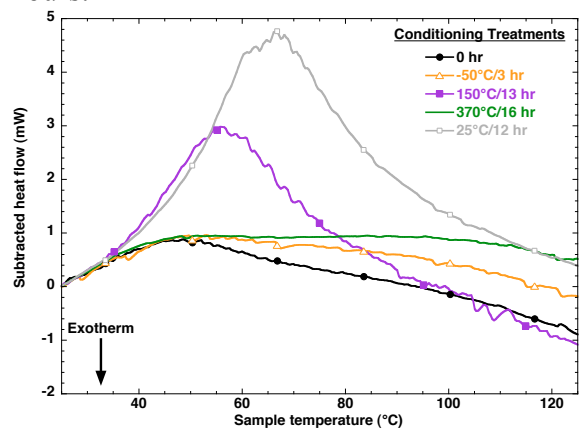


Figure 2: DSC plots showing the $\alpha' \rightarrow \delta$ reversion peak resulting from α' formation following conditioning treatments at various temperatures. The largest amount of α' forms after conditioning at 25°C for 12 hours.

This work was performed under the auspices of the U.S. Department of Energy by University of California Lawrence Livermore National Laboratory under contract No. W-7405-Eng-48.

- ¹ N. T. Chebotarev, E. S. Smotriskaya, M. A. Andrianov, and O. E. Kostyuk, in *Plutonium 1975 and Other Actinides*, edited by H. Blank and R. Lindner (North Holland Publishing Co., Amsterdam, 1975), p. 37-46.
- ² S. S. Hecker and L. F. Timofeeva, *Los Alamos Science* **26**, 244-251 (2000).
- ³ K. J. M. Blobaum, C. R. Krenn, J. N. Mitchell, J. J. Haslam, M. A. Wall, T. B. Massalski, and A. J. Schwartz, *Metall. Mater. Trans. A* (accepted, 2005).
- ⁴ S. S. Hecker, D. R. Harbur, and T. G. Zocco, *Prog. Mater. Sci.* **49**, 429-485 (2004).
- ⁵ J. N. Mitchell, M. Stan, D. S. Schwartz, and C. J. Boehlert, *Metall. Mater. Trans. A* **35A**, 2267-2278 (2004).
- ⁶ R. Becker and W. Doring, *Ann. Phys.* **24**, 719-752 (1935).

Calculated Properties of Pu-Ga Alloys Using the Modified Embedded Atom Method

M. I. Baskes*, S. Y. Hu*, S. M. Valone*, and M. A. Stan*

*Los Alamos National Laboratory, Los Alamos, NM 87545 USA

The Pu-Ga system is perhaps the most complicated binary alloy system in nature. Not only does this system have important technological importance, but also scientifically it is extremely challenging. Previously we have used the Modified Embedded Atom Method (MEAM) to describe the behavior of both Pu and Ga. This method, though semi-empirical, is able to capture most of the important unusual behavior of both of these elements.

In this presentation we show the results of recent calculations using MEAM for various alloys (phases and composition) in this complex system. Results presented will include simple bulk thermal and mechanical properties such as specific heat, thermal expansion, and elastic constants for the solid phases. Two-phase equilibrium will be discussed with respect to melting and the predicted phase diagram. Predictions will be compared with experiment when available.

Basic science on advanced plutonium fuels : new investigations on structure, thermophysical properties and radiation damage

M. Beauvy^{*}, P. Martin^{*}, S. Vaudez, L. Paret, V. Basini^{*}, J. P. Ottaviani^{*}, J. Lechelle^{*},
C. Dalmasso[†]

^{*}Commissariat à l'Énergie Atomique, Centre d'Études de Cadarache, 13115 Saint Paul lez
Durance, Cedex, France

[†]CRESA/LPES, Nice Sophia Antipolis University, Parc Valrose, 06108 Nice, France

INTRODUCTION

Primary energy consumption is near 12 Gtoe in the world. It is provided essentially by fossil matter : oil 40%, coal 20% and gas 20%, but oil reserves would be reduced dramatically during the next 50 years. In the same time, the world population could be multiplied by 1.6, and therefore the energy consumption will increase significantly. Nuclear energy well known from fission reactors represents only 7% of total primary energy, and could be more intensively used in future. Nevertheless, the quantities of natural fissile isotopes (^{235}U) are relatively low and the use of plutonium will be developed for the sustainability. Basic research on plutonium compounds is realized in our Laboratory.

The fuels of power reactors are oxides in large majority UO_2 or MOX ($\text{U}_{1-y}\text{Pu}_y$) O_2 . An important knowledge on plutonium mixed oxides exists in France after Rapsodie, Phenix and Super-Phenix FNR programs and the use of MOX in PWR. However, progress on plutonium oxide fuels must be done for the next PWR generation : EPR with 100% MOX fuel at higher Pu content and for high burn up. On the other hand, materials for new advanced high performance reactors are also studied for the future (Sodium Fast Reactors and Gas Fast Reactors, in international Forum Generation IV [1]).

BASIC SCIENCE on PLUTONIUM MIXED OXIDES

Structure and thermophysical properties

Plutonium, uranium or mixed oxides are ionic-covalent cubic face centered phases (fluorite type) with large deviation possible from stoichiometry ($\text{O}/\text{U}+\text{Pu}\neq 2$). Stable hyper stoichiometry in plutonium oxide has not been confirmed from our investigations [2]. The clusters of point defects reported in literature for hyper stoichiometric plutonium mixed oxides are not compatible with ionicity and our measured lattice parameters. New analysis on defect structure will be presented. The contribution of other species present in MOX fuels (additives, Fission Fragments) will be also analysed with some examples. Then, the effect on specific heat will be discussed and compared with our experimental results.

Radiation damage

PIE of MOX fuels have been done in our hot cell Laboratory for 40 years. Mixed plutonium oxide fuels have a good resistance to radiation. Characterisation of damage in irradiated fuels at atomic scale is very difficult, with multiple and complex mechanisms. Experimental simulation

of irradiation by Fission Fragments has been done at CIRIL/GANIL. Results on point defect, chemical properties and mechanical properties will be reported and compared with calculations.

BASIC SCIENCE on PLUTONIUM NITRIDES

Chemical and electronic structure, thermophysical properties

High melting point, high density of actinides, good thermal conductivity are in favor of nitrides and carbides for future reactor fuels. Polycrystalline plutonium nitrides have been prepared and characterized in our Laboratory. Results on lattice parameter, specific heat and thermal conductivity will be reported and analysed.

Table 1. Lattice parameters of $(Pu_yM_{1-y})N$

Nitride	Lattice parameter, nm		Radii		5f localized	
	Our measurements	atom		M ³⁺ N ³⁺		
		metallic	Covalent	M ³⁺ N ³⁺	M ⁴⁺ N ³⁺	
UN	0.4889	0.448	0.454	0.504	0.476	4.82
PuN	0.4905	0.466	0.456	0.498	0.468	6.75
$(Pu_{0.2}U_{0.8})N$	0.4891	0.451		0.503	0.474	5.2
ZrN	0.4578	0.462	0.446	-	0.440	$\cong 0$
$(Pu_{0.25}Zr_{0.75})N$	0.4635	0.463				(1.3)
$(U_{0.2}Zr_{0.8})N$	0.4638	0.459				(0.9)

Results on lattice parameters confirm the mixed bonding in plutonium nitrides : metallic and ionic (Table 1). Optical absorption spectra show tetravalent actinides and exclude practically An^{3+} in nitrides. The localized 5f electrons are respectively 4.8 and 6.7 in uranium and plutonium nitrides. The specific heat of mixed nitrides does not respect the “mixture” law (Fig. 1).

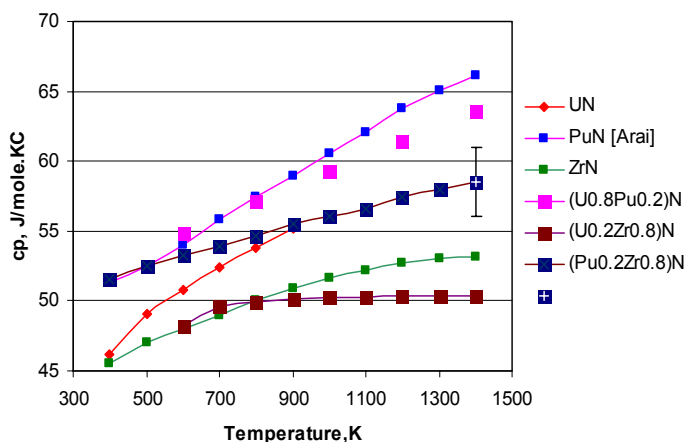


Figure 1. Specific heat of nitrides

Radiation damage

The good resistance of nitride fuels was shown after experimental simulation of irradiation by Fission Fragments : small amount of An^{3+} and defects on nitrogen lattice were detected (Fig. 2).

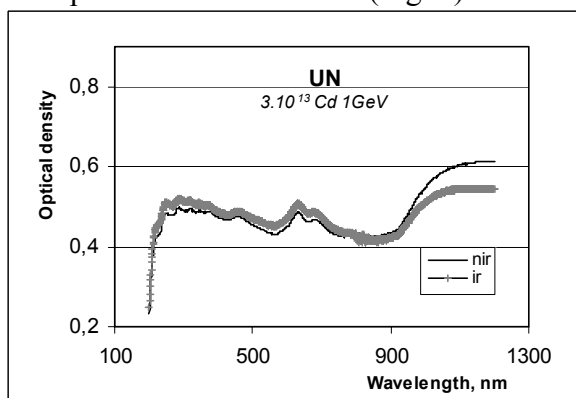


Figure 2. Optical absorption spectra of UN non-irradiated (nir) and irradiated(ir) by $5.10^{13}Cd$ $1GeV/cm^2$

REFERENCES

- [1] – AIEA, Energy to 2050-scenarios for a sustainable future, 2003; US DOE, Forum Generation IV, 2002.
- [2] – P. Martin, J. Nuc. Mat., 320(2003)138

Setups of Experimental Explosions to Study Fundamental Dynamic Properties of 4f- and 5f-metals and their Alloys

E.A.Kozlov, V.I.Tarzhanov, V.G.Vil'danov, V.M.Elkin,
S.A. Brichikov, I.V. Telichko, D.G. Pankratov, A.O.Borschevsky, D.T. Yusupov

Federal State Unitary Enterprise "Russian Federal Nuclear Center – Zababakhin All-Russia Research Institute of Technical Physics", Snezhinsk, Russia, 456770, P.O. Box 245

ABSTRACT

Of great scientific interest are (i) regular changes in physical and mechanical properties of 3d-, 4d-, 4f-, and 5f – elements as pertinent electronic shells are being filled and (ii) effects induced by changing localization extent of 3d-, 4d-, 4f-, and 5f – electrons under intensive external impacts. Therefore, methods and facilities previously developed in [1-10] to study behavior and properties of fissile materials under dynamic loading can and must be used for fundamental investigations of lanthanides and actinides.

1. 3d and 4d – transition, as well as 4f- and 5f-metals – Fe, Zr, Ce, U, Pu and their alloys – are materials, which are unique for studying the progress of polymorphous, electron, and phase transformations and these transformations-related natural changes in their physical, mechanical, and thermal properties both under static, and dynamic loading.

Explosive and shock-wave experiments provide data on (i) a wide range of changing longitudinal stresses, temperatures, and energy densities hardly attainable in static experiments, (ii) equilibrium properties of the shock-compressed matter, (iii) kinetics of high-rate visco-elastoplastic deformation, (iv) kinetics of polymorphous, electron, and phase transitions, (v) specifics of nucleation, development, and recompaction of spall and shear fractures at different scale levels and in conditions of different phases co-existence. In experiments, in addition to the time-resolved diagnostics of the structure and parameters of stress waves or profiles of sample free-surface velocity directly during loading and unloading of shock-compressed materials, sometimes after explosive loading, samples manage to be recovered for their follow-on comprehensive materials science investigations.

As distinct from experiments with Fe, Zr, Ce, and U, where these materials must be protected against oxidation only before their explosive or shock-wave loading, the explosion experiments with Pu and its alloys require that stringent environmental safety requirements be met. *The purpose of this work* - summary information on feasibility of environmentally safe explosion experiments involving Pu and its alloys with time-resolved diagnosing of wave processes in fissile materials directly under sample loading and recovery after unloading for their follow-on physical investigations. These experimental setups are of interest from the standpoint of fundamental research into behavior and dynamic properties of actinides.

2. Properties and phenomena to be studied

- phase diagrams and kinetics of polymorphous, electron, and phase (melting, evaporation) transitions;

- changes in shear and spall strength of metals and alloys in the case of their high-strain rate deformations in different phase states;
- micromechanisms of high-strain rate deformation, phase transitions, nucleation, development, and recompaction of fractured matter.

3. Methods

- 3.1 The modified photochronographic optical-lever method [1, 7, 9, 10] and the laser interferometry method
- 3.2 The photoelectric method and the manganin gage procedure
- 3.3 Shock-wave recovery experiments [1-5, 10].

Conclusions

The paper presents experimental setups with hermetical recovery and localization devices to study fundamental properties of 4f- and 5f-metals, as well as alloys – dynamic strength, polymorphous, electron, phase, and structural transformations. Methods and facilities previously developed to investigate the behavior and properties of fissile materials under dynamic (explosion and shock-isentropic) loading, can and must be used in the interest of fundamental research of lantanides and actinides.

1. E.A.Kozlov, L.F.Timofeeva, A.K.Muzyrya, Macrokinetic features of the $\delta - \alpha'$ phase transformation in the δ -plutonium under threshold pulsed loadings, *Russ. J. Chemical Physics*, 1995, v.14, № 1, pp.62-68
2. E.A.Kozlov, B.V. Litvinov, L.F.Timofeeva, V.S.Kurilo, V.K.Orlov, Structural, phase transformations, and spall fracture of the sphere made of the δ -phase alloy of plutonium with gallium in spherical stress waves, *Phys.Met. & Metallog.*, (Engl. transl.), 1996, v.81, N6, pp.679-691.
3. E.A.Kozlov, L.F.Timofeeva, G.V.Kovalenko. Features of $\alpha - \beta$ - phase transformation of unalloyed Pu in weak and strong shock waves. Abstracts of the Russian Conference MATERIALS OF NUCLEAR ENGINEERING devoted to the centenary of A.A.Bochvar, M.: VNIINM, 2002, 148p, Agoi, Krasnodarsky Territory, September 23-27, 2002, pp.20-21
4. E.A.Kozlov, L.F.Timofeeva. Dendritic liquation in delta-phase plutonium alloys and peculiarities of phase transitions proceeding in weak and strong shock waves, Abstracts of the Russian Conference MATERIALS OF NUCLEAR ENGINEERING devoted to the centenary of A.A.Bochvar, M.: VNIINM, 2002, 148p, Agoi, Krasnodarsky Territory, September 23-27, 2002, pp. 113-114;
5. E.A.Kozlov, L.F.Timofeeva. Dendritic Liquation in Delta-Phase Plutonium Alloys and Peculiarities of Phase Transitions Proceeding in Weak and Strong Shock Waves, The Fifth International Symposium on BEHAVIOUR of DENSE MEDIA under HIGH DYNAMIC PRESSURES, June 23-27, 2003, Saint-Malo, France, Tome I, pp.321-330
6. V.M.Elkin, E.A.Kozlov, E.V. Kakshina, Yu.S.Moreva, Semi-empirical equation of state and phase diagram of plutonium, Preprint of RFNC-VNIITF № 197, 2002, 25p., *Phys. Met. & Metallog.* (Engl. transl.), 2004, v.98, # 1, pp.44-50.
7. E.A.Kozlov, Phase Transitions and Spall Fracture of Zirconium under Explosive Loading, *J.Phys. (Paris)*, 1991, v.1, pp.C3-675 – C3-679
8. E.A.Kozlov, V.M.Elkin, I.V. Bychkov, Thermodynamically complete equation of state of solid phases and phase transitions of zirconium in stress waves, *Phys. Met. & Metallog.* (Engl. transl.), 1996, v.82, N 4, pp.337-342.
9. E.A.Kozlov, Shock Adiabatic Features, Phase Transition Macrokinetics, and Spall Fracture of Iron in Different Phase States, *High Pressure Research*, 1992, v.10, pp.541-582
10. E.A.Kozlov, I.V.Telichko, D.M.Gorbachev, D.G.Pankratov, A.V. Dobromyslov, N.I. Taluts, On the issue of metastability, incompleteness of the $\alpha - \epsilon$ – phase transitions in the unalloyed iron under threshold pulsed loadings. Specifics in the deformation behavior and the structure of recovered Armco-iron, *Phys. Met. & Metallog.* (Engl transl.), 2005, Vol. 99, No. 3, pp. 300–313.

Actinyl Chemistry at the Centre for Radiochemistry Research

I. May,* R. Copping,* S.M. Cornet,* M.P. Redmond,* C.A. Sharrad,* C.E. Talbot-Eecklears,* C.J. Jones,† M.J. Sarsfield† and R.J. Taylor †

*Centre for Radiochemistry Research, School of Chemistry, University of Manchester, Oxford Road, Manchester, M13 9PL.

†Nexia Solutions, Sellafield, Seascale, Cumbria, CA20 1PG, UK

THE ACTINYL CATIONS

The linear dioxo actinyl cations, $\{\text{AnO}_2\}^{x+}$ ($x = 1$ or 2), dominate the +V and +VI solution chemistry of the mid actinide elements (U, Np, Pu and Am). Usually, between 4-6 additional ligands coordinate in the equatorial plane yielding bipyramidal geometry. An increased understanding of actinyl chemistry will underpin a range of nuclear applications, from novel fuel processing technologies through to environmental waste remediation. Of particular relevance are $\{\text{UO}_2\}^{2+}$ and $\{\text{NpO}_2\}^+$, the dominant chemical forms of U and Np respectively, and $\{\text{PuO}_2\}^+$, which is thought to have environmental significance.

By far the most commonly studied actinyl cation is $\{\text{UO}_2\}^{2+}$, primarily due to its chemical stability and the comparatively low radiological hazard associated with uranium chemical research. Recent highlights include the incorporation of this moiety into liquid crystals,¹ the preparation of uranyl selenate nanotubules² and structural evidence for cation-cation interaction.³ Although prone to disproportionation, there are still ongoing investigations into $\{\text{UO}_2\}^+$ chemistry, including the structural characterisation of $[\text{UO}_2(\text{OPPh}_3)_4](\text{OTf})$.⁴ Finally, bis-imido analogues of the uranyl(VI) cation, $\{\text{U}(\text{NR})_2\}^{2+}$, have recently been synthesised and used to probe the role of the 5f and 5d U orbitals in bonding.⁵

The higher specific activity of the transuranium elements restricts experimental chemistry to specialist facilities. While there have been quite a few neptunyl (V and VI) structural studies the first structural characterisation of $\{\text{PuO}_2\}^{2+}$,⁶ and indeed $\{\text{PuO}_2\}^+$,⁷ complexes have only just been reported. This lack of basic knowledge is also reflected in solution chemistry, with a recent report on $\{\text{PuO}_2\}^{2+}$ hydrolysis providing valuable thermodynamic data.⁸ Perhaps the most interesting recent development in neptunyl chemistry has been the synthesis of $\{\text{NpO}_2\}^+$ (and indeed $\{\text{UO}_2\}^{2+}$) peroxide nanoclusters from alkaline peroxide solution.⁹ Finally, while there is no spectroscopic or structural evidence for $\{\text{PaO}_2\}^+$ a recent EXAFS study points to the existence of a Pa(V) single oxo species, $\{\text{PaO}\}^{3+}$.¹⁰

ACTINYL CHEMISTRY AT THE CENTRE FOR RADIOCHEMISTRY RESEARCH

At the Centre for Radiochemistry we have investigated several actinyl systems. Recent highlights include the use of spectroscopic techniques to prove that the pertechnetate anion, $[\text{TcO}_4]^-$, can coordinate directly to the uranyl(VI) cation¹¹ and that bioreduction of $\{\text{UO}_2\}^{2+}$ to U(IV) can occur via a $\{\text{UO}_2\}^+$ intermediate.¹² Tri-lacunary heteropolyoxometalate ligands have been shown to be very good complexants for the uranyl cation and we have used comparatively straightforward synthetic strategies to take this chemistry forward to neptunyl(V).¹³ Very recently we have made significant advances in this area of research, yielding further structural

and spectroscopic characterisation of $\{\text{NpO}_2\}^+$ complexes with different tri-lacunary ligands (see, for example, Fig. 1) and extending our investigations to $\{\text{NpO}_2\}^{2+}$ and $\{\text{PuO}_2\}^{2+}$. Both the charge on the actinyl cation (*e.g.* $\{\text{NpO}_2\}^+$ vs $\{\text{NpO}_2\}^{2+}$) and the type of polyoxometalate anion (*e.g.* A-type vs B-type) can lead to different structural types of complex being isolated.

Focusing again on uranyl chemistry, non-aqueous systems have been investigated where the ligands have been chosen with the aim of perturbing the actinyl bond. As an example of this chemistry bidentate (NCN) benzaminato ligands, $[\text{PhC}(\text{NSiMe}_3)_2]^-$, can be used to complex to $\{\text{UO}_2\}^{2+}$ and significantly distort (bending and stretching) the uranyl cation. Using this ligand system the uranyl oxygen can be activated to behave as a Lewis base, yielding the $\text{B}(\text{C}_6\text{F}_5)_3$ adduct, $[\text{UO}_2\text{B}(\text{C}_6\text{F}_5)_3\{(\text{SiMe}_3\text{N})\text{CPh}(\text{NSiMe}_3)_2\}]^-$.¹⁴ We have recently taken this chemistry transuranic, showing that $\text{R}_3\text{P}=\text{NH}$ ligands will displace $\text{R}_3\text{P}=\text{O}$ ligands coordinated to $\{\text{UO}_2\}^{2+}$ and $\{\text{NpO}_2\}^{2+}$.¹⁵

Our current research goal is to further develop transuranic actinyl research. This will be undertaken experimentally in collaboration with Nexia Solutions at Sellafield and EU ACTINET partner laboratories; particularly ROBL-ESRF, Grenoble and CEA Atalante at Marcoule. A collaborative computation programme is currently being undertaken by Kaltsoyannis and co-workers at University College London.

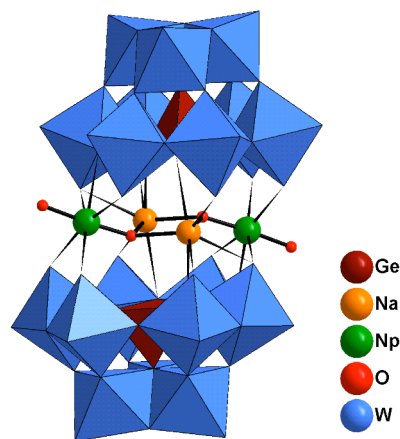


Fig. 1 Polyhedra representation of $[\text{Na}_2(\text{Np}^{\text{V}}\text{O}_2)_2(\text{GeW}_9\text{O}_{34})_2]^{16-}$

- 1 T. Cardinaels, J. Ramaekers, D. Guillon, B. Donnio and K. Binnemans, *J. Amer. Chem. Soc.* **127**, 17602 (2005).
- 2 S.V. Krivovichev, V. Kahlenberg, I.G. Tananaev, R. Kaindl, E. Mersdorf and B.F. Myasoedov, *J. Amer. Chem. Soc.* **127**, 1072 (2005).
- 3 T.A. Sullens, R.A. Jensen, T.Y. Shvareva and T.E. Albrecht-Schmitt, *J. Amer. Chem. Soc.* **126**, 2676 (2004).
- 4 J-C. Berthet, M. Nierlich and M. Ephritikhine, *Angew. Chem. Int. Ed.*, **42**, 1952 (2003).
- 5 T.W. Hayton, J.M. Boncella, B.L. Scott, P.D. Palmer, E.R. Batista and P.J. Hay, *Science*, **310**, 1941 (2005).
- 6 W. Runde, A.C. Bean, T.E. Albrecht-schmitt and B.L. Scott, *Chem. Commun.* 478 (2003).
- 7 A.A. Bessonov, M.S. Grigoriev, I.A. Charushnikova and N.N. Krot in *Recent Advances in Actinide Science*, edited by R. Alvarez, N.D. Bryan and I. May [Royal Society of Chemistry, in press].
- 8 S.D. Reilly and M.P. Neu, *Inorg. Chem.*, advanced article (2006).
- 9 P.C. Burns, K-A. Kubatko, G. Sigmon, B.J. Fryer, J.E. Gagnon, M.R. Antonio and L. Soderholm, *Angew. Chem. Int. Ed.* **44**, 2135 (2005).
- 10 C. Le Naour, D. Trubert, M.V. Di Giandomenico, C. Fillaux, C. Den Auwer, Ph. Moisy and C. Hennig, *Inorg. Chem.* **44**, 9542 (2005).
- 11 A.D. Sutton, G.H. John, M.J. Sarsfield, J.C. Renshaw, I. May, L.R. Martin, A.J. Selvage, D. Collison and M. Helliwell, *Inorg. Chem.* **43**, 5480 (2004).
- 12 J.C. Renshaw, L.J.C. Butchins, F.R. Livens, I. May, J.M. Charnock and J.R. Lloyd, *Environ. Sci. Technol.* **39**, 5657 (2005).
- 13 A.J. Gaunt, I. May, M. Helliwell and S. Richardson, *J. Amer. Chem. Soc.* **124**, 13350 (2002).
- 14 M.J. Sarsfield and M. Helliwell, *J. Amer. Chem. Soc.*, **126**, 1036 (2004).
- 15 M.J. Sarsfield, I. May, S.M. Cornet and M. Helliwell, *Inorg. Chem.* **44**, 7310 (2005).

Thermodynamic Features of Lanthanide and Actinide Solvent Extraction Reactions

K. L. Nash

Chemistry Department, Washington State University, PO Box 644630, Pullman, WA 99164-4630 (e mail, knash@wsu.edu)

The transuranium actinides were unknown on earth until the late 1930s - early 1940s. From that time through the 1950s and into the 1960s, these elements were discovered as byproducts of the irradiation of uranium (and subsequently of transuranic element targets) with subatomic particles. Separations chemistry (precipitation/co-precipitation, ion exchange, and solvent extraction) was central to the discovery of the individual actinides, to the isolation and purification of target nuclides and to the preparation of samples of sufficient purity to allow elucidation of their chemical/physical properties. Further, solvent extraction, in the form of the PUREX process, has become the single most important separations process in actinide technology.

As we move into the 21st Century, a reinvigoration of actinide separation process chemistry is in evidence. A more wide spread adoption of a closed nuclear fuel cycle approach to radioactive materials management seems inevitable. In fact, a considerable amount of research has been done around the world to develop more efficient separations methods during the last decade. In the future pyrometallurgical/electrometallurgical separations and perhaps more advanced techniques based on volatility or new materials like supercritical fluids or Room Temperature Ionic Liquids may become more important. For the present and the near future, development of new methods continues to rely on the proven techniques of solvent extraction and related methods. This emphasis arises to a significant degree from the considerable amount of insight we have gained into the chemical processes that control solvent extraction processes. The flexibility available in solvent extraction that allows ready adjustment of operational parameters and the inherent adaptability of solvent extraction to continuous operations (and thus high throughput) also favor (and justify) continuation of this dominance.

While both favorable thermodynamics and kinetics are needed for the development of a useful separation technique, the greatest insight into process and new reagent design has been gained from correlations of thermodynamic data describing liquid-liquid phase transfer reactions. Solvent extraction reactions of f elements range widely from enthalpy- to entropy stabilized. Enthalpy-entropy compensation effects and solvation energy differences also figure prominently in this chemistry. It is important to note as well that minor differences in the energetics of chemical reactions in solvent extraction can have a major impact on separation efficiency. In this presentation, the basic thermodynamics of solvent extraction reactions of actinide and lanthanide metal ions will be discussed.

Synthesis of new mixed actinides oxalates as precursors of actinides oxide solid solutions

B. Arab-Chapelet^{*}, S. Grandjean^{*}, G. Nowogrocki[†] and F. Abraham[†]

^{*}Commissariat à l'Énergie Atomique, Nuclear Energy Direction, Radiochemistry and Process Division, Valrhô Research Center, BP 17171, 30207 Bagnols sur Ceze, France

[†]Laboratoire de Cristallogimie et Physico-Chimie du Solide, UMR CNRS 8012, ENSCL-USTL, BP 108, 59652 Villeneuve d'Ascq, France

INTRODUCTION

The main objectives of the development of innovative fuel cycles such as those conceived in the Generation IV forum, are an efficient use of energetic resources by recycling together the major and valuable actinides such as uranium and plutonium, and a drastic decrease of the radiotoxicity of the ultimate wastes by partitioning and transmutating the minor ones such as americium, curium or neptunium. Whatever the choice of management in the present or future, innovative synthesis methods are studied to elaborate new mixed actinides based materials. For their synthesis, wet methods fulfill very useful requirements such as flexibility, compatibility with a hydrometallurgical fuel processing, less dissemination of highly radioactive dusts during processing, and above all a better accessibility to very homogeneous polymetallic compounds and interesting nanostructures¹. Moreover these homogeneous solids improve the proliferation resistance by diluting plutonium with other actinides.

The oxalic precipitation of plutonium(IV) or plutonium(III) is used at an industrial scale during the reprocessing of the nuclear fuel, e.g. by the PUREX process², in order to convert into oxide this energetically valuable actinide. Oxalic acid is also a very common reagent to recover actinides from liquid waste using precipitation methods because of the very low solubility of An(IV) or An(III) oxalate compounds in acidic solutions^{3,4}. The flexibility of the oxalate ligand leads to actinides-based solid compounds which are particularly suitable precursors of actinides oxide solid solutions.

AN(IV)-AN(III) OXALIC COCONVERSION

Reaction of a solution containing a tetravalent actinide An(IV) and a trivalent actinide An(III) in presence of oxalic acid in acidic media under controlled conditions, leads

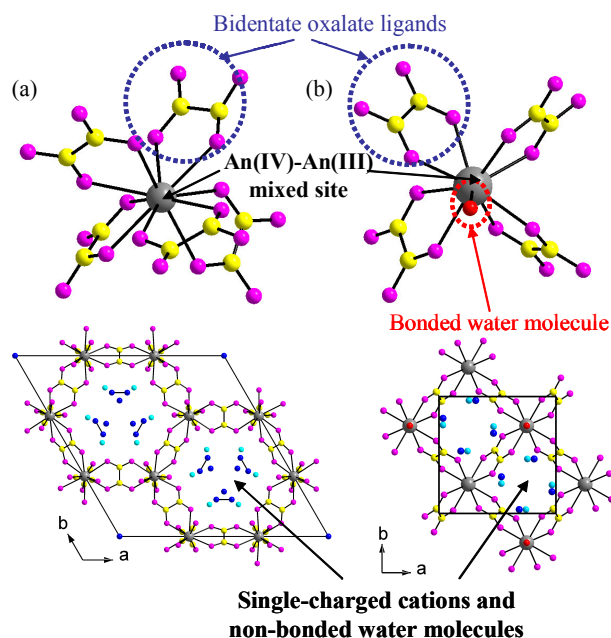


Fig 1: Environment of An(IV) – An(III) crystallographic mixed site and structural arrangement in : the hexagonal mixed oxalate (a) and in the tetragonal one (b).

to the precipitation of mixed An(IV)-An(III) oxalate compounds, with An(IV)=Th, Np, U or Pu and An(III)=Pu or Am, never described before. New mixed An(IV)-An(III) single-phase co-precipitates were obtained and characterized from powder diffraction patterns by analogy to uranium (IV)-lanthanide (III) oxalates whose structures were solved recently from single-crystal X-ray diffraction data^{5,6,7}. By varying the (An^{IV},An^{III}) pair and depending on the An^{IV}/An^{III} ratio, two original series were identified, $M_{2+x}An^{IV}_{2-x}An^{III}_x(C_2O_4)_5 \cdot 4H_2O$ (**1**) and $M_{1-x}[An^{III}_{1-x}An^{IV}_x(C_2O_4)_2 \cdot H_2O] \cdot 4H_2O$ (**2**) (M = single charged cation), with hexagonal or tetragonal symmetry, respectively. The originality of both structures is based on a mixed crystallographic site which can accept either a tetravalent actinide or a trivalent one, the charge balance being ensured by the adjustment of the single-charged ions within the structure. The main difference is that actinides are ten-coordinated in (1) and nine-coordinated in (2) (Fig 1). The honeycomb-like structure of the hexagonal compound is based on a three dimensional network of metallic and oxalate ions creating parallel tunnels. For the tetragonal series, the metallic ions are linked through oxalates ions to build a bidimensional arrangement of squared cycles.

Complementary investigations by UV-visible and Infrared spectroscopies and thermogravimetric analysis were led (Fig 2). They confirm the simultaneous co-precipitation of An(III) and An(IV) without modification neither of the ratio between A(IV) and An(III) nor of the oxidation state and highlight the role of single-charged cation and water molecules.

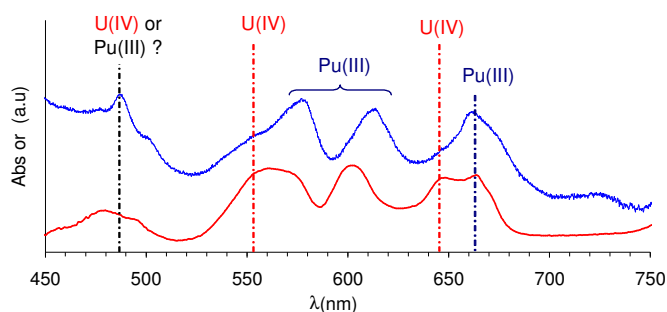


Fig 2 : UV-Vis Spectra of U(IV)-Pu(III) 50/50 nitric solution (red line) and U(IV)-Pu(III) solid co-precipitate showing the invariability of oxidation state during experiment.

CONCLUSION

In these experiments dedicated to actinides co-management using oxalic co-conversion, the simultaneous co-precipitation of the involved actinides is an important first achievement considering the specific properties of each actinide, properties which moreover differ according to various possible oxidation states.

¹ S. Pillon, J. Somers, S. Grandjean, J. Lacquement, *J. of Nucl. Mater.*, **320**, 36-43, (2003).

² F. Drain, B. Gillet, G. Bertolotti, «Oxalate process: the unique way for plutonium conversion», GLOBAL 1999 International Conference.

³ R.D. Bhanushali, *et al.*, *J. Radioanal. Nucl. Chem.*, **240**, N°2, 631-635, (1999).

⁴ P.P Mapara, *et al.*, *J. Radioanal. Nucl. Chem.*, **240**, N°3, 977-979, (1999).

⁵ B. Chapelet-Arab, S. Grandjean, G. Nowogrocki et F. Abraham., *J. Solid State Chem.*, **178**, 3046-3054, (2005).

⁶ B. Chapelet-Arab, S. Grandjean, G. Nowogrocki et F. Abraham, *J. Solid State Chem.*, **178**, 3055-3065, (2005).

⁷ B. Chapelet-Arab, L. Duvieubourg, F. Abraham, G. Nowogrocki et S. Grandjean, submitted to: *J. Solid State Chem.*, (2006).

Methods of Separations of Transuranium Elements Based on the Complex – Formation Ligands: Extraction and Sorption

B.F. Myasoedov[†], Yu.M. Kulyako[†], I.G. Tananaev[†], V.V. Yakshin*, A.Yu. Tsivadze*

[†] Vernadsky Institute of Geochemistry and Analytical Chemistry Russian Academy of Science, Moscow 199991 Russia

* Frumkin Institute of Physical Chemistry and Electrochemistry Russian Academy of Science, Moscow 199991 Russia

INTRODUCTION

The problem of high radioactive waste (HLW) treatment and storage is at present one of the most important ecological problems in Russia and in the U.S. Solution to this problem have two general aspects: (1) development of effective methods of HLW partitioning and disposal; and (2) determination, recognition, and isolation of hazardous radionuclides in the Environment. To satisfy both of these demands the main question is choice of highly accurate methods of radionuclide recognition, separation, and recovery of long-live isotopes from complex media. In practice for these purposes an extraction and sorption methods are used. In our opinion the following directions in the frame of development of fundamental knowledge of the processes of separation in nuclear technology will predominate in 21-st century: (1) The directed design and study of selective macro cyclic ionophores and another ligands with high chemical and radiolytic stability for isolation of a long-live radionuclides by means of a Liquid-Liquid, and Countercurrent Chromatography (CCC) from different media; (2) Practical realization of Supercritical Fluid Extraction (SFE) method based on quantitatively dissolution of UO_2 in some organic reagents, saturated with nitric acid in supercritical CO_2 as a solvent; (3) Development of effective sorption methods of reducing and recovery of Pu and other TRU from different man-caused and nature solutions using a fibrous “filled” sorbents. The results of a systematic study on realization of these three directions are summarized in our presentation.

EXPERIMENTAL

Extraction of U, and TRU by (4,4'(5')) bis(dialkylphosphoryl)-, bis(diphenylphosphoryl)-, bis(O-alkyl)phosphoryl)-benzo-n-crown-m ethers ($n = 18$ and $m = 6$; $n = 21$ and $m = 7$; $n = 24$ and $m = 8$, respectively) solutions in 1,2-dichloroethane and chloroform has been studied from nitric acidic media. It has been demonstrated that, during extraction, distribution coefficients (D_M) of U(VI), Pu(IV), Am(III), Eu(III) depend upon experimental conditions as well as upon structural features of the molecular complexes used. It is important that, within the range of $[HNO_3] = 0,02 - 1,0$ mol/l, the D_M values for metals depend on stereochemical orientation of phosphoryl- groups. It was found out that the extraction ability of cis(4,4'-) isomers is higher than for trans(4,5'-) isomers and for their mixtures. Using compound that has cis-oriented $(nBuO)_2P(O)$ -groups as an example, it was observed that the highest $D_U = 0,98$ in 3 mol/l HNO_3 ; $D_{Pu} = 5,1$ in 0,5 mol/l HNO_3 and $D_{Am} = 0,007$ at pH = 2. For trans-conformer under the same conditions D_M for U(VI), Pu(IV), and Am(III) are 0.091, 1.8; 0.003, respectively. It has been shown by using the BIO+(CHARMM) and MNDO computer methods, that the complexes of elements with trans-positions of the $(nBuO)_2P(O)$ - groups have larger volume, their energy

of formation is higher, and stability of the „host-guest“ complexes is lower. All this leads to the decrease of the D_M value during extraction. Under the same other conditions, the influence of the dimensions of the macrocycle (C_n) upon extraction is essential. Using extraction of Am(III) from 0.01–3M HNO_3 as an example, it has been demonstrated that for all molecules investigated, the most effective extractants are crown-ethers with $n = 21$. The shift of the D_{Am}^{max} to the higher $[HNO_3]$ was observed with the increase of n . The sequence of the coordination properties of phosphoryl-containing ligands based upon functionalized benzo-21-crown-7 under extraction of Am(III) from 0.01–3M HNO_3 is as follows: $(nBuO)(OH)P(O)- \gg (nBuO)_2P(O)- > Ph_2P(O)-$. Extraction properties of $di(nBuO)(OH)P(O)$ -dibenzo-21-crown-7 ($D_{Am} = 814$ in 0,1M HNO_3) are $>10^2$ higher for all compounds studied. The conditions of selective separation of Am(III)/Eu(III) by means of bis(O-alkyl)(OH)phosphoryl-dibenzo-21-crown-7 have been determined with separation factor of >90 at $[HNO_3] = 0.01$ mol/l.

Application of SFE technique was recently shown to be very promising for oxide nuclear fuel reprocessing thanks to using supercritical CO_2 . The main aim of realization of this process is to find and study the necessary organic ligands suitable for direct dissolution of TRU oxides for their separation. For experiments the adducts TBP- HNO_3 (**1**), methylisobutylketone - HNO_3 (**2**) and dimethyl-N,N'-dioctyl-hexylethoximalon- amide - HNO_3 (**3**) are prepared by mixing of equal volumes of the ligands with 8M HNO_3 during 15 min. The known volume of adducts used were introduced into a centrifuged test-tubes with the MOX samples (90-95% $^{233+238}UO_2$, and 10-5% $^{239}PuO_2$) at 60°C for ~3 h for dissolution. It was shown that MOX completely dissolved only in the (**1**) and (**3**) ($>99\%$ of U, and Pu in the solution). When dissolving the MOX sample in the (**2**), extraction of U only occurs ($>99\%$), resulting in separation of U(VI) from Pu(IV), which remains ($>99\%$) in the solid phase probably as PuO_2 . Hence, the system (**2**) one can find application in the future technology of oxide nuclear fuel reprocessing under SFE.

Direct dissolution of solid solution of 4.6% of PuO_2 and 95.5% of UO_2 in TBP- HNO_3 complex, conducted by us previously, requires the subsequent separation of U and Pu. Such separation may be performed by the method of CCC with the use of two-phase liquid system of TBP- HNO_3 . Influence of compositions of mobile and immobile phases on efficiency of separation of the elements was studied, and it was shown that CCC permits to separate U and Pu rather effectively under the conditions of concentration gradients both of TBP in immobile phase and of HNO_3 in mobile phase. At first, under optimal separation conditions, the fraction containing 99.7% of Pu and 0.3% of U goes out, and then uranium fraction is eluted.

At detection of TRU in natural and technological waters it is required their pre-concentration and separation from other elements. For this purpose it is most perspective sorption separation of TRU with use of the fibrous "filled" sorbents. These materials represent thin porous fibers inside which it is kept fines grain "filler" – complex forming or ion exchanger sorbent. We investigated the properties of the fibrous "filled" sorbents type POLYORGS 33-n, 34-n, and 35-n (complexing sorbents with amidoxime and hydrazidine groups) for pre-concentration of Pu(IV), U(VI), Np(V), Am(III) (~10 ppm) from solutions: **I**- 0.5M NaCl, pH=6; **II**- Ca-0.043; Mg-0.08; Na-0.045; Cl- 0.2 mg/l; pH=6.5; **III**- Ca- 42; Mg-10; Na-54; K-39; Cl-4.6; SO_4 -29; HCO_3^- - 159 mg/l. It was found that the sorption degree of the TRU used during extraction from all the model solutions by POLIORGS at ratio V : M = 100 ml/g and time contact ~2 h are exceeded 96 – 99%.

The work was supported by the U.S.DOE-OBES, Project RUC2-20010-MO-04, RFBR grant 05-03-32908, 33094; and President RF grant 1693.2003.3.

Plutonium and Other Actinides Behaviour in NEXT Process

S. Miura, M. Nakahara, Y. Sano, M. Kamiya, K. Nomura, J. Komaki

Japan Atomic Energy Agency, Tokai, Ibaraki, 319-1195, JAPAN

INTRODUCTION

In the feasibility study on the commercialized fast reactor cycle systems, which aims for ensuring safety, economical competitiveness, efficient utilization of resources, proliferation resistance, and decreasing environmental burden, Japan Atomic Energy Agency (JAEA) has been developing the advanced aqueous reprocessing system named “New EXtraction system for TRU recovery (NEXT) process” for the spent fast reactor fuel reprocessing. The NEXT process basically consists of 3 characteristic processes; the crystallization process for recovering a part of U from dissolver solution, the U-Pu-Np co-recovery process with single cycle flowsheet using TBP as an extractant and the Am-Cm recovery process with extraction chromatography¹. In this study, we will discuss the behaviour of Pu and other actinides in the crystallization process and the U-Pu-Np co-recovery process with referring to the experimental results obtained in our experimental facility, Chemical Processing Facility (CPF).

CRYSTALLIZATION PROCESS

As we reported in the previous work², Pu shows the different behaviour in the crystallization process according to its valence in the dissolver solution. If Pu(VI) exists in the dissolver solution, Pu is co-crystallized with U, which brings low decontamination factor (DF) of Pu to U (DF_{Pu}) and makes it difficult to improve DF_{Pu} by washing the crystal. On the other hand, under the condition that Pu is adjusted to Pu(IV) in the dissolver solution, Pu is not crystallized and only U crystal is obtained. Although the surface of the U crystal is contaminated with mother solution containing Pu, comparatively high DF_{Pu} can be achieved easily by washing the crystal surface with nitric acid solution. It is, therefore, important for preventing Pu co-crystallization and keeping high DF_{Pu} to adjust the Pu valence to Pu(IV) in the dissolver solution.

Under some crystallization condition, we have found that Cs contained in the dissolver solution as FP can be hardly separated from the U crystal, i.e. DF_{Cs} shows very low values³. In our recent research, it is suggested that such behaviour of Cs will be related with the formation of some kinds of Cs compounds with Pu



Photo 1: U crystal obtained in the crystallization tests with U-Pu-Cs solution (U: 409g/l, Pu(IV): 41.8g/l, Cs: 4.6g/l) (after washing). A small amount of whitish green crystals are observed in the yellow U crystal.

in the dissolver solution. It is known that whitish green crystal of $\text{Cs}_2\text{Pu}(\text{NO}_3)_6$ is composed by mixing CsNO_3 and $\text{Pu}(\text{NO}_3)_4$ in high nitric acid solution under low temperature condition. We have also obtained a small amount of similar crystals in the U crystal after some crystallization tests in which the concentration of Cs is comparatively high (Photo 1).

The analysis of these crystals is now in progress, and it will be further required for high DF_{Cs} to clarify the process condition without the formation of such Cs-Pu compounds, and/or to develop some purification methods for the U crystal contaminated with these compounds.

U-Pu-Np CO-RECOVERY PROCESS

In the U-Pu-Np co-recovery process with single cycle flowsheet, Pu partitioning section is eliminated from the conventional PUREX process, i.e. no Pu reduction to Pu(III) occurs in the process. In this process, Pu is stripped with U just by diluted nitric acid solution. The stripping reactions of Pu (Pu(IV)) and U (U(VI)) are exothermic and endothermic respectively. Therefore, it is important for the effective co-stripping of these elements to control the temperature carefully in the stripping section (Fig. 1). It is also required for preventing the generation of Pu polymer under the low acidity to adjust the nitric acid concentration to be a suitable value in the stripping section.

Among the actinide elements, Np shows the complex behaviour in the extraction section because of its variable valences in the nitric acid solution; extractable Np(IV) and Np(VI), and inextractable Np(V). These Np valences are affected by the concentration of nitric acid and nitrous acid in the process, and it is desirable for the effective Np extraction, i.e. the effective oxidation of Np to extractable Np(VI) in the extraction section, to increase the nitric acid concentration, and to control and optimize the nitrous acid concentration in this section.

Although there are some considerable points on developing and improving the flowsheet for the U-Pu-Np co-recovery process as mentioned above, we have confirmed that over 99.9% of U and Pu, and 99% of Np can be co-recovered with sufficient DF of total γ ($\sim 10^4$) under the appropriate condition^{4,5}. For optimizing the flowsheet, further investigation will be carried out.

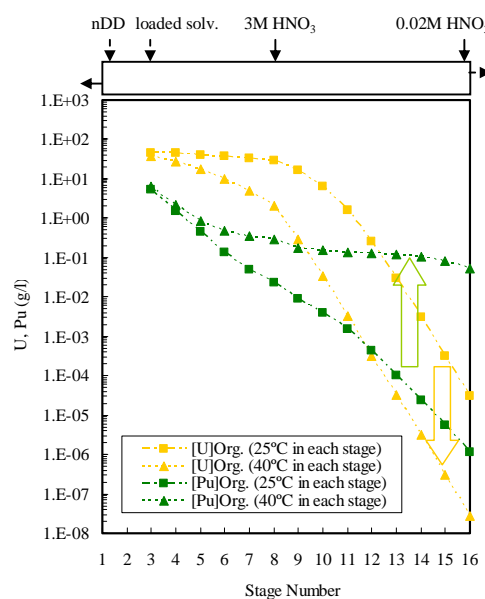


Fig. 1: Temperature dependence of U and Pu profiles in the stripping section, which was calculated with the simulation code "MIXSET-X".

- 1 Y. Takata, *et al.*, *J. Nucl. Sci. Technol.*, 41(3), **307** (2004).
- 2 K. Yano, *et al.*, *Proc. of Actinides2005*, **5P47** (2005).
- 3 K. Yano, *et al.*, *Proc. of Global2005*, **118** (2005).
- 4 Y. Sano, *et al.*, *Proc. of ISEC2005*, **B206** (2005).
- 5 M. Nakahara, *et al.*, *Proc. of Global2005*, **262** (2005).

Electrochemical studies on Plutonium in molten salts

G. Bourgès*, S. Rochefort*, D. Lambertin*, H. Chollet*, S. Delpech†, G. Picard†

* CEA – Centre d'études de Valduc – 21 120 Is sur Tille – France,

† Laboratoire d'Electrochimie et de Chimie Analytique - ENSCP, 11 rue Pierre et Marie Curie - 75231 Paris - France

INTRODUCTION

Pyrochemical separations, involving salt and metal molten media, by liquid/liquid extraction or electrorefining are studied for nuclear defence and civil applications. Both are concerned by actinides separations. Lanthanides, such as cerium, are often used as surrogates.

Early steps of such pyrochemical processes development consist of studying of the molten salt chemistry of the elements to be separated. Activity coefficients of the solute in liquid metal and salt phases are important thermochemical parameters for predicting separation efficiency and to assess the solvents influence.

CEA has been operating such processes in chloride media for more than 40 years for both plutonium metal preparation and residues recovery. In the 70's, the earlier studies concerned plutonium in NaCl/KCl/BaCl₂ mixture. More recently, Pu(III) has been investigated in NaCl/KCl eutectic mixture and in pure CaCl₂. As solvent metal such as gallium could have potentialities for the recovery of plutonium from metal scraps, the thermochemical properties of plutonium dissolved in gallium were then studied.

EXPERIMENTAL

Electrochemical investigations using cyclic voltammetry, potentiometry and chronoamperometry have been carried out to study the properties of plutonium (III) in various molten chlorides and of Pu metal in gallium metal.

The feed chlorides were previously dried. Pure commercial gallium and plutonium metal pieces prepared at CEA/Valduc were used as metal feed. The chloride salt and the metal were melted in a magnesia crucible placed under dry argon. The reference electrode was a silver wire dipped into a porous alumina tube containing a solution of silver chloride in the corresponding chloride. Tungsten wires were used as working and counter electrodes.

ELECTROCHEMICAL PROPERTIES OF PLUTONIUM IN MOLTEN CHLORIDES

The standard potential of Pu(III)/Pu redox couple in eutectic mixture of NaCl/KCl/BaCl₂ at 1073 K deduced from early studies by potentiometry is equal to -2.56 V¹(see fig.1). In NaCl/KCl eutectic mixture and in pure CaCl₂ (see fig.2), the standard potential deduced from cyclic voltammetry are respectively -2.54 V and -2.51 V, and led to the activity coefficients of Pu(III) in the molten salt². In NaCl/KCl media, the presence of plutonium seems to involve a decrease of the solvent limit (sodium reduction) so that the gap between Pu³⁺/Pu and Na⁺/Na couples is small. In more acidic melt, like CaCl₂, the standard potential is close to the reference related to pure compounds.

As oxides ions concentration in molten salts may be important for separation processes, the potential – p(O²⁻) diagrams were built from these results and literature data in order to define the stability domains of the plutonium – oxygen - chlorine compounds^{2,3}.

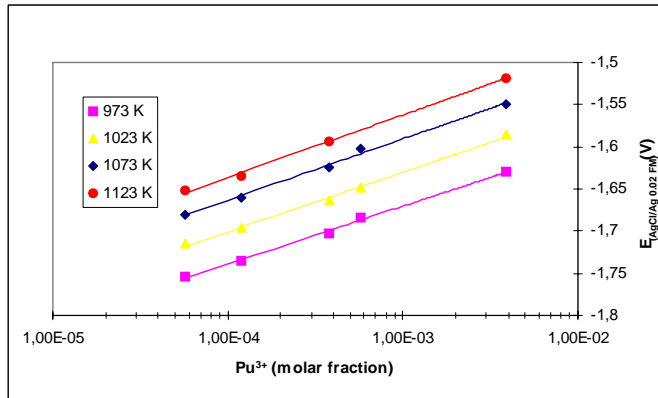


Fig. 1: Potentiometry of Pu(III)/Pu couple in NaCl/KCl/BaCl₂ (from¹).

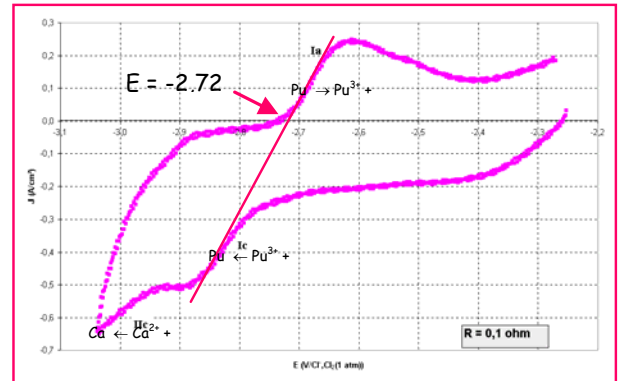


Fig. 2: Cyclic voltammetry obtained on a tungsten working electrode in CaCl₂ containing Pu(III) ions ($X_{\text{Pu(III)}} = 1.1 \times 10^{-3}$)

THERMOCHEMICAL PROPERTIES OF PLUTONIUM IN LIQUID GALLIUM

Chronoamperometry on plutonium in liquid gallium in chlorides – CaCl₂ (see fig. 3) and equimolar NaCl/KCl - led to the determination of the activity coefficient of Pu in liquid Ga, $\log \gamma = -7,2^4$.

This new data is key parameter to assess the scientific feasibility of an original process for plutonium recovery from metallic scraps after dissolution in liquid gallium by selective extraction.

As activity coefficient of cerium in gallium was previously determined⁴, it is possible to compare gallium with other solvent liquid metals such as Cd, Bi, Al for plutonium - cerium separation.

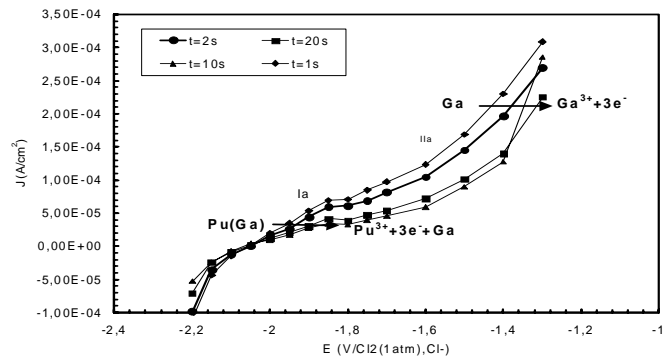


Fig. 3: Intensity-potential curve in CaCl₂ at 1073K obtained from chronoamperograms, $X_{\text{Pu(Ga)}}=0.0129$, $X_{\text{PuCl}_3}=0.0011$

The authors would like to thank J. Lannaud for his “pioneer” studies, and staff of Valduc 118 facility for their technical support.

- 1 J. Lannaud, CEA-DAM internal report (1973).
- 2 D. Lambertin, S. Ched'Homme, G. Bourgès, S. Sanchez, G. Picard, J. of Nuclear Materials, 341, (2005), 124-130
- 3 S. Sanchez, G. Picard, D. Lambertin, J. Lacquement, Proceedings “OCDE/NEA workshop on pyrochemical separations”, Avignon, (14-16 march 2000), 213-221
- 4 D. Lambertin, S. Ched'Homme, G. Bourgès, S. Sanchez, G. Picard, J. of Nuclear Materials, 341, (2005), 131-140

Systematics in PuTGa₅ Compounds

F. Wastin, E. Colineau, F. Jutier and J. Rebizant

*European Commission, Joint Research Centre, Institute for Transuranium Elements, Postfach 2340, D-76125 Karlsruhe, Germany

The recent discovery of superconductivity^{1,2} at a high transition temperature in the plutonium-based compounds PuCoGa₅ ($T_c = 18.5$ K) and PuRhGa₅ ($T_c = 9$ K) has ignited a high interest in these new materials. Prior to this discovery, no Pu-based compound was found to exhibit superconductivity. Moreover, among the known actinide or lanthanide superconductors one rarely finds a material with a T_c over 2 K. From this perspective, Pu(Co or Rh)Ga₅ can be regarded to have an astonishingly high transition temperature and the nature of the superconducting pair formation has been a point of special focus^{3,4}. Most recently, experimental studies, employing nuclear magnetic and quadrupolar resonance (NMR, NQR), proved that indeed PuCoGa₅ and PuRhGa₅ are unconventional, spin-singlet, *d*-wave type superconductors^{5,6}. However, the experimental investigations of these Pu-based compounds is complicated by the evolution of their properties as a function of time^{1-2,5-7}, due to the impact of self-radiation damage, induced by the α -decay of the Pu atoms.

At ITU-Karlsruhe, we have started a systematic investigation of PuTGa₅ (T a d transition metal) summarized in the figure 1, but no new superconducting material has been evidenced up to now, and paramagnetic type behaviour is most commonly observed in the series. However some systematics can be drawn out.

First, from the chemical point of view, we observe that moving along the 3d series beside the Co and/or going down within the Co-column, the 1:1:5s are more and more difficult to obtain as pure phase and become unstable. Thermodynamic competition with neighbouring phases (e.g. 2:1:8, 4:1:12, ...) is more and more 1:1:5 unfavourable. This observation may be related to the 1:1:5 phase stability observed in Ce-compounds (only formed with In) and other 4*f* and 5*f* elements (Th, U, Np) that reveals a marked effect of the *f*-electron count. It is marginal to conclude that the electronic structure may play an important role in the 1:1:5 phase stability and may deserve a thorough theoretical investigation.

Another systematic addresses the interesting variation of the T_c versus *c/a* ratio⁸ (Figure 2a). For each family, the differences in T_c from compound to compound (under changes in the doping on the transition metal site) from the group Co, Rh, Ir are found to correlate with the differences in

<i>3d</i>	Fe PP	Co 18.6K	Ni PP
<i>4d</i>	<i>Ru</i>	Rh 9K	<i>Pd</i>
<i>5d</i>	<i>Os</i>	Ir PP	<i>Pt</i>
	Paramagnetic	Superconductor	
	<i>element in italic: does not form or was not obtained</i>		

Fig 1: Behaviour of PuTGa₅ compounds.

c/a ratio: the plot of T_c versus c/a forms a straight line of positive slope. However, recent solid solution studies⁹ and high-pressure investigations¹⁰, have shown that this variation could not be assigned to the c/a ratio as being the main tuning parameter.

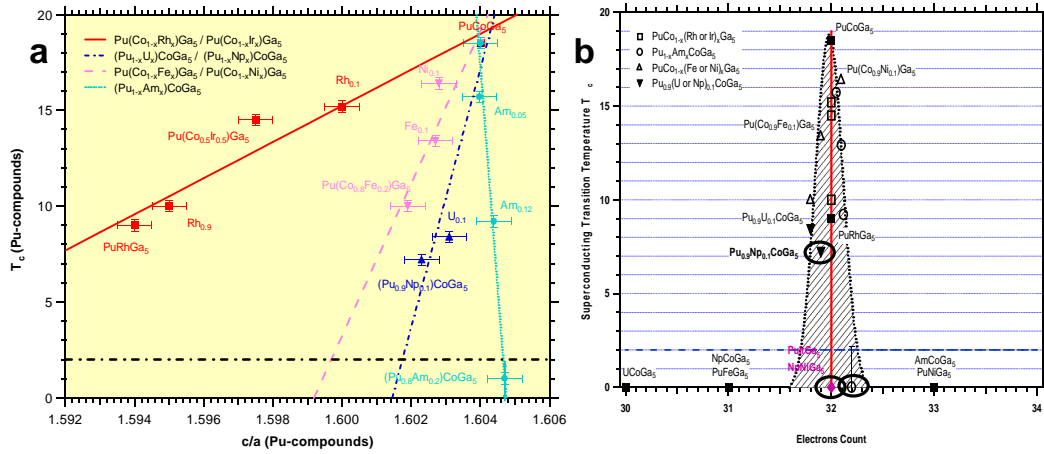


Fig 2: a) Variation of T_c as a function of the c/a ratio and b) Distribution of T_c as a function of the electron counts.

Figure 2b provides a new perspective on the influence of doping the systems investigated with different elements. Plotting the variation of T_c as a function of the electrons count (here only outer-shell electrons are counted), shows a spectacular concentration of all AnTGa₅ superconducting compounds in a narrow band at approximately 32 ± 0.2 electrons, whereas all compounds outside of this band (i.e. with different electron count) are not superconducting.

Further systematics, and in particular addressing the magnetic properties, can be drawn and will be addressed in our presentation.

The high purity Pu metals required for the fabrication of the compounds was made available through a loan agreement between Lawrence Livermore National Laboratory and ITU, in the frame of a collaboration involving LLNL, Los Alamos National Laboratory, and the US department of Energy. F. J. acknowledges the European Commission for support in the frame of the Training and Mobility of Researchers" programme.

- 1 J. L. Sarrao, *et al.*, Nature **420**, (2002).
- 2 F. Wastin, *et al.*, J. Phys. Condens. Matter **15**, (2003).
- 3 T. Maehira, *et al.*, Phys. Rev. Lett. **90**, (2003).
- 4 I. Opahle, P. M. Oppeneer, Phys. Rev. Lett. **90**, (2003).
- 5 N. J. Curro, *et al.*, Nature **434**, (2005).
- 6 H. Sakai, *et al.*, J. Phys. Soc. Jpn. **74**, (2005).
- 7 F. Jutier, *et al.*, Physica B **359-361**, (2005).
- 8 E.D. Bauer, *et al.*, Phys. Rev. Lett. **93**, (2004).
- 9 P. Boulet, *et al.*, Phys. Rev. B **72**, (2005).
- 10 P. Normile, *et al.*, Phys. Rev. B **72**, (2005).

Probing the Coulomb interaction of the unconventional superconductor PuCoGa₅ by phonon spectroscopy

S. Raymond^{*}, P. Piekarz[†], J.P. Sanchez^{*}, J. Serrano[‡], M. Krisch[‡], B. Janoušová[◊], J. Rebizant[◊], N. Metoki^γ, K. Kaneko^γ, P.T. Jochym[†], A.M. Oleś^{†,♦} and K. Parlinski[†].

^{*}CEA-Grenoble, DRFMC / SPSMS, 38054 Grenoble Cedex, France

[†] Institute of Nuclear Physics, Polish Academy of Sciences, 31342 Krakow, Poland

[‡]European Synchrotron Radiation Facility, 38043 Grenoble Cedex, France

[◊]European Commission, Institute for Transuranium Elements, 76125 Karlsruhe, Germany

^γJapan Atomic Energy Agency, 319-1195, Tokai, Japan

[♦]Max Planck Institut für Festkörperforschung, 70569 Stuttgart, Germany

Given its characteristic energy scales, the unconventional superconductor PuCoGa₅ ($T_c = 18.5$ K) is playing the central role of a missing link between the canonical heavy fermion superconductors and the high- T_c cuprates [1]. The understanding of its physical properties will thus allow progress in the global understanding of unconventional superconductivity. While a magnetic mechanism for the electron pairing is strongly suggested, the study of the phonon spectrum is nonetheless of interest. This is partly due to tremendous recent progresses in band structure calculations that allow to compute accurate phonon spectrum of strongly correlated electron systems [2,3].

We measured the phonon dispersion curves of single crystalline PuCoGa₅ samples along the [100], [110] and [001] directions by Inelastic X-ray Scattering (IXS) at room temperature. The IXS data are compared with a density functional theory (DFT) *ab-initio* calculation using the Generalized Gradient Approximation with finite U (GGA+ U) method [2]. We concluded that the inclusion of a finite on-site repulsion between f electrons, U , of approximately 3 eV is essential to describe quantitatively the lattice dynamics of PuCoGa₅. This conclusion is primarily drawn from the sensitivity of the lowest transverse optic modes to the Coulomb repulsion that undergo up to 30 % change in energy between the calculations with $U = 0$ and $U = 3$ eV. The comparison of the experimental data with the *ab-initio* calculation for $U = 0$ eV and $U = 3$ eV is

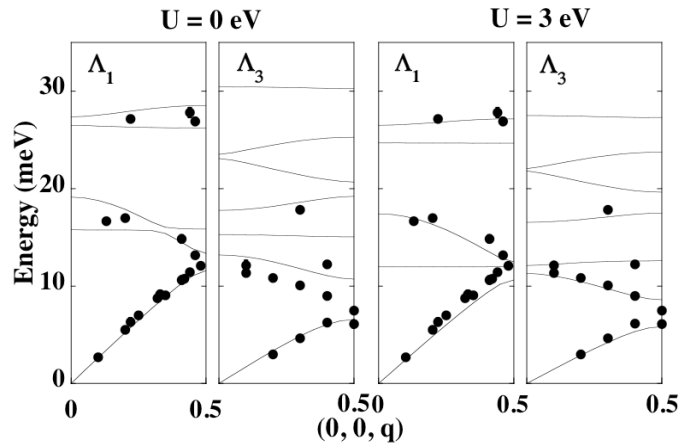


Fig. 1 : Dispersion relation of PuCoGa₅ for the [001] direction at 300 K. The experimental data (full circles) are compared with *ab-initio* calculation for $U = 0$ (left) and 3 eV (right). Branches are classified according to the irreducible representations (Λ_1 , Λ_3) along [001].

shown in Fig.1 for the direction [001]. The best agreement with the $U = 3$ eV calculation, that is found for [100], [110] and [001] directions, gives support to the existence of substantial f electrons localization in PuCoGa₅ in agreement with photoemission results [4].

In contrast, it was found that the phonon spectrum of the itinerant electron paramagnet UCoGa₅ is better described with $U = 0$ eV [5]. This is consistent with the known delocalization of f elec-

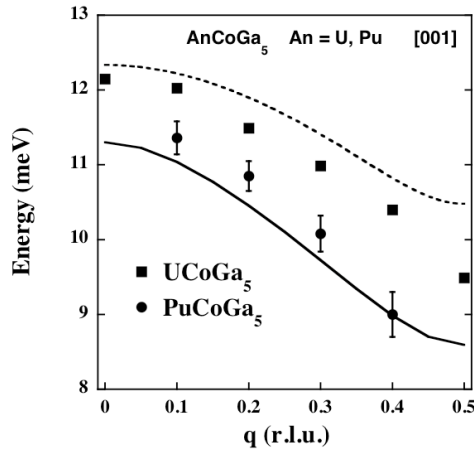


Fig. 2 : Comparison of the dispersion of the TO mode propagating along [001] and polarized along [100] for PuCoGa₅ and UCoGa₅ at 300 K. The solid line is a calculation for PuCoGa₅ with $U = 3$ eV and the dashed line is calculation for UCoGa₅ with $U = 0$ eV.

-trons in this compound [6]. The comparison between experimental data and calculation for the lowest TO branch propagating along [001] and polarized along [100] is shown in Fig.2 for the two compounds. The *ab-initio* lattice dynamics calculation shown corresponds to UCoGa₅ with $U = 0$ eV and respectively to PuCoGa₅ with $U = 3$ eV.

Our study gives new evidence for localized degrees of freedom of f electrons in PuCoGa₅ and shows that phonon spectroscopy is an alternate way of probing electronic properties of strongly correlated electron systems. This study is in line with other critical tests of theoretical treatment of $5f$ electrons, e.g. the one performed on δ -Pu [7].

- 1 N.J. Curro et al., Nature **434**, 622 (2005).
- 2 P. Piekarz et al., Phys. Rev. B **72**, 014521 (2005).
- 3 X. Dai et al., Science **300**, 953 (2003).
- 4 J.J. Joyce et al., Phys. Rev. Lett. **91**, 176401 (2003).
- 5 N. Metoki et al., Proceedings of SCES 2005, Vienna.
- 6 R. Troć et al., Phys. Rev. B **70**, 184443 (2004).
- 7 J. Wong et al., Science **301**, 1078 (2003).

Electronic Structure Investigations of Pu-Compounds: PuFeGa₅, PuNiGa₅, PuFe_{0.5}Co_{0.5}Ga₅, PuNi_{0.5}Co_{0.5}Ga₅ and PuIn₃

P.M. Oppeneer^{*}, S. Lebègue[†], O. Eriksson^{*}

^{*}Department of Physics, Uppsala University, Box 530, S-754 47 Uppsala, Sweden

[†]Laboratoire de Cristallographie et de Modélisation des Matériaux Minéraux et Biologiques, CNRS-Université Henri Poincaré, B.P. 239, F-54506 Vandoeuvre-lès-Nancy, France

SCIENTIFIC RELEVANCE OF Pu-COMPOUNDS

The interest in Pu-compounds has been revitalized considerably by the discovery¹ of superconductivity at a very high T_c of 18.5 K in the ternary Pu-compound PuCoGa₅. The mechanism of the superconducting pair formation has been a point of special attention in the scientific community. It was speculated^{1,2} that possibly an *unconventional* pairing mechanism might be responsible for the anomalously high T_c . Several investigations^{1,2} showed that PuCoGa₅ is close to magnetic ordering, and, consequently, a magnetic mechanism could be responsible for the Cooper pair formation. Recently, two experimental studies^{3,4} employing NMR and NQR showed that PuCoGa₅ as well as the isoelectronic PuRhGa₅ are unconventional, spin-singlet, *d*-wave type superconductors. This type of unconventional order parameter could possibly correspond to pairing mediated by antiferromagnetic spin fluctuations.³

In the sequel of the initiating discovery, many actinide compounds, which crystallize in the tetragonal HoCoGa₅ structure were synthesized and investigated. An important point—which yet has to be clarified—is what the essential difference is between the two superconducting Pu-115 compounds and other, non-superconducting actinide-115 compounds. Several Pu-based 115-compounds were synthesized, but the only superconducting Pu-compounds so far are PuCoGa₅ and PuRhGa₅. Moreover, substituting Co by Fe or Ni, its direct, respective neighbours in the Period Table, rapidly quenches the superconductivity.⁵ At present it is not understood why the effect of substitution on the Co site is so pronounced. Viewed from the number of electrons in the unit cell, it turns out that superconductivity appears only in a narrow “dome” around the electron filling of 32 valence electrons per unit cell (corresponding to PuCoGa₅).

ELECTRONIC STRUCTURE INVESTIGATIONS OF Pu-COMPOUNDS

With the aim to search for differences between the Pu-115 materials, we have performed a computational investigation of the electronic structures of several Pu-115 compounds. We used the density functional theory (DFT) in conjunction with the local spin-density approximation (LSDA) and the generalized-gradient approximation (GGA). The calculations were performed with the full-potential LMTO as well as with the FP-LAPW method, in which scalar-relativistic effects and the spin-orbit interaction are included. In the GGA/LSDA calculations the Pu *5f* electrons are treated as delocalized valence states. Previously the importance of Coulomb correlations within the Pu *5f* shell has been pointed out^{6,7} for PuCoGa₅. To investigate their importance, we also performed LSDA+U calculations for several Pu-115 compounds. The appropriate *5f* description has to be established through comparison with experiments.

Our GGA calculations show that there exists sensitivity to the band filling (i.e., number of electrons) in these materials. The $3d$ -states of Fe, Co and Ni are mostly retracted from the Fermi energy, although there is in the density of states (DOS) a tail, which extends to several eV above the Fermi level. A part of the Pu $5f$ states is positioned near the Fermi energy.^{2,8} To a good approximation, the filling of the $3d$ band leads to a rigid-band-like shift of the Fermi level within the narrow $5f$ band. Because the $5f$ partial DOS is rather steep near the Fermi level, the band filling leads to significant changes of the Fermi surfaces. In particular, the Fermi surface computed for PuCoGa₅ is most 2-dimensional, whereas the Fermi surfaces of PuFeGa₅ and PuNiGa₅ are computed to be more 3-dimensional. This indicates that nesting properties of the Fermi surfaces—which could be important for the pairing interaction—are different for the Pu-115 compounds.

RELATED PuGa₃ AND PuIn₃ COMPOUNDS

Closely related to the Pu-115 compounds are the binary Pu-compounds PuGa₃ and PuIn₃. An essential building block of the Pu-115's would be the cubic PuGa₃ group. However, so far only PuIn₃ was synthesized⁹ in the cubic AuCu₃ phase; it has not been possible to synthesize PuGa₃ in the cubic structure. It could be synthesized¹⁰ only in a trigonal and a hexagonal phase, both of which are magnetic. The Fermi surface of PuIn₃ was studied⁹ recently through de Haas-van Alphen (dHvA) experiments. This study revealed that one part of the Fermi surface of PuIn₃ as detected in dHvA experiments, is reasonably described by DFT calculations. We have investigated PuIn₃, too, and obtain (in variance with the previous study) one of the Fermi surface sheets to be connected across the zone boundaries (see Fig. 1). Thus, we find overall similar features of the Fermi surface, except for the topology of one Fermi surface sheet. Further de Haas-van Alphen studies would be desirable to achieve a complete picture of the Fermi surface. Also for PuFeGa₅ and PuNiGa₅ such investigations could be employed to reveal if these materials indeed have a more 3-dimensional Fermi surface.

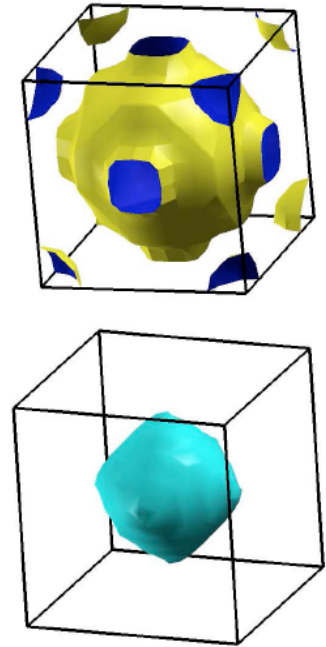


Fig 1: The calculated GGA Fermi surfaces of PuIn₃.

We gratefully acknowledge fruitful discussions with A.B. Shick, V. Janiš, J.D. Thompson, J.L. Sarrao, N.J. Curro, T. Durakiewicz, J.J. Joyce, E.D. Bauer, G.H. Lander, F. Wastin, J. Rebizant, E. Colineau, P. Boulet, D. Aoki, Y. Haga, K. Kaneko, N. Metoki, R.H. Heffner and Y. Onuki.

- 1 J.L. Sarrao *et al.*, Nature **420**, 297 (2002).
- 2 I. Opahle and P.M. Oppeneer, Phys. Rev. Lett. **90**, 157001 (2003).
- 3 N.J. Curro *et al.*, Nature **434**, 622 (2005).
- 4 H. Sakai *et al.*, J. Phys. Soc. Jpn. **74**, 1710 (2005).
- 5 P. Boulet *et al.*, Phys. Rev. B **72**, 104508 (2005).
- 6 J.J. Joyce *et al.*, Phys. Rev. Lett. **91**, 176401 (2003).
- 7 A.B. Shick, V. Janiš, and P.M. Oppeneer, Phys. Rev. Lett. **94**, 016401 (2005).
- 8 T. Maehira, T. Hotta, K. Ueda, and A. Hasegawa, Phys. Rev. Lett. **90**, 157001 (2003).
- 9 Y. Haga *et al.*, J. Phys. Soc. Jpn. **74**, 2889 (2005).
- 10 P. Boulet *et al.*, Phys. Rev. B **72**, 064438 (2005).

Fermi Surface, Magnetism and Superconducting Properties of Pu-compounds

Y. Haga^a, D. Aoki^b, H. Yamagami^c, T. D. Matsuda^a, K. Nakajima^d, Y. Arai^d, E. Yamamoto^a, A. Nakamura^a, Y. Homma^b, Y. Shiokawa^{b,a} and Y. Onuki^{e,a}

^aAdvanced Science Research Center, JAEA, Tokai, Ibaraki 319-1195, Japan

^bInstitute for Materials Research, Tohoku University, Oarai, Ibaraki 319-1313, Japan

^cDepartment of Physics, Kyoto Sangyo University, Kyoto 603-8555, Japan

^dNuclear Science and Engineering Directorate, JAEA, Tokai, Ibaraki 319-1195, Japan

^eGraduate School of Science, Osaka University, Toyonaka, Osaka 560-0043, Japan

INTRODUCTION

The discovery of high-temperature superconductivity in plutonium compounds renewed interests in plutonium and other actinide compounds. The high superconducting transition temperature of PuCoGa₅ (18.5 K)¹ and PuRhGa₅ (8 K)² is discussed based on the quasi-two-dimensionality in the electronic state predicted by the 5f-itinerant band calculations^{3,4}. On the other hand, there is no experimental work for the investigation of the Fermi surface topology because of the experimental difficulties such as strong radiation damage and self heating effect. It is therefore challenging to clarify the electronic states of plutonium compounds experimentally, by using de Haas-van Alphen Effect (dHvA) or angle-resolved photoemission spectroscopy. In this paper we report the first dHvA study in plutonium compound PuIn₃ with the cubic AuCu₃ type structure, which can be regarded as a reference compound of PuCoGa₅. The result was analyzed based on the itinerant 5f electron picture. Experimental results on magnetic and superconducting properties of PuRhGa₅ are also presented.

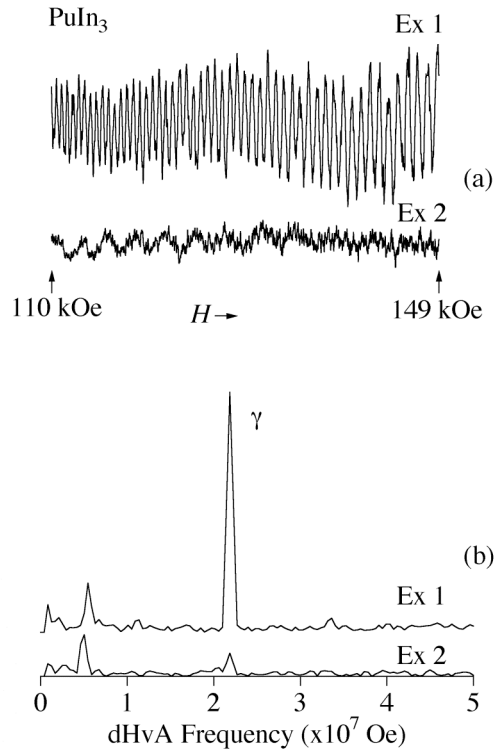
EXPERIMENTAL

Single crystals of PuIn₃ and PuRhGa₅ were grown by the flux method using an enriched ²³⁹Pu metal as the starting material^{5,6}. The sample was characterized by the x-ray diffraction. The single crystal for magnetization and dHvA measurements was encapsulated in a small polyimide tube with typical dimensions $\phi 2 \times 8$ mm. To ensure a good thermal contact between the sample and the cryostat, the sample was mounted on a silver disk. The sample was cooled down using a dilution refrigerator. Because of the self heating effect 5.2 μ W of PuIn₃, the temperature of the sample is about 10 mK higher than that of the mixture at the base temperature 30 mK. The dHvA effect was measured by the field-modulation technique. The anisotropy of the magnetic susceptibility was measured by the SQUID magnetometer where the field direction was changed by rotating the sample capsule along its axis.

RESULTS⁵

We have succeeded in observing the first dHvA oscillation in plutonium compounds, as shown in Fig. 1. The signal with the dHvA frequency 2.1×10^7 Oe shows a clear angular

dependence reflecting the crystal symmetry. The cyclotron effective mass of this branch, determined from the temperature dependence of the dHvA amplitude, is significantly larger than that of an ordinary metal, $4.8 m_0$ where m_0 is the electron rest mass. These results show that this signal is attributed to the dHvA oscillation from PuIn₃. On the other hand, the signal with a lower frequency 5.5×10^6 Oe lacks these features and therefore is considered to come from indium metal. It should also be noted that the dHvA amplitude strongly decreases as function of time, as demonstrated in Fig. 1. Ex 1 was measured 4 days after the crystal growth, while Ex 2 was measured under the same condition 10 days after Ex 1. Such decrease of the dHvA can be attributed to the radiation damage caused by the α -decay of ²³⁹Pu. In fact the mean free path of the carrier estimated from the dHvA measurements changes from 860 Å for Ex 1 to 570 Å for Ex 2.



The result of the angular dependence of the dHvA frequency, which corresponds to the extremal cross section of the Fermi surface perpendicular to the field direction, was analyzed by the band calculations. The experimental data agree well with the theory, indicating that the 5f electrons can be treated as itinerant ones. In addition to the dHvA branch detected in the experiment, band calculations predicted 2 more Fermi surfaces which have larger dHvA frequency and cyclotron mass. However, those branches are expected to have significantly small dHvA amplitude and difficult to observe because of the radiation damage as mentioned above.

From the present results, it is expected that the band calculations are valid also for PuCoGa₅ and PuRhGa₅. The experimental dHvA study for these superconductors are also desired but more challenging because the superconducting mixed state extremely weaken the dHvA amplitude.

- 1 J. Sarrao *et al.*, Nature (London), **420**, 297 (2002).
- 2 F. Wastin *et al.*, J. Phys. Condens. Matter, **15**, S2279 (2003).
- 3 I. Opahle and P. M. Oppeneer, Phys. Rev. Lett., **90**, 157001 (2003).
- 4 T. Maehira *et al.*, Phys. Rev. Lett. **90**, 207007 (2003).
- 5 Y. Haga *et al.*, J. Phys. Soc. Jpn. **74**, 1698 (2005).
- 6 Y. Haga *et al.*, J. Phys. Soc. Jpn. **74**, 2889 (2005).

What Does PuCoGa₅ Teach Us About Pu?

E. D. Bauer¹, J. D. Thompson¹, N. J. Curro¹, T. Durakiewicz¹, J. J. Joyce¹, J. L. Sarrao¹, L. A. Morales¹, J. M. Wills¹, C. H. Booth², F. Wastin³, J. Rebizant³, J. C. Griveau³, P. Javorsky³, P. Boulet³, E. Colineau³, G. H. Lander³

¹ Los Alamos National Laboratory, Los Alamos, New Mexico 87545, USA

² Chemical Sciences Division, Lawrence Berkeley National Laboratory, Berkeley, California 94720, USA

³ European Commission, Joint Research Centre, Institute for Transuranium Elements, Postfach 2340, 76125 Karlsruhe, Germany

Many of the interesting physical and mechanical properties of plutonium are derived from the behavior of its $5f$ electrons. The existence of six allotropic phases suggest an extreme sensitivity to slight variations in electronic structure, such as the f -electron localized to delocalized transition believed to be responsible for the large volume expansion ($\sim 25\%$) when Pu transforms from the α phase to the δ phase. To date, a complete description of the electronic structure of plutonium is still lacking; moreover, the strong electronic correlations that give rise to, among other things, a large Sommerfeld coefficient $\gamma \sim 55$ mJ/mol-K² and a temperature-independent magnetic susceptibility in the δ phase, cannot be adequately accounted for by theory.

By studying plutonium intermetallic compounds, we may gain unique insight into the nature of Pu itself. The strong electronic correlations in elemental Pu bear a strong resemblance to those found in the PuCoGa₅ superconductor [1]. In PuCoGa₅, the $5f$ electrons are neither fully localized nor fully itinerant [2]; elements of both kinds of behavior manifest themselves in such properties as an effective moment $\mu_{\text{eff}} = 0.7 \mu_{\text{B}}$, close to that expected for Pu³⁺ (0.84 μ_{B}) and an enhanced electronic specific heat coefficient $\gamma \sim 100$ mJ/mol-K² consistent with moderately heavy fermion behavior [1]. Recent nuclear magnetic resonance measurements [3] provide strong evidence for unconventional d -wave superconductivity in PuCoGa₅ and for a spin fluctuation energy scale that may not be too different from that of δ -Pu. In addition, a systematic investigation of ACoGa₅ (A = U, Np, Pu, Am) reveals $5f$ electron behavior quite similar to the elemental actinides where Pu is poised at the itinerant/localized boundary. In this talk, I will compare the physical properties of PuCoGa₅ and elemental Pu and discuss the implications of such a comparison.

[1] J. L. Sarrao et al., Nature **420**, 297 (2002).

[2] J. J. Joyce et al., Phys. Rev. Lett. **91**, 176401 (2003).

[3] N. J. Curro et al., Nature **434**, 622 (2005).

Local Structure, Superconductivity and Radiation Damage in PuCoGa₅ and Related Materials

C. H. Booth*, M. Daniel*, R. E. Wilson*, P. G. Allen†, E. D. Bauer††, L. Morales††, J. L. Sarrao††

*Lawrence Berkeley National Laboratory, Berkeley, California 94708 USA

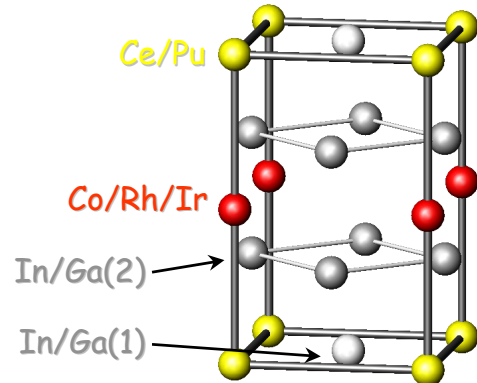
†Lawrence Livermore National Laboratory, Livermore, California 94551 USA

††Los Alamos National Laboratory, Los Alamos, New Mexico 87501 USA

In the pure form, the cerium and plutonium based 115 superconductors, such as CeCoIn₅ and PuCoGa₅, exhibit many interesting properties, not the least of which are their extraordinarily high superconducting transition temperatures (T_c 's). The structure of these materials is consistent with a superconducting, two dimensional (2D) Ce-In or Pu-In layer, flanked by non-superconducting layers (see figure). Such an enhancement of T_c in a 2D system furthers the comparisons to the high- T_c copper oxide materials that already bear many significant similarities to rare-earth intermetallics, including relations to magnetic fields and non-Fermi liquid behavior. It is therefore not surprising that there might be a similar dependence on local-structure properties.

We will present x-ray absorption fine-structure (XAFS) data on a variety of 115 materials. We find that the local structure in CeRh_{1-x}Ir_xIn₅ is remarkably insensitive to the exact stoichiometry on the transition-metal site,ⁱ consistent with the slowly varying electronic and magnetic properties ($T_c \rightarrow 0$ K only after ~75% Rh, and even CeRhIn₅ is superconducting under applied pressure). On the other hand, substituting Sn for In has a very strong effect, with $T_c \rightarrow 0$ K at only 3.6 mol% Sn. We find that this sensitivity is much stronger than expected given the known superconducting coherence length. XAFS results, however, indicate that the Sn preferentially resides on the in-plane In(1) siteⁱⁱ, thus concentrating the defects into the superconducting layers and explaining the strong sensitivity to Sn doping. Observed changes in the Kondo temperature will also be discussed in light of these results.

The PuCoGa₅ superconductor is not only fascinating as an actinide counterpart to the Ce-based 115's, but also because of its relationship to δ -Pu and the role that the radioactivity of plutonium plays in the structural, electronic and magnetic properties. For instance, this material exhibits local-moment behavior, a property that some have suspected for δ -Pu for many years. We will present Pu L_{III} -edge data that are consistent with this interpretation. Also, these materials exhibit high critical-current densities, probably due to the generation of defects by the radioactive decay of plutonium in the lattice. Our local structure data show a surprisingly large sample volume affected by these decays, suggesting that in addition to the number of Frenkel defects and holes (some estimates are as large as ~3000 pairs per decay), a relatively large sphere exists around each defect that is essentially amorphized. Our ultimate hope is to correlate the observed XAFS amplitude reductions to measurements of such properties as the superconducting coherence length to gain a better understanding of the average distortions in this material, information that would be directly applicable to other plutonium alloys.



This work was supported by the Director, Office of Science, Office of Basic Energy Sciences (OBES), Chemical Sciences, Geosciences and Biosciences Division, U.S. Department of Energy (DOE) under Contract No. AC03-76SF00098.

ⁱ M. Daniel, S.-W. Han, C. H. Booth, A. L. Cornelius, P. G. Pagliuso, J. L. Sarrao and J. D. Thompson. [Phys. Rev. B, 71, 054417 \(2005\)](#).

ⁱⁱ M. Daniel, E. D. Bauer, S.-W. Han, C. H. Booth, A. L. Cornelius, P. G. Pagliuso, and J. L. Sarrao. [Phys. Rev. Lett. 95, 016406 \(2005\)](#).

XAS study of $U_{1-x}Pu_xO_2$ solid solutions

P. Martin¹, G. Carlot¹, M. Ripert¹, S. Grandjean², C. Valot¹, P. Blanc², C. Henning³

¹CEA Cadarache, DEN/DEC/SESC, bât. 151, 13108 St Paul Lez Durance cedex, France.

²CEA Marcoule, DEN/DRCP/SCPS, BP 171, 30270 Bagnols sur cèze cedex, France

³Institute of Radiochemistry, Forschungszentrum Rossendorf, P.O. Box 510119, 01314 Dresden, Germany.

The plutonium generated in nuclear power reactors can be re-used at least partially through the exploitation of a Mixed OXide (U,Pu)O₂ fuel. Industrially, the manufacture of the MOX fuel proceeds in UO₂ and PuO₂ powders co-crushing, pelletizing and sintering. With this method, a fluorite-type solid solution (U,Pu)O₂ is obtained. Currently, rather than a mechanical mixing of pulverulent compounds, a new technique of manufacture for specific needs is under development, based on a co-precipitation of uranium and plutonium (chemical mixture). A better homogeneity of the U and Pu repartition in the solid and at lower temperature is awaited by this 'wet route'. The homogeneity of the final products may represent a significant criterion for an optimized behaviour in power reactors.

The synthesis method was optimized in the CEA Atalante facility at Marcoule [1,2] in order to obtain (U,Pu)O₂ solid solutions with a minimal content of synthesis impurities and a O/M ratio equal to 2.0. This method is based on the oxalic co-precipitation of U(IV) and Pu(III) followed by the thermal conversion of the co-precipitate into oxide. Each sample is characterized with X-Ray Diffraction. But, in order to fully investigate the ideality of the solid solution a more local probe is needed. XAFS spectroscopy using synchrotron radiation is an extremely suitable technique to study local atomic and electronic structure of mixed oxides [3,4].

EXPERIMENTAL DETAILS AND RESULTS

A series of solid solutions of $U_{1-x}Pu_xO_2$ ($x=0.07, 0.15, 0.30$ and 0.50) were prepared in the ATALANTE Facility. Both UO₂ and PuO₂ reference compounds were synthesized following the same chemical procedure. All the samples were analysed by XRD. In each case, a face centered cubic structure was observed and the cell parameter deduced obeys the Vegard's law.

The XAFS measurements were performed on the ROBL beam line of the European Synchrotron Radiation Facility (Grenoble, France). For each sample, XAS spectra were recorded at both uranium and plutonium L_{III} edges. The evolutions of the Fourier Transform are summarized on the figures 1 and 2. The overall shape of the spectra is almost always the same while the global intensity varies a lot with the plutonium content. Thus, an important decrease of oscillations for the 30 and 15% Pu samples is observed. X-ray diffraction leads to the same result showing a greater disorder than for the PuO₂ and 50 % Pu samples.

At the uranium L_{III} edge, the best fit of the 50% Pu sample leads to the following distances: $R_{U-O}=2.352(5)$ Å, $R_{U-U}=R_{U-Pu}=3.845(5)$ Å and $R_{U-O}=4.51(1)$ Å. The oxygen neighbors are the same as in UO₂ and the U/(U+Pu) ratio is 0.51. The uranium local environment is clearly the one of an

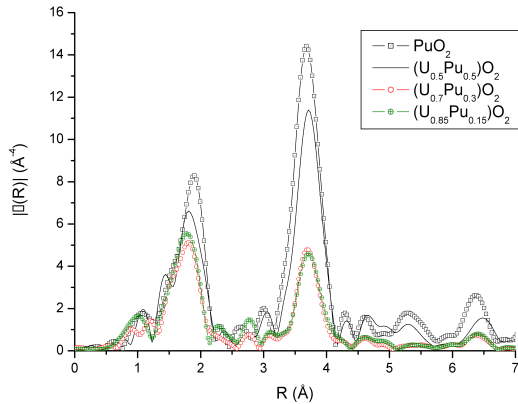


Fig 1: Fourier Transforms of the plutonium L_{III} edge EXAFS.

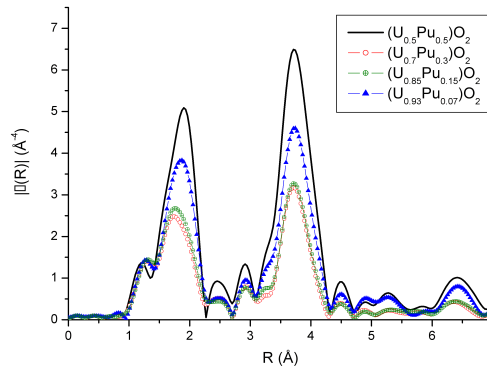


Fig 2: Fourier Transforms of the uranium L_{III} edge EXAFS.

ideal solid solution. The case of plutonium environment is a little more complicated. Indeed, the fitting of the first peak of the Fourier transform of the plutonium L_{III} edge spectra leads to values unsuitable with the fluorite structure. As seen on the figure 1, the shape of this peak (first coordination shell) is no longer gaussian. To fit it, we had to introduce an additional asymmetry term (third cumulant)[7]. Using this method, we finally obtain a shell of 8 oxygen neighbors at a distance of $2.351(5) \text{ \AA}$, which is consistent with the result obtained at the uranium edge. Considering the plutonium-metal shell, we also find an ideal solid solution structure with Pu-Pu and Pu-U distances equal to $3.845(5) \text{ \AA}$. The Pu/(U+Pu) ratio thus obtained is 47%. The results of the analysis at the two edges clearly show that the chemical procedure used to prepare the $(U_{0.5}Pu_{0.5})O_2$ sample is validated.

For the intermediate plutonium concentrations of 15 and 30%, the local environment of plutonium and uranium is highly perturbed as seen in figures 1 and 2. On the opposite to the 50% plutonium sample, a third cumulant has to be introduced in the fitting procedure even at the uranium edge. Even, if the distances obtained are in good agreement with the Vegard's Law, a doubling of the Debye-Waller ($\sigma_{U-O}^2(30\% \text{ Pu}) = 0.014 \text{ \AA}^2$ instead of $\sigma_{U-O}^2(50\% \text{ Pu}) = 0.0065 \text{ \AA}^2$) is observed. This is the signature of a higher disordered structure with a probable hyperstoichiometric composition.

Clearly, as the plutonium content is equal or below 30% at., a great distortion in the Pu local environment is observed. This disorder is incompatible with an ideal solid solution structure. It is interesting to note that EXAFS appears to be the lone technique outlining this discrepancy in plutonium and uranium local environment. Some steps of the process via the wet route checked in this study are currently modified considering their potential influence on the mechanisms of formation of ideal solid solutions, particularly with plutonium content lower than 50%.

- [1] S. Grandjean, B. Chapelet-Arab, S. Lemonnier, A-C Robisson, N. Vigier, "Actinides-Basic Science, Applications, and Technology" symposium, MRS Fall Meeting, 26 nov- 2 dec 2005 – Boston, 2005.
- [2] S. Grandjean et al, GLOBAL2005, proceeding No. 122, Oct 9-13 2005, Tsukuba, Japan, 2005.
- [3] J. Purans, et al, Physica Scripta, T115 (2005) 925-927.
- [4] Ph. Martin et al, J. of Nuc. Mat. 312(2003)103-110.
- [5] B. Ravel et al, J. Synchrotron Rad. (2005), 12:4, pp. 537-541.
- [6] J.J. Rehr et al, Rev. Mod. Phys. (2000) 72, 621-654.
- [7] E.A. Stern (1988), Chapter 9, edited by D. C. Koningsberger & R. Prins, New York, John Wiley.

Models and Simulations of Nuclear Fuel Materials Properties

M. Stan, J. C. Ramirez, P. Cristea, B. P. Uberuaga, S. Srivilliputhur, C. Deo, S. Y. Hu, S. P. Rudin, J. M. Wills.

Los Alamos National Laboratory, U. S. A.

INTRODUCTION

In a typical fuel element, cylindrical UO_2 fuel pellets are stacked in a steel cladding. The gap between the cladding and the fuel pellet is filled with helium. The fission reaction generates heat that is diffused mostly outwards in the radial direction. Due to the Soret effect, the gradients in temperature induce oxygen diffusion which in turn triggers the conventional Fickian diffusion. The counterbalancing effects of the Soret and Fickian fluxes are responsible for a variation of oxygen concentration through the fuel pellet even at steady state^{1,2}. Conversely, the temperature variation through the pellet is preserved because of the heat generation, which manifests itself as a source term in the heat equation.

To address the complexity of the phenomena that occur in a fuel element, a new multi-scale and multi-physics method was developed at LANL. The method incorporates theory-based atomistic and continuum models into finite element simulations to predict thermo-mechanical properties of alloys and ceramics. By relating micro and nano-scale models to the macroscopic equilibrium and non-equilibrium simulations, the predictive character of the method is improved. The multi-scale approach was applied to calculations of phase stability and defect concentration in PuO_{2-x} , simulations of heat and mass transport in UO_{2+x} , and simulations of irradiation effects in Fe.

MODELS

The concentration of oxygen atoms is often expressed in terms of the non-stoichiometry, x in UO_{2+x} , which is strongly related to the type and concentration of point defects. Following the pattern of a recently published model³ of PuO_{2-x} , we included in the present model four types of point defects that are considered major contributors to the lattice disorder of UO_{2+x} : U^{5+} uranium ions, Frenkel pairs, oxygen interstitials, and oxygen vacancies. The cation (U) sublattice was treated as ideal, in the sense that the concentrations of uranium vacancies and uranium interstitials were both ignored. At this stage, the Coulomb interaction between the charged species and the spatial correlations due to the exclusion effects was not included. The defect species equilibrium have been described using the general mass action equations, supplemented by charge conservation and lattice geometry constraints. This model was tested against experimental data using a Mathcad code. Given the enthalpies and the entropies of reaction between various types of defects the program predicted the concentration of various point defects and the stoichiometry as functions of temperature and oxygen partial pressure.

SIMULATIONS

We first examined the case fully radial heat conduction and oxygen diffusion, at steady state. The temperature distribution was calculated in the fuel, gap and cladding while the non-stoichiometry was only calculated in the fuel. We use typical dimensions of $R_{rod} = 4.3 \cdot 10^{-3}$ m and $R_{clad} = 4.833 \cdot 10^{-3}$ m, and a gap of 0.03 mm. For the temperature in the outer face of the steel cladding, we set Dirichlet boundary conditions by fixing the temperature at 750 K, which represents a typical operating temperature. Similarly, for the outer edge of the fuel rod, we set the non-stoichiometry to 0.001. For the heat generation rate due to the fission reaction, we used a typical ⁴ value $Q = 4.304 \cdot 10^8$ W/m³.

The temperature and non-stoichiometry distributions along the radial direction of a fuel rod were calculated. The heat generation due to the fission reaction caused the temperature within the rod to be the highest at the center. Since heat is extracted from the outer surface of the cladding, the temperature decreased with increasing radius, as expected. The oxygen atoms re-distributed such that hyperstoichiometry was higher in the hotter regions.

REFERENCES:

1. S. R. De Groot, *Thermodynamics of Irreversible Processes*, North Holland Publ. Co., Amsterdam, 1951.
2. C. Sari and G. Schumacher, *J. Nucl. Mater.*, **61** (1976) 192-202.
3. M. Stan and P. Cristea, *J. Nucl. Mater.*, **344** (2005) 213–218.
4. M. Kazimi, *et al.* “Fission Gas Release Models of Heterogeneous Fuels for Plutonium Burning”, presentation at the MIT Center for Advanced Nuclear Energy Systems.

Abstract of Presentation at International Conference
“Plutonium Future – Science 2006”
(Pacific Grove, California, the USA, July 9-13, 2006)

Development of Fuel Material with Porous Zirconium Carbide Inert Diluent for Plutonium and Minor Actinides Recycling in Fast Reactors

V.K. Orlov, E.M. Glagovsky, G.M. Blukher, A.P. Ivanov, I.A. Shlepov

A.A. Bochvar VNIINM, Moscow, Russia

An effective technique of atomic power nuclear waste treatment resulting in the waste radiotoxicity decrease is the reactor reprocessing technique that ensures the possibility to develop a closed fuel cycle. The technique is based on recycling of plutonium and minor actinides (MA) – neptunium, americium and curium extracted from spent nuclear fuel as a new fuel for fast reactors. This technique is more attractive because it allows generating an additional energy from the produced and stored plutonium and MA. The fuel with an inert diluent without uranium is of a great interest for most effective recycling of MA and plutonium [1,2].

As an option of such fuel, the authors proposed and investigate the composite material, patented at VNIINM, on the basis of zirconium carbide porous skeleton with introduction of plutonium dioxide and minor actinides oxides in the skeleton pores [3]. The skeleton type inert diluent on the basis of porous zirconium carbide has a complex of unique properties – thermalphysic, physical-mechanical, thermodynamic, radiation, high melting temperature ~ 3500 °C, thermal conductivity rising with operating temperature rise, and also chemical, thermodynamic and radiation stability. The positive characteristics of such type of fuel are a comparative simplicity of the fabrication process and its universality. Reactors with this type of fuel should have the negative sodium void reactivity effect (SVRE) that allows introducing a significant amount of MA (up to 30-40 %) in such fuel.

On the basis of calculation, the requirements are identified for characteristics of the fuel composition having the zirconium carbide porous skeleton matrix to use it in the operating fast reactor BN-600. The calculations show that it is possible to transmute 60 kg of Np-237 per year in

the reactor BN-600. Adding Pu-238 generated during transmutation of Np-237 to plutonium fuel in the active core allows making the plutonium unsuitable for weapon purposes, at that, about 200 kg of plutonium per year is burnt up. Subject to these requirements the flowsheet is developed for fabricating the fuel cores with the zirconium carbide porous matrix.

Under the developed flowsheet the cores pilot batches of compositions ZrC-simulator MA (CeO₂), ZrC-PuO₂ are fabricated. The cylindrical cores had the diameter of 5.9 mm, the length of 40–70 mm, the compression strength of 11–14 MPa.

The skeleton material had an open porosity of 60–70%. The skeleton material phase composition identified by X-ray diffractometry method (FCC with the period $a = 4.691 - 4.700 \text{ \AA}$) was consistent with the zirconium carbide stoichiometric composition.

The fissile component content in the core material changed subject to impregnation mode. The cores are fabricated with the fissile component content (CeO₂, PuO₂) over the range from 3.9 up to 38.0%.

The further investigation paths are outlined, which proximate purpose is to fabricate an enlarged batch of fuel cores having the specified composite fuel for testing in the research reactor with subsequent investigations of the irradiated material.

References

1. Bibilashvily J.K., Glagovsky E.M., Bayburin G.G., Shleпов I.A., Blukher G.M., Ivanov A.P., Khandorin G.P. "Development and study of properties of fuel materials having the skeleton type inert diluent (without ²³⁸U) for recycling of RG and WG plutonium and minor actinides in fast reactors with an advanced active core". VNIINM selected works, vol. 1. - 2002. - p.186-188.
2. C. Degueldre. "Inert matrix fuel has the potential to produce electricity while burning up more plutonium." Actinide Research Quarterly. Nuclear Materials Technology/Los Alamos National Laboratory, 1st/2nd quarter 2003, p. p. 23-30.
3. Glagovsky E.M., Bayburin G.G., Blukher G.M. The RF Patent No.2231141. "A composite fuel material and its fabrication technique". Pubd. June 20, 2004.

Ion beam irradiation of actinide-doped pyrochlores

J. Lian^{*}, R. C. Ewing^{*}, L. M. Wang^{*}, S. V. Yudintsev[†], S. V. Stefanovsky[‡]

^{*} University of Michigan, Ann Arbor, MI 48109, USA

[†] Institute of Geology of Ore Deposits RAS, Moscow 109017, Russia

[‡] SIA Radon, Moscow 119121, Russia

Email: rodewing@umich.edu

The safe disposition of fissile Pu from dismantled nuclear weapons and the “minor” actinides (Np, Am, Cm) generated by the nuclear fuel cycle remains a major challenge for the development of next generation nuclear reactors. Recently, there has been extensive interest in using materials with fluorite and fluorite-related structures, such as isometric pyrochlores, as potential host phases for the immobilization of actinides, particularly Pu [1]. Systematic ion irradiation studies of stoichiometric lanthanide pyrochlores ($\text{Ln}_2\text{B}_2\text{O}_7$) (B = Ti, Zr, and Sn) have indicated that the radiation response of the pyrochlore compounds is highly dependent on compositional changes. Both the ionic size and cation electronic configurations (e.g., bond-types) affect the structural distortion from the ideal fluorite structure and thus the response of pyrochlore-structure types to ion beam irradiation [1]. In this study, several actinide-doped pyrochlores were synthesized, including $(\text{Ca}_{0.62}\text{Gd}_{0.97}\text{U}_{0.23})(\text{Zr}_{0.84}\text{Ti}_{1.34})\text{O}_{6.90}$, $(\text{Ca}_{0.47}\text{Gd}_{0.95}\text{Th}_{0.40})(\text{Zr}_{1.29}\text{Ti}_{0.89})\text{O}_{7.05}$, $(\text{Ca}_{0.44}\text{GdTh}_{0.42})\text{Zr}_{2.13}\text{O}_{7.05}$, and $\text{Ca}_{0.91}\text{Th}_{0.84}\text{Zr}_{2.25}\text{O}_{7.09}$, and their response behaviors upon radiation damage were simulated by 1 MeV Kr^{2+} ion irradiation under in-situ TEM observation. The ion beam irradiations of Ce-doped pyrochlore ($\text{CaCeTi}_2\text{O}_7$) as well as the solid solution of $(\text{La}_{1-x}\text{Ce}_x)_2\text{Zr}_2\text{O}_7$ ($x = 0, 0.1, 0.2, 1$) were also performed, in which Ce was used as an analogue element for Pu because of their similarities in charge and size.

Figure 1 shows the critical amorphization fluences of actinide-doped pyrochlores irradiated by 1 MeV Kr^{2+} as a function of temperature. The critical amorphization temperatures of $\text{CaCeTi}_2\text{O}_7$, $(\text{Ca}_{0.62}\text{Gd}_{0.97}\text{U}_{0.23})(\text{Zr}_{0.84}\text{Ti}_{1.34})\text{O}_{6.90}$, and $(\text{Ca}_{0.47}\text{Gd}_{0.95}\text{Th}_{0.40})(\text{Zr}_{1.29}\text{Ti}_{0.89})\text{O}_{7.05}$ are ~1060, 820 and 550 K, respectively. No ion irradiation-induced amorphization has been observed in $(\text{Ca}_{0.44}\text{GdTh}_{0.42})\text{Zr}_{2.13}\text{O}_{7.05}$ and $\text{Ca}_{0.91}\text{Th}_{0.84}\text{Zr}_{2.25}\text{O}_{7.09}$, subjected to 1 MeV Kr^{2+} at room temperature. The greater radiation “resistance” of actinide-doped pyrochlores, as compared with that of Ce-doped composition, is consistent with the larger average ionic radius at the B-site with increasing concentrations of Zr. In the solid solution binary of $(\text{La}_{1-x}\text{Ce}_x)_2\text{Zr}_2\text{O}_7$ ($x = 0, 0.1, 0.2, 1$), $\text{La}_2\text{Zr}_2\text{O}_7$ can be amorphized by a 1.0 MeV Kr^{2+} ion irradiation at 25 and 293 K at doses of ~1.19 and ~3.55 dpa, respectively, similar to that observed under 1.5 MeV Xe^+ irradiation [2]. With the addition of Ce in lanthanum-zirconate pyrochlore structure ($x = 0.1$), no ion irradiation-induced amorphization has been observed at room temperature. The critical amorphization dose for $(\text{La}_{0.9}\text{Ce}_{0.1})_2\text{Zr}_2\text{O}_7$ at 25 K is ~3.55 dpa, and with increasing Ce-content, a higher dose (~5.20 dpa) is required to fully amorphize $(\text{La}_{0.8}\text{Ce}_{0.2})_2\text{Zr}_2\text{O}_7$ at 25 K. No amorphization occurred for $\text{Ce}_2\text{Zr}_2\text{O}_7$ at 25 K at a dose of ~7 dpa. The addition of Ce into the $\text{La}_2\text{Zr}_2\text{O}_7$ structure increases the radiation stability of materials (Figure 2), which may be attributed to the decreasing average radius of cations in the A-site, resulting from the smaller ionic radii of Ce^{3+} (0.114 nm) and Ce^{4+} (0.097 nm) as compared to La^{3+} (0.116 nm). These results suggest that complex pyrochlore

compositions, caused by the incorporation of actinides and lanthanides, may exhibit dramatic differences in their response to a radiation environment. The addition of actinides may enhance the radiation stability of these materials. Data such as these allow one to design a specific pyrochlore composition with a desirable radiation stability and chemical durability as a potential waste form for the immobilization of actinides, particularly Pu.

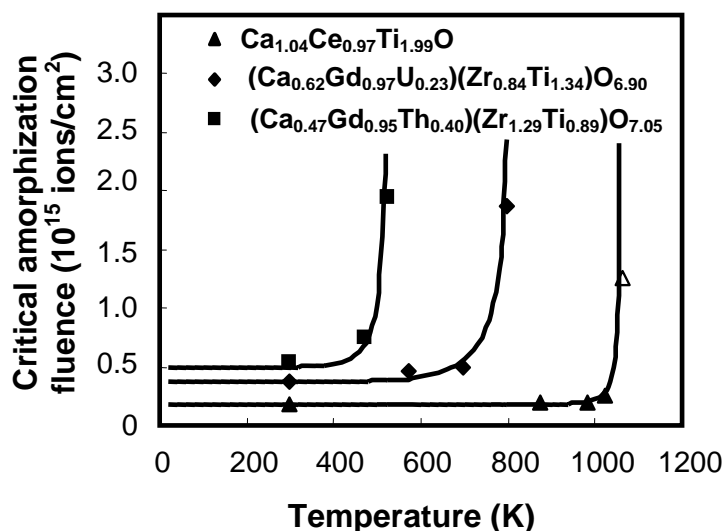


Figure 1. Critical amorphization fluences of actinide-doped pyrochlore vs. irradiation temperature.

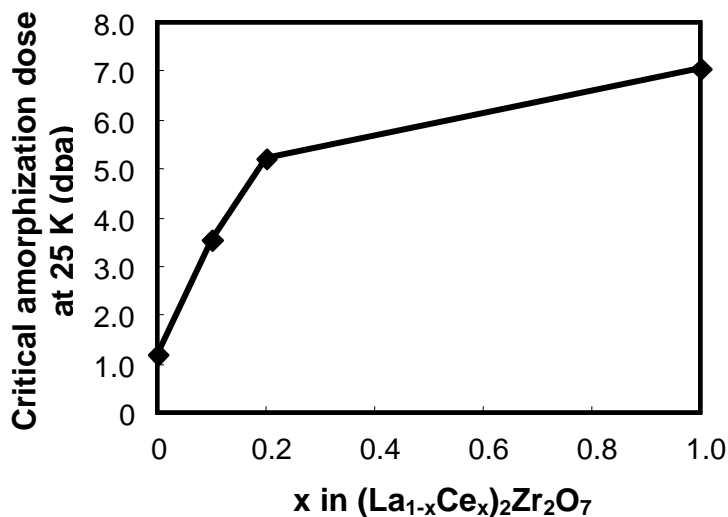


Figure 2. The addition of Ce in the solid solution of $(La_{1-x}Ce_x)_2Zr_2O_7$ enhances the radiation stability.

This work was supported by the Office of Basic Energy Sciences, USDOE under DOE grant DE-FG02-97ER45656.

1. R. C. Ewing, W. J. Weber, and Jie Lian, *Journal of Applied Physics* 95 (2004) 5949-5971.
2. J. Lian, X. T. Zu, K. V. G. Kutty, J. Chen, L. M. Wang, and R. C. Ewing, *Phys. Rev. B* 66 (2002) 054108.

High Temperature Reactivity of Mixed Uranium and Plutonium Carbide Fuels with Silicon Carbide as an Inert Matrix. Efficiency of Refractory Metals as Interdiffusion Barriers.

J. L chelle¹, E. Belval-Haltier¹, R. Belin¹

¹CEA, CEN Cadarache, DEN/Cad/DEC/SPUA/LMPC, B t 717, 13108 Saint-Paul Lez Durance

High Temperature Gas Cooled Fast Reactors for the fourth generation of reactor studies have lead to chemical compatibility studies between the foreseen fuel and matrix materials, in normal operation, incidental and accidental conditions. Reactivity experiments were first carried out for temperature incidental conditions.

A first experiment was carried out at 1650 C - 100h for a sample which consisted of a mixture of mixed uranium and plutonium carbide (14 mole %) and beta-SiC (86 mole %) powders. The temperature was representative of accidental conditions. The aim was to determine whether new liquid phases or new solid phases may appear thus disturbing the reactor core behaviour and in the case it occurs to find a way to dodge this problem by adding a thin barrier material.

The mixed uranium and plutonium carbide comes out of a fabrication made by TUI dedicated to NIMPHE2 irradiation ("NIture Mixte PHenix"). As shown by XRD powder patterns, it is made of a mixture of three monocarbide phases the lattice parameter of which is 4.979, 5.000 and 5.017   as well as a sesqui-carbide phase (8.117  ). Chemical composition of C, N and O elements can be interpreted by a partial oxidation of an initial mixture of (U,Pu)C to give these three Fm3m phases and (U,Pu)₂C₃. Under the assumption of a Vegard's law the mixture would consist of 86 w% of U_{0.78}Pu_{0.22}C_{0.9}O_{0.1} and 14 w% of (U_{0.65}Pu_{0.35})₂C₃.

The cubic polymorphic phase (3C) of silicon carbide was used for this study.

Although U-Si-C phase diagram is known, very limited thermodynamic data are available for the description of Pu-Si-C and U-Pu-Si-C phase diagrams hence limiting potential valuable computations on the expected reaction products.

XRD diffraction pattern of the mixture after the experiment shows U_{0.8}Pu_{0.2}C as main phase, beta-SiC at a lower amount, a significant amount of M₂₀Si₁₆C₃ where M could be either U or Pu, a less abundant Pu₂C₃ and tetragonal PuC₂ phases, trace amounts of hexagonal beta-PuSi₂. Guinet indicates that U₂₀Si₁₆C₃ shows a peritectic decomposition at 1600 C. Thus M₂₀Si₁₆C₃ may have appeared while cooling down the temperature. This compound shows a slight deviation of its c lattice parameter value (8.012 0.002  ) from U₂₀Si₁₆C₃ value. This high reactivity deters from using these two materials in direct contact one with the other in reactor at this temperature. Studies at a lower temperature (1400 C) are under way .

Mo, Mo-Re, W and W_{0.95}Re_{0.05} have been considered as refractory metal diffusion barriers between (U,Pu)C and SiC.

Under neutron flux W transmutes into Re and might induce a phase change of W-Re in the reactor. Ekman, Persson and Grimwall [1] have shown that under a Re mole fraction equal to

0.3, the CC phase remains stable. Re cluster spreading (after W transmutation) and cluster diffusion should maintain Re concentration under this threshold value. Phase instability is thus unlikely in the case where $\text{Re}/(\text{W}+\text{Re})=5\%$.

A sandwich material was made of a layer of Mo, a layer of NIMPHE2 mixed carbides and a layer of $\text{W}_{0.95}\text{Re}_{0.05}$. It underwent a thermal treatment at 1800°C during 6h in a HF oven. This high temperature was chosen in order to enlarge the thickness of the reactivity product layer and facilitate its observation. It was then observed by optical microscopy (Figure 1) and some material was sampled at the interfaces (Mo side of Mo/(U,Pu)C interface, (U,Pu)C side of Mo/(U,Pu)C interface, (U,Pu)C side of (U,Pu)C/W-Re interface and W-Re side of (U,Pu)C/W-Re interface) for an XRD characterization. Only two interface XRD results are yet available: the Mo side of the first interface shows evidence of Mo_2C and UMoC_2 phases while the W-Re side of the interface shows evidence of $\text{U}_2\text{W}_4\text{C}_4$ and W_2C phases.

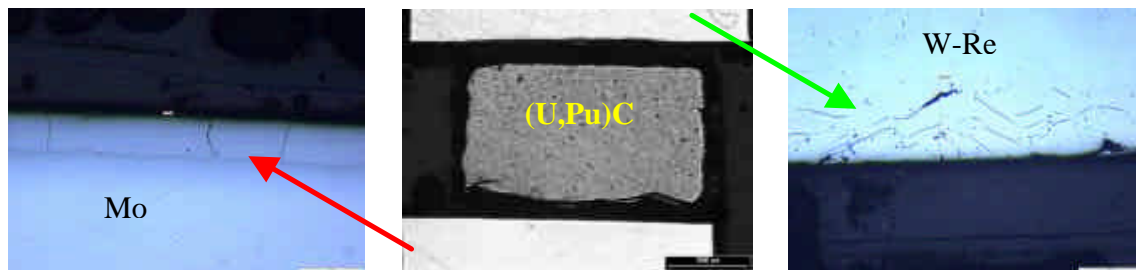


Fig. 1: optical microscopic observations of Mo/(U,Pu)C/W-Re sandwich after thermal treatment.

Mo and W-Re high temperature reactivity with SiC experiments were carried out at 1600°C for 100 hours. $60\mu\text{m}$ long Si rich fingers were observed by means of a SEM. Local W/Si ratios were measured confirming the possibility of occurrence of W_5Si_3 phase. This is in agreement with studies, reported by several authors [2, 3], which make evidence, between 1700 and 1900°C , of the succession of phases: $\text{SiC}/\text{WSi}_2/\text{WC}/\text{W}_5\text{Si}_3/\text{W}_2\text{C}/\text{W}$.

At 1600°C , even after 6 hours, a $60\mu\text{m}$ thick reactivity layer can be observed in Mo in contact with SiC. SEM local analysis of Mo and Si coupled with the measurement of their total weight percent give results compatible with Mo_5Si_3 and Mo_2C phases. These phases were observed with XRD experiments by other authors in the same conditions.

As a conclusion, at 1600°C NIMPHE2 carbide reacts with SiC. A Mo or W-Re diffusion barrier would have the drawback of consuming a part of the (U,Pu)C carbide carbon. To avoid this problem W-Re would have to be coated with Re on one of its sides in order to limit its reactivity with (U,Pu)C. The other side of W-Re would need to be protected by another material in order to limit its reactivity with SiC.

[1] Ekman, Persson and Grimwall, J. Nuc. Mat. 278 (2000) 273-276

[2] S.J. Son, T. Hinoki, A. Kohyama, in proceedings of ICAPP'05, Seoul, Korea, 15-19 May 2005, paper 5506, Interfacial properties and phase behaviour of W coated on SiC and SiC/SiC composites for advanced Nuclear Energy Systems

[3] B.V. Cockeram, BETTIS Atomic Power Laboratory, US DOE contract #DE-AC11-98PN38206, B-T-3255, November 1999, The diffusion bonding of Silicon carbide and boron carbide using refractory metals

Weapons-Grade MOX Fuel Burnup Characteristics in Advanced Test Reactor Irradiation

Gray S. Chang

Idaho National Laboratory
P. O. Box 1625
Idaho Falls, ID 83415-3885
e-mail: gray.chang@inl.gov

ABSTRACT

Mixed oxide (MOX) test capsules prepared with weapons-derived plutonium have been irradiated to a burnup of 50 GWd/t. The MOX fuel was fabricated at Los Alamos National Laboratory by a master-mix process and has been irradiated in the Advanced Test Reactor (ATR) at the Idaho National Laboratory (INL). Previous withdrawals of the same fuel have occurred at 9, 21, 30, 40, and 50 GWd/t^{1, 2, 3, 4}. Oak Ridge National Laboratory (ORNL) manages this test series for the Department of Energy's Fissile Materials Disposition Program (FMDDP).

A UNIX BASH (Bourne Again SHell) script CMO has been written and validated at the Idaho National Laboratory (INL) to couple the Monte Carlo transport code MCNP⁵ with the depletion and buildup code ORIGEN-2⁶ (CMO). The new Monte Carlo burnup analysis methodology in this paper consists of MCNP coupling through CMO with ORIGEN-2, and is therefore called the MCWO^{7, 8}. MCWO is a fully automated tool that links the Monte Carlo transport code MCNP with the radioactive decay and burnup code ORIGEN-2.

The fuel burnup analyses presented in this study were performed using MCWO. MCWO analysis yields time-dependent and neutron-spectrum-dependent minor actinide and Pu concentrations for the ATR small I-irradiation test position. The purpose of this report is to validate both the Weapons-Grade Mixed Oxide (WG-MOX) test assembly model and the new fuel burnup analysis methodology by comparing the computed results against the neutron monitor measurements and the irradiated WG-MOX post irradiation examination (PIE) data.

References:

1. R. N. Morris, C. A. Baldwin, B. S. Cowell, S. A. Hodge, et. al. "MOX Average Power Early PIE: 8 GWd/MT Final Report," Oak Ridge National Laboratory, ORNL/MD/LTR-172, November 1999.
2. R.N. Morris, C. A. Baldwin, S. A. Hodge, L. J. Ott, C. M. Malone, N. H. Packan, "MOX Average Power Intermediate PIE: 21 GWd/MT Final Report," Oak Ridge National Laboratory, ORNL/MD/LTR-199, December 2000.
3. R.N. Morris, C. A. Baldwin, S. A. Hodge, N. H. PACKAN, "MOX Average Power 30 GWd/MT PIE: Final Report," Oak Ridge National Laboratory, ORNL/MD/LTR-212, November 2001.
4. R. N. Morris, C. A. Baldwin, S. A. Hodge, N. H. Packan, "MOX Average Power 40 GWd/MT PIE: Final Report," Oak Ridge National Laboratory, ORNL/MD/LTR-241, Volume 1, August 2003.
5. J. Briesmeister (Editor), 'MCNP—A General Monte Carlo N-Particle Transport Code, Version 4C,' LA-13709-M, Los Alamos National Laboratory (2000).
6. A. G. Croff, "ORIGEN2: A Versatile Computer Code for Calculating the Nuclide Compositions and Characteristics of Nuclear Materials," Nuclear Technology, Vol. 62, pp. 335-352, 1983.
7. G. S. Chang and J. M. Ryskamp, "Depletion Analysis of Mixed Oxide Fuel Pins in Light Water Reactors and the Advanced Test Reactor," Nucl. Technol., Vol. 129, No. 3, p. 326-337 (2000).
8. G. S. Chang, " V&V of A MONTE CARLO BURNUP ANALYSIS METHOD - MCWO," Idaho National Engineering and Environmental Laboratory (INEEL) external release report, to be published in May, 2005.

Inductive Cold Crucible Melting of Actinide-Doped Murataite-Based Ceramics

Stefanovsky*, S.V., Ptashkin*, A.G., Knyazev*, O.A., Dmitriev*, S.A.

Yudintsev⁺, S.V., Nikonov⁺, B.S.

*SIA Radon, 7th Rostovskii lane 2/14, Moscow 119121 RUSSIA

⁺Institute of Geology of Ore Deposits RAS, Staromonetny lane 35, Moscow 119017 RUSSIA

Introduction

An inductive cold crucible melting (ICCM) is an effective method for growing of single crystals for various technical and jewelry purposes and production of glassy and ceramic materials.¹ The ICCM is currently developed as an alternative to vitrification of high- (HLW)^{2,3} and intermediate-level wastes (ILW)⁴ in Joule-heated ceramic melters. The ICCM seems to be very effective method of HLW ceramization due to small dimensions, high-active hydrodynamic regime, and high temperature availability. This method was used to producing numerous ceramic waste forms (see, for example⁵⁻⁸).

Murataite-based ceramics are considered as perspective matrices for complex actinide/rare earth-bearing wastes⁹ due to high chemical durability¹⁰ and capability of the murataite structure to accommodating elements with widely variable ionic sizes and radii.^{9,11,12} Therefore, it is expedient to apply the ICCM to develop high-productive, compact, and remote operable process with high volume reduction yielding leach resistant waste form.

Results

Specified chemical compositions of the ceramic were as follows (wt.%): 5 Al₂O₃, 10 CaO, 55 TiO₂, 10 MnO, 5 Fe₂O₃, 5 ZrO₂, 10 AnO₂ (An = U, Th). The UO₂-doped ceramic (U-ICCM) was produced at the Radon bench-scale cold crucible (108 mm in inner diameter, stainless steel) unit energized from a 1.76 MHz/60 kW generator. The ThO₂-doped ceramic (Th-ICCM) was produced in a lab-scale unit with a 65 mm inner diameter copper cold crucible energized from a 5.28 MHz/10 kW generator.

At the U-ICCM ceramic production starting melt formation using a SiC rod took 22 min followed by batch feeding in portions for 15 min, homogenization for 5 min and pouring into container. Totally batch in amount of 5 kg was fed and product in amount of ~2.7 kg was poured into container (about 2.3 kg remained as “dead volume” in the crucible). Because 2.7 kg of ceramic was produced for 20 min, average productivity is 8.1 kg/h or specific productivity – 900 kg/(m² h).

The Th-ICCM ceramic was produced in the lab-scale crucible in amount of ~1 kg. Both the ceramics were composed of predominant target murataite-type phases and minor extra phases: rutile, crichtonite and glass (due to melt contamination with Si from the SiC rod) in the U-ICCM ceramic, and crichtonite and traces of thorianite, pyrochlore, and low-symmetry phase in the Th-ICCM ceramic (Figure 1, a,b).

In the U-ICCM ceramic the murataite is represented by three different polytypes with five- (5×), eight- (8×), and three-fold (3×) elementary fluorite unit cell (Figure 1, c-e) composing centre, intermediate part, and rim of the murataite grains, respectively (Figure 1, a,b). Their formulae calculated from the EDS data and suggestion on formation of the murataites structure from pyrochlore and murataite-3 modules¹² are as follows: Ca_{2.54}Mn_{1.54}U_{0.56}Zr_{0.88}Ti_{7.80}Fe_{0.81}Al_{0.87}O_{27-x} (5×), Ca_{4.33}Mn_{2.99}U_{0.86}Zr_{1.10}Ti_{13.51}Fe_{1.42}Al_{1.78}O_{47-x}

(8×), and $\text{Ca}_{1.37}\text{Mn}_{1.37}\text{U}_{0.16}\text{Zr}_{0.20}\text{Ti}_{5.45}\text{Fe}_{0.95}\text{Al}_{1.50}\text{O}_{20-x}$ (3×). Maximum UO_2 content (12.1%) was found to be in the core of grains (5× polytype). UO_2 content in the rim is much lower (5.2%). In the Th-ICCM ceramic the only 5× polytype ($\text{Ca}_{2.13}\text{Mn}_{1.90}\text{Zr}_{0.82}\text{Th}_{0.55}\text{Fe}_{0.78}\text{Ti}_{7.86}\text{Al}_{0.96}\text{O}_{27-x}$) has been found and Th distribution in the grains is uniform.

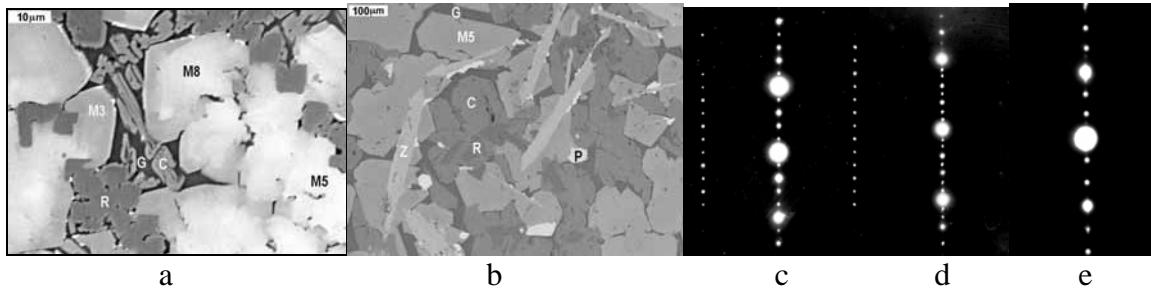


Figure 1. SEM-images of the ceramics U-ICCM (a), Th-ICCM (b) and SAED patterns from (100) plane of inverse lattice of the murataite polytypes 5× (c), 8× (d), and 3× (e).

Discussion

The ICCM is very high-productive process for actinide-waste forms fabrication. Application of a larger-scale (108 mm in diameter) cold crucible provides for low melt cooling rate in both crucible and filled container with sequential crystallization of various murataite polytypes. This yields dense ceramic with zoned structure of the grains with maximum actinide concentration in the core and minimum - in the rim thus reducing their leachability. Melt cooling rate in small cold crucible is higher and fast crystallization resulted in the only (5×) murataite polytype formation with uniform distribution of waste elements. Thus, application of large-scale cold crucibles is a perspective route to development of industrial-scale process and technology for ceramization of actinide-bearing HLW such as actinide or actinide/rare earth fraction of HLW and Am/Cm waste from conversion of excess weapons plutonium to MOX fuel.

References

- 1) Kuz'minov, Yu.S., Osiko, V.V., Fianites (Russ.), Nauka, Moscow, 2001.
- 2) Do Quang, R., Petitjean, V., Hollebecque, F., et al., Proc. Waste Management '03 Conf., Tucson, AZ, 2003. CD-ROM.
- 3) Kobelev, A.P. Stefanovsky, S.V. Knyazev, O.A. et al., The 107th Annual Meeting of The American Ceramic Society, Baltimore, MD, April 10-13, 2005. CD-ROM.
- 4) Sobolev, I.A., Dmitriev, S.A., Lifanov, F.A., et al., Glass Technol. 46 (1) 28-35 (2005).
- 5) Vlasov, V.I., Kedrovsky, O.L., Nikiforov, A.S., et al., Back End of the Nuclear Fuel Cycle: Strategies and Options, Vienna, IAEA, 109-117 (1987).
- 6) Sobolev, I.A., Stefanovsky, S.V., Ioudintsev, S.V., et al., Mat. Res. Soc. Symp. Proc. 465, 363-370 (1997).
- 7) Day, R.A., Ferenczy, J., Drabarek, E., et al., Proc. Waste Management '03 Conf., Tucson, AZ, 2003. CD-ROM.
- 8) Stefanovsky, S.V., Kirjanova, O.I., Yuditsev, S.V., Knyazev, O.A. Proc. Waste Management '01 Conf., Tucson, AZ, 2001. CD-ROM.
- 9) Stefanovsky, S.V., Yuditsev, S.V., Gieré, R., Lumpkin, G.R., in: Energy, Waste, and the Environment: a Geological Perspective, Gieré, R. and Stille, P. (eds) Geological Society, London, 236, 37-63 (2004).
- 10) Stefanovsky, S.V., Yuditsev, S.V., Perevalov, S.A., et al., Plutonium Futures – The Science – 2006. This volume.
- 11) Ercit, T.S., Hawthorne, F.C., Canad. Miner. 33, 1223-1229 (1995).
- 12) Urusov, V.S., Organova N.I., Karimova, O.V., et al., Trans. (Doklady) Russ. Acad. Sci./Earth Sci. Sec., 401, 319-325 (2005).

Phase Transformations in Pu-Al and Pu- Ga Alloys. Effects of Pressure and Temperature on the Kinetics of the Delta-Phase Decomposition

L.F. Timofeeva

A.A.Bochvar VNIINM (All-Russian Research Institute of Inorganic Materials), Moscow, Russia

EVOLUTION OF PHASE DIAGRAMS UNDER PRESSURE

The binary phase diagram at atmospheric pressure as a section of the pressure–temperature - composition PTC diagram results from a regular variation of phase areas with space. PT diagram for Pu and earlier experimental data ^{1,2,3} underlie schematic phase diagrams for the Pu-Al and Pu- Ga systems over the 0 ~3 GPa pressure range (see Figure 1). As Pu phases disappear with increasing pressure, the binary phase diagram varies from complex one at atmospheric pressure to rather simple at high pressures (see Figure 1). Features of PT binary Pu-Ga (Al) diagrams was analyzed at the pressure of triple points on PT phase diagram for Pu. Our notions on the phase diagrams evolution under pressure were used for experimental constructing of phase diagrams at different pressures.

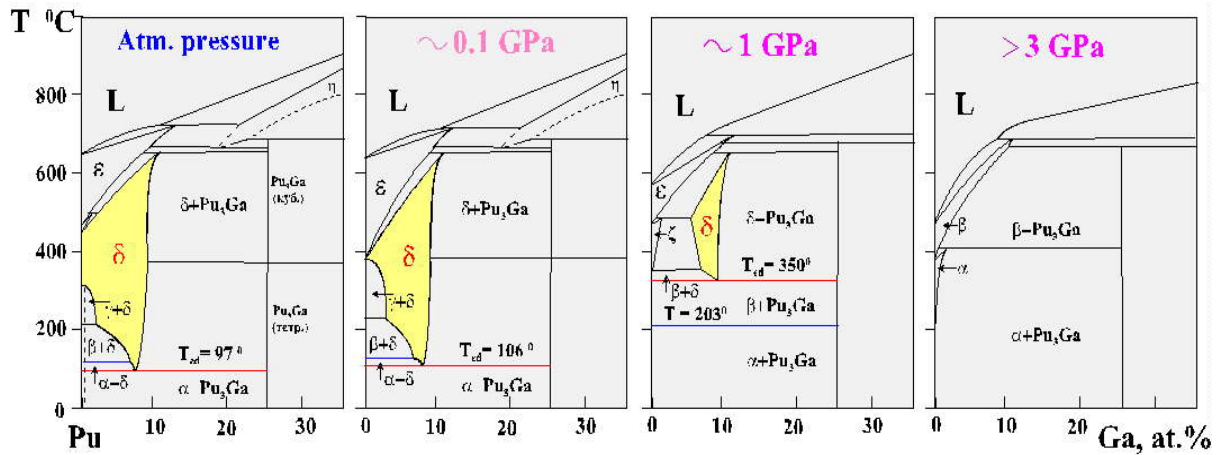


Fig1: Evolution of Pu-Ga Diagram under Pressure (scheme on a base of Experiment and Prognosis)

EXPERIMENTALLY AND THERMODYNAMICALLY DETERMINED δ-PHASE BOUNDARIES

Based on isothermal annealing results under static pressures as large as 0.6-0.8 GPa, δ-phase boundaries for the Pu-Al and Pu-Ga systems were delineated. The thermodynamic calculation of the displacement of the δ-phase boundaries to $P \cong 2-3$ GPa correlates well with the experiment. The δ-phase boundary shifts to higher concentrations of Al or Ga on the Pu-side and slightly to Pu on the intermetallic compound side. The δ-region decreases to the point of disappearance. The δ-phase eutectoid decomposition temperature at different pressures was evaluated from intersection of boundaries on the $N_{\text{МОЛБ}}^{\text{Al(Ga)}} - 1/T$ K coordinates. The eutectoid decomposition temperature (T_{ed}) versus pressure was plotted (see Figure 2). Parameters of the four-phase equilibrium ($\delta, \alpha, \beta, \text{Pu}_3\text{Ga}$) at point “H” on PT binary PuGa diagram were determined. Point “H” is a projection on the PT plane of the HH line. It is line of intersection of two three-phase equilibrium surfaces on the PTC phase diagram (see Figure 3). Above and below point H the δ-eutectoid decomposition results in $\beta\text{Pu} + \text{Pu}_3\text{Ga}$ and $\alpha\text{Pu} + \text{Pu}_3\text{Ga}$, respectively.

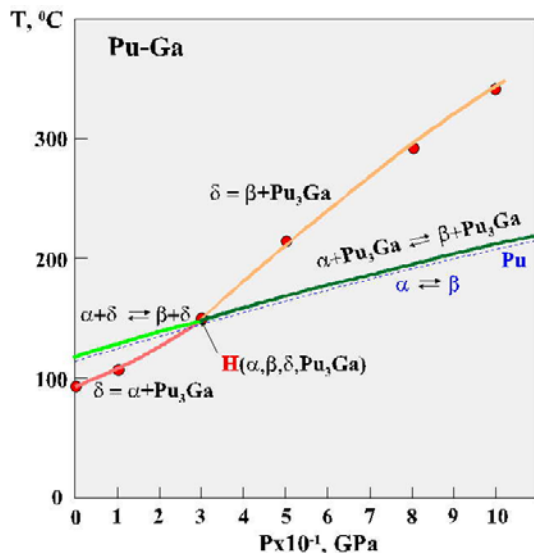


Fig 2: Effect of static pressure P on T_{ed} of PuGa alloys and $T_{\alpha \rightarrow \beta}$ Pu

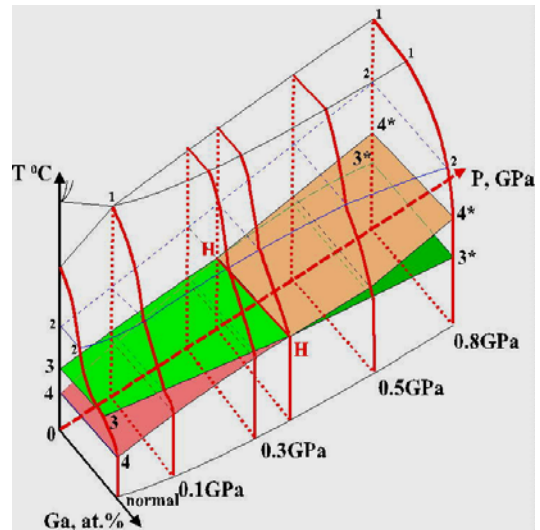


Fig 3: PTC diagram of PuGa- equilibrium
 $33HH-\alpha+\delta \leftrightarrow \beta+\delta$; $HH3*3*-\alpha+Pu_3Ga \leftrightarrow \beta+Pu_3Ga$;
 $44HH-\delta \leftrightarrow \alpha+Pu_3Ga$; $HH4*4*-\delta \leftrightarrow \beta+Pu_3Ga$

KINETICS OF δ -PHASE EUTECTOID DECOMPOSITION

As pressure and temperature increase, the rate of the δ -phase diffusion decomposition rises, the kinetics changes and the latent reaction period decreases from hundreds of hours to a few minutes as opposed to atmospheric pressure. The activation energy established for Pu-Al alloys by two methods, namely, the Avrami equation and the isothermal cross-section method, reduces from 30 kcal/mole at 0,1 GPa to 8 kcal/mole at 0,6 GPa. At a relatively low pressure, the both alloy systems show an eutectoid decomposition of different morphology: laminar for Pu-Ga (see Figure 4) and skeleton-like spheroidized for Pu-Al².

With due regard for decomposition acceleration and lower activation energy with increasing pressure, it can be suggested that the eutectoid decomposition can experience shock wave loading in a narrow pressure range.

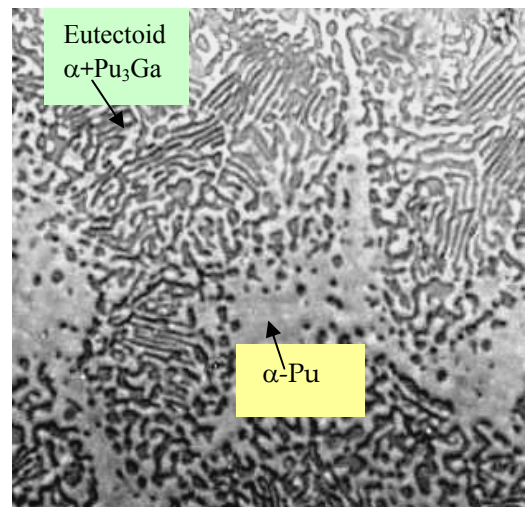


Fig 4: Microstructure of hypoeutectoid Pu-Ga alloy, $P \geq 1$ GPa

SUMMARY

Theoretical, experimental and thermodynamically calculated phase diagrams plotted for binary Pu-Al and Pu-Ga systems made it possible to clarify evolution of the phase regions under a pressure up to 2-3 GPa, to establish the temperature and pressure dependence of the eutectoid decomposition temperature. With increasing pressure, the δ -phase diffusion decomposition was shown to accelerate and the eutectoid decomposition to transform at relatively low pressures, resulting in an decrease in the activation energy.

- 1 N.T.Chebotarev, V.S.Kurilo, L.F.Timofeeva, M.A. Andrianov, V.V.Sipin .VANT(rus), seria: Materialovedenie. **37**, (1990).
- 2 L.F. Timofeeva, *in*: Ageing Studies and Lifetime Extension of Materials, ed. L. Mallinson, N-Y: Kluwer Academic /Plenum, (2001).
- 3 L.F. Timofeeva. Metallovedenie i termicheskaya obrabotka (rus). **11**, (2004).

Lattice Vibrations in α -Uranium: Non-Linearity and Localization

M. E. Manley,^{1,2} M. Yethiraj,³ H. Sinn,⁴ H. M. Volz,¹ A. Alatas,⁴ J. C. Lashley,¹ W. L. Hulst,¹ G. H. Lander,⁵ J. L. Smith¹

¹Los Alamos National Laboratory, Los Alamos, New Mexico 87545

²Department of Chemical Engineering and Materials Science, University of California, Davis, California 95616

³Oak Ridge National Laboratory, Oak Ridge, Tennessee 37831

⁴Argonne National Laboratory, Argonne, Illinois 60439

⁵European Commission, JRC, Institute for Transuranium Elements, Postfach 2340, D-76125 Karlsruhe, Germany

Non-linearity refers to a situation where small perturbations cause large shifts in the excitation spectrum. By this definition the phonons in α -uranium are quite non-linear, the phonon DOS can soften by as much as 10% when the temperature changes by as little as 100 K [1]. Although thermal softening is an expected consequence of anharmonicity, α -uranium is unusual in that it does not show behavior typically associated with a strongly anharmonic solid. First, the elastic energy of expansion can only account for about 10% of the observed softening [1]. Second, the power-spectrum derived energy exhibits linear scaling with temperature, behavior consistent with classical harmonic vibrations [1]. Finally, the features in the phonon DOS sharpen with increasing temperature, the opposite of what is expected from anharmonic lifetime broadening. Based on these observations it has been concluded that the phonon softening in uranium originates with intrinsic temperature dependence in the inter-atomic forces. By extension it has been argued that the softening originates with thermal-changes in the electronic structure [1].

The nature of the non-linearity in the lattice dynamics of α -uranium is clearly unconventional; the usual effects associated with phonon softening are not observed. There is, however, another way non-linearity might appear. Calculations have shown that non-linear dynamics can lead to the formation of spatially localized vibrations [2].

Recent measurements using both inelastic x-ray scattering (IXS) and inelastic neutron scattering (INS) have revealed that at least some of the phonon softening in α -uranium is associated with a new mode forming [3]. Figure 1 shows how the new 14.3 meV mode appears at high temperatures at a \mathbf{Q} -position on the $[01\zeta]$ zone boundary. Also appearing in Figure 1, a phonon branch that sits just below the new mode energy softens with its formation. A more detailed view of the dispersion curves (not shown here) indicates that other branches also soften, but mainly along the zone boundary [3], and also that intensity is lost in the $[00\zeta]$ longitudinal optic phonon branch [3].

Reference [3] provides detailed arguments supporting the hypothesis that the new mode shown in Figure 1 is an intrinsically localized vibration [2]. Briefly, the five main points are:

- (1) Extra modes form without a long-range crystal structure change, indicating that the required symmetry breaking must be local;

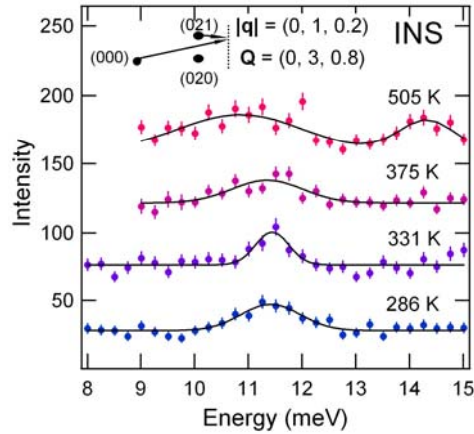


Figure 2: Data showing a new mode emerge near 14 meV at high temperature, together with the softening of the mode at about 11 meV. Data are offset for clarity. The scattering vector, \mathbf{Q} , is in the $\mathbf{b-c}$ plane. The phonon wave vector, \mathbf{q} , is at a zone boundary. Data was collected using the at the HFIR facility of Oak Ridge National Laboratory [2].

- (2) New modes appear confined to a zone boundary, implying that its spatial periodicity does not extend much beyond the lattice spacing;
- (3) Movements of defects involved in plastic deformation are impeded by the new modes while the long-range elastic moduli are not affected;
- (4) The mode forms in the presence of a strong non-linearity in the dynamical behavior;
- (5) An excess in the heat capacity is found to be consistent with the configurational entropy of having randomly distributed intrinsically localized modes on the lattice.

Interestingly many of the effects of the local mode resemble the effects of adding impurities; a reduction in mechanical ductility and the appearance of mixing entropy [2]. This is because, much like impurities, local modes are distinguishable within the crystal and they have associated strain fields. In other ways the new mode is like a vacancy, since they are thermally activated and occur randomly throughout the lattice.

Inelastic neutron and x-ray scattering measurements are revealing a surprising assortment of exotic dynamical phenomena in uranium, forcing us to rethink our basic understanding of phonon physics as well as a number of related problems including thermodynamic stability and mechanical deformation. It is likely that similar effects are also present in plutonium and other actinides and that future work will prove to be a rich area for advancing our basic understanding of condensed matter physics.

REFERENCES

- [1] M. E. Manley, B. Fultz, R. J. McQueeney, C. M. Brown, W. L. Hults, J. L. Smith, D. J. Thoma, R. Osborn, J. L. Robertson, *Phys. Rev. Lett.* **86**, 3076 (2001).
- [2] D. K. Campbell, S. Flach, Y. S. Kivshar, *Phys. Today* **57**, 43 (2004).
- [3] M. E. Manley, M. Yethiraj, H. Sinn, H. M. Volz, A. Alatas, J. C. Lashley, W. L. Hults, G. H. Lander, and J. L. Smith, *Phys. Rev. Lett.* in press.

Temperature and time-dependence of the elastic moduli of Pu and Pu-Ga alloys

Albert Migliori, D. Miller, D. Dooley, M. Ramos, R.J. Byars, J.B. Betts, I Mihut*

*Los Alamos National Laboratory, Los Alamos, New Mexico 87545

INTRODUCTION

We measured the elastic moduli of Pu and Pu-Ga alloys with three goals. They are 1) Provide accurate elastic moduli, 2) provide accurate temperature dependence, and 3) Measure the relative changes with time. We summarize here results for the time dependences with conclusions and results important to LANL and LLNL programs.

Fig. 1 shows an example of an RUS system for use with Pu and Pu-Ga alloys. A complete description of this system and a review of RUS are described by Migliori et al.[1] We have measured Pu, Pu-Ga alloys and an Accelerated-Aging Program (AAP) alloy at ambient and cryogenic temperatures. The AAP alloy “ages” at a rate 16.5 times that of normal ^{239}Pu and it was “made” on 15 May 2002. All measurements presented were performed on fine-grained polycrystal, accurately-polished RPR's of known composition. It is expected that some formation of mechanically-induced alpha-Pu has occurred in delta-Pu specimens, but because all samples are at least as large as a 2mm cube, minimal errors in absolute moduli are calculated from this effect.

TIME DEPENDENCE OF ELASTIC MODULI OF PU AND PU-GA ALLOYS

To understand the variation of the elastic moduli with time in Pu one must keep in mind several effects. These are: 1) Pu-Ga alloys are not thermodynamically stable at ambient temperature. 2) As ^{239}Pu decays radioactively, interstitial-dislocation pairs are produced, about 2200/decay. 3) Decay products include He and metals that are not Pu, and so can change physical properties. A few key referents include: 1) from radioactive decay, 3.16×10^{-9} of the Pu atoms present in a specimen decay per hour, 2) 6.9×10^{-6} Frenkel pairs/hour/atom are produced, 3) From measurements of 3.3 at. % Ga and the 3.9 at. % Ga samples, the maximum long term fractional rate of change of the bulk modulus is of order $9 \times 10^{-7}/\text{h}$, 4) The elastic moduli change at a rate much higher than that of e.g. the density or Frenkel pair retention rate. Thus from the raw Frenkel pair production rate, we can estimate that the elastic moduli change at a fractional rate of order $7 \times 10^{-5}/\text{h}$. These rates are limiting associated with radioactive decay and very low temperature. Any rate substantially different from these must be associated with other physical effects.

It is important to note that the effects seen are much smaller than the error bars for measurements presented above. This is because the precision of RUS for Pu specimens is of order 5 parts in 10^7 , but absolute accuracy is limited by errors in the measured size of specimens, of order several tenths of a percent.

Measurements were made using a very-high-precision temperature control system that held temperatures to within a few mK over many days. Good temperature control is crucial because of the strong temperature dependence of the elastic moduli of all samples.

In Fig. 2 we show the time dependence of the moduli of alpha Pu and Pu 2.36 at. % Ga. We can extract an important time scale from these measurements. Note that at 10K where Frenkel pairs are expected, from other studies, to be approximately fully retained, with less than a few tens of percent immediately annealing out, we find that delta Pu shear modulus *decreases* at a fractional

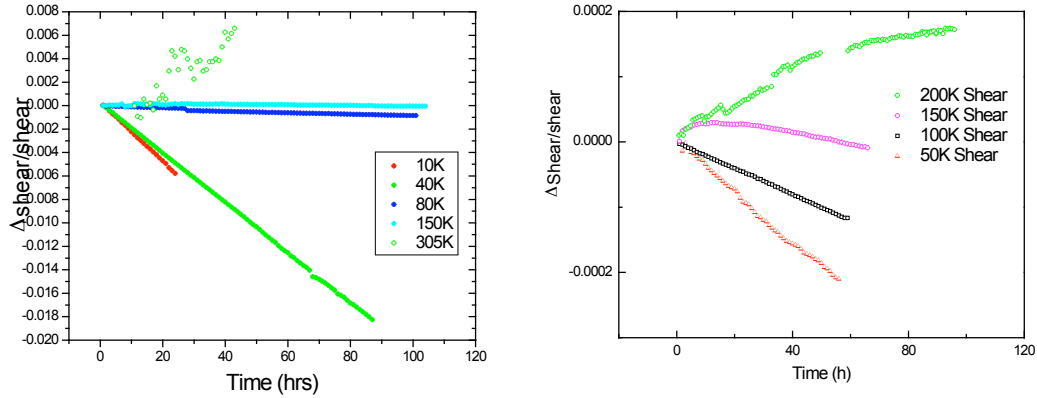


Figure 2. Left: The normalized shear modulus change for alpha Pu versus time and temperature. Right: The normalized shear modulus change for Pu 2.36 at. % Ga versus time and temperature.

rate of about $4 \times 10^{-5}/\text{h}$ and that the modulus of alpha Pu decreases at a higher rate, about $20 \times 10^{-5}/\text{h}$. The differences are not surprising in light of the differing responses of alpha and delta Pu to radiation damage. *We conclude unambiguously that radiation damage reduces the elastic moduli of Pu alloys.* Thus the time variation of these samples is strictly associated with Frenkel pair production, and *because both alpha and delta change approximately similarly, we can rule out any effects from thermodynamic reversion of the phases predicted by the Russian phase diagram.*

The time scales associated with thermal equilibration of Frenkel pairs can now be determined. Using a relaxation model, our measured difference in bulk modulus of normal and AAP Pu (about 52.3-51.3=2%), the difference in the rate of Frenkel pair production between AAP and normal Pu (a factor of 16) and, and the approximate measured rates of change near room temperature convoluted with the maximum estimated total change ($\tau B_0/B_{aging}=15$ years), we can self-consistently find the Frenkel pair main relaxation rate from

$$B = B_0 + B_{aging} e^{-\frac{t}{\tau}}$$

Where we find $B_{aging}=0.16\%$, and $\tau=8$ days. Thus in of order a month, the elastic moduli stabilize, and any further time dependences must be associated primarily with He and U production.

ACKNOWLEDGEMENTS

This work was supported by the State of Florida, the NNSA, and the LANL laboratory directed research and development program and Enhanced Surveillance.

The unique high-pressure behaviour of curium probed further using alloys

S. Heathman¹, R. G. Haire², T. LeBihan³, R. Ahuja⁴, S. Li⁵, W. Luo⁴ and B. Johansson^{4,6}

¹ European Commission, JRC, ITU, Postfach 2340, D-76125, Karlsruhe, Germany

² Oak Ridge National Laboratory, PO 2008, Oak Ridge, TN, USA 38831-6375

³ CEA-Centre de Valduc, F-21120 Is-sur-Tille, France

⁴ Dept. of Physics, Uppsala University, Box 530, S-751 21 Uppsala, Sweden

⁵ Dept. of Physics, Virginia Commonwealth University, Richland, VA 23284

⁶ Royal Institute of Technology, Brinellvägen 23, SE-10044 Stockholm, Sweden

INTRODUCTION

The role of the 5f electrons in the actinide series has been of prime interest for many years. The abrupt changes in volume and structural behaviour observed in going from plutonium to americium in the series are well documented and the subject of several reports. A few years ago the remarkable behaviour of americium under pressure¹ precipitated a strong interest in the behaviour of its 5f electrons and the structural changes observed. Very recently, both experimental and theoretical findings regarding curium under pressure were published; these findings demonstrated that curium's behaviour under pressure² was not a mirror image of that for americium. Rather, one of the five crystallographic phases observed with curium (versus four for americium) was a unique monoclinic structure whose existence was attributed to a special spin stabilization effect by curium's 5f⁷ electrons and its half-filled shell. These findings for curium have resulted in additional overall theoretical interest in these transplutonium metals, as their reduced atomic volumes affect the energies of the structures and the potential bonding that is present. In this presentation, we review briefly the behaviour of curium under pressure but also report on the behaviours of curium alloys under pressure relative to the behaviour observed with pure curium, and discuss the significance of the differences found.

RESULTS

Curium has a half-filled shell with seven 5f electrons spatially residing inside its radon core, and the element lies at the center of the actinide series. Compared to americium up to 100 GPa, curium exhibits one additional, unique structural form (identified as a Cm(III) phase, having a monoclinic symmetry) that occurs between 37 and 56 GPa. Ab initio electronic structure calculations agree with the observed experimental structural sequence², and these calculations also establish that it is the spin polarization and magnetism of curium's 5f electrons that are responsible for the formation and stabilization of this Cm (III) phase. With additional pressure, curium then adopts the Fddd and then the Pnma structures displayed by americium¹, as a result of acquiring additional participation of the 5f electrons in its bonding. The Pnma structures observed for americium and curium approaching 100 GPa are accepted as reflecting that full delocalization of their 5f electrons has occurred.

To enlighten further the influence of spin polarization for formation of the Cm (III) phase, as well as for the overall behaviour of curium, we consider here the pressure behaviours of curium alloys formed with its near neighbours, americium and berkelium: specifically, an $\text{Am}_{0.5}\text{Cm}_{0.5}$ alloy³ and two Cm,Bk alloys ($\text{Cm}_{0.7}\text{Bk}_{0.3}$ and $\text{Cm}_{0.46}\text{Bk}_{0.54}$). The experimental relative volume (V/V_0) behaviours of americium, curium and the two Cm,Bk alloys are shown in Figure 1. The behaviour of the $\text{Am}_{0.5}\text{Cm}_{0.5}$ alloy under pressure^{3,4} is similar to that for pure americium although the transitions are shifted to higher pressures. In all of these alloys under pressure, the unique Cm (III) phase is not observed.

The crystal structures of the three alloys containing curium under pressure were considered by first-principles, self-consistent total energy calculations based on the generalized full potential, linear muffin-tin orbital (FPLMTO) method together with the generalized gradient approximation by Perdew, Burke and Ernzerhof within density functional theory. The virtual crystal approximation and the spin-orbit coupling of the 5f-electrons are considered in the calculations for these alloys. Both antiferromagnetic and ferromagnetic calculations were performed for the different phases. The structural results found were in good agreement with experimental findings.

Acknowledgements

Support was from the European Commission, JRC, the Div. of Chem. Sciences, Geoscience and Bioscience, OBES, DOE with ORNL (DE-ACO5-00OR22725, UT-Battelle), the CEA and the Swedish Research Council & Swedish Foundation for Strategic Research.

References

1. S. Heathman et al, *Phys. Rev. Lett.*, **85** (2000) 2961.
2. S. Heathman et al, *Science*, **309** (July, 2005) 110.
3. T. Le Bihan et al, *J. Nuc. Science Technol.*, **Suppl. 3** (Nov. 2002) 45.
4. Sa Li et al, *Mat. Res. Soc. Symp. Proc.*, **893** (2006) 233.

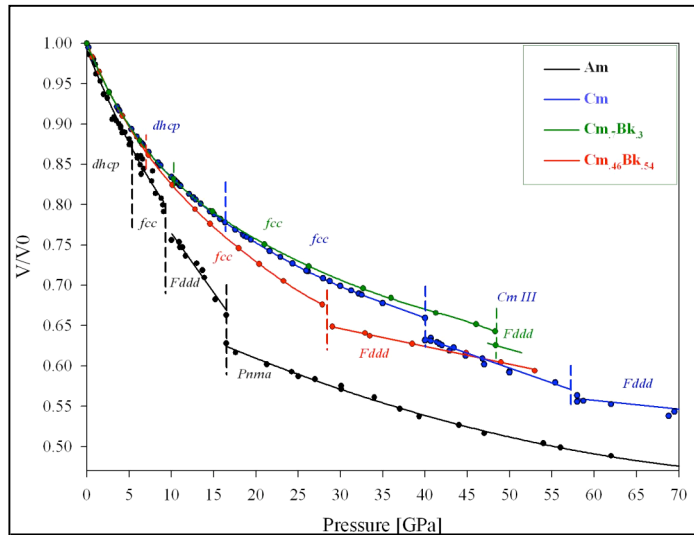


Fig. 1: The compression behaviours of Am, Cm and the two Cm,Bk alloys are displayed up to 70 GPa. (The Pnma structure for curium is observed above 90 GPa)

Correlations Magnetism and Structure Across the Actinide Series: a Dynamical Mean Field Theory (DMFT) Perspective.

K. Haule* G. Kotliar * S. Savarsov† and A. Toropova*

- * Serin Physics Laboratory Rutgers University Piscataway NJ 08854-8019 USA.
† Physics Department University of California Davis, CA 95616

In the early actinides the f electrons are well described by the itinerant model while in the late actinides they should be treated as localized.

Dynamical Mean Field Theory (DMFT), allows to treat localized and itinerant electrons within a unified approach, and properly describes the crossover between the two regimes.

We will present a comparative DMFT study of Pu³, Am², and Cm¹.

We will discuss the photoemission and inverse photoemission spectra of the different phases of these materials, and discuss the relation between structural properties electronic properties and magnetism in these materials.

Electron electron interactions are dominant for delta plutonium, while the phonon entropy has to be included for a proper description of the delta to epsilon transition. In all cases DMFT predicts a non magnetic ground state in agreement with experiments.

The theory predicts Cm to be magnetic, and predictions for the magnetic structure and the photoemission spectra of this material will be presented and compared with existing experimental data.

The Mott transition point, is located between Plutonium and Americium, and has very different character when approached from the Plutonium or the Americium side. Approaching the Mott point from the itinerant side, leads to an increase in the specific heat. The approach from the localized side is accompanied by mixed valence and superconductivity.

In plutonium, the f-valence is between f⁵ and f⁶, while in Am under pressure, it is between f⁶ and f⁷. Cm has a nearly pure f⁷ configuration.

We will conclude with a discussion of the implications of these results for alloys, and discuss the possible formation of local moments in these systems.

Acknowledgements: work supported by the Department of Energy.

- 2 S. Savrasov K. Haule and G. Kotliar PRL in press.
- 3 For a review see G. Kotliar et. al. Rev Mod Phys in press.

Plutonium and Quantum Criticality

G Chapline*, M. Fluss*

*Lawrence Livermore National Laboratory, Livermore CA 94552 USA

ABSTRACT

At its onset the Manhattan Project was bedeviled with a peculiar problem; the lattice structure and density of elemental Pu seemed to depend on how it was prepared. Perhaps even more remarkably, despite the great importance of this problem and the passage of more than 60 years, understanding why Pu occurs in these two allotropic forms has proved elusive. Adding to this enigma are many other puzzles such as why attempts to calculate the densities and binding energies of Pu from first principles seem to typically require that the Pu ions have local moments that are antiferromagnetically ordered, while there is considerable experimental evidence that there are no local magnetic moments in elemental Pu.

Fortunately a solution to these puzzles may be on the horizon. A hint that elemental Pu lies close to a quantum critical point (QCP) of some kind is that as a function of relatively modest changes in temperature and pressure there are a variety of complex phase transitions in Np, Pu, and Am that apparently involve changes in both the lattice structure and the electronic organization of the 5f electrons [1]. Consideration of atomic volumes suggests that it is δ phase of Pu that is nearest to the QCP point. Indeed, the negative thermal expansion of δ Pu for low impurity doping is by itself indicative of quantum critical behavior. A possible clue to the origin of the quantum critical behavior of Pu is provided by the pressure versus atomic volume curves for many rare earth materials that show a discontinuous decrease in volume at a critical pressure. In elemental Sm though this volume collapse becomes a continuous transition, and the proliferation of complex phases on the high pressure side of this transition is reminiscent of Am/Pu. Although these transitions occur at finite temperature the evolution of the first order volume collapse transition into a continuous transition as the atomic number of the rare earth approaches that of Sm is remarkably similar to the changes in P vs V curves of a quantum fluid near to zero temperature that result from changing some parameter in the Hamiltonian (cf Fig1). In general, for some particular value of the parameter there is no longer a discontinuous change in volume, but only a critical point. Very recently direct evidence has been obtained for the evolution of volume collapse in CeTh doped with La into a continuous transition at zero temperature as the La doping approaches 15% [2].

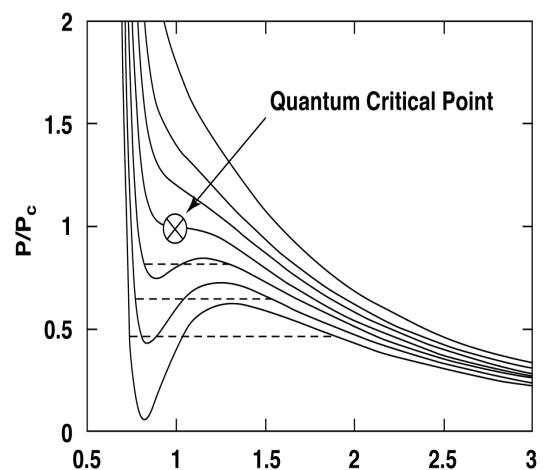


Fig 1: Pressure versus condensate density for a quantum fluid at zero temperature for various values of a parameter in the Hamiltonian such as the strength of repulsion between constituent particles.

An obvious question that arises in connection with associating the behavior of the elemental rare earths and actinides with a QCP is what is the physical nature of the organizational changes in the ground state? It cannot be a Mott metal-insulator transition because Mott transitions are always first order. In the case of the actinides it does not appear to be a change in magnetic order; although Np and Pu have rather large magnetic susceptibilities, neither are magnetic at accessible temperatures, while Am is superconducting at low temperature. The answer may be that in both the rare earths and actinides the metallic electrons form a “gossamer condensate”; i.e. the ground state wave function has BCS-like pairing of mobile charge carriers. The idea of a gossamer condensate was originally introduced to explain the close relationship between antiferromagnetism and high T_c superconductivity in the hole doped cuprates. Subsequently it was suggested [3] that there is a gossamer condensate in all materials that have metal \rightarrow bad metal phase transitions similar to the $\alpha \rightarrow \gamma$ volume collapse transition in Ce. The presumed reason that these gossamer materials are metallic and not superconducting is that the quasi-particle excitation gap is very small. In this talk I argue that both the rare earth volume collapse transitions and the strange behavior of the actinides near to Pu have their origin in the presence of a gossamer condensate that is strongly coupled to the crystal lattice.

In a superconductor the condensate density is equal to the density of metallic electrons. In gossamer metals the spectral weight assigned to conduction electrons near to the Fermi surface is significantly reduced in comparison with ordinary metals due to electron repulsion. On the other hand decreasing the spectral weight of mobile electrons decreases the binding energy of the lattice. As a result of competition between the changes in spectral weight for conduction electrons and Fermi pressure the P vs V curve for a gossamer metal will be qualitatively similar to the pressure versus atomic volume curves for the elemental rare earths. The photoemission amplitudes will also behave at least qualitatively as observed for both elemental rare earths and actinides. In addition, the magnetic susceptibility near to the critical point will be quite large.

The physical origin of the gossamer condensate in rare earth and actinide materials may be spin orbit effects. It is well known that spin orbit effects are important for core states in f-electron materials. Spin orbit effects may also be important for conduction states if the screening length is not too small and lattice distortions give rise to a Rashba effect. Under these circumstances the charge carriers are localized and carry a monopole-like charge. The BCS-like pairing is a result of the fact that spin up and spin down carriers carry opposite monopole charge. The picture that emerges for impurity stabilized δ Pu is that it is a mixture of two phases: a nearly uniform condensate with only transient distortions of the fcc lattice mixed with “gossamer insulae”, where the condensate density is substantially larger and the lattice is permanently distorted. This phenomenon is similar to the occurrence of low temperature textures in the manganites, except that the δ Pu texture involves continuous variations rather than domain walls. Thus δ Pu provides a prototype for heterogeneous quantum ground states which occur because of proximity to a quantum critical point rather than a metal-insulator transition.

The authors are grateful to Scott McCall, Jason Lashley, and Jim Smith for discussions

- 1 G Chapline and J. L. Smith, LA Science **26**, 1 (2000).
- 2 J. C. Lashley, *to be published*.
- 3 G. Chapline, Z. Nazario, and D. Santiago, Phil. Mag. **85**, 867 (2005).

INSTABILITY OF ACTINIDE ELECTRON STRUCTURE UNDER HIGH PRESSURE

B.A. Nadykto

RFNC-VNIIEF, Arzamas-16 (Sarov), Nizhni Novgorod region, 607190,

E-mail:nadykto@vniief.ru, Fax: 83130 45772

1. Refs. [1], [2] show the course of transformation of four plutonium-gallium alloys with 1, 1.7, 2.5 and 3.5 at. % Ga under isostatic pressure at 25°C in Bridgman dilatometer. As expected, large-volume δ phase collapses at low enough pressures and transfers directly from δ to α' phase with possible γ' -phase traces. Everything indicates that $\delta \rightarrow \alpha'$ transformation proceeds by the martensite mechanism much like it has been found in cooling.

The data presented shows that when δ -phase alloy volume changes under applied positive pressure above a body the work is done which is expended for the $\delta \rightarrow \alpha'$ transformation. This means that the energy level of the alloyed δ -phase is lower than that of the α' phase. At the same time, it is well known that the unalloyed α phase is more beneficial energetically than the unalloyed δ phase and the transition from the α phase to the δ phase at room temperature occurs when tensile stresses of 0.35 GPa are applied [3].

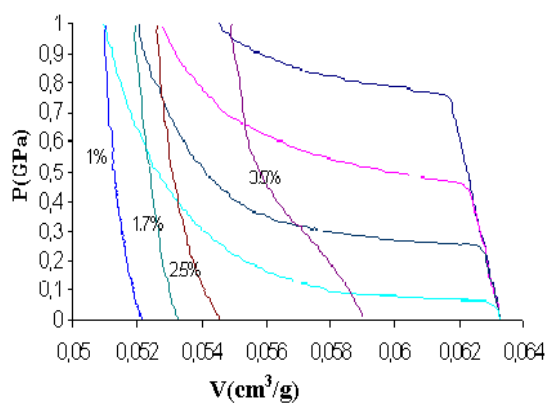


Fig. 1. Pressure versus specific volume of Pu-Ga alloy with different contents of Ga (at. %) in loading and pressure release

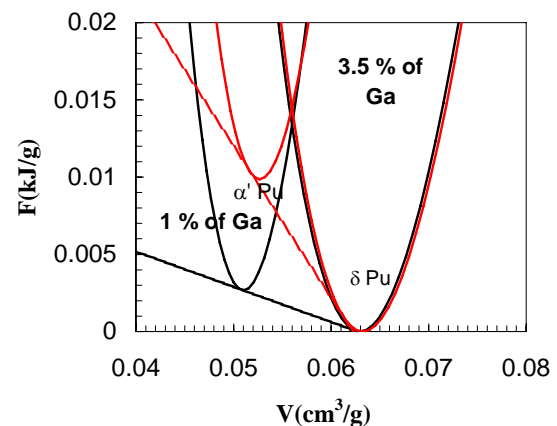


Fig. 2. Energy of α' and δ plutonium alloys as a function of specific volume.

The presented curves can be used to determine from Fig. 1 the energy of the $\delta \rightarrow \alpha'$ transformation as a function of gallium concentration in alloy through calculation of $\int PdV$ at the inelastic segment of the compression curve. Energy per gallium mole in alloy is almost independent of gallium content, which suggests the existence of some stable gallium complex in δ plutonium, which manifests itself identically in alloys with Ga content ranging from 1 at. % to 3.5 at. %. Energy of this complex can be represented as $\Delta E = 67 - 100x$ kJ/mole Ga, where x is the relative fraction of Ga in Pu-Ga alloy. In this case the enthalpy of intermetallic compound Pu_3Ga is 42 kJ/mole, which is close to the data evaluated in the literature [4].

The pattern of the transition of gallium-alloyed δ -plutonium alloy under pressure to

the α' -phase state can be represented in the graph of Helmholtz free energy as a function of specific volume. Internal energy of different plutonium phases is given by

$$E_i(\sigma) = \frac{9B_i}{2\rho_i}(\sigma^{1/3} - 1)^2 + C_i,$$

where B_i and ρ_i are the bulk modulus and equilibrium density of each phase at standard conditions (at $\sigma = 1$), C_i are constants determining minimum energy for each phase. In Fig. 2, the calculation uses 30 GPa bulk modulus for δ phase, 50 GPa for α' phase and experimental equilibrium densities of either phase. The slope of the common tangent to curves $F(V)$ for the two phases determines the phase transition pressure in the thermodynamic equilibrium state.

The plots in Fig. 2 show that the transition occurs with changing pressure, and this is evidence of thermodynamic disequilibrium. The thermodynamic disequilibrium is also testified for by the presence of hysteresis. It is well known (at least, at elevated temperatures of 130-150 °C) that the remaining δ phase gets enriched in gallium during the $\delta \rightarrow \alpha'$ transformation. This kinetic process can be responsible for the thermodynamic disequilibrium.

The α -plutonium tension of $P = -0.35$ GPa [3] that fits the $\alpha \rightarrow \delta$ transformation in unalloyed plutonium at standard temperature is correspondent with the phase energy difference of 1.2 kJ/mole. This value is less significantly than $T\Delta S$ in the $\alpha \rightarrow \delta$ transformation (3.6 kJ/mole at 300 K and $\Delta S = 12$ J/mole). Because of scarcity of information about the $\alpha \rightarrow \delta$ transformation in tension the transition energies in pure and alloyed plutonium cannot be compared, as the fraction of δ phase that therewith results is unknown. The transition from the α' phase to the pure α phase may be attended with energy release from 3.6 to 10 kJ/mole depending on gallium concentration. This can be energy of pure α -phase lattice deformation in α' -phase formation due to gallium atom capture in random sites of the α -phase lattice. The α' phase is known to be of a lower density than the pure α phase, that is its lattice is expanded.

If it is taken that in gallium-stabilized δ phase there is chemical bond of gallium and plutonium similar to that in Pu_3Ga , while in the α' phase the chemical bond disappears, then Helmholtz free energy difference evaluated experimentally from the $\delta \rightarrow \alpha'$ transformation under pressure at constant temperature is close to plutonium-gallium alloy formation enthalpy. Fig. 3 plots the δ plutonium alloy calculated enthalpy, divided by mole of the sum of nuclei of plutonium and complexes Pu_3Ga depending on atomic fraction of gallium in Pu-Ga alloy. Two experimental points obtained with the method of drop calorimetry [5] fall exactly on this calculated curve. In other words, the results of the measurements and experiments on the $\delta \rightarrow \alpha'$ transformation under pressure agree. The results of drop calorimetry for Pu-Al alloy are presented in ref. [12].

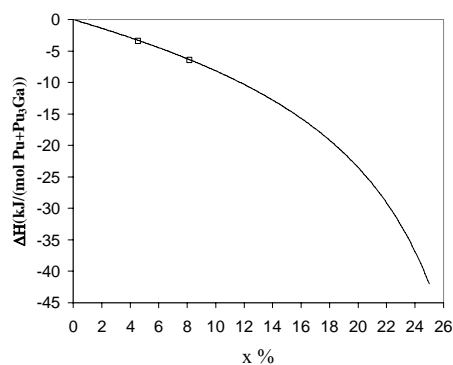


Fig. 3. δ plutonium alloy formation enthalpy (kJ/mole/(mole of Pu + Pu_3Ga)) versus Ga concentration in Pu-Ga alloy

2. The recent experiments using diamond anvils and synchrotron radiation sources have supplied interesting, important information about crystalline and electron structure of actinides in the megabar pressure range [6-10].

Ref. [7] studies compressibility of Pa to 129 GPa pressure. The computational analysis shows that up to $P \approx 95$ GPa the experimental points fall on the computed curve with parameters $\rho_0 = 15.37 \text{ g/cm}^3$ and $B_0 = 115$ GPa. At higher pressures the experiment deviates significantly from the computed dependence and can be described as the state of another Pa electron phase with parameters $\rho_0 = 19.827 \text{ g/cm}^3$ and $B_0 = 400$ GPa. Ref. [7] notes that at $P = 77$ GPa the tetragonal structure of protactinium changes to low-symmetry orthorhombic structure of α uranium. At 77 GPa, however, there is no noticeable change in slope of the curve $P(\rho)$, which is evidence that the initial electron structure of Pa remains unchanged. The slope and electron structure change abruptly at 95 GPa, evidently, at unchanged orthorhombic crystalline structure. Previously [11] it was noted that the experimental data on compressibility of thorium and uranium also indicated the existence of a stiff phase in them (with $B_0 = 400$ GPa) at pressure above 100 GPa.

Compressibility of curium metal to 100 GPa pressure is studied in ref. [10]. The parent phase of Cm (of equilibrium density 13.3 g/cm^3) has bulk modulus $B_0 = 40$ GPa, which is somewhat higher than that of americium metal and δ -phase plutonium. At pressure about 10 GPa the electron structure of Cm metal changes. The new phase parameters are $\rho_0 = 13.96 \text{ g/cm}^3$, $B_0 = 60$ GPa. According to [10], at 17 GPa the parent dhcp structure changes to fcc structure. In the 10-37 GPa pressure range, however, the experimental points are described well as states of one electron phase. Phase CmIII (monoclinic structure) has somewhat lower bulk modulus ($B_0 = 53$ GPa) at the same equilibrium density ($\rho_0 = 13.96 \text{ g/cm}^3$). For $P > 57$ GPa the points for phases CmIV and CmV can be described as states of one and the same electron phase with $\rho_0 = 20.35 \text{ g/cm}^3$, $B_0 = 280$ GPa. The parameters of this electron phase are close to those of phase Am IV at pressure 55-100 GPa.

At standard conditions, there are three electrons in the outer shell in thorium metal and four in uranium. In compression by high pressure the electron structure rearrangement takes place leading to the increase in the number of outer electrons to five or even six. In americium and curium the number of outer electrons increases under pressure to five.

References

1. S.S. Hecker, D.R. Harbur, T.G. Zocco. Phase stability and phase transformation in Pu-Ga alloys. // *Progress in Materials Science*. 49 (2004) 429-485.
2. S.S. Hecker, D.R. Harbur, T.G. Zocco. Phase stability in plutonium-gallium alloys. // Proceedings of International Workshop "Fundamental Properties of Plutonium", Sarov, 30 August – 2 September 2004. P. 3.
3. S.S. Hecker. Plutonium and its alloys. // *Los Alamos Science*. 26. 2000. P. 290.
4. Химия актиноидов. Т. 2. Ред. Дж. Кац, Г. Сиборг, Л. Морсс. М.: Мир. 1997. С. 558-621.
5. Stan M., Baskes M.I., Muralidharan K., Lee T.A., Hu S., Valone S.M. Thermodynamic properties of Pu-Ga alloys. // *Fundamental Plutonium Properties. Abstracts of V International Workshop, September 12-16, 2005. Snezhinsk. Russia*. P. 73-75.
6. Vohra Y.K., Akella J. *Phys. Rev. Lett.* 1991. V. 67. P. 3563
7. Haire R.G., Heathman S., Idiri M., Le Bihan T., Lindbaum A., Rebizant J. *Phys. Rev.*, 2003, **B67**, 134101
8. Le Bihan T., Heathman S., Idiri M., Lander G.H. et al. *Phys. Rev.*, 2003, **B67**, 134102
9. Lindbaum A., Heathman S., Litfin K. et al. // *Phys. Rev.* 2001. Vol. B63. 214101
10. Heathman S., Haire R.G., Le Bihan T., Lindbaum A. et al. // *Science*. 2005. Vol. 309. P. 110-113.
11. Nadykto B.A., Nadykto O.B. // *Plutonium Future – Science 2003. Conference Transactions*. Ed. by G.D. Jarvinen. Albuquerque. New Mexico, USA, July 6-10, 2003. P. 184-186.
12. Akhachinskiy V.V., Timofeeva L.F. // *Thermodynamic of Nuclear Materials*. 1979. Proc. of Sympos. Julix, 29 Jan. – 2 Feb. 1979. Vol. II. IAEA, Vienna, 1980. P. 161-169.

Oxygen Exchange and Diffusion in Uranium Dioxide Single Crystals

SA Joyce^{*}, JA Stultz[†], MT Paffett^{*}

^{*} Los Alamos National Laboratory, Los Alamos NM 87544 USA

[†] US Borax, Boron, CA

There are a number of solid uranium oxides ranging from U(II)O to U(VI)O₃, with essentially a continuous range of stoichiometries from UO_{2-x} up to UO₃. UO₂ is fairly stable under normal ambient conditions and is the form often used in oxide fuels and in many waste forms. There are concerns related to changes in the chemical and mechanical properties of the UO₂ upon bulk oxidation. Bulk oxidation proceeds by at least two steps: 1) oxygen incorporation into surface and 2) subsequent diffusion into the bulk. We have examined both steps using water adsorption on single crystal UO₂. In the first set of experiments, a U¹⁶O₂ sample is exposed ¹⁸O-labeled water and investigated using electron stimulated desorption (ESD). In ESD, electron irradiation leads to the desorption of oxygen ions from the surface layer only. For clean UO₂ surfaces, only ¹⁶O⁺ is observed; both ¹⁸O and ¹⁶O are seen for water-exposed surfaces, even at cryogenic temperatures. The exchanged ¹⁸O, however, remains at the surface up to temperatures as high as 650K, above which it decreases due to diffusion into the bulk. In the second set of experiments, a UO₂ surface is made oxygen deficient by ion sputtering. This reduced surface is reactive to water leading to H₂ desorption at 400K. By annealing the sample to various temperatures prior water exposure, we find the surface reoxidizes by diffusion of oxygen out of the bulk at ~700K. From these studies, we can determine the diffusion constant of oxygen in UO₂ at 700K. The calculated D (~10⁻¹⁷ cm²/sec) is in good agreement with extrapolations from previous high temperature (>1200K) studies.

Acknowledgements: This work was supported by Los Alamos National Laboratory LDRD. JS acknowledges the Seaborg Institute for postdoctoral support.

Molecular Magnetism in Some Neptunyl (+1, +2) Complexes

A. Nakamura^{*}, M. Nakada^{*}, T. Nakamoto^{*}, T. Kitazawa[†] and M. Takeda[†]

^{*} Advanced Science Research Center, Japan Atomic Energy Agency, Tokai, Ibaraki 319-1195, Japan

[†] Department of Chemistry, Faculty of Science, Toho University, Funabashi, Chiba 274-8510, Japan

The magnetic-property study of actinide (5f) complexes is few, compared with its intermetallic systems where the so-called heavy-fermion type exotic physical (electronic and magnetic) properties have been intensively studied. However, to elucidate the magnetic property of actinide complexes is of particular interest from the viewpoint of 5f low-dimensional (low-D) molecular magnetism. We are interested in the magnetic property of neptunyl (+1,+2) (Np(V,VI): $5f^{2,1}$) complexes in which strongly-bonded linear neptunyl ($O=Np=O$)^{+1,+2} monocations form unique 0, 1 to 3D network structures extended by the so-called 'cation-cation bond (CCB)'. Lately, transition-metal (3d) and lanthanide (4f) clusters, rings and complexes have been receiving increasing attention as a nanoscale and/or molecular magnet.¹ Also in this context, actinide complexes where the 5f electrons are known to exhibit a marginal character between the 3d and 4f electrons are expected to represent a novel class of nanomagnetic materials.

Though only a few of them are investigated up to now, magnetic-susceptibility and ²³⁷Np Mössbauer study of our group² has revealed that oxygen-coordinated neptunyl (+1) (Np(V)) complexes exhibit intriguing common feature as a neptunyl-molecular magnet and yet diversified magnetic character depending on the specific neptunyl network structure from a Curie-Weiss paramagnet to ferro- and meta-magnets.

We are lately extending such study to neptunyl (+2) (Np(VI)) complexes; a trinitrato complex, $NH_4[NpO_2(NO_3)_2]$ (**1**), and two (acetyl-aceton ($acac=C_5H_7O_2^-$) or trinitrato) pyridine ($py=C_5H_5N$) complexes, $NpO_2(acac)_2py$ (**2**) and $NpO_2(NO_3)_2byp$ (**3**) (where byp (bipyridine) $=C_{10}H_8N_2$).³ In the latter two (**2**, **3**) systems, one or two of the coordinating non-nyl oxygens are substituted with nitrogen(s). Plausibly related to this O→N substitution in the Np coordination environment, **2** and **3** are found to exhibit many striking magnetic features (peculiar field-dependent paramagnetic behavior up to room temperature, very large magnetic relaxation effect at low temperature, etc.) different from those of **1** and other known neptunyl (+1, +2) systems. These results are discussed in connection with their microscopic ²³⁷Np Mössbauer data.

1. O. Kahn, 'Molecular Magnetism', Wiley-VCH (N.Y), 1993.
2. T. Nakamoto, M. Nakada and A. Nakamura, J. Nucl. Sci. Technology, Suppl.3, 102 (2002).
3. A. Nakamura, M. Nakada, T. Nakamoto, T. Kitazawa and M. Takeda, submitted to J. Phys. Soc. Jpn. Suppl. (2006) (Proc. ASRC-WYP-Symp.(2005)).

Nanostructured Actinide Compounds

S.V. Krivovichev*, P.C. Burns†, I.G. Tananaev‡, B.F. Myasoedov‡

* St. Petersburg State University, St.Petersburg 199034 Russia

† University of Notre Dame, Notre Dame IN 46556 USA

‡ Institute of Physical Chemistry, Russian Academy of Sciences, Moscow 119991 Russia

INTRODUCTION

Nanostructure is the term generally used to describe the structure with at least one dimension in the nanometer range (1-1000 nm). These include nanocrystals and clusters (quantum dots), nanowires, nanotubes, thin films and superlattices (3-D structures). Usually, nanostructures have more reactive surfaces and exhibit new functions for the same chemical composition in comparison with the bulk material. Investigations of organization of matter at the nano-level are under way in many chemical systems with present and potential applications in nanotechnology. Recently, nanoscale structures were reported for the first time for actinide-containing compounds as well [1] and here we briefly summarize our recent results in the field.

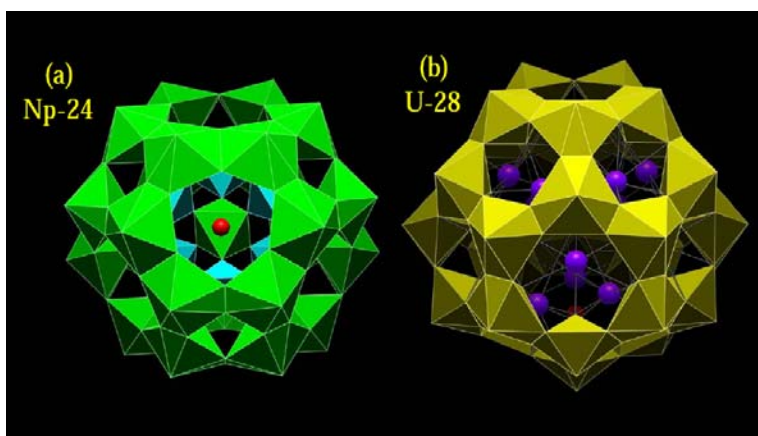


Fig. 1. Np-24 and U-28 nanospheres [2].

NANOCLUSTERS: 0D NANOSTRUCTURES

Burns et al. [2] reported the synthesis and characterization of a new family of self-assembling, f-ion (An) nanospheres with compositions such as $K_{16}(H_2O)_2(UO_2)(O_2)_2(H_2O)_2[(UO_2)(O_2)_{1.5}]_{28}^{14-}$ and $Li_6(H_2O)_8NpO_2(H_2O)_4[(NpO_2)(O_2)(OH)]_{24}^{20-}$ that are comprised of linear actinyl-peroxide building blocks. Their molecular units are composed of 24, 28 or 32 uranyl peroxide polyhedra (designated U-24, U-28 and U-32), or 24 neptunyl peroxide polyhedra (designated Np-24). The nanospheres have diameters of approximately 16.4, 17.7, and 18.6 Å (between the centers of bounding O atoms). The nanospheres are comprised of two types of actinyl peroxide polyhedra. U-24, U-32 and Np-24 contain topologically identical $(AnO_2)(O_2)_2(OH)_2$ hexagonal bipyramids, with O atoms of the actinyl ions constituting apices of the bipyramids, and peroxide groups form two of the equatorial edges of the polyhedra.

1D NANOSTRUCTURES: URANYL-BASED NANOTUBULES

Krivovichev et al. [3,4] reported synthesis and structures of two uranium(VI) compounds, $K_5[(UO_2)_3(SeO_4)_5](NO_3)(H_2O)_{3.5}$ (**1**) and $(C_4H_{12}N)_{14}[(UO_2)_{10}(SeO_4)_{17}(H_2O)]$ (**2**), containing nanometer-sized tubules formed by corner sharing of $U^{6+}O_7$ pentagonal bipyramids and SeO_4 tetrahedra. The most intriguing feature of the structures of compounds **1** and **2** is in that they contain isolated nanotubules formed by corner sharing of $U^{6+}O_7$ pentagonal bipyramids and SeO_4 tetrahedra (Fig. 2). Such nanometer-scale tubules formed by two types of coordination polyhedra are new for inorganic oxosalts. The uranyl selenate nanotubules in the structures of **1** and **2** have circular cross-sections with outer diameters of 17 and ~ 25 Å (= 1.7 and 2.5 nm), respectively. The crystallographic free diameters of the tubules are 4.7 and 12.7 Å for **1** and **2**, respectively.

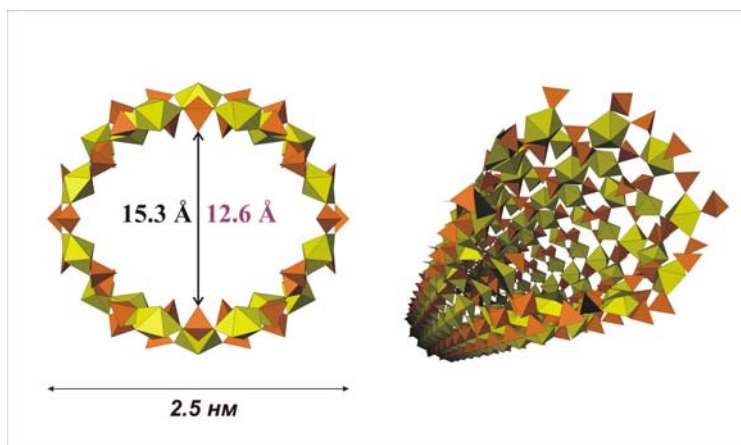


Fig. 2. Uranyl selenate nanotubules in the structure of **2**.

2D NANOSTRUCTURES: NANOCOMPOSITES

Hybrid organic-inorganic highly ordered nanocomposites have been recently reported by Krivovichev et al. [5,6]. In these structures, interfacial interactions between organic and inorganic substructures can be studied by charge-density matching principle. Application of this principle to actinide compounds requires special attention since surface area of actinide-based 2D units is higher than that of other inorganic oxosalts units (i.e. metal phosphates). The charge-density matching principle is, however, observed either through tail interdigitation (for long-chain monoamines) or incorporation of acid-water interlayers into organic substructure (for long-chain diamines). In some compounds, protonated amine molecules form cylindrical micelles that involves self-assembly governed by competing hydrophobic/hydrophilic interactions [5]. The flexible inorganic complexes present in the reaction mixture could then form around cylindrical micelles to produce highly undulated 2D sheets or nanotubules.

Thanks are due to the Ministry of Science and Education of the Russian Federation and RFBR for financial support.

- 1 Th. Albrecht-Schmitt, *Angew. Chem. Int. Ed.* **44**, 4836 (2005).
- 2 P.C. Burns, K.-A. Hughes Kubatko, G. Sigmon, B.J. Fryer, J.E. Gagnon, M.R. Antonio, L. Soderholm, *Angew. Chem. Int. Ed.* **44**, 2135 (2005).
- 3 S.V. Krivovichev, V. Kahlenberg, R. Kaindl, E. Mersdorf, I.G. Tananaev, B.F. Myasoedov, *Angew. Chem. Int. Ed.* **44**, 1134 (2005).
- 4 S.V. Krivovichev, V. Kahlenberg, R. Kaindl, E. Mersdorf, I.G. Tananaev, B.F. Myasoedov, *J. Amer. Chem. Soc.* **127**, 1072 (2005).
- 5 S.V. Krivovichev, V. Kahlenberg, R. Kaindl, E. Mersdorf, *Eur. J. Inorg. Chem.* **2005**, 1653 (2005).
- 6 S.V. Krivovichev, I.G. Tananaev and B.F. Myasoedov, *MRS Proceedings*. *In press* (2006).

Hydrous PuO_{2+x}(s): Solubility and Thermodynamic Data

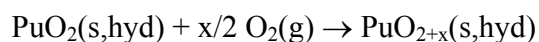
V. Neck^{*}, M. Altmaier^{*}, C.M. Marquardt^{*}, A. Seibert[†], J.I. Yun^{*}, Th. Fanghänel^{*}

^{*}Institut für Nukleare Entsorgung, Forschungszentrum Karlsruhe, D-76021 Karlsruhe, Germany

[†]European Commission, JRC, Inst. for Transuranium Elements, D-76125 Karlsruhe, Germany

SOLUBILITY AND REDOX POTENTIALS

The solubility and redox reactions of Pu(IV) hydrous oxide were analyzed by comparing total Pu concentrations, oxidation state distributions and simultaneously measured redox potentials under air (Rai et al.¹) and under Ar containing only traces of O₂ (present work). Combing all information strongly indicates that O₂ is scavenged by solid PuO₂(s,hyd) yielding mixed valent PuO_{2+x}(s,hyd) = (Pu^V)_{2x}(Pu^{IV})_{1-2x}O_{2+x}(s,hyd) according to the net reaction of the water-catalyzed oxidation mechanism proposed by Haschke et al.²:



At pH < 3 (region A in Fig.1), the oxidized fractions of PuO_{2+x}(s,hyd) (ca. 10 % in the studies of Rai et al.¹ under air and 0.5 % in the present experiment) are completely soluble and lead to a constant level of [Pu(V)] + [Pu(VI)] (under air), which is correlated and limited to the amount of oxygen in the system and/or the amount of oxidized Pu in the original Pu(IV) stock solution. In the present study under Ar, the samples at pH < 2.5 did not contain Pu(VI) but predominantly Pu(V) and Pu(III). At pH > 3, the aqueous Pu concentration is dominated by Pu(V) for both the studies under air or Ar. The maximum concentration of PuO₂⁺, decreasing with slope -1 in a logarithmic plot vs. pH (regions B and C in Fig.1), is limited to the solubility of PuO_{2+x}(s,hyd) considered as solid solution (PuO_{2.5})_{2x}(PuO₂)_{1-2x}(s,hyd). Defining the solubility product as

$$K_{\text{sp}}(\text{PuO}_{2.5} \text{ in PuO}_{2+x}(\text{s,hyd})) = [\text{PuO}_2^+][\text{OH}^-]$$

all experimental data in dilute to concentrated electrolyte solutions lead to a consistent value at I = 0, log K_{sp}^o = -14.0 ± 0.8 (2σ), which is comparable to the value for NpO_{2.5}(s)³. The low redox potentials at pH 4 - 13 (regions C in Fig.1) could not be explained¹. We have shown that they are reproducible (pe + pH = 12.5 ± 1.2), independent of the initial O₂ in the system, and caused by equilibria between PuO_{2+x}(s,hyd), PuO₂⁺(aq) and small Pu(IV) colloids/polymers (1.5 - 2 nm) predominant at pH > 7 (log [Pu(IV)]_{coll} = -8.3 ± 1.0).

THERMODYNAMIC DATA

The molar standard Gibbs energy for PuO_{2+x}(s, hyd) = (PuO_{2.5})_{2x}(PuO₂)_{1-2x}(s, hyd) can be estimated from the solubility data for x = 0.003 (present study) and x = 0.05 (under air¹):

$$\begin{aligned} \Delta_f G_m^\circ(\text{PuO}_{2+x}(\text{s,hyd})) &= 2x \Delta_f G_m^\circ(\text{PuO}_{2.5}(\text{s, hyd})) + (1-2x) \Delta_f G_m^\circ(\text{PuO}_2(\text{s,hyd})) \\ &= \{2x (-971.2 \pm 5.4) + (1-2x)(-965.5 \pm 4.0)\} \text{ kJ/mol} \end{aligned}$$

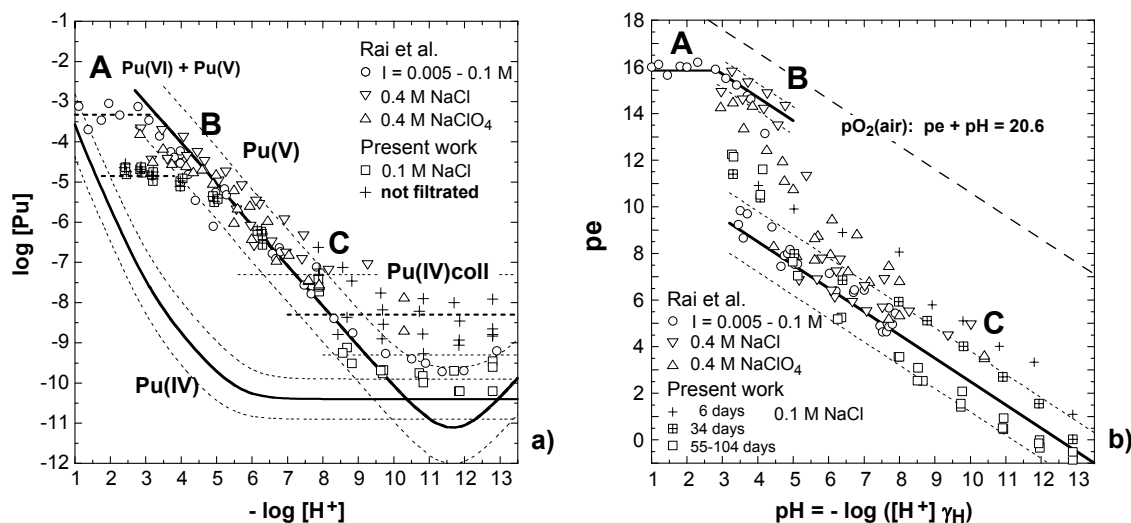
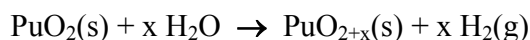


Fig 1: a) Solubility of $\text{PuO}_{2+x}(\text{s,hyd})$ at 20 - 25°C; calculated Pu(IV) concentration⁴, Pu concentration measured after ultrafiltration (open symbols) and $[\text{Pu}]_{\text{tot}}$ including Pu(IV) colloids/polymers (crosses), b) simultaneously measured redox potentials ($\text{pe} = 16.9 \text{ Eh(V)}$ at 25°C). Comparison of data from Rai et al.¹ under air and present work under Ar (traces O_2).

Accordingly, $\Delta_f G^\circ_m(\text{PuO}_{2+x}(\text{s,hyd}))$ is only slightly lower than $\Delta_f G^\circ_m(\text{PuO}_2(\text{s,hyd})) = -965.5 \pm 4.0 \text{ kJ/mol}$ ³. Since the experimental data for $\text{PuO}_{2+x}(\text{s,hyd})$ include a certain solid solution stabilization energy, it is not clear whether $\text{PuO}_{2+x}(\text{s,hyd})$ can be oxidized to values of $x > 0.27$, the maximum value observed². Possibly, the molar standard Gibbs energy for $\text{PuO}_{2.5}(\text{s,hyd})$ is slightly less negative than $\Delta_f G^\circ_m(\text{PuO}_2(\text{s,hyd})) = -965.5 \pm 4.0 \text{ kJ/mol}$. Anhydrous Pu(IV) dioxide ($\Delta_f G^\circ_m(\text{PuO}_2(\text{cr})) = -998.1 \pm 1.0 \text{ kJ/mol}$)³ cannot be oxidized by $\text{O}_2(\text{g})$. Known analogous data and observations for hydrated and crystalline $\text{NpO}_2(\text{s})$ and $\text{NpO}_{2.5}(\text{s})$ support the calculated thermodynamic data for $\text{PuO}_{2+x}(\text{s})$. The values reported by Haschke et al.², $\Delta_f G^\circ_m(\text{PuO}_{2.25}(\text{s})) = -1080 \text{ kJ/mol}$ and $\Delta_f G^\circ_m(\text{PuO}_{2.5}(\text{s})) = -1146 \text{ kJ/mol}$ are much too negative. They are calculated assuming the oxidation of $\text{PuO}_2(\text{s})$ by water according to



For thermodynamic reasons this reaction is not possible ($\Delta_f G^\circ_m > 200 \text{ kJ/mol}$).

- 1 D. Rai et al., a) *Soil Sci. Am. J.* 44, 490 (1980), b) *Radiochim. Acta* 35, 97 (1984), c) *Radiochim. Acta* 89, 491 (2001).
- 2 J.M. Haschke, T.H. Allen, L.A. Morales, a) *Science*. 287, 285 (2000), b) *J. Alloys Comp.* 314, 78 (2001), c) *J. Alloys Comp.* 336, 124 (2002).
- 3 R. Guillaumont et al. (OECD-NEA TDB), Update on the Chemical Thermodynamics of Uranium, Neptunium, Plutonium, Americium and Technetium, Elsevier, 2003.
- 4 V. Neck, J.I. Kim, *Radiochim. Acta*, 89, 1 (2001).

A Look Toward the Future of Solid-State Transuranium Chemistry

T. E. Albrecht-Schmitt*

*Department of Chemistry and Biochemistry and E. C. Leach Nuclear Science Center, Auburn University, Auburn, Alabama 36849

Abstract

In this talk we will investigate recent breakthroughs in solid-state actinide chemistry with a focus on oxide-type materials. We will attempt to look into the crystal ball to see what the future holds in store for this field by looking at recent developments of great importance that will likely have a transforming affect on solid-state actinide chemistry. There have been many exciting disclosures over the past five years that are worthy of highlighting. These topics will including a discussion of nanoscale bonding features in uranyl and neptunyl compounds, magnetic ordering phenomena derived from super-exchange interactions in neptunyl networks, the isolation of a series of Pu(V) compounds that were once thought to be unstable, and unusual bonding in actinide-containing extended networks (Fig. 1). We will look closely at advances in “designing” actinide structures for specific applications, such as ion exchange and nonlinear optics. This will be a far ranging talk intended to peak interest in many aspects of this discipline.

Acknowledgments

This research was sponsored by the U.S. Department of Energy through the Heavy Elements Program.

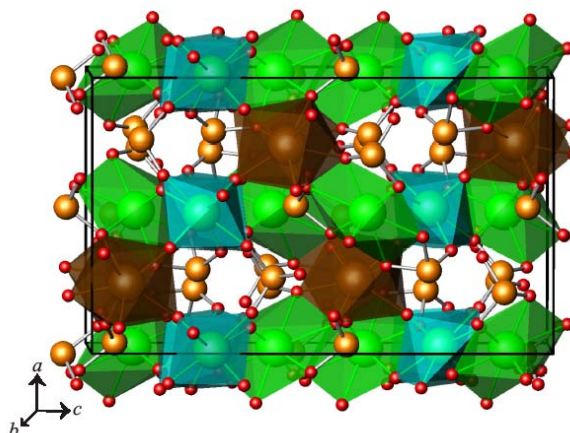


Fig 1: A view of the structure of mixed-valent Np(IV)/Np(V) Selenite, $\text{Np}(\text{NpO}_2)_2(\text{SeO}_3)_3$.

Self-irradiation effects in plutonium alloys

N. Baclet*, B. Oudot*, R. Grynszpan[†], L. Jolly*, B. Ravat*, L. Berlu*, G. Jomard[#]

* Commissariat à l'Énergie Atomique, Centre de Valduc, F-21120 Is sur Tille, France

[†] SERAM, Ecole Nat. Sup. d'Arts et Métiers, F-75013 Paris, France

[#] Commissariat à l'Énergie Atomique, Centre Ile de France, F-91680 Bruyères le Châtel, France

INTRODUCTION

Among the actinides, plutonium is certainly the most complex element due to its intermediate position in the 5f-series, at the edge between localized and itinerant electrons. Most studies focus on plutonium alloys since they can be stabilized at room temperature in the face-centered-cubic phase (δ) by adding deltagen elements such as aluminum, gallium, cerium or americium. The plutonium decay results into the creation of helium and uranium ions, which produce defects through displacement cascades.

EXPERIMENTAL EVIDENCE OF AGING EFFECTS

The self-irradiation defects may affect the plutonium properties and, for instance, induce swelling which amplitude depends on the nature of the solute element and its tendency to segregate in the matrix. Dilatometry and X-ray Diffraction (XRD) have revealed differences in swelling. While XRD shows a microscopic swelling that saturates after about 0.08 displacements per atoms (dpa) for well homogenized PuGa alloys, macroscopic swelling (as measured by dilatometry) follows a linear trend after a transient period. Swelling might then be the sum of several contributions that affect differently macroscopic and microscopic scales. A better understanding of the basic mechanisms involved in the production of the radiation damages, especially at the early stages, is then required in order to predict their effects on alloyed plutonium. Positron annihilation spectroscopy is an appropriate method to tackle this problem, owing to its specific sensitivity to vacancy-type defects in solids, while lessening radiological constraints by remote measurements. This technique was implemented to monitor the early stages of defect production in as-prepared δ -stabilized PuGa alloys, and to correlate the results with those obtained by dilatometry and XRD. Both types of swelling were investigated versus time. The increase of the positron mean lifetime observed just after casting is associated with an increase in the concentration of vacancy clusters, rather than with an increase in the defects average size, according to the increase in microscopic swelling observed by XRD [1]. Indeed, a size increase of the defects tends to deform the lattice, resulting in the broadening of X-ray lines, whereas an increase in concentration leads to a lattice parameter increase, detected in the present case.

AGING MODELING

However, even if the description of this first stage of defects creation is essential to understand further evolutions, it remains necessary to quantify the changes in physical properties, especially swelling, for much longer periods, for which samples are not available. A multi-scale (time and size) modeling of self-irradiation effects, was therefore developed to

predict the changes. The prime aim was to compare modeling and experiments regarding the swelling data. Moreover, multi-scale modeling might unveil the presence of specific defects required for a more realistic assessment of aging phenomena, and in turn also suggest additional specific experiments for their characterization.

The ab-initio method allows to calculate physical characteristics such as elastic constants, bulk modulus, that are crucial input data to estimate the interatomic potential used for molecular dynamics calculations. Displacement cascades were calculated using the Modified Embedded Atom Model, with a progressive increase in the energy of the uranium recoil atom. Preliminary results for 10 keV reveal that, in the first stage, displacement cascades lead to the formation of an amorphous core of 5 nm average radius containing approximately 5000 Frenkel pairs. At the end of the defects recombination stage (after a couple of nanoseconds), only a few interstitials remain outside the melting zone with an equal number of mono-vacancies within the melting zone [2]. Initial results concerning a 64 keV displacement cascade suggest that sub-cascades appear rapidly. Subsequent diffusion of the defects formed are described with a mesoscopic Monte-Carlo approach, that allows to calculate swelling induced by the remaining defects, and to compare directly to experimental data. In parallel, a more phenomenological approach, based on rate equations has been developed and compared to the Monte Carlo approaches.

Whatever the scale, modeling must be validated through comparison with experimental data. Dedicated experiments have therefore been designed to measure the plutonium physical properties required by the theoretical approach. For example, molecular dynamics simulation of displacement cascades depends strongly on the choice of the interatomic potential. This complex potential is adjusted using experimental data such as elastic constants. Consequently, we designed X-ray diffraction (XRD) experiments to extract single crystal elastic constants from measurements performed on a polycrystal of δ -Pu alloy. Moreover, the number of defects induced by a α -decay is directly determined by the displacement threshold energy E_d , not hitherto measured for plutonium. Hence, a low-temperature electrical resistivity setup was designed to measure E_d in electron-irradiated plutonium. Furthermore, isochronal annealing should also allow the measure the migration energy of the various defects. All these experimental results should contribute to the validation of both ab-initio and molecular dynamics calculations and will be used as input data in Monte-Carlo methods.

Recent results regarding the different physical properties cited above will be presented.

1 B. Oudot, PhD Thesis, Université de Franche-Comté, Besançon, France (2005).

2 L. Berlu, G. Rosa, P. Faure, N. Baclet and G. Jomard, MRS Fall Meeting, Boston, (2005).

First principles determination of the vacancy formation energy in δ -plutonium

G Robert^{*}, A. Pasturel[†], B. Siberchicot^{*}

^{*}CEA-DIF BP 12, F-91680 Bruyères-le-Châtel, France

[†]Laboratoire de Physique et Modélisation des Milieux Condensés, CNRS
25 avenue des Martyrs, BP 106, F-39042 Grenoble, France

Abstract :

One of the most tricky problems concerning the δ fcc-stabilized phase of plutonium consists in predicting its properties under long-term aging.

Due to its radioactive nature, the unstable plutonium nucleus decays principally by α -decay. Two types of defects, namely vacancies and self-interstitials, are formed in metals by this self irradiation.

The evolution of defect population can lead to significant changes in the microstructure and causes a number of radiation-induced macroscopic properties changes such as density, ductility or elastic constants.

Due to the special location of plutonium at the boundary between light actinides (delocalized 5f electrons) and heavy actinides (localized 5f electrons) a slight change in atomic volume or internal stresses could affect its stability.

Concerning the knowledge of the thermodynamic and kinetic behavior of metals, one of the most important quantity is the vacancy formation energy. Its determines the equilibrium vacancy concentration and contributes to the self-diffusion coefficient in the monovacancy mechanism, which is the main diffusion process in the closed-packed metals. Then the activation energy is the sum of the vacancy formation energy and of the migration energy of the vacancy. Due to the lack of experimental values concerning defects in plutonium [1] and its alloys, first-principles calculations are of considerable interest to estimate the formation energies of point defects in these phases.

In this aim, we study the stability and formation energies of vacancies in plutonium with spin-polarized PAW calculations using the Vienna ab initio simulation package VASP [2][3].

Even if magnetism in δ -Pu has not been confirmed by experiment [4][5], taking into account magnetic exchange interaction leads to major improvements compared to standard non-magnetic LDA or GGA results.

As already shown in these previous papers [6][7][8][9] spin polarized GGA approximation is able to reproduce the main equilibrium properties and energy differences of pure and alloyed plutonium.

In these presentation, we follow these ideas and expand the investigation to study the influence of magnetic configuration on the vacancies energies in δ -plutonium. The calculations were performed for three different configurations, namely : antiferromagnetic (AF), ferromagnetic (FM) and disordered magnetic structures (DM). We also evaluate box-size effects and local relaxations with these three magnetic configurations. Some results have already been reported in an earlier paper [10].

The first interesting result is that the unrelaxed values of both mono and divacancies are not very sensitive to the long range magnetic ordering.

The other important point is that the formation of divacancies do not require an additional energy with respect to the formation of two isolated monovacancies. This indicated that vacancy clusters are as stable as isolated vacancies.

Now, if we allow atomic relaxation, the inward relaxation is of order of 3 % (7 % for divacancies), as usually obtained for transition metals.

The energy of the divacancy is still similar to the energy of two isolated vacancies. Nevertheless, the relaxed energy and forces acting on atoms is function of magnetic configuration.

- 1 M.J. Fluss, B.D. Wirth, M. Wall, T.E. Felter, M.J. Caturla, A. Kubota, T. Diaz de la Rubia, J. Alloys. Comp. **368**,62, 2004
- 2 G. Kresse and J. Furthmüller, Phys Rev B **54**,11169 (1996)
- 3 G. Kresse and J. Furthmüller, Comput. Mater. Sci. **6**,15 (1996)
- 4 N.J. Curro and L. Morales, Mat. Res. Soc. Symp. Proc. **802**, 53 (2004)
- 5 R.H. Heffner, G.D. Morris, M.J. Fluss, B.Chung, D.E. MacLaughlin, L. Shu and J.E. Anderson, in press, Physica B
- 6 Y. Wang and Y.F. Sun, J. Phys. Condens. Mater. **21**,L311 (2000)
- 7 P. Soderlind, A. Landa, B. Sadigh, Phys. Rev. B **66**,205109 (2002)
- 8 G. Robert, C. Colinet, B. Siberchicot and A. Pasturel, Modelling Simul Mater Sci. Eng **12**,693 (2004)
- 9 B. Sadigh, W.G. Wolfer, Phys. Rev B **72**,205122 (2005)
- 10 G.Robert, A. Pasturel, B. Siberchicot, Europhysics Letters **71**,3,412 (2005)

Monte Carlo + Molecular Dynamics simulation of radiation damage evolution in Pu

V.V. Dremov, P.A. Sapozhnikov, S.I. Samarin, D.G. Modestov, N.E. Chizhkova

Russian Federal Nuclear Centre – Zababakhin Institute of Applied Physics (RFNC-VNIITF)
Snezhinsk, Russia 456770

ABSTRACT

The paper presents results obtained in the simulation of damage cascades in self-irradiated unalloyed and gallium-alloyed delta-plutonium. The fast cascade stage was simulated by Monte Carlo method. It follows from Monte Carlo calculations that in a cascade formed by a uranium nucleus of energy 86 keV, about 40% of the initial energy is lost in inelastic collisions with electrons and the rest energy resides in the crystal lattice. When the energies of cascade particles became close to the displacement energy, the cascade configuration resulted (coordinates + particle velocities) was transferred to a molecular dynamics (MD) code which helped track the further evolution of the system to ~1-2 ns. The Modified Embedded Atom Model (MEAM) [1,2] was used to describe particle interactions.

Our simulations show that a cascade from the uranium recoil nucleus causes a large energy release into a lattice subsystem within a local region measuring about 20-25 nm; this causes material melting and subsequent recrystallization. Preliminary estimates showed that the energy transferred to the lattice is enough to cause melting in a region which characteristic size reaches 15 nm; the region contains ~200 000 atoms. MD simulations show that lattice heat conductivity reduces the characteristic size of the melting region to ~8-10 nm (~35 000 atoms) in a sample whose initial temperature was 300K.

The evolution of temperature and density fields in the damaged region was tracked in simulations. The time of recrystallization was estimated to be ~1ns. The distribution of point defects in the recrystallized region was obtained. Most of point defects created during a fast stage of the cascade vanish when melting and recrystallizing, residual defects evolve much slower than the nano-second time scale

The calculations have also been carried out for polycrystalline samples. If the damaged region is inside a single-crystal grain, the melted material undergoes complete recrystallization when cooling. If radiation melting occurs in a region which contains a grain boundary, the recrystallization in the melted regions adjacent to different grains will differ. Such a process results in grain boundary sagging and broadening with time. As an illustration Figure 1 shows the same fragment of a sample containing a grain boundary at the moment of maximum size of melted region (left picture, $t=20$ ps) and at the moment 1 ns (right picture) when the process of recrystallization is almost completed.

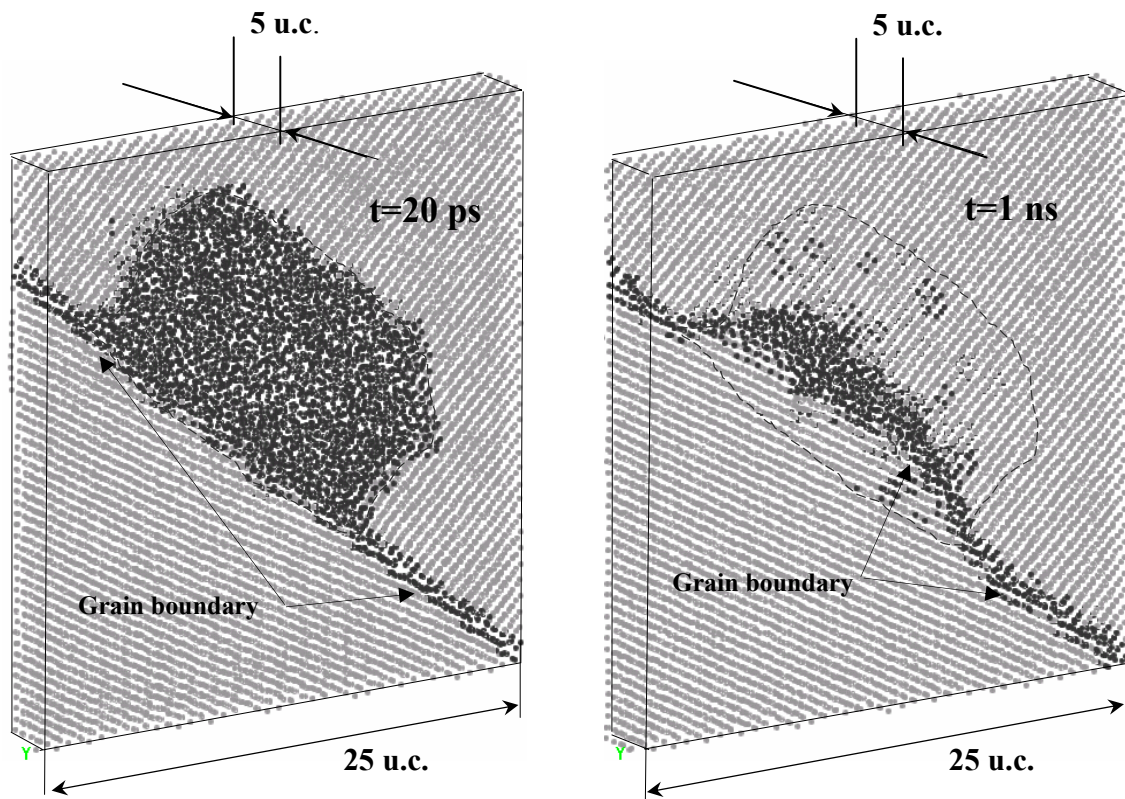


Fig.1 Fragments of a polycrystalline sample containing grain boundary adjacent to the damaged (melted) region. Taupe color is for disordered structure (grain boundary, melted region), light grey color if for fcc δ -Pu. Dashed line contours the region where the recrystallization took place.

1. M. I. Baskes, *Phys. Rev. B*, v. 62 (2000), p. 15532.
2. M. I. Baskes, K. Muralidharan, M. Stan, S. M. Valone, F. J. Cherne, *JOM* 55 (2003), p. 41.

Collective Effects in PuGa Alloys and Their Effects on Structure, Phase Stability, and Radiation Damage Mechanisms

Steven D. Conradson

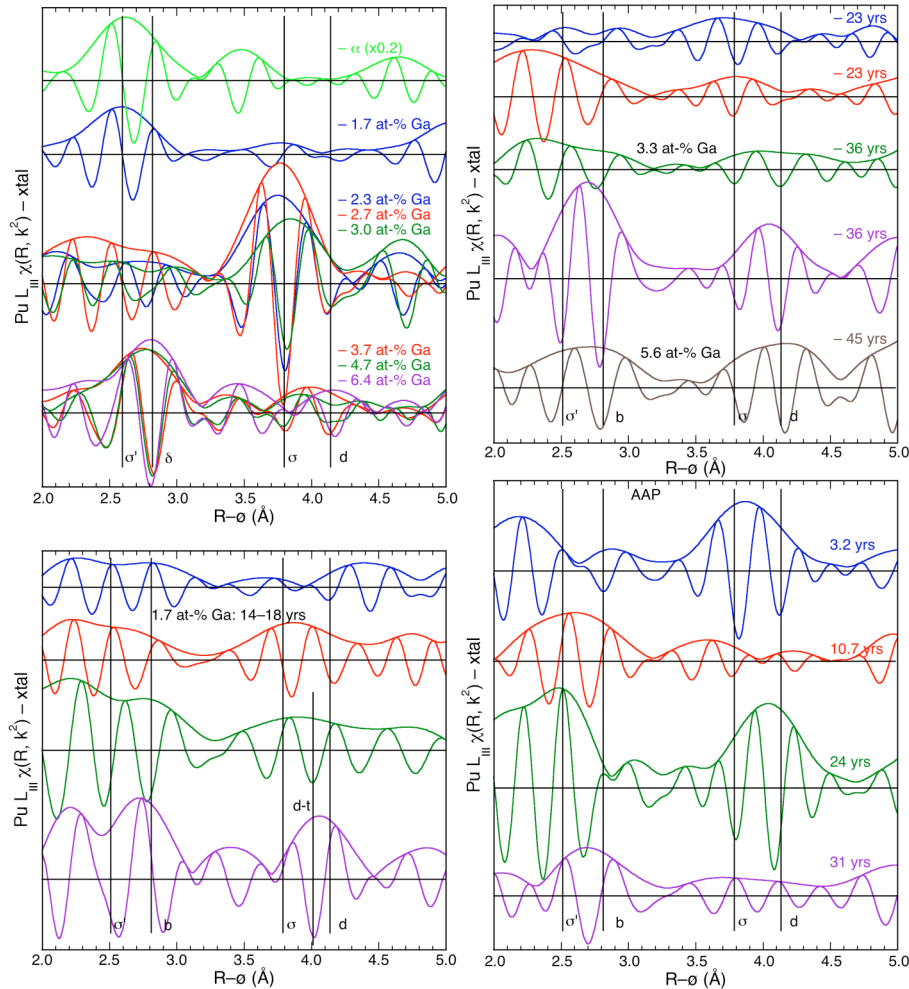
Los Alamos National Laboratory, Los Alamos NM 87544 USA

Local structure measurements, particularly the element specific information afforded by EXAFS studies at the Pu, Ga, In, Ce, and U edges, show evidence for collective behavior among these minority elements that are present at only a few atom percent and are never observed to be directly bonded in significant amounts. Certain aspects of the concentration dependence of the EXAFS are consistent with the Ga atoms being "organized" within the delta host to give a semi-ordered, quasi-intermetallic phase with a Pu:Ga ratio of around 30:1. In this the Ga atoms would have higher probabilities of being at certain distances and angles with respect to each other without being at positions specific enough to modify the diffraction pattern from that of a random solid solution with a cubic structure. However, this long-range clustering is sufficient to promote the formation of nanoscale regions that are locally depleted in Ga below the saturation limit at around 3.3 at-% Ga. If separated from the host delta lattice the up to 20% of the Pu atoms within these volumes would form alpha Pu. However, because of the tensile stress (negative pressure) and epitaxial constraints exerted by the host, it instead forms a second, ordered, novel structure called "sigma" (Fig. 1). Sigma Pu consists of a modulated, expanded Fm3m arrangement of atoms that must also contain some interstitials to retain the delta density. In addition, In- and Ce-based delta Pu alloys show analogous kinds of behavior that imply that, even when the elastic strain is minimal because the alloys atoms are close in size to Pu, there are still strong interactions between relatively distant minority atom sites that disrupt the arrangement of Pu atoms around them and also cause long range organization and clustering.

This heterogeneity and corollary nanophase separation is critical in aging, most likely accounting account for the very large (tens of percent) numbers of Pu atoms displaced from the delta lattice in aged materials. As with the sigma structure, these atoms appear to form additional types of ordered structures so that the radiation damage does not result in the Pu becoming "glassy" through decades of normal aging (Fig. 1). The radiation effects do ultimately affect phase stability however, so that causing the reversible martensitic transformation through the alpha phase that does not foster radiation damage produces some very unusual effects. These results are perhaps best explained and reconciled with other macroscopic properties in terms of describing the material with a dynamic energy landscape incorporating rehybridization induced by local composition and strain that results in multiple stable shapes for the Pu atoms and multiple structures for the nanophases.

Figure 1. Pu $\chi(R, k^2)$ residuals obtained by subtracting the curve-fit with only the δ shells of atoms from the spectra from $k=3.7-14.8 \text{ \AA}^{-1}$. Over this range a simple Pu shell will give a spectral feature in which the real component gives a minimum close to where the modulus peak is located and somewhat symmetric maxima on each side, features with a different pattern indicate more complex types of structures. The lines act as approximate guides to features

exhibited by several spectra that are associated with the σ and σ' structures, the δ structure, initial radiation damage in 1.7 at-% Ga materials (d-i) and longer duration damage in materials with higher [Ga] and AAP (d). Features below 2.5–3.0 Å that are not common to several samples are most likely low frequency residuals from incomplete background subtraction due to, e.g., a small Am edge in the spectrum or other low frequency artifacts. A spectrum of α Pu reduced in amplitude by a factor of 5 is included with the standards for comparison with the σ' feature.



Acknowledgements. This work was supported by the Heavy Element Chemistry Program, Chemical Sciences, Biosciences, and Geosciences Division, Office of Basic Energy Sciences, and the Enhanced Surveillance Campaign, National Nuclear Security Administration, U.S. Department of Energy under contract W-7405. XAFS and XRD were performed at SSRL (Stanford Linear Accelerator Center) and APS (Argonne National Laboratory), which are operated by the US Department of Energy, Office of Basic Energy Sciences. Health Physics operations at SSRL and APS were supported by the Seaborg Institute for Transactinium Science at LANL.

The Actinides – a beautiful ending of the Periodic Table

B. Johansson^{*,†}

^{*}Condensed Matter Theory Group, Department of Physics, Uppsala University, BOX 530, SE-751 21, Uppsala, Sweden

[†]Applied Materials Physics, Department of Materials Science and Engineering, Royal Institute of Technology, SE-100 44 Stockholm, Sweden



The series of heavy radioactive elements known as the actinides all have related elemental properties. However, when the volume per atom in the condensed phase is illustrated as a function of atomic number, perhaps the most dramatic anomaly in the periodic table becomes apparent. The atomic volume of americium is almost 50% larger than it is for the preceding element plutonium. For the element after americium, curium, the atomic volume is very close to that of americium. The same holds also for the next elements berkelium and californium. Accordingly from americium and onwards the actinides behave very similar to the corresponding rare-earth elements – a second lanthanide series of metallic elements can be identified. This view is strongly supported by the fact that all these elements adopt the dhcp structure, a structure typical for the lanthanides.

The reason for this behavior is found in the behavior of the 5f electrons. For the earlier actinides, up to and including plutonium, the 5f electrons form metallic states and contribute most significantly to the bonding. In Np and Pu they even dominate the bonding, while all of a sudden they become localized in Am, very much like the 4f electrons in the lanthanide series, and contribute no longer to the cohesion. This withdrawal of 5f bonding gives rise to the large volume expansion between plutonium and americium. This difference between the light and heavy actinide suggests that it would be most worthwhile to strongly compress the transplutonium elements, thereby forcing the individual 5f electron wave functions into strong contact with each other (overlap). Recently high pressure experiments have been performed for americium and curium and dramatic crystal structure changes have been observed. These results and other high pressure data will be discussed in relation to the basic electronic structure of these elements. We will also discuss some other recent high pressure data for the earlier actinides. Here it becomes important to establish to what extent standard density functional theory can account for the observed behavior.

Announcing Publication of the Third Edition of *The Chemistry of the Actinide and Transactinide Elements*


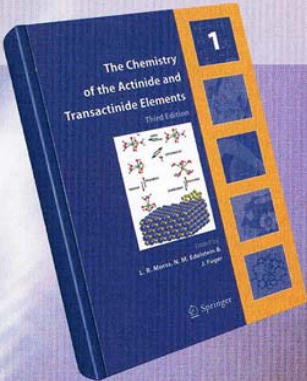
A team of international experts was invited to co-author the third edition of a classic text, *The Chemistry of the Actinide and Transactinide Elements*. Edited by Lester Morss, Norman Edelstein, and Jean Fuger, the book will be released in early 2006 by Springer Publishers. The five-volume set is critically acclaimed as the most authoritative and comprehensive compilation of the chemical properties of the actinide and transactinide elements to date and is anticipated to be the definitive work on actinides for the next twenty-five years.

The first edition of *The Chemistry of the Actinide Elements*, edited by Joseph Katz and Glenn Seaborg, was published in 1957 before the discovery of nobelium and lawrencium and the transactinide elements. The second edition of *The Chemistry of the Actinide Elements*, edited by Katz, Seaborg, and Morss, was published in 1986 by Chapman and Hall, London and New York. The third edition, containing thirty-one chapters, will include a contemporary and definitive compilation of the chemical properties of the elements from actinium (atomic number 89) to hassium (atomic number 108). Also included are authoritative review chapters on specialized topics such as thermodynamics, electronic theory, spectroscopy, magnetic properties organoactinide chemistry, coordination chemistry, solution chemistry separations science and technology, environmental science, analysis, and future element predictions. The book editors assembled teams of authors who are active practitioners and recognized experts in their specialty to write each chapter. The editors and authors have endeavored to provide a thorough, balanced, and perceptive treatment of the fascinating elements at the frontier of the Periodic Table.



Most comprehensive and definitive work in the field

- ▶ Review of actinide chemistry in the laboratory and in the environment, spectroscopic properties, thermodynamics, separations science
- ▶ Authoritative chapters on all actinide elements, transactinide elements, and speciality topics
- ▶ New chapters on emerging actinide speciality topics: X-ray spectroscopy, tracer analytical chemistry, theory



THE CHEMISTRY OF THE ACTINIDE AND TRANSACTINIDE ELEMENTS

- Chapter 1: Introduction
- Chapter 2: Actinium
- Chapter 3: Thorium
- Chapter 4: Protactinium
- Chapter 5: Uranium
- Chapter 6: Neptunium
- Chapter 7: Plutonium
- Chapter 8: Americium
- Chapter 9: Curium
- Chapter 10: Berkelium
- Chapter 11: Californium
- Chapter 12: Einsteinium
- Chapter 13: Fermium, Mendeleevium, Nobelium and Lawrencium
- Chapter 14: Transactinide Elements and Future Elements
- Chapter 15: Summary and Comparison of Properties of the Actinide and Transactinide Elements
- Chapter 16: Spectra and Electronic Structures of Free Actinide Atoms and Ions
- Chapter 17: Theoretical Studies of the Electronic Structure of Compounds of the Actinide Elements
- Chapter 18: Optical Spectra and Electronic Structure
- Chapter 19: Thermodynamic Properties of Actinides
- Chapter 20: Magnetic Properties
- Chapter 21: 5f-Electron Phenomena in the Metallic State
- Chapter 22: Actinide Structural Chemistry
- Chapter 23: Actinides in Solution: Complexation and Kinetics
- Chapter 24: Actinide Separation Science and Technology
- Chapter 25: Organoactinide Chemistry: Synthesis and Characterization
- Chapter 26: Homogeneous and Heterogeneous Catalytic Processes Promoted by Organoactinides
- Chapter 27: Identification and Speciation of Actinides in the Environment
- Chapter 28: X-ray Absorption Spectroscopy of the Actinides
- Chapter 29: Handling, Storage, and Disposition of Plutonium and Uranium
- Chapter 30: Trace Analysis of Actinides in Geological, Environmental, and Biological Matrices
- Chapter 31: Actinides in Animals and Man
- Appendix I: Nuclear Spins and Moments of the Actinides
- Appendix II: Nuclear Properties of Actinide and Transactinide Nuclides

For the complete table of contents and author listing, see the web site at:

<http://www.springeronline.com>

LA-UR-06-1234

Actinides Research Capabilities at the Lujan Neutron Scattering Center at LANSCE.

A.J. Hurd*

*Los Alamos National Laboratory, Los Alamos NM 87545 USA

NATIONAL SECURITY AND ACADEMIC RESEARCH

The Lujan Center has a new set of tools for users in neutron scattering and nuclear physics research. These tools further the Center's unique position for performing national security research including actinide science.

Since 2000, four new scattering instruments have been commissioned and three scattering instruments were substantially upgraded. For nuclear physics and nuclear chemistry, two new instruments have been built; these complement the Isotope Production Facility at LANSCE commissioned in 2004. This new suite of tools, along with user-support facilities in chemistry, x-ray scattering, and Raman scattering, plus new sample-environments in extreme pressure, magnetic fields, and temperature, provide the research community a superb environment to address both academic and national security issues.

The ability to perform research requiring special security is a key unique factor at the Lujan Center. Alliances with Theory Division, the Center for Integrated Nanotechnologies (LANL and SNL), the National High Magnetic Field Laboratory (LANL), and the Molecular Foundry (LBNL) expand the possibilities for applying unique tools to the most challenging problems.

The Lujan Neutron Scattering Center at LANSCE is funded by the Department of Energy's Office of Basic Energy Sciences and Los Alamos National Laboratory, operated by the University of California under DOE Contract W-7405-ENG-36.



Figure 1 The Lujan Center's 11-Tesla superconducting magnet has an internal sample goniometer ($\pm 15^\circ$ about the neutron beam) and wide sample

Plutonium and other *f*-Element Complexes With 'soft' Donor Ligands

Andrew J. Gaunt, Sean D. Reilly, Alejandro E. Enriquez, Brian L. Scott, Mary P. Neu

*Los Alamos National Laboratory, Los Alamos, NM 87545, USA

There are fundamental unanswered and intensely debated questions in the coordination chemistry of the early actinides (Th-Cm). For example, to what extent and generality is covalent bonding important? What are the limits of 'hard-soft' interactions? And, expressed in a way to illustrate the role of coordination chemistry in industrial processes, do relativistic effects impact *f*-element coordination chemistry such that bonding differences between An(III) and Ln(III) ions of similar ionic radii,¹ can be exploited to minimize the cost and environmental impact of waste in advanced nuclear fuel cycles? The prevailing thesis is that An(III) complexes display greater covalency than corresponding Ln(III) complexes and this difference in covalency decreases across the actinide series, and is thought to be negligible for actinides beyond Bk. However, systematic studies are needed to understand and support or dispel the thesis. Towards addressing these questions and discerning differences that may be developed into separations processes, we are preparing actinide and Ln(III) complexes with N, S, Se and Te donor ligands. We have prepared trivalent Pu, U, La and Ce complexes with $[N(EPR_2)_2]^-$ ligands (E = S, Se, Te; R = Ph, *i*Pr) allowing systematic variation of the 'softness' of the donor atom in isostructural compounds. Most directly related to the Cyanex agents that have shown great promise for An/Ln separations, low-valent *f*-element complexes with dithiophosphinates and diselenophosphinates have also been prepared. In addition, thiolates and selenolates have been synthesized by oxidation of actinide metal with dichalcogenides.

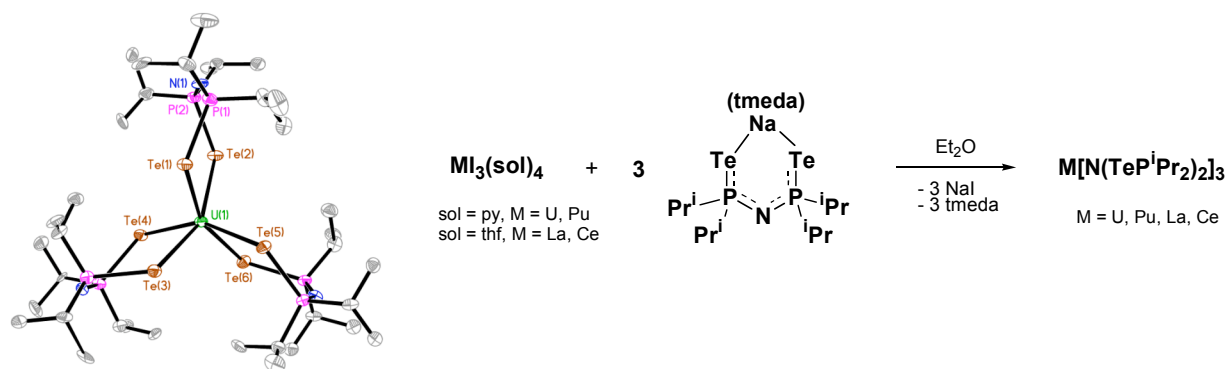


Fig. 1: ORTEP (left) and synthetic scheme (right) of trivalent *f*-element imidodiphosphinotellurido complexes.

The synthesis, structural analysis by single crystal X-ray diffraction, and traditional spectroscopic characterization (multi-nuclear NMR, IR, UV/vis/nIR) have been completed. From these studies, we find stronger bonding in U(III) 'soft' donor complexes compared to La(III), reflected by shorter U-E than La-E bonds, and that the difference is greater the 'softer' the donor atom. Collaborative studies have been initiated to more directly characterize the bonding in these molecules using X-ray spectroscopy and photoemission methods. Comparable theoretical analyses, using density functional theory, are also in progress.

References:

- 1 M. P. Jensen and A. H. Bond, J. Am. Chem. Soc. **124(33)**, 9870, (2002).

Structural Studies of Pu(VII) Under Extreme Alkaline Solution Conditions

D. L. Clark*, S. D. Conradson*, P. L. Gordon†, D. W. Keogh†, C. D. Tait†

*Los Alamos National Laboratory, Los Alamos, NM 87545

†present address: Applied Marine Technology, Inc., Virginia Beach, VA 23452

BACKGROUND

Light actinide ions (U, Np, Pu, Am, Cm) in their higher oxidation states (V) and (VI) form a unique series of linear trans dioxo ions (AnO_2^{n+} ; $n = 1, 2$) that pervade the chemistry of these elements in aqueous, nonaqueous and solid-state media. Over the last 60 years, a great deal of effort has gone into study of this inorganic functional group, and to understand its physico-chemical properties. These cations are remarkably stable, showing a high degree of covalency and chemical inertness with respect to the axial $\text{An}=\text{O}$ bonds that can be traced to the ability to use a combination of valence 5f, and 6d, and semi-core 6p atomic orbitals in chemical bonding.¹ The ability of the $6p_z$ orbital to hybridize with $5f_{z^2}$ can lead to unusually strong σ -bonding, and this type of σ -hybridization was shown to be a predominant contributor to the strong covalent bonds in linear hexavalent AnO_2^{2+} ions ($\text{An} = \text{U}, \text{Np}, \text{Pu}$).² For transuranium elements, even higher oxidation states are possible. For the heptavalent (VII) state for Np and Pu, it is known that other highly unusual, polyoxo units can form. In general, very little is known about these functional groups in comparison to the linear trans dioxo unit. In alkaline aqueous solutions between 1-10 M NaOH, An(VII) ions form unusual square planar tetra-oxo units of general formula $\text{AnO}_4(\text{OH}_2)_2^-$, and $\text{AnO}_4(\text{OH})_2^{3-}$ that have gained recent attention and study.^{3,4} At even higher alkalinity, between 10-18 M NaOH, it is thought that penta- or hexa-oxo units $\text{AnO}_5(\text{OH})^{4-}$ and AnO_6^{5-} of unknown structure can form.⁵ For plutonium, Tananaev reported that between hydroxide concentrations of 10-17 M, the Pu(VII) ion displays profound changes in the electronic absorption spectra, and the results were interpreted as evidence for the formation of either $\text{PuO}_5(\text{OH})^{4-}$ or PuO_6^{5-} .⁵ These unusual inorganic ions are exceedingly rare in actinide chemistry, and little is known about their molecular and electronic structure. The present study aims to examine the molecular structure of the Pu(VII) species formed under these extreme alkaline solution conditions.

RESULTS AND DISCUSSION

Heptavalent plutonium solutions are only stable for about 12 hours, making it impossible to prepared them in a radiological laboratory and ship them to a synchrotron facility over 1000 miles away for XAS study. Due to this inherent instability of Pu(VII) solutions, we developed an electrochemical XAFS cell for *in situ* preparation of samples based on the seminal work of Antonio and co-workers,⁶ and tested it's utility on Np(VII) under moderate hydroxide conditions. The *in situ* electrochemical cell was made of polyethylene, and consisted of working and counter compartments approximately $25 \times 10 \times 6$ mm, separated by a Nafion membrane. The working compartment held a Pt mesh electrode, a Ag/AgCl reference electrode, a magnetic stir bar, and the sample. The counter compartment contained a Pt mesh electrode with a surface area greater than that of the working electrode and an electrochemical buffer solution consisting of 0.05 M $\text{Na}_3\text{Fe}(\text{CN})_6$ in 18 M NaOH. The plutonium sample contained 0.008 M Pu(VI) and 18 M NaOH.

The high NaOH concentration was chosen to shift the Pu(VII/VI) couple below that of H₂O oxidation and inhibit O₂ generation in the cell for use at a synchrotron radiation source.

The *in situ* cell was tested using the transformation from Np(VI) to Np(VII) in 3M NaOH. Using XANES spectroscopy at the Np L_{III} edge, we observed the clear transformation of dioxo to tetraoxo forms upon oxidation of Np(VI) to Np(VII), similar to that reported by Williams and coworkers,³ and shown in Fig. 1a. We found a rather small 0.4 eV shift in the edge between Np(VI) and Np(VII) hydroxide complexes and a double “white line” peak of the tetraoxo species, as observed previously.³ These spectral changes were reversible when the electrochemical potential was changed to promote reduction of Np(VII) back to Np(VI). In these experiments the reversible oxidation, concomitant transformation to the tetraoxo geometry, the energy shift, and change in the shape of the XANES are all observed in real time (Fig. 1a), demonstrating the effectiveness of the *in situ* cell. EXAFS analysis of the resulting Np(VII) species produces four Np=O units at 1.88 Å, and two Np-OH units at 2.32 Å consistent with the formulation of NpO₄(OH)₂³⁻ (shown in 1) as reported previously.^{3,4}

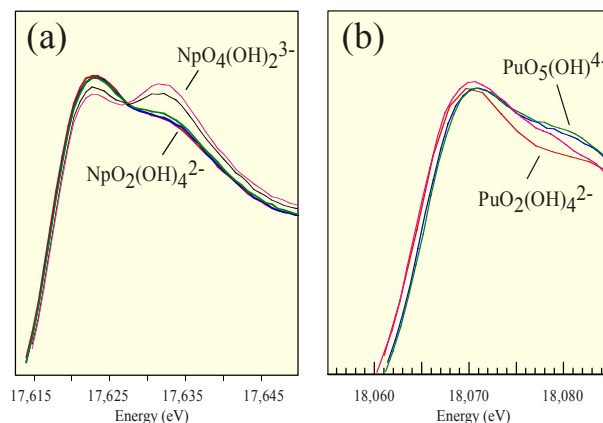
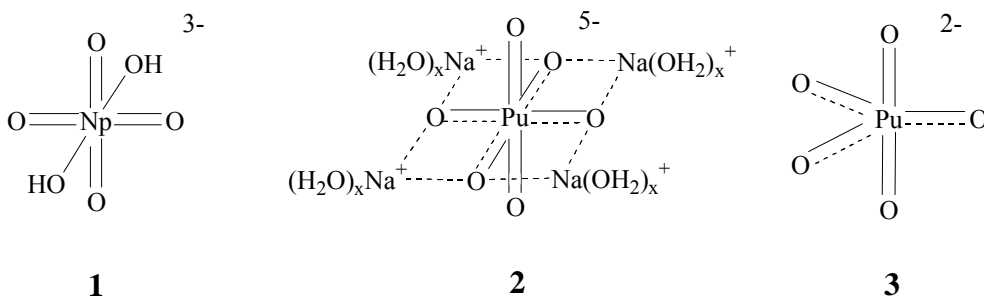


Figure 1. (a) XANES spectra of a Np solution as a function of electrolysis time, showing the reversible transformation from dioxo Np(VI) to tetraoxo Np(VII). (b) XANES spectra showing the reversible transformation of Pu(VI) to Pu(VII) in 18 M NaOH.

the shape of the XANES are all observed in real time (Fig. 1a), demonstrating the effectiveness of the *in situ* cell. EXAFS analysis of the resulting Np(VII) species produces four Np=O units at 1.88 Å, and two Np-OH units at 2.32 Å consistent with the formulation of NpO₄(OH)₂³⁻ (shown in 1) as reported previously.^{3,4}



Using the same cell setup, we recorded Pu L_{III} XANES spectra during the oxidation of Pu(VI) to Pu(VII) in highly concentrated 18 M NaOH in search of evidence for either PuO₅(OH)⁴⁻ or PuO₆⁵⁻ as shown in Fig. 1b. A 1.0 eV edge energy shift was observed similar what we found in Np(VII), yet the characteristic double “white line” and first EXAFS oscillation (Fig. 1a) did not develop as for the Np(VII) series. EXAFS data analysis for the Pu(VII) species under these highly alkaline conditions indicate that the two inner shells of Pu-O bonds are both contracted, in contrast to NpO₄(OH)₂³⁻ (1) where both shells lengthened relative to the Np(VI) starting compound. For Pu(VII) under these extreme alkaline conditions, EXAFS analysis reveals two O atoms at 1.83 Å, and 4 O atoms at 2.29 Å, thus the ion is clearly not the tetraoxo PuO₄(OH)₂³⁻ ion, consistent with Tananaev’s proposal for a species of formulation PuO₅(OH)⁴⁻ or PuO₆⁵⁻ under these conditions. In interpreting our data, we recognize that 18M NaOH is

essentially NaOH·2H₂O, and therefore there is no free water in the “solution”. Therefore, even the Na ions must be highly coordinatively unsaturated. We postulate therefore, that under these conditions, a PuO₅(OH)⁴⁻ or PuO₆⁵⁻ ion is likely to have interactions with Na ions, and we propose the structural motif indicated in **2**. At first the result of a trans dioxo unit seems puzzling, but we note that Straka and coworkers recently reported DFT calculations on the related hypothetical octavalent PuO₅²⁻ ion, and found, remarkably, that the most stable configuration is to convert back to a trigonal bipyramidal trans dioxo form as shown in **3**,⁷ with calculated axial and equatorial Pu-O bond lengths of 1.84 and 1.95 Å, respectively. Experimental details and interpretation of data leading to these conclusions will be discussed.

Acknowledgements. All experimental measurements were performed at the Stanford Synchrotron Radiation Laboratory, a national user facility operated by Stanford University on behalf of the U.S. Department of Energy, Office of Basic Energy Sciences. Health Physics support was provided by the G. T. Seaborg Institute for Transactinium Science at Los Alamos. This work was supported by the Division of Chemical Sciences, Geosciences, and Biosciences, Office of Basic Energy Research, U.S. Department of Energy under Contract W-7405.

REFERENCES

- (1) Denning, R. G. *Structure and Bonding (Berlin, Germany)* **1992**, 79, 215-276.
- (2) Denning, R. G.; Green, J. C.; Hutchings, T. E.; Dallera, C.; Tagliaferri, A.; Giarda, K.; Brookes, N. B.; Braicovich, L. *Journal of Chemical Physics* **2002**, 117, 8008-8020.
- (3) Williams, C. W.; Blaudeau, J. P.; Sullivan, J. C.; Antonio, M. R.; Bursten, B.; Soderholm, L. *J. Am. Chem. Soc.* **2001**, 123, 4346-4347.
- (4) Bolvin, H.; Wahlgren, U.; Moll, H.; Reich, T.; Geipel, G.; Fanghaenel, T.; Grenthe, I. *Journal of Physical Chemistry A* **2001**, 105, 11441-11445.
- (5) Tananaev, I. G.; Rozov, S. P.; Mironov, V. S. *Radiokhimiya* **1992**, 34, 88-92.
- (6) Antonio, M. R.; Soderholm, L.; Williams, C. W.; Blaudeau, J.-P.; Bursten, B. E. *Radiochim. Acta* **2001**, 89, 17-25.
- (7) Straka, M.; Dyllal, K. G.; Pyykko, P. *Theoretical Chemistry Accounts* **2001**, 106, 393-403.

Quantum Mechanical studies of the Cation Cation interaction.

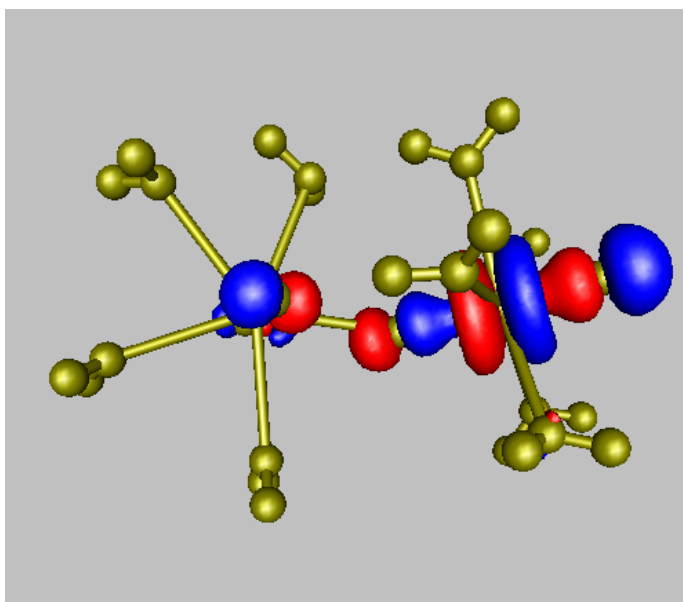
H.M. Steele, R.J. Taylor and M Sarsfield.

Nexia Solutions, Hinton House, Warrington WA3 5AS

INTRODUCTION

The tendency for pentavalent actinides to form so-called cation cation (CC) complexes is clearly a ubiquitous feature of actinyl chemistry and although first reported by Sullivan¹ in the 1960's their potential role within separation processes is still not fully quantified. There is now substantial evidence, including crystal structures of solid Np(V) compounds, that a CC complex contains at least one actinyl molecule acting as a ligand through its actinyl oxygens to another 'active cation', which can be either another actinyl or other positively charged metals.

Experimentally, the presence of a CC complex is typically characterized by short An-An separations and considerable change in the UV and IR spectra's of the actinyl group. The ability of the CC complex to perturb the IR and UV spectra, the dominance of Np CC complexes with respect to U and Pu actinides, the type of 'bonding' which exists within the CC complex and the roles played by ligands and solvation, are still not fully understood². We have used quantum mechanical (QM) approach to start to address some of these key questions.



COMPUTATIONAL APPROACH

Initial atomic co-ordinates were taken from experimentally determined crystal structures and optimised.^{3,4} The affects of interchanging actinide species in both donator and acceptor sites, altering the actinide oxidation state between V and VI, changing the complexing ligands, adjusting the electronic structure of the actinyl species and changing the dielectric of the solvation were all studied. All calculations were performed using Gaussian '03 employing the Hartree-Fock, Moller-Plesset and Density Functional levels of theory, relativistic pseudopotentials and a range of basis sets were employed.

KEY OBSERVATIONS

By following the orbital occupancy, it was shown that when the actinyl acts as a ligand its symmetry is reduced from $D_{\infty h}$ to C_{v} . This leads to orbital rearrangement which enables the oxygen on the actinyl donor molecule to carry significantly more electron density than usual for actinyl oxygen atoms, this is shown in the figure above. A much stronger electrostatic interaction can then occur between the donor actinyl oxygen and the cation centre. Further, the strength of the CC interaction is specific to the actinides involved, their oxidation state and whether they occupy the donor or acceptor sites.

From our calculations of the vibrational frequencies we obtained similar values for the asymmetric stretching vibrations to those observed experimentally. It is well known that CC complexation causes shifts in $O=An=O$ vibrational frequencies compared to those normally expected for the actinyl group². However, the calculations also showed that each of these lower energy bands has a higher energy partner. Hence we conclude that this is not a shift in the vibrational frequency as usually suggested but a splitting due to the broken symmetry of the actinyl group.

Finally, the affect of altering the solvent surrounding the CC complex was studied and initial calculations have shown that increasing the solvent dielectric constant decreased the stability of the CC complex.

Acknowledgements. The Nuclear Decommissioning Authority for funding.

- 1 J.C. Sullivan, *et al.*, J. Am. Chem. Soc. **82**, 5288, (1960).
- 2 N.N. Krot and M.S. Grigoriev Russ. Chem. Rev. **73**, 89, (2004).
- 3 M.S. Grigoriev, *et al.*, Radiokhimiya **37**, 15, (1995).
- 4 M.S. Grigoriev, *et al.*, Radiokhimiya **33**, 46, (1991).

Heteropolyanion Ligand Sensitised Uranyl Luminescence

Caytie Talbot-Eeckelaers, Simon Pope and Iain May*

*Centre for Radiochemistry Research, School of Chemistry,
University of Manchester, Oxford Road, Manchester, M13 9PL, UK

INTRODUCTION

A systematic analysis of the photophysical properties of uranyl containing tri-lacunary heteropolyanions (HPA) is presented. HPA stimulated emission of lanthanide and actinide complexes, is well documented, as is the emissive nature of the uranyl moiety.¹⁻⁴ However, no studies to date have explored the photophysics of uranyl complexed HPAs. We report the effects of heteroatom, cluster type, counter-cation, solvent and concentration on the lifetime, intensity, excitation and emission wavelengths observed for these clusters in solution.

Both A- and B-type tri-lacunary heteropolyanion ligands (of general formula $[A-X^mW_9O_{34}]^{n-}$, $X = As^V, P^V, Ge^{IV}, Si^{IV}$; $n = m - 14$ or $[B-Y^pW_9O_{33}]^{q-}$, $Y = As^{III}, Bi^{III}, Sb^{III}$ and Te^{IV} ; $q = p - 12$) are observed to sequester $\{UO_2\}^{2+}$ ions forming 2:2 sandwich clusters in solution and in the solid state.⁵⁻⁸ Complexes with A-type ligands, such as the $[(UO_2)_2Na_2(A-PW_9O_{34})_2]^{12-}$ anion form closed-type structures containing encapsulated Na^+ ions (Fig. 1).⁵ B-type ligands are unable to form this type of complex due to the presence of a lone-pair of electrons located on the heteroatom and form an open-type structure such as observed in $[(UO_2)_2(H_2O)_2(B-SbW_9O_{33})_2]^{16-}$ (Fig.2).⁸

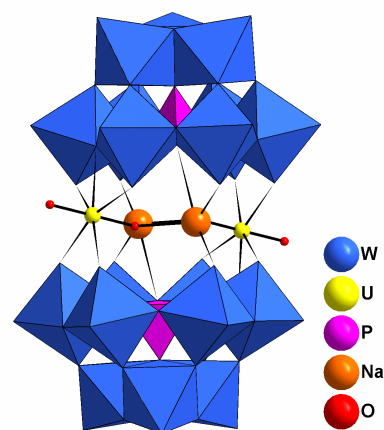


Fig. 1: Polyhedral representation of the $[(UO_2)_2Na_2(A-PW_9O_{34})_2]^{12-}$ anion

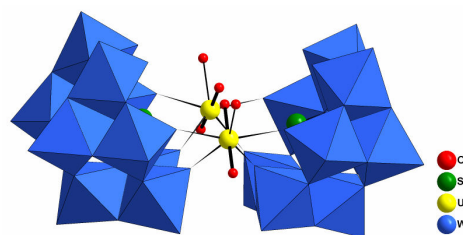


Fig. 2: Polyhedral representation of the $[(UO_2)_2(H_2O)_2(B-SbW_9O_{33})_2]^{16-}$ anion

RESULTS

Emission from tri-lacunary heteropolyoxotungstate uranyl complexes is observed between 500 and 600 nm, the typical region for uranyl complexes (Fig. 3). The corresponding excitation wavelengths show two bands, at ~ 350 nm and ~ 440 nm. The former relates to the $O \rightarrow W$ LMCT and the latter to the $O \rightarrow U$ LMCT in the absorption spectra. Variation in heteroatom, for a given complex type, leads to subtle differences in excitation frequency. Luminescence life-times

(ranging from 0.05 ms to 0.5 ms) and degree of vibronic fine structure are similarly determined by choice of heteroatom and ionic strength of the solution.

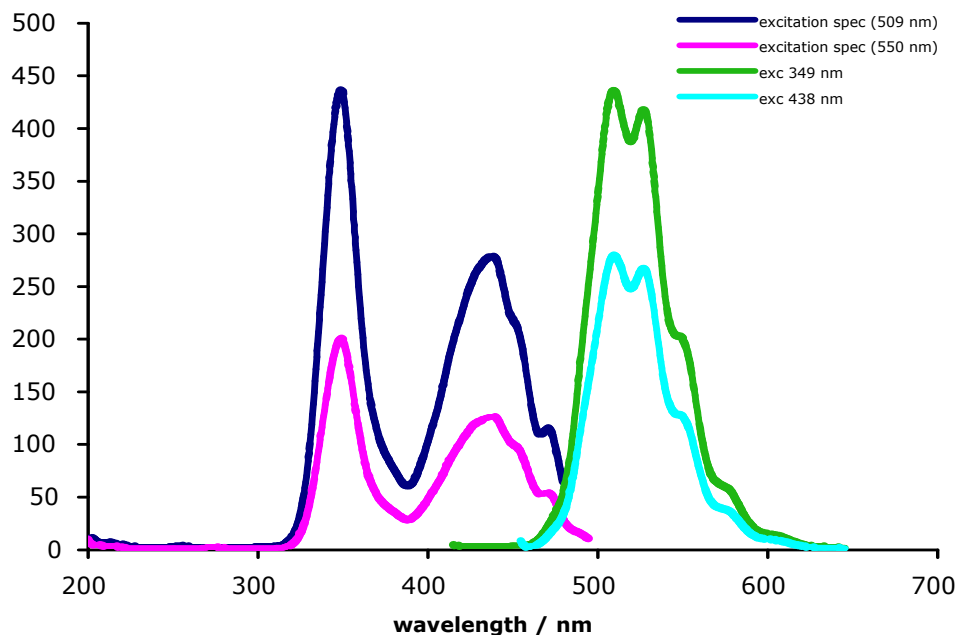


Fig. 3: Excitation and emission spectra of the $[(\text{UO}_2)_2\text{Na}_2(\text{A-PW}_9\text{O}_{34})_2]^{12-}$ anion in 1M NaCl

References

- 1 T. Yamase, H. Naruke, and Y. Sasaki, *J. Chem. Soc., Dalton Trans*, (1990), 1687.
- 2 A. B. Yusov and V.P. Shilov, *Radiochemistry*, **41**, (1999), 3.
- 3 S. Lis and S. But, *J. Alloys and Compounds*, **300-301**, (2000), 370.
- 4 S. Lis, S. But, R. Van Deun, T. N. Parac-Vogt, C. Görrler-Walrand, K. Binnemans, *Spectrochimica Acta Part A*, **62**, (2005), 478.
- 5 K. C. Kim and M. T. Pope, *J. Am. Chem. Soc.*, **121**, (1999), 8512.
- 6 K. C. Kim, A. J. Gaunt and M. T. Pope, *J. Cluster. Sci.*, **13**, (2002), 423.
- 7 A. J. Gaunt, I. May, R. Copping, A. I. Bhatt, D. Collison, O. D. Fox, T. Holman and M. T. Pope, *Dalton Trans*, (2003), 3009.
- 8 Roy Copping, PhD thesis, University of Manchester, 2006

Uranium complexes with newly designed tetraketones for active materials of redox flow battery

K. Shirasaki, T. Yamamura, S. Ohta, Y. Shiokawa

Institute for Materials Research, Tohoku University, Sendai, Miyagi 980-8577, Japan

The light actinide such as uranium and neptunium are known to show two couples of reversible or quasi-reversible electrode reactions as seen in Np(III)/Np(IV) and Np(V)/Np(VI) [1]. By utilizing these two couples of fast reactions suppressing the overvoltage at electrodes, a redox-flow battery using the light actinide as an active material with the high efficiency has been proposed [2]. Though redox flow batteries benefit the battery for the electric power storage, the energy efficiency of the existing battery with vanadium ions for positive and negative electrolytes is rather high [3]. However, because of the slow kinetics especially for the positive reaction ($\text{VO}^{2+}/\text{VO}_2^+$), the large reaction overvoltage lowers the energy efficiency.

Active materials of the uranium battery require several conditions to be satisfied for the high-energy efficiency. At the first, the materials for both positive and negative electrolytes should dissolve in an aprotic solution at a high concentration, in order to avoid the disproportionation reaction of U(V) from degrading to U(IV) and U(VI) in the presence of the proton [4, 5]. Since uranium β -diketone complexes show relatively high solubility in the aprotic solution, they have been investigated for the active material [6]. Recently, we reported that a quantitative electrolysis of the dimethyl sulfoxide (DMSO) solution of U(VI) to give the U(V) solution which was relatively stable as the half-life of 2 days at 16°C [7, 8]. In the course of the electrochemical investigation of U(VI) and U(IV) β -diketones, both complexes were found to display the ligand dissociation and association reactions during the electrode reactions as



where D^- denotes the β -diketone ligands. These side reactions would be originated from the instability of U(V) and U(III) complexes compared with U(IV) and U(VI) complexes, respectively, and this consideration agrees with the general tendency of the stability of uranium complexes; $\text{U(IV)} > \text{U(VI)} > \text{U(III)} > \text{U(V)}$. With an aim in the development of the high-energy efficiency battery, these side reactions are not desired because of the rearrangement makes the kinetics slower and also the change in the redox potential results in the energy loss [6]. The simple redox reaction without these side reactions would be realized by stabilizing the U(V) and U(III) complexes by using long-chained or macrocyclic ligands, which utilizes the entropy effect as can be seen in crown ethers capable of complexation even with alkaline metal ions. Previous study, two tetraketones with two units of acetylacetonate ligand in their molecule,

8-oxo-2,4,12,14-teraoxapentadecane (**1**; keto-form in Fig. 1) and *m*-bis(2,4-dioxo-1-pentyl)benzene (**2**; keto-form in Fig. 1) were synthesized [9]. Detailed NMR measurements were conducted to reveal the keto-enol tautomerism of the tetraketones in CDCl₃ and titration measurements were carried out in water-dioxane (1:1 (v/v)) solutions to evaluate formation constants with metal ions at III-VI valences. Although the first acid dissociation constants for **1** and **2** were close to that for the acetylacetonone, the formation constants of them at large coordination numbers are larger than those of acetylacetonone. On the basis of these formation constants, the thermodynamic distributions of tetraketone complexes are evaluated in the solution to

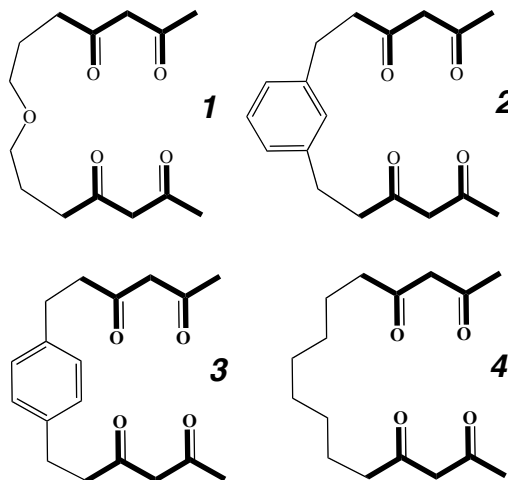


Fig 1: Tetraketone ligands prepared according to A.H. Alberts and D.J. Cram (**1**, **2**) and newly designed (**3**, **4**)

demonstrate that the change in the coordination number is not expected during the redox reactions contrary to the case of the acetylacetonone. Recently, we observed dimer formation with uranyl(VI) was observed for **2** in single crystal x-ray crystallography. This could mean that cavity radius of these ligands (**1** and **2**) is larger than ionic radius of uranium and it is not desirable for active materials of the battery.

In the present study, new tetraketones, *m*-bis(3,5-dioxohexyl)benzene (**3**; keto-form in Fig. 1) and 1,6-bis(2,4-dioxo-1-hexyl)hexane (**4**; keto-form in Fig. 1), which is expected to form monomer complex with uranium, were synthesized. Uranium(V) and uranium(III) complexes with these new tetraketones were characterized by electrode reaction and also by electrolytic reduction.

We would like to thank Prof. Y. Nakamura of Tokyo Institute of Technology for his kind measurements.

- [1] T. Yamamura, N. Watanabe, T. Yano, Y. Shiokawa, *J. Electrochem. Soc.*, 152 (2005) A830.
- [2] Y. Shiokawa, H. Yamana, H. Moriyama, *J. Nucl. Sci. Tech.*, 37 (2000) 253.
- [3] M. Skylas-Kazacos, M. Rychcik, R.G. Robins, A.G. Fane, M.A. Green, *J. Electrochem. Soc.*, 133 (1986) 1057.
- [4] G. Gritzner, J. Selbin, *J. Inorg. Nucl. Chem.*, 30 (1968) 1799.
- [5] A. Ekstrom, *Inorg. Chem.*, 13 (1974) 2237.
- [6] T. Yamamura, Y. Shiokawa, H. Yamana, H. Moriyama, *Electrochim. Acta*, 48 (2002) 43.
- [7] K. Shirasaki, T. Yamamura, Y. Shiokawa, *J. Alloys Compds.*, 408-412C (2006) 1296.
- [8] K. Shirasaki, T. Yamamura, Y. Monden, Y. Shiokawa, *Royal Soc. Chem.*, (in press).
- [9] A.H. Alberts, D.J. Cram, *J. Am. Chem. Soc.*, 99 (1977) 3880.

Studies of Gluconate Complexation with U(VI) and Np(V) In Acidic to Neutral Solutions

Z. Zhang,^{a,b} S. B. Clark,^a G. Tian,^b L. Rao^b

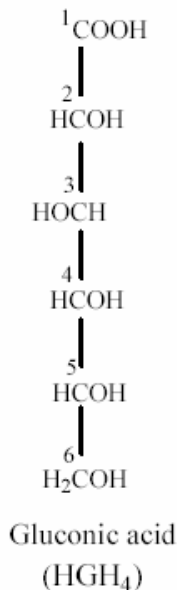
a. Washington State University, Pullman, WA 99164

b. Lawrence Berkeley National Lab, Berkeley, CA 94720

INTRODUCTION

The complexation of actinide cations by gluconate is of interest due to their existence in the Hanford high-level radioactive waste tanks. Gluconic acid, a polyhydroxycarboxylic ligand, has strong complexation ability with metal cations.¹ To develop effective treatment strategies for high-level radioactive wastes, the interaction of gluconate with actinides must be understood.

While this ligand has been investigated for many years, the majority of the studies have been focused on systems involving transition metals, with very few reports relating to complexation with lanthanides and actinides.^{2,3} Furthermore, molecular-level interactions between actinide cations and gluconate are not well defined. In this work, multiple techniques have been used to study the complexation of gluconate with U(VI) and Np(V) as dioxo cations, e.g. $\text{Np}^{\text{V}}\text{O}_2^+$ and $\text{U}^{\text{VI}}\text{O}_2^{2+}$ in acidic to neutral solutions. The uranyl and neptunyl cations serve as analogs for the $\text{Pu}^{\text{V}}\text{O}_2^+$ and $\text{Pu}^{\text{VI}}\text{O}_2^{2+}$ cations, respectively.



COMPLEXATION WITH NEPTUNYL

The thermodynamic parameters of gluconate complexation with NpO_2^+ have been measured by spectrophotometric titrations and calorimetry under the conditions: $t = 25\text{ }^\circ\text{C}$, $I = 1.0\text{ M}$ and $pH \sim 6.0$.⁴ As indicated in Figure 1 (next page), near-IR data collected during titrations of the Np(V) cation with gluconate yield two species, NpO_2GH_4 and $\text{NpO}_2(\text{GH}_4)_2^-$. The formation constants and enthalpies of complexation are: $\log \beta_1 = (1.48 \pm 0.03)$ and $\Delta H_1 = -(7.42 \pm 0.13)\text{ kJ}\cdot\text{mol}^{-1}$ for $\text{NpO}_2(\text{GH}_4)$, $\log \beta_2 = (2.14 \pm 0.09)$ and $\Delta H_2 = -(12.08 \pm 0.45)\text{ kJ}\cdot\text{mol}^{-1}$ for $\text{NpO}_2(\text{GH}_4)_2^-$. Comparison of those parameters to the thermodynamic data for complexation of NpO_2^+ with other carboxylic ligands, it is observed that gluconic acid, like α -hydroxycarboxylic acids, forms stronger complexes than simple monocarboxylic acids. It is therefore suggested that α -hydroxyl group of the gluconate probably participates in coordination to the NpO_2^+ cation. Analysis of extended x-ray absorption fine structure (EXAFS) state also supports this observation.

COMPLEXATION WITH URANYL

For the uranyl-gluconate system, we have used potentiometry and calorimetry to measure the thermodynamic properties under the conditions: $t = 25\text{ }^\circ\text{C}$, $I = 1.0\text{ M}$ and $pH\ 2.0 - 3.5$. In this case, ^{13}C NMR was employed to determine coordination sites for the uranyl cation to the gluconate ligand (Figure 2). With addition of uranyl into gluconate solutions, significant line

broadening of the peaks corresponding to the first (data not shown) and second carbons of the gluconate indicates that both the carboxylic group and α -hydroxyl group most probably take part in complexation. In combination with the structural information obtained by ^{13}C NMR, the structural characteristics of those complexes has been analyzed by EXAFS.

SUMMARY

In this presentation, our results will be described and discussed in terms of the impact of effective cationic charge on the metal cation and steric effects for the ligand and the dioxo cations. Comparison to other systems of similar ligands will also be made.

Acknowledgements: This work was supported by U.S. DOE's Environmental Management Science Program at Washington State University and by the Director, Office of Science, Office of Basic Energy Sciences, U. S. Department of Energy, at Lawrence Berkeley National Laboratory.

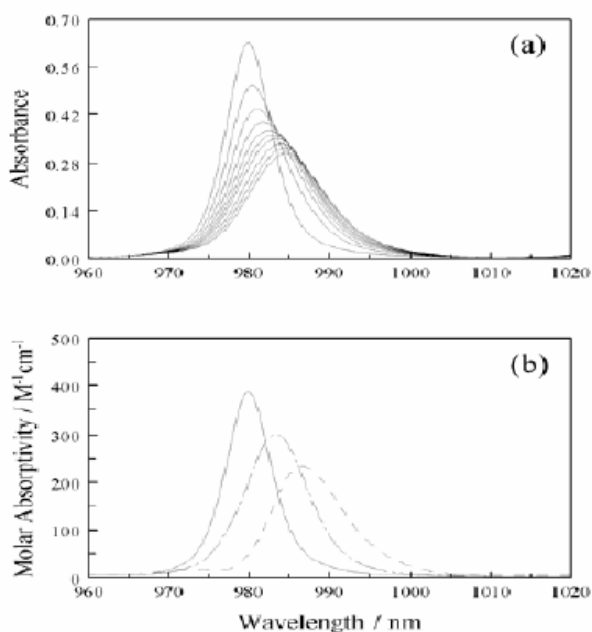


Fig 1: Spectrophotometric titration of Neptunyl – gluconate. $t = 25^\circ\text{C}$, $I = 1.0 \text{ M}$, $\text{pH} \sim 6.0$. (a) Raw spectra for one titration. (b) Resolved molar absorptivity spectra of Np(V) species: NpO_2^+ (solid line), $\text{NpO}_2\text{GH}_4(\text{aq})$ (dotted-dash), $\text{NpO}_2(\text{GH}_4)_2^-$ (dash)

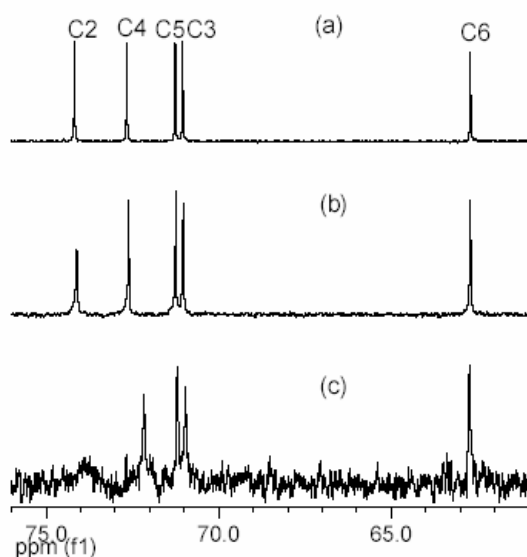


Fig 2: ^{13}C NMR of uranyl – gluconate. $t = 22^\circ\text{C}$, $[\text{NaGH}_4]_0 = 25 \text{ mM}$. (a) $\text{U}/\text{NaGH}_4 = 0/25$, $\text{pH} = 6.0$; (b) $\text{U}/\text{NaGH}_4 = 1/25$, $\text{pH} = 4.0$; (c) $\text{U}/\text{NaGH}_4 = 8/25$, $\text{pH} = 3.2$.

1. D. T. Sawyer, Chem. Rev. **64**, 633 (1964)
2. S. Giroux, P. Rubini, B. Henry, S. Aury, Polyhedron, **19**, 1567 (2000).
3. D. T. Sawyer, R. J.Kula, Inorg. Chem. **1**, 303 (1962).
4. Z. Zhang, et al., accepted in: Radiochim. Acta, (2005).

**ENVIRONMENTAL CONSIDERATIONS IN THE WEST SINAI AND
ROSSETTA BEACH ON THE MEDITERRANEAN**

Dr.ASHRAF EL SAYED MOHAMED MOHAMED

ENS/IMANUF/GNS.

**SOUF SHAMAA-TALON-STREET#1-HOUSE#28-ALEXANDRIA,21351-
EGYPT.**

amohamed@loftmail.com

amohamed@hushmail.com

ABSTRACT

**THE NUCLEAR MATERIALS AUTHORITY IS TAKING OVER THE
RESPONSIBILITY FOR EXPLOITATION OF
THE BLACK SAND DEPOSITS AT THE ROSSETTA BEACH ON THE
MEDITERRANEAN COAST AND AT THE
WEST SINAI AREA WHERE THE REMAINING PROSPECTING DRILL
HOLES OFFER SUITABLE SITES FOR HYDROGEOLOGICAL AND
GEOCHEMICAL STUDIES.THESE DEPOSITS CONTAIN
MONAZITE,ZIRCON AND RUTILE AS WELL AS ILMENITE AND
MAGNETITE.A RESEARCH PROGRAMME ON RADIONUCLIDE
TRANSPORT ANALOGY CONTINUES IN THE SURROUNDINGS OF THE
ROSSETTA AND WEST SINAI DEPOSIT. IN THIS PAPER WE
DETERMINE AND STUDY THE PROCEDURES THAT UNDERTAKE AT
THE SITES.ALSO,WE ,AS INDEPENDANT SPECIALISTS,WILL
DESCRIBE THE GOVERNMENTAL POLICY OF THE
NUCLEAR WASTE AND OUR FEARS.**

Plutonium Uptake by Brucite and Periclase

J. D. Farr^{*}, M. P. Neu^{*}, Roland K. Schulze and B. D. Honeyman[†]

^{*}Los Alamos National Laboratory, Los Alamos, NM 87545 USA

[†]Colorado School of Mines, Golden, CO 80401 USA

Batch adsorption experiments and spectroscopic investigations consistently show that aqueous Pu(IV) is quickly removed from solution and becomes incorporated in a brucite or hydroxylated MgO surface to a depth of at least 50 nm, primarily as Pu(IV) within a pH range of 8.5 to 12.5. This adsorption behavior is unaffected by the presence of the organic ligand, citrate.^[1]

Further studies on colloidal brucite, natural crystalline brucite and MgO crystals that were exposed for longer times (70 hours) to solutions containing Pu(IV) confirmed the presence of subsurface Pu and demonstrated a continuation of the Pu uptake behavior previously observed. X-ray photoelectron spectroscopy (XPS), x-ray absorption fine structure (XAFS), Rutherford backscattering spectroscopy (RBS) and x-ray diffraction (XRD) were used to estimate Pu penetration depth and provide information about its chemical state.

Periclase (MgO) and brucite (Mg(OH)₂) are not commonly used as substrates in batch adsorption experiments because they dissolve readily and are highly basic. A large body of research involving metal adsorption from solution has been performed on less soluble oxides such as silica or hematite. At first, it was not clear to us how plutonium could be removed from solution by a substrate that so rapidly dissolves. Another mystery was how Pu got so deep in the crystal so rapidly. The 50 nm penetration depth of Pu in such a short time precludes solid state diffusion as a mechanism.

The initial adsorption of Pu(IV) is expected to occur rapidly due the easy availability of sorption sites on the hydroxylated MgO and brucite surfaces. In most systems, sorption of cations will commence at the pH of initial hydrolysis. The first hydrolysis constant for Pu+4 is 0.6^[2], so hydrolysis and adsorption occur below pH 1. Under the solution conditions of these experiments, Pu will exist primarily as the neutral tetra hydroxide.^[2] The MgO and brucite

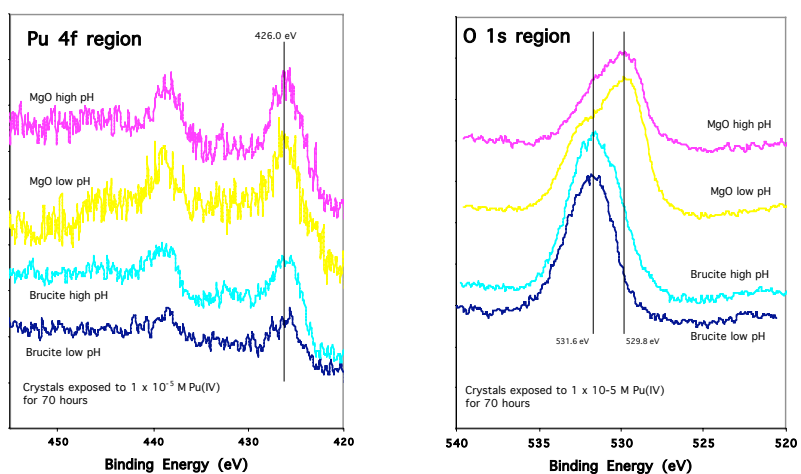


Fig. 1. XPS spectra for Pu 4f and O 1s regions of the MgO and brucite crystals that were exposed to 1×10^{-5} M Pu(IV) for 70 hours. Pu intensities are less than those seen for crystals exposed for only 7 hours, but alpha activity is much greater, indicating more subsurface Pu oxides and hydroxides.

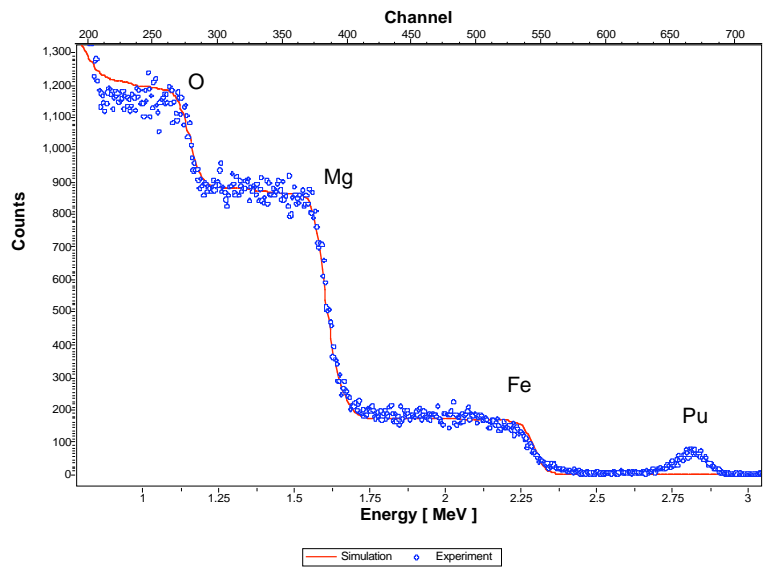


Fig. 2. Rutherford backscattering spectroscopy. Pu was detected 60 – 100 nm below the surface of the hydroxylated MgO(100) crystal. The sample holder is the source of the Fe signal.

surfaces will be hydroxylated and have a hydration layer that extends from the solid into the solution. MgO dissolution is believed to occur by first converting to brucite^[3, 4]. A flocculent, gel-like adherent film was observed on MgO crystals that were exposed to water for several months at a time. The observed film is assumed to be composed of disordered and extended polynuclear Mg oxide and hydroxide moieties and water, much like a gel. This film was not observed on MgO crystals that were exposed to water for shorter periods, or even the crystals that were exposed for 70 hours, but it was likely still forming and had not yet become visible. After dehydration, the hydroxylated surface layer is at least 50 Å thick

on the MgO crystals exposed to water for 7 hours, according to the XPS and RBS data. The thickness of the hydroxylated layers on crystals exposed for longer periods is expected to be greater.

Pu(IV) will diffuse through the gel-like layer and may become incorporated in the active crystal surface. Pu hydroxides are much less soluble than Mg hydroxides so remain with the solid. Upon dehydration the gel-like layer re-solidifies with the incorporated Pu.

The research presented here strengthens the technical basis for our stewardship of actinide materials, particularly Pu oxide or materials contaminated with Pu. These investigations directly support TRU waste disposal practices at the WIPP and enhance our ability to predict Pu behaviour in other environmental settings. Pu ions adsorbed from water on brucite and hydroxylated MgO form compounds on the surface that share many of the same spectral features that have been observed on water-exposed Pu oxide^[5], suggesting that Pu adsorbed on mineral surfaces will behave similarly.

RBS analysis was provided by Chris Wetteland and Yongqiang Wang of LANL. XANES data is courtesy of Jeff Terry.

1. Farr, J.D., R.K. Schulze, and B.D. Honeyman, *Radiochimica Acta*, 2000. **88**(9-11): p. 675-679.
2. Runde, W., et al., *Applied Geochemistry*, 2002. **17**(6): p. 837-853.
3. Wogelius, R.A., et al., *Geochimica et Cosmochimica Acta*, 1995. **59**(9): p. 1875-1881.
4. Jordan, G., S. Higgins, and C. Eggleston, *American Mineralogist*, 1999. **84**(1-2): p. 144-151.
5. Farr, J.D., R.K. Schulze, and M.P. Neu, *Journal of Nuclear Materials*, 2004. **328**(2-3): p. pp. 124-136

Actinide Interactions with Iron Oxide/Oxyhydroxide

S. A. Stout, E. Bauer, S.D. Reilly, P. Lichtner, J. D. Farr, and M. P. Neu

Los Alamos National Laboratory, Los Alamos, NM 87544

INTRODUCTION

Actinides (An) are commonly found as contaminants at sites performing nuclear material production, processing, and storage. The fate and transport of these radionuclides is largely controlled by interactions occurring at the solid-solution interface of vadose zone minerals. Thermodynamic adsorption data is needed to accurately model behavior and to produce reliable risk assessments. Adsorption experiments were conducted to determine the affect of pH (2–10) and concentration (10^{-6} – 10^{-4} M An) on the adsorption of U(VI), Np(V), and Pu(VI) onto hematite (Fe_2O_3) and goethite (FeOOH). Spectroscopic data show that Pu(VI) was reduced in solution to Pu(V) by goethite, while no reduction of Np(V) was observed.

RESULTS

Hematite and goethite have very similar binding sites and points of zero charge (PZC); therefore, it is not unexpected that the actinide adsorption isotherms for a given actinide have very similar pH-dependence and edge positions. Although the surface areas of the mineral

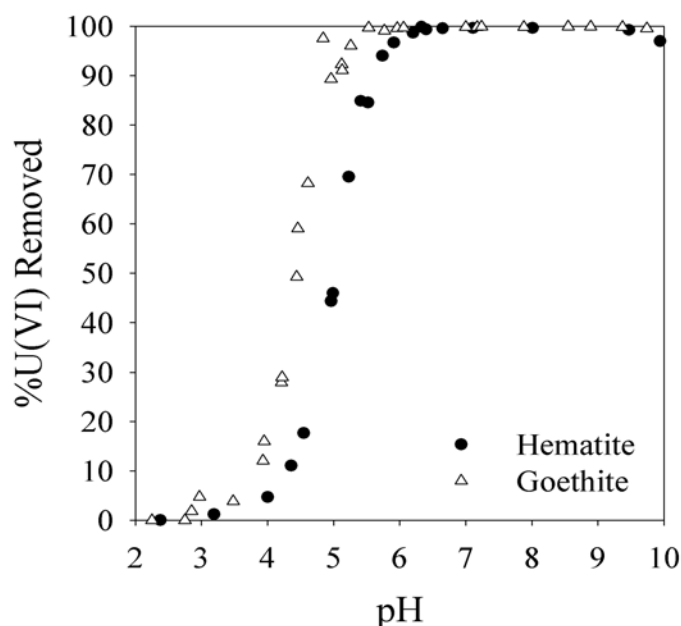


Figure 1. pH-dependent adsorption of U(VI) onto Fe_2O_3 and FeOOH . $[\text{U(VI)}]_{\text{initial}} = 10^{-6}$ M.

suspensions were normalized, the adsorption edges for like actinides were not identical. The adsorption edges for actinides reacted with goethite occurred at slightly lower pH than those reacted with hematite under similar concentrations. Figure 1 shows the pH-dependent adsorption isotherm for U(VI) adsorption onto the iron minerals after a 24 h reaction time. Decreasing the initial concentration of actinide reacted with the mineral phases also decreased the pH where the adsorption edge occurred. Figure 2a shows the adsorption of U(VI), Np(V), and Pu(VI) onto goethite. The shape and position of the Pu adsorption edge was more similar to that of the Np(V) than to U(VI) suggesting that the Pu was bound as Pu(V).

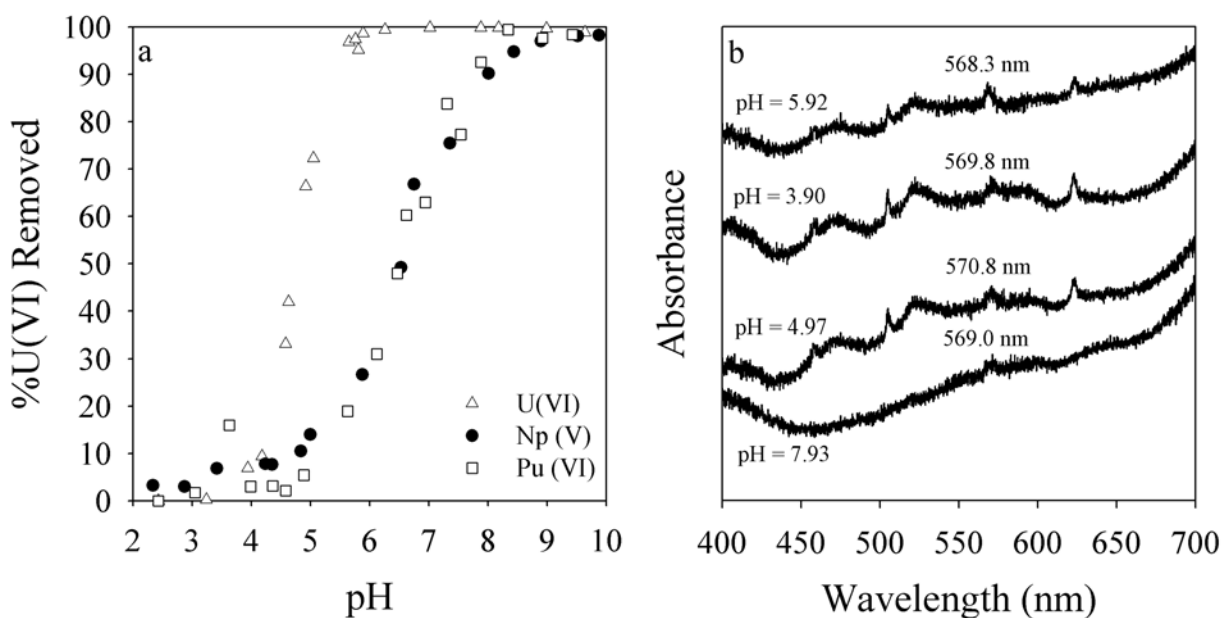


Figure 2. a.) pH dependent adsorption of U(VI), Np(V), and Pu(VI) onto FeOOH. $[An]_{\text{initial}} = 10^{-5}$ M. b.) UV/Vis spectra of Pu(VI) solution in contact with FeOOH. $[Pu(VI)]_{\text{initial}} = 10^{-4}$ M and time = 24 h.

To test this hypothesis, Pu(VI) (initially 10^{-4} M) was reacted with goethite for 24 hr. The solution phase contained Pu(V) as was evident by the presence of a characteristic Pu(V) adsorption band at ~ 569 nm indicating that Pu(VI) was reduced in solution by the FeOOH; however, no Pu(IV) absorption bands were observed (Figure 2b). These results contrast those observed previously when studying Pu(V) interactions with δ -MnO₂. In the presence of δ -MnO₂, Pu(V) was completely oxidized to Pu(VI) and bound to the manganese oxide as a Pu(VI) inner-sphere surface complex. The goethite solids were filtered from the reaction solutions, washed, and air-dried for ~ 1 month in a glovebox prior to analysis with x-ray photoelectron spectroscopy (XPS). The XPS results indicated that at near neutral pH Pu was bound to the mineral surface primarily as Pu(IV) with a small percentage of Pu(V) also present. These experiments were conducted under CO₂ free conditions and even at high pH no carbonate species were detected by XPS. As expected, under similar experimental conditions no reduction of Np(V) was observed in solution by UV-Vis or on the goethite solid by XPS.

DISCUSSION

The oxidation states of U(VI) and Np(V) are stable under our experimental parameters, and we are attempting to fit this data using hexavalent and pentavalent surface complexes, respectively. These fits will then be compared to those for Pu(VI). Initial surface complexation modeling efforts for Pu(VI) interaction with hematite required the use of both Pu(VI) and Pu(IV) surface complexes to accurately fit our experimental data. These predictive geochemical models will enhance our ability to produce more accurate risk assessments and support the use of monitored natural attenuation.

Speciation of Plutonium in Aqueous Systems

N. L. Banik^{*}, R. A. Buda^{*}, S. Bürger^{**}, J. V. Kratz^{*}, N. Trautmann^{*}

^{*} Institut für Kernchemie, Johannes Gutenberg-Universität, D-55099 Mainz, Germany

^{**} Chemical & Isotope Mass Spectrometry Group, Oak Ridge National Laboratory, Oak Ridge, TN 37831, USA

To assist the safety assessment of high-level nuclear waste repositories, a profound knowledge about the speciation of plutonium in aqueous systems is necessary. The knowledge of physical and chemical processes responsible for the behavior of plutonium in a geogenic system enables to predict the migration of plutonium and thus advances the long term safety assessments of nuclear waste repositories or facilitates the development of new remediation strategies for contaminated sites.

Capillary electrophoresis (CE) coupled online to ICP-MS has been developed as a method for the speciation of plutonium oxidation states [1]. The detection limit is 20 ppb ($10^{-12} - 10^{-13}$ g) for one oxidation state. To improve the sensitivity further, the coupling of CE to resonance ionization mass spectrometry (RIMS) has been explored. The detection limit of RIMS [2] enables to decrease the concentration of plutonium by 2 to 3 orders of magnitude compared to the CE-ICP-MS. Thus, the speciation of the oxidation states of plutonium at ultra trace levels of 10^{-9} to 10^{-10} mol/L appears to be possible [3].

For the speciation of plutonium in aqueous systems, the (I) redox kinetics, (II) complexation, and (III) sorption behavior of plutonium under environmental conditions have to be studied.

(I) Redox kinetics: Ubiquitous humic substances (HS) play an essential role in the migration of plutonium due to their complexation and reducing abilities. The redox speciation of plutonium in contact with HS has been investigated by CE-ICP-MS. A reduction of Pu(VI) by Aldrich humic acid (HA) and Gorleben fulvic acid (FA) to Pu(IV) and Pu(III) occurs within a couple of days or weeks, a short time on the scale of nuclear waste disposal in a deep geological formation. Therefore, the speciation of trivalent and tetravalent plutonium in aqueous solution was mainly studied. The reduction of Pu(VI) with FA shows an approximately linear behavior (in half-logarithmic scaling) and a significant dependence on the pH value, similar to the behavior of HA. The enhanced reduction of Pu(VI) by increasing the pH may be explained by the increased fraction of dissociated groups of the HA [4].

(II) Complexation: The time dependence of the plutonium(IV) complexation with Aldrich humic acid has been investigated and the complex formation constants ($\log\beta_{LC}$) of Pu(III) and Pu(IV) at different pH values have been determined using the ultrafiltration method. Different concentrations of plutonium (10^{-6} to 10^{-8} M) and Aldrich humic acid (0.01 to 25 mg/l) were applied.

(III) Sorption: The sorption of trivalent and tetravalent Pu on kaolinite has been studied as a function of pH. The sorption studies were performed by batch experiments under aerobic and anaerobic conditions. A pH range of 0 - 12 was examined with Pu(III) and Pu(IV) concentrations of 10^{-7} - 10^{-9} M and a solid phase concentration of 4 g/L kaolinite. Plutonium carbonate complexes are the dominant species in aqueous solution in the presence of CO₂ at higher pH for both tri- and tetravalent Pu. A similar sorption behaviour can also be reported for the trivalent americium and the tetravalent thorium. The desorption of Pu(IV) from kaolinite is only 1 - 10% for the studied pH range.

The obtained results will be briefly discussed.

Acknowledgement

This work was supported by the 'German Bundesministerium für Wirtschaft und Technologie' (Projekt 02 E 9309 5 and 02 E 9653') and the 'Deutsche Forschungsgemeinschaft' ('Graduiertenkolleg GRK 826/1')

References

- [1] B. Kuczewski, et al., Analytical Chemistry **75**, 6769-6774 (2003).
- [2] C. Grüning, et al., International Journal of Mass Spectrometry **235**, 171-178 (2004).
- [3] S. Bürger, et al., Radiochimica Acta, submitted (2005).
- [4] T. Jianxin, et al., Radiochimica Acta **61**, 73-75 (1993).

Speciation of actinides in contaminated groundwaters from Russian nuclear waste repository sites

A. Novikov^{*}, S. Kalmykov[†], B. Myasoedov^{*}, W. Halsey[‡]

^{*}Vernadsky Institute of Geochemistry and Analytical Chemistry, Moscow, Russia,

[†]Lomonosov Moscow State University, Moscow, Russia,

[‡]Lawrence Livermore National Laboratory, USA.

The study on environmental behavior of the actinides (U, Np, Pu and Am) at contaminated sites of Russia has been the major task of this work. It includes the study on speciation, transport properties and processes in both sites of deep underground disposals and near surface aquatic ecosystems.

Several sites exist in Russia to study actinide behavior in the environment including:

- Deep borehole injection of liquid radioactive wastes near Tomsk (SCC) and Krasnoyarsk.
- Near surface groundwater, soil, lake and river sediments contamination at the territory of PA “Mayak”.

The field studies include sampling of groundwater from the contaminated area and outside it with aquifer and outside this with *in-situ* measurement of groundwater hydrogeochemical characteristics. The multi-channel hydrogeochemical probe was used for this purpose. The sampling was performed by the pumping of the aqueous samples with electrical pump. The pumping rate was 2-2,5 m³/hour. The glass bottles were used for sampling previously purified by blowing of nitrogen with 1% carbon dioxide. The samples were placed to the bottles in nitrogen atmosphere avoiding contact with air. The same method was used for collecting the sub-samples after the micro- and ultrafiltration in the laboratory.

It was established that at Mayak site U and Np are presented as U(VI) and Np(V). Plutonium behaves as if it is a mixture of Pu(IV) and Pu(V). Despite highly oxidic conditions near Karachay Lake Pu in hexavalent form was not found. The presence of Pu(V) in groundwater samples should be considered as one of the main mechanisms of migration however the share of pentavalent Pu is not high since mostly this element is bound to solid phases including Fe-, Mn-oxides and clays. For surface waters of some industrial reservoirs the share of Pu(V) is 50-80% from the total concentration of true soluble species, however 99,9% of this element is bound to bottom sediments and is presented in tetravalent form¹.

For SCC contaminated groundwaters the main fraction of actinide including uranium are presented in low oxidation states. However despite the anoxic conditions in uncontaminated waters (well A-15) the natural U is presented as U(VI). Therefore it is possible that either U is present in tetravalent form in waste effluents that were injected or it is reduced upon interaction with surrounding geologic media. The following facts should be taken into consideration:

- The concentration of complexing substances is significant in waste solutions that possibly can shift the equilibrium between different redox forms.
- Nitrite ions are formed due to radiolysis in the injection well².
- The high sorption affinity of actinides in low oxidation states towards colloids can alter the initial redox equilibrium.

Therefore the reduction of actinides in water proof horizon is possible. This is also supported by the fact that the share of U(IV) and Np(IV) in groundwater samples from SCC is proportional to the total U concentration.

For groundwater samples from Mayak site actinides are bound to relatively small colloid particles (5-10 nm) and filtrate fraction. The mass fraction of actinides bound to colloids decrease in the following sequence: $\text{Pu} > \text{Zr} \geq \text{Am} \geq \text{Eu} \gg \text{Np} > \text{U}$. The share of U and Pu bound to colloidal matter increase upon dilution of waste effluents with preferential association of U with small particles (filtered by 3-10 kDa ultrafilter) and Pu with larger particles of 10 kDa and more. It is probably that U forms true hydroxo-colloids upon shifting of equilibrium between carbonate complexes and hydrolyzed complexes. In case of Pu it is sorbed on the clay particles with formation of pseudo-colloids.

In case of SCC U and other actinides are found to be bound to relatively large colloid particles. In the first case U is in hexavalent form and is not bound to colloids. In contrast to Mayak site the groundwater samples from SCC the following sequence of inclusion of radionuclides to colloid particles is observed: $\text{U} > \text{Np} > \text{Pu} \geq \text{Am} \geq \text{Zr} \geq \text{Zn} \geq \text{Eu}$.

The manner of actinide inclusion to colloid particles for Mayak site is reasonable taking into account the results of redox speciation. For SCC groundwater samples one would expect another manner of actinide distribution. However since they are represented in low oxidation states (IV or III for TPU), this sequence is governed by their total concentration that changes in the following sequence: $\text{U} \gg \text{Np} \gg \text{Pu} > \text{Am}$.

The elemental distribution on the surface of colloid particles were studied using secondary ion mass spectrometry with nanometer scale resolution (nanoSIMS-50, Cameca, France).

Sample from Mayak. According to the high-resolution TEM measurements performed as well with the same sample the mineral composition of colloids is formed by amorphous Fe oxide or hydroxide, MnO_2 , TiO_2 , CaCO_3 , BaSO_4 , clays and zeolites. The aim of this study was to determine the main colloidal phase responsible for sorption of ^{238}U . For this purpose the following U, Fe, Mn, Al, Si, Ca and Ti distribution was studied. It was observed from the experimental data that ^{238}U distribution follows the distribution of Fe while Al, Mn or Si containing particles were not enriched with U. The main chemical form of ^{238}U is uranyl sorbed onto Fe oxide colloids.

Sample from SCC. According to the measurements of actinide redox speciation uranium is present in tetravalent state (U, Np and Pu are present in tetravalent form). Therefore the possibility of formation of U(IV) true colloids is possible. The elemental distribution of U, Fe, Mn, Ti, Ca, Si, Al was studied. In contrast to sample collected at the Mayak site the distribution of U is anti-correlated with major elements that is due to the formation of U true colloids.

Acknowledgements: The study was financially supported by the U.S. Department of Energy (DOE Projects RGO-20102, RUC2-20006,20008MO).

¹ B.F. Myasoedov, A.P. Novikov. Radiochemical procedures for speciation of actinides in the environment. Methodology and data obtained in contaminated by radionuclides regions of Russia. Proceedings of Speciation Work Shop, October 25-28, 1999, Tokai-Mura, Japan, P.3-21.

² Rybaltchenko A.I., Pimenov M.K, Kostin P.P. et al. The deep injection of LNW, Moscow IzdAT, 1994, p. 256 (in Russian).

Neptunium Sorption onto Hematite and Goethite in Presence of Different Humic Acids

A.B. Khasanova*, St.N. Kalmykov*, I.V. Perminova*, S.B. Clark†

* Lomonosov Moscow State University, Chemistry Department, Moscow, 119992, Russia

† Washington State University, Chemistry Department, Pullman, WA 99164-4630, USA

INTRODUCTION

Organic and mineral colloids may enhance the mobility of pollutants in subsurface environment, including actinides. The effect of humic substances in actinide-mineral interaction is essential for modeling of actinide behavior in the far-field conditions of nuclear wastes repository sites. The goal of this work is to study the effect of humic acids (HA) with different content of hydroquinone groups on Np(V) sorption by goethite (α -FeOOH) and hematite (α -Fe₂O₃) colloids in the broad pH range.

EXPERIMENTAL

Samples of hematite and goethite were synthesized according to Penners and Koopal¹ and Atkinson et al.² accordingly. Their physical characteristics were obtained using XRD, SEM, potentiometric titration and BET surface analysis.

The hydroquinone-enriched derivative of HA was synthesized according to Perminova et al.³ using the reaction of formaldehyde copolycondensation between parent humic material (leonardite humic acid, CHP) and hydroquinone. The derivative was obtained for monomer : CHP ratio of 100 mg per 1 g and marked as HQ-100.

The batch sorption and kinetic experiments were studied in 50-ml polypropylene tubes in NaClO₄ solution in a glove-box in N₂-atmosphere and in the absence of UV-light.

Micro- and ultrafiltrations were used for solid/liquid separation. The redox speciation of Np(V) and Pu(V), formation of actinide-humate complexes and determination of HA concentration in the solution were studied by solvent extraction⁴, Vis-NIR spectrophotometry and X-ray photoelectron spectroscopy.

RESULTS AND CONCLUSIONS

The batch kinetic experiments indicated that the steady state equilibrium of Np(V) sorption in binary goethite / Np and hematite / Np systems was achieved for 3 days while in case if HA are present it took more than one

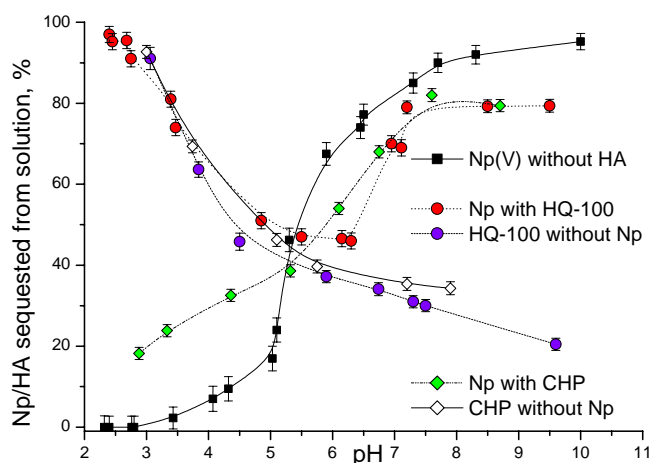


Fig 1: The pH dependences of Np(V) sorption by α -FeOOH ($c=0.22$ g/l) in the presence of HQ-100 (44 ppm) or CHP (43 ppm); $c(\text{Np})=5.8 \cdot 10^{-7}$ M.

month to reach steady state equilibrium.

The sorption of Np(V) onto goethite in binary and ternary systems is presented in Fig. 1 for CHP and HQ-100. The presence of hydroquinone-enriched HQ-100 sample enhanced Np(V) sorption at the pH < 6 with slight effect in case of CHP sample (Fig. 1). The explanation of these effects is due to the reduction of Np(V) by Np(IV) by HQ-100 at low pH values that is not the case for CHP sample. The distribution of Np fits the distribution of HQ-100 at low pH values in case of goethite that is demonstrated in Fig. 2. It was established that the sequestration of Np at low pH values upon interaction with quinone enriched HA was observed only in case of goethite colloids and not in case of hematite colloids.

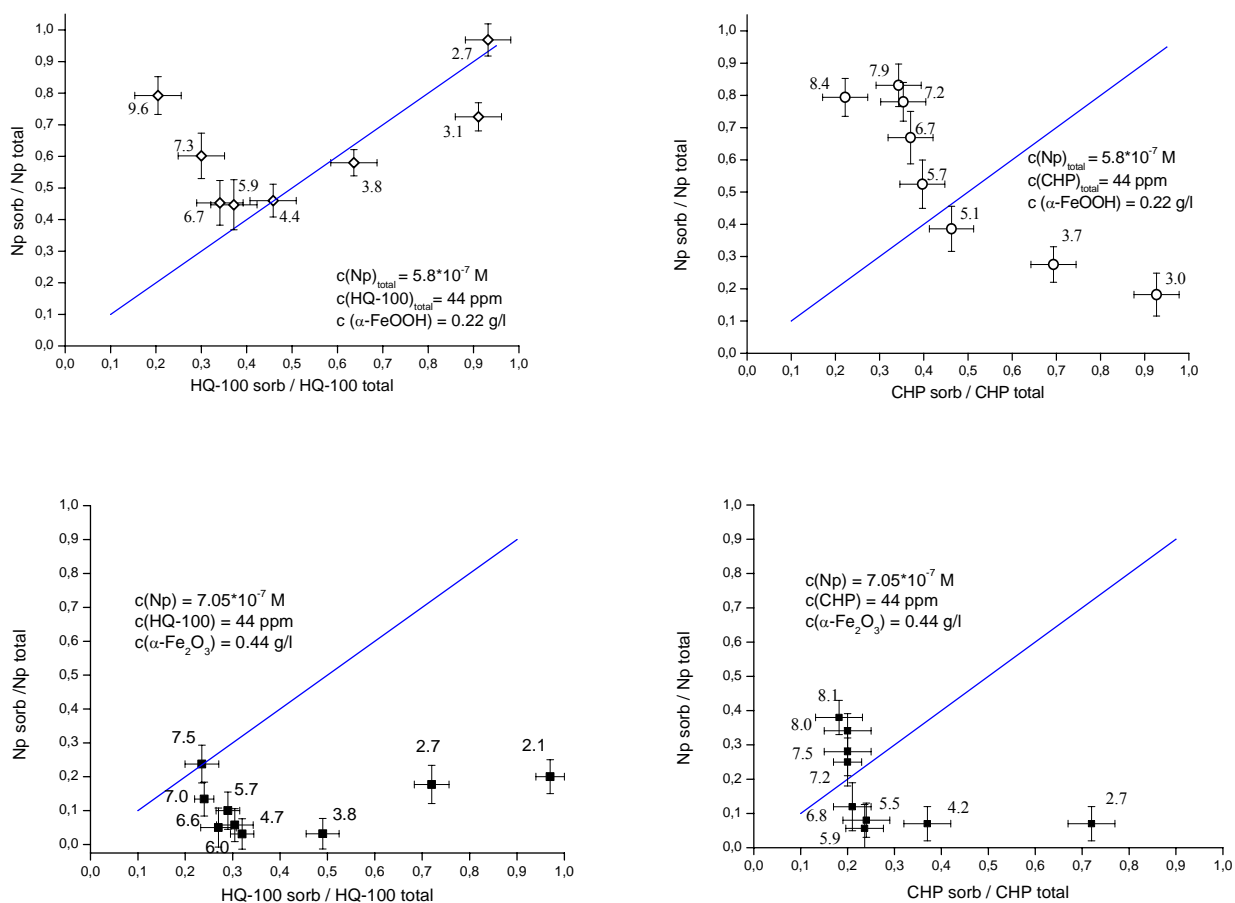


Fig 2: The correlation of Np sorbed / Np total concentrations to HA sorbed / HA total concentrations for studied ternary systems at different pH values.

This work was supported by US DOE (RUC2-20008-MO04) and by RFBR (grant 05-03-33028).

- 1 N.H.G. Penners, L. K. Koopal, J.Coll.Surf. **19**, (1986).
- 2 R.J. Atkinson, A.M. Posner, J.P. Quirk, J. Phys. Chem. **71(3)**, (1967).
- 3 I.V. Perminova, A.N. Kovalenko, *et al.*, Environ. Sci. Technol. **39(21)**, (2005).

Pu(V) and Np(V) Reduction by Hydroquinone Enriched Humic Derivatives

N.S. Shcherbina^{*}, St.N. Kalmykov[†], I.V. Perminova[†], A.N. Kovalenko[†]

^{*}Vernadsky Institute of Geochemistry and Analytical Chemistry, Laboratory of Radiochemistry, Moscow 119991 Russia

[†]Department of Chemistry, Lomonosov Moscow State University, Moscow 119992, Russia

INTRODUCTION

The concept of deep underground repositories in geological formations is accepted in many countries as a final step of nuclear fuel cycle. The multi-barrier systems are designed at the repository sites and are aimed to prevent radionuclide release into the environment. Materials commonly used as engineered barriers should have high sorption properties towards radionuclides, maintain low Eh values of groundwaters and have low hydrolytic conductivity. Among proposed materials are bentonite clays, cements, etc. This study deals with the possible application of humic substances (HS) derivatives as nano-sized material for sequestration of actinides from aqueous solutions.

Natural HS are known to reduce Pu(V) and Pu(VI) to less mobile Pu(IV) and even to Pu(III). Marquardt et al.¹ established stepwise reduction of Pu(VI) to Pu(IV) and Pu(III) by humic materials from Gorleben groundwater. Similar results were obtained by Andre and Choppin². However, the ambiguous results were reported for Np(V). According to Choppin³, Np(V) is not reduced by natural HS, while Artinger et al.⁴ showed slow reduction of Np(V) by HS from Gorleben groundwater. The capability of HS to reduce Pu, Np, and other actinides offers their use as reducing agents for in situ remediation technologies. It was hypothesized that reducing performance of natural humics can be enhanced by incorporating additional hydroquinone moieties. The aim of this research was to evaluate reducing performance of leonardite humic acids and of their hydroquinone-enriched derivatives with respect to Pu(V) and Np(V).

EXPERIMENTAL PART

The quinonoid-enriched humic derivatives were obtained as described in Perminova et al.⁵ using the reaction of formaldehyde copolycondensation between parent humic material (leonardite humic acid, CHP) and hydroquinone at hydroquinone (HQ): CHP ratio of 100 mg per 1g of CHP. The obtained derivative was designated as HQ100.

The reduction of Pu(V) by humic derivatives at tracer level concentrations of plutonium ($2.3 \cdot 10^{-8}$ M) and HS concentrations of 10 mg/l was studied by solvent extraction technique². The visible-near-IR spectrophotometry⁴ was used to study reduction of Np(V) at macro-concentrations ($3.5 \cdot 10^{-5}$ M) and HS concentrations of 250 mg/l. Reduction of Pu(V) was studied using solvent extraction described by Andre and Choppin which allows tracing trivalent form². Np(V) reduction was studied by tracing of NpO_2^+ and Np(V)-humate absorbance at 980.9 and 987.5 nm respectively.

Pu(V) and Np(V) reduction was studied in plastic 20 mL vials foiled to prevent HS photolysis. In case of Np(V), all manipulations were carried out in the glove box under N_2 atmosphere. Pu(V) reduction was studied on the air. All experiments were carried out at pH of 4.5 ± 0.2 without a

background electrolyte. The oxidation states were tracked by sampling 1.5 ml aliquots for solvent extraction in case of Pu(V), and for NIR-spectrophotometry - in case of Np(V).

RESULTS AND DISCUSSION

Reduction of Pu(V) and Np(V) by HQ100 sample is presented in Figure 1. As it can be seen, only slight reduction was observed for Np(V). At the same time complete reduction of Pu(V) was observed in the presence of HQ 100 within 180 h despite the presence of air oxygen. No Pu(III) was found in the reaction mixture over total exposure time (180 h) that indicates a predominance of Pu(IV). Hence, under environmental conditions reduction of Pu(V) to Pu(III) is hardly possible and Pu immobilization could be achieved. It appears that hydroquinone groups play a major role in Pu(V) and Np(V) reduction by HS.

The obtained results demonstrate a viability of the undertaken approach to producing humic materials of the enhanced redox properties. This opens a way for broad application of the humic materials in the practice of remediation technologies.

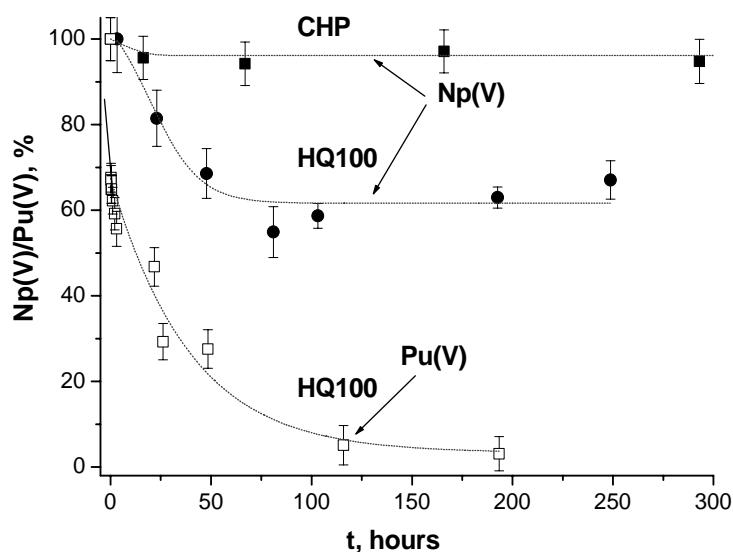


Fig. 1 Pu(V) and Np(V) reduction by CHP and HQ100; $C(\text{Pu})=2.3 \cdot 10^{-8}$ M, $C(\text{Np})=3.5 \cdot 10^{-5}$ M, $\text{pH } 4.5 \pm 0.2$, $I=0$ M

The work was supported by US DOE and Russian Academy of Sciences Program (project RUC2-20006 MO-04).

- 1 C.M. Marquardt, A. Seibert, R. Artinger, M.A. Denecke, B. Kuczewski, D. Schild, Th. Fanghanel, *Radiochim. Acta* **92**, 617-623 (2004).
- 2 C. Andre, G.R. Choppin, *Radiochim. Acta* **88**, 613-616 (2000)
- 3 G.R. Choppin, *Proceedings of NEA Workshop, Bad Zurzach, Switzerland, 14-16 Sept. 1994*, p.75-79, NEA OECD, (1994)
- 4 R. Artinger, C.M. Marquardt, J.I. Kim, *Radiochim. Acta* **88**, 609-612 (2000)
- 5 I.V. Perminova, A.N. Kovalenko, P. Schmitt-Kopplin, K. Hatfield, N. Hertkorn, E.Y. Belyaeva, V.S. Petrosyan, *Environ. Sci. Technol.* **39**(21), 8518-8524 (2005).

U – Pu Coprecipitation Experiments in granitic-bentonitic groundwater under oxidizing and anoxic conditions.

J. Quiñones*, E. Iglesias*, S. Perez de Andres*, A. Martínez Esparza†

*CIEMAT. Avda Complutense, 22. 28040 – Madrid. SPAIN

†ENRESA. C/ Emilio Vargas 7, 28043 – Madrid. SPAIN

ABSTRACT

The definition and the evolution of the source term of the High Level Waste repository are some of the key issues related to the performance assessment studies. In this way, it is essential to determine which is the most conservative and realistic concentration for each radionuclide under repository conditions. The stability of spent fuel and its ability to retain radionuclides is not an inherent materials property but it rather depends on the waste package and the properties of containment and corrosion behaviour by groundwaters. Important processes controlling radionuclide release in case of water access are: dissolution of gap and grain boundary inventories of segregated radionuclides, radiolytic production of oxidants, oxidative dissolution of the fuel matrix, sorption of radionuclides on solid phases surface in the near field and formation of secondary solid alteration products by precipitation or coprecipitation providing new host phases for retention of radionuclides^{1,2}.

This empirical approach is particularly important as thermodynamic databases but is not complete enough to predict unambiguously solubilities in multicomponent systems such as aqueous media in contact with spent fuel. Furthermore, the ongoing work will help realistic geochemical modelling of spent fuel/groundwater interactions by identifying radionuclides, elements thermodynamic properties are needed in order to be described in terms of solid solution, which solubility is better described by pure phases.

As the title remarks this is one of a group of papers related to coprecipitation phenomena with initially dissolved spent fuel in different media²⁻⁴. This paper is focussed on the results obtained on studying precipitation and coprecipitation from a supersaturated solution on U–Pu under granitic-bentonitic groundwater. In addition to assess the influence of the α radiation field (Pu in solution) on the U secondary phases formed and the final concentration value obtained for U and Pu.

EXPERIMENTAL PROCEDURE & RESULTS

The experimental procedure followed is exactly the same that those described in previous papers²⁻⁴. These experiments were carried out (in glove box) under different pH and redox conditions, i.e., oxidizing conditions and anoxic conditions (air and Ar – CO₂ atmosphere, respectively; see Figure 1). Aliquots of filtered (membrane pore diameter 220 nm) and ultrafiltered (membrane pore diameter 8 nm) solutions were analysed by α -spectroscopy and ICP-MS (represented in plots as solid and open symbols, respectively).



Fig 1: Reactor vessel used.

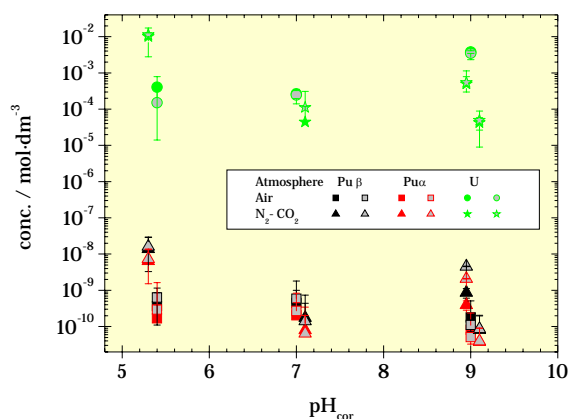


Fig 2: Evolution of the U & Pu conc. vs pH and

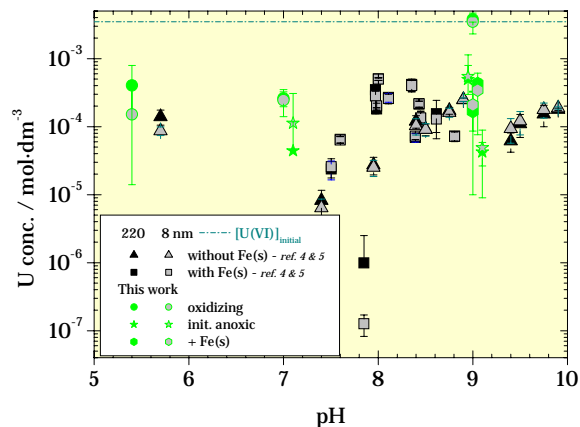


Fig 3: Influence of redox, pH and presence of Pu on the U concentration in solution.

Figure 2 shows the mean U & Pu concentration data obtained for each one selected value (both filtered and ultrafiltered data). The behaviour observed points out that with independence of the initial redox conditions the differences between the U concentration values achieved is small. However, in the case of Pu concentration values this difference it is not observed. When these results are compared with other performed in similar conditions but in absence of α -radiation field⁴ (see Figure 3) for $\text{pH} > 8$, similar U concentration behaviour is observed. This U behaviour observed could be explained as a consequence of the water α -radiolysis. Radiolysis generates oxidant species that produce an increase of the final U concentration in solution measured. In the case of Pu the final concentration in solution measured is very similar to those measured both in spent fuel⁵ and/or Pu-doped pellet leaching⁶ experiments. This experimental evidence demonstrates that a coprecipitation process between U-Pu is not observed in the studied system, under the environmental conditions simulated. Furthermore, the physicochemical characterization of the solid precipitated (by ICP-MS and XRD) shows the following evidences: i) the Pu/U ratio in the solid is the same than in the initial solution; ii) unlike with those previous experiences performed in absence of Pu⁴, amorphous structure (XRD-pattern) of all solid phases were found.

Acknowledgements

This work was financially supported by ENRESA (00/137 agreement and ACACIAS project)

REFERENCES

- ¹ B. Grambow, SKB Technical Report **TR-89-13** (1989).
- ² J. Quiñones, B. Grambow, A. Loida, and H. Geckeis, *J. Nucl. Mater.* **238**, 38 (1996).
- ³ J. Quiñones, J. A. Serrano, and P. P. Díaz Arocas, *J. Nucl. Mater.* **298** (2001).
- ⁴ J. Quiñones, A. González de la Huebra, and A. Martínez Esparza, in *Scientific Basis for Nuclear Waste Management XXVIII; Vol. 824*, edited by S. Stroes-Gascoyne, J. Hanchar, and L. Browning (Material Research Society, San Francisco, USA, 2004), p. 425-430.
- ⁵ J. A. Serrano, V. V. Rondinella, J. P. Glatz, E. H. Toscano, J. Quiñones, and P. P. Díaz, *Radiochimica Acta* **82**, 33-37 (1998).
- ⁶ J. Quiñones, J. Cobos, P. P. Díaz Arocas, and V. V. Rondinella, in *Scientific Basis for Nuclear Waste Management XXVII; Vol. 807*, edited by V. M. Oversby and L. O. Werme (Materials Research Society, 2004), p. 409-414.

MEASUREMENT OF ENVIRONMENTAL LEVELS OF PLUTONIUM IN SOIL

Thompson P., Thomas M.A., and Thomas N.

AWE, Aldermaston, Berkshire RG7 4PR, United Kingdom.

INTRODUCTION

Many organisations, including AWE, are required to measure environmental levels of plutonium in soil. Measurements are made using isotope dilution analysis, radiochemical separation of plutonium from the matrix and preparation of sources for measurement by alpha spectrometry.

At AWE, the recovery of plutonium from environmental samples for the past ten years has used two separate methods. The two methods were designed for different sample sizes, 1 and 10 grams. The aim was to develop a single generic method to be used for both sample sizes. It was desired that analysis time be shorter, resources used to be minimised and if possible the purity and recovery of the plutonium to be improved.

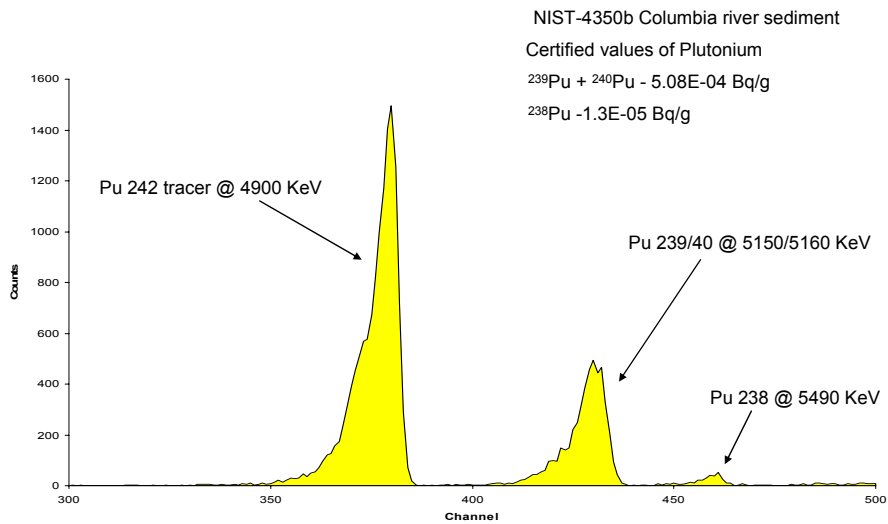
RESULTS AND DISCUSSION

Samples requiring measurement of environmental levels of plutonium in soil are first treated by ashing and addition of ^{242}Pu tracer. The plutonium is removed from the soil matrix by acid leaching and then separated and purified by ion exchange chromatography. Sources are prepared by electrodeposition for alpha spectroscopy. Further measurements of the isotopes present can be made using mass spectrometry.

The original method for analysis of 10g soil samples utilised a cation exchange resin for initial separation of the plutonium. This step required large amounts of acid for conditioning and elution and took several days to complete. The Pu eluate was purified by anion exchange chromatography using BioRad AG1 x 4 resin. For gram size samples, boric acid was used following the acid leaching process to neutralise the fluoride ions present. Successive ammonia precipitations were then performed to remove insoluble hydroxides prior to anion exchange purification using BioRad AG1 x 8 resin.

Using these original methods, a generic method for samples up to 10g of soil has been developed. Following acid leaching and complexing of the fluoride ions as boron trifluoride, the leachate is reduced to low bulk and converted to a nitrate form. The hydroxide is precipitated using ammonia which once dissolved in 8M nitric acid is passed through an anion exchange column using BioRad AG1 x 8 resin. Hydriodic acid is used as a reducing agent for this and the eluate is passed through a second anion exchange column to further reduce the level of impurities.

Alpha spectrum of Standard Reference Material.



The benefits of the method development are that there is now a generic method for use with the range of soil samples. It has led to faster analysis time, reduction in the amount of chemical waste and a reduction in the costs of materials and manpower required. The additional purification step has also reduced the impurities present in the plutonium fraction. Future development work will focus on achieving total dissolution of the soil matrix and investigating new resins available which may further improve separations.

Synthesis and Use of Humic Derivatives Covalently Bound to Silica Gel for Np(V) Sequestration

I.V. Perminova[†], L.A. Karpouk[†], N.S. Shcherbina^{*}, S.A. Ponomarenko[§], St.N. Kalmykov[†], and K. Hatfield[‡]

[†]Department of Chemistry, Lomonosov Moscow State University, Moscow 119992, Russia

^{*}Vernadsky Institute of Geochemistry and Analytical Chemistry, Russian Academy of Sciences, Moscow 119991, Russia

[§]Institute of Synthetic Polymer Materials, Russian Academy of Sciences, Moscow 117393, Russia

[‡]Department of Civil and Coastal Engineering, University of Florida, Gainesville, FL-32611, USA

INTRODUCTION

The most commonly applied technology for treatment of groundwater contaminated with metals and/or radionuclides is “pump and treat”, followed by disposal or re-injection of treated water. This process can be costly and inefficient due to difficulties arising from the ineffective capture of contaminated groundwaters and the sorption of contaminants on mineral surfaces¹. A permeable reactive barrier (PRB) is an alternative technology to “pump & treat” systems. A PRB is a subsurface wall of reactive permeable medium emplaced across the flow path of a contaminant plume². The most commonly used reactive materials are zero valent iron (ZVI), activated carbon, zeolites, and cellulose solids. Most PRBs use ZVI to treat chlorinated hydrocarbons, while a limited number remove nitrate, hexavalent chromium, and radionuclides³. A typical PRB is costly to install but economical to maintain. Much of the installation cost is related to excavation of aquifer material that is then replaced with reactive porous medium².

The goal of this study was a proof of the concept that the reactive agents of a new technology can be designed that can be used for creating broad spectrum sorptive PRBs without excavation. As those agents, the proposed innovative technology uses soluble Humic Substances (HS) that have been specifically modified to adhere to the surfaces of the mineral support and to mediate redox-transformations of actinides. These customized humic materials are immobilized onto silica gel to imitate reactive media of in situ created PRB and to assess their sequestering performance with respect to highly mobile actinide species – NpO₂⁺.

EXPERIMENTAL PART

A sample of leonardite humic material of enhanced redox activity with incorporated hydroquinone moieties (HQ100) was synthesized as described by Perminova et al.⁴ and kindly provided by A.N. Kovalenko. Parent and modified leonardite materials (CHP and HQ100, respectively) were used for preparing alkoxysilyl-derivatives as described in our PCT-application⁵. 3-amino-propyltrimethoxy-silane (APTS) was used to incorporate alkoxysilyl-groups into both humic materials. To prepare solid-phase humic scavengers, aqueous solutions of either HA-APTS or HQ-APTS at concentrations of 5 g/L (10 mL) were added with 0.1 g of silica gel and mixed for 24 hours. The silica gel with immobilized APTS-derivatives was centrifuged

and washed with distilled water. The carbon content in HA-APTS, immobilized on silica gel, was 9.2% mass, and in HQ-APTS, immobilized on silica gel, – 3.3% mass.

The experiments on Np(V) sequestration were conducted under anoxic conditions in the dark in the glovebox. Solutions of Np(V) at concentration of $3.5 \cdot 10^{-5}$ M (20 mL) were added with 40 or 70 mg of solid HA-APTS-SiO₂ or HQ-APTS-SiO₂, respectively, and adjusted to pH 4.5. The prepared solutions were sampled over 9 days exposure. The content of Np(V) in the solution was determined using extraction with HDEHP followed by liquid scintillation counting⁵.

RESULTS AND DISCUSSION

Figure 1 shows the sequestration kinetics of Np(V) in the presence of pure SiO₂, HA-APTS-SiO₂ containing not enriched leonardite HA and of HQ-APTS-SiO₂ containing hydroquinone enriched leonardite HA at pH 4.5. As it can be seen from the shown kinetic curves, both humic containing scavengers efficiently sequester Np(V) from solution with efficiency of hydroquinone-enriched scavenger being higher, as compared to that of the non-enriched scavenger.

The obtained results demonstrate a viability of the undertaken approach to producing reactive humic materials applicable for in situ installation of sorptive PRBs in actinide-contaminated aquifers. This opens a way for broad application of the humic materials in the practice of remediation technologies.

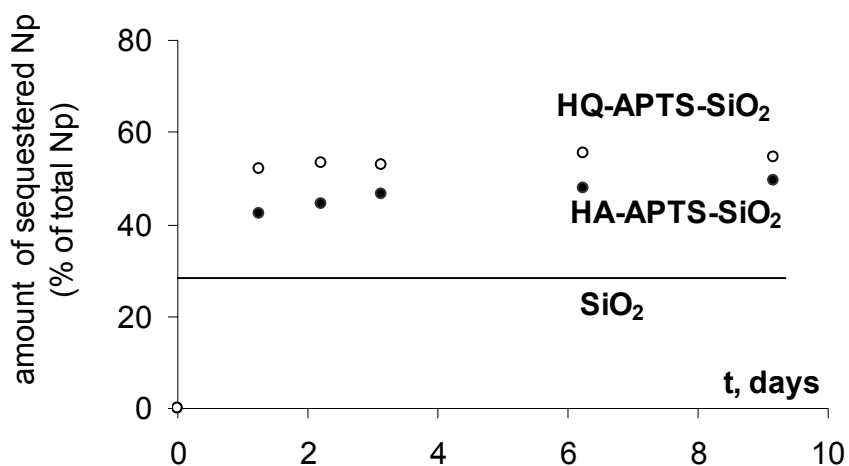


Fig. 1. Sequestration kinetics of Np(V) in the presence of pure SiO₂ and of SiO₂ with covalently bound leonardite HA (HA-APTS-SiO₂) and of their hydroquinone enriched derivative (HQ-APTS-SiO₂) at pH 4.5.

This research was supported by US DOE (project RUC2-20006) and NATO-CLG (grant 980508).

- 1 R. Renner, Environ. Sci. Technol./News **31**: 30A-31A (1997).
- 2 M. Scherer, S. Richter, R. Valentine, P. Alvarez, Crit. Rev. Environ. Sci. Technol. **30**, 363-411 (2000)
- 4 I.V. Perminova, A.N. Kovalenko, P. Schmitt-Kopplin, et al. Environ. Sci. Technol. **39**, 8518-8524 (2005).
- 5 I.V. Perminova, et al. Humic derivatives, methods of preparation and use. Patent pending. (PCT application)
- 6 A. Morgenstern, G.R. Choppin, Radiochim. Acta **90**, 69-74 (2002)

Combined Procedure for the Determination of Actinides in Environmental and Radioactive Waste Samples

M. H. Lee, K. K. Park, J. Y. Kim, Y. J. Park, W. H. Kim

Nuclear Chemistry Research Division, Korea Atomic Energy Research Institute, 150 Deokjindong, Yuseong, Daejeon, Korea

Recently, several studies have been reported on the combined procedure for the determination of the radionuclides in environmental samples with extraction chromatographic materials such as TRU Spec, TEVA Spec resins and Diphonix [1,2]. However, the combined methods for the nuclides in soil or sediment samples are limited because it is somewhat difficult to purify the radionuclides due to major salt ions in the soil. Also, these combined methods were focused on only Pu and Am isotopes, not including the Np and U isotopes. In this study, an extraction chromatography method using anion exchange resin and TRU Spec resin was developed for rapidly and reliably determining the low levels of Pu, Np, Am and U isotopes in environmental samples and radioactive waste samples. The developed analytical method for Pu, Np, Am and U isotopes was validated by an application to IAEA-Reference samples.

A total of 20 g of soil was weighed into a porcelain dish and ashed in a muffle furnace with a gradual heating program up to 600 °C to eliminate the organic matter. To compensate for the chemical recovery, ^{242}Pu , ^{243}Am and ^{232}U , as yield tracers, were added into the soil sample. The calcined samples were dissolved with each 10 mL of concentrated HNO_3 and HF and evaporated to a dryness. The residue was dissolved with 30 mL of 9 M HCl or 8 M HNO_3 . The oxidation states of Pu and Np were adjusted to tetravalent plutonium and hexavalent neptunium with 0.2 M NaNO_2 . The fractions of Pu and Np were purified by an anion exchange resin, and those of Am and U were purified by a TRU Spec resin and anion exchange resin [3]. The purified Pu, Np, U and Am isotopes were electroplated onto stainless steel planchets and measured by alpha spectrometry [4].

The measured concentrations of $^{239,240}\text{Pu}$ in the IAEA-375 and IAEA-326 were consistent with the reference values reported by the IAEA. There was no significant difference in the chemical recoveries for Pu between the 9 M HCl / 0.1 M HNO_3 media and the 8 M HNO_3 media. However, with the anion exchange method in the 8 M HNO_3 medium, the tracer level of U was often detected in the final Pu fraction during the routine analysis. There was not ^{237}Np detected in the IAEA reference soil. The concentrations of ^{241}Am and ^{238}U in the IAEA-375 and IAEA-326 were within the confidence interval. Also, the chemical recoveries for Am and U isotopes with TRU resin in the 8.0 M HNO_3 media were lower than those in the 9.0 M HCl media. This result means that a lot of irons which leached from the soil hinder adsorption of Am and U isotopes onto the TRU resin, even if ascorbic acid is added to the sample solution to reduce the Fe (III). Therefore, in the nitric acid media, it is necessary to remove Fe by means of an oxalic coprecipitation before loading the solution containing Am and U isotopes onto the TRU resin. On the other hand, in the 9 M HCl media, lots of irons are strongly adsorbed onto the anion exchange resin and thus only a

small portion of Fe was eluted in the passing and washing solution. Hence, it is not necessary to remove Fe before loading the solution onto the TRU resin.

Sequential separation method of the Pu, Np, Am and U Isotopes in the soil samples investigated in this study is rapid and reliable. The activity concentrations of the $^{239,240}\text{Pu}$, ^{241}Am and ^{238}U in the IAEA-375 and IAEA-326 reference samples were close to the reference values reported by the IAEA. In the separation of Pu and Am using an anion exchange resin and TRU resin, a hydrochloric acid medium is favoured over a nitric acid medium. The sequential method of the Pu, Np, Am and U Isotopes will be applied for the low level radioactive waste samples.

Acknowledgements

This study has been carried out under the Nuclear R & D program by the Ministry of Science and Technology of Korea.

1. E. P. Horwitz, M. L. Dietz, D. M. Nelson, J. J. La Rosa, W. D. Fairman, *Anal. Chim. Acta* **238**, 263 (1990).
2. E. P. Horwitz, R. Chiarizia, M. L. Dietz, H. Diamond, *Anal. Chim. Acta* **281**, 361 (1993).
3. J. Moreno, N. Vajda, P. R. Danesi, J. J. Larosa, E. Zeiller, M. Sinojmeri, *J. Radioanal. Nucl. Chem.* **226**, 279 (1997).
4. M. H. Lee, C. W. Lee, *Nucl. Instr. and Meth. A* **447**, 593 (2000).

Kinetics of redox reactions of Pu(V) in solutions containing different fractions of humic substances

O.A. Blinova*, A.P. Novikov[†], I.V. Perminova⁺, R.G. Haire[‡]

*A.N.Frumkin Institute of Physical Chemistry and Electrochemistry, Moscow, Russia,

[†]Vernadsky Institute of Geochemistry and Analytical Chemistry, Moscow, Russia,

⁺Lomonosov Moscow State University, Moscow, Russia,

[‡]Oak Ridge National Laboratory

Humic substances (HS) play an important role in speciation of actinides in the environment due to complexing, redox and sorptive interactions. Actual work is devoted to plutonium speciation studying on hematite (α -Fe₂O₃) -natural water interface with presence of humic substances.

Sorption of Pu(V) onto low-temperature hematite was studied in presence of natural occurring and synthetic humic acid (HA) under different concentration of HA. Sorption was carried out at pH 6.0 – 6.1 in 0.01M NH₄ClO₄ (as a background electrolyte) and at range of HA concentration from 57.0 to 0.57 ppm. It was shown by solvent extraction method that all Pu adsorbed onto hematite surface in presence of HA posed as Pu(IV).

To study the reduction of Pu(V) by natural occurring HS was humic and fulvic acids (FA) were eluted from sod-podzol and chernozem soils sampled near PA “Mayak” (Russia) using conventional method and separated to fractions depending on their nature (FA or HA), solubility and affinity to mineral part of soil. Obtained fractions of humic substances then were separated by molecular size for more detail studying of their reducing ability. Kinetic curves were obtained for each fraction and compared with results obtained for synthetic HS.

On the base of curve slope, reducing ability is increased in order: HA < FA < low molecular size fraction.

Obtained data show that different HS can play different parts in Pu(V) migration ability due to different reducing and complexing properties that allow to estimate influence of different HS to actinides behavior in actual geological system (prevention or promotion their sorption on minerals and clays).

Acknowledgements: The study was financially supported by the U.S. Department of Energy (DOE Projects RUC2-20006MO).

Partitioning of Pu between organic matter fractions in the contaminated soils and bottom sediments

O.A. Blinova*, T.A. Goryachenkova[†], A.P. Novikov[†], S. Clark[‡]

*A.N.Frumkin Institute of Physical Chemistry and Electrochemistry, Moscow, Russia,

[†]Vernadsky Institute of Geochemistry and Analytical Chemistry, Moscow, Russia,

[‡]Washington State University

The aim of the study is to develop the optimized scheme for sequential extraction of radionuclides from soil or bottom sediment samples. Several procedures were used as described in:

- Smith, G.E. Fractionation of Actinides Elements in Sediments Via Optimized Protocol for Sequential Chemical Extraction, Masters Thesis, Florida State University, (1998),
- Miller W.P., Martens D.C., Zelasni L.W. J. Soil Sci. Soc. Am, V.50, P.598-601 (1986),
- Tessier A., Campbell P.G.C., Bisson M. Anal. Chem., V.51, P.844-851 (1979),
- Pavlotskaya F.I. Problems of Radiochemistry and Cosmochemistry, Moscow, Nauka, P.148-179 (1992).

The bottom sediment sample with high plutonium content from the reservoir 10 located at “Mayak” Production Association Plant has been chosen for carrying out of comparative researches. The reservoir was constructed for storage of low activity waste solutions and self-cleaning of water by sorption on bottom sediments. The sample used in this study was light loam of dark gray color with high peat content. Chemical and mineralogical content of the sample was thoroughly studied. The major part of plutonium (92 - 93%) is bound to amorphous compounds. This is in good agreement with earlier obtained data for various soils and sediments. The major part of plutonium in organic fraction (86-91%) was associated with low soluble humic compounds and their compounds with $R_2O_3 \cdot nH_2O$ (where R=Fe, Al). The pentavalent plutonium compounds are the most soluble among other oxidation states that was demonstrated by speciation experiments. Only about 1% of total plutonium is extracted by water but 80% of it is found in Pu(V) form. The share of Pu(V) in exchangeable fraction (extracted by acetate) reach 55%.

Acknowledgements: The study was financially supported by the U.S. Department of Energy (DOE Projects RUC2-20008MO).

Pu(VI) Speciation In Environmentally Relevant Solutions

S. D. Reilly, W. Runde, M. P. Neu

Los Alamos National Laboratory, Los Alamos NM 87545 USA

INTRODUCTION

Plutonium exists in the environment as a result of nuclear energy and weapons production. Plutonium has rich redox chemistry and can exist in the environment in the four oxidation states III through VI. Each oxidation state has unique solubility and complexation chemistry that contributes to the overall speciation and mobility of Pu. Cations of all the oxidation states form molecular complexes with anions that are common in environmental media. The higher valent species Pu(V) and Pu(VI) tend to adsorb to minerals and other matrices to a lesser extent than lower valent species, and are therefore particularly important to characterize. Carbonate and hydroxide compounds are of interest because they form strong and sparingly soluble complexes. Chloride complexes are comparatively weak, being significant primarily in areas containing brine. The extent to which these anions stabilize plutonium(VI) and influence the behavior of Pu in the near field of radioactive waste repositories and other nuclear sites is being determined.

RESULTS

We have investigated the environmentally-relevant equilibria shown in Figure 1 using a variety of experimental techniques. We studied the chloride complexation of Pu(VI) in NaCl media using visible-near infrared (vis-NIR) spectrophotometry and determined the stability constants of the PuO_2Cl^+ and $\text{PuO}_2\text{Cl}_2^0(\text{aq})$ complexes.¹ The initial hydrolysis of Pu(VI) was studied using complementary potentiometric and vis-NIR techniques.² We found evidence for both monomeric and dimeric initial hydrolysis species, depending upon the Pu(VI) concentration, but not trimeric species that are important in U(VI) hydrolysis.

We determined the solubility product of $\text{PuO}_2\text{CO}_3(\text{s})$ in NaCl and NaClO_4 media as a function of electrolyte concentration using vis-NIR spectrophotometry and potentiometry. Vis-NIR spectra of Pu(VI) in solutions containing excess carbonate relative to Pu (Fig 2) show absorbances characteristic of both carbonate and hydroxide species. We are analyzing spectrophotometric and potentiometric data to determine the stoichiometries and stabilities of the species formed under these conditions.

We have also studied the redox and speciation of Pu in synthetic brine solutions that were stored in contact with actual TRU waste for several years. For example, spectra of Pu(VI) in these brine solutions show absorbances attributable to Pu(VI) hydroxides and carbonates (Fig 3).

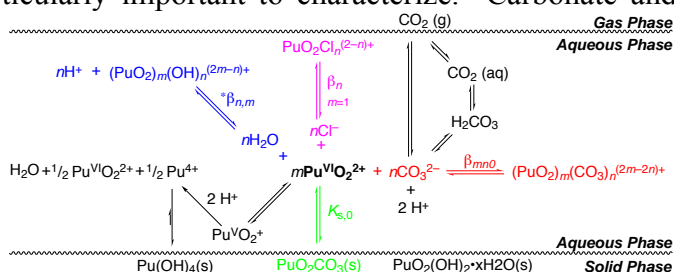


Fig 1: Numerous plutonium(VI) species can exist in aqueous solution. Complexation, solubility, sorption, and redox equilibria exist.

Interestingly, spectra of Pu in brine that had been in contact with pyrochemical TRU waste for weeks to months showed the presence of Pu(VI) hydroxide (Fig 3).

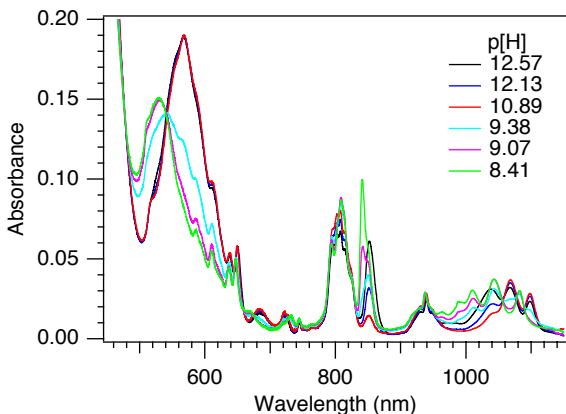


Fig 2: Spectrophotometric titration of 4 mM Pu(VI) in the presence of excess CO_3^{2-} .

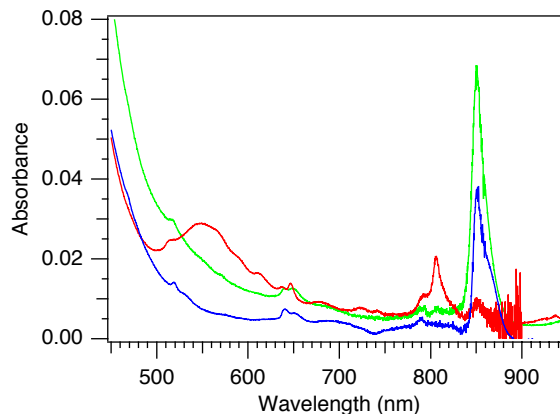


Fig 3: Spectrum of synthetic WIPP brine contacted with TRU waste (blue). Reference spectra of 0.5 mM Pu(VI) in Castile brine (green) and Brine A (red).

DISCUSSION

Plutonium solution thermodynamics and speciation studies are often complicated by multiple complexation, redox, and solubility equilibria. Based on analyses of environmental samples from Pu contaminated sites and from seawater, Pu(VI) species account for a relatively small fraction of the total Pu present. However, common soluble carbonate and hydroxide complexes are highly stable and likely contribute to the overall environmental mobility of Pu. Additional ligands, such as chloride in brines, further increase the stability and solubility of Pu(VI) under oxic conditions.

We and others have found that plutonium(VI) exhibits concentration-dependent initial hydrolysis behavior. Monomeric Pu(VI) hydrolysis species persist at sub-millimolar concentrations. The solubility of $\text{PuO}_2\text{CO}_3(\text{s})$ is greater in solutions containing high chloride concentrations due to the formation of Pu(VI)-chloro complexes, and the mono-carbonato solution species, $\text{PuO}_2\text{CO}_3(\text{aq})$, has a relatively large stability field. The unexpected observation of Pu(VI) hydroxide in brine contacted with test TRU waste confirms that Pu(VI) complexes should not be neglected from plutonium speciation models.

This work was sponsored by the D.O.E. Office of Science Programs in Heavy Element Chemistry Program and in Environmental Remediation Sciences (BES and BER), the Los Alamos National Laboratory Directed Research & Development program, and the Actinide Source Term Waste Test Program.

- 1 W. Runde, S. D. Reilly, and M. P. Neu, *Geochim. Cosmochim. Acta* **63**, 3443 (1999).
- 2 S. D. Reilly and M. P. Neu, *Inorg. Chem.* **45**, 1839 (2006).

Neptunium Dioxide Precipitation Kinetics in Aqueous Solutions

A.M. Johnsen^{*†}, K.E. Roberts[†], S.G. Prussin^{*†}

^{*}Department of Nuclear Engineering, University of California, Berkeley CA 94720 USA

[†]Lawrence Livermore National Laboratory, Livermore CA 94552 USA

The proposed Yucca Mountain nuclear waste repository poses many questions about the behavior of nuclear materials stored underground for tens of thousands of years. The chemical and transport behavior of ²³⁷Np in such a repository is of particular interest, as it has a 2.14 million year half-life.

Previous studies of Np solubility in Yucca Mountain groundwaters supersaturated with Np(V) and performed at temperatures below 100°C for up to a year reported different solid phases, although all were Np(V) solid phases¹⁻³. However, thermodynamic modeling of Np indicated that Np(V) under those conditions should have resulted in the precipitation of the slightly more thermodynamically stable NpO₂(cr); it was hypothesized that the Np(IV) solid phase was not seen in earlier experiments because of kinetic limitations⁴. Roberts, *et al.* performed solubility experiments with aqueous Np(V) in very dilute NaCl solutions at near neutral pH at 200°C, resulting in the precipitation of crystalline NpO₂ and suggesting that the Np(IV) solid phase was indeed kinetically limited⁵.

We are continuing studies of aqueous Np(V) solutions at elevated temperatures. Experiments at varying temperatures near 200°C are being performed to determine the activation energy for the reduction/precipitation reaction. This will allow for the estimation of relevant time scales for the reaction at lower temperatures, such as those found in Yucca Mountain. Studies are also being conducted to evaluate the effect of ionic strength on precipitation kinetics. This is also an important issue, as the ionic strength of Yucca Mountain groundwaters varies by a factor of approximately 10. Finally, we are investigating the effects of O₂ and CO₂ on the equilibrium concentration of various species.

This work was performed under the auspices of the U.S. Department of Energy by University of California Lawrence Livermore National Laboratory under contract No. W-7405-Eng-48. This work was also supported by the National Science Foundation and the University of California, Berkeley.

- 1 H. Nitsche, *et al.* Los Alamos National Laboratory Report No. LA-12562-MS, 1993.
- 2 H. Nitsche, *et al.* Los Alamos National Laboratory Report No. LA-12563-MS, 1994.
- 3 D.W. Efurud, *et al.* Environ. Sci. Technol. **32** (1998).
- 4 T.J. Wolery, *et al.* "The Neptunium Solubility Problem in Repository Performance Assessment: A White Paper," Lawrence Livermore National Laboratory, 1995 (unpublished).
- 5 K.E. Roberts, *et al.*, Radiochim. Acta. **91**, (2003).

Interactions of Heavy Elements with Microorganisms

T. Ohnuki^{*}, T. Yoshida^{*,†}, T. Ozaki^{*}, F. Sakamoto^{*}, N. Kozai^{*}, T. Nankawa^{*}, Y. Suzuki[‡], A. J. Francis[§]

^{*}Japan Atomic Energy Agency, Tokai, Ibaraki, 319-1195 Japan

[†]National Institute of Advanced Industrial Science and Technology, Tsukuba, Ibaraki, 305-8567 Japan

[‡]Graduate School of Engineering, Nagoya University, Furo-cho, Chikusa, Nagoya 464-8603, Japan

[§]Brookhaven National Laboratory, Upton, NY, 11973, USA

INTRODUCTION

The presence of actinides in nuclear reactors and radioactive wastes is a major environmental concern due to their long radioactive half-lives, their high-energy radiation emissions, and their chemical toxicity. In order to determine the mobility of actinides in the environment, studies have been designed to examine its interactions with soils and subsoils composed of abiotic and biotic components, principally minerals, organic matter and bacteria^{1,2}. Among the biotic components, microorganisms have been shown to sorb actinides on cell surfaces^{2,3}. The high capacity of microbial surfaces to bind actinides may affect the migration of actinides in the environment. However, we have only limited knowledge of the role of microorganisms in the migration of actinides in the environment.

The interaction of actinides with microorganisms involves (i) adsorption, (ii) oxidation/reduction, (iii) degradation of actinide-organic component complexes and (iv) mineralization. The interaction of actinides with microorganisms results in changes in the chemical state of actinides (biotransformation). We have been conducting basic scientific research on microbial interactions with actinides in order to elucidate the environmental behavior of actinides under relevant microbial process conditions.

ADSORPTION OF ACTINIDES-DFO COMPLEXES WITH BACTERIA

Adsorption of Pu(IV)-, Th(IV)- and Eu(III)- desferrioxamine B (DFO) on bacteria was studied⁴. A Gram-negative bacterium *Pseudomonas fluorescens* or a Gram-positive bacterium *Bacillus subtilis* was exposed to Pu(IV), Th(IV) or Eu(III) solution in the presence of DFO. At 3 hours after contact of the 1:1 Th(IV)- and Eu(III)-DFO complexes with the cells, the sorption of Pu(IV) and Th(IV) on the cells increased with a decrease in pH from 7 to 4. On the contrary, without DFO most of Pu(IV), Th(IV) and Eu(III) were precipitated in the solution of pH between 7 and 4. Adsorption of DFO on the cells was negligible in the solution with and without metals. Adsorption of Pu(IV), Th(IV) and Eu(III) on *P. fluorescens* cells decreased in the order Eu(III) > Th(IV) > Pu(IV), which corresponds to the increasing the stability constant of the DFO complexes. These results indicate that Th(IV), Pu(IV) and Eu(III) dissociate by contact with cells, after which the metals are adsorbed, and that pH dependence of adsorption density of metal ions on cells is dominated by the stability of the metal-DFO complexes.

REDUCTION OF Pu(IV) BY SULPHATE REDUCING BACTERIUM

Reduction of Pu(IV) by *Desulfovibrio desulfuricans* was studied in the presence of citric acid at pH 7.0⁵. Plutonium(III) in spent medium was determined by the extraction with

thenoyltrifluoroacetone (TTA) solution after oxidizing with $\text{Cr}_2\text{O}_7^{2-}$ solution. Effect of 2,6-anthraquinone disulfonate (AQDS) was also examined. After the exposure of Pu(IV) to *D. desulfuricans* approximately 10% of Pu was present as Pu(III). No Pu(III) was detected in the solution without bacterium. These findings suggested that Pu(IV) is reduced to Pu(III) by the activity of sulphate reducing bacteria. Fraction of Pu(III) in the spent medium containing AQDS was nearly the same as that without AQDS, suggesting that AQDS does not enhance the reduction of Pu(IV) to Pu(III).

BIOMINERALIZATION OF H-AUTUNITE BY YEAST

Mechanism of uranium mineralization by the yeast *Saccharomyces cerevisiae* was examined by batch experiment at pH 3.2³. FESEM-EDS analyses revealed the formation of a U(VI)-bearing precipitate on the yeast cells. Analysis of the U(VI)-bearing precipitates by FESEM-EDS, TEM, and visible diffuse reflectance spectrometry demonstrated the presence of H-autunite, $\text{HUO}_2\text{PO}_4 \cdot 4\text{H}_2\text{O}$. Thermodynamic calculations suggest that the chemical compositions of the solutions were undersaturated with respect to H-autunite, but were supersaturated with ten-times more U(VI) and P than were actually observed. Apparently, the sorbed U(VI) on the cell surfaces reacts with P released from the yeast to form H-autunite by local saturation. These findings indicate that the yeast's cell surfaces, rather than the bulk solution, offer the specific conditions for this geochemical process.

EFFECT OF Eu(III) ON DEGRADATION OF MALIC ACID BY A SOIL BACTERIUM

We studied the effect of Eu(III) on the degradation of malic acid by the bacterium *Pseudomonas fluorescens*⁶. Its breakdown depended upon the ratio of Eu(III)- to malic acid-concentrations; the higher the ratio, the less malic acid was degraded. The resulting chemical species of Eu(III), determined by calculations using thermodynamic data, indicated that predominant species were $\text{Eu}(\text{Mal})_2^-$ and EuMal^+ ; free Eu(III) was less than 1% of the total Eu(III). The degradation of malic acid was independent of $\text{Eu}(\text{Mal})_2^-$, and was hindered by the presence of EuMal^+ , as well as by free Eu(III). These results suggest that Eu(III) retards the degradation of malic acid, and the effect can be masked through its complexation with malic acid. The degradation of malic acid was followed by the production of unidentified metabolites which were associated with Eu(III). One of the metabolites was analysed to be pyruvic acid.

Our findings indicate that biotransformation of actinides caused by adsorption, reduction, mineralization and degradation should be taken into account for predicting environmental behaviors of actinides.

- 1 T. D. Waite, et al., *Geochim. Cosmochim. Acta* **58**, 5465(1994).
- 2 A. J. Francis, et al., *Radiochim. Acta* **92**, 481(2004).
- 3 T. Ohnuki, et al., *Chem. Geol.* **220**, 237(2005).
- 4 T. Yoshida, et al., *J. Nucl. Radiochem. Sci.*, **6**, 77(2005).
- 5 T. Yoshida, et al., To be submitted (2006).
- 6 T. Nankawa et al., *J. Nucl. Radiochem. Sci.*, **6**, 95(2005).

Selective extraction of Pu by a calix[6]arene bearing hydroxamic groups. Application to bioassays

B. Boulet*, C. Bouvier-Capely*, G. Cote[†], L. Poriel*, C. Cossonnet*¹

*IRSN/DRPH/SDI/LRC, BP 17, 92262 Fontenay aux Roses - FRANCE

¹Present address: IRSN/DEI/STEME/LMRE, Bat 501, Bois des Rames, 91400 Orsay - FRANCE

[†]ENSCP/LECA - UMR 7575 - 11, rue Pierre et Marie Curie, 75231 Paris Cedex 05 - FRANCE

INTRODUCTION

Individual monitoring of workers exposed to a risk of internal contamination with actinides is achieved through *in vivo* measurements (anthroporadiometry) and *in vitro* measurements (urine and feces). The procedures currently used for actinides analysis in urine are well established and validated but are time-consuming, which limits the frequency and the flexibility of individual monitoring. The aim of this work is to propose an alternative radiochemical procedure for plutonium and possibly in the presence of uranium. Indeed when Pu and U are both analyzed, it is necessary to separate them prior to alpha spectrometry measurement.

In our previous work, a calixarene-based uranophilic extractant, the 1,3,5-OCH₃-2,4,6-OCH₂CONHOH-*p*-*tert*butylcalix[6]arene (LH₃) (see Figure 1), has been selected and has already shown a very good affinity towards uranyl ion¹. Furthermore, the hydroxamic chelating functions (CONHOH) of LH₃ are supposed to present a very high affinity towards Pu(IV)².

The aim of this work is to study the affinity of LH₃ towards plutonium by solvent extraction and to define experimental conditions allowing to separate plutonium from uranium.

RESULTS

To be representative of the concentrations currently measured in routine monitoring, Pu and U concentrations were in the order of 10⁻⁹M.

Preliminary experiments have been realized to study the affinity of LH₃ towards plutonium at the three most stable oxidation states in aqueous phase (III, IV, and VI) using typical oxidizing or reducing agents (ClNH₂NOH, NaNO₂, and KMnO₄). The results have confirmed that LH₃ presents the best affinity for Pu(IV). Thus, a protocol has been chosen to control the Pu oxidation state to have only the Pu(IV) species in solution prior to the extraction by LH₃.

Then, the affinity of LH₃ towards Pu(IV) has been studied as a function of pH. The results have shown that LH₃ extracts quantitatively Pu from pH 2. At this pH, the 1,3,5-OCH₃-

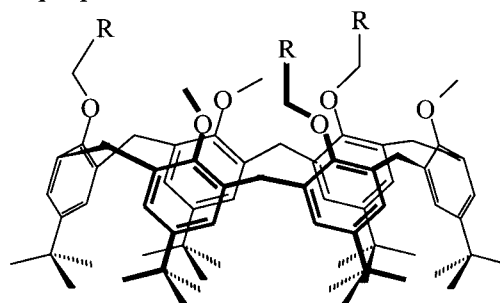


Fig 1: Structure of
1,3,5-OCH₃-2,4,6-OR-*p*-*tert*butylcalix[6]arene

R = CONHOH (LH₃)

R = COOH (L'H₃)

2,4,6-OCH₂COOH-*p*-*tert*butylcalix[6]arene (L'H₃) (see Figure 1) does not extract Pu(IV). This result confirms the very good affinity of hydroxamic functions for Pu(IV).

Lastly, in order to determine experimental conditions to isolate Pu from U, we have compared the extraction of Pu(IV) and of U(VI) by LH₃ as a function of pH (see Figure 2). The extraction curves show that both elements can be selectively extracted in function of the pH value of the aqueous phase. Indeed, a first step allows to extract quantitatively plutonium at pH 2. Then, the increase of the pH of the aqueous phase at pH 5 allows to extract quantitatively uranium.

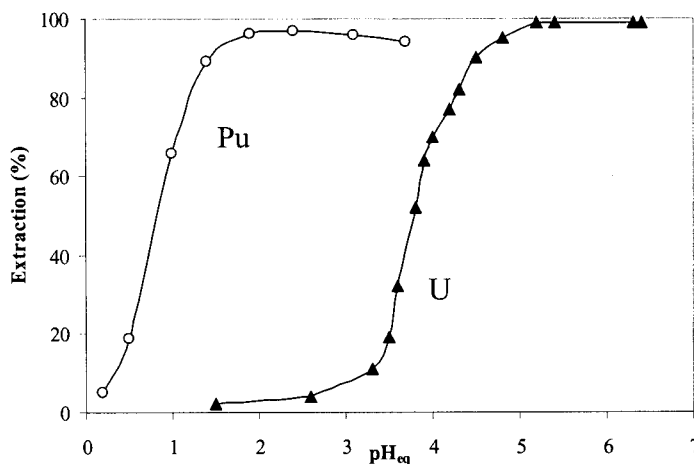


Fig 2: Extraction (%) of Pu and U by LH₃ versus pH

CONCLUSION

In this work we have studied the affinity of a calix[6]arene bearing hydroxamic groups towards plutonium and uranium. The results have shown the very good affinity of this molecule for Pu(IV) and the possibility to separate Pu from U at the extraction step by choosing the adequate pH value.

- 1 B. Boulet, C. Bouvier-Capely, C. Cossonnet, G. Cote, *to be published to: Solvent extraction and Ion exchange*.
- 2 R.J. Taylor, I. May, A.L. Wallwork, I.S. Denniss, N.J. Hill, B.Ya. Galkin, B.Ya. Zilberman, Yu.S. Fedorov, *J. Alloys and Compds*, **271**, 534 (1998).

Plutonium Interactions with Aerobic Microorganisms and Microbial Chelators.

Hakim Boukhalfa, Sean, D. Reilly, and Mary. P. Neu*

* *Chemistry Division, Los Alamos National Laboratory Los Alamos, New Mexico 87545*

Microorganisms and their metabolites affect the chemistry of metals present in their environment through solubility and speciation changes, chelation, biosorption, bioaccumulation and other transformations. Bio-molecules can solubilize, oxidize, reduce or precipitate major metal contaminants in soils and ground water and affect their distribution, mobility and bio-availability. We are studying the fundamental interactions between actinides and natural microorganisms to gain an understanding of how they could affect environmental contaminant behavior. The specific interactions we have focused on are bacterial cell surface and bi-products such as siderophores and extracellular polymeric substances (EPS) interaction with Pu species. We examined Pu(IV) binding by classes of natural siderophores, including pyoverdin, desferrioxamine B, desferrioxamine E and rhodotorulic acid; characterized the redox properties of the complexes formed; examined Pu accumulation by biofilms and EPS substances; and quantified Pu uptake through multi-protein siderophore mediated uptake systems in aerobic bacteria.

We found that siderophores have strong binding affinity for Pu(IV) and that all Pu species (III, IV, V, and VI) rapidly and irreversibly form Pu(IV)-siderophore complexes. We will show that Pu(IV)-siderophore complexes are as stable as their Fe(III)-siderophore complexes analogues with the same composition, and that additional complexes can form due to the exceptionally large Pu coordination sphere. We have also found that Pu-siderophore complexes can be recognized by protein membrane transporters and transported across the cell membrane and thereby accumulated intracellularly. Selected data from this broad range of experiments, including biosorption of plutonium, spectroscopic characterization of plutonium-siderophore complexes, the thermodynamic values of the stability constants of the complexes formed and their electrochemical behavior will be presented.

The Surface Properties of UO_2 Related to Disposal of SNF and Possible Application of Depleted Uranium

St. N. Kalmykov^{*}, O.N. Batuk^{*}, V.P. Petrov^{*}, E.V. Zakharova[†], Yu.A. Teterin^{††},
B.F. Myasoedov^{†††}, V.I. Shapovalov^{††††}, T.V. Kazakovskaya^{††††}

^{*}Radiochemistry Division, Chemistry Department, Lomonosov Moscow State University, Moscow 119992, Russia

[†]Frumkin Institute of Physical and Electrochemistry RAS, Moscow, Russia

^{††}Science centre "Kurchatovskiy institute", Moscow, Russia

^{†††}Vernadsky Institute of Geochemistry and Analytical Chemistry RAS, Moscow, Russia

^{††††}Russian Federal Nuclear Centre – VNIIEF, Sarov, Russia

INTRODUCTION

The behavior of UO_2 under different conditions and its interaction with fission products and actinides is a key parameter in modeling radionuclide release from irradiated nuclear fuel. Such information is essential in case of direct disposal of spent nuclear fuel (SNF). On the other hand huge quantities of depleted uranium (DU; primarily as UF_6) is accumulated worldwide. Despite DU being considered a low-level waste, its conversion to stable oxide forms and subsequent emplacement in a near-surface disposal facility is not an appropriate means of disposal. Use of DU in deep repositories for high level nuclear waste (HLW) may be beneficial. DU can be used in the form of UO_2 for heavy concrete casks as shielding over-pack, as a floor material component (drift "invert"), or as fill and backfill material¹. The goal of this study is to develop a molecular-level understanding of the interaction of Np(IV) and Np(V) with UO_{2+x} .

METHODS

Industry produced sample of DU dioxide was studied. The sample was prepared from UF_6 and then annealed at 625°C in H_2/Ar gas mixture. The average particle size was about $1.5\ \mu\text{m}$ with low free surface area about $1.5\ \text{m}^2/\text{g}$ as determined by dynamic light scattering technique, scanning and by N_2 -sorption and fitting by BET equation.

Partial oxidation of U(IV) to U(VI) takes place for sample as a result of oxygen diffusion to its crystal structure. This leads to the decrease of lattice constant value. The bulk ratio of U/O of the sample was studied by powder X-ray diffraction and surface ratio of U/O was studied by X-ray photoelectron spectroscopy. According to the measurements the bulk composition was close to UO_2 while the surface composition was close to $\text{UO}_{2.25}$.

The solubility and the sorption of the sample were studied in aqueous solutions at constant pH x Eh values in Ar atmosphere. Redox speciation of uranium in solutions was determined by solvent extraction technique. Sorption of Np(IV) and Np(V) by UO_{2+x} was studied in batch mode at total Np concentration of $1 \cdot 10^{-10}\ \text{M}$ (using ^{237}Np and ^{239}Np mixture). The radioactivity of solution aliquots was measured by liquid scintillation counting after filtration. For the comparison the sorption of Th(IV) was studied under exactly the same conditions using ^{232}Th and ^{234}Th mixture.

RESULTS AND DISCUSSION

The sorption of Np(IV), Np(V) and Th(IV) by the studied sample is presented in Fig. 1. It was established that at steady state equilibrium the sorption of Np(IV) and Np(V) was almost similar. The decrease of sorption at neutral pH values is established that is not typical for cation sorption. The explanation of this phenomenon is due to the redox reactions that take place at different pH values. At $\text{pH} < 3.5$ - 4.0 due to high solubility of U(VI) (Fig. 2) the sample surface is "washed" and its composition is close to UO_2 . The reduction of Np(V) takes place at these pH values upon contact with UO_2 that favors its high sorption. This is supported by Th(IV) sorption that is close to 100% at $\text{pH} > 2$. Due to low free surface area it is not possible to use any spectroscopic methods for Np redox speciation on the surface.

At $\text{pH} > 3.5$ the surface composition changes from UO_2 to UO_{2+x} that prohibit the reduction of Np(V). This is the reason of that sorption decrease at $\text{pH} = 3.5 - 8$. At higher pH values Np(V) is stabilized and is sorbed by the surface complexation mechanism.

The effect of surface mediated redox reactions at different pH values and their influence should be considered in case of direct SNF disposal and use of DU dioxide in HLW repositories.

We acknowledge Dr. M.J. Haire and Dr. R.G. Wymer (Oak Ridge National Laboratory) for collaboration in this study as well as ISTC for financial support (project 2694).

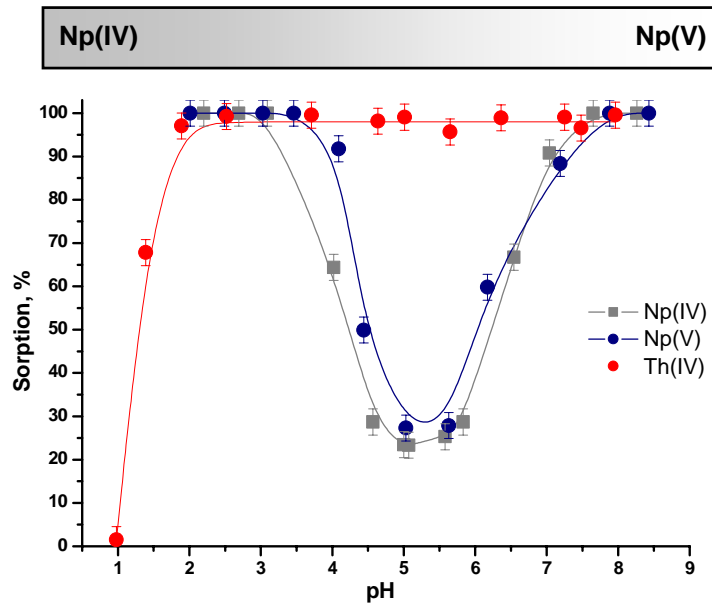


Fig 1: Sorption of Np(IV), Np(V) and Th(IV) by DU dioxide sample.

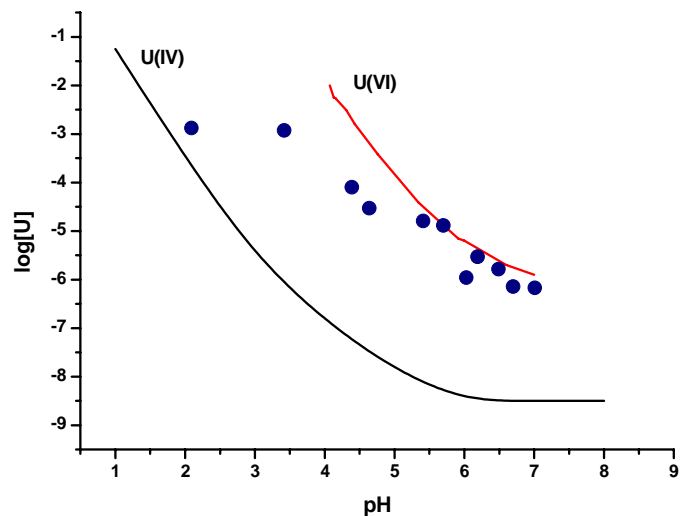


Fig 2: Solubility of DU dioxide sample as a function of pH.

Actinide Analysis and Leaching of Samples Collected from the Glovebox Excavator Method Project

W. F. Bauer, G. S. Groenewold, R. V. Fox, B. J. Mincher, A. K. Gianotto

Department of Chemical Sciences, Idaho National Laboratory, Idaho Falls ID, USA

INTRODUCTION

The transport of radionuclides in the subsurface is a topic of concern, which is motivated by the disposal of contaminated material in unlined waste pits. At the Idaho National Laboratory (INL), these practices were used from the 1950s to the early 1970s to dispose of radioactive wastes from a wide range of activities, most notably plutonium milling operations conducted at the Rocky Flats, CO plant. Estimation of transport involves modelling hydrologic flow occurring in the geologic subsurface that is coupled to the geochemistry of the radionuclides of interest. The modelling requires knowledge of the contents of the source term, and of the solubilisation properties of the radionuclides. Source term contents are normally inferred from disposal records, and substantiated by subsurface gamma probes. Solubilization behavior generally is derived from solid-solution partitioning studies conducted on model systems in the laboratory. However, there are few studies where samples from radioactive waste disposal pits were measured for radionuclide content and solubilisation properties. This is because sampling would require disinterring the burial zones, which is onerous on account of exposure and environmental concerns.

In late 2003 – early 2004 waste and soil samples were collected during a waste retrieval demonstration (Glovebox Excavator Method Project) in Pit 9, which is part of the Subsurface Disposal Area. The Subsurface Disposal Area (SDA) is a radioactive waste landfill located in the Radioactive Waste Management Complex at the INL in southeastern Idaho. The samples presented a unique opportunity to measure actinide contamination, leaching, and speciation in material that has been buried more than 30 years.¹

EXPERIMENTAL METHODS

The Glovebox Excavator Method consisted of a backhoe housed in an enclosure that was constructed over the Pit 9 dig area, and was designed to eliminate release of airborne particulate contamination during operations (Figure 1). The excavation was not designed for sample collection, however grab samples of both soil and waste were intentionally collected from the waste zone to ensure acquisition of actinide contaminated material.

The samples were dissolved using a sodium peroxide fusion procedure, and then analyzed using inductively coupled plasma-mass spectrometry, with mass acquisition focused on actinide contaminants. Leaching studies were conducted by contacting the solid samples with a leachate



Fig 1: Backhoe bucket grabbing a barrel.

solution, and analyzing the actinide concentrations that were partitioned into the solution. Sequential aqueous extractions were conducted using a modified Tessier-type procedure.

RESULTS

Nearly all of the soil and waste samples were contaminated with plutonium, and most had elevated levels of uranium, americium, or neptunium. This observation was consistent with the grab sampling procedure that targeted collection of contaminated material. Samples that were not visually contaminated contained ^{239}Pu at concentrations ranging from 80 ppb to not detected, and had uranium concentrations consistent with the natural background. On the other hand, highly contaminated soil samples were collected (a) from soil caked to graphite mold fragments, and (b) after rupture of a jar containing graphite mold scarfings that contaminated the excavation area: [^{239}Pu] ranged from 30 to 80 ppm in these samples. The $^{239}\text{Pu}/^{240}\text{Pu}$ and $^{239}\text{Pu}/^{241}\text{Am}$ isotope ratios indicated that much of the actinide contamination was derived from weapons-grade plutonium originating from Rocky Flats Plant.

Leaching of plutonium at ambient pH generated operational soil/aqueous distribution coefficients (K_d) of about 10^3 mL/g for organic waste, 10^4 to 10^5 mL/g for low-contamination soil, and about 10^6 mL/g for highly contaminated soil (Figure 2). The excavation logs indicate that the highly contaminated soil was probably exposed to Pu-bearing graphite dust. The K_d values are consistent with sequential aqueous extraction results that showed large percentages of plutonium in the nonextractable fraction. High K_d values were also measured for americium. Leaching studies of uranium and neptunium showed enhanced aqueous partitioning at pH values of $< \sim 4$. Complete leaching as a function of pH and ionic strength and studies of sequential aqueous extraction were reported for uranium, neptunium, plutonium, and americium.

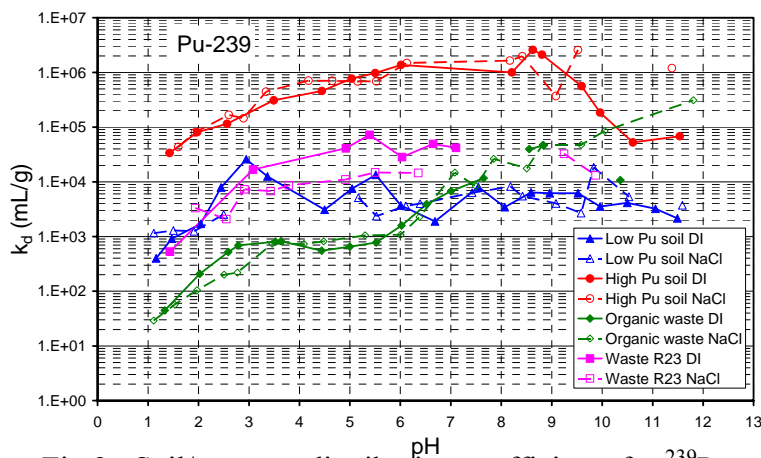


Fig 2: Soil/aqueous distribution coefficients for ^{239}Pu plotted versus pH. Note that the soils containing high levels of Pu were probably contaminated with graphite dust, and displayed very little leaching.

Work supported by the U.S. Department of Energy under DOE Idaho Operations Office Contract DE-AC07-05ID14517.

¹ G. S. Groenewold, et al., "Actinide Analysis and Leaching of Samples Collected from the Glovebox Excavator Project for OU 7-13/14", DOE Report ICP/EXT-04-00439, April, 2005.

Uranium (VI) Solubility from Over-saturation in Carbonate-free Brines

Jean-Francois Lucchini, Marian Borkowski, Michael K. Richmann, Donald T. Reed
Los Alamos National Laboratory, EES-12 Carlsbad Operations, Actinide Chemistry and
Repository Science Program, Carlsbad, NM, USA

Introduction

The environmental chemistry and the subsurface mobility of actinides are of primary importance for a transuranic waste repository such as the Waste Isolation Pilot Plant (WIPP). In WIPP Performance Assessment (PA), the uranium (VI) solubility was estimated to be $(8.8 \pm 0.1) \times 10^{-6}$ M in the absence of carbonate, but this value has not been experimentally confirmed under the WIPP specific conditions (highly concentrated brines at $\text{pH} \leq 12$)¹. At high pH, carbonate complexation is expected to compete with hydrolysis, leading to lower uranyl U(VI) solubility in the absence of an amphoteric effect². Determination of the relative importance of these two processes is the objective of our experimental program.

This study was conducted with carbonate-free simulated WIPP brines to establish a baseline for the effect of carbonate on the solubility of the +VI oxidation state of actinides (including Pu) in the WIPP. Herein we present the results of uranium (VI) solubility experiments, performed using the over-saturation approach in two simulated WIPP brines, for 250 days, at $\text{pH}=6-12$ and in the absence of carbonate.

Results

The over-saturation approach of these solubility experiments consisted of sequentially adding dissolved uranyl until precipitation was observed, and a steady-state concentration was achieved.

The two simulated WIPP brines used were ERDA-6 brine (multi-component sodium chloride-based brine at ionic strength = 5.0 M) and GW brine (multi-component magnesium chloride-based brine at ionic strength = 6.8 M). Significant effort was made to establish carbonate-free conditions. The removal of carbonate from the brines was a two-step process: acidification of the brines to convert carbonate into carbon dioxide, and a smooth removal of the dissolved gases using a slow pump-down process. The solutions were continuously kept in a nitrogen-controlled atmosphere glove box (oxygen level ≤ 10 ppm).

Because of the high ionic strength and strong buffer capacity of the brines, the negative logarithm of the hydrogen ion concentration, called pC_{H^+} , was determined by adding an experimentally measured constant (0.94 for ERDA-6 brine, 1.23 for GW brine) to the measured pH.

The experiments were initiated by first adding uranyl-spiked brine (1.7×10^{-5} M) into pC_{H^+} -adjusted brines. The solutions were periodically sampled, ultra centrifuged, filtered (30,000 Daltons cut off) and analyzed for uranium content by ICP-MS. A second addition of uranyl-spiked brine (8.6×10^{-5} M) was performed into pC_{H^+} -adjusted brines at day 215. The pC_{H^+} values of the solutions were experimentally checked and did not change during the 250 days of the experiment.

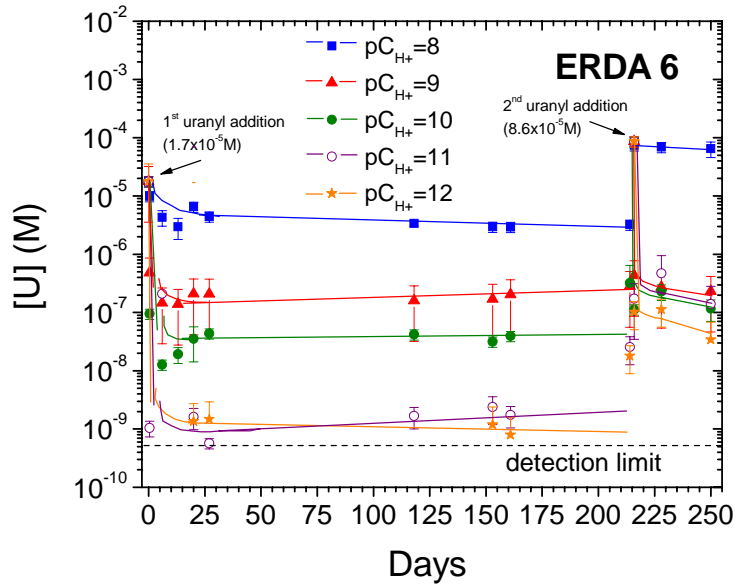


Fig. 1: Concentration of uranium, in ERDA 6 brine and a nitrogen atmosphere, with time. Data are shown consecutively for $pC_{H^+}=8$ (top) to 12 (bottom). The effective detection limit of uranium in brine with our sampling protocols, is 5×10^{-10} M.

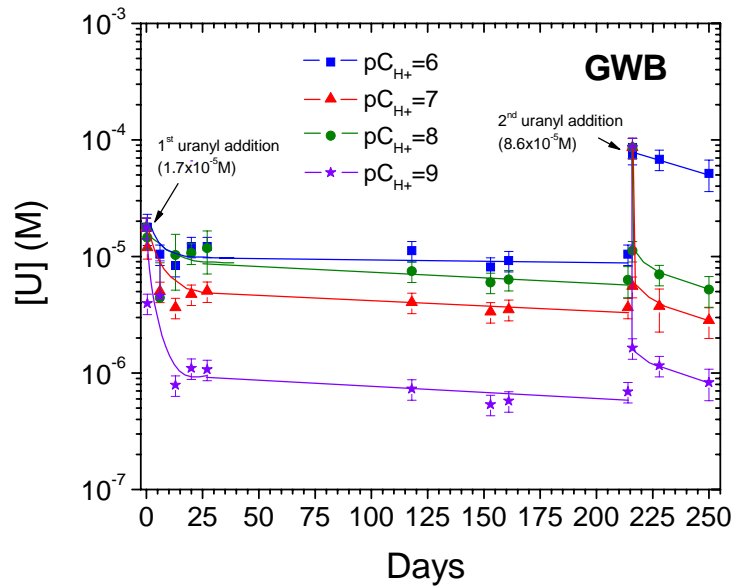


Fig. 2: Concentration of uranium, in GW brine and a nitrogen atmosphere, with time. Uranium concentration profiles correspond to $pC_{H^+}=6, 7, 8$ and 9.

Discussion

The uranium concentration profiles (in Figure 1 for carbonate-free ERDA-6 brine and in Figure 2 for carbonate-free GW brine) suggest that before the second uranyl addition, the uranium solubility was close to equilibrium in all solutions when the initial uranium concentration introduced in solution was above the uranium solubility. The decrease of the uranium concentration to the apparent equilibria obtained before the second uranyl addition seemed faster in GW brine than in ERDA-6 brine. Based on these results, we estimate that the uranium (VI) solubility in carbonate-free brines at high pC_{H^+} is about 10^{-6} - 10^{-5} M in GW brine and below 10^{-6} M in ERDA-6 at $pH \geq 9$, which are lower than the PA theoretical predictions. Further work will be performed to establish the role of the ionic strength in the uranium (VI) solubility difference between the two brines.

A strong pC_{H^+} dependence was observed in carbonate-free ERDA-6 brine. Uranium (VI) concentrations were lower when pC_{H^+} increased (Fig.1). They were slightly less than the second uranyl addition concentration at $pC_{H^+}=8$, but about 3 orders of magnitude lower at $pC_{H^+} \geq 9$. This pH dependence was mostly a hydrolysis effect. We observed a yellow precipitate, presumably a uranyl hydroxide phase, in ERDA-6 in nitrogen-controlled atmosphere at $pC_{H^+}=12$. We will characterize the precipitate at the end of the experiments.

The uranium concentration trends observed over time at pC_{H^+} values up to 12 in carbonate-free ERDA-6 brine indicate that uranium (VI) does not exhibit amphoteric behavior under the conditions investigated.

We compared our data with the most similar published work, performed by Diaz Arocas and Grambow³. They performed uranium (VI) solubility experiments in 5 M NaCl at 25°C and different basic pH values, under an argon atmosphere using an over-saturation approach³. The uranium solubility data measured in our ERDA-6 experiments at $pC_{H^+}=9$ are lower by two orders of magnitude than Diaz and Grambow's data. Some identical experiments were performed with less stringent CO₂ controls in sealed vessels kept in room air, leading to CO₂ uptake during sampling. The uranium concentrations obtained were two orders of magnitude higher than in our nitrogen-controlled atmosphere and comparable with Diaz and Grambow's data.

These data on solubility of uranium (VI) in WIPP brines are the first at high pC_{H^+} under what we believe to be a truly carbonate-free system. They establish a uranium solubility, in the absence of carbonate, that is 10-100 times lower than published results. These estimated values define a "baseline" carbonate-free uranium solubility that will be used to evaluate the effect of carbonate on uranium (VI) solubility in future studies.

References

- 1) Hobart, D.E., Moore, R.C.: Analysis of Uranium (VI) Solubility Data for WIPP Performance Assessment. Unpublished report, May 28, 1996. Albuquerque, NM: Sandia National Laboratories. WPO 39856.
- 2) Clark, D.L., Hobart, D.E., Neu, M.P.: Actinide carbonate complexes and their importance in actinide environmental chemistry, *Chemical Reviews* 95, 25 (1995).
- 3) Diaz Arocas, P., Grambow, B.: Solid-liquid Phase Equilibria of U(VI) in NaCl Solutions, *Geochimica et Cosmochimica Acta* 62/2, 245 (1998).

Aerosol Monitoring During Works inside the Object “Shelter”: Analysis of Dispersity and Concentration for Different Work Types

P. Aryasov, S. Nechaev, N. Tsygankov

Radiation Protection Institute, 04050, Kiev, Ukraine

INTRODUCTION

Results of aerosol monitoring inside the Object Shelter (OS) are presented in the given work. Taking into account the fact, that dispersity of aerosol is one of the main dose-forming factors of internal exposure dose, principal task of the investigation was determination of radioactive aerosol distribution an aerodynamic diameter (AD). At that, special attention was paid on content in the aerosol of transuranium elements as the main dose-forming radionuclides for the OS conditions. At present, works on stabilization of unstable constructions of the OS are in their active stage. Most of the works inside the OS lead to increased generation of radioactive aerosols. At that these works are carried out in highly contaminated premises of the OS, where radioactive situation is unstable and has been formed during the accident.

DESCRIPTION OF EXPERIMENTS

Results on two major directions of the experiments are presented in the work: the first – dispersity and radionuclide composition determination directly in breathing zone of the personnel during works, and, the second - experiments on aerosol distribution determination in

different radiationally dangerous rooms with stationary impactor equipment usage. Six- and eight-cascade Marple personal impactors 290 Series and air pumps GilAir-5 and Gilian 3500 were used for the first task, and two set of Hi-Q Environment company impactors SA-235 model was used for the second task. Special program of monitoring was developed. This program included four major directions: preparation and organization; quality assurance program; air



Fig 1: Personal air sampling by individual impactor during work area preparation, room G 635/3, mark +33

sampling procedure; radiometric measurements. According to the analysis results, works were divided into 5 major types. In fact all radiationally-dangerous works with the increased probability of radioactive aerosols generation were covered, namely: preparation of the workplace (see Fig. 1), elements mounting and cleaning, welding, drilling, cutting of metal.

RESULTS

According to the developed program, for the period from September 2005 till February 2006 more than 100 impactor measurements were carried out. Data on aerosol distribution, radionuclide composition and concentrations of the radioactive aerosols during the works inside the OS is analysed. All air samples obtained during the monitoring underwent measuring of total activity of alpha- and beta-emitters, and selected - for further radiometric analysis of Cs-137 content and radiochemical separation of Pu-239, Am-241. Generalized results on dispersity, radionuclide composition and concentrations of the radioactive aerosols dependences on the type of work are presented in the paper. Analysis of experimental data allows to determine the most radiationally-dangerous types of works. Results of the investigations are used for planning and optimization of radiation protection.

XANES IDENTIFICATION OF PLUTONIUM SPECIATION IN RFETS SAMPLES

V. LoPresti, S. D. Conradson, D. L. Clark

Los Alamos National Laboratory, Los Alamos, NM 87545 USA

Using primarily X-ray Absorption Near Edge Spectroscopy (XANES) with standards run in tandem with samples, probable plutonium speciation was determined for 13 samples from contaminated soil, acid-splash or fire-deposition building interior surfaces, or asphalt pads from the Rocky Flats Environmental Technology Site (RFETS). Save for a single extreme oxidizing situation, all other samples were found to be of Pu (IV) speciation, supporting the supposition that such contamination is less likely to show mobility off site. EXAFS analysis conducted on two of the 13 samples supported the validity of the XANES features employed as determinants of the Pu valence.

References:

1. J. M. Haschke et al., *Science* **287**, 285 (2000).
2. W. Runde, et al., *Applied Geochem.* **17**, 837 (2002).
3. S. D. Conradson et al., *J. Am. Chem. Soc.* **126**, 13443 (2004).

REDOX REACTIONS OF PLUTONIUM WITH HYDROQUINONE AND HUMIC SUBSTANCES

C.M. Marquardt*, A. Seibert*†, Th. Fanghänel*

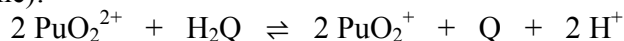
* Institut für Nukleare Entsorgung (INE, Forschungszentrum Karlsruhe, P.O. Box 3640, 76021 Karlsruhe, Germany

INTRODUCTION

The interaction of humic substances, a ubiquitous compound in natural aquifers, with radionuclides in aqueous solutions are manifold, e.g. complexation of metal ions, sorption of metal colloids and redox reactions. For the migration behaviour of plutonium in aquifers nearby nuclear waste repositories in deep geological formations, the redox stability of plutonium species is one of the key questions. Therefore we wanted to know, what are the dominant species in presence of humic substances and under anaerobic conditions and can this redox behaviour be described with a thermodynamic approach? For that studies have been performed on the interaction of plutonium with GoHy-573 fulvic and humic acid. Unfortunately, the exact composition of reducing entities of humic substances are not known and this makes the interpretation of experiments difficult. Therefore it is convenient to use simultaneously more simple reducing compounds as model substances in the experiments. As one model substance hydroquinone has been chosen, because it is generally accepted that hydroquinone-like entities can act as redox centres in humic substances.

RESULTS AND DISCUSSION

To hydroquinone (H₂Q) solution hexavalent plutonium (PuO₂²⁺) was added at various pH values between pH 1 and 7 and 0.1 M NaClO₄ as background electrolyte. The final Pu and H₂Q concentrations were typically 1·2·10⁻⁴ M and 2·3·10⁻³ eq/L, respectively. The process of the reduction has been followed by absorption spectroscopy and solvent extraction with BMBP¹ as chelating agent. In a first step, the reduction of PuO₂²⁺ to pentavalent Pu (PuO₂⁺) was studied. We have observed that the reduction is fast and complete within less than one minute. To get the stoichiometry of the reaction, 1·2·10⁻⁴ M Pu(VI) was titrated with 1·10⁻³ M H₂Q until all Pu(VI) is reduced. At pH 3 for each mol of hydroquinone 2 mol of Pu(VI) are reduced that confirms the following redox reaction, where H₂Q stands for C₆H₄(OH)₂ (Hydroquinone), and Q stands for C₆H₄O₂ (Benzoquinone):



This result coincides with observations from Newton², who has performed the experiment in 1 M HClO₄.

The next step in the reaction sequence is the reduction of Pu(V) to lower oxidation states Pu(III) and (IV). Here, we have focused first on the rates and on the Pu oxidation state distribution. For that excess of H₂Q was added to the solutions from the titration experiment and the evolution of the lower oxidation states were observed with time. The rate of this step is much

† Present address: European Commission, JRC, Inst. for Transuranium Elements, D-76125 Karlsruhe, Germany

slower and reduction is completed after about two months. Depending on the pH value Pu(III) or Pu(IV) is the prevailing Pu oxidation state. At pH below 3 mainly Pu(III) is formed, but Pu(IV) is dominating at pH values above 3. The results are illustrated in Fig. 1. On the left the characteristic absorption bands of the Pu(III) are observed in the absorption spectrum at pH 1 and 3. At pH 3 a tilted background spectrum evolves coming from colloidal Pu(IV) and superposes the Pu(III) spectra. At higher pH values, that is shown on the right, only the background spectra of colloidal Pu(IV) is observed. At the present conditions, the main part of Pu(IV) precipitates as a brownish solid, indicating that the colourless hydroquinone was converted to a brown reduction product, that was sorbed on the Pu(OH)₄(am). Similar experiments have been done with Pu and purified GoHy-532 fulvic acid. From the results so far the prevailing Pu species are Pu(III) or Pu(IV) depending on the pH range. Pu(III) is dominating in the acidic pH range below pH 3, whereas Pu(IV) is the most stable oxidation state in the near neutral pH range.

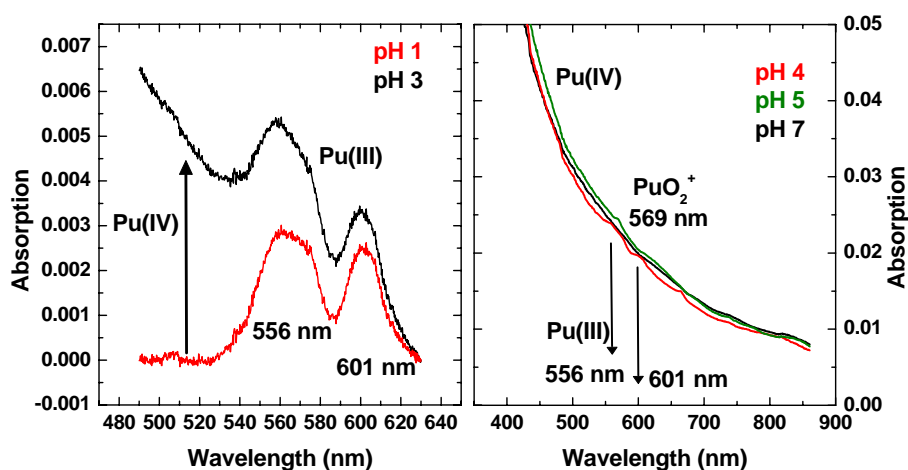


Fig 1: Absorption spectra of Pu, added as Pu(V), in hydroquinone solutions after a reaction time of 2 months at pH 1 and 3 (left hand) and pH 4, 5, 7 (right hand).

CONCLUSIONS

From our results we can conclude that Pu(V) and Pu(VI) are not stable in solutions containing hydroquinone and hydroquinone-like organic compounds like humic substances, and under oxygen free conditions. The tetravalent Pu will be the main species in solution at pH values relevant for aquifers in deep geological formations (pH 5-9), provided that similar redox conditions prevail like in our experiments. It cannot be excluded, that the Pu(III) might be more stable in aquifers containing stronger reducing organic compounds than the GoHy-573-FA batch we used. This batch was separated and purified under air conditions from a Gorleben groundwater and has presumably changed its redox state.

REFERENCES

- 1 Nitsche, H., Roberts, K., Xi, R., Prussin, T., Becraft, K., Mahamid, I.A., Silber, H.B., Carpenter, S.A., Gatti, R.C., *Radiochim. Acta*, **66**, 3 (1994)
- 2 Newton, T.W., *J. Inorg. Nucl. Chem.*, **36**, 639-643 (1974).

Neodymium Analog Study of An(III) Solubility in WIPP Brine

M. Borkowski, J-F. Lucchini, M. Richmann and D. Reed

Los Alamos National Laboratory, Carlsbad Operations, NM 88220 USA

The solubility of An(III) and An(IV) in brine is important to the Waste Isolation Pilot Plant, WIPP, primarily from the point of view of release of transuranium elements to the near-field environment. The solubility of Am(III) and Nd(III), which is an established analog for Am(III), was measured in low ionic strength solutions¹⁻⁶, as well as in 3-4 M NaCl and NaClO₄ solutions^{7,8}. These data were used by WIPP PA for modeling An(III) solubility in brines⁹. The goal of the present work, conducted using an Nd(III) analog, was to measure the effect of pC_{H+}, carbonate concentration, and brine composition on Nd(III) solubility to verify model calculations. Long term experiments (>150 days) were performed in three kinds of brine: ERDA-6, GWB and in 5 M NaCl in the basic pC_{H+} range, in the presence and absence of carbonate ions at a temperature of ~25 °C. Both over-saturation and under-saturation approaches were used.

CARBONATE FREE EXPERIMENTS

These experiments were designed to provide baseline data for the effect of carbonate. Carbonate was carefully removed from the brine. The brine solution was acidified and bubbled with high-purity nitrogen. The brine was then placed in a nitrogen glove box and the atmosphere was controlled for the duration of experiment. The desired pC_{H+} was adjusted in each bottle and a stock neodymium solution at pH~4 (HCl) was used as a spike in the over-saturation approach. For the under-saturation experiments, commercially-available neodymium hydroxide was used as the solid phase. The results of these experiments are presented in Figure 1.

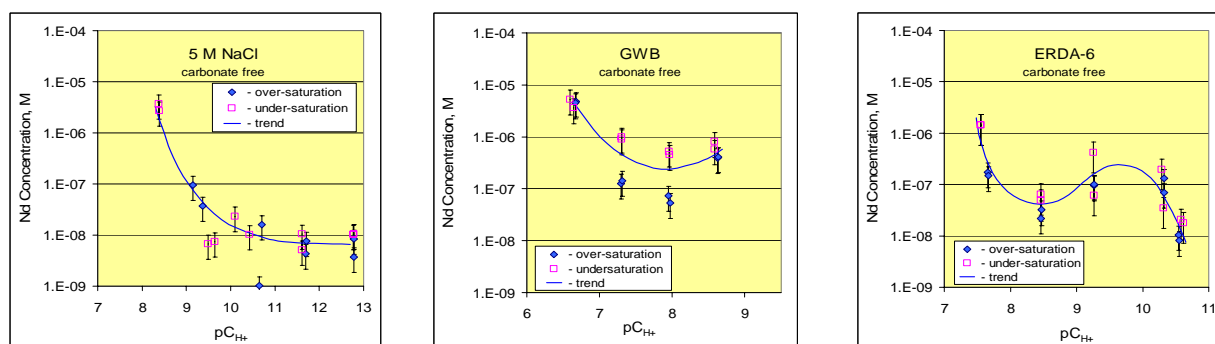


Fig 1. Solubility of Nd(III) measured after 150 days of equilibration without carbonate ion as a function of hydrogen ion concentration. Neodymium concentrations measured for over-saturation and under-saturation were very close to each other.

The pC_{H+} neodymium concentration trend for 5 M NaCl is analogous to the Am(III) solubilities reported for low ionic strength solutions¹⁻⁴ but is shifted up by about two orders of magnitude. At pC_{H+} ~8.5, the likely value expected in the WIPP, the lowest Nd(III) solubility was found in ERDA-6 (the low magnesium brine) and was almost one order of magnitude lower than in GWB (high magnesium brine). The shoulder observed for ERDA-6 brine with a

maximum at $pC_{H^+} = 9.6$, can be assigned to neodymium complex formation with brine components. This shoulder probably exists in GWB brine but could not be measured due to the precipitation of this brine at $pC_{H^+} \geq 8.9$.

EFFECT OF CARBONATE, pC_{H^+} AND BRINE COMPOSITION

The carbonate effect was measured in similar systems. Four concentrations of total carbonate were used: 10^{-2} , 10^{-3} , 10^{-4} and 10^{-5} M. In each sample, pC_{H^+} was adjusted to the desired value and stock neodymium solution at $pH \sim 4$ (HCl) was used as a spike in the over-saturation approach. The initial neodymium concentration was equal to 5×10^{-5} M. For under-saturation experiments, $NdCO_3OH$, prepared in our laboratory, was used as a solid phase. The results of these experiments are presented in Fig. 2.

The solubility of neodymium measured as a function of pC_{H^+} in GWB and ERDA-6 brines for all carbonate concentrations used, reproduces to a good approximation the dependencies found in the carbonate free experiments. In 5 M NaCl solution with $pC_{H^+} > 9$, a shoulder similar to the ERDA-6 case in the carbonate free system was found. This change in neodymium solubility observed in the 5 M NaCl solution with carbonate in respect to carbonate free system, can be explained as carbonate complexation, however this effect did not increase with increased carbonate concentration. Characterization of solids controlling solubility collected in broad range of pC_{H^+} values will give us more information to better explain this phenomenon.

The Nd(III) complexation with carbonate ion does not appear to play a significant role for neodymium solubility in the WIPP brine. The solubility of neodymium is mostly controlled by the hydroxyl ion concentration and decreases as pC_{H^+} increases. For $8.5 < pC_{H^+} < 10.5$, a shoulder in neodymium solubility was found in some cases. This shoulder was assigned to complexation of neodymium with carbonate ion or with brine component (e.g. borate) in carbonate free system. These observations are consistent with the literature data^{4,6}. However, the literature data are reported for low ionic strength solutions and hydroxyl ion concentrations used were not high enough to observe the further decrease we noted at higher pC_{H^+} .

The An(III) solubilities calculated in GWB and ERDA-6 brines using the Pitzer model⁹ at $pC_{H^+} \sim 8.5$ are equal to 3×10^{-7} M and 1.7×10^{-7} M respectively and are in good agreement with the neodymium solubility data measured in the present work.

References

- 1 Rai D., Strickert R.G., Moore D.A., Ryan J.L., Radiochim. Acta, **33** (1983) 201-206.

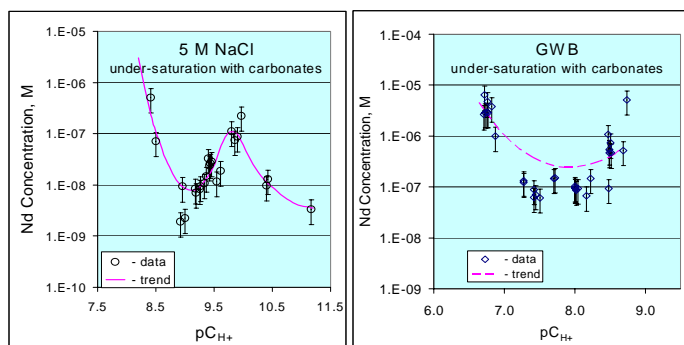


Fig 2. Neodymium concentrations as a function of pC_{H^+} after 220 days of equilibration. Experimental points are presented for various carbonate concentrations. The trend curve (dashed line) was transferred from the graph in Fig 1 for the carbonate free GWB system to the carbonate GWB under-saturation case for comparison.

- 2 Stadler S., Kim J.I., *Radiochim. Acta*, **44-45** (1988) 39-44.
- 3 Silva R.J., Report LBL-15055, Lawrence Berkeley Laboratory, Berkeley, California, 1982, 57 pp.
- 4 Kim J.I., Bernkopf M., Lierse Ch., Koppold F., *ACS Symp. Ser.*, No. **246**, Washington, D.C.: American Chemical Society, (1984) 115-134.
- 5 Meinrath G., Kim J.I., *Radiochim. Acta*, **52/53** (1991) 29-34.
- 6 Felmy A.R., Rai D., Fulton R.W., *Radiochim. Acta*, **50** (1990) 193-204.
- 7 Robouch P.B., Report CEA-R-5473. Commissariat à l'Energie Atomique, Gif-sur-Yvette, France, 1989, 216 pp.
- 8 Giffaut E., Vitorge P., *Mat. Res. Soc. Symp. Proc.*, **294** (1993) 747-751.
- 9 Title 40 CFR Part 1991 Subparts B and C Compliance Recertification Application 2004, Appendix PA, Attachment SOTERM, November 10, 2003, DOE CBFO.

The effect of extracellular polymeric substances (EPS) on adsorption of Pu(IV) and (V) on silica particles.

K.A. Roberts^{*}, P.H. Santschi^{*}, K.A. Schwehr^{*}, C.C. Hung[†]

^{*}Laboratory for Oceanographic and Environmental Research, Texas A&M University at Galveston, 5007 Ave. U Galveston, TX 77551

[†] Institute of Marine Environmental Chemistry and Ecology, National Taiwan Ocean Univ., Keelung, Taiwan

ABSTRACT

Phytoplankton and bacteria exude extracellular polymeric substances (EPS) that are acid polysaccharide-rich and expected to affect the mobility and adsorption of actinides in surface and ground water. EPS are predicted to enhance adsorption onto particles, especially if they are amphiphatic and contain hydrophobic moieties, such as proteins. Because plutonium can occur in several oxidations states under normal environmental conditions, the focus of the work presented here will be on comparing the adsorption of Pu(IV) and Pu(V) onto silica particles in the presence or absence of EPS harvested from laboratory cultures. The hypothesis that will be tested is that EPS also contains reducing moieties capable of reducing Pu (V) to Pu (IV), thereby favoring Pu immobilization by rendering Pu more particle active. Preliminary data on particle-water partition coefficients (K_d) for Pu(IV) and Pu(V) to EPS from *Pseudomonas fluorescens* Biovar II with and without proteins, in 0.1M NaClO₄ and Tris buffer at pH of 8.4±0.1, after 2 days exposure of Pu tracer to EPS, and subsequent separation by ultrafiltration through 1 kDa ultrafilters, will be presented. Log K_d of Pu(IV) to EPS without protein was significantly lower (7.51 vs. 7.93), when EPS was dissolved in EPS for less than one day before a short-term sorption experiment. However, the more mobile Pu(V), prepared according to Saito et al.¹, equilibrated for 4 days with EPS that was pre-equilibrated for 4 days in distilled water, showed much lower log K_d than the more particle-reactive Pu(IV), regardless of protein content (6 vs 7.3). The experimental results will also be compared to chemical composition data of the EPS used such as carbohydrate and protein content, and the relative hydrophobicity of EPS as characterized by the hydrophobic contact area.

1 A. Saito *et al.*, Anal. Chem. **57**, (1985).

The Effects of Extracellular Polymeric Substances (EPS) on Plutonium Sorption Behavior

R. M. Tinnacher^{*}, B. D. Honeyman^{*}, J. B. Gillow^{*,†}

^{*}Laboratory for Applied and Environmental Radiochemistry, Environmental Science and Engineering Division, Colorado School of Mines, Golden CO 80401 USA

[†]Environmental Sciences Department, Brookhaven National Laboratory, Upton NY 11973 USA

EXTRACELLULAR POLYMERIC SUBSTANCES AND PLUTONIUM MOBILITY

Until relatively recently, the potential for plutonium (Pu) transport through soils and sediments as a constituent of the mobile aqueous phase was considered to be limited. The aqueous solubility of Pu ranges from atamolar to femtomolar, and its solubility may be further reduced through sorption onto mineral surfaces¹. The implication of mineral colloids² in facilitating Pu transport through groundwater systems has been demonstrated to be a reasonable mechanism for enhanced Pu transport. Biocolloids (biologically-generated organic macromolecules and bacteria) may also serve to enhance Pu mobility in some circumstances.

RESEARCH GOALS

In this study, we investigate the effects of microbial extracellular polymeric substances (EPS) on plutonium sorption behavior in bench-scale laboratory systems. EPS is defined as “extracellular polymeric substances of biological origin that participate in the formation of microbial aggregates”³. These microbially produced ligands represent an organic matter fraction at the very beginning of the microbial food-chain. In the early stages of biofilm research, polysaccharides had been considered the most abundant components of EPS; however, proteins, nucleic acids as well as amphiphilic compounds are now also known to contribute substantially to biofilm formation. Previous research indicates that EPS has the ability to strongly complex plutonium in solution⁴, and preliminary data also suggest that plutonium sorption is affected by the presence of EPS in solution.

This investigation focuses on two aspects of the role of EPS on Pu mobility: (1) the potential decrease of plutonium sorption to the mineral phase due to Pu-EPS complexation in solution, and (2) the potential remobilisation of sorbed plutonium as a result of the presence of mobile-phase EPS. The first question is



Fig 1: Experimental static column setup used for the investigation of the effects of EPS on plutonium sorption behavior.

essential to determine if Pu-EPS complexes found in solution can possibly be further transported in the subsurface. The latter question represents an attempt to simulate seasonal changes in the soil column during spring run-off, when moisture and nutrient conditions improve, and microorganisms tend to release EPS from cell surfaces.

EXPERIMENTAL SETUP

EPS used in experiments has been extracted from *Pseudomonas fluorescens* Biovar II and gone through a detailed characterization concerning its chemical composition⁵. EPS found in nature is probably more heterogeneous in composition and affected by the microbial diversity of the soil of interest than is our target EPS. The use of EPS from one particular soil bacteria culture, however, provides a controllable and reproducible organic matter composition throughout the course of the experiments. Pretreated silica sand (Q-ROK #1, U.S. Silica) was used as a soil surrogate to minimize the contribution of soil organic matter other than EPS to the organic carbon content of pore water solutions. In addition to the silica sand, which represents a complex 'geomedia' due to commonly found surface impurities, we also evaluate Pu sorption to goethite. Goethite provides a good reference material and has been used for plutonium batch sorption studies in the past⁶. Further, solution conditions, such as pH and ionic strength, are controlled during the course of experiments.

This investigation includes two types of experimental setups, the commonly used batch sorption experiments and a static-column setup⁷ (see Fig. 1). Static columns represent pseudo-advective systems with a high solid-to-liquid ratio, which allow the controlled exchange of pore volumes during experiments. Therefore, static columns can be used as a good screening tool prior to the performance of advective column experiments.

Supported by the U.S. Department of Energy, Office of Science, Natural and Accelerated Bioremediation Research Program (NABIR). The authors acknowledge Peter Santschi's Group at Texas A&M at Galveston, Texas for providing the Pseudomonas fluorescens Biovar II EPS.

- 1 T. R. Garland and R. E. Wildung. In *Biological Implications of Metals in the Environment*, Proceedings of the Fifteenth Annual Hanford Life Sciences Symposium, CONF-750929, 254, (1977).
- 2 A. B. Kersting, *et al.*, *Nature*, **397**, 56 (1999).
- 3 G. G. Geesey, *ASM News*, **48**, 9 (1982).
- 4 C. Kantar, R. M. Harper, B. D. Honeyman (unpublished).
- 5 Ch.-Ch. Hung, P. H. Santschi, J. B. Gillow, *Carbohydrate Polymers*, **61**, 141 (2005).
- 6 L. Duro, *et al.*, *Mat. Res. Soc. Symp. Proc.*, **807** (2004).
- 7 J. P. Loveland, *et al.*, *Colloids and Surfaces A: Physicochemical and Engineering Aspects*, **107**, 205 (1996).

Effect of Microbial Activity on the Release of Plutonium from, and the Transport within, Contaminated Soils

A.D. Diaz*, J.B. Gillow*†, B.D. Honeyman*

*Laboratory for Applied and Environmental Radiochemistry, Environmental Science and Engineering Division, Colorado School of Mines, Golden, CO 80401 USA

†Environmental Sciences Department, Brookhaven National Laboratory, Upton, NY 11973 USA

PLUTONIUM IN THE ENVIRONMENT

The behavior of plutonium (Pu) in natural environments is generally poorly understood; it is the objective of this work to help elucidate the effect of microbial activity on the fate of Pu. Although there is a comprehensive knowledge base for the microbial transformation of uranium under various redox conditions, relatively little information is available for Pu on the major microbially-catalyzed processes that are expected to affect its transport behavior.

PLUTONIUM AND MICROORGANISMS

Over the last several years, mounting evidence has indicated that small amounts of Pu are mobile in saturated groundwater systems. For the most part, models of Pu transport via the ‘colloid pathway’ have focused on Pu transport by inorganic colloidal species [1]. However it is clear from our recent laboratory studies that bacterial metabolic products such as citric, alginate and galacturonic acids, and exocellular polymeric substances (EPS), are capable of complexing Pu; such complexes have the potential of fostering the transport of Pu under advective flow conditions. In addition, microbial activity can alter the local geochemical environment through such processes as the reductive solubilization of Fe(III) oxides.

PRELIMINARY RESULTS

Batch reactors and ‘static columns’ [2] were used to examine the microbially-stimulated release (i.e., solubilization) and transport (i.e., mobilization) of Pu from Rocky Flats, Colorado, USA soil samples. Soils under study have $^{239,240}\text{Pu}$ activities ranging from 50-300 pCi/gram. Metabolic activity of indigenous soil microorganisms was stimulated by the addition of electron donors. Amendments of soil isolates with glucose under batch conditions resulted in the production of Fe(II) and potentially mobile Pu (approximately 4% of the soil Pu was found in the solution phase as compared to deionized water-amended controls). These results indicate that microbial

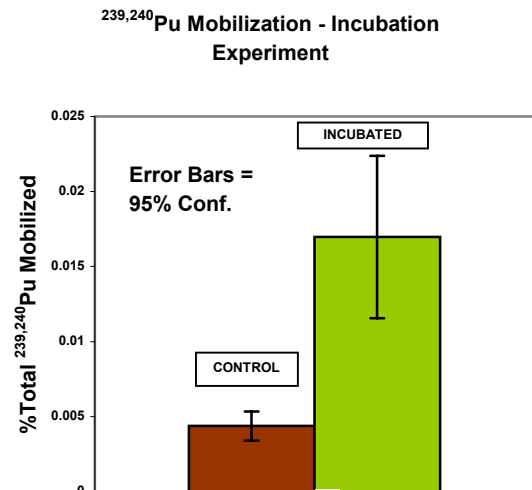


Figure 1: Enhanced $^{239,240}\text{Pu}$ transport resulting from incubation of indigenous Rocky Flats soil microbes in static columns. Note: batch studies resulted in 4% total Pu released.

activity may mobilize Pu as Pu colloids in contaminated soil, possibly due to dissolution of iron phases and or complexation with microbial exudates.

While batch experiments allow for the investigation of Pu release, static columns permit the assessment of Pu release and transport as a result of microbial activity at solid/solution ratios more appropriate for saturated groundwater systems without the complexity of full column studies. Static column experiments conducted include incubation experiment where glucose is the electron donor provided to indigenous microbes and EPS experiments where *Pseudomonas fluorescens* EPS is introduced into the column to determine if enhanced transport occurs and to assess EPS biodegradation and the resulting fate of Pu. In both batch and static column experiments where glucose is provided as the electron donor products of metabolic activity were identified and microbial activity resulted in both the enhanced release and transport of Pu.

Batch and static columns have substantially different soil/solution ratios (e.g., 0.125 g/mL vs. 1.5 g/mL, respectively). Initial results indicate that the greater soil/solution ratio in the static columns results in a decreased microbial activity compared to batch systems and a greater amount of Pu released in the batch studies when compared to the amount of Pu released and transported in the static column experiments (Figure 1). The magnitude of acid production and the percent of total soil Pu released/mobilized also is a function of the soil/solution ratio. While iron release was detected in the batch systems, there was no detectable iron present in the effluent of the static columns after ten days of incubation; we also believe this to be a consequence of the soil/solution ratio.

Preliminary static column experiments conducted in the presence of *P. fluorescens* EPS, a microbially produced ligand, indicate that the transport of Pu is enhanced in the presence of the EPS. The potential for microorganisms to utilize EPS as their primary carbon source exists [3]. This work will investigate such a potential for *P. fluorescens* EPS and indigenous Rocky Flats soil microbes in static columns. Changes in molecular weight will be determined with 2-dimensional polyacrylamide gel electrophoresis (2D PAGE) while high performance liquid chromatography (HPLC) will detect the production of organic acid metabolites as a result of biodegradation.

This work also involves sequencing extracted DNA from “raw” Rocky Flats soil, non-amended static column soil (i.e., control), and amended static column soil (i.e., incubated with either glucose or EPS). DNA sequencing will provide information regarding the link between microbial community and changes in biogeochemistry responsible for enhanced Pu transport. Knowledge in this area is currently lacking.

This work was supported by the U.S. Department of Energy, Office of Science, Natural and Accelerated Bioremediation Research Program (NABIR). The authors acknowledge Peter Santschi's group at Texas A&M University at Galveston, TX for providing Pseudomonas fluorescens EPS.

- 1 B.D. Honeyman and J.F. Ranville. Soil Geochemical Process of Radionuclides. Chapter 7. Soil Science Society of America Special Publication. p. 131 – 163 (2002).
- 2 J.P. Loveland, J.N. Ryan, G.L Amy, and R.W. Harvey. Colloids and Surfaces A: Physiochemical and Engineering Aspects, **107**, 205 (1996).
- 3 M. Ratto, A. Mustranta, and M. Siika-aho. Applied Microbiology and Biotechnology, **57**, 182 (2001).

Effect of HEDPA on Partitioning of Np(V) and Pu(V) to Synthetic Boehmite (γ -AlOOH)

B. A. Powell^{*}, L. Rao^{*}, K. L. Nash[†]

^{*}Lawrence Berkeley National Laboratory, Berkeley, CA 94720 USA

[†]Washington State University, Pullman, WA 99164 USA

INTRODUCTION

A fundamental understanding of actinide partitioning to natural and synthetic minerals is necessary for the reliable prediction of hydrogeochemical behavior of the actinides, to evaluate the risk posed by subsurface contamination, and to design remediation strategies for contaminated sites and high-level wastes. Sorption of actinides to aluminum oxides and oxyhydroxides is proposed to be a primary control of migration¹⁻². Therefore, a detailed description of Pu(V) and Np(V) interactions with aluminum oxyhydroxides will aid in the refinement of models predicting subsurface actinide transport. Additionally, aluminum oxides are a principle component of the sludge phase within the underground storage tanks at the Hanford site. In order to develop an efficient waste treatment process, interactions between Pu/Np and this predominant sludge component must be understood. To reduce the cost of vitrification of the sludge, reduction of the sludge volume via dissolution of the aluminum oxide phase is desirable. For such a process to be effective, the partitioning of the actinides during dissolution must be examined.

Pentavalent actinides generally have a lower affinity for solid phases relative to other actinide oxidation states due to their low effective charge of approximately +2.2⁴. At low pH values where metal oxide solid phases possess an overall positive charge, electrostatic repulsion prevents sorption of the cationic AnO_2^+ species. As the pH increases and the surface develops an overall negative surface charge, sorption generally increases. The presence of naturally-occurring or synthetic organic ligands will drastically affect the partitioning of Np/Pu through formation of Np/Pu complexes and dissolution of the solid phase. The objective of this study was to investigate the effect of 1-hydroxyethane-1,1-diphosphonic acid (HEDPA) on the sorption of Pu(V) and Np(V) to synthetic boehmite (γ -AlOOH). HEDPA is a diphosphonate complexant that forms strong complexes with actinides and aluminum in acidic to neutral and basic solutions.

RESULTS and DISCUSSION

The effect of HEDPA on sorption of Np(V) and Pu(V) over time was examined via batch sorption experiments. Np(V) and Pu(V) were equilibrated with 600 mg L⁻¹ boehmite suspensions until a steady state was reached. Then HEDPA was added and the concentration of Np and Pu in the aqueous phase was measured over time. Data describing the effect of HEDPA on Np(V) and Pu(V) sorption to boehmite are shown in Figure 1. In the absence of HEDPA, sorption edges for Pu(V) and Np(V) (defined as the point at which 50% is sorbed) occurred at approximately pH 6.6 and 8.0, respectively. This is consistent with the point-of-zero-charge of 8.1 for boehmite measured via potentiometric titration.

Addition of HEDPA effects the partitioning of Np and Pu through formation of Np/HEDPA and Pu/HEDPA complexes and by dissolution of the solid phase, although these reactions occur

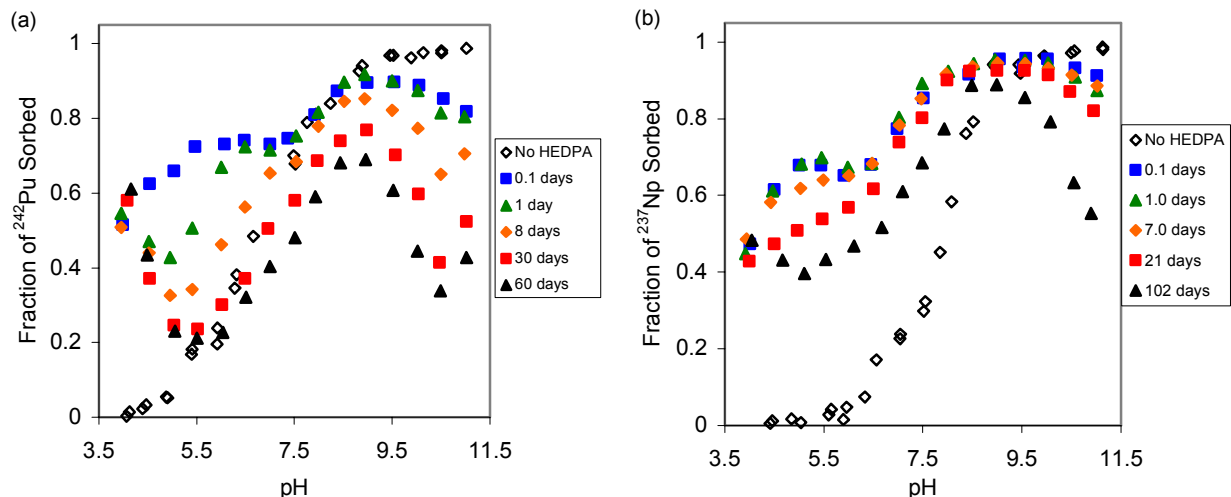


Fig 1: Effect of HEDPA on Pu(V) (a) and Np(V) (b) sorption to boehmite ($\gamma\text{-AlOOH}$). System parameters: $[\text{HEDPA}] = 5.4 \text{ mM}$; $[\gamma\text{-AlOOH}] = 600 \text{ mg L}^{-1}$; $[\text{NaCl}] = 1.0 \text{ M}$; $[^{242}\text{Pu(V)}] = 1.9 \text{ }\mu\text{M}$; $[^{237}\text{Np(V)}] = 9.4 \text{ }\mu\text{M}$. Open symbols represent steady state distribution (10 day equilibrium) of Pu(V) (a) and Np(V) (b) without HEDPA present.

on different time scales. Within the first few days following HEDPA addition, formation of Np/HEDPA and Pu/HEDPA complexes modified the distribution of Np and Pu between the solid and aqueous phase. At pH values below the original sorption edge, where the surface is predominantly positively charged, addition of HEDPA caused increased sorption of Np and Pu relative to the HEDPA free system. Conversely, at pH values above the original sorption edge, HEDPA caused leaching of Np and Pu into the aqueous phase. These results indicate that Np/HEDPA and Pu/HEDPA complexes are primarily anionic.

At extended time periods, the fraction of Np and Pu in the aqueous phase slowly increased. This is likely due to dissolution of boehmite facilitated by HEDPA. The change in Np and Pu partitioning in this system was concurrent with dissolution of boehmite by HEDPA⁵. Maximum boehmite dissolution was observed at pH 4 and 11. As the pH increased from pH 4 and decreased from pH 11, the Al concentration decreased monotonically until converging at pH 7.5. Addition of HEDPA clearly effects the partitioning of Np and Pu in these systems through dissolution of the solid phase and formation of Np-HEDPA and Pu-HEDPA complexes.

This work was supported by the Director, Office of Science, Office of Biological and Environmental Research of the U.S. Department of Energy under Contract No. DE-AC02-05CH11231 at the Lawrence Berkeley National Laboratory.

- 1 L. Righetto, G. Bidoglio, B. Marcandalli, I. R. Bellobono, *Radiochim. Acta*, **44/45**, 73-75 (1988).
- 2 J. D. Prikryl, R. T. Pabalan, D. R. Turner, B. W. Leslie, *Radiochim Acta*, **66/67**, 291-296 (1994).
- 3 J. W. Morse and G. R. Choppin, *Rev. Aqu. Sci.*, **4**, 1-22, (1991).
- 4 B. A. Powell, L. Rao, K. L. Nash, L. Martin, in *Basic Science, Applications, and Technology*, Eds. J. Sarrao, A. Schwartz, M. Antonio, P. Burns, R. Haire, H. Nitsche (Mat. Res. Soc. Symp. Proc. Vol. 893, Warrendale, PA, 2005), 0893-JJ07-02.

Actinides in Sediment and Submerged Plants of the Yenisei River

A. Bolsunovsky and L. Bondareva

Institute of Biophysics SB RAS, Akademgorodok, Krasnoyarsk 660036 Russia

INTRODUCTION

The Yenisei is one of the world's largest rivers, over 3000 km long, flowing into the Kara Sea. The Mining-and-Chemical Combine (MCC) at Zheleznogorsk is situated on the right bank of the Yenisei River, 60 km down of the city of Krasnoyarsk. The Combine has been producing weapons-grade plutonium in uranium-graphite reactors since 1958, when the first reactor was started up. The irradiated uranium is reprocessed at the radiochemical plant to separate uranium, plutonium, and fission products. The reactor plant houses three reactors. Two of them used the Yenisei water as coolant, i.e. the water was taken from the river to remove heat from the core, passed through the reactor fuel channels, and returned to the Yenisei. Both of these reactors were shut down in 1992, but the third reactor is still working. It has been proposed to put it out of service in 2007-2009. This reactor also uses the Yenisei water as coolant for some channels and releases radionuclides of activation origin into the river.

Scientific expeditions revealed that the Yenisei River flood plain is contaminated with artificial radionuclides, including plutonium isotopes, within 2000 km downstream of the plutonium complex¹. However, earlier investigations ignored the radioactive contamination of components of the aquatic ecosystem. Gamma-spectrometric and radiochemical analysis of samples of aquatic plants and animals collected from the river near the MCC during the 1997-2004 expeditions revealed a broad spectrum of long-lived and short-lived radionuclides². Among the short-lived radionuclides the highest activity concentration in aquatic plants and animals was recorded for ²³⁹Np. The Yenisei River continuously receives a wide range of radionuclides, both long-lived and short-lived, and, thus, the aquatic ecosystem of the Yenisei River is a unique object that can be used to study the migration mechanisms of various radionuclides in the environment.

The aim of our investigation was to assess the levels of actinides in sediments and aquatic plants both near the MCC and at a considerable distance from it, down the Yenisei River.

MATERIALS AND METHODS

During the expeditions of 1997-2005, samples of sediment and aquatic plants were collected from the Yenisei River at different distances downstream of the MCC. The aquatic plants sampled were of two species: *Potamogeton lucens* (shining weed) and *Fontinalis antipyretica* (water moss). As control, we used samples of aquatic plants collected upstream of the MCC. Samples of sediments and aquatic plants were prepared for investigations following standard procedures. In some cases, parts of the aquatic plant *Potamogeton lucens* (leaves and stem) were measured separately. For radiochemical and some γ -spectrometric investigations samples of sediments and aquatic plants were ashed. For the radiochemical analysis to determine the content of actinides in samples of aquatic plants, the ash was treated with acid in an MLS 1200 mega microwave system (Milestone) equipped with high pressure TFM vessels. Methods of radiochemical analysis of samples for actinides and ⁹⁰Sr were

described in detail elsewhere^{1,3}. Radiochemical determination of actinides in sediment and plant samples was performed at the RPA RADON (Moscow)¹ and γ -spectrometric measurements of ^{241}Am and ^{239}Np – at the Institute of Biophysics (Krasnoyarsk). Sequential extraction technique proposed by Tessier and modified by Klemt and his colleagues⁴ was used to investigate sediment samples. An abbreviated procedure was used to perform sequential extractions in aquatic plant samples and the obtained fractions were exchangeable, adsorbed fractions, organics, and mineral residue.

RESULTS AND DISCUSSION

Investigations of the Yenisei River sediment samples revealed high activity concentrations of transuranic elements (^{238}Pu , $^{239,240}\text{Pu}$, and ^{241}Am), which were 10 and more times higher than those reported earlier and 100 times higher than their global levels. These local anomalous spots can be found both in the top and in the deep layers of sediments. In these spots specific activities of transuranic elements can be very high: $^{239,240}\text{Pu}$ up to 280 Bq/kg, ^{241}Pu up to 1429 Bq/kg, ^{241}Am up to 48 Bq/kg, ^{237}Np up to 5.6 Bq/kg. These anomalies are indicative of mobile behavior of transuranic radionuclides in the environment and of continued disposals of artificial radionuclides by the MCC².

Sequential extraction of samples of sediments collected near the MCC showed that the amounts of extracted ^{152}Eu and ^{241}Am were the largest (60-80% of initial activity), then followed ^{60}Co (30%), and, last, ^{137}Cs (5-15%). The largest amounts of the radionuclides are extracted from such fractions as organics, sesquioxides and hydroxides, and amorphous silicates. Exchangeable fractions contain not more than 2% of total radionuclides. In the sediment – Yenisei River water systems spiked with ^{241}Am the distribution of the actinides released at different extraction stages was not the same as in the unspiked samples.

It was found that aquatic plants of the Yenisei River collected both near the MCC discharge site and at a distance up to 200 km downstream contained a wide range of artificial radionuclides, including actinides (plutonium isotopes, americium, and neptunium). The aquatic moss *Fontinalis antipyretica* was found to have the highest radionuclide concentration factors. Leaves of *Potamogeton lucens* contained higher levels of radionuclides, including ^{239}Np , than stems. Sequential extraction of radionuclides from samples of aquatic plants showed that ^{239}Np levels in exchangeable and adsorption fractions of *Potamogeton lucens* biomass were higher than in the respective fractions of *Fontinalis antipyretica* biomass.

The study was supported by RFBR Grant No.06-04-48124 and Integration Project SB RAS No.30.

- 1 A.Ya. Bolsunovsky, *et al.*, Doklady Rossiiskoi Akademii Nauk. **387**, (2002).
- 2 A. Bolsunovsky, Aquatic Ecology. **38(1)**, (2004).
- 3 I.A. Kashirin, *et al.*, Applied Radiation and Isotopes. **53**, (2000).
- 4 E. Klemt, *et al.*, Environmental Radioactivity in the Arctic & Antarctic. (Ed. Per Strand, Torun Jolle and Ase Sand). Norwegian Radiation Protection Authority, Norway. (2002).

Biotransformation of Plutonium (IV) Adsorbed to Iron Oxides

J.B. Gillow^{*,†}, B.D. Honeyman[†], and A.J. Francis^{*}

^{*}Brookhaven National Laboratory, Upton, NY 11973 USA

[†]Colorado School of Mines, Golden, CO 80401 USA

INTRODUCTION

Iron oxide coatings and mineral phases are an important sorptive phase for radionuclides in the natural environment and in nuclear waste repositories (1). Plutonium (IV), (V), and (VI) has been shown to adsorb to iron oxides including goethite and hematite. Sorption of Pu onto iron oxides may facilitate colloidal transport; adsorbed Pu(V) has also been shown to be reduced to Pu(IV) in the case of goethite (2,3). Once adsorbed the sequestered Pu(IV) may be transformed due to biogeochemical processes. A moderately stable, crystalline iron oxide common in the natural environment and on corroding steel surfaces is goethite (α -FeOOH). Anaerobic fermentative microbial activity can profoundly affect the stability of the iron oxides due to reductive dissolution caused by direct and indirect action including lowering of the Eh and pH and electron transfer processes that alter the mineral phase (4). We studied the fate of Pu(IV) adsorbed to goethite in the presence of an actively growing culture of *Clostridium* sp.

MATERIALS AND METHODS

Goethite was synthesized according to the methods of Schwertmann and Cornell (5). $^{242}\text{Pu(IV)}$ nitrate was obtained from New Brunswick Laboratory (Argonne, IL). The oxidation state was determined by extraction with thenoyltrifluoroacetone at pH 0 and 4. Pu was added to 10 mg of the oxide to achieve a concentration of $1.8 \times 10^{-7}\text{M}$ and pH adjusted to 2-9; adsorption to the solid oxide was determined after 19 hours by centrifugation (6,000xg) and liquid scintillation counting (LSC). The goethite with adsorbed ^{242}Pu was then added to culture medium containing the following: glucose, 28 mM; Na^+ , 2.0 mM; Ca^{2+} , 3.4 mM; Mg^{2+} , 0.8 mM; NH_4^+ , 12 mM; Cl^- , 16 mM; SO_4^{2-} , 0.8 mM; PO_4^{3-} , 0.08 mM; glycerol-1-phosphate, 1.22 mM; peptone, 0.1 g/L; yeast extract, 0.1 g/L ($I=0.1\text{M}$, pH = 6.8). Triplicate samples were inoculated with the actively growing anaerobic bacterial culture *Clostridium* sp. and pH, Eh, inorganic phosphate (ascorbic acid method) and iron dissolution (Fe(II) determined by o-phenanthroline) were monitored in a time course experiment. Soluble ^{242}Pu was determined by filtration using a $0.45\ \mu\text{m}$ syringe filter followed by LSC of the filtrate. Similar experiments were performed with ^{230}Th ($2.4 \times 10^{-8}\text{M}$). Geochemical modelling of the Pu speciation was performed using PHREEQCi with hydrolysis

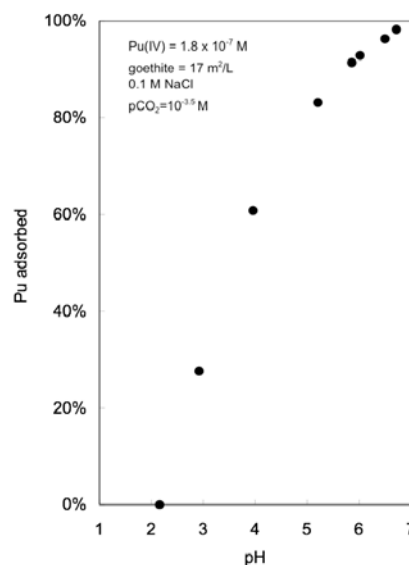


Figure 1. Sorption edge of Pu(IV) onto synthetic goethite.

constants for Pu(IV) and for formation of carbonate and phosphate species from the NEA TDB project and Lemire (6).

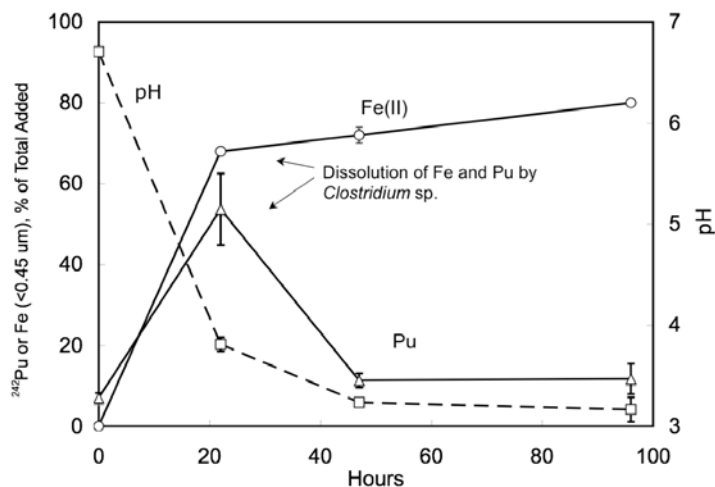


Figure 2. Reductive dissolution of iron and release of Pu due to growth of *Clostridium* sp. BC1.

Concomitant with microbial growth is an increase in biomass and increase in the inorganic phosphate concentration in the medium (47 hrs., 0.3 mM orthophosphate). Reductive dissolution of goethite stimulated the release of phosphate (in the absence of the solid iron oxide phosphate was not detected in solution at 47 hours). Studies of ^{230}Th in this system showed that the Th(IV) was solubilized over the same period of time and rapidly precipitated at 48 hours. Geochemical modelling of Pu(IV) in the growth medium reveals that at pH 3 and in the presence of 0.3 mM PO_4^{3-} , actinide phosphate species dominate and could precipitate Pu as insoluble or colloidal phases. In addition, phosphate rich functional groups at the bacterial cell surface, and exudates released in the medium stimulated by solid iron oxide dissolution, can interact with the mobilized actinide. These studies demonstrate the redistribution of Pu due to anaerobic microbial activity.

This research was supported by the Environmental Remediation Sciences Division, Office of Biological and Environmental Research, Office of Science, US Department of Energy under Contract No. DE-AC02-98CH10886.

1. C.J. Dodge, A.J. Francis, J.B. Gillow, G.P. Halada, C. Eng, C.R. Clayton. *Environ. Sci. Technol.* **36** (2002).
2. W. Keeney-Kennicutt and J.W. Morse. *Geochim. Cosmochim. Acta* **49**, (1985).
3. B.A. Powell, R.A. Fjeld, D.I. Kaplan, J.T. Coates, and S.M. Serkiz. *Environ. Sci. Technol.* **39**, (2005).
4. A.J. Francis, and C.J. Dodge. *Environ. Sci. Technol.* **24** (1990).
5. U. Schwertmann and R.M. Cornell, *Iron Oxides in the Laboratory*. New York: Wiley-VCH (2001).
6. R.J. Lemire. *Chemical Thermodynamics of Neptunium and Plutonium*. OECD-NEA (2001).

RESULTS AND CONCLUSIONS

The pH sorption edge for Pu(IV) onto goethite was characterized by a steep increase in adsorption between pH 3 and 6 with >95% uptake at pH 6-7 (the pH_{pzc} of goethite is ~ 7) (Figure 1). Biotransformation of the Pu adsorbed to the goethite resulted in dissolution of iron and a corresponding release of ^{242}Pu into solution ($<0.45 \mu\text{m}$) (Figure 2). At 22 hours $66 \pm 3\%$ of the iron and $54 \pm 9\%$ of the Pu was released into solution at pH 3.5. However the Pu was removed from solution by 47 hours, with only $15 \pm 1\%$ of the total detected in the $<0.45 \mu\text{m}$ fraction.

Plutonium in seawaters of the Pacific Ocean

K. Hirose*, M. Aoyama*, C.S. Kim†

*Meteorological Research Institute, Nagamine 1-1, Tsukuba, Ibaraki 305-0052, Japan

†Korea Institute of Nuclear Safety, Daeduk-Danji Daejeon 305-336, Korea

INTRODUCTION

Plutonium in seawater of the Pacific has been introduced in ocean surface by global fallout due to atmospheric nuclear weapons testing, from which the major fallout occurred in the early 1960's.^{1,2} A significant amount of plutonium was injected into seawater by close-in fallout from the US nuclear explosions conducted at the Pacific Proving Grounds in the Marshall Islands in the 1950's^{3,4} and the French nuclear explosions conducted at the French Polynesia.⁵ As a result, the Pacific waters have been contaminated by plutonium. The vertical and horizontal distributions of plutonium in the Pacific as did its temporal trend and biogeochemical behaviour have been reviewed by Livingston et al. (2000)⁶, Hamilton et al. (1997)⁷, and Hirose and Aoyama.⁸

Until 1997, there is a little information on the spatial distribution of plutonium concentrations in seawater of the Pacific except the GEOSECS expedition³ and the continuous monitoring of the western North Pacific.⁹ Recently, some research projects have been conducted to survey artificial radioactivity contamination in the World Ocean, in which Worldwide Marine Radioactivity Studies (WOMARS: an IAEA's Co-ordinated Project)¹⁰ and Southern Hemisphere Ocean Tracer Study (SHOTS: MRI, JAMSTEC, IAEA-MEL, KINS and others) were included.¹¹ These projects provide new data of plutonium concentrations and plutonium isotope ratios in seawaters of the Pacific, especially the South Pacific. As a result, we can depict the current features of plutonium contamination levels in the Pacific waters as do the transport processes of plutonium in the ocean and the interaction of plutonium with biogenic particles in seawater.

SAMPLING AND METHOD

Surface water samples were collected during cruises on board the R/V Ryofu-maru (the Japan Meteorological Agency) and the R/V Mirai (the Japan Marine Science and Technology Center), respectively, over the period from 1997 to 2004. All water samples were filtered through a fine membrane filter (Millipore HA, 0.45 µm pore size) immediately after sampling.

Plutonium isotopes dissolved in seawater were coprecipitated with Fe hydroxides from 50 to 200 L of seawater samples. Plutonium (^{239,240}Pu) concentrations were assayed using α-spectrometry and SF-ICPMS¹² following radioanalytical separation using anion exchange resin and extraction chromatographic resin (TEVA), described in detail elsewhere.⁹ The chemical yield was determined by the addition of a known amount of ²⁴²Pu.

PLUTONIUM IN THE PACIFIC

In the 1970s, ^{239,240}Pu concentrations in surface waters of the Pacific showed a typical latitudinal distribution of high in mid-latitudes of the North Pacific and low in the South Pacific.⁸ This pattern has been considered to reflect the geographical distribution of global fallout due to the atmospheric

nuclear weapons testing. We examined the latitudinal distribution of surface $^{239,240}\text{Pu}$ in the period from 1997 to 2004. The present $^{239,240}\text{Pu}$ concentrations in surface waters of the North Pacific were in the range of 1.5 to 9.2 mBq m^{-3} , whereas the $^{239,240}\text{Pu}$ concentrations in surface waters of the South Pacific were in the range of 0.8 to 4.1 mBq m^{-3} . Surface $^{239,240}\text{Pu}$ showed no marked inter-hemisphere distribution in the North Pacific, although spatial variation of surface $^{239,240}\text{Pu}$ has been observed. In fact, there is the longitudinal variation of surface $^{239,240}\text{Pu}$ along 30°S as shown in Fig. 1. The result suggests that the current level of surface $^{239,240}\text{Pu}$ in the Pacific is controlled by oceanographic processes such as advection and diffusion as well as biogeochemical processes.

The vertical profiles of $^{239,240}\text{Pu}$ observed in mid-latitudes of the North Pacific are characterized by a typical distribution pattern with surface minimum, subsurface maximum (700 - 750 m depth) and gradual decrease with increasing depth. In the South Pacific, the vertical profiles showed the similar pattern as that in the North Pacific. However, the $^{239,240}\text{Pu}$ concentrations in deep waters (> 700 m depth) of the South Pacific were significantly lower than that in the North Pacific. It has been reported that the subsurface maximum of $^{239,240}\text{Pu}$ in mid-latitudes of the North Pacific has moved into deeper water.⁶ This pattern of vertical $^{239,240}\text{Pu}$ profiles and their temporal change has been demonstrated by particle-scavenging processes, the removal of $^{239,240}\text{Pu}$ by sinking particles following regeneration of dissolved $^{239,240}\text{Pu}$ due to the biological degradation of particles.

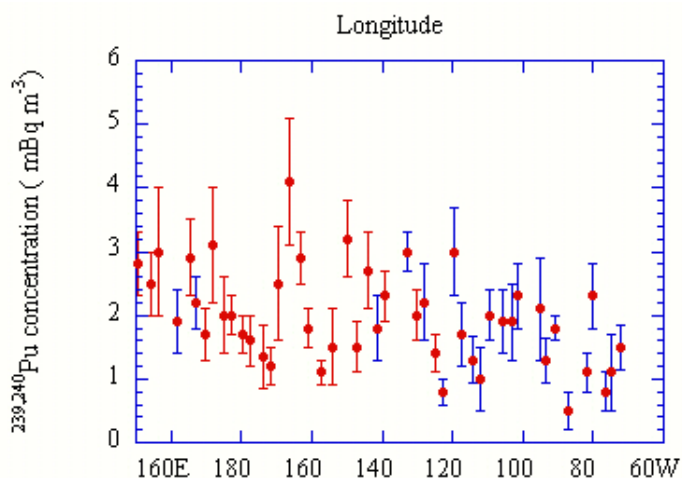


Fig. 1 Longitudinal distribution of $^{239,240}\text{Pu}$ concentrations in the mid-latitude region of the South Pacific

- 1 J.H. Harley, *J. Radiat. Res.*, 21, 83 (1980).
- 2 K. Hirose, *et al.*, *Plutonium in the Environment*, A. Kudo, Ed, Elsevier Science (2001).
- 3 V.T. Bowen, *et al.*, *Earth Planet. Sci. Let.*, 49, 411 (1981).
- 4 K.O. Buesseler, *J. Environ. Radioact.*, 36, 69 (1997).
- 5 R. Chiappini, *et al.*, *Sci. Total Environ.*, 237/238, 269 (1999).
- 6 H.D. Livingston, *et al.*, *Plutonium in the Environment*, A. Kudo, Ed, Elsevier Science (2001).
- 7 T.F. Hamilton, *et al.*, *Radionuclides in the Ocean Inputs and Inventory*, eds., P. Guéuati, et. al., (1996).
- 8 K. Hirose and M. Aoyama, *Deep-Sea Res. II*, 50, 2675 (2003).
- 9 K. Hirose *et al.*, *J Radioanal Nucl Chem* 248, 771 (2001).
- 10 P.P Povinec *et al.*, *J. Environ. Radioact.*, 81, 63 (2005)
- 11 M. Aoyama *et al.*, *Intern. Conf. on Isotopes in Environmental Studies- Aquatic Forum 2004*, (IAEA-CN-118)
- 12 C.S. Kim, C.K. Kim and K.J. Lee, *Anal. Chem.*, 74, 3824 (2002).

On the possibility of application of ultrashort pulses of laser radiation to study the properties of metallic Pu under extreme conditions

A.Ya. Uchaev, V.T. Punin, N.I. Sel'chenkova, E.V. Kosheleva

Russian Federal Nuclear Center – VNIIEF, Russia, 607188, Nizhni Novgorod region, Sarov, Mira avenue 37, uchaev@expd.vniief.ru

At present the knowledge of matter behavior under extreme conditions is acute as, for example, ultimate capabilities of current technology and unique scientific facilities are related to the processes caused by powerful impulse action on the matter.

The knowledge of behavior of metallic *Pu* under extreme conditions is acute at present due to insufficient knowledge of properties of metallic *Pu* of different age and its behavior at high-intense pulse action.

To study the dynamic failure phenomenon¹⁻³, there were applied the methods of explosion and shock-wave loading (longevity is $10^{-5} < t < 10^{-8}$ s), the heat shock method (HS - longevity range $t \sim 10^{-6} \div 10^{-10}$ s); as well as to study the dynamic failure in subnanosecond range ($10^{-9} \div 10^{-11}$ s), there were applied ultrashort pulses of laser radiation (USPLR) with power density J of laser radiation up to $J \sim 10^{14}$ W/cm².

The paper contemplates a possibility for applying the critical phenomena theory and theory of second-kind transitions to the description of failure process at the final stage in the dynamic longevity range (submicro-subnanosecond range).

As a result of a large scope of research^{1,2} it was shown that arising dissipative structure – failure centers cascade - puts up the resistance of the body to the external action in the dynamic longevity range. The failure centers cascade is a fractal cluster.

A model of lattice gas was applied for adequate mathematical modeling of the arising failure centers cascade which is a percolation cluster at the stage of macro-failure.

At present it is known that canonical distribution function in the Ising model is similar to the function of distribution of large canonical ensemble in the lattice gas model. This reflects the analogy between the model of Ising ferromagnet and the lattice gas model.

Application of the apparatus of critical phenomena theory and second-kind transition theory in an effort to describe the dynamic failure processes at the final stage allowed determination of universal attributes of metals behavior in the dynamic failure phenomenon conditioned by self-organization and instability in dissipative structures.

On the basis of complex approach to the work there is considered a possibility for obtaining quantitative characteristics of behavior of a number of metals including metallic Pu, under extreme conditions on the macro-level on the basis of analysis of quantitative characteristics of dissipative structures, arising on different scale levels, whose behavior is similar to behavior of systems near the second-kind transition.

The approach proposed specifies the possibility for predicting behavior of a number of metals, including metallic Pu⁴ on different scale-time levels basing upon experimental studies performed in the laboratory environment on small samples.

1. R. I. Il'kaev, A.Ya. Uchaev, S. A. Novikov, N.I. Zavada, L. A. Platonova, N. I. Sel'chenkova. Universal metal properties in the dynamic failure phenomenon // DAN, 2002, vol. 384 (3), P. 328-333.

2. R. I. Il'kaev, V. T. Punin, A. Ya. Uchaev, S. A. Novikov, E.V. Kosheleva, L. A. Platonova, N. I. Sel'chenkova, N. A. Yukina. Time regularities of metals dynamic failure process conditioned by hierarchic properties of dissipative structures – failure centers cascades //DAN, 2003, vol. 393 (3), P.326-331.
3. A.Ya. Uchaev, V.T. Punin, S. A. Novikov, E.V. Kosheleva, A.P. Morovov, L. A. Platononva, N. I. Sel'chenkova, N.A. Yukina. “Substantiation of the possibility of obtaining of quantitative characteristics of metals behavior under extreme conditions on the macro-level on the basis of regularities of behavior on meso-level”. Matter extremal states. Detonation. Shock waves. Proceedings of the International Scientific Conference, the VII Khariton Readings. 14-18 March 2005. Edited by the Doctor of Sciences, Engineering, A.L. Mikhailov. RFNC-VNIIEF Sarov. 2005. P. 356-361.
4. Plutonium Handbook A Guide to the Technology, volume I. Edited by O.J. Wick Pacific Northwest Laboratories Battelle Memorial Institute. 1967 by Gordon and Breach, Science Publishers, Inc. 150 Fifth Avenue, New York.

Neutron Resonance Spectroscopy Measurements of Temperature and Velocity During Shock Wave Experiments

D.C.Swift and V.W.Yuan

Los Alamos National Laboratory, Los Alamos, NM 87545, USA

INTRODUCTION

Most of the applications of high-pressure physics, and many of the experimental measurements, involve dynamic loading and shock waves. A key outstanding problem is the measurement of temperatures within condensed matter during dynamic loading. Temperature is a critical quantity in many aspects of the response of condensed matter to dynamic loading, as it governs the activation of processes including phase transitions, chemical reactions, and plastic flow. Without reliable measurements of the temperature within a sample, the value and effects of temperature can be deduced only indirectly, for instance from surface measurements.

Neutron resonance spectroscopy (NRS) is a very powerful technique, offering the possibility of direct measurements of internal temperature on short time scales, even for opaque materials such as metals. A small number of shock wave experiments have been performed to investigate the feasibility of the technique. Temperatures measured in a model system thought to be well understood were higher than expected, highlighting unresolved issues either with the experimental technique or with the theoretical model. Here we discuss contributions to the temperature from plastic flow, and newly-quantified details of the shock-loading system which may appear as a higher apparent temperature.

PREVIOUS RESULTS FOR MOLYBDENUM

NRS measurements¹ of temperature in shock-loaded systems have been performed at the LANSCE accelerator at Los Alamos National Laboratory. In each experiment, a pulse of 800 MeV protons was used to generate a pulse of neutrons from a nuclear spallation target. The neutrons were moderated to epithermal temperatures before use in the resonance spectroscopy measurement. The sample material was dilutely doped with an element possessing suitably-chosen neutron resonances: energies of a few tens of electron-volts, fairly narrow, and clearly distinct from resonances in the sample material. A region of high and (close to) constant shock pressure was induced by the impact of a projectile. The neutron pulse was synchronized to arrive while the shock state was as constant as possible over the doped region. The neutrons interacted with the resonances in the dopant nuclei according to the energy of the neutrons in the rest frame of each nucleus; thus, in the laboratory frame, the interaction varied with the material velocity and temperature of the doped material, in a calculable way. Essentially, each absorption peak was shifted according to the relative velocity of the material and broadened according to its temperature. The modified resonance spectra were measured using time-of-flight discrimination of the neutrons at the detectors. Calibration experiments were performed on samples heated in an oven. Dynamic experiments were performed on Mo as a material for which it was expected that shock heating would be predicted accurately by continuum dynamics, and on a chemical explosive.²

The Mo was doped with ^{182}W , which has a usable resonance at 21.1 eV. In two experiments, samples were shocked to ~ 63 GPa, a value obtained by calculation using the laser Doppler velocimetry measured free surface velocity of the shocked sample and Mo equation of state, which describe the pressure-volume-energy relation. The experimentally-measured temperatures were 150-300 K higher than predictions using plausible equations of state (Figure 1).

THE EFFECT OF PLASTIC HEATING

Recently a new model and numerical method of solving the shock jump conditions for general forms of material response was used to predict the magnitude of plastic heating consistent with the shock jump conditions. Using the Steinberg-Guinan model of plastic flow stress in shocked Mo, the temperature was predicted to be significantly closer to the measurements (Figure 1). The flow stress may deviate from the Steinberg-Guinan predictions by tens of percent at high pressures, though the velocimetry records indicated that the difference may not be this large.

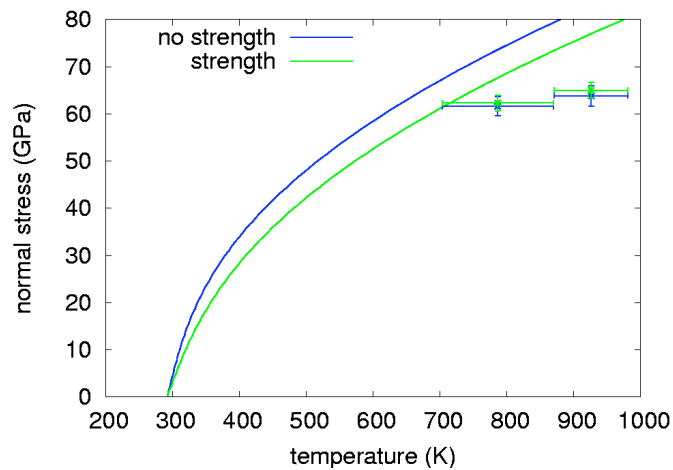


Figure 1: Comparison of shock Hugoniot with and without strength (curves), and NRS measurements (points). Note that the stress is inferred from the particle speed using the material model, and varies slightly depending on the strength.

POSSIBLE NON-IDEALITIES IN THE SHOCK SYSTEM

The shock-inducing projectile was launched using a high-explosive system.³ New simulations of the system and interpretation of the velocimetry record indicate that the projectile might have been accelerating on impact, and if so the shock pressure was not constant. Simulations also suggest that the projectile may be distorted on impact. Both effects would appear as a higher apparent temperature, suggesting that the NRS technique itself is likely to be more accurate than previously thought.

Discussions with C.Greeff, A.Seifert, and L.Bennett are gratefully acknowledged.

- 1 V.W.Yuan *et al.*, Phys Rev Lett, **94**, 125504 (2005).
- 2 D.J.Funk *et al.*, Proc. 11th Intl Detonation Symposium, 1998, U.S. Office of Naval Research.
- 3 C.A.Forest *et al*, *ibid*.

Future Capability for Experiments on the Dynamic Behavior of Materials at the LANSCE Scientific Firing Site

D.C.Swift, W.V.Anderson, and K.Schoenberg

Los Alamos National Laboratory, Los Alamos, NM 87545, USA

INTRODUCTION

This is an exciting time in shock physics. Recently, great advances have been made in developing new techniques for applying the load to the sample, and in probing the response of the sample. It is now possible to investigate the response at the atomic level as well as the average or bulk response, and thus to explore the contribution of different physical processes to the behavior of the material. Atomic-level measurements and simulations are also converging so that direct comparisons can be made.

Some of the new experimental capabilities require large facilities such as particle accelerators, and it is common for an experimental facility to specialize in a subset of the capabilities desirable for a thorough characterization of material response and underlying physics. We are proposing to develop a new experimental facility based around an enhancement to the LANSCE accelerator at Los Alamos National Laboratory, which would build on the exceptional diagnostics afforded by LANSCE and combine them with a selection of loading techniques other diagnostics to maximize the rigor and accuracy with which dynamic loading measurements can be made. The configuration is designed to allow great flexibility in experimental configurations and efficiency in acquiring data.

The new facility will also allow experiments on warm dense matter and the development of applications for high-energy short-pulse lasers.

DYNAMIC LOADING AND DIAGNOSTIC CAPABILITIES

The LANSCE enhancement is expected to lead to a factor of $\sim 10^2$ increase in proton current, along with changes in pulse structure. The spallation neutron source will be reconfigured to allow shock experiments to be probed without the degree of disruption currently caused to other users. A prime driver for locating the Scientific Firing Site at LANSCE is to enable experiments to use proton radiography (pRad) and neutron resonance spectrometry (NRS) more routinely and with large improvements in signal, etc. Density and damage distributions can be reconstructed from pRad measurements, with the possibility of discriminating between materials of different composition. NRS measurements can detect the temperature and velocity within materials, even if optically opaque.

Loading methods will include a gas/propellant gun, containment vessels for high-explosive drives, a ~ 100 kJ class capacitor bank to launch flyers or induce ramp loading, and ~ 5 kJ class lasers capable of inducing shock or ramp loading by surface ablation (~ 1 to 10 ns pulse length) or of inducing loading or launching flyer plates by tamped ablation (~ 0.1 - 2 μ s pulse length). Nanosecond laser pulses will also be used to generate x-rays for radiography and diffraction. It will be possible to preheat or precool the sample.

A suite of optical techniques will be available to measure velocity, displacement, electronic band structure (e.g. from multi-band ellipsometry), vibrational modes (e.g.

from Raman spectrometry), emission spectra, and particulate holography. These will require additional, lower-power probe lasers. A pulsed-power x-ray source will be used for radiography, diffraction, and *in-situ* imaging of defects during loading. A high-power short-pulse laser (100 J class, ~100 fs-1 ps pulse length) will be included in the facility, and could be used as an x-ray source, or even to accelerate electrons or ions. The facility will be configured and managed so that the core loading and diagnostic capabilities are readily accessible and well-maintained, while making it possible to develop new capabilities. Dynamic electron microscopy is a diagnostic which we plan to develop, possibly using a short-pulse laser pulse to accelerate the electrons. An important consideration will be the synchronization of the different loading methods and diagnostics: this will be made as straightforward, reliable, and reproducible as possible for users.

The experimental area will be laid out so that several different experiments can be performed simultaneously. In particular, this means that laser – and possibly proton – beams will be designed with flexibility in the beam transport. The facility will be licensed to perform experiments on toxic and radioactive materials, including plutonium.

EXPERIMENTS ON THE BEHAVIOR OF CONDENSED MATTER

The mainstay of shock physics experiments will be the well-diagnosed single-shot measurement. There is a huge opportunity to perform experiments on the effect of the microstructure of materials on their plastic flow properties, tensile damage leading to spall and ejecta, and phase changes. For these experiments, the microstructure must be well-characterized and often constructed to investigate some particular conformation of crystals or voids, and the loading history must be controlled and understood very well. For some studies, it may be advantageous to operate at a high repetition rate, e.g. to collect statistics of the onset of a phase change in a single crystal, translating the crystal automatically between shots. It may be possible to perform some such multi-shot experiments with laser loading.

We envisage a series of experimental campaigns exploring different aspects of shock physics and material dynamics, and employing a few basic experimental configurations:

- Equation of state to a few hundred gigapascals, driven by gun, pulsed power or laser, and using velocimetry and NRS, and possibly radiography.
- Phase change dynamics from a few to a few hundred gigapascals, loaded using all of the techniques, and probed using velocimetry, ellipsometry, Raman spectrometry, and x-ray diffraction.
- Plasticity, mainly at a few to a few tens of gigapascals, loaded by all techniques and probed with velocimetry, NRS, x-ray diffraction, and x-ray imaging of defects.
- Tensile damage and ejecta, loaded mainly by gun, pulsed power and explosives, and probed with velocimetry, pRad, x-ray radiography, and holography.
- Experiments on configurations representing parts of application systems, such as inertial fusion capsules.

A huge amount of science will be accessible in this way, and we anticipate that this flexible facility will make it possible to add currently unforeseen capabilities relatively painlessly further in the future.

Actinide Sample Preparation for Materials Science, Chemistry, and Physics

M. A. Wall, J. J. Welch, A. J. Schwartz, and M. J. Fluss

Lawrence Livermore National Laboratory, Livermore CA 94550 USA

Abstract

The development of the Actinide Sample Preparation Laboratory commenced in 1998 driven by the need to perform transmission electron microscopy studies on aged plutonium alloys. Remodeling and construction of laboratory space in the Chemistry and Materials Science Directorate at LLNL was required to turn a radiological laboratory into a type III workplace. A dry-train glove box (Figure 1) with a baseline atmosphere of 1 ppm oxygen and 1 ppm water vapor was installed to facilitate sample preparation with a minimum of oxidation or corrosion. This glove box continues to be the most crucial element of the laboratory allowing essentially oxide-free sample preparation for LLNL-based characterizations such as transmission electron microscopy, electron energy loss spectroscopy, optical microscopy, electrical resistivity, ion implantation, and differential scanning calorimetry. In addition, the glove box is used to prepare samples for experiments at world-class facilities such as the Advanced Photon Source at Argonne National Laboratory, the European Synchrotron Radiation Facility in Grenoble, France, the Stanford Synchrotron Radiation Facility, the National Synchrotron Light Source at Brookhaven National Laboratory, the Advanced Light Source at Lawrence Berkeley National Laboratory, and the Triumph Accelerator in Canada.

Preparation Methodology

Nearly all of the sample preparation procedures are based upon the fundamental metallographic preparation procedures of dicing, lapping, polishing, etching, and electrochemical polishing¹. The experimental methodology for sample preparation and design is based upon a lowest common denominator shaped sample. Simple put, a standard 3mm diameter transmission electron microscopy (TEM) sample shape is the basic geometry for virtually all of the small scale science experiments. For example, prior to thinning a 3mm diameter by 100 μ m thick TEM disc to electron transparency it is possible to (i) prepare one side of the sample for optical microscopy (figure 2), (ii) perform standard X-ray diffraction, (iii) measure resistivity² (Figure 3), (iv) further thin for EXAFS³ (Figure 4) and/or in-elastic X-ray studies⁴ (Figure 5a,b), (v) finally thin for TEM studies (Figure 6a,b).

Conclusion

The combination of small sample methodologies, adapted conventional sample preparation techniques, and custom built laboratory and glovebox designs has lead to versatile, efficient sample preparation of actinide samples for a wide variety of small-scale experimentation.

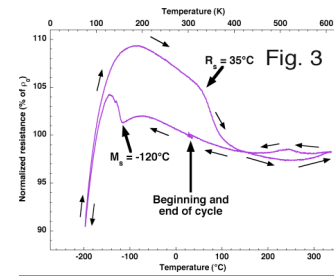
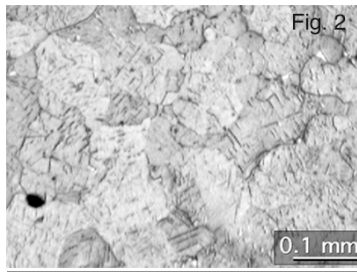
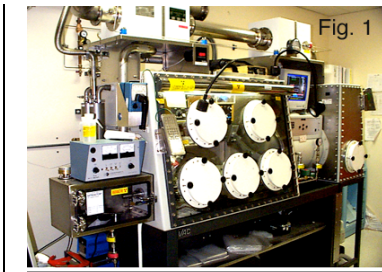


Figure 1. Glove box for small-scale sample preparation. **Figure 2.** Optical micrograph of a delta phase Pu-Ga sample after partial transformation to alpha-prime as a result of quenching to -120°C for ≈ 100 minutes. **Figure 3.** Resistivity data from a cooling and heating cycle of a Pu-Ga “TEM” disc specimen.

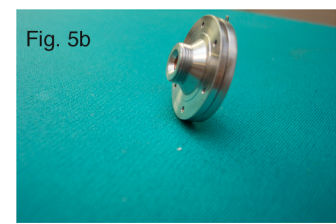
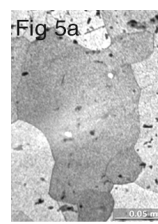
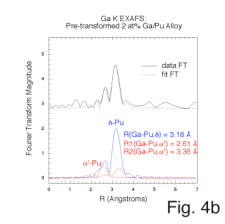
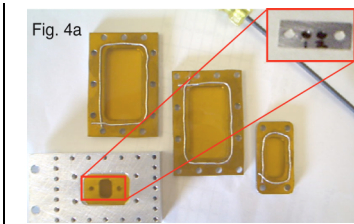
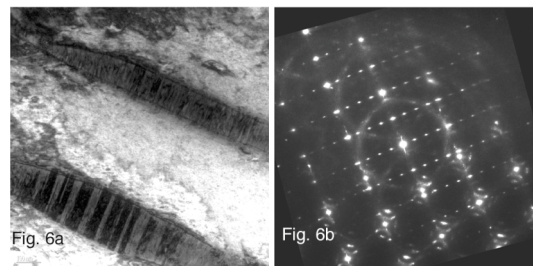


Figure 4.a) Insert shows 2 each, $\approx 10\mu\text{m}$ thin, “TEM” disc specimens that will be sealed inside a double Kapton windowed holder for EXAFS experiments. **b)** EXAFS data from a two-phase delta-alpha Pu-Ga sample. **Figure 5.a)** Optical micrograph of a large grain grown by stain-annealing for in-elastic X-ray experiments that produced the first measurements of the FCC Pu phonon dispersion curves. **b)** Double Kapton windowed sample holder for $\approx 8\mu\text{m}$ thick “TEM” disc samples used for the phonon dispersion experiments. **Figure 6 a)** Bright field TEM image of alpha-prime plates in a delta matrix. **b)** Electron diffraction from the alpha-prime plates and the delta matrix showing the Zocco orientation relationship.



This work was performed under the auspices of the U.S. Department of Energy by the University of California Lawrence Livermore National Laboratory under contract No. W-7405-Eng-48.

References:

- 1) Sample Preparation for Transmission Electron Microscopy Characterization of Pu Alloys, M. A. Wall, A. J. Schwartz and M. J. Fluss, LLNL report, # UCRL-ID-141746..
- 2) Phase Transformation Hysteresis in a Plutonium Alloy System, J.J. Haslam, M.A. Wall, D.L. Johnson, D.J. Mayhall, and A.J. Schwartz, MRS Proceedings, 2001, UCRL-JC-144283.
- 3) Local structure and vibrational properties of Alpha-Pu, Alpha-U, and the Alpha charge density wave, E. Nelson, P. Allen, K. Blobaum, M. Wall, C. Booth, *Phy. Rev. B* 71, 184113 (2005).
- 4) Phonon Dispersions of fcc -Plutonium-Gallium by Inelastic X-ray Scattering, Joe Wong , M. Krisch, D. Farber, F. Occelli, A. Schwartz, T.C. Chiang, M. Wall, C. Boro and Ruqing Xu, *Science*, 301, 1078 (2003).

Reinvestigating plutonium phase transitions using high purity electro-refined metal

A. Perry, M. Boyd, P. Roussel

AWE Aldermaston, Berkshire, UK, RG7 4PR

Plutonium is a unique element. In the pure state it has six temperature induced metallic phases. These phases start in the unusual monoclinic α -phase progressing through monoclinic β , orthorhombic γ to cubic (face centred) δ -allotrope. The transition from α to δ is accompanied by a 20 % density decrease. In the δ phase plutonium undergoes negative thermal expansion changing to the tetragonal δ' and finally increasing density by 4.6 % to the cubic (body centred) ϵ phase. It should be noted that there is some discrepancy within the literature on the actual transition temperatures. For example, the α to β transition has been reported in the range of 119 to 127 °C. This may arise from differences in sample purity and scan rates. Indeed, the δ' phase was only detected when metal of high purity became available.

These six temperature induced phases have been investigated in detail using a high purity electro-refined plutonium sample by dilatometry, differential scanning calorimetry and X-ray diffraction as a function of heating rate.

Evaluation of the nucleation and growth of helium bubbles in aged Plutonium alloys

D.W.Wheeler, P.D. Bayer, A. Perry, S. Kitching

AWE, Aldermaston, Reading, Berkshire, RG7 4PR, UNITED KINGDOM.

The processes of radioactive decay that take place in plutonium alloys can result in significant changes to their physical, chemical and mechanical properties. In order to understand the ageing behaviour of Pu alloys it is necessary to construct a model which will enable these changes to be quantified. The present study was undertaken to determine experimentally the fundamental parameters needed for such a model. Pu alloys of different ages and compositions were analysed using dilatometry to measure bubble growth and void swelling. The specimens were subjected to isothermal heat treatments for extended durations followed by metallographic examination in order to study the microstructures. Density measurements were also performed on the alloys while the effect of ageing on the mechanical properties was studied by hardness testing.

The results have enabled the calculation of the diffusion coefficient of He in Pu from the bubble size, bubble density and inter-bubble distances. The diffusion coefficients of He in Pu at elevated temperatures appear to be close to that of Ga in Pu. Extrapolation of the swelling rates from the elevated temperatures has predicted a density decrease of 0.0004 g cm^{-3} per annum at ambient temperature. However, there are no indications of the onset of steady state void swelling in 40 year old Pu.

© British Crown Copyright 2006 / MOD.

“PuGa and PuAl alloys density measurements using gas pycnometer: first results.”

O. Ast, S. Carlet, M. Perez, Boiteux.O.

CEA Valduc, DRMN/SEMP, 21120 Is sur Tille, FRANCE.

Plutonium alloys density is an important data to determine some metallurgical and mechanical parameters like martensitic (α') phase fraction (in relation with delta phase stability study) and elastic constants versus pressure (in relation with ultra sonic waves measurements). Density also gives some information about the quality of casting through its sensitivity to impurities contents. Generally, Archimede's technique is used to measure the volume of sample¹ and the density is determined by using the following equation: M/V (where M is the mass and V the volume of the sample). This technique has however a lot of limits:

- performing this measurement is difficult due to the difficulty to put the sample in the right location;
- accuracy is limited (from 0.05 to 0.1 g/cm^3) and depends on the weight of the sample;
- as it follows, large samples are necessary which is not always possible.

The gas pycnometer technique has been developed in glove box to improve the quality of density measurements. This presentation describes the principle of this technique and the process which is used. The second part is devoted to the first results on plutonium alloys and the accuracy of measurements.

The pycnometer determines density and volume by measuring the change in pressure of helium in a calibrated volume. The principle of this process is based on Mariott's law. The process frequently used, shown on figure 1, is described below.

The expansion chamber contains a volume of helium at a precise pressure. After introducing the sample in the sample chamber, difference in pressure is precisely measured between the expansion chamber and the sample chamber which allows determining the sample's volume.

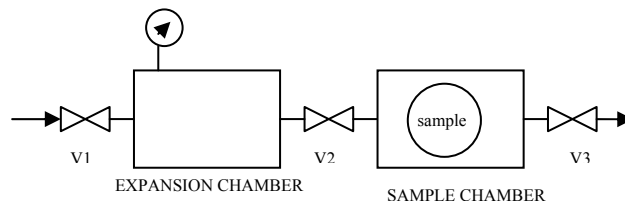


Fig 1: Schematic diagram explaining the gas pycnometer's process.

Steel and tantalum density measurements using this technique, have been performed and the accuracy has been improved (accuracy of tantalum density with pycnometry is 0.006 g/cm^3 whereas it is 0.02 g/cm^3 with Archimede's technique). Density measurements on nuclear materials are more difficult, especially for the plutonium alloys, for which we have to consider :

- the temperature instability (due to self heating and thermal expansion),
- the pressure instability due to the pressure variation in the glove box.

The second part of this work presents the study of the capability of the process (repeatability and reproducibility measurements). Some experiments have been performed on different delta stabilized plutonium alloys: PuGa 2,2 and 3,7 at% and PuAl 5 and 2 at%.

A metallurgical characterization of the alloys has been performed:

- grain size and microhardness;
- impurities (gallium, aluminum, carbon, oxygen, iron and nickel) X maps;
- alloying element contents profiles (microsegregation profiles) using EPMA.

First density measurements will be presented and compared with crystallographic density deduced from XRD measurements on the same batch of samples and from literature ².

The future studies aim at improving accuracy by working on the sample geometry and by using the real temperature of the sample given by modeling. Concerning aging studies, it will be interesting to study the density changes versus time. A comparison of swelling measurements by thermal expansion and density will also be done.

References

- 1 R.D Nelson, C. R. Becker, T. K. Bierlen, F.E. Bowman, AEC Research and Development Report, HW-80841, UC-25, Metals, Ceramics, and materials (TID-4500, 34th Ed.), (1964).
- 2 D.C. Miller and J.S White, Journal of Nuclear Materials 10, 4. 339-345, (1963).

Delta-phase stability in plutonium-aluminum alloys

P Bruckel*, B. Ravat*, L. Jolly*, N. Baclet*, V. Honkimaki†, G. González Avilés†

*CEA Centre de Valduc, 21120 Is-sur-Tille FRANCE

†ESRF, beamline ID15, 38000 Grenoble FRANCE

INTRODUCTION

The δ -phase of plutonium is stable between 592K and 724K but can be retained at room temperature by alloying plutonium with so-called deltagen elements (gallium, aluminum, americium, cerium...). The stability of the δ -phase strongly depends on several parameters such as the deltagen-element concentration, the metallurgical state of the alloy, the temperature and the pressure¹.

In this paper, the stability of the δ -phase in Pu-Al alloys is investigated. In a first part, the degree of stability of the δ -phase at low temperatures is discussed whereas a second part deals with the mechanisms of stabilization of the δ -phase.

EXPERIMENTAL

After casting and cutting of Pu-Al alloys with various aluminum concentrations (1.8, 2.3, 3.0 and 5.8 at%Al), one half of the Pu-Al samples is homogenized during 200 hours at 723K. The second half (as-cast samples) is considered as segregated (Figure 1). A 6 hours annealing at 533K is then performed to restore the metallic structure. Before any experiments, samples are electropolished to remove surface oxides and other possible impurities.

Chemical analyses are performed by Electron Probe MicroAnalysis (EPMA). Lattice parameters are deduced from Rietveld analysis of the X-Ray Diffraction patterns (XRD). Metallurgical state is characterized by using Optical Microscopy (OM) and EPMA (elements imaging).

The degree of stability of the δ -phase in Pu-Al alloys is characterized by the martensitic transformation temperature (M_S) determined from electrical resistivity measurements performed from 300K down to 4K. Influence of both the Al-concentration and the metallurgical state is investigated.

To go further, the mechanisms of stabilization of the δ -phase are studied by X-ray Total Scattering (XTS). Experiments are performed at room temperature at ESRF on the Pu-Al samples described before. The beamline ID15 allows working with an incident beam of high energy (~90 keV) that is particularly suitable for Pair Distribution Function analysis (PDF)². The PDF-method requires a good counting statistic and thus small and equiaxed grains. Therefore, samples of 300 μ m thick are rolled to get a final thickness of 140

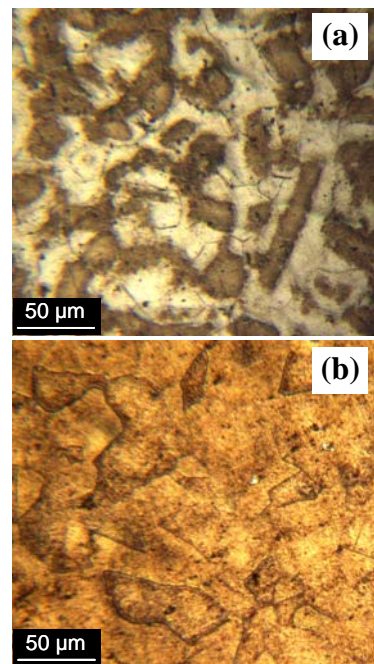


Fig 1: Micrographs of a PuAl 3at% alloy (a) in the segregated state and (b) in the homogenized state.

μm : the high mechanical strain (53%) associated to the rolling of the samples is used, in combination with an annealing treatment of 20 hours at 723K, to get small and equiaxed recrystallized grains.

DEGREE OF STABILITY OF THE δ -PHASE

For δ -stabilized Pu-alloys and depending on the delta-tagen concentration, a decrease in temperature can lead to a martensitic transformation which product, labeled “ α' ”, is monoclinic with solute atoms trapped in the structure¹. The martensitic transformation is characterized both by the temperature at which the transformation starts (M_S) and the amount of α' -phase formed. An increase in the aluminum content leads to a decrease in both the M_S temperature and the amount of α' -phase formed¹ (Figure 2), in agreement with a higher stability of the δ -Pu alloys.

Another parameter that might have an influence on the martensitic transformation is the metallurgical state of the Pu-Al alloys. In the segregated state, local micro-segregations of the Al-solute are observed (MO and EPMA): consequently, both the α - and δ -phases are present on XRD-patterns. The question lies on whether the already present α -phase makes it easier for the α' -phase to form.

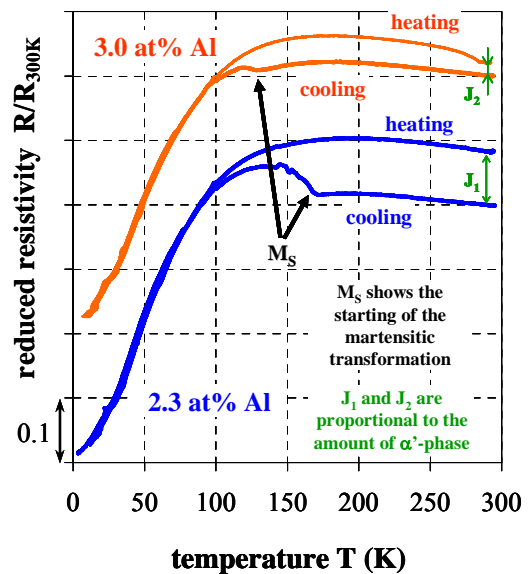


Fig 2: Electrical resistivity versus temperature for the homogenized PuAl 2.3 and 3 at% Al alloys.

STABILIZATION MECHANISM OF THE δ -PHASE

The mechanisms for δ -phase stabilization in δ -Pu alloys have been widely studied, though they are still not well understood, and are known to be strongly related to the electronic structure of the plutonium atoms. Furthermore, the electronic structure of Pu-alloys is directly related to their local structure.

The aim of XTS experiments coupled to PDF-analysis is to characterize the local atomic arrangement in Pu-Al alloys, depending on their composition and metallurgical state. By now, Conradson *et al.* have shown that a new phase labeled “ σ ” coexists with the δ -phase in Pu-Ga alloys containing 1.70 at %Ga to 3.35 at %Ga³: the σ -phase is assumed to be organized in nano-domains acting as precursors for a further martensitic transformation. Since the electronic structure of aluminum and gallium are equivalent, it might be assumed that the same mechanism is responsible for the stabilization of the δ -phase in Pu-Al and Pu-Ga alloys.

1 S.S. Hecker, Los Alamos Science, **2**, (2000).

2 T. Egami and S.J.L. Billinge, Underneath the Bragg peaks: structural analysis of complex materials, Pergamon Materials Series, **7**, (2003).

3 S.D. Conradson, Applied Spectroscopy, **52**, (1998).

THE INFLUENCE OF INTERNAL STRESSES INDUCED BY DECAY PRODUCTS ON ORIGINATION ON β - PHASE NUCLEATION DURING $\alpha \rightarrow \beta$ TRANSFORMATION OF UNALLOYED PLUTONIUM UNDER ISOTHERMAL CONDITIONS.

A.V. Troshev, A.M. Lyasota, S.I. Abramenko, Yu.N. Zuev, B.V. Litvinov

*Academician E.I. Zababakhin All-Russia Research Institute of Technical Physics,
456770, Snezhinsk, Chelyabinsk region, PO Box 245*

INTRODUCTION

It has been found that α -decay of plutonium leads to ‘self-induced’ defects in the lattice and to changes of chemical composition. It is expected that these changes at atomic level should modify of plutonium physical properties with time.

Successes in research of the problem of ‘plutonium self-irradiation’ at cryogenic temperatures so far do not allow prediction of plutonium behavior at high temperatures. There are at least two reasons explaining difficulties of plutonium research at high temperatures. First, as well known “general observations of self-irradiation damage show no major macroscopic changes for at least 40 years – in other words, plutonium does not “crumble” [1]. That is critical changes of plutonium properties do not occur during this time. However relying on results of studies of irradiation effects on metals and alloys we can make a reasonable assumption that plutonium is so far in so called ‘incubation period’ of properties alteration. In this case we need research techniques quite sensitive to plutonium changes at nano- and micro-level. Second, it is clear from general notions, that thermodynamically stimulated processes transpire in metal at high temperature and these process are associated with a trend of reduction of the system intrinsic energy. Stress relaxation as a rule occurs as a result of plastic strain and diffusion processes. It is clear that this evolution of metal structure without reference to specific experimentally observed structure-dependent phenomena complicates interpretation of experimental data.

Technique of plutonium research based on measurements of kinetic dependencies in phase transformations will meet the points above as we know that kinetics of plutonium phase transformations is highly sensitive to kinetics of structure defects alteration [2].

In the present paper we report the results of the first experimental studies of kinetics of $\alpha \rightarrow \beta$ -transformation in plutonium after long self-irradiation and the issues of measurement of quantities of excess energy accumulated as a result of α -decay and experimental studies of these energy relaxation kinetics.

EXPERIMENTAL RESULTS

Results of studies of isothermal phase transformation kinetics directly in plutonium performed with samples containing different levels of impurities and with nearly equal low rate of self-irradiation one more time confirm in our view the appropriate sensitivity of this technique to the level of structural defects (Fig.1).

Curves recorded from the sample with high rate of self-irradiation have demonstrated noticeable change of transformation parameters compared with initial state (Fig.2). Thus the change of chemical composition as a result of accumulation of α, β -decays products had a value by several orders of magnitude lower than initial level of impurities content. This indicates to significant (for transformation kinetics) change of metal structure specifically as a result of self-irradiation. Kinetic curve describing phase transformation in a sample with even higher rate of self-irradiation is illustrated in Fig.3. Here kinetic curve demonstrates not only noticeable alteration of transformation parameters, but also it has specific features: smooth trend of the curve is changed by stops at transformation that occur many times and are clearly observed.

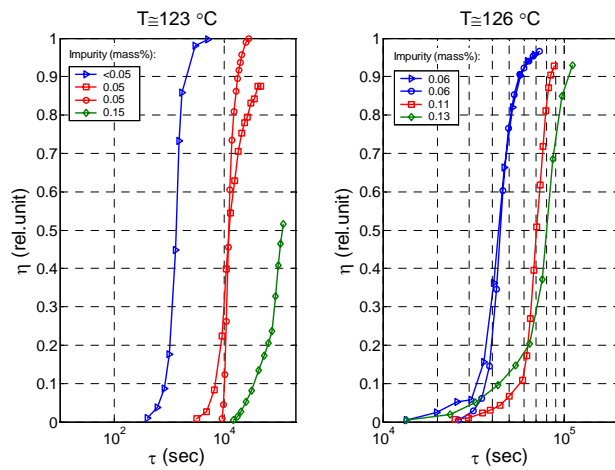


Fig.1 Kinetic curves of transformation for the samples with different content of impurities.

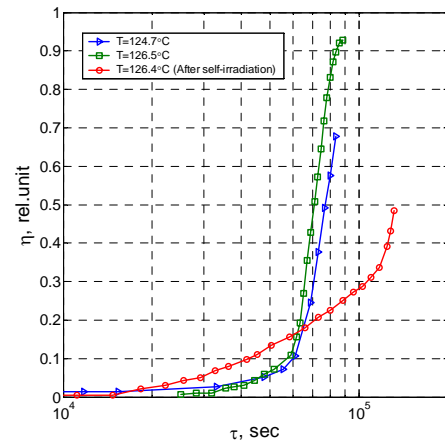


Fig.2 Changes of transformation kinetics as a result of self-irradiation

We have applied a classical approach to the issue of new phase origination at polymorphous transformation in single-component solid body for interpretation of these data [2]. According to this theory nucleation of new phase in a solid body occurs when the group of atoms overcomes the potentials barrier due to fluctuations and the energy of this barrier is proportional to the energy on the interface between the old and the new phase. It is assumed generally that the surface energy is an insurmountable barrier to transformation. Therefore the rate of phase transformation is essentially determined by the depth of elastic stress relaxation in subsurface zone of two phases interface. Accepted that the most efficient relaxation of elastic stress occurs as a result of plastic strain. Then two phases interface should be surrounded by a mesh of dislocations. Noteworthy that such dislocations mesh should have certain mobility sufficient for coalescence and growth of a new phase nuclei. We now from hardening theory that mobility of dislocations is finally determined by the dislocation elastic stress fields and the barriers to this mobility glide. Hence we come to a hypothesis that centers of elastic deceleration occur in a metal as a result of self irradiation and these centers decelerate dislocations (reduce dislocation mobility). Therefore extent of hardening will be determined by location and dimensions of these centers. Stops at the curve (Fig.3) correspond to kinetic processes leading to softening. According to this curve the softening process has several stages that testifies to the range of structure defects having different energies.

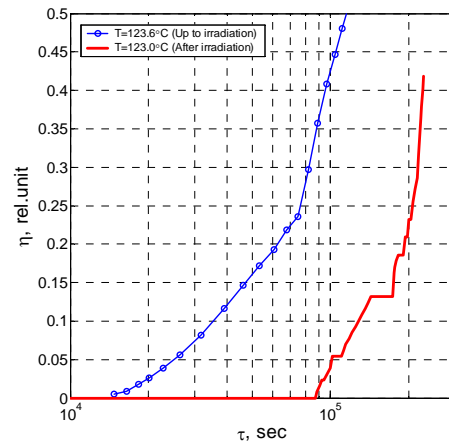


Fig.3 Variation of transformation kinetics at increase of self-irradiation rate.

Thus the energy of structural defects may be apparently determined from the ratio of transformation driving force proportional to exposure temperature and the sum of elastic stresses involved in nucleus origination.

References:

1. Sigfried S. Hecker, Joseph K. Marts. Ageing of plutonium and its alloys. Los Alamos Science. Number 26, (2000).
2. J. W. Christian. The theory of transformations in metals and alloys. Part 1: Equilibrium and general kinetic theory. Pergamon press. 1975.

Semiempirical Models for Describing Thermodynamic Properties of f-metals

V. M. Elkin, E.N. Mikhaylov, E.A. Kozlov

Institute of Technical Physics (RFNC-VNIITF), Snezhinsk, Russia 456770

ABSTRACT

The unusual thermodynamic properties (the abnormal behavior of elastic and thermophysical characteristics and the complicated and contradictory phase diagram) of some metal with unfilled f-shells (4f and 5f) are attributed to the close energies of electronic configurations. According to the present views, the electronic states differ either in the degree of spin screening of localized f-electrons (Kondo volume collapse model), or in localization and delocalization of f-electrons (Mott transition). At finite temperatures, thermodynamically stable states of a compound of atoms of different electronic structures may exist. From the literature we know about two, very similar semiempirical models which describe the states of a compound of different atoms. These are Strässler-Kittel two-level model and Aptekar-Ponyatovsky model for pseudo-binary solid solutions.

This paper studies capabilities of these models to describe the thermodynamic behavior of unalloyed cerium (4f metal), and unalloyed δ -plutonium and δ -plutonium-based alloys (5f-metals). It shows that with a small number of fitting parameters, both models adequately describe the abnormal behavior of these metals under varying temperature and pressure. However, Aptekar-Ponyatovsky model is preferable for practical purposes because it relates electronic structures to polymorphic modifications thus providing a basis for the construction of a multi-phase equation of state.

Experiments and model of dynamic deformation of U-238 and its alloy with Mo

B.Glushak, V.Pushkov, O.Ignatova

Russian Scientific-Research Institute of Experimental Physics, 607190, Sarov, Russia

INTRODUCTION

The results presented in this communication were gained by an analysis of the dynamic diagrams of uniaxial compression and tension of U-238 and its alloy with Mo (~1 wt %). The yield strengths presented in this study were assessed from the diagrams at different strain rates of $\dot{\epsilon} \leq 1800$ 1/s and initial temperatures $T \leq 600^\circ\text{C}$. The data obtained served as a basis for a semi-empirical model at the heart of which was an equation of state of U-238 and its alloy with Mo^{1,2}. Measurements were taken by the split Hopkinson pressure bar (SHPB) method³.

EXPERIMENTAL RESULTS

Compression. Yield strengths $\sigma_{-0,2}$ calculated from the σ - ϵ diagrams at different T and $\dot{\epsilon}$ values for uranium and its alloy with Mo are summarized in Table 1. The yield strength $\sigma_{-0,2}$ of the uranium alloy with molybdenum increased in proportion to the strain rate $\dot{\epsilon}$ and decreased almost linearly with increasing temperature^{2,3}.

Tension. The yield strength and tensile strength of uranium measured at $T \sim 0^\circ\text{C}$ and $\dot{\epsilon} = 1000$ 1/s were $\sigma_{+0,2} = (470 \pm 78)$ MPa and $\sigma_{+B} = (650 \pm 83)$ MPa, respectively. The samples failed at a percent elongation from 4,0 to 4,2%. The yield strength and tensile strength of the uranium alloy with Mo were $\sigma_{+0,2} = (900 \pm 56)$ MPa and $\sigma_{+B} = (1080 \pm 62)$ MPa, respectively, at $T \sim 0^\circ\text{C}$ and $\dot{\epsilon} = 1200$ 1/s. The samples were destroyed at a percent elongation of 15%^{1,2,3}.

Table 1. Yield strengths data

T, °C	U-238		U-238+Mo	
	$\dot{\epsilon}$, 1/s	$\sigma_{-0,2}$, MPa	$\dot{\epsilon}$, 1/s	$\sigma_{-0,2}$, MPa
20	100-420	565±42	280-360	760
	1300-1600	660±80	600-880	868±54
			1000-1400	990±70
100	520-1040	446±48		
200	160-1440	440±30	350-510	580±30
			800-1100	665±18
			1300-1800	720±67
400	540-890	300±13	200-520	370±40
			800-1000	426±52
			1200-1700	500±35
600			200-500	275±35
			850-1000	330
			1200-1400	360±26

MODEL FOR DYNAMIC DEFORMATION OF U-238 AND ITS ALLOY WITH MO

Consider U-238 and its alloy with Mo as an elastoplastic medium such that its stress strength σ_i can be represented as a function of four variables defining its strained state; in the simplest case, σ_i is a product of four simple functions f_i , each dependent on only one variable^{2,4}:

$$\sigma_i = \sigma_i(\varepsilon_i, \dot{\varepsilon}_i, P, T) = A f_1(\varepsilon_i) f_2(\dot{\varepsilon}_i) f_3(P) f_4(T) \quad (1)$$

Function $f_1(\varepsilon_i)$ in Eq.(1) allows for strain strengthening, $f_2(\dot{\varepsilon}_i)$ and $f_3(P)$, for the effects of the rate of plastic strain and pressure, respectively, and $f_4(T)$, for thermal softening. Function $f_3(P)$ looks as^{2,5} $f_3(P) = 1 + \alpha_0 P$, where $\alpha_0 = \text{const}$.

Dependence (1) was approximated by the following analytical function

$$\sigma_i = A \cdot [1 + a(\varepsilon_i)^m] \cdot \left[1 + b \left(\frac{T}{T_{ml}} \right)^n + d \left(\frac{T}{T_{ml}} \right)^k \right] \cdot \left[1 + c \left(\ln \frac{\dot{\varepsilon}_i}{\dot{\varepsilon}_{i0}} \right)^l \right] \cdot f_3(P); \quad (2)$$

here, A, a, b, c, d, n, m, l, and k are constants, $\dot{\varepsilon}_{i0} = 1 \text{ s}^{-1}$, and T_{ml} is the melting point.

Poisson's ratio μ is supposed to be a linear function of temperature, $\mu = 0,205 + 8,7 \cdot 10^{-5} T$, where T is an absolute temperature. By way of illustration, the experimental values of the conditional yield strength $\sigma_{-0,2}$ measured under dynamic compression are compared to their theoretical counterparts² calculated from Eq.(2) in Figure 1.

The range of validity of the proposed model for dynamic deformation of U-238 and its alloy with Mo is²: $P \leq 5 \text{ GPa}$, $\varepsilon_i \leq 0,12$, $\dot{\varepsilon}_i \leq 2 \cdot 10^3 \text{ 1/s}$, $293 \leq T \leq 873 \text{ K}$.

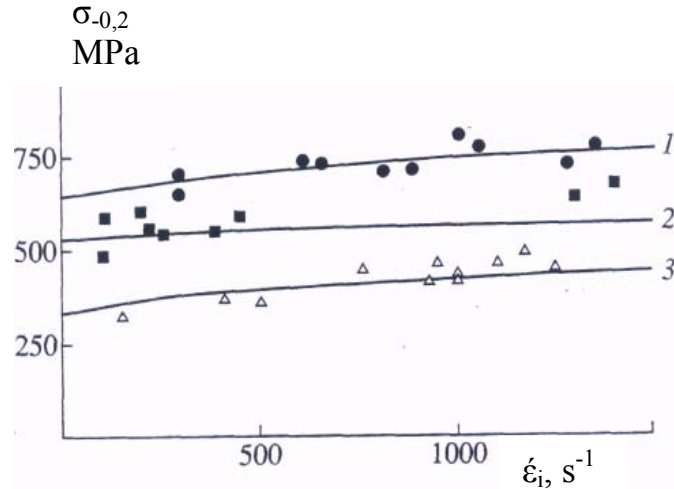


Fig 1: Conditional yield strength in the case of dynamic compression: (1)- $T=293\text{K}$, U-238+Mo; (2)- $T=293 \text{ K}$, U-238; (3)- $T=673\text{K}$, U-238+Mo; (■, Δ, ●) experimental data; solid curves were calculated.

1. B.L. Glushak, *et al.*, Proceedings of abstracts of papers for the XIV International Conference "Effect of intensive flows of energy on substance", Terskol, Russia, 96, (1999).
2. S.A. Novikov, V.A. Pushkov, *et al.*, J. Chemical Physics (Rus), **18**, №10, 22-25, (1999).
3. S.A. Novikov, V.A. Pushkov, *et al.*, Mechanical Properties of Uranium under Quasi-static and Shock-Wave Loading, Preprint No.54-97, Russia, RF Nuclear Center: Scientific-Research Institute of Experimental Physics, (1997).
4. D. Steinberg, S. Cochran, and M. Guinan, J. Appl. Phys., **51**, No.3, 1498, (1980).
5. B.L. Glushak O.N. Ignatova, J. VANT (Rus). Matematicheskoe Modelirovanie Fizicheskikh Protssessov, **2**, (1998).

Melting and Crystallization Front Induced Processes in a d-phase Pu Alloy Exposed to Laser Pulses*

A.V. Laushkin, V.K. Orlov, P.P. Poluectov, M.Yu. Bakursky, S.A. Kiselev, I.A. Larkin

A.A.Bochvar Research Institute of Inorganic Materials (VNIINM), Moscow, Russia

Behavior of gas pores in a liquid gas-saturated plutonium over a temperature range from the melting point to ~ 2000 °C is phenomenologically described. A d-phase plutonium alloy was tested. The elapsed time from the Pu alloy production was 13 years. In this period the sample accumulated about 500 ppm of helium.

Pore formation and growth processes (metallography, calculation of pore size changes) are described. Photos are presented showing the pore coagulation instant. A process initiated by motion of a crystallization front is discussed that is most likely responsible for the pore structure (Figure 1).

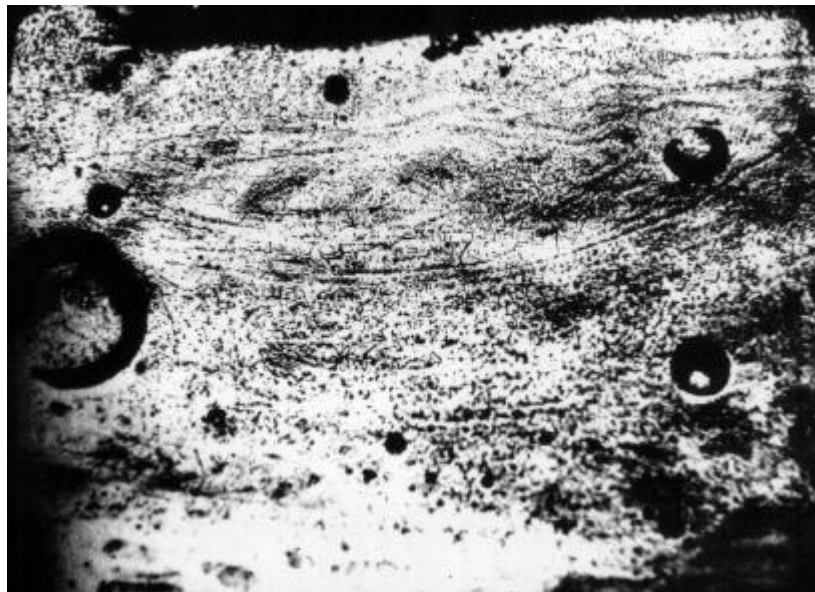


Fig 1: Photomicrograph of a cross-sectional microsection.

The kinetic viscosity of the alloy at about 1900 °C was estimated from eddy flows generated in a bath of the molten alloy.

* The sanction to an information exchange: dd-2071.

RFNC-VNIIEF Capabilities to Production High Enriched ^{242}Pu and ^{244}Pu

S.Vesnovskiy

Russia Federal Nuclear Center - VNIIEF, Sarov, Nizhni Novgorod Region, 607188, Russia

The report considers the possibilities of producing highly enriched isotopes ^{242}Pu and ^{244}Pu using a method of electromagnetic separation of **plutonium** isotope mixtures with different content of ^{242}Pu and ^{244}Pu . Different isotope compositions that can be produced in Russia through neutron irradiation of ^{242}Pu in a nuclear reactor with high density of neutron flux at various start materials and different irradiation duration are studied as original material. There are proposed optimal versions of ^{244}Pu production at the rates enough to realize investigations of fundamental plutonium properties and processes of its ageing. Preliminary estimations of the cost of these isotopes production are given.

Isothermal martensitic phase transformations in plutonium gallium alloys

B. Oudot, K.J.M. Blobaum, M.A. Wall, A.J. Schwartz

Lawrence Livermore National Laboratory, Livermore CA 94552 USA

INTRODUCTION

Under ambient conditions, the thermodynamically stable phase of pure plutonium is the brittle monoclinic alpha phase. However, the high-temperature delta phase (δ) can be retained at room temperature by alloying plutonium with a few atomic percent of gallium [1]. For Pu-Ga systems at ambient conditions, the retained δ phase is metastable and undergoes an extremely slow eutectoid decomposition to alpha (α) + Pu₃Ga. When the metastable δ phase is cooled to sub-ambient temperatures, a partial transformation to the alpha-prime (α') martensitic phase occurs. This α' phase is similar to the α phase, but it has Ga trapped in the lattice. Previously, the δ to α' phase transformation (at about -100 °C) and its reversion (at about 30°C) have been studied using cooling and heating cycles in a differential scanning calorimeter (DSC) [2]. Here, we investigate the kinetics of the δ to α' transformation in a Pu-2.0 at% Ga alloy under *isothermal* conditions. This δ to α' transformation is reported by Orme, *et al.* [3] to have unusual double-C curve kinetics in a time-temperature-transformation (TTT) diagram. Our work extends this TTT diagram from 200 minutes to 18 hours.

RESULTS AND DISCUSSION

The amount of α' formed during long isothermal holds at specific sub-ambient temperatures between -90°C and -160°C was investigated using DSC. For each experimental run, the sample was cooled from 25°C to the isothermal hold temperature at 20°C/min. Then it was held at a subambient temperature for 18 hours, heated to 350°C and cooled back to 25°C at 20°C/min. Prior to each experimental run, the sample was annealed at 375°C for 8 hours and then conditioned at 25°C for 12 hours [4, 5]. The amount of α' formed during each isothermal hold was quantified using the area of the α' to δ peak observed during the heating portion of the scan.

Orme, *et al.*'s work does not explicitly define time zero, but the TTT diagram indicates that transformation does not occur above -120°C. Therefore, for the present experiments, we define time zero as the time when the sample temperature reaches -100°C. This time is indicated on the cooling portions of the DSC scans shown in figure 1. The data shown in figure 1 was collected as the samples were cooled to the isothermal hold temperature. In this figure, it is clear that some δ to α' transformation did occur prior to each isothermal hold, except before the hold at -90°C.

The transformation prior to the isothermal hold is observed as several overlapping exothermic peaks beginning at about -102°C. These peaks are very reproducible and are believed to be the result of different kinds of δ to α' martensitic transformation. This may be due to the presence of different nucleation sites and/or different morphologies.

The results of the 18 hour isothermal holds give a cross-section of the TTT diagram at 18 hours, as shown in figure 2. Instead of plotting a contour line of constant amount of transformation, as is traditionally done in TTT diagrams, the contour in figure 2 is for constant time. This data suggests a confirmation of the double-C behavior because there are two temperatures at which local maxima in the amount of transformation occur (-130°C and -155°C). Between these two temperatures, there is a valley at -145°C where isothermal holds result in smaller amounts of transformation. Thus, the results presented here suggest that the isothermal δ to α' transformation has double-C curve kinetics, even when the transformation is allowed to proceed for times significantly longer than those included in the TTT diagrams published by Orme, *et al.*

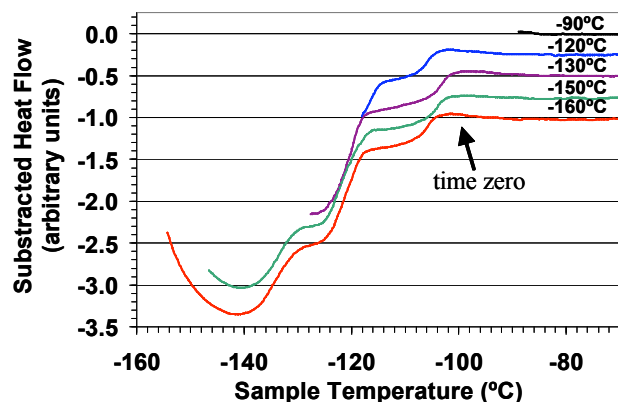


Figure 1. DSC thermograms corresponding to the δ to α' transformation during continuous cooling at 20°C/min before each 18 hour anneal. Transformation begins at about -102°C. The transformation results in and is evidenced by 3 overlapping exothermic peaks. The data have been offset along the y-axis for clarity.

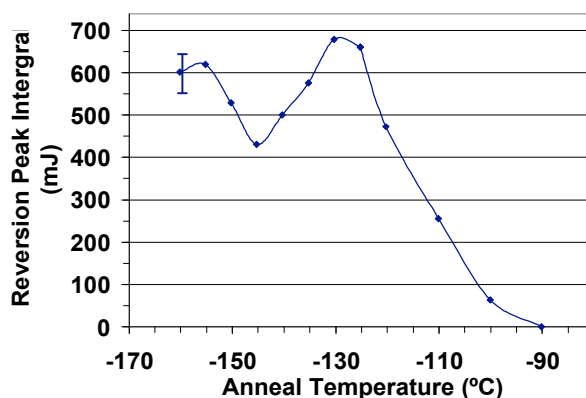


Figure 2. Integrated peak areas of the α' to δ reversion peaks following 18 hour isothermal holds versus anneal temperature. The amount of α' formed is related to the integrated area of the α' to δ reversion peak. Several runs with holds at -160°C give an approximation of the error, which is less than ± 50 mJ.

ACKNOWLEDGMENTS: *This work was performed under the auspices of the U.S. Department of Energy by University of California, Lawrence Livermore National Laboratory under contract No. W-7405-Eng-48 and the Commissariat à l’Energie Atomique (CEA) of Valduc located in France.*

REFERENCES

- [1] F.H. Ellinger, C.C. Land and V.O. Struebing, *J. Nucl. Mater.*, **12**, 226,(1964).
- [2] K.J.M. Blobaum, C.R. Krenn, J.N. Mitchell, J.J. Haslam, M.A. Wall, T.B. Massalski, and A.J. Schwartz, *accepted by Metallurgical and Materials Transactions*, 2005.
- [3] J.T. Orme, M.E. Faiers and B.J. Ward, *Plutonium 1975 and Other Actinides*, (edited by H. Blank and R. Lindner, North-Holland Publishing Company, Amsterdam, 1975), pp. 761.
- [4] K.J.M. Blobaum, C.R. Krenn, M.A. Wall, T.B. Massalaki and A.J. Schwartz : *to be submitted to Acta Mat.*, 2006
- [5] See a separate paper entitled “Evidence for formation of alpha embryos in a Pu-Ga alloy at ambient temperature” by K.J.M. Blobaum, C.R. Krenn, M.A. Wall, T.B. Massalski, and A.J. Schwartz in this volume.

Mechanical Property Measurements using Micro Test Bar for Pu Alloy Aging Study

B. Choi^{*}, B. Ebbinghaus[†], G. Gallegos[†]

^{*} Lawrence Livermore National Laboratory, Livermore CA 94552 USA

[†] Lawrence Livermore National Laboratory, Livermore CA 94552 USA

ABSTRACT

Modeling of the mechanical strength as a function of helium bubble in growth predicts that there can be a significant increase in the yield strength of plutonium if the helium bubbles are pressurized. For example if there is a He to vacancy ratio of 2, the increase in yield strength is about 30% in 100 years. Such a change is potentially important in assessing the lifetime of plutonium phase stabilities and in order to confirm the predictions of the model and the limited experimental data systematic tensile testing and possibly some hardness testing have been conducted on new and aged alloys.

This paper summarizes how strain rate (quasi-static), fabrication process history and prior thermal history affect the tensile property change observed from both naturally and accelerated aged plutonium alloys. For this study, the “micro tensile” test bar (about 0.060 inch diameter) and corresponding tensile test fixture has been developed and verified for use in measurement of tensile properties for the plutonium alloys under general tensile loading conditions. Initial testing has been conducted using 1100-H18 as a surrogate.

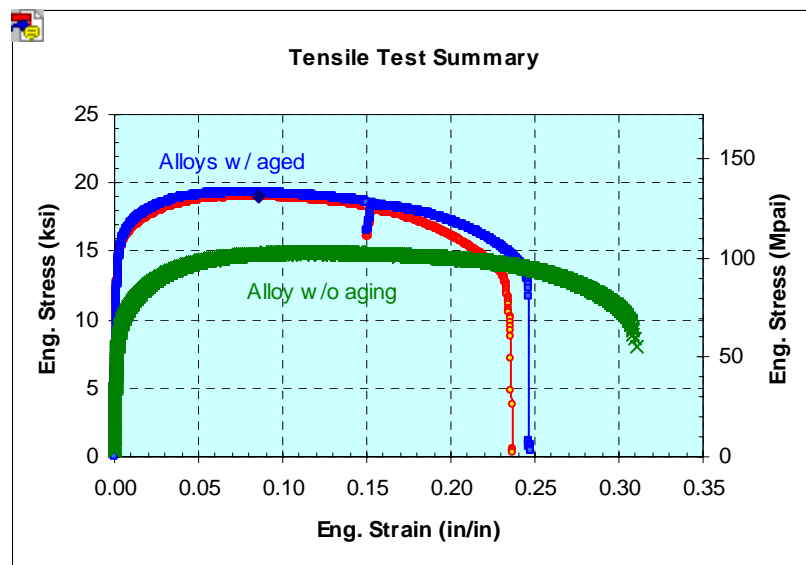


Fig 1: Engineering stress and strain curve from tensile test results for the delta-stabilized plutonium alloys

X-Ray Diffraction of Aged U-Nb Alloys

H.M. Volz, R.E. Hackenberg, A.M. Kelly, W.L. Hulst, A.C. Lawson, R.D. Field, D.F. Teter, and D.J. Thoma

Los Alamos National Laboratory, Los Alamos, NM, 87545 USA

ABSTRACT

Uranium alloys exhibit many different stable and metastable phases, including martensite. An improved understanding of phase stability of actinides would be advantageous. In particular, we are interested in the aging of U-Nb alloys. To this end, compositionally homogeneous U-5.5 Nb and U-7.5 Nb (wt%) experimental specimens have been artificially aged by heating to temperatures of 373K, 473K, 523K, and 573K for times ranging from 10 to 100,000 minutes. It is desirable to understand any long-term changes in the structure of these materials in order to improve predictions of materials properties over time, but changes may be subtle and elude standard metallographic techniques. Therefore, we collected powder diffraction patterns on these aged polycrystalline U-Nb samples using a laboratory X-ray diffractometer (CuK α source) along with a CeO₂ standard (Figure 1, below) and analyzed using full pattern Rietveld analysis with GSAS (Figure 2, next page). Surface preparation was achieved by mechanical and

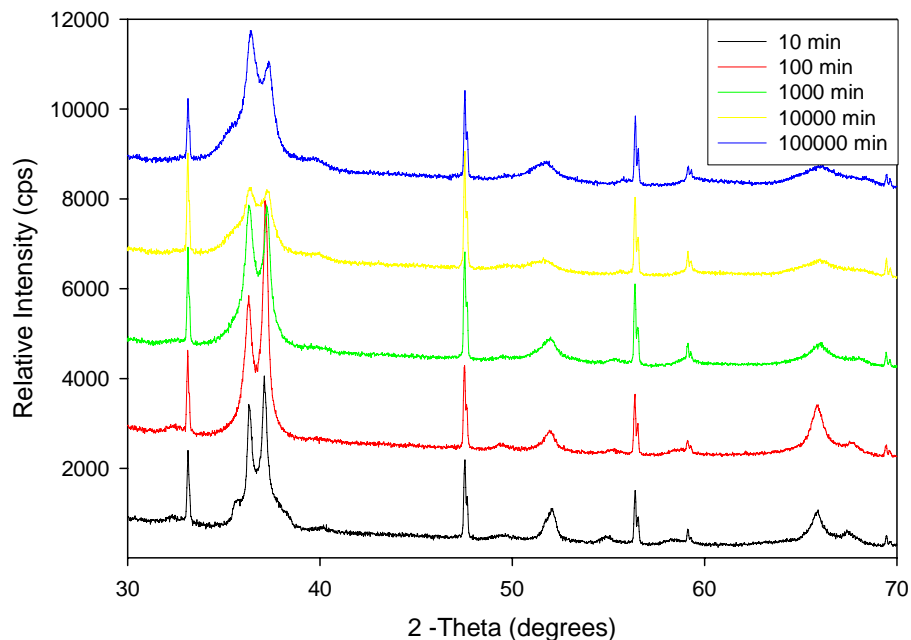


Fig 1: X-ray diffraction data of a U-7.5Nb alloy artificially aged at 573K for the times shown. Sharp peaks at 33°, 47°, 56° are from a ceria standard.

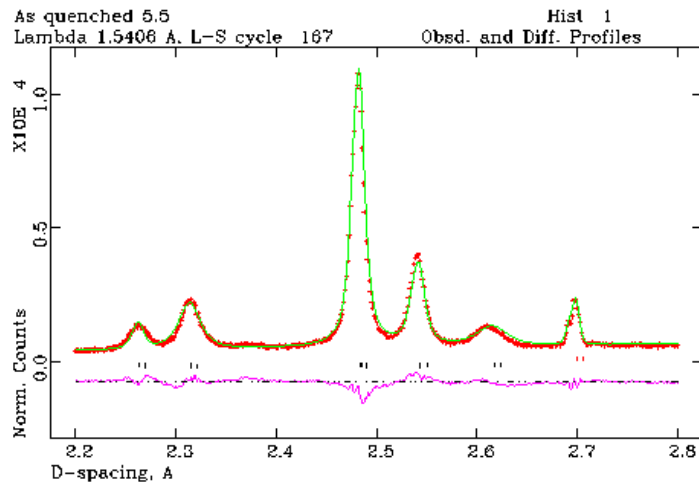


Fig 2: X-ray diffraction data of an as-quenched U-5.5Nb alloy showing the monoclinic α'' phase. Red are data points, green is refined Rietveld fit, black tick marks show positions of α'' phase, and purple is the difference curve between the data and fit.

electrochemical polishing. Multiple metastable and equilibrium phases are possible in the range of 0 to 10 wt% niobium, making interpretation challenging. At the time of this writing, trends in crystallographic parameters that would indicate mechanisms involved are ambiguous. We will present and interpret observations of aging-induced changes (or lack thereof) in lattice parameters, unit cell volume, atomic positions in the crystal structure, and composition of phases.

Acknowledgements: This research is sponsored by the US Department of Energy National Nuclear Security Administration under contract W-7405-ENG-36. LA-UR-06-1104.

The $\gamma \leftrightarrow \delta$ Transformation in Pure Pu: Thermal and Volumetric Characteristics and the Effect of Thermal Cycling

D. S. Schwartz*, J. N. Mitchell*, R. A. Pereyra*

*Los Alamos National Laboratory, Los Alamos NM 87545 USA

BACKGROUND

Plutonium is an excellent material for studying solid-state phase transformations because it goes through 6 allotropic phase transformations between room temperature and its 640°C melting point. We are using Differential Scanning Calorimetry (DSC), dilatometry, optical microscopy, and scanning electron microscopy to study solid-state transformations in pure Pu in detail. The $\gamma \leftrightarrow \delta$ (orthorhombic \leftrightarrow fcc) transformation is particularly interesting, and will be the focus of this paper. The $\gamma \leftrightarrow \delta$ transformation displays extreme asymmetry with respect to heating and cooling (Figure 1). On heating, the $\gamma \rightarrow \delta$ transformation is a conventional solid-state transformation, characterized by a single well-defined heat absorption event initiating at $\sim 323^\circ\text{C}$, spread over roughly 10°C at $10^\circ\text{C}/\text{min}$ scanning rate. The $\delta \rightarrow \gamma$ reversion on cooling has a completely different character. First, it initiates at 260°C , which is an unusually large supercooling of $> 60^\circ\text{C}$ below the onset temperature of the heating transformation. Secondly, the cooling transformation is characterized by a diminishing series of narrow heat release spikes, spread over an 80°C temperature range. This unusual transformation upon cooling was first reported several decades ago by Pascard¹, who suggested that the transformation was martensitic.

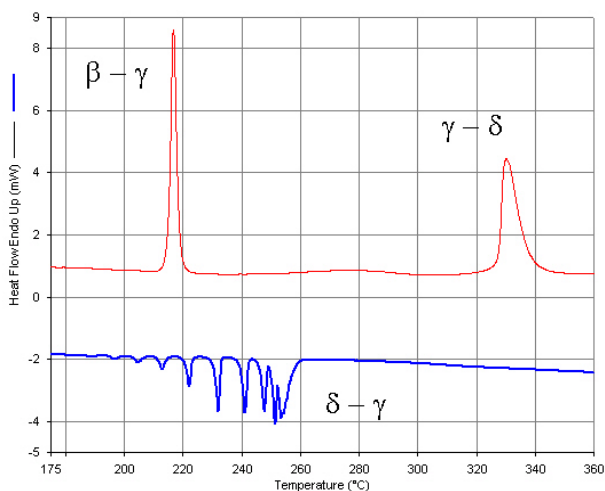


Figure 1. DSC thermal scans comparing enthalpic absorptions on heating (red curve) to enthalpic releases on cooling (blue curve) for the $\gamma \leftrightarrow \delta$ transformation.

RESULTS

The effect of cooling rate was explored over the range $1^\circ\text{C}/\text{min}$ to $50^\circ\text{C}/\text{min}$. The structure of the reversion was significantly dependent upon cooling rate in this range. The spacing and amplitude of the heat release spikes at the slower cooling rate was much more stochastic in character, while at the high rate the heat bursts were almost completely suppressed.

Dilatometry shows similar burst behavior to DSC. A significant difference is that the $\delta \rightarrow \gamma$ reversion shows a clear onset at $\sim 300^\circ\text{C}$ in the form of a slope change in the $\Delta L/L$ vs.

temperature curve. This indicates that the δ -phase begins to transform, or at least contract discontinuously, without releasing heat, as no heat release is seen by DSC before reaching $\sim 260^\circ\text{C}$. This pre-transformational phenomenon was explored by varying cooling rate and through the use of isothermal holds at different temperatures above the reversion onset.

If the heat release during cooling through the entire 260°C to 180°C temperature range is summed, it totals ~ 2.14 J/g, about 10% less than the heat absorbed during the $\gamma \rightarrow \delta$ heating transformation. This suggests that some δ -phase may be retained below 180°C . To explore this further, a series of heat-cool cycles was performed through the $\gamma \leftrightarrow \delta$ transformation where the Pu was cooled to different temperatures, all above the β -phase field stability region. These controlled cycles will be described in detail, and their effect on phase retention and the character of the $\gamma \leftrightarrow \delta$ transformation will be discussed.

The heating-cooling asymmetry of $\gamma \leftrightarrow \delta$ transformation has some features in common with another martensitic transformation that occurs in Pu stabilized into the δ -phase with small amounts of Ga². In this case, heat release bursts are seen when the martensitic phase (α') formed by cooling to $< -100^\circ\text{C}$ reverts to the δ -phase upon heating. The $\delta \rightarrow \gamma$ and $\alpha' \rightarrow \delta$ transformations both involve significant volume changes for a phase nucleating within a δ -phase matrix. However, significant differences exist and a detailed comparison will be drawn between the two transformations.

Los Alamos National Laboratory performed this work under the auspices of the US Department of Energy, (contract W-7405-ENG-36).

- 1 R. Pascard, Plutonium 1960, eds. E. Grison, W. B. H. Lord, R. D. Fowler, Cleaver-Hume Press, London, pp. 16-25 (1960)
- 2 K.J.M. Blobaum, C.R. Krenn, J.N. Mitchell, J.J. Haslam, M.A. Wall, T.B. Massalski, A.J. Schwartz, Metall Mater Trans A [in press].

High-load anionic chromatography of An(IV) for recovery and purification of neptunium

T. Yamamura, T. Miyakoshi, Y. Shiokawa

Institute for Materials Research, Tohoku University, Sendai, Miyagi 980-8577, Japan

Actinide metals with very high purity are essential for the reliable studies of the physical nature of actinide compounds, especially of the physical properties such as the Kondo effect where the infinitesimal quantity of magnetic elements plays an important role. For the neptunium compounds the purity of the prepared compounds is governed by the purity of the metal because the metal is required to be produced from the supplied neptunium oxide whose purity is as low as 99.9%. Moreover, the reuse and the recovery of the neptunium element from the used compounds are strongly desired because the neptunium is the precious man-made element. The purification system for preparing the gram-amount neptunium with high-purity should be simple and easy to be handled in laboratories. Recently new method of preparing the gram-amount actinide metals has been developed by our research group [1, 2]. This method, which only requires an aqueous acidic solution of metal ion as the starting material, is especially suitable to prepare the highly radioactive neptunium metal at the high purity. The most suitable method for the extensive purification prior to this metal preparation is the anion exchange chromatography because the formation of the stable anionic complex with nitrate ion $An(NO_3)_6^{2-}$ is characteristic to the actinide (An) chemistry.

Though purification condition for actinide(IV) at its tracer scale is already established, that at gram-amount scale generally becomes difficult due to decrease in distribution coefficient. In purification systems, both of load amount and purity should be satisfied by quantitative investigation of column condition. Anion exchange chromatography of thorium(IV) nitrate anion was examined quantitatively with a small column formerly [3]. When the amount of thorium loaded to the column is increased, the elution curve changed from Gaussian function type curve to tailing. Simultaneously, peak position moved forward and distribution coefficient decreased substantially. Optimization of these column condition based on an experiment, however, is prohibitedly difficult due to large amount (150-200 times of column volume) of radioactive effluent, as well as its long period and large costs. Therefore,

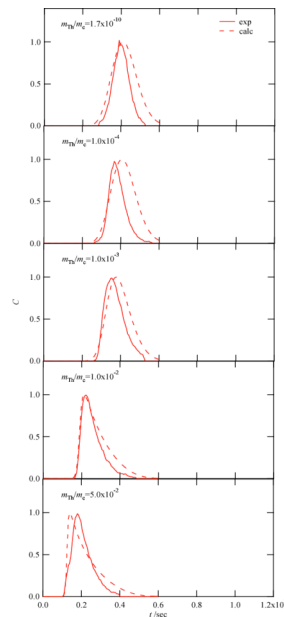


Fig 1: Comparison of elution curve of thorium(IV) in 6M HNO₃ at variety of load amount obtained in experiments (solid curves) and calculation (dashed curves).

estimation of elution curve of anion exchange chromatography should be desirable in an aid of using numerical calculation.

Though the estimation of elution curve by numerical calculation had been used in purification of gram quantity of organic compounds such as medicinal compounds [4], there is little use in purification of an inorganic compounds. Guiochon reported investigation of elution curve in highly-loaded state by numerical calculation based on adsorption isotherm [5, 6].

In this research, elution curves of actinide(IV) obtained in experiments were compared with those calculated. Excellent agreement was attained in the case of thorium(IV) (Fig. 1) and uranium(IV) with an inclusion of rate equation of Langmuir type as non-linear kinetics equation, which is contrary to model by Guiochon. Based on the above-mentioned result, elution curve for neptunium(IV) was obtained on basis of $k=10^3$ according to literatures. That estimation of the purification condition which says purity/recovery because calculation of elution curve in such a high load became possible is enabled can be expected.

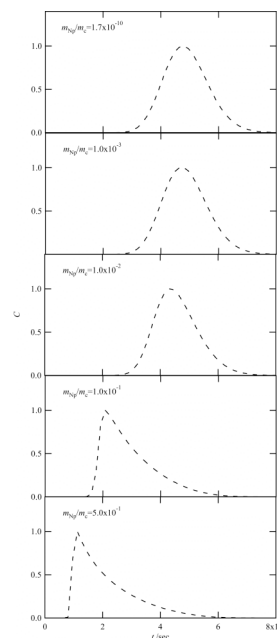


Fig 2: Calculated elution curves for neptunium(IV) in 6M HNO₃ at variety of load amount.

We would like to thank Prof. S. Mitsugashira of Tohoku University and Prof. H. Yamana of Kyoto University for their encouraging discussions. We wish to acknowledge valuable discussions on numerical calculations with Prof. Y. Nibori of Tohoku University and Mr. H. Iwase of Nippon Sheet Glass, Co., Ltd.

- [1] Y. Shiokawa, K. Hasegawa, K. Konashi, M. Takahashi, K. Suzuki, J. Alloys Compd., 255 (1997) 98.
- [2] Y. Shiokawa, K. Hasegawa, Isotope News, 525 (1998) 6.
- [3] T. Yamamura, Y. Shiokawa, T. Mitsugashira, Research Report of Laboratory of Nuclear Science, Tohoku Univ., 32 (1999) 31.
- [4] Y.-L. Li, N.G. Pinto, J. Chromatogr. A, 702 (1995) 113.
- [5] G. Guiochon, S. Golshan-Shirazi, A. Jaulmes, Anal. Chem., 60 (1988) 1856.
- [6] L.R. Snyder, J.W. Dolan, G.B. Cox, J. Chromatogr., 483 (1989) 63.

THE SELF-CONSISTENT ONE ASSOCIATION MODEL FOR STRATIFYING MELTS OF THE BINARY SYSTEMS WITH STRONG CHEMICAL INTERACTION BETWEEN ATOMS OF COMPONENTS

A.L.Udovsky

Baikov Institute of Metallurgy and Material Science of Russian academy of sciences, Moscow, Russian Federation

The row of the binary systems, for example, the U-O, Pu-O, Fe-O, Cr-O, Fe-S, Cr-S and others systems have a phase diagrams, containing both chemicals compounds, and miscibility gap of melts. On the one hand presence of the chemical compounds in these systems are indicative of presence in these systems strong attracting inter-atomic interactions, bring about formation of these compounds. On the other hand presence of the miscibility gap is indicative of that that free energy mixing of melts as function of composition within some temperature range have local concavity, which is be situated between family of points of inflexion (or spinodal curve). At first thought simultaneous presence these fragment (chemical compound and miscibility gap) on phase diagram brings about contradiction.

In purpose of the permission this logical contradiction in persisting work is designed the self-consistent one association model (SCAM) for description of thermodynamic, as well as structured properties (distribution of atoms different kinds between single, as well as associated states) properties of melts in binary system with strong chemical interaction [1].

In work is received and analyzed the equation of the state for calculation of local stable mole fractions of associates for melts depending on composition and temperature. In work is shown that often used the law acting masses, being quotient event of the equation of state, does not allow to describe the thermodynamic characteristic stratifying melts for systems, containing chemical compounds as well as miscibility gap. While the SCAM allows modeling miscibility gap of melts for binary systems with strong inter- atomic interactions. Within the framework of the SCAM is built the algorithm of the calculation of miscibility gap for melts, here under appears the possibility of the description within the framework of one model thermodynamic, as well as structural properties of melts for system with strong chemical interaction between atoms of components.

The SCAM has applied to modeling the thermodynamic properties and miscibility gap of melts for the U-O system [2]. The optimized values of model's parameters were obtained by solution of the inverse problem. As input data have been used experimental data [3], which have obtained for two ends of tie-line at 3090 K. The two critical points of miscibility gap were calculated. Between these critical points the miscibility gap is located. The top critical point agreement with experimental phase diagram of the U-O system. The lower critical point is situated in meta-stable part under thermodynamic stable (the uranium-base liquid + solid state UO_{1-x}) – tie-lines of phase diagram of the U-O system.

Good agreement have been obtained between calculated two-phase tie-lines and experimental data for stratifying melts of the U-O system under 2700 and 3100 K measured by different researchers is received.

This approach allows to consider the interaction between of various kinds of atoms, which can form by dynamic reaction of the associations (or the reaction of dissociation) localized group of atoms (associate) either different chemical components, or atoms of one component differing some internal parameter (the varied valences or others properties).

Acknowledgements: The work supported by Dutch-Russian Program NWO-RFBR (Project № 047.011.2001.011), the Russian Federation Target Program "Integration" (Project B0056) and the Russian Foundation of Basic Researches (Project RFBR 02-03-32621).

- 1 A.L.Udovsky, Doklady of RAS, in press (2006)
- 2 A.L.Udovsky, M.V.Kupavtsev, H.A.J.Oonk The application of self-consistent on one association model for calculation miscibility gap of melts for uranium-oxygen system. Abstracts and Program. CALPHAD XXXIV Conference, May ,2005, Maahstriht, The Netherlands.
- 3 C. Gueneau, V.Dauvouis, P.Perodeaud, C.Gonella, O.Dugne. J. Nucl. Mater. 254 (1998) 158-174.

Phase-field Modeling of Coring Structure Evolution and Ga Homogenization Kinetics in Pu-Ga Alloys

S. Y. Hu* , M. Baskes and M. Stan

MST-8, Los Alamos National Laboratory, Los Alamos, NM 78545

During the casting of Pu-Ga alloys, the huge difference of Ga diffusivity in ϵ and δ phases results in the formation of coring structures which consist of Ga-rich cores with Ga-poor edges. On the other hand, the elastic interaction among different oriented δ grains and diffusive Ga might lead to an inhomogeneous diffusion and δ grain growth. In this work, the phase-field approach has been used for modeling the coring structure evolution and Ga homogenization kinetics in three dimensions. We assume that the transition from ϵ (bcc) to δ (fcc) follows the Bain distortion. The chemical free energy is constructed according to the phase diagram. The effect of diffusivity inhomogeneity, internal stresses, anisotropy of interfacial energy and cooling rate on the coring structure evolution is systematically studied. Fig.1 presents the coring structures obtained with and without the effect of internal stresses on the coring structure evolution in two dimensions. The color denotes Ga composition, Red means higher Ga composition while Blue lower Ga composition. The letters "A" and "B" denote two different oriented δ grains. The results demonstrate that the internal stresses speed up the growth in the a-direction, but slow down the growth in the c-direction to minimize the elastic energy, leading to the elongation of the grains as seen in experiments.

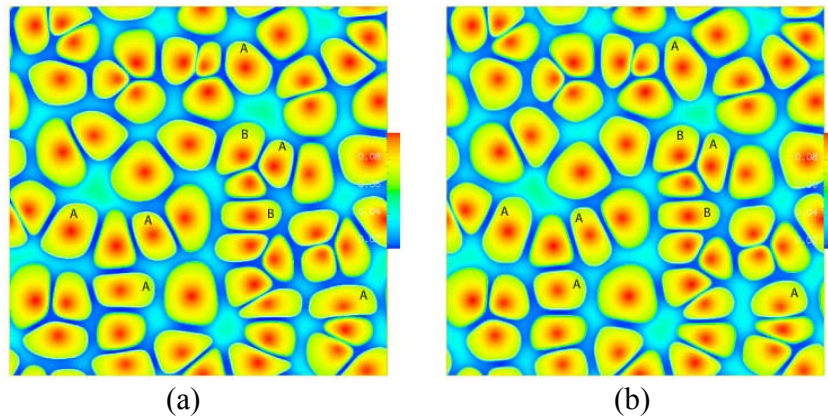


Fig 1: Effect of internal stresses on multi-particle growth in 2D, (a) without internal stresses and (b) with internal stresses

Acknowledgement: This work was supported at Los Alamos National Laboratory by the US Department of Energy under contract W-7405-ENG-36.

Tantalum Corrosion with Pu-Ti alloys

T. Paget, R. Watson, S. Slade

AWE plc. Aldermaston, Reading, RG7 4PR, UK

INTRODUCTION

Reported here are recent observations during the processing of plutonium-titanium alloys. Six runs were conducted, where plutonium metal was treated with ~10 wt% MgCl₂ in CaCl₂. The metal was introduced into a magnesia crucible and the salt mixture poured on top. The crucible was heated to around 850°C under an argon atmosphere and stirred for 3.5 hours. The stirrer was removed while the salt and plutonium were still molten and the furnace allowed to cool. The product metal was recovered by breaking away the ceramic crucible and salt.

The flat paddle stirrers were fabricated from tantalum (99.9% pure, ASTM B708-86 GRAIN 5-7). Two stirrers of the same design were studied, both had been used previously to process plutonium of a similar purity, but without added titanium. Stirrer 1 was used on eight previous occasions, Stirrer 2 was used on twenty previous occasions, no signs of corrosion were observed at the end of any of these runs.

Run1/1 was carried out at half batch size using Stirrer 1. Figure 1 shows the stirrer following processing. The corrosion is in the form of pitting and occurred on one face only, close to the salt-metal interface. The lighter grey portion indicates the depth to which the stirrer extended into the molten plutonium during processing. Chemical analysis shows the metal contains between 0.1-0.3 wt% Ta and 0.6 wt% Ti.

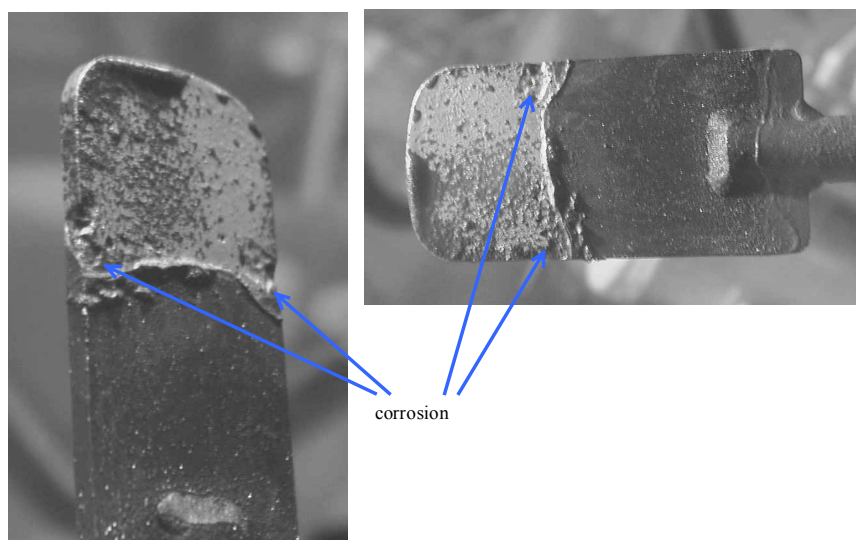


Figure 1. Stirrer 1 following Run 1/1

Run 2/1 used similar feed to Run1/1 at the same batch size. There was no sign of corrosion of the stirrer at the end of the run. The product had a similar appearance to the product of Run

1/1 with an apparent surface layer. Chemical analysis shows the Ti content was between 0.3 and 0.4 wt% and the Ta content was around 100-300 ppm.

Stirrer 2 was re-used in Run 2/2 which processed metal that did not contain Ti. A full batch was treated in this run, the salt-metal interface being close to the top of the stirrer blade during processing. Corrosion of the stirrer, similar to that in Run1/1, was observed approximately halfway up the blade. The location of the corrosion is consistent with the depth of the metal during the previous run, Run 2/1.

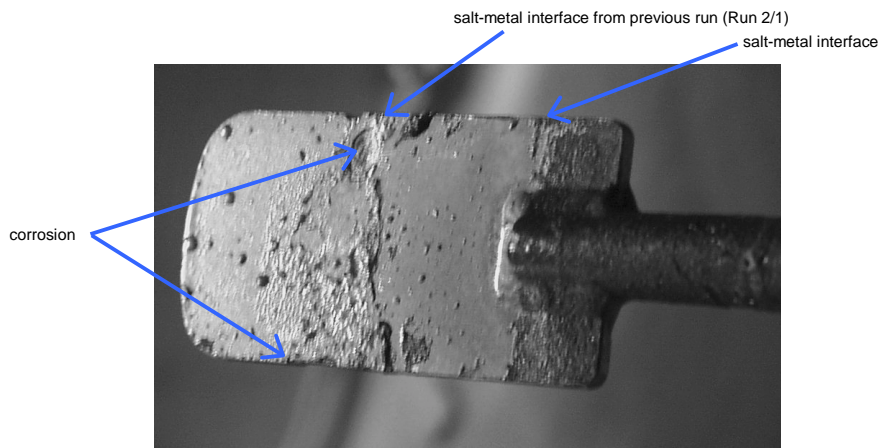


Figure 2. Stirrer 2 following Run 2/2

The Stirrer 2 was subsequently used in Run 2/3 and Run 2/4 without further corrosion. Run 2/5 processed a full size batch of Pu-Ti alloy and used Stirrer 2. Noticeable corrosion of the stirrer blade occurred at a location consistent with the upper surface of the molten metal during processing (Figure 4). No further corrosion was observed at the earlier sites from Run 2/2. Chemical analysis show the product contains between 0.3 and 0.6 wt% Ti and between 0.02 and 0.2 wt% Ta.

Unusual Appearance of Plutonium Metal in Electrorefining Product

R Campbell-Kelly, R Watson

AWE plc, Aldermaston, Reading, RG7 4PR, UK

INTRODUCTION

The electrorefining process is used to produce high purity plutonium metal. The product usually forms a well coalesced uniform ring in the outer annulus of the ceramic process crucible. In a small number of cases the process has operated with reduced current efficiency at the anode and cathode and a lower process yield. In two instances the process electrolyte, CaCl_2 , has been significantly depleted in plutonium. In these runs the product metal is not uniform but exhibits an area with a most unusual structure. The majority of the product is well formed, but there is a $\sim 90^\circ$ sector of the annulus which appears to comprise two vertical layers of plutonium. An example is shown in Figure 1. The cathode was withdrawn from the crucible while the contents were at 850°C and the crucible held at this temperature for 1 hour before cooling started. The vertical face of the metal bears the impression of the rivets used in the construction of the cathode. This area corresponds to a gap in the cathode and reduction of Pu(III) may be taking place on both surfaces.

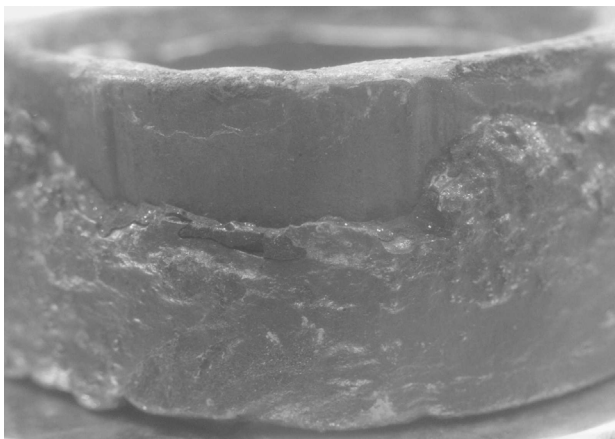


Figure 1. Unusual electrorefining product

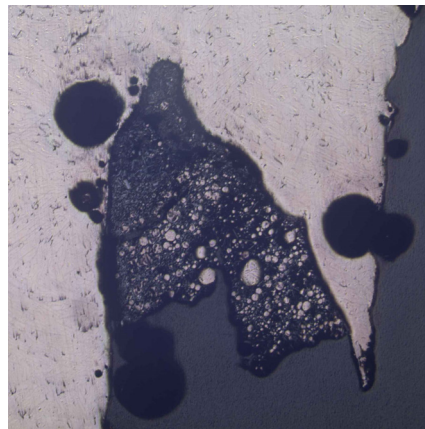


Figure 2. Metallographic image of recast material

As the salt was depleted in plutonium it was thought possible that reduction of the CaCl_2 salt may have taken place to generate calcium. Examination of the applied potential in these runs does not show an increase to potentials where calcium could form. Chemical analysis is inconclusive in showing if calcium metal is formed. Metallography of recast material shows the bulk metal is alpha phase, but there are also metal spheres suspended in a salt matrix. The large globules have a two phase structure which may indicate the presence of calcium, Figure 2.

Possible explanations for this unusual behaviour are either a high viscosity of liquid plutonium or surface effects. A number of studies have shown that additions of up to 5 at% impurities such as iron, gallium and cerium can result in increases in the viscosity of the metal of more than 25%. Chemical analysis does not show any impurities at levels which could explain a significant increase in the viscosity of the metal. There is very limited data on the surface tension of plutonium and none examining the effect of impurities.

In a number of cases the metal has been drip cast to produce a well formed, uniform, product. About 5% of the metal is retained as a casting skull. Analysis of this material shows high levels of gallium and probably CaCl_2 salt to be present.

The cause of the unusual formation of plutonium metal in electrorefining is not fully understood. Detected impurities are not present at high enough concentrations to significantly affect the viscosity of the metal. The influence of solid phases on the surface properties of the metal may be an important factor.

On the fcc \rightarrow monoclinic Martensitic Transformation in a Pu-1.7 at. % Ga Alloy

T. E. Mitchell^{*}, J. P. Hirth^{*}, J. N. Mitchell[†], D. S. Schwartz[†]

Los Alamos National Laboratory, Los Alamos NM 87545 USA

^{*}Structure-Property Relations Group, MST-8, Mail Stop G755

[†]Nuclear Materials Science Group, NMT-16, Mail Stop

The face-centered cubic $\delta \rightarrow$ monoclinic α' martensite transformation in a Pu-1.7 at. % Ga alloy is analyzed in terms of the defect-based topological model¹. The crystallography of the $\delta \rightarrow \alpha'$ transformation, and of twinning, is greatly facilitated by the replacement of the monoclinic phase by a hcp pseudostructure. Both have ABAB stacking and, in spite of the distorted arrangement of atoms in the (010) plane of the monoclinic structure, this structure can be mapped into the hcp structure without changing atom neighbors. After analyzing transformations from δ to the hcp pseudostructure, and the formation of twins therein, the pseudostructure can be transformed to α' by means of shuffles and one shear of 3.2° . There is also a large volume change of $\sim 20\%$. Another important feature is the near parallelism of the $\{111\}_\delta$ and $(010)_\alpha$ planes as well as of the $\langle \bar{1}10 \rangle_\delta$ and $[100]_\alpha$ directions. Because of the large strains involved in the transformation, there are significant differences between the predictions of the topological model and the standard phenomenological theory of martensitic transformations.

In the topological model, the Burgers vectors of the disconnections along the terrace planes for the transformation are deduced from the transformation strains. The habit plane is determined from the height and spacing of the disconnections. The predicted habit plane is in good agreement with experimental results. Observed twinning is associated directly with the transformation strain. The lattice invariant deformation due to strain parallel to the disconnection line direction is connected with slip in the α' plates. Implications for hysteresis in the transformation as observed by dilatometry and calorimetry are discussed.

This project was funded by the United States Department of Energy under Contract No. W-7405-ENG-36.

1. J. P. Hirth, J. N. Mitchell, D. S. Schwartz and T. E. Mitchell, *Acta Materialia*, in press.

NMR Studies of Neptunium and Plutonium Compounds

Y.Tokunaga, S.Kambe, H.Sakai, T.Fujimoto, R.E.Walstedt and H.Yasuoka

ASRC, Japan Atomic Energy Agency, Tokai, Naka, Ibaraki, 319-1195 Japan

Octupole Ordering in NpO_2

Multipolar degrees of freedom in the f-electron shell bring rich and complex physics to rare-earth and actinide compounds. Recently, it has been suggested that the phase transition in NpO_2 can be understood as the spontaneous ordering of octupolar degrees of freedom [1]. Soon after, resonant X-ray scattering (RXS) measurements gave evidence for the appearance of a longitudinal triple- q antiferro-quadrupolar (AFQ) structure in the ordered state [2]. This AFQ structure, however, has been regarded as a secondary order parameter driven by a primary longitudinal triple- q antiferro-octupolar (AFO) order, since the AFQ order alone cannot successfully explain the breaking of time reversal invariance suggested by susceptibility [3] and μSR [4] measurements. The longitudinal triple- q AFO ordered ground state has also been corroborated by recent microscopic calculations [5].

In order to elucidate the nature of the exotic ordered phase of NpO_2 , we have initiated the first NMR measurements on this system [6]. Figure 1 shows the angular dependence of the NMR spectrum obtained recently in a single crystal, where θ is the tilting field angle from $[110]$ to $[001]$ through the $[111]$ direction for the cubic crystal axes. From this field-angle dependence, the occurrence of a hyperfine interaction which stems from a field-induced AFO moment has been confirmed. This field-induced AFO moment appears as a result of the longitudinal triple- q AFQ structure in the ordered state. We have also observed characteristic spin echo modulation behavior caused by quadrupole splittings created by the AFQ ordering. This reveals that the AFQ structure is directly observable with NMR.

In general, multipole order is hard to investigate by conventional means. Although there are several indirect methods, recent identification of multipole order parameters can be credited mostly to RXS, which can directly probe the anisotropy of the f-electron shell. In the present work, we show that direct observation of multipole order parameters is also possible by means of NMR. Our NMR results provide further insight into the microscopic nature of

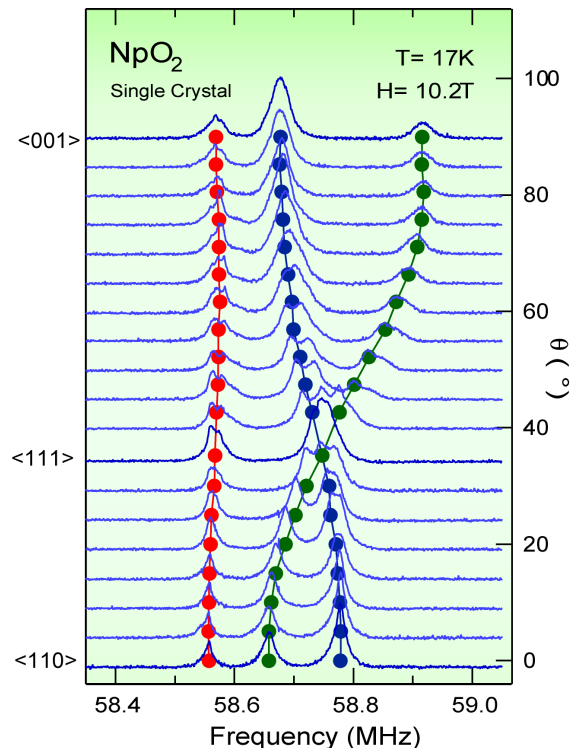


Figure 1: The field-angle dependence of the NMR spectrum at $T=17$ K.

multipole phase transitions in f-electron systems.

Unconventional Superconductivity in PuRhGa₅

In 2002, the Los Alamos group reported that PuCoGa₅ exhibited superconductivity with a transition temperature $T_c = 18\text{K}$ [7]. A few months after that discovery, the ITU group at Karlsruhe reported that its sister compound PuRhGa₅ also exhibits superconductivity below 9K [8]. The relatively high T_c values of these PuTGa₅ compounds has stimulated interest in the mechanism of their superconductivity. It has been suggested that the superconducting (SC) state may be unconventional, similar to other classes of strongly correlated electron systems.

To investigate the SC pairing symmetry, we have performed ^{69,71}Ga NMR/NQR studies on a single crystal of PuRhGa₅ [9]. We have observed a ⁶⁹Ga NQR line at 29.15 MHz, and have assigned it to the 4i Ga site (Ga(2) site) using NMR data. The spin-lattice relaxation rate $1/T_1$ shows no coherence peak just below T_c and obeys T^3 behavior below T_c , as seen in Fig. 2. This result strongly suggests that PuRhGa₅ is an unconventional superconductor having an anisotropic SC gap. We have obtained the gap amplitude $2\Delta(0) = 5k_B T_c$ and found the residual density of states to be $N_{\text{res}}(0)/N_{\text{res}}(T_c) \cong 0.25$, assuming a simple polar function. For PuCoGa₅, Curro, *et al.*, have obtained $2\Delta(0) = 8k_B T_c$ [10].

Recently, we have also measured the Knight shift at the Ga(2) site. The Knight shift has been confirmed to decrease below T_c . This gives strong evidence for spin singlet SC pairing in PuRhGa₅. Together with the NQR results for $1/T_1$, it is entirely plausible that the d-wave SC pairing is realized in PuRhGa₅.

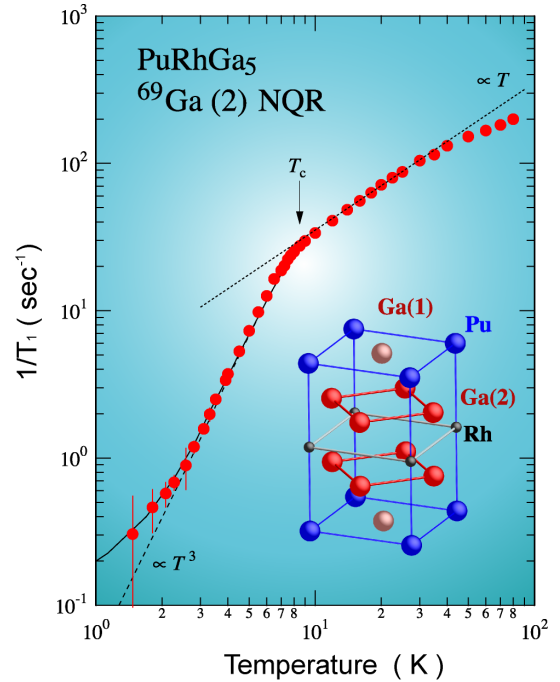


Figure 2: Temperature dependence of $1/T_1$ in PuRhGa₅.

The authors would like to thank D.Aoki, Y.Homma, Y.Haga, K.Nakajima, Y.Arai, T.D.Matsuda, Y.Ônuki, E.Yamamoto, A.Nakamura, and Y.Shiokawa for preparing high quality single crystals. The authors also would like to thank K.Kubo T.Hotta T.Maehira, R.Shiina and O.Sakai for valuable discussions. This work was partly supported by a Grant for Basic Science Research Projects from the Sumitomo Foundation, and a Grant-in-Aid for Scientific Research of Ministry of Education, Culture, Sports, Science and Technology (Grants No.14340113).

- 1 P. Santini and G. Amoretti, Phys. Rev. Lett. **85**, 2188 (2000).
- 2 J. A. Paixão *et al.*, Phys. Rev. Lett. **89**, 187202 (2002).
- 3 P. Erdős *et al.*, Physica B **102**, 164 (1980).
- 4 W. Kopmann *et al.*, J. Alloys Compd. **271**, 463 (1998).
- 5 K. Kubo and T. Hotta, Phys. Rev. B **71**, 140404(R) (2005).
- 6 Y. Tokunaga *et al.*, Phys. Rev. Lett. **94**, 137209 (2005).
- 7 L. J. Sarrao *et al.*, Nature **420**, 297 (2002).
- 8 F. Wastin *et al.*, J. Phys.:Condens. Matter. **15**, S2279 (2003).
- 9 H.Sakai *et al.*, J.Phys.Soc. Jpn. **74**, 1710 (2005).
- 10 N. J. Curro *et al.*, Nature **434**, 622 (2005).

GGA and LDA+U calculations of Pu phases and Pu-Ga system

J. Bouchet*, R.C. Albers†, G. Jomard*

*CEA-DAM, DPTA, Bruyères-le-Châtel, 92690 France

†Theoretical Division, Los Alamos National Laboratory, Los Alamos NM 87545, USA

INTRODUCTION

It is well known that the unique position of Pu in the periodic table is responsible for its unusual physical properties. Before its melting point Pu passes through six different phases, where the low temperatures distorted structures, α or β (monoclinic with 16 and 34 atoms/cell respectively) contrast with the high-temperature simple structures δ (fcc) or ϵ (bcc). This crystallographic sequence is surprisingly very close to the crystallographic sequence of the actinide series with open structures for the light actinides (Ac-Np) and close-packed structures for the heavy actinides. This transition, directly related to the delocalized (light actinides) and the localized (heavy actinides) behaviour of the f electrons, places Pu in the middle of a discontinuity and indicates that the delicate balance between itinerant and localized states must be responsible for its anomalous properties and for its structural diversity.

Söderlind¹ used density functional theory (DFT) and the generalized gradient approximation (GGA) to study the α phase. They found a good agreement with experiment, confirming α as the most favourable structure for Pu, and explained the presence of this structure by a narrow $5f$ bands with approximately 5 electrons. On the other hand, in despite of the simplicity of the δ phase, DFT with GGA completely failed to describe this structure. Recently a new understanding has emerged, with the assumption of δ -Pu as a strongly correlated system, that requires going beyond GGA in order to take into account the Coulomb interaction between the f electrons. The LDA+ U approach^{2,3} reproduces the experimental equilibrium volume and the stability of the fcc structure for plutonium. Söderlind⁴ included an energy shift of the $5f$ orbital via the Racah parameter to reproduce the volume of the six phases of Pu. But the problem of all these approaches is that they predict a long-range magnetic order for δ -Pu, not observed experimentally, despite a compensation between the orbital and the spin magnetic moments. Recently Savrasov⁵ combined dynamical mean field theory (DMFT) with density functional methods to obtain the total energy of a correlated system. They showed the possibility of a double well for the total energy of δ -Pu as a function of volume, with one minimum assigned to the α phase and the other one, at high volume, assigned to the δ phase. But a major problem with DMFT is the complexity of the calculation and the computational time, which makes it very difficult to treat structures with more than one atom per primitive cell, such as the α , β and γ phases of Pu.

RESULTS AND DISCUSSION

We have recently proposed a pseudo-structure to model α plutonium⁶, which is an orthorhombic structure with two atoms per unit cell. We found a surprisingly simple path between α and γ phases. Here we have used this pseudo-structure to study the complete phase diagram of Pu and supercells of Pu with Ga, using the GGA, and LDA+ U approximations. We use the simplicity of the pseudo phase to understand the main differences between low and high temperatures phases of Pu. We have compared the total energies of the α , pseudo- α , γ , δ , ϵ phases, using different functionals and magnetic order. The total energies of pseudo- α and α phase are very similar for a long range of volumes and are much lower than for the other phases. This gives us confidence to use the pseudo structure instead of the real α in more computationally intensive techniques. The volumes of the different structures are well reproduced, compared to the experiments, as found in Ref.[4]. To see the effects of the correlations, we have performed calculations with LDA+ U , allowing U to vary between 0 and 4 eV. As U increases, the γ , δ , ϵ phases rapidly develop a magnetic and high-volume solution, whereas the pseudo- α stays non-magnetic and at low volume. These two kinds of behavior are interpreted in terms of the interatomic distances of the different phases, and we show that the short bonds in the pseudo phase suppress correlations effects. Moreover, since the pseudo- α and the γ structures are orthorhombic but with different b/a and c/a ratios, we can easily simulate a transition path between low and high volume structures and follow the effects of the correlations. This would be, of course, impossible

without the pseudo phase. We show a threshold in the nearest-neighbor distance, independent of structure, which controls the occurrence of magnetism and the high volume solution. Finally, we have included a Ga atom in supercells of Pu. This allows us to study the influence of an alloying element of the surrounding Pu atoms, and to see its effect on the phase stability. We show that Ga stabilizes the high volume structures as found experimentally.

- 1 P. Söderlind, J. Wills, B. Johansson and O. Eriksson, Phys Rev B **55**, (1997)
- 2 J. Bouchet, B. Siberchicot, F. Jollet and A. Pasturel, J Phys : Condens Matter, **12**, (2000)
- 3 S. Y. Savrasov and G. Kotliar, Phys Rev Lett, **84**, (2000).
- 4 P. Söderlind, and B. Sadigh, Phys Rev Lett **92**, (2004).
- 5 S. Y. Savrasov, G. Kotliar and E. Abrahams, Nature, **410**, (2001).
- 6 P. Söderlind, and B. Sadigh, Phys Rev Lett **92**, (2004).

Hysteresis of the $\delta \leftrightarrow \alpha'$ Transformation in Pu-Ga alloys

J.N. Mitchell, D.S. Schwartz, and T.E. Mitchell

Los Alamos National Laboratory, Los Alamos NM 87545 USA

BACKGROUND

Face-centered cubic δ -phase plutonium stabilized with <2 at. % Ga will undergo a transformation to monoclinic α' Pu at temperatures of ~ 100 C or less. This transformation is martensitic, meaning that it appears to be diffusionless and that there is a shear-induced change in the shape of the unit cell. A variety of factors can affect the onset of the $\delta \rightarrow \alpha'$ transformation, including the concentration and distribution of the stabilizing solute, grain size, cooling rate, and possibly age. This transformation has several unusual characteristics, including its incompleteness, a $>20\%$ volume contraction, and a $150\text{-}200$ °C reversion hysteresis. A second type of hysteresis is also found where thermal cycling displaces the transformation to lower temperatures and decreases the amount of transformation. In this presentation, we will explore in detail these two types of hysteresis.

EXPERIMENTS

All experiments were performed on well homogenized δ -phase Pu alloys stabilized with 1.7 to 2 at. % Ga. Measurements were made using a Netzsch 402C dilatometer with cooling and heating rates of 1-10 C/min and in a ultra-high purity He gas environment. Two types of experiments were performed: (1) single-cycle cooling to induce the transformation followed by heating to induce the reversion and (2) multiple-cycle cooling and heating to observe the effect of these cycles on the transformation behavior. Typical minimum temperatures were -165 °C; maximum temperatures ranged from $200\text{-}375$ °C. In one experiment, the sample was held at room temperature following the high temperature phase for 2-5 hours before beginning the next cryogenic cycle.

RESULTS

A typical single-cycle hysteresis loop is shown in Figure 1. In this experiment, the sample was heated to 200 °C prior to cooling and holding at -155 °C. Several interesting features are present in this hysteresis loop, including the very sharp transformation onset and distinctive steps during the reversion. The latter feature is best represented in the dL/dt curve, where they appear as bursts [1, 2].

In the experiment shown in Figure 2, the sample was cycled three times between RT, -155 °C, and 200 °C. After the first 200 °C segment (second cycle), the sample was held at RT for 2 hours prior to cooling to -155 °C. After the second 200 °C segment (third cycle), the sample was held at RT for 5 hours before cooling to -155 °C. This experiment shows that although cycling reduces the amount of transformation, a RT rest stage will inhibit further hysteresis of the transformation.

We have also studied the effects of the maximum temperature on thermal cycling hysteresis. In Figure 3, the sample was cycled twice through the transformation up to 200 °C and once up to

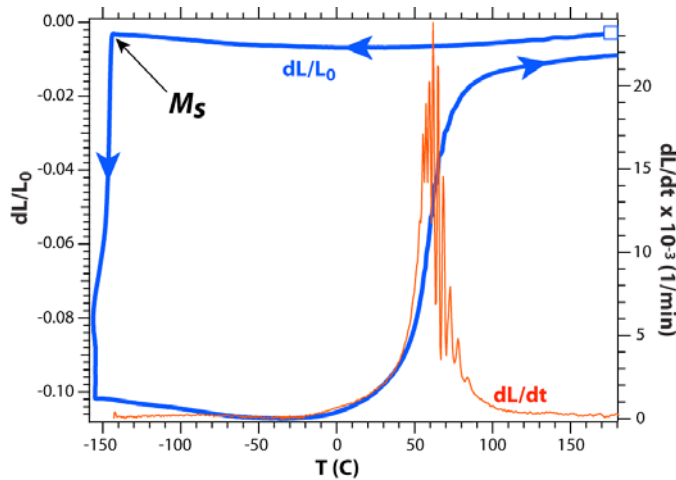


Fig. 1: Hysteresis loop of the $\delta \leftrightarrow \alpha'$ transformation.

375 °C. The curves show that the transformation was displaced to lower T and resulted in less alpha prime, but that the 375 °C anneal produced more alpha prime during the subsequent cryogenic stage.

These experiments show that there are several factors that can influence the transformation behavior during thermal cycling. Resting at RT for as little as two hours limits and heating to temperatures well above the reversion temperature range limits hysteresis. We will discuss in detail the role that microstructure plays in these phenomena.

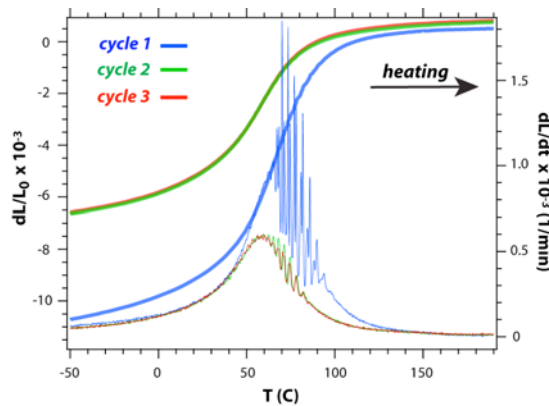


Fig. 2: Detail of the $\alpha' \rightarrow \delta$ reversion during separate heating phases of a three-stage thermal cycle. Cycle 2 and 3 include 2 and 5 hour rests, respectively, at RT before cooling. The thin lines are the dL/dt curves.

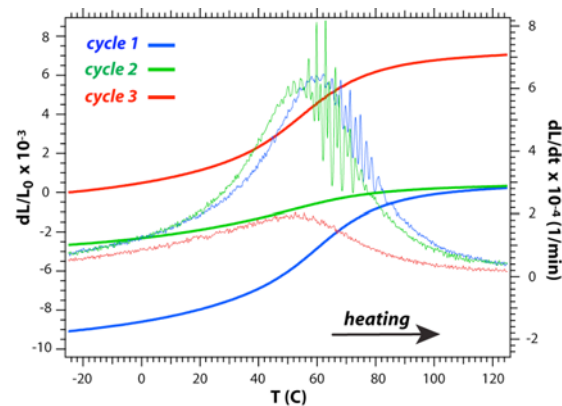


Fig. 3: Detail of the $\alpha' \rightarrow \delta$ reversion during separate heating phases of a three-stage thermal cycle. Cycle 2 finished with a 375 °C anneal, allowing more transformation in Cycle 3. The thin lines are the dL/dt curves.

- 1 J. N, Mitchell *et al.*, Metall. Mater. Trans. 35A, 2267 (2004).
2. K.J. Blobaum *et al.*, Metall. Mater. Trans. 37A, 567 (2006).

A Study of the Novel C5BTBP-PAN Solid Phase Extractant for the Partitioning of Minor Actinides from High Level Waste

J. Sulakova*, J. John*, M. J. Hudson†, M. R. S. Foreman†

* Czech Technical University in Prague, Department of Nuclear Chemistry and Centre for Radiochemistry and Radiation Chemistry, Brehova 7, 115 19 Prague 1, Czech Republic

† School of Chemistry, University of Reading, Whiteknights, RG5 4BD Reading, UK

With respect to the management of spent nuclear fuels, several European countries have chosen the closed fuel cycle involving reprocessing. The nuclear wastes produced by the reprocessing contain the fission products and the minor actinides; they are vitrified and supposed to be deposited in deep geological repositories. Selection of the sites for these repositories must consider the fact that these vitrified wastes contain long-lived radionuclides (LLR), essentially belonging to the family of the actinide elements (An), which induce important radiotoxicity for the long-term. The elimination of these LLR, which are mainly minor actinides (MAn), from the vitrified wastes would significantly decrease the long-term radiotoxicity of these wastes and would simplify the selection of geological sites. After separation, the actinides may be either transmuted into short-lived or stable nuclides by nuclear means or conditioned into stable solid matrices¹.

The 6,6'-bis-(5,6-dipentyl-[1,2,4]triazin-3-yl[2,2']bipyridinyl (C5BTBP) extractant, developed and synthesized at the University of Reading, UK has been recently demonstrated to separate efficiently MAn from the reprocessing waste using liquid-liquid extraction. At the same time very high separation factors between MAn and lanthanides can be achieved in one stage.²

At the Czech Technical University in Prague, a novel C5BTBP-PAN solid phase extractant (SPE) was prepared. The beads of the C5BTBP-PAN material were composed of the solid powdered C5BTBP extractant (33 % w/w) and a binding matrix of modified polyacrylonitrile (PAN). For the preparation of the C5BTBP-PAN, a modification of the earlier developed procedure³ was used.

In an introductory study, the dependences of mass distribution ratios D_g on the nitric acid concentration have been determined for europium(III) and americium(III) for the original C5BTBP-PAN material. The D_g values for europium were below the limit of detection (3.5 mL/g) in all the nitric acid concentration range tested whilst for americium, the D_g values did not exceed the value of ~ 30 mL/g (in 3M HNO₃) and, contrary to the data on the C5BTBP behaviour in liquid-liquid extraction², further decreased with increasing nitric acid concentration. The high hydrophobicity of the solid C5BTBP extractant and its low solubility are assumed to be the reasons for these unsuccessful results.

Therefore, the next experiments were directed towards conversion of the C5BTBP-PAN material into a material used in standard extraction chromatography by introducing octanol solvent into the system. Alternatively, addition of pure liquid N,N'-dimethyl-N,N'-dibutyl-tetradecylmalonamide (DMDBTDMA) extractant was tested alone or in conjunction with the octanol.

The performance of these wetted materials was then evaluated by comparing the mass distribution ratios D_g for americium(III) at two nitric acid concentrations (0.01 mol/L and 3 mol/L). The results obtained have shown that the most significant improvement of the performance of the original material can be achieved by wetting it with octanol that dissolves a part of the solid C5BTBP extractant and thus converts the material into a standard extraction chromatography system. However, the overall C5BTBP concentration in this material is much higher than could be achieved by impregnating the support with C5BTBP solution.

Since the difference between the performances of the materials with and without DMBTDMA was not very significant, the simpler two-component C5BTBP[octanol]–PAN system has been selected for the further studies. For this system, the dependences of mass distribution ratios D_g of Eu(III), Am(III), Pu(IV) and U(VI) on nitric acid concentration were determined. The results obtained are presented in Figure 1.

It can be seen that the C5BTBP[octanol]–PAN material offers the possibility of easy separation of americium from europium in the nitric acid concentration range 0.5–3 mol/L, where a Am/Eu separation factor $SF_{Am/Eu} > 100$ was achieved. No deterioration of the properties of this material was observed after 20 hours of contact with 3M HNO_3 . The results obtained also show that the tetravalent actinides [Pu(IV)] are co-extracted with the trivalent ones, while the hexavalent ones are rejected.

In further experiments, the kinetics of uptake of americium by C5BTBP[octanol]–PAN material was followed in detail.

The results obtained are very encouraging, the system has been proposed for further more detailed study.

This research was supported by EC FP6 F16W-CT-2003-508854 project EUROPART and by Czech grant MSM 6840770020. Prof. F. Sebesta is acknowledged for the preparation of the C5BTBP–PAN material.

- 1 G. R. Choppin, *et al.*, *Chemical Separation in Nuclear Waste Management. The state of the art and look to the future*. Tallahassee (USA): Florida State University, (2002)
- 2 M. R. S. Foreman, *et al.*, *Solv. Extr. Ion Exch.* **23**, (2005)
- 3 F. Sebesta: Preparation of Granular Forms of Powdered Materials for their Application in Column Packed Beds, In: P. Misaelides, *et al.*, eds.: *Natural Microporous Materials in Environmental Technology*, Kluwer Academic Publishers, (1999)

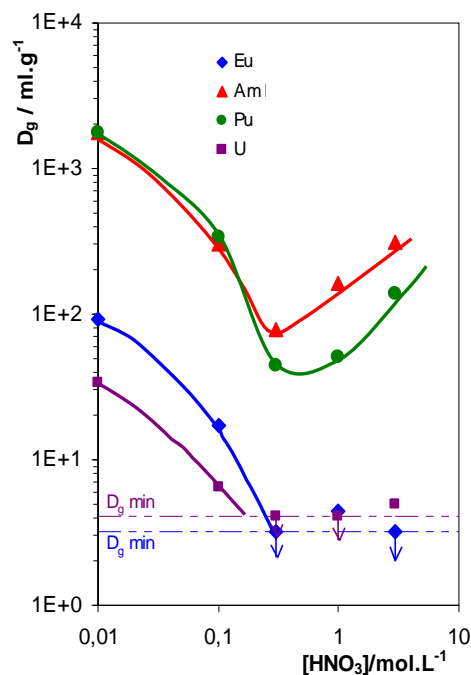


Fig 1: Dependence of mass distribution ratios D_g of Eu(III), Am(III), Pu(IV) and U(VI) on C5BTBP[octanol]–PAN solid extractant on nitric acid concentration. (V/m = 250 mL/g, 20 hrs of contact)

Kinetic Model of Actinides and Lanthanides Extraction in None Stationary Conditions

M.A. Afonin, A.A. Kopyrin, A.A. Fomichev

Saint-Petersburg Institute of Technology, 26 Moskovsky av., 190013, Saint-Petersburg, Russia

INTRODUCTION

Separation of similar elements in none steady state conditions are a prospective method to increase elements separation factor. Realisation of the process in non stationary non equilibrium conditions using phenomena of oscillating extraction allows the exploitation of differences in kinetics of ion complexation and extraction rates, using their transport through the boundary area in both directions for elements separation¹. One of the possible procedures to deviate extraction system from equilibrium is oscillatory changing of the temperature of the extractors. However, the influence of oscillatory temperature changing in the extractor(s) is not described in the literature.

EXPERIMENTAL

The influence of periodical oscillations of the temperature on extraction and stripping processes in the extraction systems is studied. Two extraction system with tri-n-butyl phosphate (TBP) were investigated, №1: 6M NaNO₃ – Nd(NO₃)₃ – Pr(NO₃)₃ – TBP – kerosene and №2: [Nd(NO₃)₃·3TBP] – [Pr(NO₃)₃·3TBP] – kerosene – 0.1M HNO₃. The setup flow sheet (fig. 1.) is described as following: the emulsion is pumped from thermostatic extractors 16, 17 to centrifugal separators 5, 6 through the turbidimeters 11, 12 by peristaltic pump 10. After separation from the separator 5 the organic phase flows to the extractor 17 and from the separator 6 the organic phase flows to spectrophotometer 8 for analysis and it flows to the extractor 16, passing through both aqueous phases organic phase forms bulk liquid membrane. After spectrophotometers 7, 9 the aqueous phases come back to their corresponding extractors. Data acquisition of pH, red/ox potential of the aqua phase, temperature and emulsion turbidity are performed with frequency above 1 Hz using the DAQ board in computer 18 and specially designed software. Diode-array spectrophotometers are used to obtained spectra every 6-15 seconds. By deconvolution of each spectrum, using specially designed software concentration of several elements can be obtained.

RESULTS AND DISCUSSION

Dependence of rate constants of extraction on temperature according to Arrhenius equation has been included into existing mathematical model of none stationary membrane extraction. The values of activation energy and Arrhenius pre-exponential factor for the rate constants of extraction and stripping reactions of Pr and Nd were calculated from experimental temporal dependencies of metal concentration and temperature by solving reverse kinetics problem using proposed mathematical model and software package. The difference between the activation energy of extraction and the activation energy of stripping of Pr, and Nd from 6 Mol/l NaNO₃ by TBP in the temperature range 293-329 K were -25±3 kJ/Mol and -30±3 kJ/Mol respectively. The

rate constants of Pr and Nd extraction and stripping in 6 M NaNO₃ and 0.1 M HNO₃ were also calculated.

The series of experiments with influence of periodical oscillations of the temperature on the extraction system for separation of rare earth elements using bulk liquid membrane between two extractors are performed. The mathematical model describes experimental data adequately.

On the basis of the extraction and stripping rate constants and corresponding activation energies the optimization of the extraction process of separation of rare earth elements by liquid membrane under the influence of periodical oscillation of the temperature is carried out. The optimal conditions of separation by liquid membrane were found: frequency and amplitude of thermal oscillations, effective boundary area and liquid membrane flow rate.

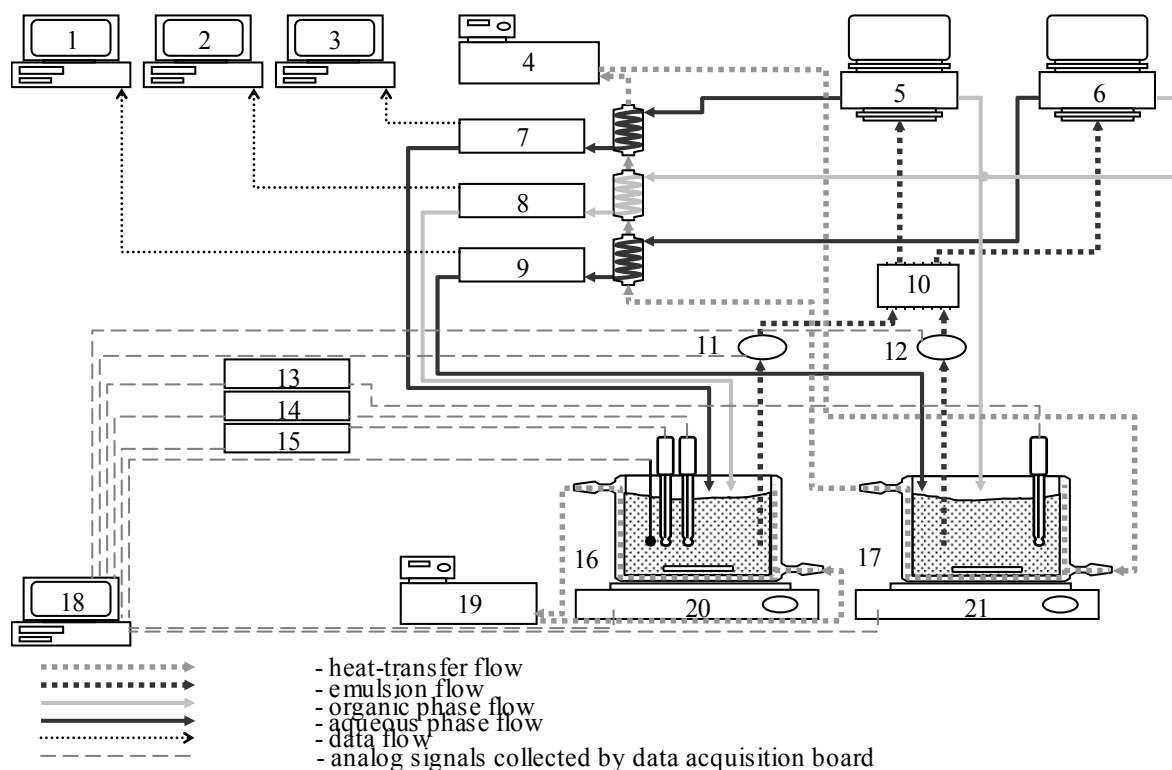


Fig 1: Experimental setup: 1-3, 18 computers; 4, 19 – thermostats; 5, 6 – centrifugal separators EC-33 NIKIMT; 7, 8, 9 – spectrophotometers SF 2000 OKB Spectrum; 10 – peristaltic pump; 11, 12 – turbidimeters; 13 –pH-meter; 14, 15 potentiometers; 16, 17 – extractors; 20, 21 – magnetic stirrers

Acknowledgements. This work was supported by the U.S. Department of Energy, Office of Basic Energy Sciences, under grant RUC2-20011-ST-04 administered by the Civilian Research and Development Foundation..

Electrochemical behaviour and dissolution of UC in acidic media.

A. Maslennikov^{*}, B. Fourest[†], Ph. Moisy[§], V. Sladkov[†], M. Lecomte[§]

^{*} A.N. FRUMKIN Institute of Physical Chemistry and Electrochemistry, RAS, Moscow, Russia

[†] Institute of Nuclear Physics, University Paris-XI, F-91406 Orsay Cedex, France

[§] CEA, Research Center VALRHO, BP 17171, 30207 Bagnols-sur-Cèze Cedex, France

AIM OF THE STUDY

Uranium-based carbides cause a renewed interest as possible fuels for the future high temperature gas cooled reactors (HTGR). Since the minor actinides (MA) and most of long-lived fission products (FP) could be incinerated in HTGR, its reprocessing process should be strongly simplified. Certain aqueous flowsheets for the HTGR fuel reprocessing preview the actinides (An) and FP separation already at the step of the fuel dissolution. In order to develop the dissolution process, providing feasible and effective reprocessing, the knowledge of the fundamental redox properties of actinides and fission products carbides in aqueous solutions is essential.

The present work is aimed to study UC electrochemical behavior in 0.1 – 4.0 M HClO₄. The boundaries of UC passivation, and transpassivation, as well as charge transfer resistance (R_{ct}), double layer capacitance (C_{DL}) and conditional charge transfer rate constants (k_{ct}^0) and their changes with solution acidity and applied potential were determined.

METHOD AND MAIN RESULTS

UC spherical ingot ($\varnothing = 4$ mm) was prepared by arc melting, pressed into a Teflon tip and connected to an EDI101T rotating disk electrode (RDE) assembly (Radiometer). This assembly served as working electrode in a three-electrode system comprising also an Hg/Hg₂Cl₂ reference electrode (SCE) and a Pt wire counter electrode. Cyclic voltammetry (CV), electrochemical impedance spectroscopy (EIS) and multistep potential sweep coulometry (MPSC) were applied while carrying out the study.

CV and MPSC curves in 0.1- 4.0 M HClO₄, presented in Fig. 1, give general information about the electrode reactions occurring at the UC electrode. In the interval of potentials from open circuit potential ($E_{i=0}$) to +400 mV/SCE, a slow anodic reaction with a rate increasing with the H⁺ concentration is observed. The Nyquist plots associated with this reaction (Fig. 2) represent straight lines with a slope increasing from 0.1 to 0.58 with the increase of H⁺ concentrations. The latter observation indicates that in this region of potentials the UC oxidation is diffusion controlled. The slopes of Z_i - Z_r curves, less than 1, show that the diffusion in the double layer is complicated by the surface film formation.

The increase of anodic reaction rate is observed in the range of potentials from 400 to 700 mV/SCE (Fig. 1). This increase is much greater in 1.0 M HClO₄, than in 0.1 M HClO₄ (Fig. 1), and is practically independent on HClO₄ concentration with a further increase to 4.0 M. The Nyquist plots for these potential values (Fig. 2) contain a semi-circular part indicating the increase of charge transfer limitations to the kinetics of the UC oxidation.

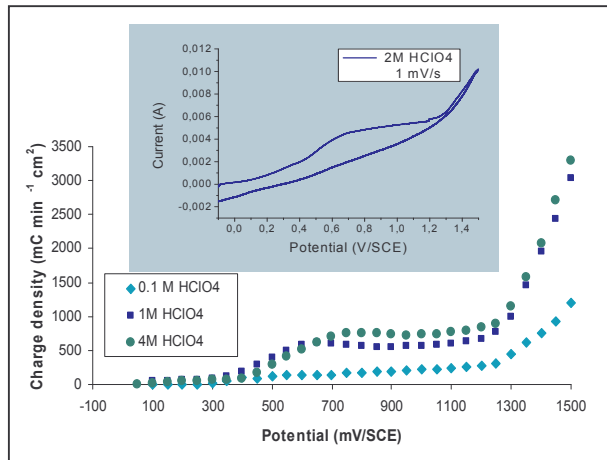


Fig. 1: MPSC and LV (inset) curves at a UC sphere electrode ($S = 0.145 \text{ cm}^2$) in HClO_4 solutions of different concentrations.

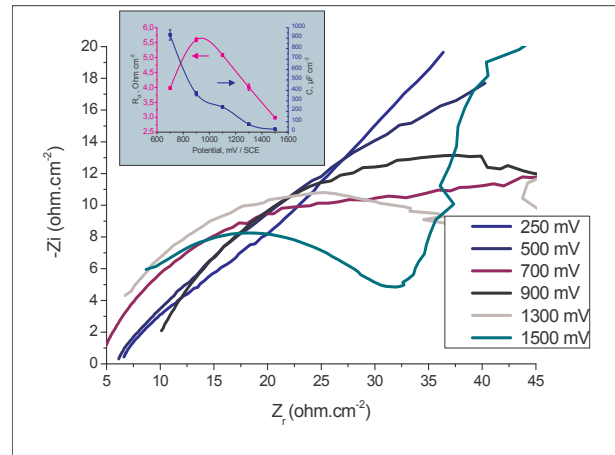


Fig. 2: EIS Nyquist plots of UC sphere electrode ($S = 0.145 \text{ cm}^2$) in 2M HClO_4 and calculated R_{ct} , C_{DL} values (inset) as a function of the applied potential.

The plateau of the anodic current in the potential range from 700 to 1100 mV/SCE, may be associated with the formation of a pseudopassive film on the UC surface. The oxidation rate in this potential region is limited by the electron transfer (Fig. 2), R_{ct} achieving its maximum at 900 mV/SCE. The formation of the passive film is proved by the decrease of C_{DL} with the increase of the applied potential (Fig. 2, inset).

At potential values exceeding 1100 mV/SCE, the transfer of UC electrode to a transpassive state, characterized by a drastic increase of the anodic current (Fig. 1), is observed. Corresponding Nyquist plots indicate a R_{ct} decrease, while the C_{DL} values decrease only slightly in the range of potentials 1100 - 1500 mV /SCE, indicating no further growth of the passive film thickness.

The k_{ct} values are found to increase from $(2.69 \pm 0.17) \cdot 10^2$ to $(1.12 \pm 0.02) \cdot 10^4 \text{ s}^{-1}$ with the increase of the UC potential from 700 to 1500 mV/SCE. The fitting of the obtained values with the equation $k_{ct} = k_{ct}^0 \exp[-\alpha n F / RT (E - E^0)]$ provides $k_{ct}^0 = 7.9 \pm 1.8 \text{ s}^{-1}$ and shows that the electrochemical reaction is strongly irreversible ($\alpha n = 0.119$).

CONCLUSION

LV, MPSC and EIS measurements at the UC electrode in 0.1 – 4.0 M HClO_4 demonstrated that UC charge transfer controlled oxidation becomes possible at $E > 449 \text{ mV/SCE}$ resulting in the formation of a pseudopassive film at the electrode surface. UC is transferred to a transpassive state at the potentials exceeding 1100 mV/SCE. The UC electrochemical dissolution rate in the transpassive region may achieve $50 \text{ mg cm}^{-2} \text{ h}^{-1}$ according to MPSC data.

Spectroelectrochemical Studies of Actinides in Ionic Melts

C. A. Sharrad^{*}, H. Kinoshita^{*}, I. May^{*}, I. B. Polovov[†], J. M. Charnock[§], C. Hennig[‡], A. C. Scheinost[‡] and B. Kralj[#]

^{*}Centre of Radiochemistry Research, School of Chemistry, Oxford Road, Manchester, M13 9PL, U.K.

[†] Department of Rare Metals, Ural State Technical University – 14 Mira Street, UPI, Ekaterinburg, 620002, Russia.

[§] CCLRC Daresbury Laboratory, Daresbury, Warrington, Cheshire, WA4 4AD, U.K.

[‡] Forschungszentrum Rossendorf, Institute of Radiochemistry, P. O. Box 510119, 01314 Dresden, Germany.

[#] Nexia Solutions, B13022, Sellafield, Seascale, Cumbria, CA20 1PG, U.K.

INTRODUCTION

Ionic melt technologies, at both high and room temperature, have been considered for a range of applications in the nuclear industry,^{1,2} including the electrolytic separation of uranium from irradiated nuclear fuel and plutonium purification for military applications. Many of these processes are relatively poorly understood from a fundamental chemical viewpoint due to the harsh chemical environment, from the very high melting points of some of the salts used to radiological hazards.

Several groups, including ours, have investigated *in situ* actinide speciation in ionic melts using a variety of spectroscopic techniques including electronic absorption spectroscopy (EAS), Raman spectroscopy and X-ray absorption spectroscopy (XAS).³⁻⁵ Our previous molten salt XAS experiments were performed using chemically generated U species, with measurements made in transmission mode.⁵ However, our main interest is the linking of our understanding of actinide speciation in ionic melt systems with electrochemical properties, including the industrially relevant processes of anodic dissolution and cathodic deposition. The air and moisture sensitivity of these systems, and the thermal resistivity required, renders the development of a spectroelectrochemical cell more challenging than for conventional systems.

RESULTS

We wish to report studies into the speciation of uranium in oxidation states III, IV, V and VI in high temperature alkali chloride salts and room temperature ionic liquids using spectroelectrochemical techniques (EAS and XAS). In doing so we have developed a cell-furnace system (Figure 1) to probe electrolytically generated uranium species in high temperature melts. This has allowed us to perform the first *in situ* XAS spectroelectrochemical studies of uranium in high temperature melts. Anodic dissolution of uranium metal and cathodic reduction of U(IV) to U(III) in LiCl-KCl eutectic at 450 °C were probed using the X-ray absorption near edge structure (XANES) region of the XAS experiments (Figure 2). The U L_{III}-edge position is observed to shift to more negative values as the cathodic reduction of U(IV) to U(III) proceeds but a relatively pure U(III) melt was only obtained by anodic dissolution of uranium metal. Modelling of the extended X-ray absorption fine structure (EXAFS) of the U(III)

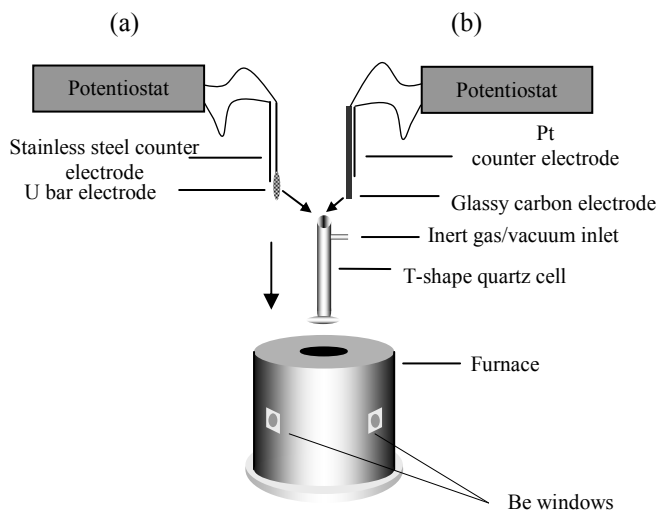


Fig. 1 Schematic diagram of the experimental apparatus used for *in situ* EXAFS spectroelectrochemistry on U species in high temperature melts using (a) anodic dissolution and (b) cathodic reduction processes.

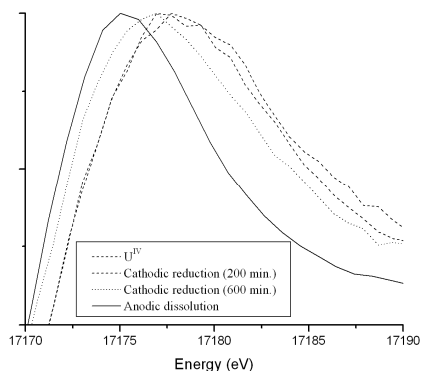


Fig. 2 U L_{III}-edge XAS spectra of uranium cathodic reduction ($\text{U}^{\text{IV}} \rightarrow \text{U}^{\text{III}}$) and anodic dissolution ($\text{U metal} \rightarrow \text{U}^{\text{III}}$) in LiCl-KCl at 450 °C.

spectrum was able to obtain a U-Cl distance of $2.83 \pm 0.02 \text{ \AA}$, typical for the +III oxidation state, with six chlorine atoms surrounding the uranium atom.

Investigations into $\{\text{UO}_2\}^+$ species in the room temperature ionic liquid (RTIL), trimethylbutylammonium bistriflimide ($\text{Me}_3\text{BuN}^+\text{TFSI}$), have been conducted through the electrolytic reduction of $\text{UO}_2(\text{TFSI})_2$ in the RTIL. EAS indicated the slow disproportionation of $\{\text{UO}_2\}^+$ to $\{\text{UO}_2\}^{2+}$ and U(IV). XAS studies have been conducted using a specially designed electrochemical cell.⁶

Finally, the first EAS spectroelectrochemical studies of ^{237}Np in high temperature chloride melts have also been undertaken with the cathodic reduction of Np(IV) to Np(III) in LiCl-KCl eutectic (450 °C) studied.

CONCLUSIONS

The *in situ* speciation of electrochemically generated actinide species in ionic melts has been achieved using EAS and XAS techniques. This can lead to a better understanding of electrolytic methods for actinide separation processes in such media.

We would like to thank Nexia Solutions for financial support, INTAS for a fellowship for I. B. P., and CCLRC and ESRF for the provision of synchrotron radiation facilities.

- 1 D. G. Lovering, Ed. *Molten Salt Technology*, Plenum, New York, (1982); R. J. Gale and D. G. Lovering, Eds. *Molten Salt Techniques*, Plenum, New York, 1984.
- 2 V. A. Cocalia, K. E. Gutowski and R. D. Rogers, *Coord. Chem. Rev.* in press.
- 3 V. A. Volkovich, A. I. Bhatt, I. May, T. R. Griffiths and R. C. Thied, *J. Nucl. Sci. Technol.* **Suppl. 3**, 595 (2002); V. A. Volkovich, T. R. Griffiths, D. J. Fray and R. C. Thied, *Phys. Chem. Chem. Phys.* **2**, 3871 (2000).
- 4 G. M. Photiadis and G. N. Papatheodorou, *J. Chem. Soc., Dalton Trans.* 3541(1999).
- 5 A. I. Bhatt, E. F. Kerdaniel, H. Kinoshita, F. R. Livens, I. May, I. B. Polovov, C. A. Sharrad, V. A. Volkovich, J. M. Charnock and R. G. Lewin, *Inorg. Chem.* **42**, 2 (2005); V. A. Volkovich, I. May, J. M. Charnock, *Rasplavy* **2**, 76 (2004).
- 6 C. Hennig, J. Tutschuku, A. Rossberg, G. Bernhard and A. C. Scheinost, *Inorg. Chem.* **44**, 6655 (2005).

Effect of Hydrogen on Dissolution of the Spent Fuel Matrix and UO₂ pellets doped with Plutonium : A Threshold Phenomenon?

C. Jégou, B. Muzeau, V. Broudic

Commissariat à l'Énergie Atomique (CEA/Valrhô), DTCD/SECM/LMPA
BP 17171, 30207 Bagnols-sur-Cèze Cedex, France

INTRODUCTION

The option of direct disposal of spent nuclear fuel in a deep geological formation raises the need to investigate the long-term behavior of the UO₂ matrix in aqueous media subjected to $\alpha\beta\gamma$ radiation. Molecular hydrogen, produced as a result of the anoxic corrosion of iron container, appears to be capable of inhibiting oxidizing dissolution of the spent UO₂ fuel matrix due to water radiolysis in a α and/or $\beta\gamma$ radiation field¹, although the mechanisms behind this phenomenon have not been clearly identified. The effect of molecular hydrogen on radiolytic decomposition of pure water subjected to a mixed radiation field combining high-LET charged α particles and low-LET $\beta\gamma$ radiation has nevertheless been investigated in relation with radiolysis problems in nuclear reactor primary systems². This work has demonstrated that molecular hydrogen was capable of reducing the concentration of oxidizing species in the medium through a radical chain reaction. This chain reaction occurs in the presence of hydrogen with a sufficient radical concentration, which requires low-LET radiation and assumes that the molecular species such as O₂ and H₂O₂ likely to stop the chain reaction are not in excess, i.e. when the high-LET radiation is not too intense. The competition between these phenomena results in a threshold effect above which water decomposition is observed. The objective of this study is to determine to what extent the spent fuel UO₂/water interface inherently subjected to a mixed $\alpha\beta\gamma$ radiation field reacts according to similar mechanisms in the presence of hydrogen, and whether a threshold effect may be applicable.

EXPERIMENTAL PROCEDURE

An aqueous solution initially containing 8×10^{-5} mol/L hydrogen (Ar + 4% H₂ at 2.5 bars, with no hydrogen renewal during the experiment) was irradiated for 14 days by a 260 Ci cobalt (⁶⁰Co) source. The γ dose rate in the homogeneous solution determined by Fricke dosimetry was 650 Gy/h. Various materials containing UO₂ were placed in the experimental reactor to vary the intensity of the α radiation field at the UO₂/water reaction interface. The H₂O₂ concentration in the homogeneous solution was determined by chemiluminescence³ after 14 days of irradiation. The materials used consisted of spent fuel fragments (UO₂ with a burnup of 60 GWd/t_{HM}), UO₂ pellets doped with different ²³⁸Pu concentrations to vary the alpha radiation intensity at the reaction interface, and Simfuel pellets (6 at%)⁴. The Simfuel did not supply a significant self-irradiation field but—with some reservations—its chemistry was comparable to that of the spent fuel. The alpha irradiation fields corresponding to these materials are summarized in Table I.

EXPERIMENTAL RESULTS AND DISCUSSION

Two H₂O₂ concentrations were determined experimentally in the homogeneous solution depending on the materials used (Table I). For the materials having the most intense alpha irradiation fields a concentration of $2 (\pm 0.2) \times 10^{-7}$ mol/L was measured after 14 days, compared with

$3 (\pm 0.5) \times 10^{-8}$ mol/L for the materials with the lowest alpha irradiation fields. The Chemsimul kinetic code⁵ was used for radiolysis calculations to assess the H₂O₂ concentrations in the homogeneous solution irradiated by a 650 Gy/h cobalt source versus the initial hydrogen concentration. The calculations revealed a threshold (Fig. 1) depending on the hydrogen concentration. Based on these calculations, initially adding 8×10^{-5} mol/L of hydrogen to the homogeneous solution should result in the onset of steady-state conditions near 3×10^{-8} mol/L (Fig. 1) in the homogeneous solution for all experiments. This calculated concentration is in full agreement with the experimental results for the materials with the lowest alpha irradiation field. For the materials with an intense alpha irradiation field, an experimental value of 2×10^{-7} mol/L was obtained. This value is consistent with the calculated value obtained in absence of a substantial effect of hydrogen on the production of oxidants (i.e. low hydrogen concentrations). The results clearly show that in a high-intensity alpha irradiation field at the UO₂/water interface the initial hydrogen concentration in comparison with the molecular species formed under alpha radiation is probably not sufficient to sustain the chain reaction.

Table I. Alpha dose rate at the reaction interface for the test materials and H₂O₂ concentrations in the homogeneous solution

Material	α dose rate (Gy/h)	[H ₂ O ₂] (mol/L)
Spent fuel	1600	$2 (\pm 0.2) \times 10^{-7}$ mol/L
²³⁸ Pu-doped UO ₂	1100	$2 (\pm 0.5) \times 10^{-7}$ mol/L
²³⁸ Pu-doped UO ₂	110	$3 (\pm 0.5) \times 10^{-8}$ mol/L
Simfuel	< 0.01	$3 (\pm 0.5) \times 10^{-8}$ mol/L

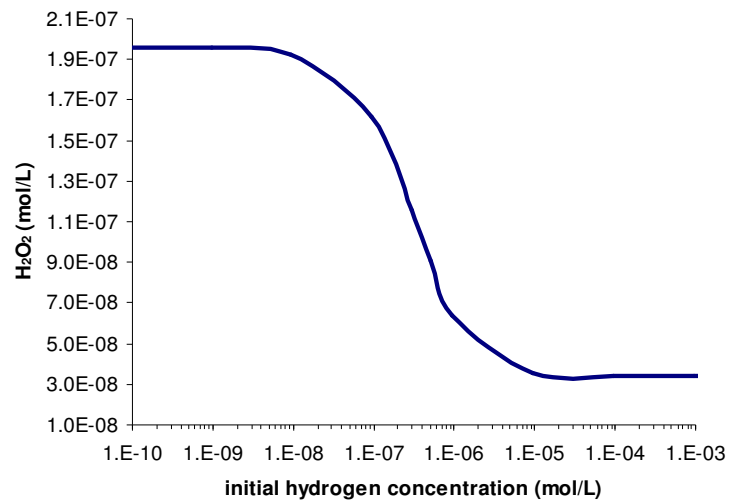


Fig. 1. Model of H₂O₂ concentration in the homogeneous solution versus the initial hydrogen concentration (650 Gy/h for 14 days)

- 1 K. Spahiu, L. Werme, U-B. Eklund, The influence of near field hydrogen on actinide solubilities and spent fuel leaching, *Radiochim. Acta* 88 (2000) 507-511.
- 2 B. Pastina, Ph.D Thesis, Université Paris-Sud, Paris, France, 1997; no. 4862.
- 3 V. Broudic, B. Muzeau, C. Jégou, M. Bonnal, A. Gavazzi, C. Marques, Application of chemiluminescence to the study of alpha, beta and gamma radiolysis of water. *Atalante 2004* international conference, June 21-24, 2004: Nîmes, France. P2-11.
- 4 P.G. Lucuta, R.A. Verrall, Hj. Matzke and B.J. Palmer. *Journal of Nuclear Materials* 178 (1991) 48-60.
- 5 P. Kirkegaard and E. Bjergbakke, *CHEMSIMUL, A program package for numerical simulation of chemical reaction systems*. November 20, 1998. Riso National Laboratory DK-4000 Roskilde Denmark (1998).

Engineering-Scale Distillation of Cadmium for Actinide Recovery

B.R. Westphal, J.C. Price, and D. Vaden

Idaho National Laboratory, Idaho Falls ID 83415 USA

BACKGROUND

The electrometallurgical treatment of Experimental Breeder Reactor-II (EBR-II) spent nuclear fuel at the Idaho National Laboratory (INL) comprises a set of operations designed to recover actinides from radioactive fission products and place the fission products into acceptable waste forms [1]. A glass-bonded ceramic waste form and a stainless steel-based metallic waste form are the two types of high-level waste forms being qualified for disposal in a geological repository [2]. Two actinide products are recovered during the spent fuel treatment process; a primarily uranium product and a plutonium-uranium product. The low enriched uranium products recovered from spent fuel treatment are currently being stored pending a decision by the Department of Energy on final disposition. To date, several plutonium-uranium products have been produced and are the subject of this paper.

Treatment of the EBR-II spent fuel is performed in the Fuel Conditioning Facility (FCF), a shielded hot-cell environment located at the Materials and Fuels Complex of the INL. The treatment program was initiated in June 1996 and continues presently on the balance of the spent fuel. Batch operations on the spent fuel include a chopping step, electrorefining, cathode processing, and casting. The electrorefiner and cathode processor are the primary recovery steps for the actinide products. During electrorefining, fuel is anodically dissolved in a LiCl-KCl eutectic salt such that the transport of actinides as cathode material is feasible. In addition to the LiCl-KCl, other chloride species are present in the electrorefiner salt due to the oxidation of fission products, bond sodium, and actinides present in the spent fuel. Once transported, uranium cathode products are collected and further processed by a vacuum distillation operation for the removal of the adhering salts. The plutonium-uranium products are produced by utilizing a liquid cadmium cathode for electrorefining and then removing the cadmium by distillation. Both distillation operations are performed in the same piece of equipment, the cathode processor, to produce consolidated actinide ingots.

EXPERIMENTAL

The cathode processor (Fig. 1) is an induction-heated furnace capable of temperatures to 1400°C and

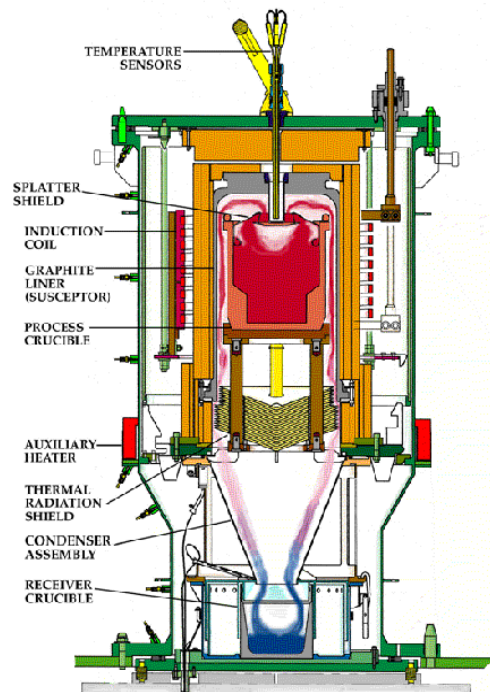


Fig 1. Schematic of Cathode Processor

pressures less than 0.1 Torr. The furnace region contains a passively cooled induction coil and a graphite furnace liner that acts as the susceptor to heat the process materials. Separation of the chloride salts and cadmium from the actinide products in the cathode processor is accomplished by reducing the internal pressure to approximately 1 Torr and heating to at least 1200°C to consolidate the actinide products. A more detailed description of the cathode processor and its general operation is given elsewhere [3].

Of the four experiments performed at the cathode processor for cadmium distillation, three have been with plutonium-uranium products from the electrorefiner. The first test in the cathode processor utilized surrogate materials to confirm operating parameters developed during qualification testing. For cadmium distillation, the process conditions consist of evacuating the cathode processor vessel to 1 Torr, isolation of the vacuum system from the vessel to prevent the migration of cadmium vapor, heating to 700°C at 8 kW, and then heating to a maximum temperature of 1200°C at 15 kW. The reduced power level controls the rate of cadmium distillation initially while the 700°C temperature is considered high enough to achieve thermal decomposition of any plutonium-cadmium compounds. The overall run time (from induction power start to finish) for the four cadmium distillation experiments averaged less than nine hours per run. The three consolidated plutonium-uranium ingots are then processed in the casting furnace where samples are taken for chemical analyses. Due to facility safeguard issues, dilution with depleted uranium is necessary for the plutonium-uranium products. Additionally, the actinide product ingots are returned to the electrorefiner salt to enable continued testing.

RESULTS

For the four cadmium experiments performed in the cathode processor, at least 25 kg of cadmium was distilled and greater than 99 wt.% was recovered for reuse. An average cadmium distillation rate of 0.41 g/min/cm² was determined which compares favorably with previous investigators. The final plutonium-uranium products for three experiments contained levels of cadmium below the detection limits of analytical chemistry; typically 50 ppm. Similar to cadmium, negligible amounts of rare earth impurities were detected in the samples taken following casting. Additional sampling was performed following cathode processing on the cadmium and process waste streams and their analyses will also be reported. In conclusion, a successful separation of cadmium from actinide products was achieved at the engineering-scale to support further research efforts in actinide recovery.

The authors would like to acknowledge the cathode processor designers, FCF operations support, and analytical laboratory personnel for their contributions to the testing program. Work supported by the U.S. Department of Energy, Office of Nuclear Energy, Science, and Technology, under DOE-NE Idaho Operations Office Contract DE-AC07-05ID14517.

- 1 K.M. Goff, K.L. Howden, G.M. Teske, and T.A. Johnson, "Pyrochemical Treatment of Spent Nuclear Fuel", Proc. Global 2005, (Tsukuba, Japan: AESJ, 2005).
- 2 K. Marsden et al., "Process and Equipment Qualification of the Ceramic and Metal Waste Forms for Spent Fuel Treatment", Proc. Global 2005, (Tsukuba, Japan: AESJ, 2005).
- 3 A.R. Brunsvold, P.D. Roach, and B.R. Westphal, "Design and Development of a Cathode Processor for Electrometallurgical Treatment of Spent Nuclear Fuel," Proc. Eighth Int. Conf. Nucl. Eng. (ICONE), (New York, NY: ASME, 2000).

The LLNL Heavy Element Facility -- Facility Management, Authorization Basis, and Readiness Assessment Lessons Learned in the Heavy Element Facility (B251) Transition from Category 2 Nuclear Facility to Radiological Facility

Mark Mitchell*, Brian Anderson, Erik Brown, Leonard Gray

*Lawrence Livermore National Laboratory, Livermore CA 94552 USA

UCRL-ABS-218323

This presentation discusses Facility Management, Readiness Assessment, and Authorization Basis experience gained during the Risk Reduction Program (RRP). These lessons can help facilitate similar activities at other sites, including facilities restarting operations or new facilities starting new operations. The RRP successfully downgraded the Heavy Element Facility (B251) from a Category II Nuclear Facility to a Radiological Facility. Leading up to this major achievement were significant safety accomplishments, completing objectives on time and on budget, achieving the November 2003 Milestone for reducing Inventory to 20% of the initial inventory, and reducing Inventory to < 0.03 ^{241}Am -equivalent curies by the April 2005 Milestone.

B251 was constructed at LLNL to provide research areas for conducting experiments in radiochemistry using transuranic elements. B251 capabilities once included the preparation of tracer sets associated with the underground testing of nuclear devices and basic research devoted to a better understanding of the chemical and nuclear behavior of the transuranic elements. Facility safety and experimental systems were deteriorating with age, even with preventative maintenance. A variation of seismic standards were used in a design that encompassed eight building increments constructed over a period of 26 years. The RRP was created to mitigate the risk of dispersal of radioactive material during an earthquake by removing the radioactive materials inventory and glove box contamination. The cost to bring the facility into compliance with the current requirements was quite high, and simply maintaining B251 as a Category 2 nuclear facility posed serious cost considerations under a changing regulatory environment. LLNL adopted the goal of reaching Radiological Facility status.

To support the RRP, B251 transitioned from a standby to fully operational, Category 2 Nuclear Facility, compliant with current regulations. A work control process was developed, Authorization Basis Documents were created, work plans were written, off-normal drills practiced, a large number of USQ reviews were conducted, and a type II Readiness Assessment (RA) was conducted to start up operations. Subsequent RA's focused on specific operations. Finally, a four-step process was followed to reach Radiological Status: 1) Inventory Reduction and D&D activities reduced the inventory and radiological contamination of the facility below the Category 3 threshold (DOE-STD-1027), 2) Radiological Safety Basis Document (SBD aka HAR) was approved by NNSA, 3) the inventory control system was in place, and 4) verification by NNSA of radiological status was completed.

Key to this success is the RRP philosophy in a schedule driven paradigm.

- “Expect the unexpected and confirm the expected”
- Recognize when you reach the point of diminishing returns,
- Develop robust processes that anticipate and can handle surprises,
- Plan, plan, and re-plan “Measure twice, cut once”

This presentation will discuss:

- History of the Heavy Element Facility, B251
- Risk Reduction Program
 - Objectives
 - Accomplishments
- Lessons Learned
 - Transitioning from Standby to Operating Facility
 - Robust processes that “Expect the Unexpected”
 - Authorization Basis Strategies
 - Facility Infrastructure Strategies
 - Readiness Assessment (RA) Strategies
 - Operational Strategies
- Conclusions



Staff from multiple organizations played significant roles in downgrading B251 from Nuclear Category 2 to Radiological

Impressive safety accomplishment
No one had decontaminated facilities with this level and variety of high specific activity isotopes (e.g. ^{244}Cm , ^{238}Pu)
Dramatic cost savings, \$250 million under current regulations



Reference: Mark Mitchell et al, *The LLNL Heavy Element Facility -- Facility Management and Authorization Basis Lessons Learned in D&D Environment: Transition from Category II Nuclear Facility to Radiological Facility*, UCRL-PRES-213765, Proceedings of the 2005 Tri-Lab Conference, Monterey, CA, September 2005.

Photochemical Oxidation of Oxalate, Urea, and Hydroxylammonium in Pu-238 Process Streams

K. Long, D. Ford, G. Jarvinen

Los Alamos National Laboratory, Los Alamos NM 87544 USA

For over forty years, NASA has relied on plutonium-238 in Radioisotope Thermoelectric Generator (RTG) units and Radioisotope Heater Units (RHUs) to provide power and heat for many space missions including Transit, Pioneer, Viking, Voyager, Galileo, Ulysses and Cassini. RHUs provide heat to keep key components warm in extremely cold environments found on planets, moons, or in deep space. RTGs convert heat generated from the radioactive decay of plutonium-238 into electricity using a thermocouple. Plutonium-238 has proven to be an excellent heat source for deep space missions because of its high thermal power density, useful lifetime, minimal shielding requirements, and oxide stability.

At Los Alamos, a plutonium-238 scrap recovery system has been built at Technical Area 55 (TA-55) and will be operational in the near future. This glovebox facility will purify Pu-238 from scrap material and residues from past production operations to provide RTGs and RHUs for additional NASA missions. The scrap material is balled-milled to give a mean particle size < 5 microns and then dissolved in a mixture of nitric acid and hydrofluoric acid. The plutonium solution is purified using an ion exchange column, if necessary, or it is sent directly to oxalate precipitation. During the oxalate precipitation step, urea is added to scavenge nitrite, hydroxylamine nitrate is added to adjust the valence of plutonium to Pu(III), and oxalic acid is added to precipitate plutonium as $\text{Pu}_2(\text{C}_2\text{O}_4)_3$. The plutonium oxalate is isolated and calcined in a gas stream containing oxygen-16 enriched water vapor to produce the PuO_2 used in the RTGs and RHUs. The filtrate after oxalate precipitation still contains a significant amount of Pu-238, most of which is precipitated by addition of sodium hydroxide to give a pH of 10-13. An ultrafiltration process with water-soluble chelating polymers is used to selectively bind with most of the remaining plutonium in the solution, reducing the alpha radioactivity to meet regulatory

discard limits. The hydroxide precipitation and the polymer filtration process are both more efficient at removing plutonium if the oxalate is not present to compete with hydroxide or the water-soluble polymer for the plutonium. We are investigating using UV irradiation to oxidize the oxalate (along with urea and hydroxylamine nitrate) before the hydroxide precipitation or ultrafiltration operations.

Surrogate solutions comprised of oxalic acid, urea, and hydroxylamine nitrate in a nitric acid have been used for experimentation. The test solutions were placed in a glass reactor containing a water-cooled quartz immersion well. A 1200-watt or 2000-watt mercury vapor lamp was used to irradiate the solution and compressed air or argon was used to continuously sparge the solution. The oxidation rates of oxalic acid and urea were measured throughout each irradiation period by monitoring the total organic carbon content of the solutions. The concentrations of oxalate, hydroxylammonium, ammonium, and nitrate were monitored by ion chromatography. A number of variables, including concentrations of oxalic acid, urea and hydroxylamine, type of sparge gas, and additions of iron as an oxidation catalyst were studied to help optimize the processing conditions. Figure 1 gives an example of the time dependence of the concentration of the solution constituents during irradiation. An overview of the irradiation test results to date will be presented.

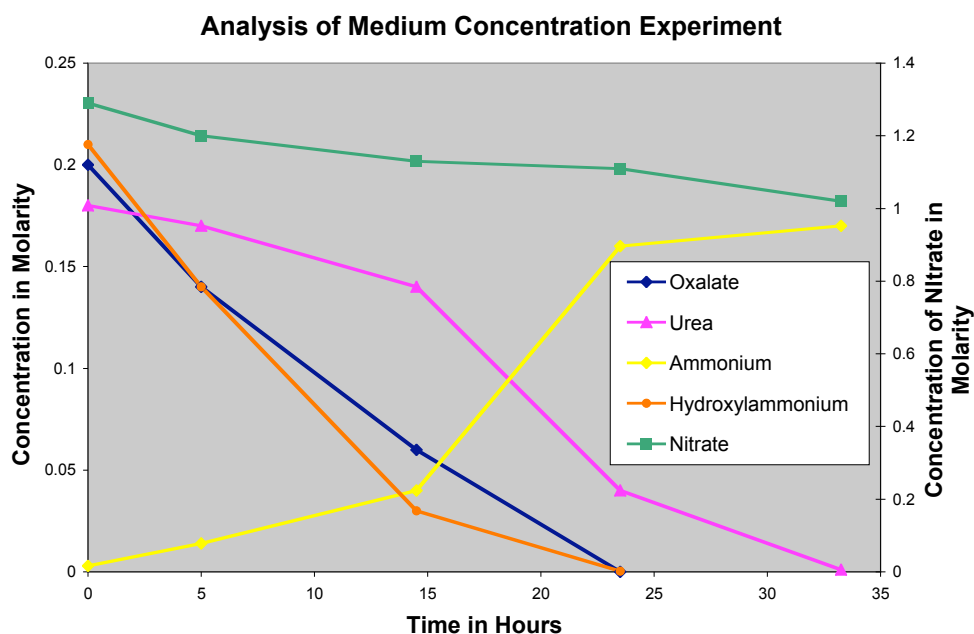


Figure 1. Time dependence of the concentration of solution constituents during irradiation.

Diffusion Behavior of Actinide and Lanthanide Elements in Molten Salt for Reductive Extraction

D Yamada¹, T. Murai¹, K. Moritani¹, T. Sasaki¹, I. Takagi¹, H. Moriyama¹,
K. Kinoshita², H. Yamana³

¹ Department of Nuclear Engineering, Kyoto University, Yoshida, Sakyo-ku, Kyoto 606-8501

² Central Research Institute of Electric Power Industry, Tokyo 201-8511

³ Research Reactor Institute, Kyoto University, Kumatori, Osaka 590-0494

INTRODUCTION

In recent years, there has been a renewed interest for new nuclear fuel cycles or new nuclear waste management strategies, especially for efficient transmutation of long-lived radionuclides in order to minimize the radiological toxicity of nuclear wastes. Reductive extraction process, which has been developed for reprocessing molten salt reactor fuels, is expected to be more useful for separation and recovery of transuranic elements. Up to date extensive studies have been performed concerning the thermodynamics of reductive extraction.^{1,2} However little is still known about the kinetics. For the development of reductive extraction process the rate of extraction of actinide and lanthanide elements in a two-phase system of molten LiCl-KCl eutectic salt and liquid cadmium was measured at 723-873K in our previous study.³ The mass transfer coefficients were found to be as high as expected. In some cases, however, it was found that the rate of reductive extraction was possibly affected by the solubility limits of the solute elements in the metal phase.

For comparison, in the present study, the diffusion coefficients of actinide and lanthanide elements were measured as a function of temperature in LiCl-KCl for reductive extraction. By combining the present results with the previous ones on the rate of extraction, the extraction mechanism and the system performance will be discussed for further development of the extraction system.

EXPERIMENTAL

Diffusion coefficients were measured by a capillary method.⁴ All the chemicals were of reagent grade obtained from Nacalai Tesque, Inc., and the radioactive tracers were produced by neutron irradiation of metal specimens. All experiments used high-purity reagents and were performed in a glove box under argon atmosphere containing <0.5ppm of O₂ and <0.2ppm of H₂O.

In the measurement, a quartz capillary tube of an i.d. of 0.2 or 0.3mm and a length of about 50mm sealed from one end was used. The open end of the evacuated capillary was immersed into molten LiCl-KCl containing the radioactive tracers in order to allow the liquid to rise up. The capillary filled with the LiCl-KCl was then immersed into a pure LiCl-KCl. The temperature of the system was controlled within ± 0.5 K. After a known diffusion time, the capillary was removed, allowed to cool, and cut into several sections. The concentration profile of each

radioactive tracer was determined by a direct γ -ray spectrometry. No significant differences were observed for the capillaries of 0.2 and 0.3mm, and it was concluded that thermal convection was not important source of uncertainty.

RESULTS

In Fig. 1, the diffusion coefficients of solute elements in LiCl-KCl are plotted as a function of inverse temperature and compared with literature values for La⁵ and U⁶. Similar temperature dependences are found for all the elements, although some differences are observed possibly due to the different interactions of solute elements with the solvent and due to different sizes of the diffusing species. The obtained results are discussed for the kinetics of reductive extraction process.

- 1 T. Inoue, M. Sakata, H. Miyasiro, A. Sasahara and T. Matsumura, *J. Nucl. Technol.* **93** (1991) 206.
- 2 K. Kinoshita, T. Inoue, S. P. Fusselman, D. L. Grimmett, J. J. Roy, R. L. Gay, C. L. Krueger, C. R. Nabelek and T. S. Storvick, *J. Nucl. Sci. Technol.* **36** (1999) 189.
- 3 H. Moriyama, D. Yamada, K. Moritani, T. Sasaki, I. Takagi, K. Kinoshita, and H. Yamana, *J. Alloys and Compounds* **408-412** (2006) 1003.
- 4 H. Moriyama, K. Moritani and Y. Ito, *J. Chem. Eng. Data* **39** (1994) 147.
- 5 M. V. Smirnov, Yu. N. Krasnov, V. E. Komarov and V. N. Alekseev, *Electrochem. Molten Solid Electrolytes*, **6**, 47, (1968).
- 6 S. A. Kuznetsov, H. Hayashi, K. Minato and M. Gaune-Escard, *J. Nucl. Mater.* 344 (2005) 169.

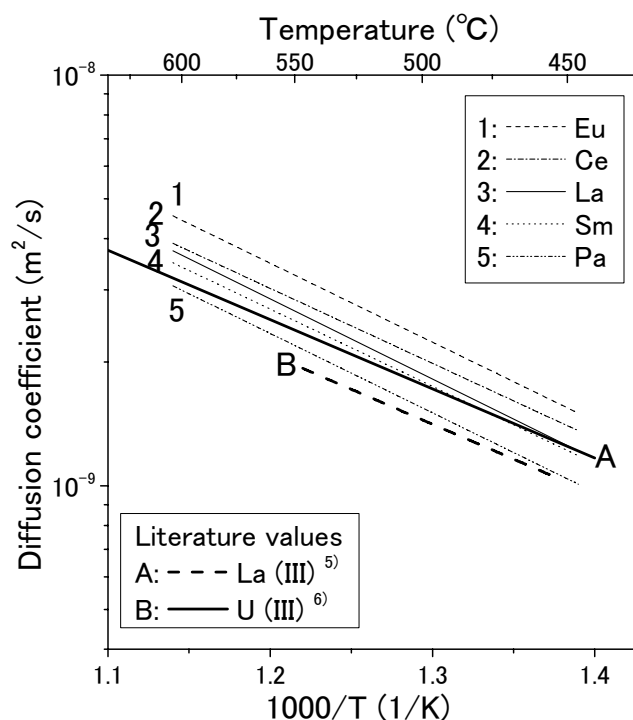


Fig. 1. Diffusion coefficients of actinide and lanthanide Elements in LiCl-KCl.

Plutonium and americium ceramic matrices: Structure and resistance to self-irradiation damage

R. Belin^{*}, J. Cambedouzou^{*}, D. Bregiroux^{*†}, P. Valenza^{*} and F. Audubert^{*}.

^{*} Commissariat à l'Énergie Atomique - CEA Cadarache - DEN/DEC/SPUA
- 13108 Saint-Paul-lez-Durance, FRANCE

[†] Laboratoire Science des Procédés Céramiques et de Traitements de Surface
- UMR 6638 - 123 avenue Albert Thomas - 87060 Limoges, FRANCE

INTRODUCTION

Management of minor actinides (MAs) is one of the main concerns of the nuclear industry. The proposed strategies have to take into account large volumes, strong activities and political issues. Both once-through transmutation and direct long-term storage are viable options. In any case, matrices have to handle long-term containment. It is well known that a potential alpha-decay induced amorphization of the material causes an increase of several orders of magnitude of lixiviation. Thus, a better understanding of resistance to self-irradiation damage is of major importance. In that prospect, we have performed comparative studies on pyrochlores and monazites ceramic oxides, respectively prominent candidates for once-through transmutation and long-term immobilization. Plutonium and americium compounds were synthesized, their structures characterized by XRD and compared. Finally, the evolution of the americium compounds under the effect of self-irradiation was followed and discussed.

SYNTHESIS AND XRD CHARACTERIZATION

All compounds were prepared on the scale of a few milligrams and AmO₂ was handled in a special glove-box equipped with biological protections. Pu₂Zr₂O₇ and Am₂Zr₂O₇ pyrochlores were prepared starting from polycrystalline PuO₂ or AmO₂ and ZrO₂. Both compounds were ground/mixed with the appropriate ratios and fired in a Mo crucible under a reducing atmosphere (Ar/5% H₂) at 1673 K for 55 hours, the process repeated twice. The following monazites were prepared: PuPO₄, (Pu⁺³Pu⁺⁴)_{1-x}Ca_xPO₄ and AmPO₄. These samples are not representative of the considered material for storage as, based upon observations on mineral monazite [1], the actinide incorporation ratio will not exceed 10wt%. Nevertheless, pure actinide monazites allow a plain comparison with the pyrochlores. The compounds were made by solid-state reaction between PuO₂ or AmO₂ and NH₄H₂PO₄ (and CaO for PuCaPO₄) at 1400°C for 2 hours and the entire process repeated. Both plutonium monazites were synthesized under air and argon, whereas AmPO₄ synthesis was only carried out under argon. X-ray samples were prepared according to a procedure previously described [2]. The pyrochlore structure was investigated in detail by the Rietveld method, which allowed us to refine the 48f oxygen position. This parameter is critical for the structural stability of the compound. Regarding monazites, the effect of the atmosphere and the incorporation of tetravalent plutonium in the structure were studied.

RESISTANCE TO SELF-IRRADIATION DAMAGE

The effects of alpha irradiation on the structure were followed as a function of time for $\text{Am}_2\text{Zr}_2\text{O}_7$ and AmPO_4 . It was found that the pyrochlore structure progressively disappeared to the benefit of a fluorite-type solid solution in correlation with the alpha dose-rate, as shown by the fading of superstructure peaks marked by * (see Fig. 1). The stability of the pyrochlore phase versus the fluorite phase has been examined. Interestingly, the compound shows a significant resistance to radiation damage as no amorphization is observed even after 400 days (2.13×10^{25} α -decay/ m^3).

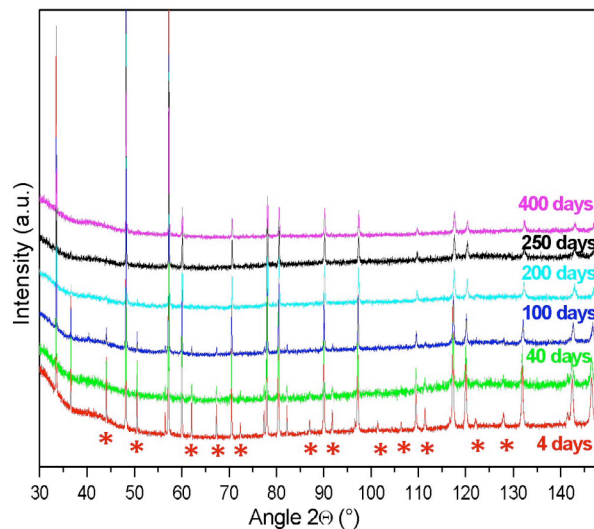


Fig.1: Evolution of X-ray patterns for $\text{Am}_2\text{Zr}_2\text{O}_7$ as a function of time.

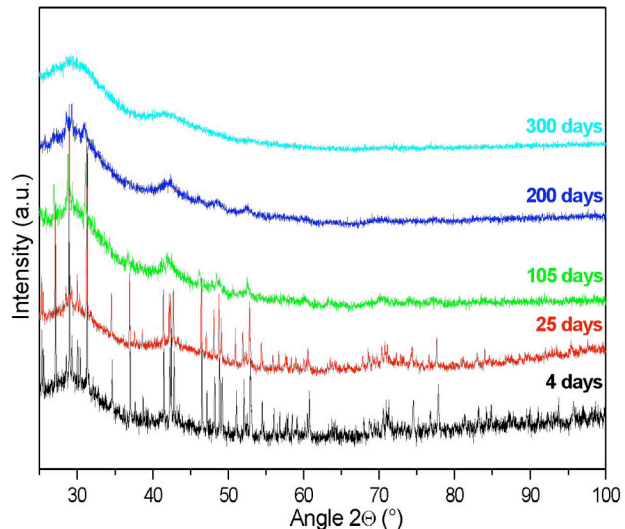


Fig.2: Evolution of X-ray patterns for AmPO_4 as a function of time.

On a reverse fashion, AmPO_4 shows a complete amorphization after 300 days and a dose of 1.65×10^{25} α -decay/ m^3 as no more diffraction peak is observed (see Fig. 2). This result is in agreement with Burakov who found that ^{238}Pu doped PuPO_4 turns amorphous for an equivalent dose [3]. Resistance to amorphization can be seen as the structure's ability to regain the initial crystalline state following the damage. Bonds ionicity - the competition between the short-range covalent and long-range ionic forces - is considered as an important factor to understand this behavior [4,5].

In the presentation we shall give a precise description of $\text{Am}_2\text{Zr}_2\text{O}_7$ and AmPO_4 structures and, by comparing their electronic density maps, discuss how the type of interatomic forces involved is relevant for resistance to amorphization.

- 1 L. A. Boatner and B. C. Sales, Monazite. In *Radioactive Waste Forms for the future* (ed. W. Lutze and R.C. Ewing), 495-564. Elsevier (1988)
- 2 R. C. Belin *et al.*, *J. Appl. Cryst.* 37, 1034-1037 (2004)
- 3 B.E. Burakov *et al.*, *Mater. Res. Soc. Symp. Proc.* 824, 219-224 (2004)
- 4 K. Trachenko, *J. Phys.: Condens. Matter* 16, R1491-R1515 (2004)
- 5 H. M. Naguib and R. Kelly, *Radiat. Eff.* 25, 1-12 (1975)

Leaching of Plutonium and Americium from Perovskite-Based Ceramics

Merkushkin^{*}, A.O., Ochkin^{*}, A.V., Rovniy⁺, S.I., Bobylev⁺, A.I. Stefanovsky^{*,+}, S.V.

^{*}University of Chemical Technology, Miusskaya sq,9, Moscow 125047 RUSSIA

⁺FSUE PA "Mayak", Lenin st., 31, Ozersk, Chalyabinsk reg. 456780 RUSSIA

^{*,+} SIA Radon, 7th Rostovskii lane 2/14, Moscow 119121 RUSSIA

Introduction

Perovskite, ideally CaTiO_3 , is orthorhombic structure phase (space group P_{nma}) capable to form continuous solid solutions with lanthanide aluminates, LnAlO_3 and ferrites LnFeO_3 .¹ General formula of such modified perovskites is $\text{M}^{\text{I}}\text{M}^{\text{II}}\text{O}_3$, where M^{I} and M^{II} are eight- and six-coordinated cations with ionic radii about 0.10 nm and 0.06 nm, respectively. Thus, the perovskite structure compounds are promising host phases for trivalent rare earths, actinides, such as Am and Cm, and iron group elements (corrosion products) of high level waste (HLW) as well as gallium. In our previous works we have demonstrated low leachability of trivalent actinides and lanthanides from perovskite ceramics.²⁻⁴ On the next stage of the work we studied leaching of Pu, Am and Cm from the perovskite-based ceramics doped with actual actinide-bearing HLW. Some preliminary data were published in ref.³

Experimental

Two oxide mixtures with specified formulations $0.2 \text{La}_2\text{O}_3 \cdot \text{Al}_2\text{O}_3$ and $0.4 \text{La}_2\text{O}_3 \cdot \text{Fe}_2\text{O}_3$ were milled, mechanically activated and homogenized in a planetary mill. The precursors obtained were soaked with radioactive solution containing Pu, Am, Cm, and Pm, dried at 150°C , and calcined at 750°C for 30 min. The batches were compacted in pellets ~7 mm in diameter and ~5 mm in height under a pressure of 300 MPa, heat treated in a resistive furnace in an Ar atmosphere to either 1300°C (ferrite ceramic) or 1400°C (aluminate ceramic) kept at this temperature for 5 hours followed by cooling to a room temperature in turned-off furnace. Total Pu, Am, and Cm concentrations in the pellets were 13, 0.336, and 0.002 mg/g, respectively.

The ceramics were examined by X-ray diffraction. Open porosity and relative density were measured using standard procedures. Specific surface area was measured using a BET method. Leach measurements were performed using a MCC-5 Soxhlet test⁵ for 10 days at a temperature close to 100°C (boiling water). Activities of individual radionuclides were measured by α -, β -, and γ -spectrometry. Leach rates of radionuclides were calculated by eq. (1)⁶: $w = (A \times m) / (A_0 \times S \times t)$ (1), where w - leach rate, $\text{g}/(\text{cm}^2 \times \text{day})$, A - activity of the radionuclide in leachate, s^{-1} , t - leaching time, days, A_0 - initial activity of the radionuclide in the sample, s , S - surface area, cm^2 , m - sample mass, g. The data obtained were treated using an eq. (2): $w = a_1 \times \exp(-b \times t) + a_2$ (2), where a_1 is a leach rate of radionuclide from relatively highly soluble minor phases, a_2 is "equilibrium" leach rate from the major host phase, and b is constant depended on test conditions.

Results

As follows from XRD data the aluminate ceramic is composed of major perovskite type phase (ideally LaAlO_3) and minor β -alumina (ideally $\text{LaAl}_{11}\text{O}_{18}$). The ferrite ceramic consists of predominant perovskite structure phase (ideally LaFeO_3) and minor partially reacted hematite ($\text{Fe}_{1-x}\text{La}_x\text{O}_3$). These data are consistent well with the data obtained for samples containing HLW surrogate.^{3,4} The open porosity, theoretical and relative density values for the ceramics $0.2 \text{La}_2\text{O}_3 \cdot \text{Al}_2\text{O}_3$ were found to be 28%, $4.75 \text{g}/\text{cm}^3$, and 75% of theoretical value, respectively. The same values for the $0.4 \text{La}_2\text{O}_3 \cdot \text{Fe}_2\text{O}_3$ ceramic were 0.3%, $6.10 \text{g}/\text{cm}^3$, and 85% of theoretical value, respectively. Thus aluminate ceramic is much more porous than the ferrite one. As a result at similar geometric surface areas (14.06 and 10.44cm^2) their actual surface areas measured by

BET-method are strongly different (~ 28100 and <1000 cm^2).

Leach rates (a_2) of individual radionuclides from the monolithic ceramic samples are given in Table. For the aluminate ceramic leach rates calculated using geometric surface area are higher than those measured by the BET-method by on average a factor of 2000 because leaching takes place from both outer surface of the sample and inner surface of its open pores. Pu and Am leach rates from the aluminate ceramic with surface area measured by the BET-method were found to be almost the same as those from the aluminate ceramic doped with trace amounts of radionuclides.³

Table. Leach rates of radionuclides, in $\text{g}/(\text{cm}^2 \times \text{day})$, from monolithic ceramic samples.

Radionuclide	0.2 $\text{La}_2\text{O}_3 \cdot \text{Al}_2\text{O}_3$		0.4 $\text{La}_2\text{O}_3 \cdot \text{Fe}_2\text{O}_3$
	$S_{\text{geom}} = 14.06 \text{ cm}^2$	$S_{\text{BET}} = 28100 \text{ cm}^2$	$S_{\text{geom}} = 10.44 \text{ cm}^2$
²³⁹ Pu	5.8×10^{-7}	2.9×10^{-10}	6.1×10^{-8}
²⁴¹ Am	4.2×10^{-8}	2.1×10^{-11}	2.0×10^{-8}
²⁴⁴ Cm	3.1×10^{-8}	1.6×10^{-11}	2.8×10^{-8}
¹⁴⁷ Pm	2.2×10^{-8}	1.1×10^{-11}	6.7×10^{-8}

Pu and Am leach rates from the ferrite ceramic calculated by geometric surface area are higher than those found for the ceramic doped with radionuclide tracers where surface area was measured by the BET-method by approximately 10 times. It may be suggested that this difference is due to porosity of the samples used in the given work and should disappear in the case of the samples with zero open porosity. Leach rate of ²⁴⁴Cm has approximately the same level as ²⁴¹Am. Pu exhibits higher leach rate from the aluminate ceramic as compared with that of Am and Cm by about one order of magnitude probably due to occurrence of some Pu in a tetravalent form.

Leach rate of ¹⁴⁷Pm as a matrix constituent allows to make some conclusions on long-term stability of the matrix. Using density values (ρ , g/cm^3) corrosion rates (R , cm/day) of the aluminate and ferrite matrices calculated by eq.: $R = w/\rho$ (3) are 5.2×10^{-9} and 1.1×10^{-8} cm/day , respectively. This corresponds to average matrix corrosion depth of 1.9 mm and 4.0 mm, respectively, providing for mechanical integrity even under incidental conditions when repository is flooded with water.

Discussion

According to a HLW partitioning concept HLW a long-lived REE/An fraction must be separated from a short-lived Cs/Sr fraction to be converted in ceramic and glass waste forms, respectively. The REE/An fraction contains major rare earths and minor actinides (Am, Cm, and traces of residual Pu). Because actinides are the most dangerous HLW constituents requiring their storage for a period of up to half of billion years it is expedient to separate them and process into ceramic waste form with high chemical durability and radiation resistance. The components of this An fraction - Am, Cm, residual Pu and lanthanides are mainly trivalent and the perovskite structure phases seem to be the most suitable hosts for these elements.

References

1. Phase Diagrams of High-Fusible Oxide Systems (Russ.), Nauka, Leningrad, 5 (1985-1991).
2. Ochkin, A.V., Chizhevskaya, S.V., Archakova, N.E. et al. Mat. Res. Soc. Symp. Proc. 757, 303-308 (2003).
3. Merkushkin, A., Ochkin, A., Rovniy, S., Stefanovsky, S. In: Proc. 35th Journées des Actinides, Baden, Austria, April 23-26, 2005. Abstract P-27, CD-ROM.
4. Merkushkin, A., Ochkin, A., Rovniy, S., Stefanovsky, S. In: Proc. 35th Journées des Actinides, Baden, Austria, April 23-26, 2005. Abstract P-28, CD-ROM.
5. Nuclear Waste Materials Handbook (Test Methods), DOE Technical Information Center, Washington, DC. Report DOE/TIC-11400 (1981).
6. Chemical Durability and Related Properties of Solidified High-Level Waste Forms, Technical Reports Series No.257, IAEA, Vienna (1985).

SHS method for immobilization of plutonium-containing waste

Levakov Eu.V., Postnikov A.Yu.

(RFNC - VNIIEF, Russia, Sarov)

Glagovskyi E.M., Kuprin A.V., Bogdanov A.I., Pelevin L.P.

(VNIINM, Russia, Moscow)

The main results of work in the area of technology development for immobilization of highly active waste (HAW) and, in particular plutonium-containing ones into mineral-like array compounds using the method of self-spreading high-temperature synthesis (SHS) are presented.

The choice of mineral-like arrays for HAW immobilization is proved. According to the results of thermodynamic calculations the availability of systems' formation based on zirconolite, pyrochlorine and other mineral-like compounds under SHS mode has been shown. The conditions influencing on both characteristics of SHS systems combustion and quality of obtained materials have been studied to optimize the technological parameters of SHS mineral-like arrays.

Base technological modes for SHS compacting of arrays based on pyrochlorine containing HAW simulators have been tested.

It is shown that the parameters of hydrothermal stability of arrays formed by SHS methods are similar to the same ones in arrays got by the method of cold compacting- sintering. Based on the experimentally got results the stands for immobilization of HAW simulators by SHS have been created.

An Improved Method To Dissolve Alloyed Plutonium Residues

L. Pescayre, C. Passot, D. Cardonna, H. Chollet
CEA/DAM, Centre d'Etude de Valduc – 21120 IS SUR TILLE – France

INTRODUCTION

The activities of the Valduc nuclear centre generate various plutonium metal residues which do not meet the required purity specifications to be directly reused. A nitric acid based process enables the recovery of the majority of the plutonium scrap in a purified form since the seventies. It consists in four main stages:

- Direct dissolution of the metal in $\text{NH}_2\text{SO}_3\text{H}$,
- Transformation in plutonium nitrate,
- Purification,
- Conversion into plutonium dioxide and metal.

However this process is not efficient or not safe for alloyed plutonium residues (alloyed elements > 15 wt %). A new method has been developed for four years to dissolve it. The first step is an oxidation of the metal. The second step is an aqueous dissolution in a mixture of HNO_3/HF (10 N/0.05N). The purpose is to develop a procedure and equipment for efficiently recovering the residues: complete burning (no metal remaining), good kinetics and recovery yield > 80%.

EXPERIMENTAL PROCEDURE

The first apparatus, which leads to the production of oxide, consists in a large horizontal muffle oven (Figure 1). A gas line feeds a mixture of oxygen (15% O_2) and argon into the furnace. The flow is measured before entering the glove box (45 l/h). The water vapour concentration varies between 0 and 14 000 vpm. The temperature is maintained at 550°C for 2 hours. The sample is placed in a “stainless steel/tantalum/stainless steel” cell (Figure 2).



Fig 1: Horizontal Furnace



Fig 3: Vessel used for dissolution

The second apparatus consists in a stainless steel (Uranus B6) vessel surrounded by an electric resistance (Figure 3). A wet cooling component is present on the top of the vessel head. The HNO_3/HF mixture is thermostated at 70°C for 2*6 hours with a coated thermometer and agitated with a mechanical stirrer.



Fig 2: Pu alloyed sample

MAIN RESULTS

As noted in many works before, the rate of corrosion of alloyed plutonium increases substantially with moisture. For a water vapour concentration of 14000 vpm, the burning rate is about 20 g/h/cm². A greater rate could be performing with a mechanical system which breaks the protective dioxide layer. A general trend is that the burning rate is not very sensitive to the impurities present in the metal.

The observed increase of the sample weight is that expected for a complete oxidation to PuO₂. X-ray diffraction on one of the product exactly shows the pattern and lattice constants of c.f.c. PuO₂.

It seems there is no residual plutonium metal. However metallic grains or droplets appear inside the product (Figure 4). They are extracted from the plutonium oxide and spread with a blade on the surface of the container. SEM analysis shows that they are alloyed elements that segregated during the combustion because of good resistance to oxidation (Figure 5).



Fig 4: Burning product

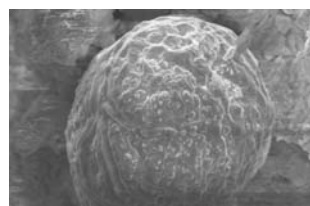


Fig 5: Alloyed element (SEM)

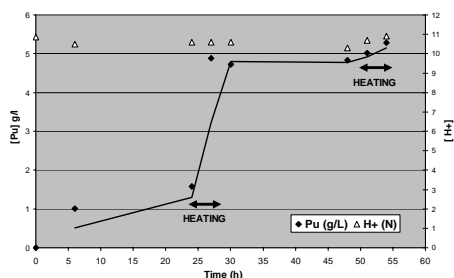


Fig 6: [Pu] during dissolution

Plutonium powder dissolution is efficient. The yield is higher than 97 %. The dissolution kinetic results from the burning temperature, the HF concentration and the dissolution temperature (Figure 6). The plutonium content of the residual undissolved powder was estimated by gamma counting. After rinsing, the insoluble solid residue contains less than 2g of plutonium for about 150g of impure oxide to be dissolved.

CONCLUSION - PERSPECTIVE

In order to recycle alloyed plutonium residues, an improved method has been successfully tested. The recovery yield is higher than 97 %.

New furnace device is in progress to improve the burning kinetic. A mechanical system will break the protective dioxide layer.

High Temperature Behaviour of Irradiated Mixed Nitride Fuel during Post Heating Tests

I. Sato*, K. Tanaka, T. Hirosawa, S. Miwa, K. Tanaka

*Japan Atomic Energy Agency, 4002 Narita-cho, Oarai-machi, 311-1393 IBARAKI, JAPAN

INTRODUCTION

In the Feasibility Study on Commercialized Fast Reactor Cycle System in Japan (F/S), a uranium-plutonium mixed nitride fuel with good thermal properties was selected as a candidate fuel form¹ with which conceptual design studies have been performed. Fast reactor design candidates suitable for the nitride fuel include middle and small size reactor cores using a coolant of Pb-Bi alloy and pellet type fuel. In a safety study for these concept reactors, it is quite important to recognize the behaviour of the nitride fuel under abnormal fuel temperatures such as in core damage accidents (CDAs). This is because a large amount of fission gases could remain in the nitride fuel due to the lower irradiation temperature experienced as compared to that for oxide fuel and these gases might be rapidly released as the temperature rose during CDAs. Moreover, if the temperature exceeds 2000 °C, decomposition (the nitride fuel changes to metals and nitrogen gas) of the nitride fuel may occur², which can complicate the fission gas release behaviour. However, hardly any fission gas release data from irradiated mixed nitride fuel under abnormal temperature conditions have been obtained. The same holds for the decomposition behaviour.

JAEA is studying the applicability of nitride fuel for fast reactors by heating tests using uranium-plutonium mixed nitride fuels irradiated in the experimental fast reactor, "JOYO." In this work, the fission gas release and the decomposition behaviours were evaluated for the safety study of a Pb-Bi cooled fast reactor. The gas release behaviour and metallographic observations during and after the tests are shown and discussed.

EXPERIMENTAL PROCEDURE

The characteristics and irradiation conditions of nitride fuel pellet are shown in Table 1. Results for other post irradiation examinations (PIEs) for this fuel pellet have been given in the literature³. A pellet was removed from the fuel pin and the cladding was cut away to get the test specimens. The test specimens were heated in an induction heating furnace in an atmosphere of flowing high-purity Ar. The heating tests were designated Nifti-1 and Nifti-2 (Nifti: Nitride fuel heating test after irradiation). In Nifti-1, the temperature was slowly elevated to the maximum of 2400 °C to allow observation of the fission gas release and decomposition behaviour in detail. In Nifti-2, a relatively rapid heating rate (approx. 20K/s) was applied from 1700 °C (equivalent

Table 1: Characteristics and irradiation conditions of the uranium-plutonium nitride fuel pellet

N/M	1.00
Diameter	7.28 mm
Pu/(Pu+U)	18.6 wt%
U235 enrichment	19.6 wt%
Density	84.8 %T.D.
Burn up	Approx. 4 at%
Max fuel temperature	Approx. 1700 °C

to the centre line temperature under irradiation) to 2500 °C, which simulated a transient timescale, “slow TOP.” During the tests, the released gases were analysed in-site by gas mass spectrometry, and then the concentrations of released gases were evaluated depending on the heating temperature. Details of analysis systems have been given in the literature⁴. After these heating tests, metallographic observations and EPMA for these specimens were carried out to get microstructures and elemental distributions.

RESULTS AND DISCUSSION

In Nifti-1, a concentration profile of fission gases and nitrogen in the carrier gas was obtained as shown in Fig. 1. The fission gas release starts around the heating temperature of 1730 °C. Although the heating temperature is sufficiently high compared to the normal fuel temperature, a few dozen percent of fission gases remain in the fuel after the heating test from results of the other gas quantitative analysis. Concerning the relationship between the fission gas release and nitrogen release by the decomposition, the main nitrogen release starts around 1900 °C, but is not dependent on the fission gas release. Fig. 2 shows the metallographic images of a specimen before and after

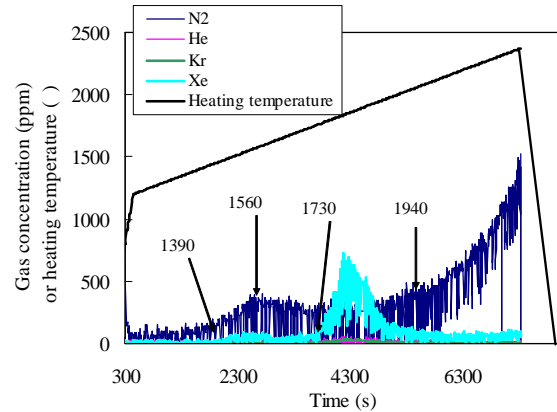


Fig. 1: Heating temperature and released gas concentration histories during Nifti-1.

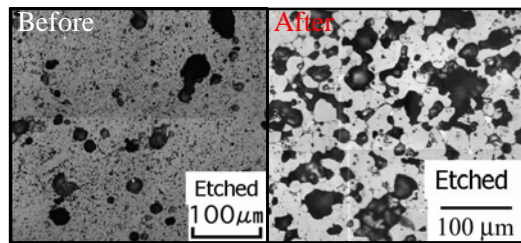


Fig. 2: Metallographic images obtained before and after Nifti-1.

The quite small pores existing before the heating test could connect with each other and grow by heating to become larger ones. Therefore, the fuel density before heating (approx. 13 g/cm³) is 9 g/cm³ which is smaller than the coolant density (10 g/cm³). The fuel pellet could float above the coolant during CDA with cladding melting. However, in the Nifti-2 specimen, there are still small pores after heating. This implies that the pore size and number depend on the heating rate applied in each test.

EPMA for the Nifti-1 specimen shows some inclusions containing Pu and Rh without U. This indicates that Pu preferentially except U can precipitate along with the decomposition.

Acknowledgements

The authors are grateful to Dr. Ikken Sato for suggestions and discussions about this work. They also wish thank the technical staff members, Mr. T. Ishida and Mr. S. Sekine.

- 1 M. Konomura, et al., JNC report, JNC TN9400 2004-035 (2004) [in Japanese].
- 2 K. Richter and C. Sari, J. Nucl. Mater. **184** (1991) 167.
- 3 K. Tanaka, K. Maeda, K. Katsuyama et al., J. Nucl. Mater. **327** (2004) 77 .
4. I. Sato, T. Nakagiri, T. Hirose, et al. J. Nucl. Sci. Technol. **40** (2003) 104.

Oxygen Chemical Diffusion in Hypostoichiometric MOX

M. Kato*, K. Morimoto*, T. Tamura†, T. Sunaoshi†, K. Konashi††, M. Kashimura*

*Nuclear Fuel Cycle Engineering Laboratories, Japan Atomic Energy Agency, 4-33 Muramatsu, Tokai-Mura, Ibaraki 319-1194, JAPAN

†Inspection Development Company, 4-33 Muramatsu, Tokai-Mura, Ibaraki 319-1194, JAPAN

††Tohoku University, 2145-1313 Narita-cho, Oarai-machi, Ibaraki 311-1313, JAPAN

INTRODUCTION

Plutonium and uranium mixed oxide (MOX) has been developed to use as the fuel for fast reactors. The oxygen to metal ratio (O/M) of the MOX fuel is an important parameter to control fuel and cladding chemical interaction. The oxygen potential and the oxygen diffusion coefficient of MOX are essential data to understand oxygen behaviour in MOX. The oxygen potentials of MOX were measured previously with good accuracy as a function of O/M and temperatures¹. In the present work, the oxygen chemical diffusion coefficients in $(\text{Pu}_{0.2}\text{U}_{0.8})\text{O}_{2-x}$ and $(\text{Pu}_{0.3}\text{U}_{0.7})\text{O}_{2-x}$ were investigated using a thermo gravimetric technique.

EXPERIMENTAL

Two kinds of MOX powder with 20%Pu and 30%Pu contents were prepared by a direct microwave heating denitration process. Each powder type was pressed and sintered into needle-like samples, which were about 1.4mm in diameter and 5.7-7.2mm in length, weighed about 120mg and had 87.8-92.9% TD.

Measurements of the changing rate of O/M ratio were carried out by thermal gravimetry and differential thermal analysis (TG-DTA) at temperatures of 1250, 1300 and 1350°C. Details of the apparatus were reported previously¹. The oxygen partial pressure in the atmosphere was controlled rapidly by changing hydrogen content in the atmosphere and the change of sample weight was measured as a function of time.

RESULTS AND DISCUSSION

Figure 1 shows measurement results of the reduction process in the range of hypostoichiometric composition. The average concentration \bar{c} of an infinite cylinder sample of radius r_0 is given by Eq. (1) when the change is dominated by chemical diffusion².

$$F = \frac{\bar{c} - c_f}{c_i - c_f} = \sum_{v=1}^{\infty} \frac{4}{\xi_v^2} \exp\left(-\frac{\xi_v^2 \tilde{D}t}{r_0^2}\right) \quad (1)$$

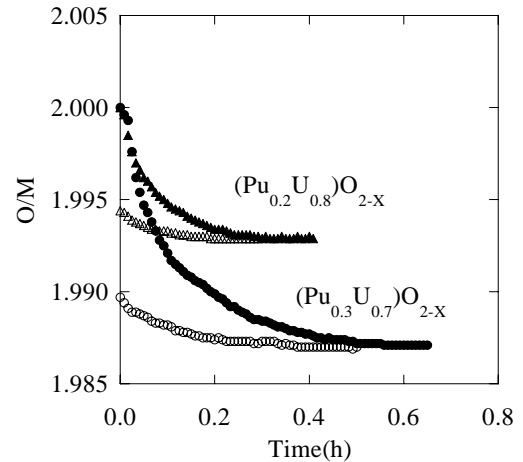


Fig.1 Kinetics of reduction process of $(\text{Pu}_{0.2}\text{U}_{0.8})\text{O}_{2-x}$ and $(\text{Pu}_{0.3}\text{U}_{0.7})\text{O}_{2-x}$ at 1300°C as a function time.

Here c_i , c_f , t and ξ_v are the initial concentration, the final concentration, time and the roots of the equation $J_0(x)=0$, respectively, where $J_0(x)$ is the Bessel-function of zero order. The measurement results were analyzed using Eq. (1), since the infinite cylinder is a good approximation for the needle-like samples. Eq. (1) represents the curves of the reduction processes very well. The oxygen chemical diffusion coefficients \tilde{D} of hypostoichiometric MOX with 20%Pu and 30%Pu are estimated to be $3.2 \times 10^{-6} \text{ cm}^2/\text{s}$ and $1.6 \times 10^{-6} \text{ cm}^2/\text{s}$, respectively, from the results of reduction curves at 1300°C.

The oxygen chemical diffusion coefficients of $(\text{Pu}_{0.2}\text{U}_{0.8})\text{O}_{2-x}$ and $(\text{Pu}_{0.3}\text{U}_{0.7})\text{O}_{2-x}$ are expressed by the following equations.

$$\ln \tilde{D} = \left(-\frac{68.4 \times 10^3}{RT} \right) + \ln(5.486 \times 10^{-4}) \quad \text{for } (\text{Pu}_{0.2}\text{U}_{0.8})\text{O}_{2-x} \quad (2)$$

$$\ln \tilde{D} = \left(-\frac{116.1 \times 10^3}{RT} \right) + \ln(1.16 \times 10^{-2}) \quad \text{for } (\text{Pu}_{0.3}\text{U}_{0.7})\text{O}_{2-x} \quad (3)$$

Figure 2 shows the oxygen chemical diffusion coefficients calculated by Eqs. (2) and (3) using the experimental values as a function of $1/T$. The oxygen chemical diffusion coefficient in $(\text{Pu}_{0.2}\text{U}_{0.8})\text{O}_{2-x}$ is larger than that in $(\text{Pu}_{0.3}\text{U}_{0.7})\text{O}_{2-x}$. Data from other works are also plotted in the figure³⁻⁵. The results of this work are smaller than the literature data which were obtained from measurement results of oxidation of $(\text{Pu}_{0.2}\text{U}_{0.8})\text{O}_{2-x}$.

CONCLUSION

The kinetics of the reduction processes of $(\text{Pu}_{0.2}\text{U}_{0.8})\text{O}_{2-x}$ and $(\text{Pu}_{0.3}\text{U}_{0.7})\text{O}_{2-x}$ were measured by TG-DTA. The oxygen chemical diffusion coefficients were estimated from the reduction curves. It was concluded that the oxygen chemical diffusion coefficient in $(\text{Pu}_{0.3}\text{U}_{0.7})\text{O}_{2-x}$ was smaller than that of $(\text{Pu}_{0.2}\text{U}_{0.8})\text{O}_{2-x}$.

REFERENCES

- 1 M. Kato, et al., Journal of Nuclear Materials, 344, 235, (2005)
- 2 W. Jost, Diffusion in solid, liquids, gases, Academic press, (1960)
- 3 A. S. Bayoglu, Solid State Ionics, 12, 53, (1984).
- 4 F. D'annucci and C. Sari, Journal of Nuclear Materials, 68, 357, (1977)
- 5 C. Sari, Journal of Nuclear Materials, 78, 425, (1978)

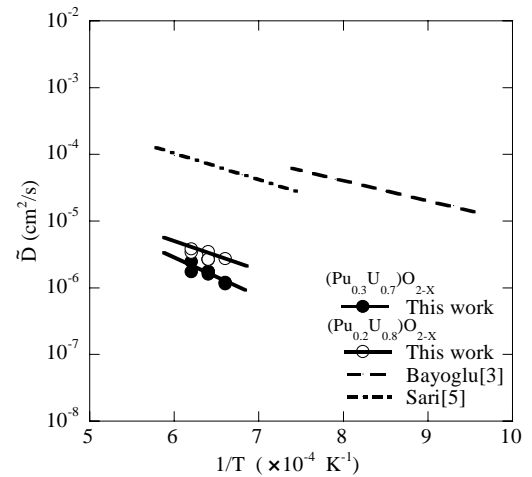


Fig.2 Oxygen chemical diffusion coefficients plotted in an Arrhenius diagram.

The oxidation rate of $(U_{0.7}Pu_{0.3})O_{2-x}$ with two fcc phases

K. Suzuki^{*}, M. Kato^{*}, T. Tamura[†], S. Aono^{*}, M. Kashimura^{*}

^{*}Nuclear Fuel Cycle Engineering Laboratories, Japan Atomic Energy Agency, 4-33 Muramatsu, Tokai-Mura, Ibaraki 319-1194, JAPAN

[†]Inspection Development Company, 4-33 Muramatsu, Tokai-Mura, Ibaraki 319-1194, JAPAN

INTRODUCTION

It has been reported that sintered MOX pellets of hypostoichiometric composition were oxidized at room temperature in an atmosphere of inert gas and air^{1,2}. The region of two fcc phases exists at room temperature in the $(Pu,U)O_{2-x}$ with Pu content of greater than 20%.^{3,4} In this study, using a thermogravimetric technique, we investigated the oxidation rate of $(Pu_{0.3}U_{0.7})O_{2-x}$ with two fcc phases to contribute to understanding of the oxidation behavior.

EXPERIMENTAL

The sintered pellets of $(U_{0.7}Pu_{0.3})O_{2-x}$ were prepared by a mechanical blending method and were sliced into disc-like samples with about 1 mm thickness and 85-93% theoretical density. The samples were annealed under appropriate conditions to adjust the ratio of oxygen to metal (O/M) to 1.95-1.97⁵. The oxidation rate of the samples were measured using thermal gravity and differential thermal analysis (TG-DTA) at 60, 125 and 150°C in an atmosphere of air, N₂ and air/N₂ gas mixture with moisture content of 1 - 700ppm. The X-ray diffraction patterns of samples were analyzed before and after the TG-DTA.

RESULTS AND DISCUSSION

Figure 1 shows kinetics of the isothermal oxidation reaction in air as a function of time and temperatures. In the isothermal oxidation, under 150°C, the O/M of sample did not exceed 2.00 and the oxidation rate increased with an increase of temperature. In the results of X-ray diffraction measurement, the amount of fcc phase with O/M \approx 2.00 was observed to increase by the oxidation of sample. It was reported that the $(Pu_{0.3}U_{0.7})O_{2-x}$ exists as two fcc phases at room temperature and the O/M ratios of the two fcc phases are estimated to be O/M=1.85 and 1.985, respectively^{3,4}. Therefore, we think that the oxidation of $(Pu_{0.3}U_{0.7})O_{2-x}$ with two fcc phases is explained by diffusion of the higher O/M phase formed on the surface.

Jost⁶ treated diffusion in a system

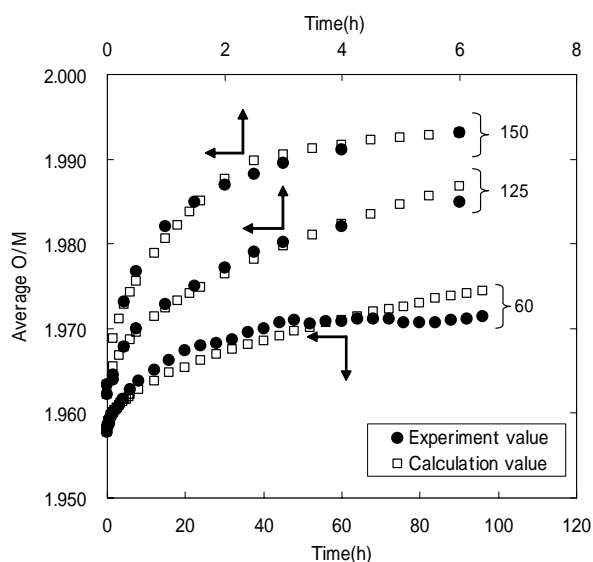


Fig.1 Kinetics of the oxidation reaction in air plotted as a function of time and temperatures

consisting of two phases as shown in Fig.2. The distribution of O/M is expressed by following equation as a function of x-direction

$$O/M_x = O/M_s - B \cdot \operatorname{erf}\left(\frac{x}{2\sqrt{\tilde{D}t}}\right),$$

for $0 < x < \xi \dots (1)$

$$O/M_x = O/M_i, \text{ for } x \geq \xi.$$

Here $O/M_x = O/M$ at x , $O/M_s = O/M$ at sample surface, $O/M_i =$ initial O/M, $B =$ arbitrary constant, $t =$ time, $\tilde{D} =$ oxygen chemical diffusion coefficient and $\xi =$ discontinuous point of O/M distribution. The average O/M ratio of the sample was calculated using equation (1) as shown in Fig.1. We see the calculation results are good agreement with measurement results.

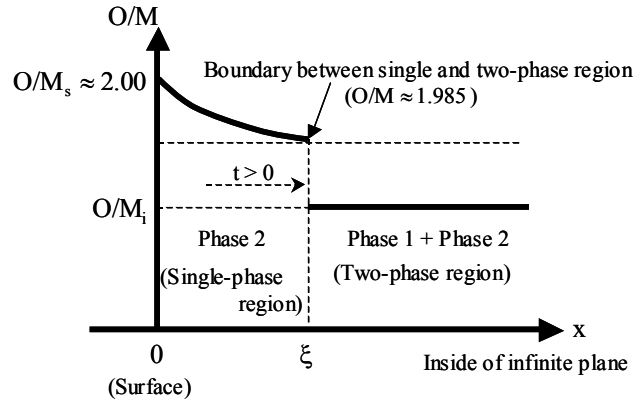


Fig.2 Diffusion into the two-phase system. Discontinuous point of O/M distribution ξ is located in the surface for $t=0$, where Phase 1=the lower O/M phase and Phase 2=the higher O/M phase.

CONCLUSION

The oxidation of $(U_{0.7}Pu_{0.3})O_{2-x}$ with two fcc phases was evaluated at temperatures up to 150°C and the curve of the isothermal oxidation was analyzed by the model of diffusion in a system consisting of two phases. The diffusion model could represent the oxidation curve as a function of time and temperature. The oxidation of the $(U_{0.7}Pu_{0.3})O_{2-x}$ proceeded by diffusion of the phase with $O/M \approx 2.00$ which was formed on the sample surface.

REFERENCES

1. R. E. Woodley and R. L. Gibby, HEDL-SA-592 (1973)
2. R. Eicher, *et al.*, J. Nuclear Materials, 124, (1984) 9
3. C. Sari, U. Benedict and H. Blank, J. Nuclear Materials, 35, (1970) 267
4. M. Kato, *et al.*, Proceedings of Actinides 2005, Manchester, 4P04, (2004), 108
5. M. Kato, *et al.*, J. Nuclear Materials 344, (2005) 235
6. W. Jost, Diffusion in solids, liquids and gases, Academic Press, Inc., (1960), 69

A New Method of Describing Uranium Oxidation in Water Vapor

V.K. Orlov, A.A. Karnozov, T.B. Karnozova

The Federal State Unitarian Enterprise A.A. Bochvar All-Russian Scientific Research Institute of Inorganic Materials (VNIINM), P/Box 369 Moscow, 123060 Russia

It is shown that uranium oxidation rate in water vapor depends on water evaporation rate from glassy capillary vessels (moisture bearer).

A new method of describing gaseous products accumulation kinetics is offered. The method is based on an assumption that dynamic equilibrium between water vapor consumption rate during uranium oxidation and water evaporation rate from moisture source can be achieved in the studied system by providing constant temperature.

The figure 1 shows dependence rate of water evaporation and rate of water vapor consumption during Uranium oxidation on water vapor pressure. With water vapor pressure dropping below the pressure of saturated water vapor the rate of metallic Uranium oxidation decreases (blue arrow), while the rate of water evaporation from the source increases (red arrow).

The process of uranium oxidation in water vapor can be relatively shared in two parts: transitional one and stationary one. In the first part (transitional) water vapor pressure is decreased by saturated water vapor pressure to stationary pressure, which is accompanied by gaseous products accumulation rate increase in the reaction vessel.

In the second part (stationary) water vapor pressure keeps constant (stationary) up to complete evaporation of liquid water from capillary vessel (moisture bearer); gaseous products accumulation rate keeps constant in the reaction vessel.

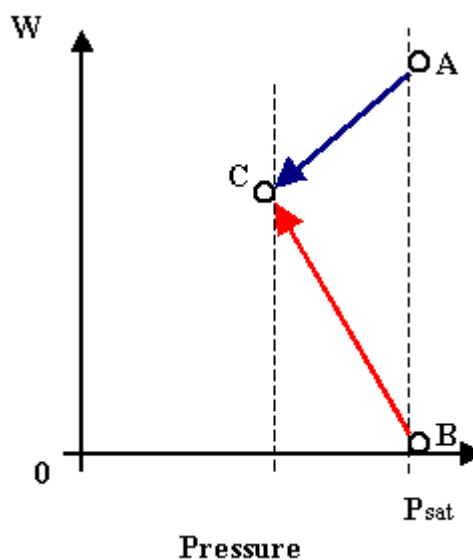


Fig.1: The dependence of water evaporation rate and water vapor consumption rate during Uranium oxidation on water vapor pressure.

Physical-Chemical and Radiation-Chemical Processes in the PuO₂ - Sorbed Water System

M.V. Vladimirova, A.A. Karnozov

The Federal State Unitarian Enterprise A.A. Bochvar All-Russian Scientific Research Institute of Inorganic Materials (VNIINM), P/Box 369 Moscow, 123060 Russia

Turning weapons-grade plutonium into dioxide and its further use for MOX -fuel is one of major activities on conversion of excessive plutonium stocks. PuO₂ is a hygroscopic substance. When exposed to plutonium's alpha-radiation, the sorbed water is decomposed resulting in the formation of hydrogen and oxygen, to constitute a potential hazard associated with a possible detonating mixture formation and a buildup of pressure inside sealed vessels. The special containers will be created to ensure safe storage and handling of plutonium dioxide. With this aim in view, it is necessary to have the data on kinetics of H₂ and O₂ formation, and a mathematical model to calculate amounts of the evolved gases and their pressure in a container for any initial data.

The presentation generalizes the experimental data on kinetics of hydrogen and oxygen formation depending on water content, a technique of water sorption onto PuO₂ (from a liquid or gas phase), specific surface area of powder, radiation dose rate, time and temperature of plutonium dioxide storage.

As for the system including the water sorbed from the liquid phase, it has been shown that the H₂ and O₂ formation rates increase with increasing radiation dose rate and H₂O amount. On long storage of PuO₂, the gas-phase hydrogen amount reaches the steady-state value that is equal in moles to the initial amount of sorbed water. It has been concluded that kinetic characteristics of formation of the water radiolysis products depend on water content, and the rates of the H₂ and O₂ formation reaction have the first order relevant to the sorbed water amount.

Based on this and on the results of comparison of calculated and experimental data, there has been created a mathematical model of sorbed water radiolysis, including the reactions of radiolysis product formation, the reaction of PuO₂ with H₂O₂ resulting in formation of water and overstoichiometric plutonium oxide, and the reaction of H₂ and O₂ recombination to form water. The mathematical model was used to calculate the amounts of H₂ and O₂ for various initial conditions. Good agreement has been shown between the calculated and experimental data obtained for the water sorbed onto PuO₂ from the liquid phase.

Outlined have been the main lines of the experimental and calculation activities required to obtain full quantitative information on radiolysis of the water sorbed onto PuO₂ from the gas phase.

Alteration of U(VI)-Phases Under Oxidizing Conditions

A.P. Deditius[†], S. Utsunomiya[†], R.C. Ewing[†]

[†] Department of Geological Sciences, University of Michigan, Ann Arbor, Michigan 48109-1005

INTRODUCTION

Uranium-(VI) phases are the primary alteration products of the UO_2 in spent nuclear fuel and the UO_{2+x} in natural uranium deposits. The U(VI)-phases generally form sheet structures of edge-sharing UO_2^{2+} polyhedra. The complexity of these structures offers numerous possibilities for coupled-substitutions of trace metals and radionuclides. The incorporation of radionuclides into U(VI)-structures provides a potential barrier to their release and transport in a geologic repository that experiences oxidizing conditions. In this study, we have used natural samples of UO_{2+x} , to study the U(VI)-phases that form during alteration and to determine the fate of the associated trace elements.

SAMPLE AND ANALYTICAL METHODS

Samples were obtained from the Marshall Pass deposit, Colorado, a unique locality because of the presence of Cu minerals; thus, this is also a potential analogue to canister interactions with spent nuclear fuel (SNF)¹ for programs considering such waste package materials. The uranium ore deposit is located close to the surface and has reacted both with ground and meteoritic waters. Primary uraninite formed under reducing conditions in veins controlled by faulting. The UO_{2+x} is intergrown with Cu, Zn, Pb, Sb, Ag, As sulfides and sulfosalts, such as tetrahedrite, covellite, chalcocite, chalcopyrite, galena and sphalerite². Five samples of different degrees of alteration were analysed by optical petrography, scanning electron microscopy/energy dispersive X-ray spectrometry (SEM/EDS), electron microprobe analysis (EMPA) and transmission electron microscopy (TEM).

RESULTS AND DISCUSSION

The chemical composition of the uraninite by EMPA is 75.1-77.6 wt% U, 1.2-2.0 wt.% Ca 1.0-2.1 wt.% Pb, 0.98-1.7 wt.% W, 0.16-1.0 wt.% As, with minor amounts (<1 wt.%) of Zr, Ti, REE, Mo, Si, P and Fe.

The first stage of alteration was caused by penetration of oxidizing fluids with W and Mo. The oxidation of U may have caused the reduction in the uraninite unit cell parameter, creating microfractures, and providing additional pathways for the fluids. Uraninite grains show grain spallation, finally resulting in lost of cohesion and subsequent separation. Sulfides and sulfosalts are unstable under these conditions, liberating Pb, As, S, Cu, Zn, Sb, Ag. The presence of Mo in the fluids with liberated Pb resulted in precipitation of wulfenite (PbMoO_4). Acidic solutions derived from the dissolution of the sulfides caused the oxidation and dissolution of uraninite. In general, the sequence of uraninite alteration is consistent with that previously reported from the Nopal I deposit (Mexico) and the laboratory experiments: uraninite, uranyl oxide hydrates, uranyl silicates, and finally, alkali + alkali earth uranyl silicates^{3,4}.

In the present samples, the sequence of formation began with ianthinite, $\text{U}^{4+}(\text{UO}_2)\text{O}_4(\text{OH})_6(\text{H}_2\text{O})_9$, followed by schoepite-type minerals, e.g., $(\text{UO}_2)_8\text{O}_2(\text{OH})_{12}(\text{H}_2\text{O})_{12}$,

with mainly preserved “dehydrated schoepite”. Subsequently, two phases formed: (i) a rare Pb-uranyl oxide hydrate and (ii) mats of fine-grained platy crystals of a Ba-Mo-W uranyl phase with the composition of: 47.4-55.2 wt.% of U, 7.27-14.8 wt.% of W, 5.73-10.9 wt.% of Mo, 3.62-4.54 wt.% of Ba, 1.25-1.65 wt.% of Ti, 0.65-1.32 wt.% of Fe, and 0.26-0.61 wt.% of Ce. The latter phase is a uranotungstite-type⁵ mineral, $(\text{Ba,Pb,Fe}^{2+})(\text{UO}_2)_2(\text{WO}_4)(\text{OH})_4(\text{H}_2\text{O})_{12}$, with possible substitution of Mo for W. A similar, but previously unknown, Cs-Ba-Mo uranyl oxide hydrate has been reported in the SNF corrosion experiments⁶. At the next stage of paragenesis, fluids with Si and Ca entered into the system leading to supersaturation for uranophane, $\text{Ca}(\text{UO}_2)_2(\text{SiO}_3\text{OH})_2(\text{H}_2\text{O})_5$, and then uranyl arsenates, (trogerite, $(\text{UO}_2)_3(\text{AsO}_4)_2(\text{H}_2\text{O})_{12}$; metazeunerite, $\text{Cu}[(\text{UO}_2)(\text{AsO}_4)]_2(\text{H}_2\text{O})_8$), precipitated partially replacing the previously formed phases.

A different alteration sequence was observed in the areas where uraninite is intergrown with sulfides and sulfosalts. The Cu-bearing minerals (tetrahedrite, covellite, chalcocite, chalcopyrite) show evidence of dissolution, such as corrosion rinds. The paragenesis of uranyl-minerals including Cu in the system may be applicable to the corrosion of Cu-based SNF containers¹. In veinlets, (meta)zeunerite precipitated replacing uraninite and the Cu-minerals, as well. A thin layer (2-5 μm) of a fine-grained unknown phase enriched in U (44.6-49.2 wt.%) and Sb (22.4-26.1 wt%) was found between uraninite, U-arsenate and tetrahedrite. This may be a new U-Sb mineral, a mixture of uranyl oxide hydrate and Sb oxide or antimonite containing U, which has been proposed as a phase that forms in the fission-product waste stream that results from the reprocessing of SNF, especially $^{90}\text{Sr}^{2+}$ and REE^{3+} in acidic waste streams⁷.

The last stage of alteration is most likely caused by reaction with meteoric water of low ionic strength. U-arsenates and silicates were replaced by “dehydrated schoepite” (II). Finally, uranyl minerals were altered to swamboite, $\text{U}^{6+}(\text{UO}_2)_6(\text{SiO}_3\text{OH})_6(\text{H}_2\text{O})_{30}$.

CONCLUSIONS

In Marshall Pass, Colorado, oxidizing fluids of various compositions resulted in a complex sequence of alteration phases. The most common trace element is As, forming uranyl arsenates as a major phase. In case of supersaturation with W and Mo, an unknown U-W-Mo phase precipitated. Additionally, crystallization of a U-Sb phase reflects substantial local variability in Sb-concentration. This occurrence provides a good example of the complexity one may expect in anticipating the results of the corrosion of SNF in an open system under oxidizing conditions.

Acknowledgements

This work was supported by the Office of Science and Technology and International (OST&I) of the Office of Civilian Radioactive Waste Management (DE-FE28-04RW12254). The views, opinions, findings and conclusions or recommendations of the authors expressed herein do not necessarily state or reflect those of DOE/OCRWM/OSTI.

- 1 T. Hedmann, *et al.*, C. R. Physique. **3**, (2002).
- 2 D. Zhao and R.C. Ewing, Radiochim. Acta. **88**, (2000).
- 3 D.J. Wronkiewicz, *et al.*, J. Nucl. Mater. **238**, (1996).
- 4 E.C. Percy, *et al.*, Appl. Geochem. **9**, (1994).
- 5 K. Walenta, Tschermaks Mineral. Petrol. Mitt. **34**, (1985).
- 6 E.C. Buck, *et al.*, J. Nucl. Mater., **249**, (1997).
- 7 M.V. Siviaiah, *et al.*, Radiochim. Acta. **92**, (2004).

Enthalpy of Formation of $\text{Pu}_{(1-x)}\text{Zr}_x\text{O}_2$ Fluorite and $\text{CaPuTi}_2\text{O}_7$ Pyrochlore

T. Lee^{*}, J. Mitchell^{*}, A. Navrotsky[†], B. Ebbinghaus[‡]

^{*}Los Alamos National Laboratory, Los Alamos, NM, USA 87545 USA

[†]University of California at Davis, Davis, CA 95646 USA

[‡]Lawrence Livermore National Laboratory, Livermore CA 94552 USA

ABSTRACT

The total inventory of high-level radioactive nuclear waste in the US alone is projected to exceed 100,000 metric tons by the year 2035. Oxides with the fluorite and pyrochlore structures, are chemically and thermally durable, radiation tolerant, and proliferation resistant, and, thus, are of great interest as nuclear waste forms suitable for burial.¹ These properties also make oxides with the fluorite structure attractive as potential inert matrix nuclear fuels.² Such nuclear waste forms or nuclear fuels, however, must also be thermodynamically stable. For example, recent studies have suggested that the $\text{CaPuTi}_2\text{O}_7$ pyrochlore could be thermodynamically unstable with respect to an oxide-perovskite phase assemblage.³ We will use high temperature high temperature oxide melt drop solution calorimetry to investigate the thermodynamic stability of the $\text{Pu}_{(1-x)}\text{Zr}_x\text{O}_2$ fluorite phase and the $\text{CaPuTi}_2\text{O}_7$ pyrochlore phase. Our preliminary results show that mixing in the analogous $\text{Ce}_{(1-x)}\text{Zr}_x\text{O}_2$ fluorite phase is ideal. That is, unlike in other fluorite oxide systems, there is no thermodynamic driving force to order, and the inherent disorder in this and the $\text{Pu}_{(1-x)}\text{Zr}_x\text{O}_2$ fluorite solid solutions should result in exceptional tolerance to radiation damage.

This work supported in part by the Seaborg Institute Postdoctoral Fellowship.

- 1 R. C. Ewing, *Canadian Mineralogist* **39**, (2001).
- 2 G. Ledergerber, *et al.*, *Progress in Nuclear Energy* **38**, (2001).
- 3 K. B. Helean, *et al.*, *Journal of Nuclear Materials* **303**, (2002).

An Experimental Investigation on Phase Relation of Americium-doped PuO₂

S. Miwa^{*}, M. Osaka^{*}, H. Yoshimochi^{*}, K. Tanaka^{*}, K. Kurosaki[†], M. Uno[†], S. Yamanaka[†]

^{*}Oarai Research and Development Center, Japan Atomic Energy Agency, Oarai-machi, Higashi-ibaraki-gun, Ibaraki, 311-1393, Japan. E-mail: miwa.shuhei@jaea.go.jp

[†]Department of Nuclear Engineering, Graduate School of Engineering, Osaka University, Yamadaoka 2-1, Suita-shi, Osaka 565-0871, Japan

INTRODUCTION

Japan Atomic Energy Agency (JAEA) is promoting R&D programs for future nuclear cycle technology based on fast reactors, which is essential to a reduced environmental burden and a sustainable energy supply [1]. Development of the mixed oxide (MOX) fuel and target containing minor actinides (MAs), which are considered as promising candidates for the future fast reactor, is underway [1,2]. The target is composed of actinide oxides and non-radioactive support materials such as MgO [2].

Among MAs, americium (Am) is of special concern because of its high and lasting radiotoxicity, together with several noticeable properties such as its effect on oxygen potential [3-5]. It was revealed through these studies that only a small amount of Am addition to oxides had significant effects on various properties [3-5]. Am-doped PuO₂, (Pu,Am)O_{2-x}, is considered as a candidate form for MAs-including oxide of the target [2]. Since phase relation is one of the most fundamental properties especially for the evaluation of irradiation behaviour, an experimental investigation on phase relation of (Pu,Am)O_{2-x} is carried out in this study. In particular, effects of Am addition to PuO_{2-x} on the phase relation are focused on.

EXPERIMENTAL

The (Pu_{0.91}Am_{0.09})O_{2-x} solid solutions were prepared by a conventional powder metallurgical route; i.e., ball-milling of (²⁴¹Am,Pu)O_{2-x} powder, uni-axial pressing into pellets, followed by sintering in moisture added Ar containing 5 % H₂ for 3 h at 1973 K. Density of the stoichiometric (Pu_{0.91}Am_{0.09})O₂ was about 79 % of theoretical. There were no cracks in the sintered body.

The sintered pellets were then thermally treated under moisture added Ar/H₂ at different oxygen potentials to adjust the O/M ratio from 1.90 to 2.00 [4]. The O/M ratios at various oxygen potentials were calculated from the weight change relative to the stoichiometry. X-ray diffraction (XRD) analysis was carried out for the (Pu_{0.91}Am_{0.09})O_{2-x} having different O/M ratios at room temperature. Phase transition temperatures of (Pu_{0.91}Am_{0.09})O_{2-x} at the O/M range mentioned above were investigated by Differential Thermal Analysis (DTA).

RESULTS AND DISCUSSION

XRD patterns showed a single phase of the fluorite structure for (Pu_{0.91}Am_{0.09})O_{2.00}. Figure 1 shows lattice parameter dependence of (Pu_{0.91}Am_{0.09})O_{2-x} solid solution on O/M ratio. It is seen

that the lattice parameter decreases with decrease of O/M ratio. The lattice parameters of $(\text{Pu}_{0.91}\text{Am}_{0.09})\text{O}_{2.00}$ and $(\text{Pu}_{0.91}\text{Am}_{0.09})\text{O}_{1.92}$ agreed with those of calculated by using Vegard's law, in which assumes $(\text{Pu}_{0.91}\text{Am}_{0.09})\text{O}_{2-x}$ as an ideal solid solution of PuO_2 , $\text{PuO}_{1.62}$, AmO_2 and $\text{AmO}_{1.61}$.

Figure 2 shows peak locations observed in the DTA plotted on the phase diagram of temperature versus O/M ratio for $(\text{Pu}_{0.91}\text{Am}_{0.09})\text{O}_{2-x}$. DTA peaks were observed on both increasing and lowering the temperature at constant O/M ratios. The DTA peaks were so small that they should be derived from quasi-stable phase transition. It is seen that there are phase transition temperatures at about 1000°C and 300°C through the investigated O/M ratio, while there are also indications of the phase transitions at about 600°C below $\text{O/M} = 1.95$. It is considered that phase relation of $(\text{Pu}_{0.91}\text{Am}_{0.09})\text{O}_{2-x}$ has different aspects which can be divided by around $\text{O/M} = 1.95$.

Osaka et al. [4] adopted following hypothesis for the interpretation of oxygen potential isotherms of $(\text{Pu}_{0.91}\text{Am}_{0.09})\text{O}_{2-x}$: i.e., Am is reduced prior to Pu in $(\text{Pu,Am})\text{O}_{2-x}$. This hypothesis is also used for the discussion of the present aspects of phase relation in this study. With this hypothesis, the boundary O/M ratio, at which all Am in $(\text{Pu}_{0.91}\text{Am}_{0.09})\text{O}_{2-x}$ is trivalent, is 1.955. This O/M ratio is close to what divides the different phases mentioned above.

It is known that the profile of phase diagram for Am-O system is similar to that of Pu-O system [6]. However, phase transition temperatures of Am-O system are higher than those corresponding to Pu-O system, as superimposed on Fig. 2 [6]. Of note is that there are phase transition temperatures corresponding only to Am-O system above the boundary O/M ratio, while there are phase transition temperatures corresponding to those of Pu-O and Am-O systems below the boundary O/M ratio. These results suggest that the Am-O system and Pu-O system are predominant in the respective phases of $(\text{Pu,Am})\text{O}_{2-x}$ above and below the boundary O/M ratio.

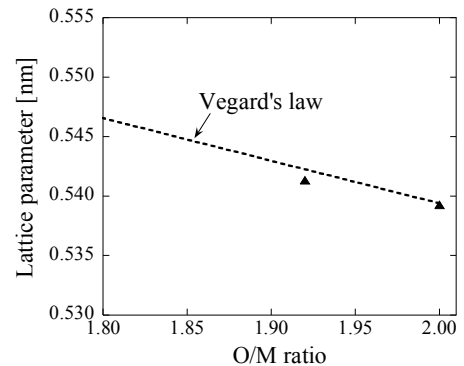


Fig. 1 Dependence of lattice parameter of $(\text{Pu}_{0.91}\text{Am}_{0.09})\text{O}_{2-x}$ on O/M ratio.

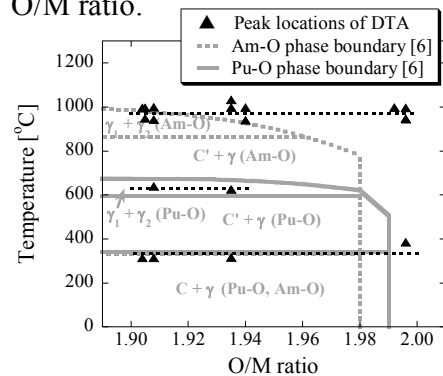


Fig. 2 Peak locations observed in the DTA for $(\text{Pu}_{0.91}\text{Am}_{0.09})\text{O}_{2-x}$.

- 1 K. Aizawa, Proc. Int. Conf. on Back-End of the Fuel Cycle, Paris, France, Sept. 9-13, 2001, p.50 (2001)
- 2 M. Osaka, H. Serizawa, M. Kato, M. Inoue, K. Nakajima, Y. Tachi, R. Kitamura, S. Ohki, S. Miwa, T. Iwai, K. Tanaka, S. Ukai, Y. Arai, Proc. GLOBAL 2005, Japan, Oct. 10-13, 2005, No. 240 (2005)
- 3 M. Osaka, I. Sato, T. Namekawa, K. Kurosaki and S. Yamanaka, J. Alloys and Comp. 2005, **397**, 110.
- 4 M. Osaka, K. Kurosaki and S. Yamanaka, submitted to J. Nucl. Mater..
- 5 M. Osaka, S. Miwa, H. Yoshimochi, K. Tanaka, K. Kurosaki and S. Yamanaka, Proc. Actinides 2005, England, July 4-8, 2005, 4P13 (2005)
- 6 C. Sari and E. Zamorani, J. Nucl. Mater., **37** (1970) 324.

Speciation of Pu in Aged Wastes and Wasteforms

Alayna Rodriguez, Juan Lezama-Pacheco, Steven D. Conradson
Los Alamos National Laboratory, Los Alamos NM 87544 USA

In the original discovery (or confirmation) of PuO_{2+x} the contention was made that it increased the environmental hazard of Pu because it should increase the solubility of PuO_2 . Subsequent XAFS measurements showed that, whereas the adventitious O was incorporated as Pu(V) oxo groups analogous to the mononuclear solution chemistry of Pu, the Pu(V) was not necessarily preferentially leached from PuO_{2+x} compounds but was present at times even in colloids prepared by both hydrolytic and reductive precipitation from aqueous solution as well as in materials prepared by oxidation with H_2O vapor at both elevated and ambient temperature. An additional type of disorder was also identified in these measurements; a multisite O distribution even in compounds without the oxo groups that most likely originates in the incorporation of H_2O as OH^- in the PuO_2 lattice. This moiety also occurred in PuO_2 samples prepared at both ambient and elevated temperatures including, surprisingly, materials that had been fired at temperature in excess of 1000°C where sorbed H_2O should be eliminated. These laboratory experiments raise the question of whether long term equilibration with the environment, whether the natural environment for Pu in soils or other more extreme ones for certain kinds of Pu wastes, will affect Pu speciation. For example, although curve-fit results of the EXAFS of PuO_{2+x} samples are very similar for both types of preparation methods, the white line amplitudes in the XANES of those prepared from aqueous solution are always higher than in the XANES of those that have been exposed to elevated temperatures. Similarly, the Fourier transformed spectra of aqueous-based materials exhibit broader features.

We are fortunate in having obtained XAFS spectra of some Pu wastes that have been subjected to long term exposure to various conditions, including size fractionated particles from the Pu cribs at Hanford and from an ion exchange resin used in Pu purification. The PuO_2 from the cribs was the insoluble fraction following HF extraction of Pu that had been air oxidized at high temperature. As expected, the Pu XAFS from the large particles resembles those of PuO_2 materials prepared at elevated temperatures. The spectra of the smaller fraction is very similar to those prepared by aqueous methods, indicating that exposure to H_2O over long periods actually can slowly modify the Pu speciation of the solid, converting it to the form that is equilibrated with liquid H_2O . The XAFS of the purification stream waste shows a Pu-O bond length that, while previously unobserved in the PuO_{2+x} system, is close to that expected for Pu(IV) coordination complexes with H_2O or NO_3^- . The formation and aging of colloidal PuO_2 in the presence of chelators – either the resin or the HNO_3 in the system – may therefore cause the surface Pu ions on the particles to remain coordinated to these ligands, resulting in a unique kind of PuO_2 structure.

Additional results on other systems will also be presented.

This work was supported by the Heavy Element Chemistry Program, Chemical Sciences, Biosciences, and Geosciences Division, Office of Basic Energy Sciences, U.S. Department of Energy under contract W-7405. XAFS measurements were performed at SSRL (Stanford Linear

Accelerator Center), which is operated by the US Department of Energy, Office of Basic Energy Sciences. Health Physics operations at SSRL and APS were supported by the Seaborg Institute for Transactinium Science at LANL.

Moisture Content of Impure Plutonium Oxide in Long-Term Storage

J. M. Berg

Los Alamos National Laboratory, Los Alamos NM 87544 USA

INTRODUCTION

Extensive campaigns to stabilize and package excess plutonium holdings in sealed stainless steel containers for long-term storage have recently been completed at several United States Department of Energy facilities. These activities were governed by the criteria in the US DOE Standard "Stabilization, Packaging, and Storage of Plutonium-bearing Materials".¹ A few thousand such packages containing plutonium metal or plutonium oxides have been created and are now being monitored under formal surveillance programs in several storage facilities.

The surveillance is designed in part to look for any indications of internal pressurization or container degradation. Pressurization, if it occurs, is expected to be highly correlated with residual moisture content on impure oxides. Therefore the packaging protocols specifically required that moisture content of oxides be measured prior to packaging. A maximum moisture threshold of 0.5 mass % of the package contents assures that the design pressure of the container will not be exceeded in storage under a set of worst-case assumptions.

As a result of these required moisture measurements, there is now a wealth of data on the moisture content of a wide variety of impure plutonium oxides following controlled treatment and handling protocols. This paper will summarize those data, discuss their limitations, and illustrate trends based on impurities, processing history and handling conditions.

DISCUSSION

It was recognized before these packaging campaigns began that some pre-treatment of plutonium oxide feed materials would be necessary to assure that potential chemical and radiolysis reactions associated with impurities would not over-pressurize and/or corrode the containers. Water was identified the common reactant in the pressure generating and corrosion reactions of greatest potential concern. Therefore the specified pre-treatment for oxides, calcination in air at either 950 °C or 750 °C, was selected principally as a simple means to reduce the moisture content. Calcination was presumed to also decompose residual organics, nitrates and carbonates.¹ Substantial quantities of halide salts were presumed to remain in the materials.

Packaging protocols required measurement of the final moisture content of each batch after calcination. If the measurement did not show conclusively that the moisture content was below 0.5 mass %, further pre-treatment was performed and the measurement was repeated. The 0.5 % threshold was chosen to assure that even if complete conversion of the hydrogen content of the water to H₂(g) occurred, the resulting total gas pressure would be below the design limit of the container in all cases.

Several analytical techniques of varying specificity were employed to measure moisture content depending on the facility and the type of material. The most common technique employed for plutonium oxides was thermo-gravimetric analysis (TGA). Mass changes of

samples (~ 3 grams) from each batch were measured as a function of time during a temperature ramp to 1000 °C under a flowing stream of argon. For the purposes of certifying that a container met the 0.5 % criterion, all mass loss in the TGA data was assumed to be due to H₂O. This interpretation of the TGA data made it a conservative technique with considerable bias toward over-estimating moisture for some materials due to evaporation of NaCl and KCl at high temperature. In approximately 20% of the cases FTIR spectroscopy or mass spectrometry were performed on the effluent gas from the TGA to obtain more specific measurements of moisture.

The different techniques gave reported moisture content values that are quite diverse in their uncertainties and inherent biases. This was acceptable for certification that storage criteria were being met because a conservative measure of moisture was more important than an accurate measure. However, there are other potential uses for moisture content that would benefit from greater accuracy. Among these is the identification of the containers in storage with the highest moisture content for more frequent surveillance. There is also potentially useful information in the correlations between moisture content and the major impurities, the origin and processing history of the material, and the different handling protocols that were employed in the packaging campaigns.

Fortunately, the raw data from all the techniques were retained and could be analyzed later in greater depth to obtain more accurate moisture estimates. As expected, the results show that true moisture content is substantially lower in general than values estimated from total TGA mass loss. The handling atmosphere had the largest effect on residual moisture content. Where material was stabilized and packaged in a dried air atmosphere (~1000 ppm H₂O), residual moisture had a median below 0.02 mass % and rarely exceeded 0.05 mass %. Batches handled in humid air had a median moisture content between 0.05 and 0.1 % with a few as high as 0.4 mass %. To the extent that impurity contents are known, there appear to be correlations with moisture content, though we have not completed those analyses as of this writing.

Though too numerous to list here, we acknowledge the many people who developed the moisture measurement methods and who collected the data. We specifically thank Ted Venetz and G. Scott Barney for providing the raw data from the Hanford campaign and Mark Brugh for providing the raw data from the Rocky Flats campaign. This work was supported by the United States Department of Energy under the Surveillance and Monitoring Program, Materials Identification and Surveillance Project.

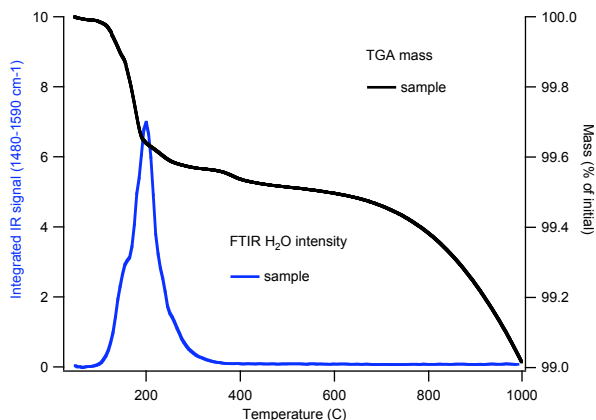


Fig.1: TGA and H₂O-specific FTIR data from a sample containing alkali halide impurities and approximately 0.4 % moisture.

1 DOE-STD-3013-2004 “Stabilization, Packaging, and Storage of Plutonium-bearing Materials”, United States Department of Energy, 2004.

Reaction mechanisms of the thermal conversion of Pu(IV) oxalate into plutonium oxide

N. Vigier¹, S. Grandjean¹, B. Arab-Chapelet¹, F. Abraham²

¹ CEA Valrhô Marcoule, DRCP/SCPS/LCA, Bât 399, BP 17171, 30207 Bagnols-sur-Cèze, FRANCE

² UMR CNRS 8012, ENSCL-USTL, LCPS, B.P. 108, 59652 Villeneuve d'Ascq Cedex, France

INTRODUCTION

During the oxalic conversion of plutonium into oxide at the end of the PUREX process, the thermal transition of Pu(IV) oxalate into oxide plays a significant role leading to the main properties of the oxide. The structure of the solid intermediates is often speculating and the reaction mechanisms are quite misunderstood and divergent from a study to another [1-7]. This work deals with a detailed structural investigation on the main solid intermediates encountered when calcining Pu(IV) oxalate into oxide under air or argon.

EXPERIMENTAL METHODS

The Pu(IV) oxalate precipitate, $\text{Pu}^{\text{IV}}(\text{C}_2\text{O}_4)_2 \cdot 6\text{H}_2\text{O}$, was prepared by mixing an acid Pu(IV) nitrate solution and a concentrated $\text{H}_2\text{C}_2\text{O}_4$ solution in a vortex effect reactor with a slight excess of $\text{H}_2\text{C}_2\text{O}_4$. The resulting crystallized powder was filtered off and dried at room temperature.

Thermogravimetric analyses (TG) were carried out with a NETZSCH STA 409C thermal analyzer using alumina crucibles, under argon or air flow at a gradient of 2°C min^{-1} up to 700°C . Solid intermediates were isolated at specific temperatures for structural investigations.

X-ray powder diffraction data were acquired with an INEL CPS 120 diffractometer (curved position sensitive detector) using $\text{Cu-K}_{\alpha 1}$ radiation isolated by a germanium monochromator. Silicon or gold was used as an internal standard. Each solid sample was mixed to an epoxy resin in order to fix up the contamination.

UV-visible spectra of the solid intermediates and products were acquired between 400 and 800 nm with a HITACHI U-3000 analyzer equipped with an integration sphere.

Infrared (IR) spectra of all samples were recorded with the NICOLET MAGNA IR 550 series II. A spectral range from 400 to 4000 cm^{-1} was typically investigated.

RESULTS

A typical TG plot is shown on figure 2 (static air). Each intermediate was identified by extrapolating the molecular formula from the mass loss, or by structural analyses (XRD, UV-Visible, IR) of the isolated solid after stopping the heating at the corresponding temperature. Only two isolated intermediates were not strictly identified due to their particular instability: $\text{Pu}^{\text{IV}}(\text{C}_2\text{O}_4)_2 \cdot \text{H}_2\text{O}$ and $\text{Pu}^{\text{IV}}(\text{C}_2\text{O}_4)_2$. Both compounds reacts quasi-instantaneously with trace amounts of water to form again $\text{Pu}^{\text{IV}}(\text{C}_2\text{O}_4)_2 \cdot 2\text{H}_2\text{O}$. Under air, the transitory reduction of Pu(IV) into Pu(III) is for the first time established directly by structural analysis of the solid intermediates: the Pu(III) intermediates are mixed oxalate-carbonate structures and not anhydrous Pu(III) oxalate as previously stated [1, 5-7].

The same investigations were led using Ar atmosphere instead of air. If transitory plutonium reduction is observed using both atmospheres, the nature of the corresponding Pu(III) solid intermediate(s) was found significantly different.

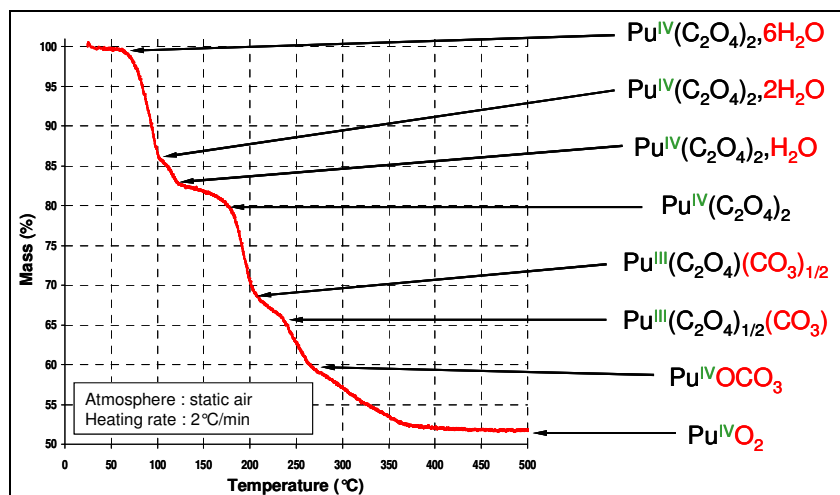


Fig. 1 : TG plot starting from a $\text{Pu}^{\text{IV}}(\text{C}_2\text{O}_4)_2, 6\text{H}_2\text{O}$ sample under static air.

The proposed reaction mechanism leading to plutonium oxide under air is detailed in figure 2. This schematic path differs very significantly from that obtained under argon stream.

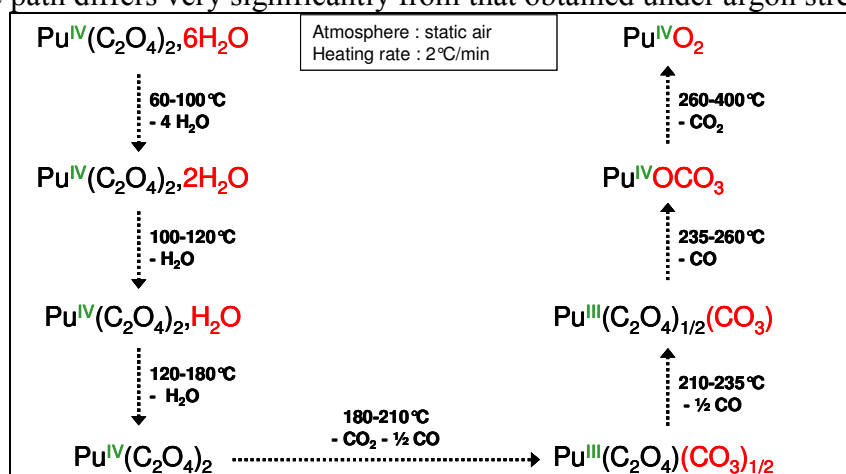


Fig. 2 : reaction path of the thermal conversion of $\text{Pu}^{\text{IV}}(\text{C}_2\text{O}_4)_2, 6\text{H}_2\text{O}$ into oxide under air.

CONCLUSION

The reaction mechanism of the thermal treatment of $\text{Pu}^{\text{IV}}(\text{C}_2\text{O}_4)_2, 6\text{H}_2\text{O}$ into oxide under air or argon was thoroughly investigated using TG analysis and structural analysis of the solid intermediates. Distinct reaction paths were established depending on the atmosphere used.

REFERENCES

- [1] M.N. Myers, U.S.A.E.C, document HW 45128 (1956).
- [2] G.S. Rao, M.S. Subramanian, G.A. Welch, J. Inorg. Nucl. Chem. 25 (1963) 1293-1295.
- [3] I.L. Jenkins, M.J. Waterman, J. Inorg. Nucl. Chem. 26 (1964) 131-137.
- [4] A. Glasner, J. Inorg. Nucl. Chem. 26 (1964) 1475-1476.
- [5] D.A. Nissen, J. Therm. Anal. 18 (1980) 99-109
- [6] R.D. Kozlova, A.I. Karelin, O.P. Lobas, V.A. Matyukha, Radiokhimiya, 26 (3) (1984) 311-316.
- [7] A.I. Karelin, N.N. Krot, R.D. Kozlova, O.P. Lobas, V.A. Matyukha, J. Radioanal. Nucl. Chem. 143 (1) (1990) 241-252.

Pu association with Corroded Magnox Sludge: Relevance to Storage Pond Management, Future Remediation Strategy and Effluent Treatment

S.A. Parry*, F.R. Livens*, L. O'Brien†

*Centre for Radiochemistry Research, School of Chemistry, University of Manchester, Oxford Road, Manchester, M13 9PL.

†Nexia Solutions, Sellafield, Seascale, Cumbria, CA20 1PG, UK.

Background: Managing Pu-contaminated Corroded Magnox Sludge

"Magnox" fuel elements were developed for use in the UK's first generation reactors, and comprise a natural uranium core supported by a magnesium-rich alloy cladding. Spent fuel rods are stored in water-filled storage ponds, mostly at the Sellafield site (Windscale, Cumbria), under carefully controlled conditions to minimise corrosion of the Magnox cladding. However, the Magnox alloy cladding corrodes readily in water, and over the last 50 years, some 12000 m³ of contaminated sludge has accumulated at UK facilities.

Corroded Magnox sludge (CMS) is generally believed to comprise brucite, Mg(OH)₂, which is very soluble at neutral and acid pH. As a result, the storage ponds are maintained at pH>10, conditions which facilitate carbonation through reaction with atmospheric CO₂.

CMS is contaminated with highly radioactive isotopes from the spent fuel, in particular Pu, which is difficult to manage in these high pH, aqueous systems, since the most stable oxidation state, Pu (IV), is very susceptible to a complex series of hydrolysis reactions leading to the formation of colloidal and/or surface reactive species, depending on conditions. In addition, Pu (IV) solubility will be further affected by the presence of carbonate, since soluble ions such as [Pu(CO₃)₅]⁶⁻ can be formed.

Because the highly radioactive, Pu-contaminated CMS dissolves easily, it is amongst the highest priority wastes for immobilisation prior to disposal. However, the nature of the waste is not well understood, indeed our current work has shown that the evolution of the CMS is more complex than originally thought. Therefore, before a remediation strategy can be developed, knowledge of the composition and evolution of the aging CMS, and the behaviour of the association of Pu with the sludge must be acquired.

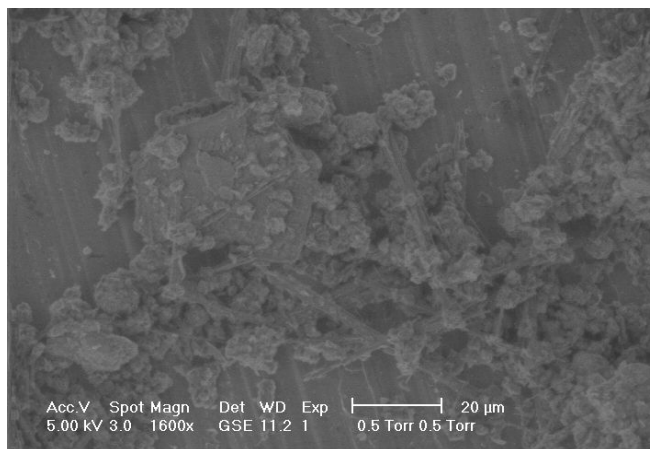


Fig. 1: Environmental scanning electron microscope (ESEM) image of CMS sludge illustrating platy brucite crystals and needle-like artinite crystals.

Experimental Assessment of Factors Controlling Pu Mobility

At present the discharge from the storage ponds passes through an effluent treatment plant prior to release into the environment. However, the complex chemistry of Pu and CMS make Pu mobility and discharge difficult to predict. Therefore, we have performed a full-factorial experiment to assess quantitatively the control a range of factors (reagents, particulate, and solution pH) have on the solubility of Pu prior to, and during effluent treatment.

Our experimental approach in addressing this problem has taken a second line to investigate the nature of the fine particulate, CMS and identify the phases present. Our initial characterisation of inactive CMS simulant has shown it to consist of brucite and additionally the mineral artinite, $Mg_2CO_3(OH)_2 \cdot 3H_2O$ (Fig. 1), likely formed through reaction of the highly alkaline waste sludge with atmospheric CO_2 .

To assess the factors controlling Pu solubility we have used filtration experiments to identify the conditions/reagents that yield hold-up of Pu on a $0.2 \mu m$ filtration membrane, either as Pu-colloid or Pu associated with particulate. The $0.2 \mu m$ molecular size cut-off prevents a conclusive assessment if the Pu remains truly in solution but provides a valuable first approximation, and an insight as to which factors may be significant in controlling Pu solubility during effluent treatment.

The results (Fig. 2) show that the presence of CMS and Si, likely to generate particulate and/or colloidal particles in aqueous solution results in filtration of Pu. The results also indicate dissolution of Pu following a reduction in pH, from pH 11 to pH 7.

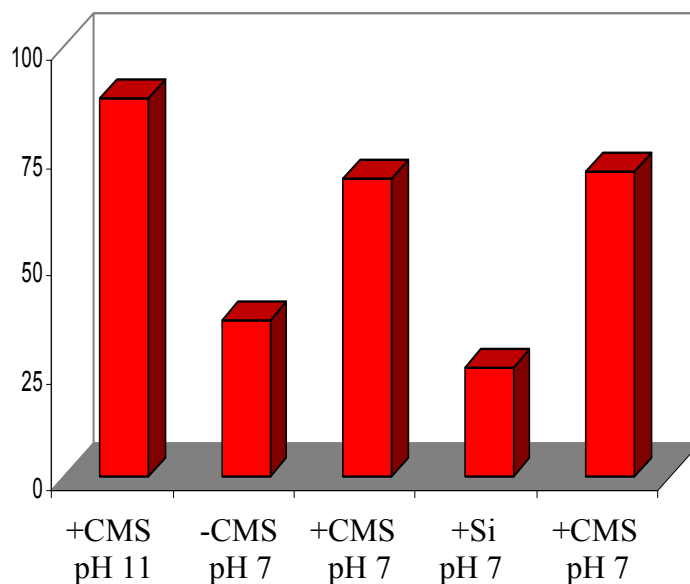


Fig. 2: % of Pu (IV) retained on a $0.2 \mu m$ filter

Self-irradiation damage in zirconolite for minor actinides immobilization

X. Deschanel, V. Broudic, S. Peugnet, C. Jegou, D. Roudil

CEA Valrhô Marcoule, BP17171, 30207 Bagnols-sur-Cèze, France

INTRODUCTION

Zirconolite is a potential host phase for the conditioning of the minor actinides arising from the reprocessing of the spent fuel [1-4]. In order to study the consequences of the self-irradiation damage on this structure, samples doped with 10wt.% of $^{238}\text{PuO}_2$ were fabricated. This article reports the result obtained on the evolution of macroscopic properties (initial alteration rate, swelling, hardness) of this material up to an integrated dose of $5 \times 10^{18} \alpha \cdot \text{g}^{-1}$.

EXPERIMENTAL

Forty ^{238}Pu doped pellets were fabricated in hot cells by natural sintering. The relative density of all these pellets exceeded 91%. Polished cross sections of these samples were examined by scanning electron microscopy (SEM) coupled with X-ray microanalysis (EDX) and X-ray diffraction analysis to check their homogeneity. The macroscopic swelling was determined from sample density measurement by hydrostatic weighing in water. The ceramic hardness was measured in air by Vickers micro-indentation on polished specimens, with indenter loads of 100 g maintained for 5 s.

The dissolution characteristics of the ceramics were determined by Soxhlet-mode dynamic leach testing at 100°C during 55 days. The mean alteration rate of the ceramics was measured by analysing the release of plutonium at the end of the test and by measuring the sample weight loss.

Some pellets were annealed continuously at 250 and 500°C in order to evaluate the evolution of their macroscopic swelling and the recovery of their crystallographic structure under these conditions.

RESULTS

The ^{238}Pu -doped pellets fabricated for this study become X-rays amorphous for a dose close to $5 \times 10^{18} \alpha \cdot \text{g}^{-1}$ at room temperature. This result is in good agreement with others published earlier [3-4].

The figure 1 shows the measured macroscopic swelling versus the integrated dose. This swelling was about 6% at room temperature for an integrated dose of $5 \times 10^{18} \text{ g}^{-1}$. Up to an integrated dose of $10^{18} \alpha \cdot \text{g}^{-1}$, the microscopic swelling estimated from X-ray diffraction analysis is close to the macroscopic one. This result suggests that both phenomena have the same origin, i.e. the production of point defects in the structure. The swelling also generates microscopic cracks within ceramics. The pellets annealed at 500°C recovered their initial density and their crystalline structure (Fig. 2).

The hardness of the samples decreases by approximately 25% compared to its initial value, when the integrated dose reached $3 \times 10^{18} \alpha \cdot \text{g}^{-1}$. Similar behaviour has also been reported by Weber [5].

The results of leaching test indicate a good behaviour of this matrix which has an initial leaching rate lower than $10^{-2} \text{ g.m}^{-2}.\text{j}^{-1}$ if it is calculated on the variation of mass, and about $10^{-4} \text{ g.m}^{-2}.\text{j}^{-1}$ if it is based on the release of plutonium in the leachate.

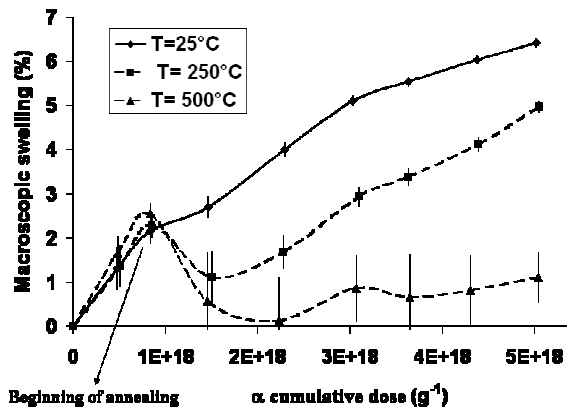


Fig. 1: Macroscopic swelling vs. Integrated dose for samples stored at room temperature, at 250 and 500°C.

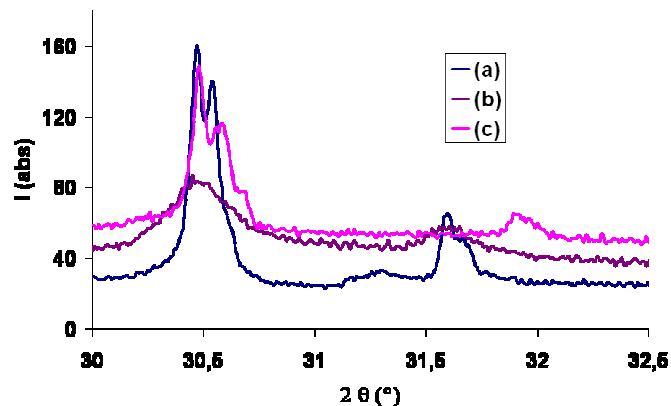


Fig. 2: Recovery of the structure for peaks corresponding to planes [221] $2\theta=30,5^\circ$ and [-402]: (a) sample after annealing at 500°C (α dose = $2,4 \cdot 10^{18} \alpha \text{ g}^{-1}$); (b) sample stored at room temperature (α dose = $2,2 \cdot 10^{18} \alpha \text{ g}^{-1}$); (c) initial state (α dose = $8 \cdot 10^{17} \alpha \text{ g}^{-1}$).

The consequences of the production of helium were not evaluated in this work. The available data on helium thermal diffusion [1] indicate that this is a relatively slow process (10 micrometers traversed in 100 years at 300°C). It is reasonable to think that a part at least of helium will remain occluded in material and that it will be able to have a long-term impact on the swelling of the pellets. Complementary work will have to be undertaken to evaluate this point.

CONCLUSION

Doping zirconolite with ^{238}Pu allows us to obtain after only 4 years interesting results on the long term behaviour of this structure. At integrated dose below $5 \cdot 10^{18} \alpha.\text{g}^{-1}$ the ceramic exhibits satisfactory resistance to self-irradiation and good defect healing behaviour at relatively low temperature. The consequence of helium production at higher concentration approaching $2 \cdot 10^{19} \text{ He.g}^{-1}$ (or 0.1 at.%) have to be investigated soon.

The authors thank T. Advocat and F. Jorion for their contribution to this study.

- 1 F. Jorion, *et al.*, *accepted in Nucl. Sci. Eng.*, (2006).
- 2 X. Deschanel, *et al.*, *accepted in J. Nucl. Mat.*, (2006).
- 3 D.M. Strachan, *et al.*, *J. Nucl. Mat.*, **345**, (2005).
- 4 F.W. Clinard, *Am. Ceram. Soc. Bull.*, **65** (1986).
- 5 W.J. Weber, J.W. Wald, H.J. Matzke, *J. Nucl. Mat.* **138**, (1986).

SHS method for immobilization of plutonium-containing waste

Levakov Eu.V., Postnikov A.Yu.

(RFNC - VNIIEF, Russia, Sarov)

Glagovskyi E.M., Kuprin A.V., Bogdanov A.I., Pelevin L.P.

(VNIINM, Russia, Moscow)

The main results of work in the area of technology development for immobilization of highly active waste (HAW) and, in particular plutonium-containing ones into mineral-like array compounds using the method of self-spreading high-temperature synthesis (SHS) are presented.

The choice of mineral-like arrays for HAW immobilization is proved. According to the results of thermodynamic calculations the availability of systems' formation based on zirconolite, pyrochlorine and other mineral-like compounds under SHS mode has been shown. The conditions influencing on both characteristics of SHS systems combustion and quality of obtained materials have been studied to optimize the technological parameters of SHS mineral-like arrays.

Base technological modes for SHS compacting of arrays based on pyrochlorine containing HAW simulators have been tested.

It is shown that the parameters of hydrothermal stability of arrays formed by SHS methods are similar to the same ones in arrays got by the method of cold compacting- sintering. Based on the experimentally got results the stands for immobilization of HAW simulators by SHS have been created.

Glass Fabrication and Product Consistency Testing of Lanthanide Borosilicate Glass for Plutonium Disposition

C. Crawford, J. Marra, N. Bibler

Savannah River National Laboratory, Aiken SC 298008 USA

INTRODUCTION AND BACKGROUND

The Department of Energy Office of Environmental Management (DOE/EM) plans to conduct the Plutonium Disposition Project (PDP) at the Savannah River Site (SRS) to disposition excess plutonium.¹ A plutonium glass waste form is the leading candidate for immobilization of the plutonium for subsequent disposition in a geological repository. Reference Lanthanide Borosilicate (LaBS) glasses, developed during the former Plutonium Immobilization Program (PIP), were originally studied in 1995/96. Current FY06 PDP research and testing being conducted at the Savannah River National Laboratory (SRNL) addresses several near term data needs identified by DOE/EM and the Yucca Mountain Repository. Our initial phase studies have examined the LaBS glass dissolution and subsequent fate of plutonium and the neutron absorbers during the dissolution processes, and the degree of macroscopic cracking that occurs during processing of the Pu glass waste form and subsequent pouring of High-Level Waste (HLW) in the Defense Waste Processing Facility (DWPF). We have also investigated frit formulations to improve durability and processability of the Pu-LaBS glass. This presentation will focus on the durability testing of a baseline Frit B LaBS glass containing 9.5 wt% PuO₂. The Frit B LaBS formulation resulted from earlier PIP testing.²

RESULTS

This study was performed with the baseline Frit B LaBS glass with frit composition shown in Table 1. A Frit X formulation is also shown in Table 1 that includes increased rare earth elements and decreased aluminum and silicon. The Frit X formulation should have improved qualities for PuO₂ immobilization and has recently been used to successfully vitrify a 9.5 wt%

Table 1. LaBS Glass Frit Compositions

Oxide	Frit B (wt%)	Frit X (wt%)
Al ₂ O ₃	21.3	9.0
B ₂ O ₃	11.6	11.7
Gd ₂ O ₃	12.8	12.15
HfO ₂	6.6	6.3
La ₂ O ₃	8.1	17.1
Nd ₂ O ₃	8.2	13.5
SiO ₂	28.9	18.0
SrO	2.5	2.25

PuO₂ LaBS glass that will be tested in upcoming studies in the SRNL. For the tests in the current program, plutonium LaBS glass was fabricated at SRNL using Frit B material that was vitrified from reagent grade chemicals in Pt/Rh crucibles at 1500 °C melt temperature for 2 hours, followed by quench-pouring. This cullet frit was ground to -325 mesh and mixed with PuO₂ powder in the SRNL shielded cells facility via remote handling. The PuO₂ LaBS glass was fabricated in Pt/Rh crucibles at 1500 °C for 4 hours, followed by water quenching. The resulting PuO₂ glass was crushed, mixed and remelted to enhance

homogenization of the glass. The glass density measured by water displacement using > 100 mesh glass powder in a pycnometer was determined to be 3.57 g/cm³. A significant finding from XRD and SEM characterization of the washed and dried powdered PuO₂ LaBS glass is the presence of trace, perhaps 1 vol%, amounts of undissolved PuO₂ in the glass. It could be that this undissolved PuO₂ in the glass is result of incomplete mixing of the glass precursors (PuO₂ powders mixed with the -325 mesh Frit B powders in a polybottle via remote handling) before fabrication. Future studies could examine other means of mixing such as mechanical mixing to better blend the PuO₂ powder in with the frit precursor powder.

The Product Consistency Test (PCT) is an ASTM standard Test (ASTM 1285-02) for leaching nuclear waste forms. This is the leach test used for the Frit B Pu-glass at SRNL discussed in this paper. As part of this SRNL program, other corrosion testing is planned at Argonne National Laboratory (ANL) involving monolithic leach tests and vapor hydration testing (VHT), as well as at the Pacific Northwest National Laboratory (PNNL) involving flow methods (Single-Pass Flow-Through (SPFT) and Pressurized Unsaturated Flow (PUF). Our PCT results performed from 7 to 56 days at 90°C, using varying surface area to volume (SA/V) ratios of 1500 m⁻¹ to 20,000 m⁻¹, indicate that normalized release of all Pu Frit B glass components including Pu are in the range of 10-100X lower than normalized release of Al, B and Si from the reference Environmental Assessment (EA) glass.³ The PCT testing was carried out in both steel and Teflon[®] vessels using ultrapure water (ASTM Type 1) as lechant. The leachates were filtered and vessels acid-stripped.

Colloidal plutonium species have been observed in previous Pu-glass corrosion studies involving the accelerated dissolution associated with the PUF test.⁴ The PCT leachates from this current study were examined after both syringe-filtration with 0.45 µm filters, and 30,000 nominal molecular weight limit (NMWL) ultrafilters capable of excluding colloids. Comparison of the different filtered leachate solutions indicates no significant differences in the plutonium concentrations (determined by ICP-MS), indicating that plutonium colloid formation does not occur under these PCT test conditions. Alteration secondary phases can form on the surface of glass powders used in long term, e.g. 120-240 day PCT's, and in PUF corrosion tests.⁴ The leached glass from our 28-day and 56-day PCT's performed in Teflon[®] at 90 °C and 20,000 m⁻¹ SA/V were thus characterized by SEM to examine the glass powder surfaces after leaching. No evidence of any alteration phases were observed from these leached glasses using SEM imaging capable of 1 to 100 µm resolution. Further details on the LaBS frit development, Pu glass fabrication, and Pu glass dissolution testing results will be presented in this paper and compared to previous published data.

REFERENCES

1. US Federal Budget, FY2006, Fissile Materials Disposition, 10 Million \$ Appropriation for Conceptual Design Activities for the Plutonium Immobilization Facility at the SRS, DOE/EM (<http://thomas.loc.gov/>).
2. N. E. Bibler, *et al.*, Mat. Res. Soc. Symp. Proc., Vol. 412, Materials Research Society, Pittsburgh, PA, (1996).
3. C. M. Jantzen, *et al.*, Ceramic Transactions, Env. And Waste Management Issues in the Ceramic Industry, Vol. 39, American Ceramic Society, Westerville, OH, (1994).
4. B. P. McGrail, *et al.*, PNNL-11834, UC-2030, Pacific Northwest National Laboratory, Richland, WA, October (1998) (and references cited therein).

Diffuse reflectance spectroscopy of actinide ions in polycrystalline ceramics designed for immobilisation of HLW

Y. Zhang, E. R. Vance, B. D. Begg

Australian Nuclear Science and Technology Organisation, PMB 1, Menai 2234, Australia

INTRODUCTION

Diffuse reflectance spectroscopy (DRS) is a useful tool for deriving information about actinide speciation in the solid state and has been used to probe uranium valences in polycrystalline brannerite¹ on which a number of intraconfigurational $f-f$ electronic absorption bands for $U^{4+}(5f^2)$ and $U^{5+}(5f^1)$ ions have been observed over the near infrared (NIR) range (4000-12000 cm^{-1}), and plutonium valences in zirconolite². It is of interest in the nuclear waste form application to study systematically the DRS spectra of actinide ions in other actinide-bearing ceramic phases, e.g. perovskite, zirconolite, pyrochlore and monazite.

EXPERIMENTAL

Samples doped with various amounts of U/Np/Pu were made by the standard alkoxide/nitrate route³ and sintered at around 1400°C for 16-20 hrs under air/argon/H₂-N₂ atmospheres as appropriate. X-ray diffraction and scanning electron microscopy confirmed that the samples were essentially single-phase.

Roughly polished (200 grit SiC) disc samples were used for DRS measurements at ambient temperatures over the NIR range (4000-12000 cm^{-1}) using a Cary 500 spectrophotometer equipped with a Labsphere Biconical Accessory. Spectra were converted into Kubelka-Munk units, $F(R)=(1-R)^2/2R$, by reference to the spectrum of a Labsphere certified standard (Spectralon).

RESULTS AND DISCUSSION

U^{4+}/U^{5+}

Like U^{4+} ions in $ThTi_2O_6$ ¹, U^{4+} ions in perovskite, zirconolite, pyrochlore-rich ceramic and zirconolite glass-ceramic show weak bands in the visible and NIR regions and show rather similar spectral features. In contrast to the DRS spectra of U^{4+} , DRS spectra of U^{5+} are much simpler with only a small number of intraconfigurational $f-f$ transition bands in the NIR region and they are fairly similar for different ceramics. The U^{5+} bands slightly shift to the IR direction when the U coordination numbers increase, from 6-fold for brannerite to 8 and/or 7 for pyrochlore and zirconolite. Compared to the free ion energy levels⁴, the observed band shifts, splittings, intensities and additional bands are related to the actual U ion site symmetries in the ceramic crystal structures.

Np^{3+}/Np^{4+}

Sintering samples in air or argon always gives rise to the formation of Np^{4+} . Np^{3+} can be formed at reducing conditions in perovskite and in monazite but not in zirconolite under reducing conditions. Reduction of perovskite samples by heating in 3.5% H₂/N₂ atmosphere to produce Np^{3+} generally led to increased absorption (with the samples turning black in color) and broadly

featureless spectra, obliterating any weak Np^{3+} absorptions. However, for samples containing 0.1 formula units (f.u.) of Np, characteristic absorption peaks for Np^{3+} at around 4100 cm^{-1} could be detected for both samples with or without Al on the Ti-site as charge compensators, and distinctly different from Np^{4+} spectra.

The DR spectrum of a zirconolite sample sintered in air with 0.01 f.u. of Np^{4+} on the Ca site is similar to that of a perovskite except an additional sharp and strong transition band at around 7000 cm^{-1} due to the lower Np site symmetry in zirconolite. There appeared to be little difference in the electronic spectra between Np^{4+} in the Ca vs the Zr site of zirconolite as the crystal field splittings in the two kinds of sites cannot be distinguished at ambient temperature due to the band broadening and overlapping.

$\text{Pu}^{3+}/\text{Pu}^{4+}$

The DR spectra of Pu ions give rise to a number of unresolved intraconfigurational f-f electronic absorption bands of a few hundred cm^{-1} bandwidth. No clear spectral differences were evident when Pu^{4+} was targeted to Ca or Zr sites in zirconolite. Samples prepared in reducing atmospheres with a view to producing Pu^{3+} were strongly absorbing, leading to suppression of Pu transitions. Evidence for Pu^{3+} in perovskite and zirconolite under reducing conditions has been obtained previously by XANES⁵.

In general, there was approximate agreement of the Kubelka-Munk absorption intensities with Beer's Law for the different actinide ions at low concentrations (0.001-0.03 f.u.) in most of the ceramics studied. It would appear that U spectra are most sensitive to valence change ($\text{U}^{4+}/\text{U}^{5+}$) and site symmetry whilst Np ($\text{Pu}^{3+}/\text{Pu}^{4+}$) and Pu ($\text{Pu}^{3+}/\text{Pu}^{4+}$) are not.

We would like to thank Alan Brownscombe and Terry McLeod for sample preparations.

- 1 K. Finnie, Z. Zhang, E. R. Vance and M. L. Carter, *J. Nucl. Mater.*, **317** (2003) 46-53.
- 2 E.R. Vance, K.S. Finnie, Y. Zhang and B.D. Begg, "Diffuse Reflectance Spectroscopy of Pu Ions in Zirconolite", *Scientific Basis for Nuclear Waste Management XXVIII*, Eds. J. M. Hanchar, S. Stroes-Gascoyne and L. Browning, Materials Research Society, Warrendale, PA, USA, pp. 261-6.
- 3 E.R. Vance, Materials Research Society, MRS Bulletin, Vol. **VIX**, **12** (1994) 28-32.
- 4 W.T. Carnall and H.M. Crosswhite, ANL-84-90, Argonne National Laboratory, USA.
- 5 B.D. Begg, E.R. Vance and S.D. Conradson, *J. Alloys Compds.*, 271-273 (1998) 221-226.

Plutonium Oxide Polishing for MOX Fuel Fabrication

F. Coriz¹, J. Danis¹, D. Gray¹, D. Martinez¹, J. Martinez¹, C. Martinez¹, Y. Martinez¹, D. Garcia¹, J. Royba¹, B. Griego¹, M. Saba¹, J. Valdez¹, K. Ramsey², J. Alwin¹, D. Costa²

¹Actinide Process Chemistry Group, NMT-2, Nuclear Materials Technology Division, Los Alamos National Laboratory, Los Alamos, NM 87545 USA

²Pit Disposition Science & Technology Group, NMT-15, Nuclear Materials Technology Division, Los Alamos National Laboratory, Los Alamos, NM 87545 USA

Los Alamos National Laboratory (LANL) was successful in polishing 120 kg of plutonium as highly purified PuO₂ for the European Mixed Oxide (MOX) Lead Test Assembly (LTA) managed by Duke, COGEMA, and Stone & Webster (DCS). The purified oxide has been successfully fabricated into fuel pellets that went into making the lead test assemblies (LTAs). The LTAs have been inserted into the Catawba nuclear reactor located in South Carolina which is presently generating electricity, using MOX fuel produced from surplus nuclear weapons.

This project has been recognized as representing the first plutonium oxide for LANL that was polished under the quality requirement of the Nuclear Regulatory Commission (NRC). In addition, the project has been credited as one of the “largest single nonproliferation project in history” by US Ambassador Linton Brooks (9/23/04). The process flow sheet for PuO₂ purification was based on aqueous recovery that included several unit operations (dissolution, ion exchange, oxalate precipitation, and calcination). Data from the chemical and physical test will be presented to show product quality and consistency in the production phase of this project. In addition, upcoming optimization experiments will be presented in preparation to polish an additional 330 kg of PuO₂ for the Fuel Pellet Fabrication Facility in Savannah River. For example, during the production phase of this project in early 2003, it was determined that the ion exchange unit operation was a waste-intensive and inefficient process that needed improvement. In order to meet the stringent impurity specification for the MOX PuO₂ Polishing Project, approximately 500 L of 7 M nitric acid was used for washing impurities from the plutonium. Yearly production capacity is projected to be at 90 kg of purified PuO₂, which would generate 30,855 L of Transuranic Waste (TRU) liquid waste to be dispositioned using an evaporation process. Currently, the distillates from the evaporation process are sent to the LANL Radioactive Liquid Waste Treatment Facility (TA-50) for further treatment.

In order to reduce or eliminate the waste stream dependency on sending the distillate to an external treatment facility and advancing the Laboratory’s mission on reducing waste generation, LANL has identified an avenue to recycle the processed distillate (7M HNO₃) back into the aqueous polishing process (ion exchange). To ensure quality assurance and control, LANL will first test the recycled acid to ensure that no additional contaminants are introduced into the ion exchange process, inadvertently causing the product oxide to fail specification requirements. The qualification exercise will include running a series of ion exchange

experiments using the recycled acid and analyzing the product oxides impurity levels. Based upon a successful qualification exercise, aqueous polishing has estimated using 24,375 L of recycled nitric acid out of the 30,855 L of effluent sent to the evaporation process. NMT-2 projects recycling 79% of the effluent as 7M acid back into the anion exchange process, reducing the nitric acid waste sent to LANL's Radioactive Liquid Waste Treatment Facility.

The role of magnesium chloride in gas generation and corrosion during storage of impure plutonium oxides

Eduardo Garcia^{*}, Patricia Bielenberg[†], Kirk Veirs^{*}, John Berg^{*}, Adam Montoya^{*}, Max Martinez^{*}

^{*}Los Alamos National Laboratory, Los Alamos NM 87545 USA

[†]ExxonMobile, Baton Rouge LA

INTRODUCTION

Of the 3322 containers packaged under DOE's 3013 Standard¹ at Hanford, Rocky Flats, and Livermore, 1290 (39%) have been identified as potentially susceptible to pressurization or corrosion.² The vast majority of these containers have chloride salt impurities. Initial studies of materials representative of this class of stored material have shown unexpectedly high rates of hydrogen generation and corrosion.³ Corrosion occurs in 304L stainless steel and in heat affected zones of welds in 316L stainless steel as shown in Fig. 1. Pure plutonium oxide with the same amount of moisture generates hydrogen at lower rates with no observable corrosion.

Electrorefining processing salts contain equimolar mixtures of NaCl and KCl with added anhydrous MgCl₂. Stabilization of these salts by calcining was thought to destroy the MgCl₂ component by hydrolysis resulting in MgO. These materials pickup moisture rapidly at low relative humidities (RH), indicating that some of the MgCl₂ survives calcination because NaCl and KCl do not pickup moisture until their deliquescent point, which is above 70% RH. Thermal gravimetric analysis of materials after calcination with FTIR identification of the evolved gases show HCl being evolved at low temperatures, ~ 200°C, which is consistent with thermal hydrolysis of hydrated MgCl₂. In order to identify the role MgCl₂ plays in these observations, we have (1) conducted x-ray diffraction studies of salt mixtures to identify the MgCl₂ containing component, (2) identified the soluble constituents of calcined salts to see if Mg is present, and (3) conducted hydrogen gas generation studies to see if MgCl₂ containing salts generate gas at sufficient rates.

X-RAY DIFFRACTION STUDIES

Magnesium chloride is known to form double salts with alkali metal chlorides of formula XMgCl₃ and X₂MgCl₄, where X is Na or K. These salts are hygroscopic but their hydration behavior has not been quantitatively characterized. However, the XMgCl₃ salts have been shown to adsorb water and form the hexahydrate just as MgCl₂ does. In the equimolar NaCl/KCl

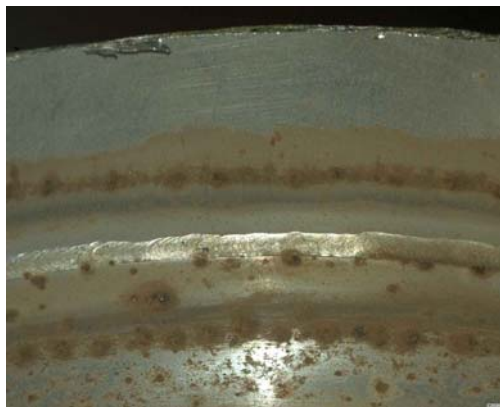


Fig 1: Pitting corrosion formed on the interior surface of a container filled with a stabilized material of 80% PuO₂ and 20% salt with 0.2wt% water. The weld joins 316L (above) to 304L (below).

mixture with small amounts of added $MgCl_2$, the magnesium component appears to be a $Na_yK_{2-y}MgCl_4$ salt where y is less than one. This salt appears to pickup water at low RH to form a hydrate in a manner very similar to $MgCl_2$.

SOLUBLE MAGNESIUM AND GAS GENERATION STUDIES

One gram samples of twelve calcined materials representative of materials in 3013 containers were dissolved in 100 ml of water and then filtered to remove the insoluble oxides, which were mainly PuO_2 . The soluble components were measured using ion selective electrodes for Na, K, Cl and F and ICP/AES for Ca, Cr, Fe, Ni, Mg, Mn, and Mo. The pH and conductivity were also measured. Chemical analysis of the starting material was also available. The fraction of the total magnesium that was soluble varied from less than 1% to 27%. The correlation between soluble magnesium and hydrogen gas generation is given in Table I. Two materials, 520610020 and 053038, have high gas generation rates for the amount of soluble magnesium. These materials have high soluble calcium content. Calcium chloride also adsorbs water and will hydrolyse thermally, but at much higher temperatures than $MgCl_2$.

Table 1 The soluble Mg and Ca content of salt bearing MIS representative materials and the hydrogen gas generation rate.

Material	Soluble Mg (wt%)	Total Mg (wt%)	Soluble Ca (wt%)	H ₂ rate (kPa/day)
520610020	0.001%	8.50%	5.526%	0.27
TS707001	0.002%	0.01%	0.024%	0.03
PMAXBS	0.016%	0.24%	0.006%	0.15
07242201A	0.023%	0.17%	0.274%	0.13
053038	0.038%	0.79%	1.583%	0.61
ARF-102-85-365	0.050%	0.56%	0.000%	0.40
CLLANL025	0.062%	0.38%	0.000%	0.52
011589A	0.086%	2.26%	0.251%	0.68
ARF-102-85-295	0.157%	4.04%	0.064%	0.60
ARF-102-85-223	0.157%	0.59%	0.002%	0.78
C00695	0.174%	0.95%	0.014%	1.37
C06032A	0.218%	2.15%	0.000%	1.29

CONCLUSION

Magnesium chloride present in plutonium processing salts survives calcination and adsorbs water from the atmosphere. The resulting hydrated salt will radiolysis producing hydrogen gas. Corrosive gases are also produced with the most likely candidate being HCl.

- 1 DOE-STD-3013-2000, "Stabilization, packaging, and storage of plutonium-bearing materials", U.S. Department of Energy, Washington, D.C. 20585.
- 2 E. Kelly, L. Peppers, K. Veirs, and J. Berg, LA-UR-05-2193.
- 3 Veirs, D. K.; Worl, L. A.; Harradine, D. M.; Martinez, M. A.; Lillard, S.; Schwartz, D. S.; Puglisi, C. V.; Padilla, D. D.; Carrillo, A.; McInroy, R. E.; Montoya, A. R., LA-14148.

Recent Studies of Uranium and Plutonium Chemistry in Highly Alkaline Radioactive Wastes

W. King*, D. Hobbs*, and W. Wilmarth*

*Savannah River National Laboratory, Aiken, SC 29808 USA

INTRODUCTION

Operation of the Department of Energy facilities at the Savannah River Site (SRS) has generated millions of gallons of highly radioactive wastes that are stored in large underground storage tanks comprised of carbon steel. The highly alkaline wastes consist of three forms: Sludge produced when acidic wastes from purification of irradiated nuclear fuels and targets are neutralized and consists of transition metal hydroxides and oxy-hydroxides along with similar compounds of aluminum; Supernate containing soluble components of the neutralized reprocessing solutions and largely a mixture of dissolved salts, predominantly sodium hydroxide, sodium nitrate and sodium nitrite; and Saltcake produced upon evaporation of the supernate and is largely sodium salts of nitrate and nitrite. Small quantities of uranium and plutonium are partitioned in the three waste types.

Retrieval of sludge began in the 1990s and is currently being vitrified at the Defense Waste Processing Facility (DWPF) in a borosilicate glass matrix for disposal in the federal repository for High-Level Waste. The alpha component of the other two waste classes (saltcake and supernate) must be reduced prior to shallow land burial at SRS. The alpha removal technology is a batch contact with monosodium Titanate and has been well tested.¹ The waste processing strategy calls for the saltcake to be dissolved with water and batched through the alpha removal process along with the supernate wastes. These operations will require numerous waste transfers and will result in the mixing of these streams.

The chemistry of uranium and plutonium is of interest in these processing steps to ensure that their concentrations do not exceed solubility limits, resulting in the precipitation of the actinides. Even though their concentrations are low, the volumes involved (millions of gallons) can lead to criticality concerns. The actinide solubilities have been previously studied. Allard compiled measured and estimated complex formation quotients for the actinides as a function of oxidation state in the pH range of 7 to 11.² Hobbs and Karraker³ have measured the uranium and plutonium solubility in simulated SRS waste solutions and have developed solubility models as a linear function of a number of anion concentrations. Additionally, the mixing of various process solutions can result in the precipitation of various compounds like aluminosilicates. Aluminosilicates have been shown to occlude actinides.⁴ As a result of these concerns, SRNL has been examining the chemistry of uranium and plutonium in these possible mixing scenarios.

RESULTS

Several supernate samples have been retrieved from selected waste tanks and characterized for actinide content. The uranium and plutonium solubilities were measured using

a technique modified from that used by Addai-Mensah, et al.⁵ The method includes the spiking of supernate solutions with small volumes of acidic uranyl nitrate and plutonium oxide solutions, and the direct addition of preformed uranium and plutonium solids to fresh supernate. Initial results revealed that a DWPF recycle stream was supersaturated in uranium, but not plutonium. Solubility test results for several other tank supernate samples reveal that Pu solubility is typically < 5 mg/L, while U solubility limits can approach 50 mg/L. The solubilities are believed to vary with the concentrations of the primary anions in solution, including hydroxide, nitrate, nitrite, carbonate, and sulfate. Statistical models have been developed to predict solubility as a function of composition and temperature.

The chemistry of uranium was also examined under the conditions whereby sodium aluminosilicate was forming. In this study, the degree of uranium supersaturation was tested as to whether it influenced the participation of uranium in the aluminosilicate reaction. Figure 1 shows the fate of uranium when highly supersaturated. In these experiments, uranium was spiked into the waste solution and held at temperature (50 °C) for 50h. Samples were taken very shortly after uranium addition and at 50 h to determine if the uranium had precipitated. An aliquot of sodium metasilicate was added to the waste solution and a second sample was taken following the dissolution of the metasilicate and periodically over approximately 200 h. Figure 1 shows the results for the test conducted with a uranium solution at a degree of supersaturation of 2.7. At the time that the second sample was collected, during the 50th hour, a concomitant reduction in the aluminum concentration occurred, indicating that formation of aluminosilicate had commenced. Evident from the silicon and aluminum data, aluminosilicate formation continued over the duration of the test.

The successful processing of High-Level Waste requires a fundamental understanding of the fate of uranium and plutonium under highly alkaline conditions. The importance of this work will assist in the successful retrieval and processing of the stored wastes at the Savannah River Site. These results along with others will be reviewed.

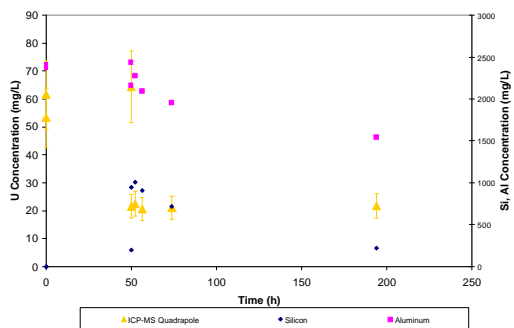


Figure 1. Uranium Concentrations during Aluminosilicate Formation.

¹ F.F. Fondeur, D. T. Hobbs, M. J. Barnes, S. D. Fink, *Separation Science and Technology*, **2005**, 40(1-3), 571-592.

² R. Allard, "Solubilities of the Actinides in Neutral and Basic Solutions," Actinides in Perspective, Edited by N. M. Edelstein, Pergamon Press, 1982.

³ D. T. Hobbs and D. G. Karraker, *Nucl. Tech.*, **114**, 318, 1996.

⁴ W. R. Wilmarth, S. W. Rosencrance, D. T. Hobbs, C. M. Jantzen, J. E. Laurinat, W. B. Van Pelt, W. L. Tamosaitis, A. J. Mattus, M. Z. Hu, D. W. DePaoli, C. F. Weber, C. P. McGinnis, S. Mattigod, "Aluminosilicate Formation in High Level Waste Evaporators: A Mechanism for Uranium Accumulation" Proceedings of Waste Management '02.

⁵ J. Addai-Mensah, J. Li, M. Zbik, and W. R. Wilmarth, "Uranium Sorption on Solid Aluminosilicate Phases under Caustic Conditions", *J. of Sep. Sci. and Tech.*, **40**, 267, 2005

DOE's Technical Requirements for Packaging of Nuclear Material Stored Outside of a Glove Box

G. D. Roberson*, D. Kirk Veirs[†]

*Department of Energy, Albuquerque NM USA

[†]Los Alamos National Laboratory, Los Alamos, NM 87545

INTRODUCTION

The storage of nuclear materials by the U.S. Department of Energy has been the subject of concern and much expense recently. The U.S. Defense Nuclear Facilities Safety Board's concern about materials left in process after production work stopped as a result of the end of the Cold War resulted in DNFSB Recommendation 94-1. In response to 94-1, DOE issued a stabilization, packaging, and storage Standard in 1994 with updates in 1996, 1999, 2000, and 2004, the 3013 Standard. Since that time over 4000 containers packaged to the 3013 Standard have been prepared and are in storage at Hanford, Savannah River Site, and Lawrence Livermore National Laboratory. Since 1994 there have been a number of events that led the DNFSB to issue recommendation 2005-1. The DNFSB cited in particular an August 5, 2003, event at Los Alamos National Laboratory's (LANL) Plutonium Facility that resulted in multiple workers receiving plutonium-238 uptakes as a result of the degradation of a package stored longer than planned and an October 6, 2004 incident at LLNL that involved the accidental drop of a package containing salt-bearing plutonium oxide. The DOE is developing a Manual to ensure all packages containing Special Nuclear Materials (including U, Np, Pu, Am, Co, Sr, Sc Th, Bk, Cf, or Cm) outside of a glove box meet minimum standards of design, construction, procurement, and testing. This presentation will present the new requirements and their technical basis.

SCOPE

The Manual, scheduled to be issued by December 30, 2006, will be applicable to all DOE facilities. Establishing packaging requirements for nuclear materials within the DOE complex requires consideration of a diverse population of material types for storage for uncertain periods of time. From a safety standpoint, nuclear material packaging must protect against a number of challenges that could breach the container and release radioactive material. Many of the materials of concern generate gases that result in container pressurization and may be pyrophoric or highly reactive. The container design must take into account corrosion, oxidative expansion of stored metal, effects of radiolysis, diurnal pumping and damage due to impacts from drops and tooling during handling. The DOE sites have not fully considered these issues for all packages within their inventories. For this reason, a consistent set of packaging requirements was found to be necessary for interim storage of Nuclear Materials outside of an approved engineered contamination barrier in order to protect workers.

This presentation will cover the limits on materials, the criteria that must be met for package design, allowable packaging configurations, and the requirements of a surveillance program.

1. U.S. Defense Nuclear Facility Safety Board Recommendation 1994-1.
2. U.S. Defense Nuclear Facility Safety Board Recommendation 2005-1.
3. DOE-STD-3013-2004.
4. HQ-EH-2004-1, OAK--LLNL-LLNL-2004-0046

The Legacy of Bolas Grande Spheres at Los Alamos National Laboratory: A Responsible Management and Disposition Plan¹

J. Kohler , W. Crooks, W. Partain, R. Villarreal, D. Martinez, E. Flores, P. Pittman, T. Harden, L. Field

Los Alamos National Laboratory, Los Alamos, NM 87545 USA

THE LEGACY

There are 14 Bolas Grande Spheres that reside at the Los Alamos National Laboratory in outdoor, above ground, uncovered storage. They were manufactured during the Cold War.

The instrumented Spheres, each used only once, provided the containment that confined the fall-out from a small-scale internal plutonium detonation.

The steel Spheres are 6 feet in diameter, weigh up to 14,000 pounds, and have a wall thickness of 1-2 inches.



Fig 2: Inside a Bolas Grande Sphere
time. Gamma flux reaches a maximum dose at 60 years.



Fig 1: Bolas Grande Spheres in outdoor storage at Los Alamos National Laboratory

Bolas Grande Spheres contain SNM consisting of plutonium-239 (^{239}Pu) in the form of actinide metals and oxides, mixed in a matrix of metal, powdered silica, graphite, electrical wires and other hardware. Each sphere is estimated to contain approximately 400 pounds of radioactive debris. The debris is settled below that level of the 20-inch port.

The primary radioactive component of the material in these spheres is americium -241 (^{241}Am) created from the decay of plutonium-241 (^{241}Pu). ^{241}Am emits a highly energetic 60 keV gamma ray. The gamma ray flux increases over time as the ^{241}Pu is decaying to ^{241}Am with

While the steel containment sphere significantly attenuates the flux from this material, several of the spheres, in their outdoor storage locations, have contact dose measurements of 3mR/hr.

THE PROBLEM

The spheres cannot reside outdoors forever, yet currently there is no clear-cut disposition path. Their outdoor storage location subjects them to uncertain environmental conditions and natural phenomenon. The two Category II nuclear facilities on the lab site that could process these spheres, Plutonium Facility-4 (PF-4) and the Chemical and Metallurgical Research Facility (CMR), each have design and engineering limitations in light of advances in safety and radiation protection standards/regulations. While several spheres were emptied in the late '90s in PF-4, that process was neither ALARA engineered nor worker friendly and, absent an emergency, could not be restarted without significant re-engineering. Space in the CMR Facility could be redesigned for sphere processing, but the facility itself does not meet modern seismic criteria.

THE CHALLENGE

Introducing new nuclear processes into aging nuclear facilities presents challenges to the regulator, the engineer, and the safety analyst. Complying with the constraints and limitations of modern regulations can present mutually exclusive alternatives. Yet doing nothing, maintaining the status quo, or postponing action to an unspecified future date is neither environmentally nor socially responsible.

THE SOLUTION

The paper will introduce the Bolas Grande Project at Los Alamos. It will describe how the Project Team plans to meet the challenge of sphere processing in a safe and expeditious manner, in light of new regulations and their impact on aging nuclear facilities.

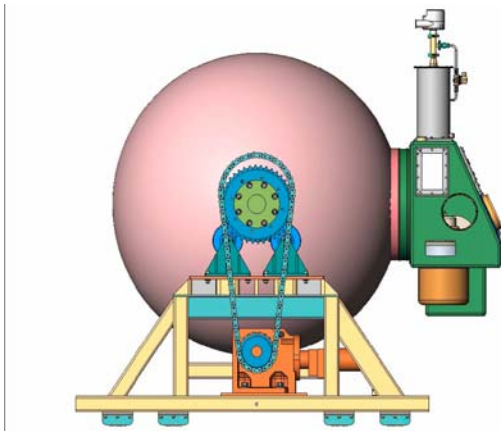


Figure 3: Bolas Grande Sphere mounted on the Sphere Support Stand with attached Dry Work Station

The Bolas Grande Project is developing a set of ALARA compliant, uniquely designed and engineered Bolas Grande structures, systems, and components (SSCs) to remediate the spheres. Central elements of the design are the Sphere Support Stand, the Dry Work Station, and the Wet Chemical acid etch decontamination process using a mixture of Nitric and Fluoboric acid. The functional safety requirements called out by the Bolas Grande Preliminary Documented Safety Analysis (PDSA) and compliance with DOE Order 420.1, "Facility Safety", directly impact the design of the SSCs.

¹ J. Kohler, *et al.*, Bolas Grande Project Critical Decision (CD)-1 Package, Title 1 Design Report and Design Package

Influence of H₂O content in test atmosphere on creep properties of (U, Pu)O₂ materials

V. Basini*, F. Bruguier*

*CEA Cadarache, DEC/SPUA/LMPC, Bat 315, 13108 St Paul lez Durance, France

INTRODUCTION

MOX fuel tested under transient conditions behaves particularly well from the pellet-cladding interaction point of view and can undergo power variations above the current standard UO₂ threshold.

To complete understanding on the specific mechanical properties of MOX fuel, experimental programs have been undertaken within the framework of the cooperation between EDF, FRAMATOME-ANP and CEA. Since the MOX benefit is largely attributed to its higher fuel creep, the influent parameters on the thermo-mechanical behaviour of MOX fuels are studied and compare to the behaviour of UO₂. Among them, influence of oxygen potential variations have been studied via creep tests under different atmospheres (dry and damp) and seem to be one of the most influent.

EXPERIMENTAL PROCEDURE

Cylindrical pellets of (U,Pu)O₂ had elaborated by classical powder metallurgy route : UO₂ and PuO₂ powders are mechanically mixed to obtain a plutonium content of about 7 %, mixed powders are shaped by uniaxial pressing and sintering under Ar+5%H₂+1000ppmH₂O atmosphere at 1700 °C, thereby ensuring the material stoichiometry. After sintering, the pellets were thermally treated under the same atmosphere during 245 h to obtain a solid solution of (U, Pu)O₂. The samples are of PWR geometry, 13 mm high and 8.2 mm diameter. Their characteristics are given on table 1. Compressive tests were conducted in a suitable adapted furnace on a screw-type Instron machine placed in glove box (Figure 1). Creep tests were performed at 1500 °C under different atmosphere : vacuum, Ar+5%H₂ and Ar+5%H₂+ x ppm H₂O (x ranges from 500 to 3000 ppm).

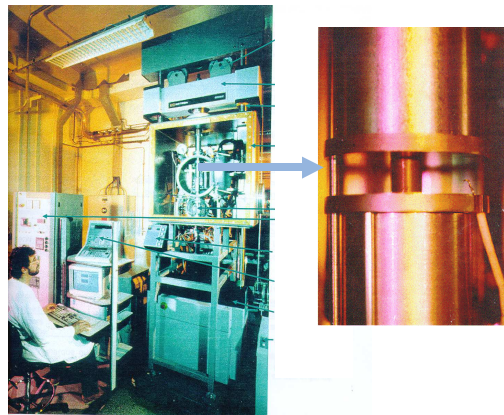


Fig 1: Mechanical test device

Pu Content (%)	Grain size (μm)	Porosity (%)	O/M Ratio ^a
7	6,5	2	2.001 ± 0.003

Table 1 : characteristics of (U, Pu)O₂ pellets

^a : obtain by thermogravimetry measurements

EXPERIMENTAL RESULTS

Creep tests have been performed at 80 MPa under varied atmospheres : vacuum, Ar/H₂ and Ar/H₂ + 1000 ppm H₂O. Creep curves, exhibit a classical primary regime followed by a stationary strain rate regime in which the creep parameters were determined. No difference is observed between vacuum and Ar/H₂ atmosphere, the stationary creep rate is about 0,6 %/h. One test was started first under Ar/H₂ atmosphere, and then, when the stationary strain rate regime was reached, vapour water was introduced in the furnace. The stationary creep rates increase rapidly with the humidification of the atmosphere, about almost 10 times the creep rate under dry atmosphere. The same rate is obtained when the test is directly performed under damp atmosphere.

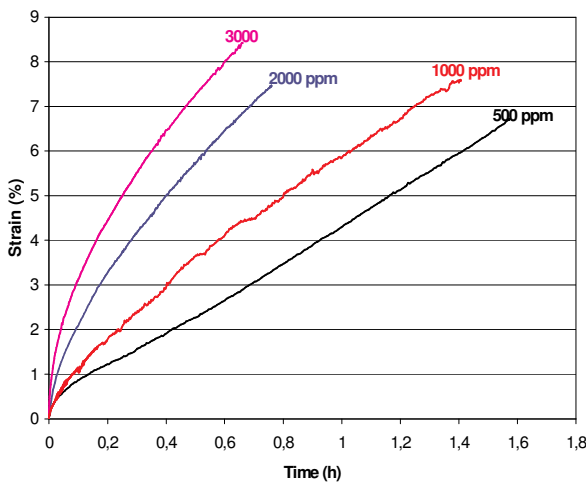


Fig 3 : Variation of primary creep under different atmospheres

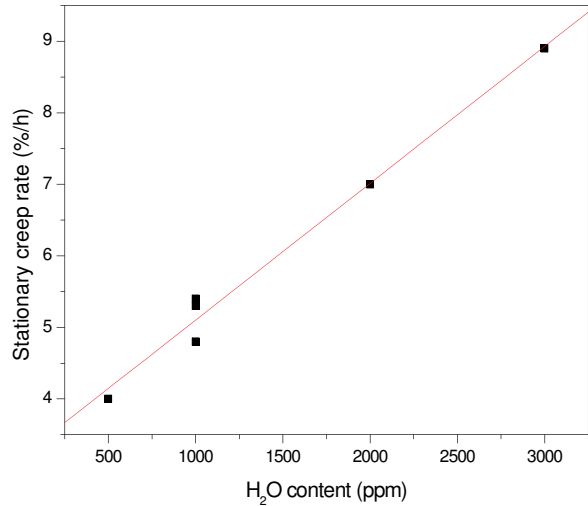


Fig 2 : Influence of H₂O content on stationary creep rate of (U,Pu)O₂

Linear increasing of the stationary creep rate is observed with H₂O content from 0 to 3000 ppm (Figure 2). The primary creep strain is also increased with the H₂O content (Figure 3). For instance, after 20 minutes, a primary creep strain less than 2 % is measured for 500 ppm H₂O content, instead of about 7% for 3000 ppm H₂O content. Same tests have been performed on UO₂ pellets and showed a low influence of the humidification of the atmosphere (stationary creep rate increase by a factor 4 from dry atmosphere to Ar/H₂ +1000 ppm H₂O) and no influence of the H₂O content from 0 to 2000 ppm is observed.

CONCLUSION

This study showed the important influence of the oxygen potential on the creep behaviour of (U, Pu)O₂ materials. Primary creep strain and stationary creep rate increase with increasing of the H₂O content. The influence is different in the case of UO₂ material and then allow us to make the assumption that it could be one of the influent factor of the better in pile behaviour of MOX fuels. Relation between oxygen potential and creep parameters on UO₂ and (U,Pu)O₂ will have to be evaluated.

Determination of elastic moduli at high temperatures for alpha-Plutonium and Uranium-Vanadium alloy with an ultrasonic method

L. Bourgeois, M.-H. Nadal, F. Clement, G. Ravel-Chapuis

CEA-Centre de Valduc, Département de Recherches sur les Matériaux Nucléaires,
21120 IS-SUR-TILLE, FRANCE

INTRODUCTION

The knowledge of the elastic moduli¹ is necessary in calculations with classical mechanical computer codes, both in the elastic and in the elastoplastic regimes. When a structure is stressed versus temperature other than room temperature, these elastic moduli must be known across the whole range of temperature investigated. For materials which are submitted to high temperatures, most of the conventional measurement methods, such as mechanical testings, are unsuitable. An alternative solution is an ultrasonic method which has the advantage to determine the elastic moduli² for a very weak strength to deformation ratio. A contact delay-line ultrasonic device³ has been developed to measure the shear and compression waves velocities up to 1000K on cylindrical specimens.

EXPERIMENTAL SET UP

The determination of the shear modulus $\mu(T)$ depends on the acoustic velocities, in particular on the shear velocity, which variation versus the temperature θ can be measured. The principle of the experiment consists in measuring the time of flight of the acoustic wave through the sample as described on the figures 1.a and 1.b. The elastic-wave velocities determination requires the accurate knowledge of the distance of propagation through the solid versus temperature $l(\theta)$. This is obtained using the thermal expansion of the material. A furnace is used so that the main heating region is located on the sample. This latter (cylindrical sample of 4.5 mm to 10 mm width and 23 mm diameter) is placed between two wave-guides. At the end of each one, two transducers are connected with the same ultrasonic characteristics. The two wave-guides are used to ensure the propagation of the waves through the sample and also to undergo the temperature gradient. Therefore, the thermal resistance of the wave-guides is sufficient to keep the transducers near the room temperature.

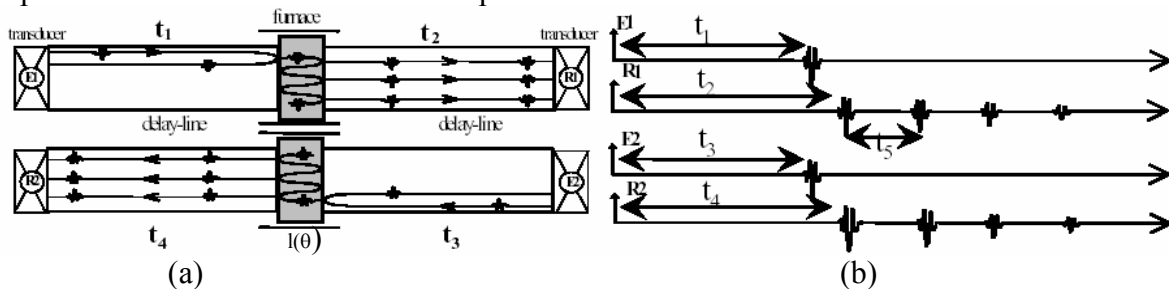


Fig 1: (a) Propagation of the ultrasonic waves in the delay-line/material/delay-line structure, (b) Echograms acquired by each transducer.

EXPERIMENTAL RESULTS

Experimental results are presented for plutonium and uranium-vanadium samples.

Figure 2 presents the evolution of the shear modulus of the uranium-vanadium alloy. The measures have been realized in the temperature range ($0.2 < T/T_m < 0.7$). The melting point of uranium-vanadium alloy is $T_m = 1400\text{K}$. The evolution of $\mu(T)$ keeps a monotonous decrease up to the first shift $\alpha \rightarrow \beta$ at 938K where the decrease is more important. We have developed a model including phase jumps and change of state to obtain a continuous description of $\mu(T)$ up to the melting point considering the second phase shift $\beta \rightarrow \gamma$ at 1040K . $\mu(T)$ results seem to exhibit enforced phase jumps comparing to Young modulus.

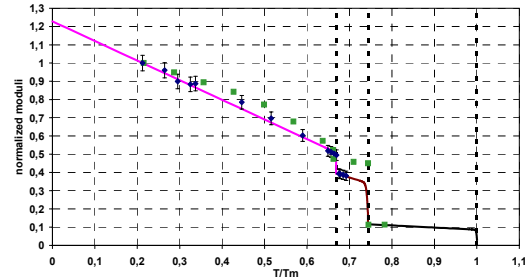


Fig 2: Normalized shear modulus variation of the U-V (\bullet) versus temperature with the associated modelling (-). Comparison to normalized Young modulus (\blacksquare).

Figure 3 shows the latest results obtained at the end of 2005 for α -Pu. The evolution of the normalized time of flight of the longitudinal wave and the normalized variation length are compared up to $T/T_m = 0.74$. It can be seen that the time of flight variation versus temperature is the same for the two samples. These changes are coherent with the curve of variation length but the amplitudes are different which means that there are probably problems on the experimental set up. Indeed, with this contact device, the samples are under strains and their dimensions are not kept, especially because of the important thermal expansion of the material.

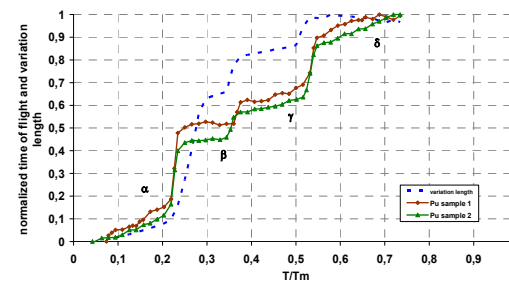


Fig 3: Normalized time of flight of longitudinal wave and variation length versus temperature for α -Pu.

CONCLUSION

Our next goal is to improve the contact device by reducing the strain on the samples, especially to improve characterization of materials having an important thermal expansion coefficient. Our measurements have to be completed by longitudinal and shear wave velocity measurements to determine all the elastic moduli of U-V alloy and α -Pu. For this latter, dilatometric measurements have to be realized with respect to the temperature kinetic of ultrasonic measurements and the material composition.

REFERENCES

1. M.-H. Nadal and P. Le Poac, J. Applied Physics 93, 5, 2472-2480, (2003).
2. M. Fukuhara, A. Sanpei, J. of Mat. Sci. Let., 12, (1993).
3. M.-H. Nadal, C. Hermerel, C. Gondard and L. Paradis, 14th World Conference on NDT & INTEXT NDT, New Delhi (Inde) (1996).

Determination of single crystal elastic constants from polycrystalline material using X-ray diffraction: prospects for plutonium

B. Ravat^{*}, N. Baclet^{*}, E. Lépine[†], C. Valot[◇], Ch. Valot[◇], K. Inal[†]

^{*}CEA Centre de Valduc, Is sur Tille F-21120, France

[†]MECASURF, ENSAM, 2 cours des Arts et Métiers, 13617 Aix en Provence, France

[◇]CEA, Centre de Cadarache, 13108 St Paul les Durances, France

INTRODUCTION

The knowledge of the single crystal rigidity tensor is fundamental to define interatomic potentials used for the modelling of self-irradiation in plutonium alloys. Ultrasonic technique allows the determination of the elastic tensor components, but it requires single crystal, which is very difficult or even impossible to obtain for materials such as plutonium alloys. Thus, X-Ray diffraction (XRD) has been revealed to be an interesting technique since it allows to determine the X-ray Elastic Constants (XEC) which, combined with a polycrystalline model (self-consistent model^{1,2}), can be used to determine Single Crystal Elastic Constants (SCEC) from a polycrystalline material.

However, due to the difficulties in handling plutonium, the method has been first tested on copper, which has a face centred cubic structure and a high mechanical anisotropy, properties similar to those of δ -Pu.

ANALYTICAL AND EXPERIMENTAL APPROACHES

The SCEC are determined by applying a uniaxial stress to the polycrystalline sample thanks to a small 4-points bending device and measuring by using XRD the lattice planes spacing which is used as an internal strain gauge. The XEC corresponding to the $\{hkl\}$ lattice planes can then be determined. A scale transition relationship remains necessary to link the mesoscopic strains (scale of the crystallites) to the macroscopic stresses. First, a relationship between strains at different scales can be written with an equation of localisation:

$\varepsilon^m(\Omega) = A(\Omega) \cdot \varepsilon^l$, where ε^l and ε^m are the macro and mesoscopic strains, Ω is the crystallites orientation and $A(\Omega)$ is the localisation tensor of the self-consistent model defined as:

$A(\Omega) = [E \cdot (c(\Omega) - C) + I]^{-1}$ where E is the Morris tensor, c is the single crystal rigidity tensor, C is the macroscopic stiffness tensor and I is the identity matrix. This form for the localisation tensor takes into account the nature, orientation and shape (spheroidal grains) of crystallites. Moreover, the elastic behaviour within the limits of the anisotropic Hooke's law for the single crystal is expressed by: $\sigma^l = C \cdot \varepsilon^l$. Considering that the material is elastically isotropic at the macroscopic scale (not textured), neglecting the strain of second order and performing XRD experiments for $\phi = 0^\circ$ (which is the direction of the applied uniaxial stress), the following relationship, called "sin² Ψ ", is obtained: $\varepsilon_{\phi\Psi\{hkl\}} = [\frac{1}{2}S_2\{hkl\} \cdot \sin^2\Psi + S_1\{hkl\}] \cdot \sigma_{11}^l$ where $\frac{1}{2}S_2$ and S_1 are the XEC, σ_{11}^l is the applied stress and (Φ, Ψ) are the XRD measurement directions. An analytical expression of the self-consistent model, which takes into account the mechanical interactions between each grain and the elastic polycrystalline matrix, is then obtained. It allows to deduce the SCEC from the components of the macroscopic stiffness tensor C_{ij} (determined by

ultrasonic method) and the XEC: $\frac{1}{2}S_{2\{h00\}}$ and $\frac{1}{2}S_{2\{hhh\}}$. For cubic materials, the latter are calculated from the XEC experimentally determined for two $\{hkl\}$ lattice planes.

RESULTS

In order to validate the analytical and experimental approaches described above as well as the bending device accuracy, a first experiment has been performed on a rolled copper sample which ultimate tensile strength is 160 MPa. A second experiment has then been performed on annealed copper to reduce its ultimate tensile strength down to 50 MPa, closer to the one for the δ -PuGa alloys, which limited the range of applied stress. XRD experiments have also been performed to control that the sample was not textured since this can not be taken into account in the analytical expression of the self-consistent model. The components C_{ij} of the stiffness tensor have also been determined on the annealed sample. Since the diffractometer is out of glove box, the XRD experiments on plutonium alloys will have to be performed on samples confined in a 80 μ m thick polymer Rilsan sealed film. The last experiment on copper has been performed on a confined sample to check that the Rilsan film did not modify the applied stresses. All the results (values of c_{ij}) for the different experiments are presented in the figure 1. The values have been compared to those obtained from ultrasonic technique on a copper single crystal³. The results show a good agreement with a dispersal of values less than 10%, which validates both the analytical and experimental approach.

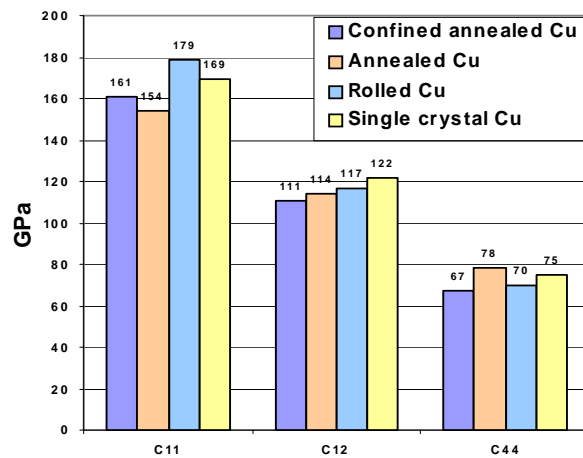


Fig 1: Copper single crystal elastic constants.

The values have been compared to those obtained from ultrasonic technique on a copper single crystal³. The results show a good agreement with a dispersal of values less than 10%, which validates both the analytical and experimental approach.

CONCLUSION

XRD experiments combined with an analytical expression of the self-consistent model have been revealed to be very satisfying for the determination of Single Crystal Elastic Constants from a polycrystalline material. The next step of this work, in progress, is to perform this experiment on radioactive materials and especially on δ -PuGa alloys.

1 Morris P.R., Int. J. Eng. Sci., **8**, 1970, 49

2 E. Kröner, Acta Metall., **9**, 1961, 155

3 Landolt-Börnstein, New Series, 18 Springer Verlag, Berlin, 1984

Shear modulus determination versus temperature up to the melting point using a laser-ultrasonic device

M.-H. Nadal, C. Hubert

CEA-Centre de Valduc, Département de Recherches sur les Matériaux Nucléaires
21120 IS-SUR-TILLE, FRANCE

INTRODUCTION

The shear modulus μ is one of the parameters needed to implement the constitutive laws. These mechanical properties can be measured for a solid or a liquid with different ultrasonic methods [1, 2]. This paper deals with the determination of $\mu(T)$ especially during the solid-liquid phase transition. Elastic wave velocity determination is performed by an original laser-ultrasonics device [3]. Indeed, owing to its non-contact characteristic, this technique has demonstrated its potential for high temperature measurement [4]. The present work focuses on Tin and proposes the simultaneous determination of the longitudinal and the shear velocities from the room temperature T_0 up to the melting point T_m . Indeed, a special effort was made to measure shear-wave velocity despite a strong attenuation function of the temperature. A continuous function $\mu(T)$ from T_0 to T_m is proposed, taking into account the drastic jump of the shear modulus at T_m , validated by experimental measurements.

EXPERIMENTAL SET UP

This study is devoted to the characterization of white Tin samples obtained by cold rolling ($T_m = 505$ K) in the temperature range [300 – 600] K. The samples have a parallelepiped shape with a square surface (15×15 mm²) and their thicknesses range from 1 mm to 5 mm. The experimental setup is composed of three main components: a Q-switched Nd:YAG laser operating at the wavelength of 1.064 μ m to generate ultrasounds; a Mach-Zehnder heterodyne interferometer [3] to measure the normal component of the mechanical displacement; a furnace with infrared lamps to control the temperature of the sample (1-10 K/min - temperature level better than 1/10 K). A sample is introduced inside a quartz cell located in a greater quartz tank filled by inert gas (Ar) to avoid oxidation effects, especially around the melting point.

EXPERIMENTAL RESULTS

The experiment principle is to determine the times of flight respectively of the longitudinal and shear waves in the solid, and of the longitudinal waves in the liquid. Measurements are performed in a transmission configuration at the epicenter. Correcting the thickness for thermal expansion, velocity is then determined versus temperature (V_{SL} longitudinal wave velocity in the solid; V_{LL} longitudinal wave velocity in the liquid; V_{SS} the shear waves velocity in the solid) (figure 1). These values of V_{SL} are in good agreement with the results of Nakano *et al* [5], even if a difference exists around the melting point because of a shift in the measurement of the temperature (in the quartz cell and not in the sample). The shear-wave attenuation, due to the approach of the melting, leads to a crucial difficulty of the shear velocity measurement. The elastic moduli are deduced from the previous results by using the well known following equations given for an isotropic solid. Furthermore, the density of the liquid Tin is given by a linear function versus temperature.

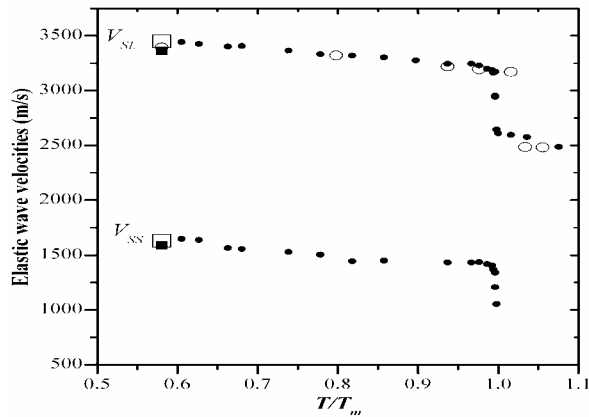


Figure 1: Elastic velocities of Tin versus temperature up to the melting point, (●) this study, (○) [5].

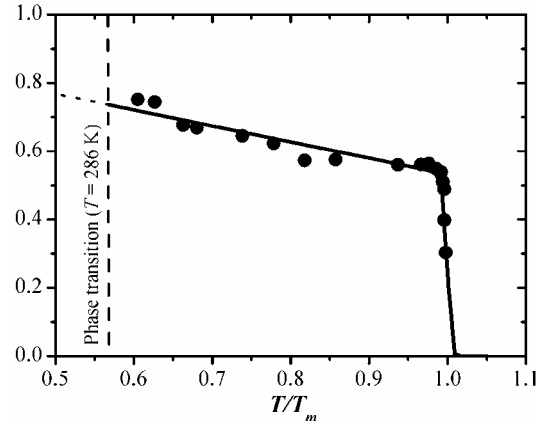


Figure 2: Evolution of the shear modulus μ/μ_0 of Tin versus T/T_m up to the melting point: (●) experiment and (—) the model.

For pure polycrystal metals, a $\mu(T)$ modeling [6] is proposed made of a continuous analytical expression over a large temperature range, from the absolute temperature to the melting point leading to:

$$T/T_m \in [0; 1+\varepsilon] \quad \mu(T) = \frac{\mu_0 [1 - a (T/T_m)]}{\mathfrak{Z}(T/T_m)}, \quad \mathfrak{Z}(T/T_m) = 1 + \exp \left[\frac{T/T_m - 1}{\varepsilon \left\{ 1 - \frac{T}{T_m(1+\varepsilon)} \right\}} \right] \quad (1)$$

where a is a positive factor, μ_0 is the shear modulus at 0 K. According to the intrinsic characteristics of the material, the model [Eq. (1)] becomes a full consistent model to describe the $\mu(T)$ evolution versus the complete temperature range of our study ($T/T_m \in [286/T_m; 1+\varepsilon]$). Figure 2 shows the comparison between some experimental data of the shear modulus versus temperature and the modeling. The fall of $\mu(T)$ around $T/T_m = 1$ is described rather well by the modeling. The results show $\varepsilon = 0.05$. It can be noted that the drastic fall of $\mu(T)$ around the melting point can be described by a function falling down to zero in a weak temperature range.

CONCLUSION

This paper shows the high potential of Laser-Ultrasonics to study the solid to liquid transition. Applied to Tin, this work succeeded in the determination of both longitudinal and shear wave velocities and the elastic moduli from ambient to the liquid. An analytical and continuous description of $\mu(T)$ is proposed and validated by the experimental data. The drastic fall of $\mu(T)$ at T_m is then described. Future projects deal with an innovating ultrasonic device to measure accurately surface-wave velocities connected to $\mu(T)$.

REFERENCES

- [1] H.J. McSkimin, Physical Acoustics, E. P. Mason, New York, Vol. 1A, Chap. 4, p.271, 1964.
- [2] D. J. Steinberg, S.G. Cochran, and M.W. Guinan, J. Appl. Phys. 51, 1498, 1980.
- [3] D. Royer and E. Dieulesaint, Appl. Phys. Lett. 49, 1056, 1986.
- [4] M. Paul, B. Haberer, and W. Arnold, Mater. Sci. Eng. A168, 87, 1993.
- [5] H. Nakano, Y. Matsuda, and S. Nagai, Meas. Sci. Technol. 9, 217, 1998.
- [6] E. Fraizer, M.-H. Nadal, R. Oltra, J. Appl. Phys., Vol 93, No 1, pp. 649-654, 2003.

The Effect Of Pressure On Phase Stability In The Pu-Ga Alloy System

D.R. Harbur

Los Alamos National Laboratory, Los Alamos NM 87544 USA

Abstract

In examining and analyzing over three decades of research on the transformations involved in the Pu-Ga alloy system, it has become evident that the data is comprised of many seeming incongruities and contradictions. Plutonium is not the easiest material to generate data on, and because of the complexities in its phase relationships, and its sensitivities to alloying, temperature and pressure, the analysis of the data is not always straightforward. The best technique that the metallurgy community has for identifying the different phases in Pu is x-ray diffraction, and many capable scientists have well developed the art as it is applied to Pu and its alloys. X-ray diffraction, however, is not a very good tool for studying non-diffracting disordered materials. In this paper we have shown that under certain processing methods large amounts of a non-diffracting disordered-state are formed in Pu-Ga alloys, which we call the amorphous-state. The amorphous-state is certainly not an equilibrium-state, but it nevertheless can be formed under certain pressure-states, and more surprisingly once formed can persist for extended times and temperatures at ambient pressures. Being a physical-state, the amorphous-state has distinct physical properties, meta-stability and sensitivities to Ga content.

When Pu is alloyed with small amounts of Ga and homogenized, the δ -phase can be stabilized over a reasonable temperature and pressure range. At low temperatures, the δ -phase will begin to transform to the α' -phase, with the transformation temperature being dependent upon the amount of Ga. At very low Ga contents near 1 at. % Ga the δ -phase will begin to transform very near room temperature and the transformation products are a mixture of the α' -phase and the amorphous-state. At 0.68 at. % Ga all of the δ -phase transforms into the α' -phase and the amorphous-state upon cooling to room temperature.

The δ -phase also becomes unstable at high hydrostatic-pressures, and this instability is also strongly related to the Ga content. The higher the Ga content, the higher the pressure before the δ -phase transforms to a denser-state. The transformation path is dependent upon the overall Ga content of the δ -phase.

At a Ga content of 1.0 at. % Ga the transformation begins by forming a mixture of the α' -phase and the amorphous-state. For this alloy, the α' -phase and amorphous-state mixture is stable upon pressure release even after small incremental pressure cycles just above the initiation of the transformation. It is believed that the large amount of amorphous-state formed early in the transformation cycle for this alloy disrupts the crystallographic alignment between the martensitic α' -phase and the parent δ -phase and is responsible for the martensitic α' -phase not transforming back to the δ -phase upon pressure release.

At a Ga content of 1.7 at. % the δ -phase first transforms directly to the α' -phase. After about 50% α' -phase is formed, the transformation changes to a $\delta \rightarrow$ amorphous-state transformation with a little more α' -phase forming either from the δ -phase or the amorphous-state. The amorphous-state in this mixture begins to transform to the α' -phase at pressures of 5-7 kbars. Pressure release at low pressures, where little of the amorphous-state has formed, results in the martensitic α' -phase transforming back to the δ -phase. The amorphous-state in these two lower Ga alloys slowly crystallizes into the δ -phase upon heating. When the α' -phase transforms into the β -phase, near the normal $\alpha \rightarrow \beta$ transformation temperature, the rejected Ga moves into the amorphous-state causing it to spontaneously crystallize into the δ -phase. This behavior shows that the relative stability of the amorphous-state to that of the δ -phase is dependent upon the Ga content.

At 2.5 at. % Ga the δ -phase initially transforms to the α' -phase. Only as the pressure approaches 10 kbars and the amount of α' -phase approach 60 % does any significant amount of the amorphous-state form in this alloy, and only after a 10 kbar pressure cycle does the phase-mixture remain stable upon pressure release. Even after a 10 kbar pressure-cycle the martensitic α' -phase transforms directly back to the δ -phase when heated. It appears that at this alloy content enough amorphous-state forms at 10 kbars to disrupt the $\alpha' \rightarrow \delta$ transformation on pressure release, but not enough forms to disrupt the $\alpha' \rightarrow \delta$ transformation during the heating cycle. The small amount of amorphous-state that forms in this alloy crystallizes into the δ -phase over a wide temperature range extending even into the normal β -phase temperature range.

In addition to the transformation start pressure being dependent upon the Ga content, the rate at which the δ -phase transforms to a denser material is also dependent upon the Ga content. As one would expect, the δ -phase in the lower Ga content alloys transforms faster than in the higher Ga content alloys. As pointed out above the rate at which the δ -phase transforms does not necessarily relate to the rate of formation of the products of that transformation. The δ -phase is transforming to two products in the lowest Ga alloy, but is only transforming to the α' -phase early on in the transformations of the two higher Ga alloys.

The existence of the amorphous-state requires innovative new tools for identification and analysis. The density/compressibility data presented in this paper is one such tool for analyzing the amorphous-state, but it requires other knowledge of the material for proper analysis. Disordered states are common in irradiated materials. In the on-going studies of aging effects in Pu, the existence of radiation damage, and irradiation particles and effects requires careful examination for the possibilities of amorphous-state development.

Strong Electron-Phonon Coupling in δ -Phase Stabilized Pu

Matthias J. Graf, Turab Lookmann, John M. Wills, Duane C. Wallace, Jason C. Lashley

Los Alamos National Laboratory, NM 87545 USA

ABSTRACT

Heat capacity measurements of the δ -phase stabilized alloy $\text{Pu}_{0.95}\text{Al}_{0.05}$ suggest that strong electron-phonon coupling is required to explain the moderate renormalization of the electronic density of states near the Fermi energy. We calculate the contributions of the heat capacity from the lattice and electronic degrees of freedom, as well as from the electron-lattice coupling term, and find good overall agreement between experiment and theory assuming a dimensionless electron-phonon coupling parameter of order unity, $\lambda \sim 0.8$. This large electron-phonon coupling parameter is comparable to reported values in superconducting metals with face-centered cubic crystal structure, for example, Pd ($\lambda \sim 0.7$) and Pb ($\lambda \sim 1.5$). In addition, our analysis shows evidence of a sizable residual low-temperature entropy contribution, $S_{\text{res}} \sim 0.4 k_B$ (per atom), which can be fit by a two-level system. Therefore, we speculate that the observed residual entropy originates from crystal field effects of the Pu atoms or from self-irradiation induced defects frozen in at low temperatures.

The actinide metal plutonium (Pu) exhibits six unique crystal structures in the solid state at ambient pressure between absolute zero and its melting temperature. The phases range in symmetry from simple monoclinic (sm) to body-centered cubic. The easily worked face-centered cubic (fcc) phase, denoted by δ , is thermodynamically stable in pure plutonium from 592 K to 736 K, and can be stabilized down to room temperature by small additions of trivalent elements such as gallium or aluminum. The effects of alloying have a profound impact on the electronic structure. Specifically, the low-temperature α phase (sm) of pure Pu has an enhanced Sommerfeld coefficient of $\gamma_S = 17 \text{ mJ}/(\text{mol K}^2)$ compared to a simple metal with typically $\gamma_S \sim 1 \text{ mJ}/(\text{mol K}^2)$, while the stabilized δ phase exhibits a moderately heavy electron mass with an enhanced Sommerfeld coefficient $\gamma_S = 50\text{-}70 \text{ mJ}/(\text{mol K}^2)$. It is believed that the high-volume δ phase has localized, nonbinding electrons, while in the low-volume α phase the electrons are itinerant and binding. This behavior resembles the Mott transition in correlated electron systems. In a recent calorimetry study, Lashley and coworkers [1] pointed out that the low-temperature data of the heat capacity of $\text{Pu}_{0.95}\text{Al}_{0.05}$ exhibit a moderately enhanced Sommerfeld coefficient, $\gamma_S = 64 \text{ mJ}/(\text{mol K}^2)$, and a λ -shaped anomaly around 60 K in C/T . These observations were suggestive to those authors to describe $\text{Pu}_{0.95}\text{Al}_{0.05}$ as an incipient heavy-fermion system.

The purpose of this study [2] is to give a quantitative description of the electron-phonon interaction on the conduction electrons in a plutonium alloy and whether the observed low-temperature λ -shaped anomaly in C/T is associated with a martensitic phase transformation. From this study we conclude that the observed anomaly is unlikely due to a full or partial martensitic phase transformation from the high-temperature δ phase into the low-temperature α' phase (note the substitutional binary alloy α' and α have the same crystal structure). Because on

cooling this transformation finishes around 130-180 K and is completely reversed on heating around 380 K. Instead of a structural transformation, we speculate that crystal field effects or self-irradiation induced defects and vacancies, for example, Frenkel pairs, are responsible for the reported excess entropy.

A direct consequence of our analysis is that the relatively strong electron-phonon coupling of order unity, necessary for describing the measured specific heat data, would suggest that the alloy PuAl should become superconducting below a few Kelvin. So far no evidence of superconductivity has been observed down to roughly 3 K.

We divide the calculation of the total heat capacity of a metal into a vibrational, electronic, electron-phonon coupling, and residual (everything else) term, $C = C_{ph} + C_e + C_{ep} + C_{res}$. One by one, we calculate their contributions and importance. Furthermore, we assume that the thermodynamic properties are dominated by the fcc δ -Pu crystal structure and any possible admixture of α' is negligible.

In Figure 1 we are comparing the combined total theoretical heat capacity with experiment. The agreement is excellent. Here we combine the individual contributions to the heat capacity, assuming an electron-phonon coupling parameter $\lambda \sim 0.8$ with Eliashberg's $\alpha^2 F(\omega)$ function that has an Einstein mode at 2.8 THz, a two-level system (TLS) with an occupation factor $n \approx 0.5$ and level splitting $T_{TLS} \approx 120$ K, as well as an electronic density of states peaked at the Fermi level.

In conclusion, we studied heat capacity measurements of a δ -phase stabilized PuAl alloy and calculated the vibrational, electronic, electron-phonon, anharmonic, crystal field, and structural transformation contributions. Thereby, we found several important aspects: (1) electron-phonon coupling is strong and cannot be neglected at low temperatures; (2) a residual excess entropy of order $S_{res} \sim 0.4 k_B$ (per atom) can be understood in terms of an additional internal degree of freedom, for example, crystal field effects or self-irradiation induced defects at plutonium sites; (3) a structural transformation from $\delta \rightarrow \alpha'$ occurs at temperatures too high, and is too small in magnitude, to account for the low-temperature excess entropy.

Acknowledgements

This work was supported by the U. S. Department of Energy at Los Alamos National Laboratory under contract No. W-7405-ENG-36.

1 J. C. Lashley et al., Phys. Rev. Lett. **91**, 205901 (2003).

2 M. J. Graf, T. Lookman, J. M. Wills, D. C. Wallace, J. C. Lashley, Phys. Rev. B **72**, 045135 (2005).

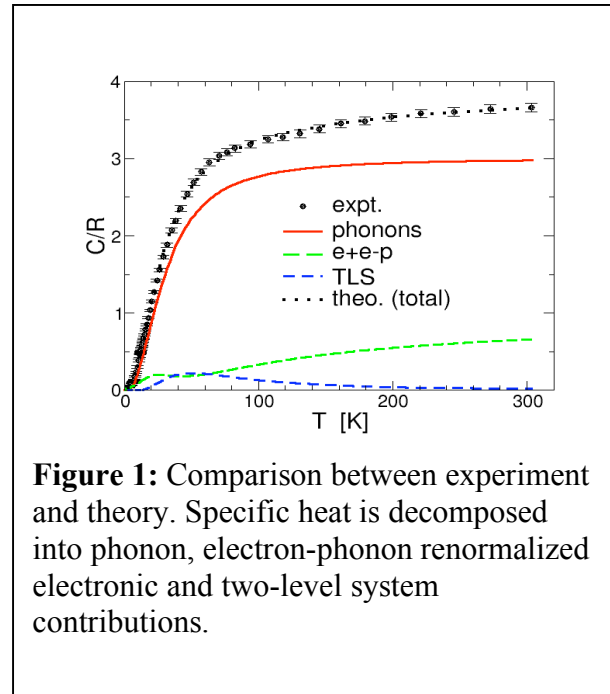


Figure 1: Comparison between experiment and theory. Specific heat is decomposed into phonon, electron-phonon renormalized electronic and two-level system contributions.

Bulk and Shear Modulus of Polycrystal Plutonium through the (α - β) and (β - γ) Phase Transitions¹

I. Mihut, J. B. Betts, H. Ledbetter, D. Dooley, D.A. Miller, A. Migliori

We used resonant-ultrasound spectroscopy to measure simultaneously the bulk and shear moduli of pure polycrystal Pu from 295K to 475K. Our measurements span the α - β and β - γ phase transitions. We used the known volume changes to obtain absolute values for the moduli of β and γ . When we add these measurements to our previous work, we obtain the behavior of the bulk modulus and the polycrystal shear modulus of pure Pu from 18K to 475K.

¹This work was supported by the National Nuclear Security Administration, The State of Florida, and the National Science Foundation.

Cerium Isomorphism and the δ - α Transformation in Plutonium

Andrew C. Lawson^{*}, Jason C. Lashley^{*} and Peter S. Riseborough[†]

^{*}Los Alamos National Laboratory, Los Alamos NM 87545 USA

[†]Physics Department, Temple University, Philadelphia, PA 19122-6082 USA

MODEL

Aptekar' and Ponyatovskiy (A-P) gave a model for the isomorphous γ - α transformation in cerium metal that is based on a putative binary phase equilibrium between the α and γ phases with energy difference ΔE , entropy difference ΔS , volume difference ΔV and energy of mixing U , all of which are materials parameters to be found from experiment. The difference in free energies of the two phases is

$$\Delta G(p, T, \Delta E, \Delta S, \Delta V, U) = RT[C \ln(C) + (1-C) \ln(1-C)] + [\Delta E - T \Delta S + p \Delta V]C + UC(1-C)$$

The phase diagram is determined by minimizing the Gibbs free energy with respect to C , the relative concentration of the phases. Excellent agreement with experiment is found for the choices $\Delta E = 505$ Cal/mole, $\Delta S = 3.69$ Cal/mole-K, $\Delta V = 3.4$ cm³/mole and $U = 2200$ Cal/mole, as shown in the calculated phase diagram of Figure 1.

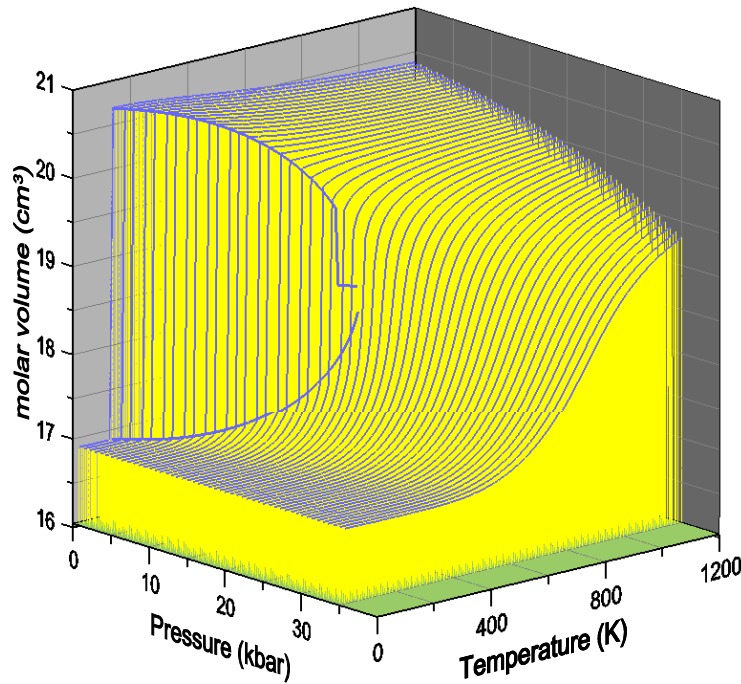


Fig.1. Phase diagram of cerium metal calculated with the A-P model.¹

PU-GA LATTICE CONSTANTS

Chemical periodicity indicates the possibility of describing the extreme properties of plutonium with a cerium model. We used the Aptekar'-Ponyatovskiy model to describe the δ - α transformation in plutonium metal. The α -phase is not isomorphous with δ , but it is nearly so, and the volume change is comparable with that observed for cerium. For appropriate choices of the parameters we can fit the lattice constant versus temperature curves of Pu-Ga alloys, where the parameters ΔE etc. are now assumed to depend on gallium concentration. The discontinuity in the lattice constant of unalloyed Pu is a consequence of the model.

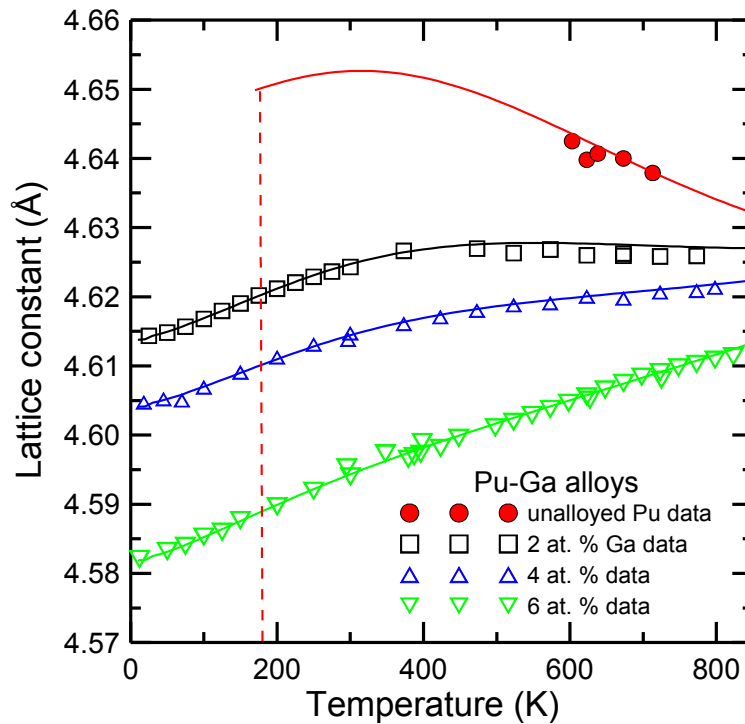


Fig.2. Lattice constants of δ -phase Pu-Ga alloys measured by neutron diffraction² (points) and their fit with the A-P model¹ (lines).

The energy of mixing, U is found to be ~ 2600 Cal/mole, equivalent to the energy of 1300K used in the invar model² of the lattice constants. We will give further details on the application of the A-P model to the problem of δ -phase stabilization.

This research was conducted under the auspices of the United States Department of Energy.

1. I. L. Aptekar' and Ye. G. Ponyatovskiy, Fiz. metal. metalloved. **25** 777 (1968) and Fiz. metal. metalloved. **25** 1049 (1968).
2. A. C. Lawson, J. A. Roberts, B. Martinez and J. W. Richardson, Jr., Phil. Mag. B **82** 1837 (2002).

Crystallographic anisotropy in the compression of some f-electron metals

Jagan Akella, Reed Patterson, Chantel Aracne-Ruddle
Lawrence Livermore National Laboratory, Livermore, CA 94550

The complex crystal and electronic structures of the f-electron metals give rise to interesting behavior when these materials are subjected to high pressures and temperatures. Several of these metals show a symmetry lowering transition, which is attributed to delocalization of the f-electrons. In recent high-pressure experiments on low symmetry α -Uranium, we have observed anisotropic compression. Although condensed matter physics theory has predicted Uranium should undergo a phase transition, there is to date no experimental evidence for this from studies up to 1 Mbar. We will present a detailed study of the metal, showing interesting variation in both axial ratios b/a and c/a with increasing pressure. This observation is in accord with the proposal made by Akella et al., (1990) that the orthorhombic axes in Uranium show “differential” compression. In addition, we will compare our data with that from Behan et al., 2003. It is evident from our study that more detailed and careful studies are needed to ascertain whether other lighter actinides show similar anisotropic compression.

THE ASSESSMENT OF PHASE DIAGRAM OF THE U-ZR SYSTEM

A.L.Udovsky*, D.A.Vasilyev*, H.A.J. Oonk†

* A.A. Baikov Institute of Metallurgy and Material Sciences RAS, Moscow, Russia

† Chemical Thermodynamics Group, Faculty of Chemistry, Utrecht University, CD Utrecht, The Netherlands

In [1] we have calculated preliminarily different parts of phase diagram of the uranium - zirconium system, which have not included phase equilibria with $U_{0.333}Zr_{0.667}$ – base solid solution (δ – phase). In [2] we have calculated stabilities parameters for metastable ω –phases, which is isomorphic with δ – phase, for pure Zr and U as well as calculated phase diagram of the U-Zr system into 850 – 2100 K. It is necessary note that calculated stability parameters for metastable ω – and HCP-phase of the pure uranium to put in difficulties, since the δ – phase become metastable at temperature interval below 800 K. These calculated results were contradicted with experimental phase diagram.

In present report we have assessed stability parameters for metastable HCP – phase of pure uranium by using ab-initio pseudopotential calculated results for cohesive energies and bulk modulus for different phases of uranium at 0 K. We have obtained differences enthalpy and entropy (only vibrational part) between HCP- and BCC-phases of uranium as well as re-calculated interaction parameters for different phases of the U-Zr system.

We have applied a new minimization algorithm with the goal function (the generalized χ^2 – method [4]) to calculate phase diagrams and thermodynamic properties of binary system for solution of indirect task (calculation interaction parameters for BCC- phase, β -U – base solid solution, δ – phase solid solution, α -U – base solid solution, HCP-Zr – base solid solution) for the uranium - zirconium system. We have compared calculated as thermodynamic properties as function of composition and temperature for as phase diagram with experimental data obtained by different scientists, which have been assessment in the review [5].

As a result we have calculated phase diagram of the U-Zr system in temperature interval from 600 up to 2123 K, at that δ – phase become thermodynamic stable in temperature interval from temperature of peritectoid reaction up to 600 K and below.

As test we have compared predicted temperature dependencies of thermodynamic properties of alloys different compositions for the uranium - zirconium system [6], which we have not used in optimisation procedure, with experimental data.

Acknowledgements

The work supported by Dutch-Russian Program NWO-RFBR (Project № 047.011.2001.011) and Russian Federation Target Program “Integration” (Project B0056)

- 1 A.L.Udovsky, D.A.Vasilyev, M.Jacobs, H.A.J.Oonk. Program & Abstracts of CALPHAD XXXII, La Malbaie, Quebec, Canada, May 25-30, 2003, p. 122.(2003)
- 2 A.L.Udovsky, D.A.Vasilyev, H.A.J.Oonk. CALPHAD XXXIV, May 22-27, 2005, Maastricht, The Netherlands. Programme and Abstracts. Univ.Utrecht, p.77. (2005).
- 3 M.Freyss, Th.Petit, J.-P. Crocombette. J.of Nucl. Mater. V.347 p.44-51 (2005).
4. A.L.Udovsky. Russian Metally, № 2, p.136-157 (1990).
5. R.I. Sheldon, D.E. Peterson. The U-Zr (Uranium-Zirconium) System. Los Alamos National Laboratory. Bulletin of Alloys Phase Diagrams. Vol.10, № 2, 165-181 (1989).
6. Y.Takahashi, K.Yamamoto, T.Ohsato, H.Shimada, T. Terai. J. Nuclear Materials, v.167, p.147-151 (1989).

Lattice dynamics and thermodynamics of light actinides

J. Bouchet and G. Jomard

CEA-DAM, DPTA, Bruyères-le-Châtel, France

INTRODUCTION

Despite the general interest in f -electron elements, details about their phonon-dispersion relationships are very limited. Experimentally, this fact is due to the great difficulty of realizing such experiments. The most developed technique for the study of phonons, based on neutrons scattering, needs crystals large enough and isotopes with a small neutron absorption cross section. Lanthanides and actinides hardly satisfy these two conditions, not to mention the radioactivity of some of them. But recently, a new hope has emerged with several works, using inelastic x-ray scattering, mostly on U^{1,2} and Pu³. Nevertheless all this experimental issues show that theoretical works are needed to tackle the f electrons systems elastic properties. Unfortunately these calculations are far from straightforward. The most important problem comes from the difficulty to treat correctly the f -electrons and the relativistic effects, as the spin-orbit coupling, needed in such heavy materials. To our knowledge there is only one *ab-initio* spectrum for a f element, which was obtained by Dai⁴ on fcc plutonium.

Density functional perturbation theory (DFPT) is a well established tool for calculating the vibrational properties from first principles in the framework of the harmonic approximation. The crystal free energy is easily built by adding to the phonon contributions the 0 K isotherm, accessible to standard density functional theory (DFT) calculations. A step beyond the harmonic approximation can be made by allowing phonon frequencies to depend on crystal volume, the so-called quasiharmonic approximation. This approach has been shown to give an accurate description of the thermodynamic quantities of many bulk materials below the melting point. Taking into account the anharmonic effects through the volume dependence gives access to thermal expansion, phase transition and crystal stability.

RESULTS AND DISCUSSION

Here we apply the quasiharmonic approximation to the study of the thermal properties of Th metal, such as thermal expansion, bulk modulus or Debye temperature. In Fig.1 we display the phonon dispersion curves as calculated along several symmetry directions at zero pressure conditions (equilibrium volume). Our results⁵ are in very good agreement with neutron-scattering data at ambient condition⁶. We have also calculated the phonons spectrum of Th in the bct structure. The results are presented in Fig.2., and compared to the phonon dispersions of fcc. The T₁ branch strongly softens during the phase transition in fcc and becomes imaginary near the Γ point, in contrary, the frequencies of this branch increase with pressure in bct. This observation indicates that the fcc structure at this pressure is dynamically unstable. The soft phonon mode near the zone center is expected for the second order transition between fcc and bct since both

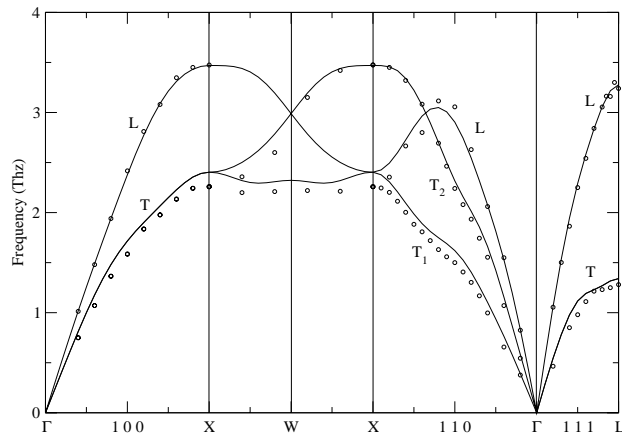
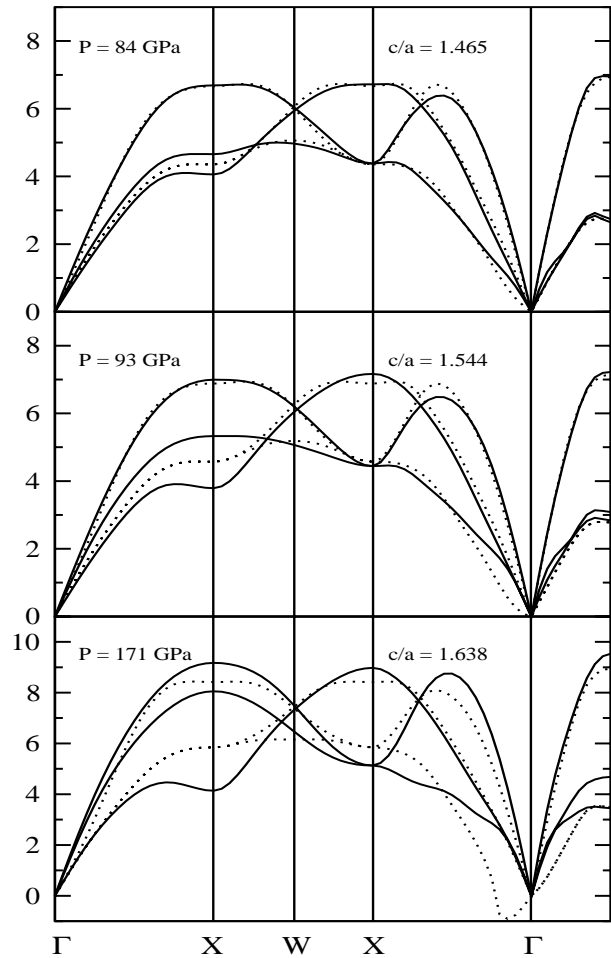


Fig 1: Calculated phonon dispersion curves for fcc Th at the lattice parameter corresponding to static equilibrium. Experimental neutron-scattering data are denoted by circles.

structures have one atom in their respective unit cell. We have also calculated thermodynamic properties of Th, as the linear thermal expansion or specific heats.

Using DFPT we have studied the pressure dependence of the elastic constants of the light actinides (Th, Pa, U, Np and Pu), the results help to understand the stability of the complex structures adopt by these metals. The phonons spectrum of U has also been calculated, this will shed light on the origin of charge density waves in this material and the nature of vibrational softening observed experimentally¹. Phonons spectrum for fcc Pu obtained in GGA are compared to the DMFT results⁴.

This work will help to understand the effect of electronic structure on lattice dynamics in *f*-electron metals.



Calculated phonon dispersion curves for bct (solid lines) and fcc (dashed lines) Th for pressure and *c/a* ratios in the transition region. The symmetry directions are those of fcc.

- 1 M. E. Manley, *et al.*, Phys Rev Lett **86**, (2001).
- 2 M. E. Manley, *et al.*, Phys Rev B **67**, (2003).
- 3 J. Wong, *et al.*, Science **301**, (2003).
- 4 X. Dai *et al.*, Science **300**, (2003).
- 5 J. Bouchet, F. Jollet and G. Zerah, submitted to Phys Rev B, cond-mat.
- 6 R.A. Reese, S.K. Sinha and D.T. Peterson, Phys Rev B **8**, (1973).

Contribution to the U-Ga Phase Diagram

Shai Salhov^a, Giora Kimmel^a, and M P. Dariel^b

^aNuclear Research Centre - Negev, P O Box 9001, IL-84190 Beer-Sheva, Israel

^bDepartment of Materials Engineering, Ben-Gurion University of the Negev,
P O Box 653, IL-84105 Beer-Sheva, Israel.

INTRODUCTION

Three Ga-rich intermetallic compounds, namely UGa_3 , UGa_2 and U_2Ga_3 were reported by Buschow¹ in the U-Ga binary system. No information was provided regarding the U-rich side of the diagram, in particular, regarding the solubility of Ga in the three allotropic phases of uranium. Dariel et al.² have shown that the compound with the highest uranium content was actually U_3Ga_5 , space group Cmc₂m, Pu₃Pd₅-type, and not the previously reported U_2Ga_3 . In a series of studies, Dayan et al.³⁻⁶ reported that U(Ga) β -phase alloys can be retained at room temperature where they eventually transform via a shear-like transformation into a mixture of α' -U(Ga), a monoclinic variant of orthorhombic α -U³, and the U_3Ga_5 compound. In the present communication we provide further information regarding the uranium-rich side of the U-Ga diagram.

EXPERIMENTAL

Uranium metal lumps with 300 ppm metallic impurities and Ga, 99.95% pure were melted on the water cooled copper hearth of an arc furnace under a 0.4 bar, gettered argon atmosphere and cast into split copper crucibles. The U(Ga) alloy samples, wrapped in thin Ta foils underwent various heat treatments in evacuated pyrex ampoules. The samples were characterized using conventional optical microscopy, XRD, SEM, DTA techniques.

The solubility limit of Ga in the high temperature γ and β -phases of uranium was determined by electron microprobe measurements on a U15at.%Ga sample. Since the U_5Ga_3 compound has the highest U content in the phase diagram, the U15at.%Ga samples were in all instances two-phase alloys containing some U_5Ga_3 compound and a U-rich solid solution. As had been shown previously³⁻⁶, β -phase alloys can be retained at ambient temperature by quenching; moreover, γ -phase alloys also transform by fast quenching into β -phase alloys retained at room temperature. Lengthy anneal in the U- γ temperature range leads to segregation of the U_5Ga_3 compound particles at the grain boundaries of the Ga-saturated U_γ grains, as shown in Fig.1. Upon quenching from this γ -range, the interior of the well and clearly delineated U_γ grains undergoes a transformation into Ga-saturated U_β as shown unambiguously by x-ray diffraction. Composition measurements of the Ga content, using WDS, at the interior of these grains quenched from different temperatures in the U_γ range, allows determining the temperature dependence of solubility limit of Ga in U_γ phase.

After aging treatments carried out in the U_β temperature range, using a similar procedure as the above-described one, it was possible to determine the solubility limit of Ga in the U_β phase. The solubility of Ga in U_β and in U_γ is reported in Table I. Clearly the solubility in U_β is much lower than in U_γ , nevertheless the latter when quenched to ambient temperature retains a greatly supersaturated in U_β structure. The rapid transformation of the U_γ solid solution into the in U_β solid solution during quenching suggests that it proceeds via a massive

transformation mechanism. The resulting 2-phase, $U_{\beta} + U_3Ga_5$, microstructure, shown in Fig. 1, is retained at room temperature and allows determining the composition dependence of the in U_{β} lattice parameters well beyond the solubility limit of Ga in the U_{β} phase, shown in Fig.2.

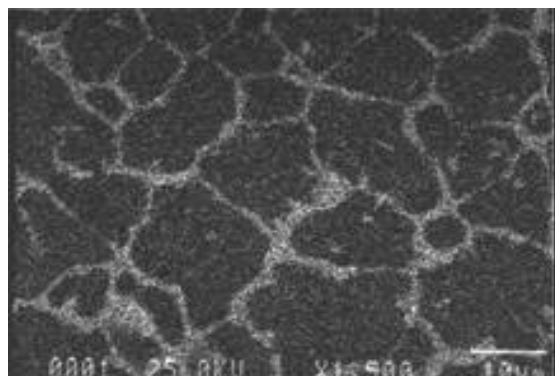


Fig.1. Ga distribution by $Ga_{K\alpha}$ mapping in a U-10at%Ga alloy annealed at 900°C and quenched to room temperature. The grain boundaries of the U_{γ} phase are clearly delineated by segregation of the U_3Ga_5 compound.

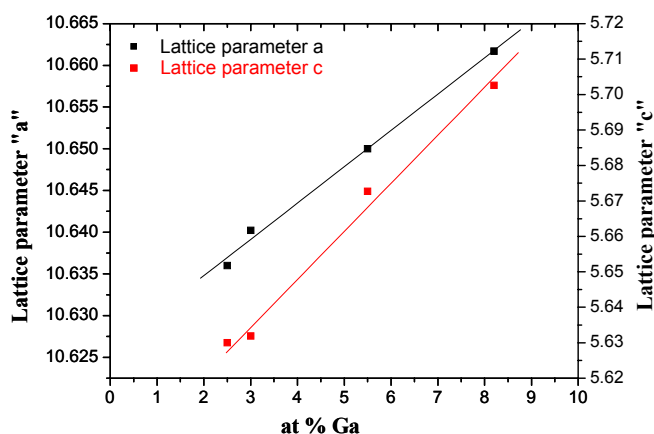


Fig.2. Composition dependence of the lattice parameters of the metastable $U_{\beta}(Ga)$ phase at ambient temperature.

Table I.
Solubility limit of Ga in U_{β} and U_{γ}

The kinetics of the greatly supersaturated U_{β} phase, quenched from the U_{β} temperature range are currently under investigation.

matrix	Temp.	Solubility limit
γ -U	1000°C	8.5±0.1 at%
	900°C	5.7±0.1 at%
	800°C	2.5±0.4 at%
β -U	710°C	1.8±0.2 at%
	680°C	1.2±0.4 at%

REFERENCES

1. K. H. J. Buschow, J. Less-Common Met. 31, (1973) 165.
2. D. Dayan, G. Kimmel and M. P. Dariel, J. of Nuclear Materials 135 (1985) 40.
3. D. Dayan, M.P. Dariel and M. Dapht, J. Less-Common Metals 121, 399 (1986).
4. D. Dayan, H. Klimker and M.P. Dariel, Met. Trans. 19A, 909 (1988).
5. D. Dayan, M. Talianker and M.P. Dariel, Met. Trans. 20A, 1163 (1989).
6. D. Dayan, H. Klimker, M. Talianker and M.P. Dariel, Met. Trans. 21A, 2125 (1990).

Formation of Higher Chloride Complexes of Np(IV) and Pu(IV) in Water Stable Room Temperature Ionic Liquid [BuMeIm][Tf₂N]

S.I. Nikitenko¹, P. Moisy²

¹ CNAB - UMR5084, BP 120 Le Haut Vigneau, 33175 Gradignan Cedex, France,

² CEA Valrho, DEN/DRCP/SCPS, Bat.399, BP 17171, 30207 Bagnols sur Cèze Cedex, France

A UV/VIS/NIR spectroscopic study shows that in [BuMeIm][(CF₃SO₂)₂N] hydrophobic room-temperature ionic liquid solutions, [BuMeIm]₂[AnCl₆] complexes, where BuMeIm⁺ is 1-*n*-butyl-3-methylimidazolium and An(IV) is Np(IV) or Pu(IV), have an octahedral An(IV) environment similar to that observed in solid complexes.

Water has no influence on the absorption spectra of AnCl₆²⁻ complexes, indicating their stability to hydrolysis in ionic liquid. Adding [BuMeIm]Cl modifies the UV/VIS/NIR absorption spectra of An(IV) in the ionic liquid and causes solids to precipitate. The solid-state reflectance spectra of the precipitates reveal considerable differences from the corresponding An(IV) hexachloro complexes. A voltammetric study indicates that AnCl₆²⁻ complexes are electrochemically inert in [BuMeIm][(CF₃SO₂)₂N] at the glassy carbon working electrode.

By contrast, quasi-reversible electrochemical reduction An(IV)/An(III) and An(IV) oxidation are observed in ionic liquids in the presence of [BuMeIm]Cl. The oxidation wave of noncoordinated chloride ions interferes with the An(IV) oxidation waves. The spectroscopic and voltammetric data clearly indicate the formation of nonoctahedral An(IV) chloride complexes with a Cl⁻/An(IV) ratio exceeding 6/1 in [BuMeIm][(CF₃SO₂)₂N] in excess chloride ions.

Study of Np Speciation in Citrate Medium

L. Bonin¹, E. Ansoborlo¹, C. Den Auwer¹, G. Cote², Ph. Moisy¹

¹CEA Vlarh  - DEN/DRCP/SCPS; BP 17171 - 30207 Bagnols sur C ze, France

²ENSCP, UMR 7575; 11, rue Pierre et Marie Curie 75231 Paris Cedex 05, France

In the framework of the French Environmental Nuclear Toxicology program, additional experiments related to the decorporation of actinides are planned. The lack of information on the neptunium behavior within blood and the inefficiency of therapeutic treatments, led us to study the complexation of this element with basic anions. Within this purpose, the *in vitro* behavior of Np(IV) and Np(V) in simple media simulating biological media was studied.

This study was more specifically focused on the behavior of neptunium with citrate ion. In order to determine the speciation of this system, spectrophotometry was more particularly used. Concerning the complexation phenomenon, the existence of several complexes of Np(V) with various acido-basic forms of the citrate anion was observed; regarding Np(IV), complexes with Cit^{3-} have been observed.

From the quantitative study of these equilibriums, the values of the absolute constants for the complexation of Np(IV) and Np(V) with citrate were determined: $\log K_{4,0,1}=16.3\pm 0.3$ and $\log K_{4,0,2}=15.0\pm 0.3$, $\{\log K_{5,0,1}=2.5\pm 0.2, \log K_{5,1,1}=1.6\pm 0.5, \log K_{5,2,1}=1.2\pm 0.2\}$ and $\{\log K_{5,0,2}=1.5\pm 0.3, \log K_{5,1,2}=0.9\pm 0.5, \log K_{5,2,2}=0.5\pm 0.3\}$. From those constants, E-pH diagrams were built, allowing thermodynamical predictions for the behavior of neptunium in citrate medium. Those predictions are in accordance with the experimental instability of Np(V) in presence of citrate, and lead to the conclusion that this instability is due to Np(V) disproportionation.

Given the pH and the citrate concentration in blood plasma, the state of a Np-Cit system at room temperature has been inferred, as well as the speciation of Np in citrate solution before *in vivo* injection.

Separation of Similar Elements and Isotopes Separation in Non-Stationary conditions

A.A. Kopyrin^{*}, M.A. Afonin^{*}, K. Moody[†]

^{*}Saint-Petersburg Institute of Technology, 26 Moskovsky av., 190013, Saint-Petersburg, Russia

[†]Lawrence Livermore National Laboratory, Livermore CA 94552 USA

INTRODUCTION

Extraction methods based on the achievement of a chemical equilibrium traditionally have received the greatest attention. If the separation factor of two elements approaches the value one, then the required number of extractors in the separation cascade increases infinitely. The problem of separation of elements with similar properties is still vital. Separation of similar elements and isotopes in a non-steady state condition is a prospective method to increase the separation factor. Liquid-liquid extraction driven by an oscillatory oxidation-reduction reaction in the aqueous phase could provide an opportunity for the separation of similar elements using the repetition of extraction/stripping in a single extractor. The multiple extraction scenarios should improve the separation by exaggerating the small kinetic differences between similar metal ions. The same effect is possible to apply to the separation of isotopes.

EXPERIMENTAL

To induce the oscillatory extraction-stripping process, the cyclic Belousov-Zhabotinsky (BZ) reaction (a cyclic electrochemical oxidation-reduction reaction) was used. The experimental set up consisted of two extractors coupled by a bulk liquid membrane (extractant – 0.5 M TBP in tetradecane). The aqueous phase of both extractors consisted of a solution of cerium, praseodymium and neodymium nitrates in sodium nitrate media in the presence of potassium bromate and malonic acid. The experimental set up is described elsewhere¹.

RESULTS AND DISCUSSION

A new separation-extraction method was created based on an oscillatory extraction/stripping process in two extractors coupled by a bulk liquid membrane. The experimental setup, designed to investigate the kinetics of non-stationary processes, was constructed at the Saint Petersburg State Institute of Technology in the Rare Earth department. This setup can be used to separate macro-concentrations of similar elements or to enrich isotopes.

To induce the oscillatory extraction-stripping process, the cyclic Belousov-Zhabotinsky (BZ) reaction (a cyclic electrochemical oxidation-reduction reaction) was used. It is shown that it is possible to use an oscillatory extraction approach to separate similar elements by using the differences in their kinetic properties. We have obtained experimental evidence of the separation of uranium, cerium and neodymium isotopes. It is shown that the separation of Rare Earth Elements using the oscillatory extraction method is more complete than is the separation of these elements in classical extraction systems. A mathematical model of non-stationary oscillatory extraction systems has been created. The model results are in good agreement with the experimental results. The possibility of applying this new technique to separate similar elements and isotopes from aqueous phases is discussed.

In this work we present data on the possibility of isotope enrichment by means of the oscillatory extraction. The experimental set up consisted of two extractors coupled by a bulk liquid membrane (extractant – 0.5 M TBP in tetradecane). The oscillatory extraction method is based on exaggerating the small kinetic differences between isotopes during competitive extraction driven by the BZ reaction. Oscillations between Ce(III) and Ce(IV) concentrations driven by the BZ reaction are the cause of oscillations in the equilibrium concentration of the extractant. This leads to a difference in the partition of isotopes between aqueous phases and an organic phase. The organic phase of bulk liquid membrane is enriched by “light” isotopes, and stripping to the second aqueous phase causes a further enrichment in these isotopes as well. A possible explanation of our results is based on the fact that due to the difference in the kinetic properties of the isotopes toward extraction and complexation, differences in the average concentrations of the isotopes appear in the organic phase. Therefore the difference in the isotopic concentrations in different extractors appears.

The separation of ^{142}Ce and ^{140}Ce isotopes between aqueous phases of two extractors coupled by bulk liquid membrane in the experiments with cyclic chemical oxidation/reduction was observed, with an enrichment factor of about 2.5%. In the same conditions the separation of the Nd isotopes (heavy isotopes of Nd – ^{144}Nd , ^{145}Nd , ^{146}Nd , ^{148}Nd and ^{150}Nd from the light isotope – ^{143}Nd) in the same experiment with an enrichment factor about 0.7-1.4% was observed

Acknowledgements. This work was supported by the U.S. Department of Energy, Office of Basic Energy Sciences, under grant RC0-20000-SC14 and RUC2-20011-ST-04 administered by the Civilian Research and Development Foundation.

Leach Resistance of Murataite-Based Ceramics

Stefanovsky^{*}, S.V., Yudintsev⁺, S.V., Perevalov^{*+}, S.A., Startseva^{*}, I.V.,
Varlakova^{*}, G.A..

^{*}SIA Radon, 7th Rostovskii lane 2/14, Moscow 119121 RUSSIA

⁺Institute of Geology of Ore Deposits RAS, Starominetnii lane 35, Moscow 109017
RUSSIA

^{*+} V.I. Vernadsky Institute of Geochemistry and Analytical Chemistry RAS, Kosygin st.,
19, Moscow RUSSIA

Introduction

Pyrochlore, murataite and related phases with fluorite-derived structure are considered as host phases for actinide (An) and rare earth elements (REE)¹. Producing combined structures consisting of pyrochlore (two-fold elementary fluorite unit cell) and murataite (three-fold) modules² we can adjust ceramic formulations for immobilization of An/REE-bearing waste with variable chemical composition. In our previous work³ we have proposed a baseline composition (wt.%): 5 Al₂O₃, 10 CaO, 55 TiO₂, 10 MnO, 5 Fe₂O₃, 5 ZrO₂, and 10 (An,REE)O₂ or (An,REE)₂O₃ yielding >90% of the phases containing murataite modules in their structure. Preliminary studies have demonstrated high leach resistance of the murataite-based ceramics³. Zoned structure of the murataite grains with depletion of the rim with An and REEs protects core with the highest An/REE content from leachate attack and reduces leach rates to levels which are lower than those for zirconolite and pyrochlore by 1 to 3 orders of magnitude. In the given paper we present new data on leaching of ²³⁹Pu and ²⁴¹Am from the murataite-based ceramic and preliminary results of a SPFT test for the Th- and U-bearing murataite-based ceramics with above-mentioned formulation.⁴

Results

Major results of MCC-1 test⁵ for the ²³⁹Pu/²⁴¹Am-bearing (Am was present in the PuO₂ used for specimen preparation as an impurity in amount of 0.1 wt.%) murataite-based ceramic are given in Table I. Leach rate of both Pu and Am reduced gradually with time and achieved after 49-56 days of leaching values of $\sim 1 \times 10^{-5}$ g m⁻² d and $\sim 2 \times 10^{-4}$ g m⁻² d, respectively. Am existing in a trivalent form is more leachable element than Pu, which is tetravalent in this ceramic,⁶ due to higher electronegativity.

SPFT test was performed using an apparatus delivered by Pacific Northwest National Laboratory, USA under contract between US DOE and SIA Radon. Particle size of the U- and Th-bearing powdered ceramics were 87.5 μ m and 112.5 μ m, respectively. Measured density of both the ceramics was 4.52 g/cm³.

Main results of SPFT leach testing show that the ceramic specimens exhibit extremely low leachability of U and Th in deionized water at 90 °C and pH=7. Average leach rates for these elements were found to be 2.40×10^{-5} and 1.14×10^{-6} g/(m² d), respectively.

Discussion

Pu leach rate (MCC-1 test at 90°C in deionized water) from the murataite ceramic ($\sim 10^{-5}$ g m⁻² d) is similar to that of Pu-bearing Synroc-C⁷ and zirconolite-rich Synroc⁸.

For the pyrochlore-based ceramics designed for excess weapons plutonium immobilization 7-day Pu leach rate ranged between 4×10^{-5} and $\sim 10^{-3}$ g m⁻² d⁻¹ (depending on type and amount of impurities) reducing to $\sim 1 \times 10^{-4}$ after 50 to 100 days and to $(0.8-3) \times 10^{-5}$ g m⁻² d⁻¹ after more than 300 days of leaching⁹. Thus, Pu leach rate from the

Table I. Leach data for the Pu/Am bearing murataite ceramic (MCC-1 test in Teflon container with deionized water at 90 °C⁸).

Leach time, days	Concentration in leachate, g/L		Mass of the nuclide leached, g		Leach rate, g m ⁻² d	
	Pu	Am	Pu	Am	Pu	Am
3	2.22×10 ⁻⁵	3.39×10 ⁻⁸	3.02×10 ⁻⁷	4.62×10 ⁻¹⁰	8.37×10 ⁻³	5.48×10 ⁻³
7	4.25×10 ⁻⁶	3.23×10 ⁻⁸	5.79×10 ⁻⁸	4.41×10 ⁻¹⁰	6.88×10 ⁻⁴	5.23×10 ⁻³
14	7.19×10 ⁻⁶	3.12×10 ⁻⁸	9.79×10 ⁻⁸	4.26×10 ⁻¹⁰	5.82×10 ⁻⁴	2.39×10 ⁻³
21	2.40×10 ⁻⁶	2.88×10 ⁻⁸	3.27×10 ⁻⁸	3.93×10 ⁻¹⁰	1.30×10 ⁻⁴	1.55×10 ⁻³
28	4.73×10 ⁻⁷	4.25×10 ⁻⁹	6.44×10 ⁻⁹	5.78×10 ⁻¹¹	1.91×10 ⁻⁵	2.34×10 ⁻⁴
35	6.51×10 ⁻⁷	6.53×10 ⁻⁹	8.87×10 ⁻⁹	8.90×10 ⁻¹¹	2.11×10 ⁻⁵	2.88×10 ⁻⁴
42	6.05×10 ⁻⁷	7.28×10 ⁻⁹	8.24×10 ⁻⁹	9.92×10 ⁻¹¹	1.63×10 ⁻⁵	2.68×10 ⁻⁴
49	7.76×10 ⁻⁷	6.60×10 ⁻⁹	1.06×10 ⁻⁸	8.99×10 ⁻¹¹	1.79×10 ⁻⁵	2.08×10 ⁻⁴
56	4.99×10 ⁻⁷	9.42×10 ⁻⁹	6.80×10 ⁻⁹	1.28×10 ⁻¹⁰	1.01×10 ⁻⁵	1.90×10 ⁻⁴
63	6.64×10 ⁻⁷	1.19×10 ⁻⁸	9.04×10 ⁻⁹	1.62×10 ⁻¹⁰	1.19×10 ⁻⁵	2.14×10 ⁻⁴

murataite-based ceramic under steady-state conditions is by about one order of magnitude lower than from the pyrochlore-based ceramics. Higher leach rates at initial period (3 to 7 days) of leaching are probably due to dissolution of defect surface layer.

Ti release rate from the pyrochlore-based ceramics measured by SPFT test at 90 °C was found to be about 1×10⁻⁶ g m⁻² d⁻¹ at pH=7 and it increased to ~2×10⁻⁴ g m⁻² d⁻¹ at pH=2.¹⁰ U and Th leach rates measured in our tests were 2.40×10⁻⁵ and 1.14×10⁻⁶ g m⁻² d, respectively. Therefore, it can be expected that their release rates at pH=2 should be about ~10⁻⁴-10⁻⁵ and ~10⁻⁵-10⁻⁶ g m⁻² d⁻¹, respectively. Steady-state U and Pu release rates from the pyrochlore-based ceramics at 85 °C and pH=2 were found to be about ~10⁻⁴ g m⁻² d⁻¹.¹¹ Therefore, actinide release rates from the murataite-based ceramics are suggested to be by 1 to 2 orders of magnitude lower than those from the pyrochlore-based ceramics. Actual SPFT measurements of U and Th release from the murataite-based ceramics at pH=2 are in progress.

Acknowledgement

The work was supported from US DOE (Project RUC2-20009-MO-04).

References

1. Stefanovsky, S.V., Yudintsev, S.V., Gieré, R., Lumpkin, G.R., In Energy, Waste, and the Environment: a Geological Perspective, Geological Society, London, 236, 37-63 (2004).
2. Urusov, V.S., Organova N.I., Karimova, O.V., et. al., Transactions (Doklady) of the Russian Academy of Sciences/Earth Science Section, 401, 319-325 (2005).
3. Yudintsev, S.V., Stefanovsky, S.V., Omelianenko, B.I., Nikonov, B.S., Mat. Res. Soc. Symp. Proc. 663, 357-366 (2001).
4. Stefanovsky, S., Stefanovsky, O., Yudintsev, S., Nikonov, B. In: Proc. 35^{èmes} Journées des Actinides, Baden, Austria, April 23-26, 2005. Abstract E-19, CD-ROM.
5. Nuclear Waste Materials Handbook (Test methods), Rep. DOE/TIC-11400, Washington, DC (1981).
6. Yudintsev, S.V., Stefanovsky, S.V., Nikonov, B.S., et al/ In: Plutonium Future - The Science (2006), this volume.
7. Smith, K.L., Lumpkin, G.R., Blackford, M.G., et al/, Mat. Res. Soc. Symp. Proc. 465, 1267-1272 (1997).
8. Hart, K.P., Vance, E.R., Stewart, M.W.A., et al. Mat. Res. Soc. Symp. Proc. 506, 161-168 (1998).
9. Hart, K.P., Zhang, Y., Loi, E., et al. Mat. Res. Soc. Symp. Proc. 608, 353-358 (2000).
10. Icenhower, J.P., Strachan, D.M., McGrail, et al. Amer. Miner. 91, 39-53 (2006).
11. Strachan, D.M., Scheele, R.D., Buck, et al. Journ. Nucl. Mater. 345, 109-135 (2005).

XRD, SEM, TEM, and XPS Study of Pu-Bearing Murataite Ceramic

Yudintsev^{*}, S.V., Stefanovsky⁺, S.V., Nikonov^{*}, B.S., Teterin^{*+}, Yu.A. Ptashkin⁺, A.G.

^{*}Institute of Geology of Ore Deposits RAS, Staromonetni 35, Moscow 109017 RUSSIA

⁺SIA Radon, 7th Rostovskii lane 2/14, Moscow 119121 RUSSIA

^{*+}RRC "Kurchatov Institute", Kurchatov sq. 1, Moscow RUSSIA

Introduction

Murataite is considered as a promising host phase for actinides and rare earths as well as corrosion products and process contaminants in high level waste (HLW)¹. Murataite as well as pyrochlore has a fluorite-derived structure²⁻⁴. In general, pyrochlore, $A^{VI}{}_2B^{VI}{}_2O_{7-x}$ ($A = REE^{3+}, An^{3+/4+}, Ca^{2+}$; $B = Ti^{4+}, Zr^{4+}, Hf^{4+}$) and murataite, $A^{VIII}{}_3B^{VI}{}_6C^V{}_2O_{20-x}$ ($A = REE^{3+/4+}, An^{3+/4+}, Zr^{4+}, Ca^{2+}, Na^+$; $B = Ti^{4+}, Fe^{3+}, Mn^{3+/4+}, Al^{3+}$; $C = Mn^{2+}, Fe^{2+}$) being structure-related form a polysomatic series of the phases with modular structure and two- (2C - pyrochlore), three- (3C – murataite), five- (5C), seven- (7C), and eight-fold (8C) elementary fluorite unit cell⁴. All the phases with three-fold elementary fluorite unit cell and higher multiplicity, i.e. containing murataite modules in their structure are considered as murataite polytypes. Previously we synthesized and examined Pu-bearing murataite-based ceramics.⁵ In the present work the Pu-bearing murataite ceramic is characterized in more details in particular using X-ray photoelectron spectroscopy (XPS).

Results

The murataite ceramic with specified composition (wt.%): 5 Al₂O₃, 10 CaO, 55 TiO₂, 10 MnO, 5 Fe₂O₃, 5 ZrO₂, 10 PuO₂ was prepared by melting of oxide mixtures in a platinum ampoule at 1500 °C for 3 hours followed by quenching. The sample was characterized with X-ray diffraction (XRD), scanning electron microscopy – energy dispersive system (SEM/EDS), and transmission electron microscopy (TEM) – selected area electron diffraction (SAED). XPS spectra were measured with an electrostatic spectrometer MK II VG Scientific using AlK_α and MgK_α radiation under 1.3×10⁻⁷ Pa at a room temperature.

The ceramic is composed of predominant murataite-type phases: 5C, 8C and 3C, and minor Fe-Mn-titanate. Core of the murataite grains is composed of the 5C phase (the lightest on SEM-image) with the highest Pu content. The 8C phase with intermediate Pu content composes major bulk of the grains (light-gray). Rim is formed by the 3C phase (gray) with the lowest Pu content. Fe-Mn-titanate (dark-gray) is almost free of Pu.⁵

The low binding energy XPS from murataite exhibits the OVMO structure attributed to the outer Ca 4s, Pu 5f,7s, Zr 4d,5s, Fe 3d,4s, Ti 3d,4s, Mn 3d,4s, Al 3s,3p, and O 2p electrons, as well as the IVMO structure due to the Ca 3s,3p, Pu 6s,6p, Zr 4p, Ti 3p, Mn 3p, and O2s electrons (Table I). This binding energy range exhibits only the lines typical of the compounds studied. The Pu 4f spectrum of the sample exhibits the fine structure typical of the Pu⁴⁺ ions (Figure 1) with the doublet split at $\Delta E_{sl}=12.5$ eV. On the higher binding energy side from the basic peaks at $\Delta E_{sat}=7.4$ eV the typical shake up satellite of about 19% intensity was observed. The oxidation states of the elements were determined to correspond to the following ions: Ca²⁺, Ti⁴⁺, Mn²⁺, Fe³⁺, Zr⁴⁺, Al³⁺, Pu⁴⁺. The O1s spectrum consists of the two peaks at 530.0 and 532.1 eV. Taking into account equation $R_{M-O} = 2.27 (E_b - 519.4)^{-1}$, derived in⁶, on the basis of the O1s binding energy the interatomic distances R_{M-O} (nm) calculated are 0.214 nm and 0.173 nm. Probably the value 0.173 nm can be attributed to the hydroxide groups on the surface of the sample. The value $R_{M-O} = 0.214$ nm corresponds to average M-O distance in the murataite structure².

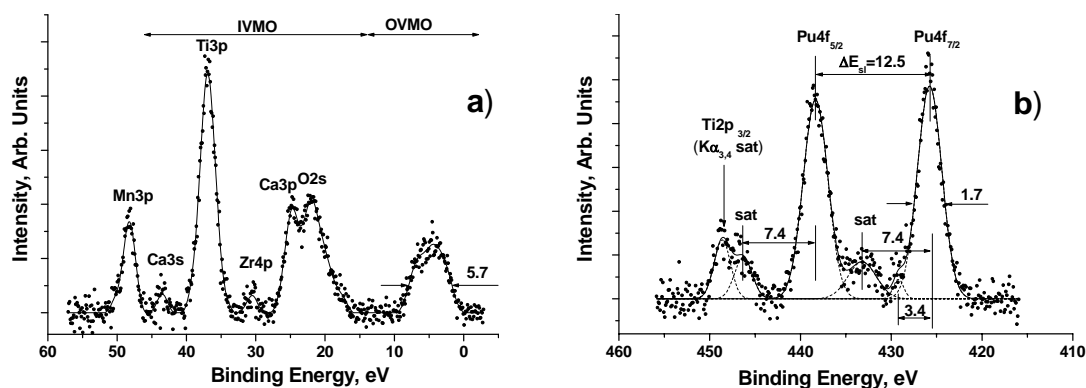


Figure 1. Low binding energy (a) and Pu 4f (b) XPS from the murataite ceramic.

Table. Binding energies E_b (eV) and FWHMs^{a)} (eV) of the outer (MO) and core electrons for the the actinide-doped murataite ceramics.

Ceramic	MO	Pu(Np) 4f _{7/2}	Ca2p _{3/2}	Ti2p _{3/2}	Mn2p _{3/2}	Fe2p _{3/2}	Zr3d _{5/2}	Al2p	O1s
Murataite	4.4; 22.0;	426.1	346.7	458.5	641.0	710.3	182.2	74.0	530.0
	24.7; 30.5;								7.4 sat
	36.9; 43.5;								(1.3)
	48.3								

^{a)}FWHMs are given in parentheses relative to the FWHM of the C1s-peak accepted to be 1.3 eV. Initial C 1s FWHM for Pu-bearing murataite is 2.1 eV.

Discussion

The phase composition and texture of the Pu-bearing murataite ceramic are typical of those for the murataite ceramics produced by melting and crystallization^{1,3-5}. Such ceramics are composed of zoned murataite grains with increasing of the number of the murataite modules in the structure of the murataite polytypes from core to rim. Because actinide content reduces in a series: 2C (pyrochlore) < 7C < 5C < 8C < 3C^{1,4,5} actinide depletion of the rim with respect to the core creates an additional barrier against their leaching into environment. As follows from XPS data such elements as Ca, Al, Ti, and Zr have their typical oxidation states (are present as Ca²⁺, Al³⁺, Ti⁴⁺, and Zr⁴⁺ ions). Transition elements - Mn and Fe were found to be mainly di- and trivalent, respectively. Occurrence of trivalent iron (Fe³⁺ ions) is consistent well with Mössbauer spectroscopy data⁷.

The work was performed under financial support from US DOE (Project RUC2-20009-MO-04).

References

1. Stefanovsky, S.V., Yudintsev, S.V., Gieré, R., Lumpkin, G.R., in Energy, Waste, and the Environment: a Geological Perspective, Gieré, R. and Stille, P. (eds) Geological Society, London, 236, 37-63 (2004).
2. Ercit, T.S., Hawthorne, F.C., Canad. Miner. 33, 1223-1229 (1995).
3. Ewing, R.C., Weber, W.J., Lian, J., Journ. Appl. Phys. 95, 5949-5971 (2004).
4. Urusov, V.S., Organova N.I., Karimova, O.V., Yudintsev, S.V., Stefanovsky, S.V., Trans. (Doklady) Russ. Acad. Sci./Earth Sci. Sec., 401, 319-325 (2005).
5. Stefanovsky, S., Stefanovsky, O., Yudintsev, S., Nikonov, B. In Proc. 35^{èmes} Journées des Actinides, Baden, Austria, April 23-26, 2005. Abstract E-19, CD-ROM.
6. Sosulnikov, M.I., Teterin, Yu.A., Rep. Acad. Sci. USSR (Russ.) 317, 418-421 (1991).
7. Urusov, V.S., Rusakov, V.S., Yudintsev, S.V., Stefanovsky, S.V. Mat. Res. Soc. Symp. Proc. 807, 243-248 (2004).

OPEN POSTER #4 Wednesday 3:30 PM



Elucidation of reactions yielding uranyl phosphate layers connected by organic amine cations.

T. Bray*, T. Albrecht-Schmitt*

*Department of Chemistry and Biochemistry, Auburn University, 179 Chemistry Building, Auburn, AL 36849, USA

ABSTRACT

Three two-dimensional uranyl phosphates, synthesized from the reaction of uranyl nitrate hexahydrate, phosphoric acid, and different organic amines, are presented in this poster. Two compounds, synthesized with 2,2'-bipyridine and 4,4'-bipyridine, are arranged in a pseudo-tectouranophosphate fashion in which the uranyl unit exists in an octahedral environment, bridged by four tetrahedral phosphate groups. The resulting layers are connected by self-assembled bipyridinium cations, directed by π -stacking. The final compound, produced in the presence of ethylene diamine, has a different structure in which the uranyl units are in pentagonal bipyramid geometry with three equatorial oxygens bridged to phosphate groups, and two equatorial oxygens allowing for dimerization between uranyl centers. This system of dimers and bridging phosphate groups allows for two-dimensional propagation. In all three, the negatively charged framework is charge-balanced by the presence of the amine cations.

Spectroscopic Studies of Intra-5*f* Fluorescence from $\text{Cs}_2\text{Np(VI)O}_2\text{Cl}_4$

M. P. Wilkerson and J. M. Berg

Los Alamos National Laboratory, Los Alamos NM 87545 USA

We have recently measured fluorescence from an excited 5*f* state of crystalline $\text{Cs}_2\text{Np(VI)O}_2\text{Cl}_4$ at room temperature following visible excitation. To date, the most successful efforts at rigorously describing the electronic structures of actinyl ions have focused on uranyl (U(VI)O_2^{2+}), which is a specific case that has no valence electrons in the 5*f* shell of the ground state.¹ The lowest-energy electronic transitions to occur in this system are ligand-to-metal charge-transfer (LMCT), in which an electron is promoted from a state of primarily ligand orbital character to a state of principally metal orbital character. These transitions are associated with an extensive series of vibronic bands with an energy spacing corresponding to the symmetric stretch, ν_1 , of the excited uranyl ion. Fluorescence-based methods have been applied quite successfully to work ranging from field surveys of uranyl dispersal in the environment to fundamental studies of electronic structure. In contrast to uranyl ions, all other chemically stable oxidation states of actinide species contain at least one electron in the 5*f* valence shell of the ground state. There are two types of transitions in the spectra of 5*f*^{*n*} (*n*>0) molecules; LMCT's and transitions that correspond to promotion of an electron from one state of predominantly 5*f* orbital character to another state of primarily 5*f* orbital character. These transitions lie in both the near-infrared and higher ultraviolet/visible region. Investigations of lower energy 5*f*-5*f* transitions of actinyl compounds are not well explored, and an insight into the nature of compounds with a single electron in the 5*f* shell could provide a unique opportunity to probe 5*f* electronic properties without introducing some of the typical complicating factors resulting from more than one electron in a valence shell.²

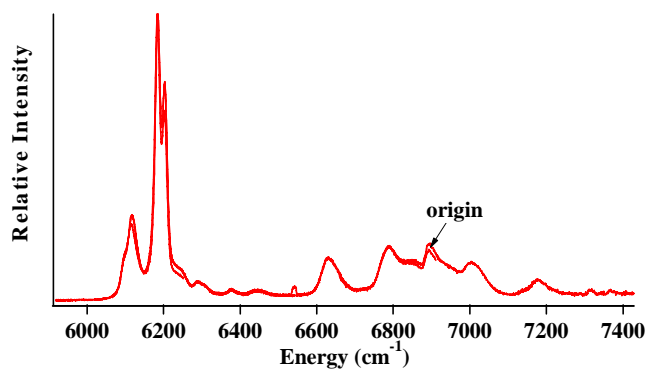


Fig 1: Fluorescence spectrum of $\text{Cs}_2\text{Np(VI)O}_2\text{Cl}_4$ at room temperature using an array detector following excitation at 633 nm (continuous wave).

Our prior work has shown that trans-dioxo forms of other actinides with partially filled 5*f* shells may also produce detectable fluorescence upon photo-excitation.³ In particular, we have demonstrated that a simple 5*f*¹ system, the neptunyl ion, luminesces with relatively high resolution and vibronic structure in the near-infrared at 77K, and more notably, it luminesces strongly at room temperature. Dilution of the luminescent analyte into host crystals was employed in order to study neptunyl fluorescence in the absence of potential self-quenching while offering some degree of control over the

local environment. In particular, neptunyl tetrachloride ($\text{Np(VI)O}_2\text{Cl}_4^{2-}$) was doped into the slightly larger isostructural uranyl tetrachloride ($\text{U(VI)O}_2\text{Cl}_4^{2-}$) matrix, which offers a large window throughout the near-infrared and most of the visible region and apparently lacks vibrational modes that could allow radiationless deactivation.

We will discuss here a more recent observation of near-infrared fluorescence from neat single crystals of $\text{Cs}_2\text{NpO}_2\text{Cl}_4$ following excitation at 633 nm. These characteristically broad spectra show that the relaxation pathway from the excited state of this material is competitive with radiationless deactivation at room temperature (Figure 1). Initial assignments of the vibronic bands, based upon energies of ground state vibrational modes of $\text{Cs}_2\text{NpO}_2\text{Cl}_4$, reveal the presence of hot bands. We will also compare time-resolved measurements of this compound with lifetimes of doped $\text{Cs}_2\text{U(Np)O}_2\text{Cl}_4$.

This research at Los Alamos National Laboratory was supported by NA-22, Office of Nonproliferation Research and Engineering, U. S. Department of Energy, National Nuclear Security Administration, and Division of Chemical Science, Office of Basic Energy Research, U. S. Department of Energy.

1. a) Denning, R. G. *Struct. Bonding (Berlin)* **1992**, 79, 215. b) Hopkins, T. A.; Berg, J. M.; Costa, D. A.; Smith, W. H.; Dewey, H. J. *Inorg. Chem.* **2001**, 40, 1820. c) Metcalf, D. H.; Dai, S.; Del Cul, G. D.; Toth, L. M. *Inorg. Chem.* **1995**, 34, 5573.
2. a) Denning, R. G.; Norris, J. O. W.; Brown, D. *Mol. Physics* **1982**, 46, 287. b) Denning, R. G.; Norris, J. O. W.; Brown, D. *Mol. Physics* **1982**, 46, 325.
3. Wilkerson, M. P.; Berg, J. M.; Hopkins, T. A.; Dewey, H. J. *J. Solid State Chem.*, **2005**, 178(2), 584.

Computational Modelling of Actinide Complexes

M. Benson, R. S. Herbst, D. Peterman

Idaho National Laboratory, Idaho Falls ID 83402 USA

The chemistry and separation of key radionuclides, primarily the actinides, lanthanides, and select fission products, figures predominately into the Global Nuclear Energy Partnership, notably in the area of advanced nuclear fuel cycles. Computational chemistry can play a role in that research by providing much needed information to the experimental scientists, information that may be extremely difficult or impossible to determine experimentally. At this time, computational efforts have been focused on one of the two most challenging and important areas in the development of an advanced fuel cycle: trivalent actinide/lanthanide (An(III)/Ln(III)) separation, with the second area being Cs/Sr separation.¹⁻³ In the concept of a closed fuel cycle, the minor actinides (Am, Cm, Np) are recycled to reactor fuels or transmuted, so efficient separation from the trivalent lanthanides is mandatory. This is due to the lanthanides high thermal neutron absorption cross-sections (they are neutron poisons), which substantially interferes with reactor efficiency.

The separation system of interest is the TALSPEAK process (Trivalent Actinide Lanthanide Separations by Phosphorus reagent Extraction from Aqueous Complexes). Separation of actinides and lanthanides is extremely difficult, though, due to their similarities. The softer donor atoms, specifically nitrogen and sulfur, coordinate preferentially to actinides.² This fact has been exploited in several separation methods, such as the nitrogen based TALSPEAK process, and the sulfur based Cyanex 301 extractants.

Modelling the actinides presents several problems, such as strong relativistic and correlation effects, that need to be addressed to obtain reliable and useful results. These problems arise from high charge, a large number of electrons, and the complexities of modelling the f orbitals. At this point, modelling has been focused on known extractants, with the goal of gaining insight into the coordination chemistry of these systems. Complexes of the minor actinides (Am, Cm, Np) and of Europium have been modelled using a variety of methods (UHF, MP2, uB3LYP, uPW91, uBLYP, and CAS, CAS-MP2 for the smaller systems). The results of these calculations will be presented.

This research was supported by The United States Department of Energy under Contract DE-AC07-05ID14517.

1. C. Madic, M. J. Hudson, J. O. Liljenzin, J. P. Glatz, R. Nannicini, A. Facchini, Z. Kolarik, R. Odoj, *New Partitioning Techniques for Minor Actinides*, Final Report, EUR 19149, Nuclear Science and Technology (2000).
2. M. Miguiritchian, D. Guillauneux, D. Guillaumont, P. Moisy, C. Madic, M. P. Jensen, K. L. Nash, *Inorg. Chem.*, **44**, 1404 (2005).
3. W. W. Schultz, L. A. Bray, *Sep. Sci. Technol.*, **22(2&3)**, 191 (1987).

Raman Studies Of Solid Plutonium Compounds

P. Rance and K. Webb

Nexia Solutions, Sellafield, Seascale, Cumbria CA20 1PG

RAMAN MICROSCOPE

A Raman Microscope has recently been installed in the active laboratories of Nexia Solutions at Sellafield in the UK and will be used as a tool in wide ranging studies covering both clean-up and decommissioning activities as well as forward looking fundamental studies investigating phenomena relevant to advanced reprocessing and waste management. This abstract describes the installation of the equipment, gives preliminary results and describes some future studies.

The Raman microscope (InVia, Renishaw) consists of Leica microscope (x5, x20 and x50 objectives) and Raman spectrometer with a peltier cooled CCD detector. Three lasers, argon ion (50 mW, 514 nm), helium-neon (17 mW, 633 nm) and near infrared diode (300 mW, 785 nm) are available.

PLUTONIUM SOLID STUDIES

Fumehood limits for active powders (3.7×10^6 Bq α) restrict plutonium dioxide holdings to somewhat less than 1 mg without resort to more exotic, long-lived isotopes (Pu-242,244). However, the focussing ability of the microscope optics is such that high quality spectra can be recorded from very small sample masses.

Figure 2, shows a Raman spectrum recorded from an approximately 10 ng sample of PuO₂ secured to an aluminium foil-backed glass microscope slide secured with adhesive cellulose tape. Spectrometer settings were 633 nm laser irradiation, 5% power, single capture. The

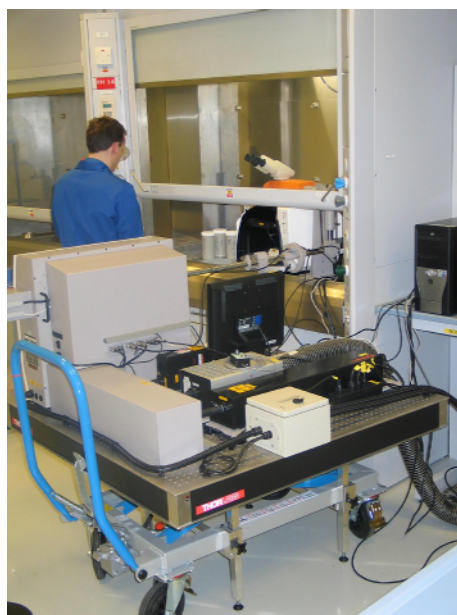


Figure 1. Raman microscope

spectrum clearly shows the single peak of PuO₂ at 476 cm⁻¹ (cf. 478 cm⁻¹ reported previously¹). The smaller peaks at just below 400 cm⁻¹ and above 800 cm⁻¹ are artefacts resulting from the mounting arrangement. Other preliminary results recorded from different samples have shown a slight variation in the peak position, down to 473 cm⁻¹, perhaps due to variation in sample stoichiometry although this is far from certain.

A range of plutonium bearing residues are to be characterised in future programmes with plutonium nitrate, chloride and oxalate samples to be analysed imminently.

Also purchased is a glovebox unit and associated fibre-optics. This is to be installed and commissioned during 2006 and will enhance significantly the utility of the spectrometer in analysing powder samples as the amount of material that can be handled will be increased substantially. This unit will be used in combination with infrared spectroscopy to study a number of aspects of plutonium chemistry relevant to its storage and encapsulation in ceramic wastefoms.

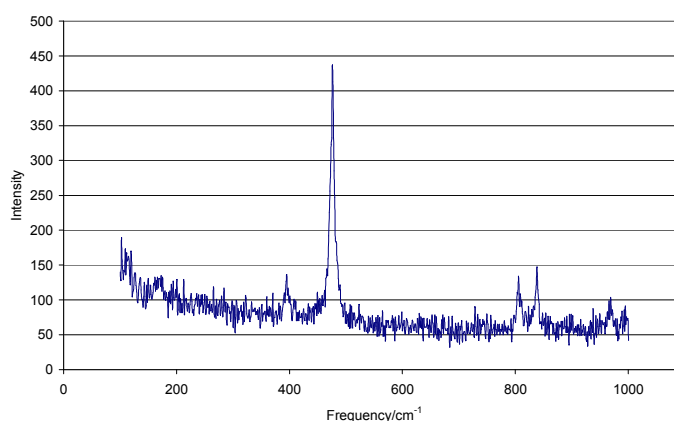


Figure 2. Raman spectrum of PuO₂

For example the interaction of water with the PuO₂ surface from monolayer coverage to 'damp powder' is being investigated in a number of ways including radiolysis of water/PuO₂ mixtures and desorption of water from PuO₂ within closed environments. Raman and infrared spectroscopy will form part of these studies in which samples are to be characterised prior to and following exposure to water vapour for varying lengths of time. Other potential applications include characterisation of non-stoichiometric oxides and analysis of amorphisation by radiation damage.

The authors would like to thank British Nuclear Fuels for financial support in purchasing the Raman Spectrometer used in this work and the [UK] Nuclear Decommissioning Authority for funding these studies as part of their commitment to supporting key skills.

1 G.M. Begun *et al.*, *J. Less-common Met.* **162**, 129 (1990)

Calculation of Low-Lying Excited States of PaO⁺ and PuO⁺

M. Mrozik,* R. Pitzer,* B. Bursten[†]

*The Ohio State University, Columbus OH 43209 USA

[†]The University of Tennessee, Knoxville TN 37996 USA

ABSTRACT

Recent experimental investigations into the reactivity of several actinide-oxide cations have identified a need for high accuracy calculations of some low-lying excited states. Questions that are still unanswered in the actinide systems regard the increased reactivity of some actinide oxide cations over their actinyl counterparts. Predictions of low energy transitions of actinide complexes have helped elucidate some of the more complicated bonding pictures that would be extremely difficult to assign without theory. The understanding of the nature of the bonding in actinide oxide cations will help explain their reactivity. Implementation of multiple-reference configuration interaction with single and double excitations (MR-CISD) including spin-orbit coupling within the *Columbus Suite* of programs allows for accurate determination of electronic configuration contributions to the overall wave function. Inclusion of medium size (68 electrons) effective core potentials (ECP) allow for determination of spin-orbit coupling effects present within the actinide species. Application of MR-CISD with ECP's has proven indispensable for actinyl ions and is used in this study to identify the ground and low-lying excited states in PaO⁺ and PuO⁺.

Acknowledgments:

This work was supported by Department of Energy Grant # DE-FG02-01ER15135.

Raman and Infra-Red Analysis of Plutonium Compounds

C. Puxley

Atomic Weapons Establishment, Aldermaston, Berkshire RG7 4PR, United Kingdom

INTRODUCTION

The unambiguous identification and characterisation of plutonium compounds rapidly by non-destructive means is a desirable goal in the area of plutonium chemistry. One of the fields that has the potential to achieve this is that of vibrational spectroscopy. The accumulation of both the Raman spectrum and the infra-red spectrum of a sample gives an unique fingerprint for the plutonium compound under study.

The hazards inherent with the manipulation of plutonium and its compounds necessitate strict containment of these materials and this has a negative effect on the ease of analysis. The options available are to either to site the analytical equipment inside the containment region or to have a link from the analytical equipment outside the containment area to a probe within the containment area. Results achieved using these two approaches will be presented.

FIBRE-OPTIC AND NON FIBRE-OPTIC SPECTROMETERS

The difficulties associated with working with plutonium make it preferable to conduct analyses of samples remotely, e.g. through fibre-optic cables interfaced to the glovebox containment. Whereas Raman spectroscopy lends itself easily to the employment of optical fibres to carry the laser radiation to the sample and the scattered laser radiation back to the detector, infra-red spectroscopy is not as pliant. Significant losses in the infra-red signal can occur through fibre-optic media and this results in a reduced sensitivity and efficiency for the analysis.



Figure 1: Miniature Infra-Red Spectrometer.

Advances in infra-red spectrometer technology have resulted in the production of spectrometers that are sufficiently small to be wholly accommodated within a glovebox (Figure 1).

The sample can be analysed using the technique of attenuated total reflectance (ATR). For this, the infra-red beam is reflected at a diamond/sample interface and directed to the detector where the infra-red spectrum is generated. Results obtained with a miniature infra-red spectrometer will be displayed.

ANALYSIS UNDER INERT ATMOSPHERES

Since certain plutonium compounds, such as plutonium tetranitrate, are oxygen and/or moisture sensitive, and other compounds of plutonium may be pyrophoric, it is necessary to obtain the vibrational spectra of these materials whilst they are under an inert atmosphere. In the case of the infra-red analysis, the siting of the entire infra-red spectrometer inside the glovebox means that the glovebox atmosphere must be inert.

In the case of the fibre-optic Raman spectrometer, cells may be constructed within which the sample is contained under an inert atmosphere. These cells may then be analysed in a glovebox with an air atmosphere without degradation of the sample. Examples of these cells and the Raman spectra obtained will be provided.

RESULTS

The Raman and infra-red spectra of a number of simple inorganic plutonium compounds will be presented. These spectra will be assigned according to the structure of the compound and the nature of the ligands attached to the plutonium.

The Use of Glovebox-Mounted High Resolution Inductively-Coupled Plasma Mass Spectrometry for the Analysis of Trace Metals in Actinide Materials

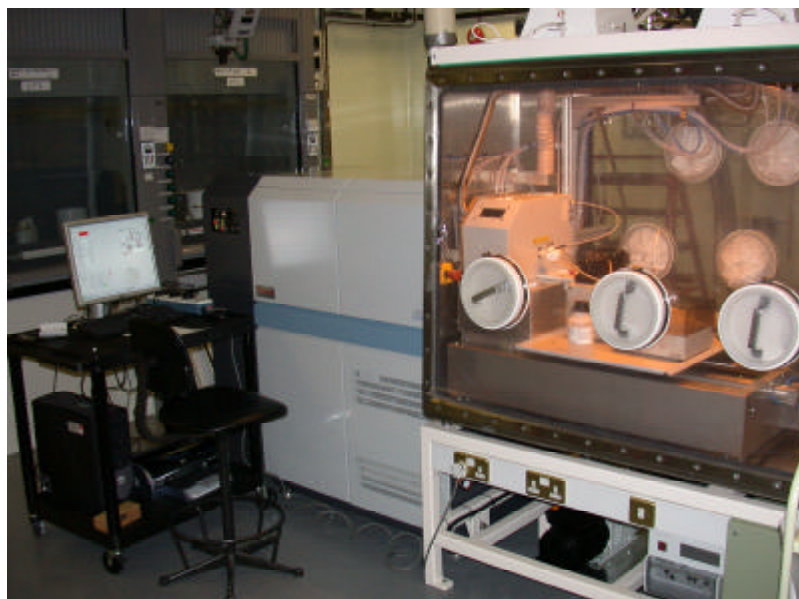
P. I. Kaye and O. J. Marsden

Atomic Weapons Establishment, Aldermaston, Berkshire, RG7 4PR, United Kingdom

INTRODUCTION

The presence of trace elements in plutonium and uranium materials can affect the mechanical, metallurgical and chemical properties of the materials. In addition, they may yield information on the source and age of the material. For these reasons, the identification and characterisation of the trace elemental content of actinide materials is of interest to AWE.

This poster will describe a glovebox mounted High Resolution Inductively Coupled Plasma Mass Spectrometer (HR-ICP-MS) recently installed at AWE (Figure 1). The performance and engineering aspects of the spectrometer will be discussed, as will the merits of double pass and cyclonic spray chambers for sample introduction.



The benefits of using ICP-MS in comparison to ICP-OES for trace metals analysis of actinide materials will also be considered¹. For example, at AWE, uranium samples are prepared for ICP-OES analysis by dissolution, followed by the extraction of uranium by tributyl phosphate (TBP). The use of ICP-MS allows the omission of the separation stage, affording significant reductions in sample preparation time and the volume of aqueous wastes generated

Figure 1: Glovebox-Mounted HR-ICP-MS

1 C. Mahan, S. Bonchin, D. Figg, D. Gerth and C. Collier. *J. Anal. At. Spectrom.*, **15**, (2000) p 929-935.

A high efficiency cavity ion source using TIMS for nuclear forensic analysis

S. Bürger^{*}, L. R. Riciputi^{*}, S. Turgeon^{*}, D. Bostick^{*}, E. McBay^{*}, M. Lavelle^{*}

^{*}Oak Ridge National Laboratory, Chemical & Isotope Mass Spectrometry Group, Transuranic Research Institute, Oak Ridge, TN 37831, USA

INTRODUCTION

The investigation of illicit trafficking of nuclear materials and non-proliferation control requires sensitive and isotope-selective detection methods to gain crucial nuclear forensic information like isotope ‘fingerprints’, allowing the origin and age of the sample of concern to be determined. One of the standard types of samples analyzed by IAEA’s Safeguards Environmental Sampling Program are environmental samples collected on cotton swipes by IAEA inspectors, which can contain picogram or even sub-picograms of plutonium. The analysis of plutonium for bioassay, or low-level environmental monitoring in the surrounding of a nuclear waste repository or nuclear facility might require the identification of even lower concentrations. Thus, sub-femtogram detection and characterization capabilities for plutonium are desirable.

Alpha-spectrometry, conventionally used for ultra trace detection of plutonium, is not well-suited for isotope resolved analysis due to the very similar alpha-energies of certain isotopes and the fact that the detection limit depends on the half-life of the isotope. In contrast, mass spectrometric methods provide detection limits independent of the half-life. Inductively coupled plasma mass spectrometry (ICP-MS), multi-collector inductively coupled plasma mass spectrometry (MC-ICP-MS), thermal ionization mass spectrometry (TIMS), and secondary ion mass spectrometry (SIMS) are routinely used for bulk or particle analysis of plutonium, with detection limits at the picogram to femtogram level [1,2]. Resonance ionization mass spectrometry (RIMS) demonstrates detection limits on sub-femtogram levels for isotope resolved analysis of plutonium [3,4], but no RIMS system is yet commercially available. Accelerator mass spectrometry (AMS) has a detection limit of low attograms of plutonium [5,6], with extremely high isotopic selectivity, but the experimental equipment of an AMS is rather complicated and costly, and sample utilization is generally inefficient.

HIGH EFFICIENCY CAVITY TIMS

The efficiency and thus the detection limit of a TIMS system can be enhanced by replacing the conventional ribbon filament with a high efficiency cavity (HEC) ion source [7]. Previous studies for uranium and plutonium at Oak Ridge National Laboratory and the IAEA’s Safeguard Analytical Laboratory showed promise for high efficiency [8] when utilizing this source. For a HEC, a rhenium, tungsten or tantalum rod with a narrow cavity bored into the end is used and the sample is loaded in the base of the cavity. The cavity is heated via electron bombardment, and the sample inside the cavity is thus evaporated and ionized. With higher operating temperatures, larger ratio of surface area to volume, and confined geometry, higher ionization efficiencies are potentially feasible.

We present here results using a HEC interfaced with a ThermoFinnigan Triton MC-TIMS to explore the accuracy, precision, efficiency and detection limit for several elements including strontium, neodymium and plutonium.

RESULTS AND CONCLUSION

For the HEC-TIMS instrument at ORNL, initial plutonium isotope ratio measurements focused on liquid samples loaded and dried in the cavity, as liquid loads allow for relatively straightforward sample handling. Isotope ratio measurements have been performed on loads down to femtogram levels of plutonium for certified reference material performed using a discrete dynode secondary electron multiplier (SEM) detector. With a total efficiency of about 0.2% (amounts of atoms loaded to ions detected), a detection limit of (0.1 - 1) fg of plutonium ($^{239-242}\text{Pu}$, ^{244}Pu) can be reported. These results were surprising, as the efficiencies were far higher in tests on previous HEC systems; similar or better efficiencies can be obtained using a normal ribbon filament. However, these earlier tests did not use liquid loads. Instead of introducing the analyte into the cavity as a solution, sub-millimeter resin beads containing adsorbed plutonium were loaded into the cavity.

To further investigate the HEC-Triton system, isotope ratio measurement experiments were performed on strontium and neodymium samples loaded using both liquid and resin bead methods. An efficiency of about 0.2% for Sr and about 1% for Nd has been achieved using liquid loads. Variable but much higher efficiencies (1 - 20%, average around 10%) are achieved when the samples are loaded on resin beads, significantly improving the sensitivity and detection limit for isotope ratio analysis of Sr and Nd. These results suggest that the use of bead loading should similarly enhance efficiency towards (5 - 25%) for plutonium and uranium [8].

The cause of the dramatic difference in efficiencies using bead and liquid loading is not currently understood. Further studies with different cavity materials (Re, W, Ta), cavity sizes, elements, and loading techniques will be performed to better understand the significant increase in efficiency using bead loading instead of solution loading.

Research sponsored by the Office of Non-Proliferation Research and Engineering (NA-22), National Nuclear Security Administration (NNSA), U.S. Department of Energy, under contract DE-AC05-00OR22725 with Oak Ridge National Laboratory, managed and operated by UT-Battelle, LLC.

- 1 R. N. Taylor et al., Journal of Analytical Atomic Spectrometry. **18**, (2003).
- 2 M. Betti et al., Analytical Chemistry. **71**, (1999).
- 3 C. Grüning et al., International Journal of Mass Spectrometry. **235**, (2004).
- 4 S. Bürger et al., Journal of Environmental Radioactivity. **in press**.
- 5 J. E. McAninch et al., Nuclear Instruments and Methods in Physics Research B. **172**, (2000).
- 6 L. K. Fifield et al., Nuclear Instruments and Methods in Physics Research B. **117**, (1996).
- 7 P. G. Johnson et al., Nuclear Instruments and Methods. **106**, (1973).
- 8 L. R. Riciputi et al., International Geological Conference Abstract. **32**, (2004).

Determination of $^{241}\text{Pu}/^{239}\text{Pu}$ Amount Ratio in PHWR-Pu Samples Using Isotope Correlations

S.K. Aggarwal and D. Alamelu

Fuel Chemistry Division, Bhabha Atomic Research Centre, Trombay, Mumbai 400 085, INDIA

INTRODUCTION

Data on the isotopic composition of Pu produced in power reactors are required to know the fissile content of Pu when used as a fuel in fast reactors. Also, this information is useful to determine the α -specific activity of Pu, which is required to calculate the weight percentage of ^{241}Am in any Pu sample as well as for the determination of Pu concentration by radiometric methods. Usually the amount ratios of different Pu isotopes in a Pu sample are obtained by thermal ionisation mass spectrometry (TIMS) which requires a detailed chemical separation procedure. This increases the amount of analytical effort, in addition to the cost per analysis. There are many instances when such data, if available with a reasonable accuracy by an alternative fast and cost-effective method, suffice for the purpose e.g. in assay of waste solutions by radiometric method. Isotope correlations can be used to generate the data, in such cases, without resorting to mass spectrometric analysis procedure.

We have developed and reported isotope correlations¹⁻³ for the determination of amount ratios of Pu isotopes, using the data obtained by alpha spectrometry and by thermal ionisation mass spectrometry. With these correlations, the amount ratios of different Pu isotopes, except for the one involving ^{241}Pu , could be obtained with reasonable accuracy (2 to 5%). The uncertainty on the correlation involving ^{241}Pu was large due to its relatively short half-life (14.4 yr) which necessitates the availability of Pu samples with known irradiation and cooling history. Thus an attempt was made to develop a simple and independent method for determining $^{241}\text{Pu}/^{239}\text{Pu}$ amount ratio. This method is based on the determination of total α and total β activity of Pu isotopes using a suitable liquid scintillation counter.

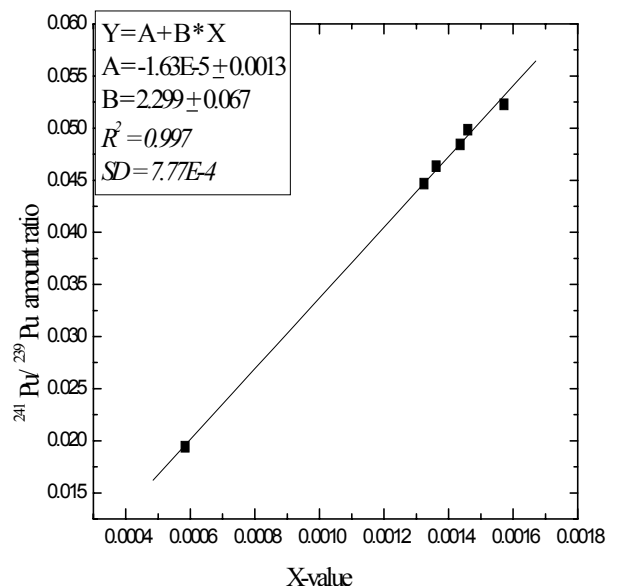


Fig 1. Correlation for the determination of $^{241}\text{Pu}/^{239}\text{Pu}$ amount ratio

The details of the experimental work carried out and the methodology developed for determining $^{241}\text{Pu}/^{239}\text{Pu}$ amount ratio are presented here. The decrease in the uncertainty of $^{241}\text{Pu}/^{239}\text{Pu}$ amount ratio along with the data on amount ratios of other Pu isotopes, obtained by isotope correlations, would improve the accuracy in the data on the percentage amounts of different Pu isotopes in the Pu sample.

EXPERIMENTAL

Five PHWR Pu samples, with varying amounts of different Pu isotopes, were used for the present study. The Pu samples were purified from ^{241}Am by anion exchange resin in 1:1 (v/v) HNO_3 using anion exchange separation and purification procedure. From each of the purified Pu samples, weighed amount (about 100 mg) of the solution was taken in a glass scintillation vial. The solution was dried under an infrared lamp. 5 mL of Ultima Gold AB scintillator (DIN based) was then added to the vial which was subjected to ultra-sonication for redissolving the Pu in the scintillation cocktail. The vials were then counted in a low back ground Liquid Scintillation Spectrometer for sufficient time in order to reduce the uncertainties due to counting. The total counts in the alpha region (100 to 400 keV) from ^{238}Pu , ^{239}Pu , ^{240}Pu and ^{242}Pu and in beta region (0 to 20 keV) from ^{241}Pu were recorded. The overall counts in the beta channel were much higher due to the high β specific activity of ^{241}Pu (half-life = 14.4 yr). In order to improve the statistics of measurements, the counts in the alpha region were recorded for 5 minutes.

Aliquots containing about 10 μg of Pu were taken for mass spectrometric analysis. The solutions were concentrated under an IR lamp and were loaded on to the vaporization filament of a double filament assembly of high purity rhenium. The TIMS used was equipped with a multi-Faraday cup detector system. $^{240}\text{Pu}/^{239}\text{Pu}$, $^{241}\text{Pu}/^{239}\text{Pu}$ and $^{242}\text{Pu}/^{239}\text{Pu}$ amount ratios were obtained by acquiring the data in static mode of multi-collection. $^{238}\text{Pu}/^{239}\text{Pu}$ amount ratios were determined by using electrodeposited sources of Pu samples and recording the alpha spectra using a 100 mm^2 PIPS semiconductor detector. The alpha spectra were acquired using a PC based multi-channel analyser. The $^{238}\text{Pu}/^{239}\text{Pu}$ amount ratios in the samples were calculated by using the $^{238}\text{Pu}/(^{239}\text{Pu} + ^{240}\text{Pu})$ alpha activity ratios determined by alpha spectrometry and $^{240}\text{Pu}/^{239}\text{Pu}$ atom ratio determined by TIMS, taking the half-life values of 87.74 yr, 24110 yr and 6553 yr, respectively for ^{238}Pu , ^{239}Pu and ^{240}Pu isotopes.

RESULTS & DISCUSSION

Using ratio of the total counts in the β region i.e. (0 - 20 keV) to total counts in the α region i.e. (100 to 400 keV) and knowing the pre-determined $^{238}\text{Pu}/^{239}\text{Pu}$, $^{240}\text{Pu}/^{239}\text{Pu}$ and $^{242}\text{Pu}/^{239}\text{Pu}$ amount ratios, a relation was established to determine the $^{241}\text{Pu}/^{239}\text{Pu}$ amount ratio ($R_{1/9}$) as given below:

$$R_{1/9} \propto (\text{Total } \beta / \text{Total } \alpha) \times [R_{8/9} \lambda_{238} + R_{0/9} \lambda_{240} + R_{2/9} \lambda_{242} + 1/\lambda_{239}] / \lambda_{241} \text{ -----(1)}$$

$$R_{1/9} \propto X \text{ -----(2)}$$

Figure 1 shows the correlation developed for the determination of $^{241}\text{Pu}/^{239}\text{Pu}$ amount ratio using the X value calculated as given in Eqs. (1) and (2), from ratio of total beta counts to the total alpha counts obtained by LSC and the amount ratios obtained from TIMS. It can be seen

that this relation is linear over the entire region of $^{241}\text{Pu}/^{239}\text{Pu}$ amount ratios expected for Pu from PHWR reactors. Table 1 gives a comparison of $^{241}\text{Pu}/^{239}\text{Pu}$ amount ratio obtained by TIMS as well as that calculated using the developed correlation for an unknown Pu sample. The two values agree well within 5 % showing the usefulness of the present methodology.

Table 1. A comparison on $^{241}\text{Pu}/^{239}\text{Pu}$ amount ratio determination by LSC and by TIMS

Atom % abundances by TIMS					β/α by LSC	$^{241}\text{Pu}/^{239}\text{Pu}$ by correlation	LSC / TIMS
^{238}Pu	^{239}Pu	^{240}Pu	^{241}Pu	^{242}Pu			
0.181	68.156	26.60	3.124	1.940	10.36	0.0452	0.987

It may be noted that since the amount ratio $^{241}\text{Pu}/^{239}\text{Pu}$ would reduce as a function of time due to radioactive decay of ^{241}Pu , the determination of the same will be possible by adopting the methodology discussed in this work. It may, however, be noted that the correlation presented here might be biased if there is a large difference in the cooling history (5 years or more), since the total alpha activity would also decrease due to the radioactive decay of ^{238}Pu (half-life 87.74 yr) in the sample.

The authors are thankful to Dr. V.Venugopal, Director of the Radiochemistry and Isotope Group of BARC, for his keen interest in this work.

1. S.K.Aggarwal and D.Alamelu, International Journal of Nuclear Energy and Science Technology **1**, 215 (2005).
2. D.Alamelu and S.K.Aggarwal, Radiochim. Acta **89**, 131 (2001).
3. S.K.Aggarwal, D.Alamelu and P.M.Shah, Radiochim. Acta **81**, 129 (1998).

High Resolution Alpha Spectrometry for the Determination of $^{240}\text{Pu}/^{239}\text{Pu}$ Amount Ratio in Pu Samples from PHWR

S.K. Aggarwal and D. Alamelu

Fuel Chemistry Division, Bhabha Atomic Research Centre, Trombay, Mumbai 400 085, INDIA

INTRODUCTION

Alpha Spectrometry is a useful analytical technique for the determination of alpha emitting isotopes in environmental, biological and nuclear fuel samples. Using the commercially available passivated and ion implanted planar silicon (PIPS/IPE) detectors, the best possible resolution that can be achieved is about 10 keV (FWHM) at 5.50 MeV using electrodeposited sources. But this resolution is not sufficient to allow complete resolution of the close-lying alpha energy groups in some of the important actinide isotopes. These include ^{240}Pu (5.168 MeV), ^{239}Pu (5.155 MeV); ^{238}Pu (5.499 MeV), ^{241}Am (5.486 MeV); ^{233}U (4.824 MeV), ^{234}U (4.784 MeV); ^{243}Cm (5.780 MeV), ^{244}Cm (5.804 MeV); ^{232}U (5.320 MeV), ^{228}Th (5.342 MeV) etc. It is nevertheless possible to employ sophisticated computer algorithms to resolve these close lying alpha energies and obtain information on $^{240}\text{Pu}/^{239}\text{Pu}$ amount ratios etc. However, most of these algorithms available previously were highly complex and could not be adopted by all the interested laboratories world-wide. Recently, under an International Atomic Energy Agency (IAEA) Coordinated Research Program (CRP) on the development of alpha spectrometry, a more generalized and user friendly version of the software (WinALPHA) for high resolution alpha spectrometry (HRAS) has been developed¹ and is now available to different users. The analytical function used in this program is a combination of an asymmetrical gaussian for the main part of the peak and a low energy exponential tail function. It was, therefore, considered interesting to employ this software for evaluating the precision and accuracy in the determination of $^{240}\text{Pu}/^{239}\text{Pu}$ amount ratios in NIST SRM-947 Pu as well as in Pu samples generated from Pressurized Heavy Water Reactors (PHWRs) using sources prepared in our laboratory and the alpha spectrometry system available with us. The values obtained from HRAS were compared with those determined experimentally by thermal ionization mass spectrometry (TIMS).

EXPERIMENTAL

For the determination of $^{240}\text{Pu}/^{239}\text{Pu}$ alpha activity ratio by HRAS, a few Pu samples obtained from PHWR reactors (burn-up about 10,000 MWD/TU) were taken up. These Pu samples were obtained after purifying the aliquots taken from irradiated fuel dissolver solutions, by using suitable anion exchange procedure in HNO_3 medium. Electro-deposited sources were prepared using electro-polished stainless steel disks as the backing material and a Pt stirrer as the anode. The sources were used as such, without heating in a flame or furnace. The alpha spectra were recorded using a 25 mm² PIPS detector, mounted in a vacuum chamber. The multiplets of $^{240}\text{Pu} + ^{239}\text{Pu}$ were resolved into individual components using the WinALPHA program, giving the abundances of all the alpha energy peaks of ^{240}Pu and ^{239}Pu as input in the software. For spectrum fitting, a region of 4.930 MeV to 5.200 MeV was used in all the spectra. Further, for the energy calibration, a value of 5.161 MeV, which corresponds to the average of the energies

of main peaks of ^{239}Pu (5.155 MeV) and ^{240}Pu (5.168 MeV) was used for the unresolved peak of $^{239}\text{Pu} + ^{240}\text{Pu}$ in addition to a value of 5.499 MeV for ^{238}Pu peak. This was found to be critical since otherwise the $^{240}\text{Pu}/^{239}\text{Pu}$ atom ratios were found to be positively or negatively biased w.r.t. mass spectrometric value when using the energy of ^{240}Pu or of ^{239}Pu peak alone, respectively for energy calibration.

RESULTS & DISCUSSION

Tables 1 and 2 give the typical results obtained after spectrum fitting on independent sources prepared from NIST-SRM-947 Pu and Pu samples from PHWR, respectively. $^{240}\text{Pu}/^{239}\text{Pu}$ atom ratios given in Tables 1 and 2 were obtained from the $^{240}\text{Pu}/^{239}\text{Pu}$ alpha activity ratios obtained by HRAS and using the half-life values of 24110 yr and 6553 yr, respectively for ^{239}Pu and ^{240}Pu . It is seen that the results obtained by HRAS for $^{240}\text{Pu}/^{239}\text{Pu}$ atom ratios in PHWR Pu samples as well as those in NIST-SRM-947 Pu² sample agree within 2 to 5% with TIMS values. These studies demonstrate the applicability of the new software developed under IAEA CRP for the determination of $^{240}\text{Pu}/^{239}\text{Pu}$ atom ratio by HRAS. Rigorous evaluation of the software by varying different parameters e.g. source quality, counting statistics etc. is planned in future.

The authors are thankful to Dr. V.Venugopal, Director of the Radiochemistry and Isotope Group of BARC, Mumbai for his keen interest in this work.

1. R.Capote Noy, E.Garcia-Torano, E.Mainegra, E. Lopez, Nucl. Instr. Methods in Phys. Res. **A 525**, 522 (2004).
2. D.Alamelu, P.M.Shah and S.K.Aggarwal, Nuclear and Radiochemistry Symposium, March 15-18, 2005, Guru Nanak Dev University, Amritsar (NUCAR 2005), (Eds. Keshav Chander, R.Acharya, B.S.Tomar and V.Venugopal), p.493 (2005).

Table 1. Typical data after spectral fitting using WinALPHA on replicate spectra for NIST-SRM-947 Pu

Source number	Area under the peak		Fitted parameters			$^{240}\text{Pu}/^{239}\text{Pu}$ atom ratio
	^{240}Pu	^{239}Pu	χ^2	Tail parameter	FWHM (keV)	
1	105761	120493	15.4	0.94	16.7	0.23856
2	212640	238013	39.2	1.06	17.8	0.24282
3	145356	157580	16.2	1.05	17.9	0.25071
4	106330	123130	11.9	1.03	17.1	0.23471

Certified $^{240}\text{Pu}/^{239}\text{Pu}$ atom ratio (corrected for decay) : 0.24099

Table 2. Typical data after spectral fitting using WinALPHA on replicate spectra for PHWR Pu samples

Sample no.	Source no.	Area under the peak		Fitted parameters			²⁴⁰ Pu/ ²³⁹ Pu atom ratio by HRAS	Mean value from HRAS/TIMS value
		²⁴⁰ Pu	²³⁹ Pu	χ^2	Tail parameter	FWHM (keV)		
1.	A	9479	5643	3.0	1.02	17.7	0.4566	1.029
	B	18843	11957	2.7	1.01	16.2	0.4283	
2.	A	20783	13031	3.5	1.02	16.9	0.4335	1.036
	B	18828	12553	2.6	0.96	15.8	0.4077	
3.	A	103041	72063	11.9	1.00	16.2	0.3886	0.986
	B	136125	97132	16.7	1.01	16.9	0.3809	
4.	A	141488	109582	11.9	1.05	17.6	0.3509	1.008
	B	150385	125655	15.9	1.04	17.7	0.3253	

A Novel Methodology for Determining Traces of Uranium in Plutonium by Thermal Ionisation Mass Spectrometry

D.Alamelu and S.K.Aggarwal

Fuel Chemistry Division, Bhabha Atomic Research Centre,
Trombay, Mumbai - 400 085, INDIA

INTRODUCTION

Determination of trace amounts of uranium (U) in plutonium (Pu) is required for variety of purposes. These include chemical quality assurance of Pu bearing fuel materials, characterisation of certified reference material for Pu amount and for determining the chemical purity of Pu obtained after reprocessing of the irradiated fuel. Most of the analytical methodologies involve prior separation of U from bulk of Pu. Isotope dilution - thermal ionisation mass spectrometry (ID-TIMS) using atomic ions (U^+) for measurements also depends upon the separation of U from Pu, prior to mass spectrometric determination of U amount ratios in the spiked sample. This becomes essential to minimise the isobaric interference of $^{238}Pu^+$ at $^{238}U^+$ peak during measurements by mass spectrometry.

Previously, studies have been reported¹⁻³ from our laboratory on the formation of atomic and molecular ions (M^+ and MO^+) using synthetic mixtures of U and Pu with different amount ratios. During these studies, it was possible to identify the filament heating conditions, using a multiple filament assembly, when only UO^+ ions are produced and no PuO^+ ions are formed. These studies prompted us to investigate the possibility of determining trace levels of U using UO^+ ions in TIMS, without involving the separation from bulk of Pu in the sample. In this work, this methodology has been adopted to the determination of U in a chemical assay standard of Pu as well as in the synthetic dissolver solutions of Indian PHWR fuels.

EXPERIMENTAL

Two synthetic samples, representing the PHWR irradiated fuel dissolver solution samples, with U/Pu amount ratios of 100 and 300, were prepared by mixing weighed aliquots of purified NIST-SRM -947 Pu and NIST- SRM - U chemical assay standard.. The synthetic mixtures were subjected to purification by anion exchange separation procedure using DOWEX 1 X 8 resin in

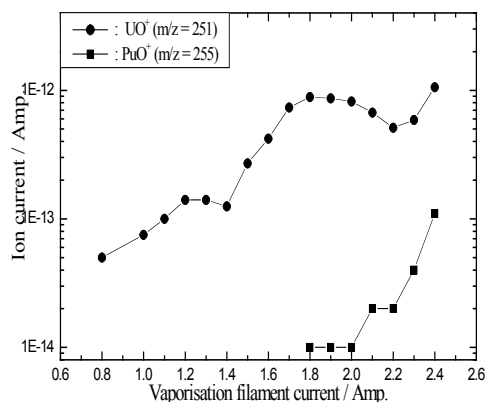


Fig 1 : Production of UO^+ and PuO^+ ions as a function of vaporisation filament heating current. The heating current of ionisation filament is kept constant.

1:1 (v/v) HNO₃. Uranium present on the column was washed with 1:5 HNO₃ and Pu was eluted with 1:50 HNO₃. The eluted Pu solutions, containing traces of U, were taken up in pre-weighed volumetric flasks. The concentration of Pu in these solutions was determined using liquid scintillation counting (LSC) and the specific activity calculated from the isotopic composition data determined by TIMS. Weighed aliquot from each of these solutions, containing 5 to 10 µg of Pu was taken and was mixed with pre-calibrated NIST-SRM- 930 U solution (²³⁵U > 93 atom%) to obtain an Pu/U amount ratio of 5 in the mixture. 2 µL solution from the mixture was loaded on to a high purity rhenium filament of a double filament assembly. The ionisation and vaporization filaments were heated to about 6 A and 2 to 2.4 A, respectively to obtain sufficient ion current of UO⁺ without PuO⁺. A thermal ionization mass spectrometer equipped with multi-Faraday cups was employed for acquiring the data in static mode of multi-collection. The amount ratios of U isotopes in the samples were obtained using UO⁺ ions at m/q values of 251 and 254 corresponding to ²³⁵UO⁺ and ²³⁸UO⁺, respectively. The concentration of U in the purified solution was then evaluated by usual equation used in ID-TIMS. Experiments were also conducted to determine the amount of uranium in the proposed chemical assay standard of plutonium viz. K₄Pu(SO₄)₄ without resorting to any ion exchange separation and using the same methodology as discussed above.

RESULTS

Tables 1 and 2 show the results of the ID-TIMS experiments on the determination of uranium at ppm levels in plutonium. The synthetic samples used to simulate U/Pu amount ratios as those expected in PHWR irradiated fuel samples (Table 1) also provide data on the decontamination factor achieved for U w.r.t. Pu in the anion exchange separation procedure employed in the present work for purification of Pu. The results given in Table 2 clearly demonstrate the applicability of the present ID-TIMS approach using enriched ²³⁵U (> 93 atom%) for the determination of trace amounts of U in Pu samples, without resorting to any separation and purification procedure.

The authors are thankful to Dr V.Venugopal, Director of Radiochemistry and Isotope Group at BARC for his keen interest in the work and constant support and encouragement.

1. S.K.Aggarwal, M.K.Saxena, P.M.Shah, S.Kumar, U.Jairaman and H.C.Jain, Int. J. Mass Spectrom. Ion Process. **139**, 111 (1994).
2. D.Alamelu, P.S.Khodade, P.M.Shah and S.K.Aggarwal, Int. J. Mass Spectrom. **239**, 51 (2004).
3. S.K.Aggarwal and D.Alamelu, Int. J. Mass Spectrom. **241**, 83 (2005).

Table 1. Determination of U in synthetic samples with U/Pu amount ratios as seen in PHWR irradiated fuel dissolver solution samples, after subjecting them to purification by anion exchange method

Initial U/Pu amount ratio in the synthetic mixture	Weight of solution (in gm)		$^{235}\text{UO}^+ / ^{238}\text{UO}^+$ amount ratio determined by TIMS in the mixture	Concentration (μg of element/gm of solution)		% of U in Pu	Decontamination factor (DF) of Pu w.r.t. U
	Sample (purified Pu solution)	Spike (NIST-SRM-930-U)		U	Pu		
100	5.97	0.1053	9.6318 (0.23 %)	0.00894	0.87	1.028	9730
300	5.96	0.0766	6.6549 (0.4 %)	0.01307	0.89	1.469	20422
300	13.46	0.0971	5.6959 (0.07 %)	0.00934	0.42	2.225	13483

Table 2. Determination of U in $\text{K}_4(\text{PuSO}_4)_4$ chemical assay standard of Pu

Weights of the solution (gms)		$^{235}\text{UO}^+ / ^{238}\text{UO}^+$ amount ratio determined in the mixture	Concentration (μg of element/gm of solution)		U/Pu amount ratio / 10^{-6}
Pu standard sample	NIST-U-930 spike		U	Pu	
1.06225	1.00905	17.1849 (0.14 %)	0.0057	71.171	80.23
1.3127	1.0123	17.1483 (0.12 %)	0.0071	87.951	80.82

Effect of Radioactive Decay of Pu Isotopes for Determination of Pu Concentration with High Accuracy by Isotope Dilution Mass Spectrometry (IDMS) and Isotope Dilution Alpha Spectrometry (IDAS)

D.Alamelu and S.K.Aggarwal

Fuel Chemistry Division, Bhabha Atomic Research Centre, Trombay, Mumbai 400 085, INDIA

INTRODUCTION

Determination of the total amount of Pu at the input point of a fuel reprocessing plant is one of the very important requirements of nuclear material accounting. This determination usually involves two measurements: (i) the total volume or weight of the solution in the tank and (ii) the concentration of Pu in the solution. The latter is generally achieved by following isotope dilution methodology due to complex nature of the irradiated fuel dissolver solution and also due to high radiation dose associated with the solution. The use of isotope dilution involves the addition of a known amount of tracer solution to an accurately known amount of the sample solution followed by the determination of change in the atom ratio by thermal ionisation mass spectrometry (TIMS) or change in the alpha activity ratio by alpha spectrometry (AS). The two methodologies are popularly known as isotope dilution mass spectrometry (IDMS) and isotope dilution alpha spectrometry (IDAS). In our laboratory, we have developed and demonstrated the use of ^{239}Pu and ^{238}Pu as spikes (tracers), respectively, for IDMS^{1,2} and IDAS³ experiments on Pu. In the IDMS experiments, we have used Pu containing about 65 atom% of ^{239}Pu as a spike for Pu from low burnt fuels with ^{239}Pu abundance of 90 atom% or higher.

The uncertainty in Pu concentration measurements by IDMS or IDAS depends upon many components including the uncertainty in the atom ratio or the alpha activity ratio determination in the spiked mixture. It is well recognised by the scientific community that any uncertainty in the data of Pu spike will contribute a systematic error in the concentration value of Pu in the sample. Thus it is essential that the isotopic composition of Pu in the spike, average atomic weight of Pu in the spike and the amount of Pu in the spike aliquot used must be known with the smallest possible uncertainty. These measurements again involve the use of thermal ionisation mass spectrometry and calibration of the spike by IDMS or IDAS by using a primary reference material of Pu. It is generally assumed that once the spike calibration is done, the aliquots of the spike distributed in different vials and stored properly may be employed for several years in future. However, due to the radioactive decay of Pu isotopes present in the spike, there would be changes in these parameters (i.e. isotopic composition, total amount of Pu in the aliquot etc.) which could contribute additional uncertainties in the Pu concentration measurements. This paper presents our experience in using two such spikes viz. ^{239}Pu about 65 atom% and ^{238}Pu about 93 atom% for IDMS and IDAS experiments. It is shown that the radioactive decay of Pu isotopes, if not considered properly, can contribute appreciable uncertainty in the Pu concentration values, particularly, when using ^{238}Pu as a spike in IDAS or in IDMS. This

assumes great importance in the present global scenario when tonnes of Pu are available and the concentration measurements are expected to have overall uncertainties of less than 0.1% .

RESULTS & DISCUSSION

Table 1 gives the isotopic composition data of ^{239}Pu and ^{238}Pu spikes used in our laboratory for IDMS and IDAS work on Pu. In the ^{239}Pu spike, the amount of ^{238}Pu was determined by alpha spectrometry whereas the amounts of all other isotopes in the two spikes were obtained by thermal ionisation mass spectrometry. Table 2 shows the changes in the atom % abundance, average atomic weight of Pu and the amount of Pu in the spike aliquot due to radioactive decay of Pu isotopes over a period of 1,2,5 and 10 years after fresh calibration of the spike (assumed as zero time). Figures 1 and 2 present the effects of these changes in ^{239}Pu and ^{238}Pu spikes respectively. It is evident that there is a combined effect to the extent of 0.25% and nearly 7%, respectively, when using pre-calibrated ^{239}Pu and ^{238}Pu spikes with amount% of different isotopes given in Table 1. These changes must be included in the isotope dilution equation used for calculation of concentration after measuring the atom ratio of alpha activity ratio in the spiked mixtures. When these measurements are carried out on a routine basis by an operator and all the calculations are made by using an excel sheet, there is a possibility of overlooking the changes in the parameters given here and the concentration values will, therefore, have uncertainties due to the radioactive decay of Pu isotopes in the spikes used. The investigation presented in this paper are extremely important when aiming at an overall uncertainty of better than 0.1% in the Pu concentration or in the total amount of Pu at a reprocessing plant.

The authors are thankful to Dr. V.Venugopal, Director of the Radiochemistry and Isotope Group of BARC, Mumbai for his keen interest in this work.

1. S.K.Aggarwal, G.Chourasiya, R.K.Duggal, R.Rao and H.C.Jain, Int. J. Mass Spectrom. Ion Processes, **69**, 137 (1986)
2. S.K.Aggarwal, R.K.Duggal, R.Rao and H.C.Jain, Ibid, **71**, 221 (1986).
3. M.V.Ramaniah, H.C.Jain, S.K.Aggarwal, S.A.Chitambar, V.D.Kavimandan, A.I.Alamula, P.M.Shah, A.R.Parab and V.L.Sant, Nucl. Technol. **49**, 121 (1980).

Table 1. Data on the amounts of different Pu isotopes in ^{239}Pu and ^{238}Pu spikes

S.No.	Amounts (atom%) of different isotopes in spike		
	Nuclide (<i>Half-life in yr</i>)	^{239}Pu spike	^{238}Pu spike
1.	238 (87.74)	0.225	92.254
2.	239 (24110)	65.14	7.3017
3.	240 (6553)	28.62	0.4143
4.	241 (14.4)	3.604	0.0277
5.	242 (3.76×10^5)	2.406	0.00212

Table 2. Change in atom % abundance, average atomic weight of Pu and the amount of Pu in the spike aliquot due to radioactive decay of Pu isotopes

Spike (methodology)	Decay period (Yrs)	Spike isotope	Correction factor due to radioactive decay			
			Atom fraction (a)	Average atomic weight (b)	Pu amount (c)	Combined effect of (a), (b) and (c)
^{239}Pu (IDMS)	0	^{240}Pu	1.00	1.00	1.00	1.00
	1		1.001658	0.999989	0.99824	0.999905
	2		1.003241	0.999978	0.996559	0.99981
	5		1.007574	0.999949	0.991958	0.999522
	10		1.013571	0.999909	0.985568	0.999034
^{238}Pu (IDAS)	0	^{238}Pu	1.00	1.00	1.00	1.00
	1		0.999401	1.000003	0.992727	0.99213
	2		0.998799	1.000005	0.985511	0.984322
	5		0.996964	1.000012	0.964205	0.961266
	10		0.993814	1.000025	0.929807	0.924032

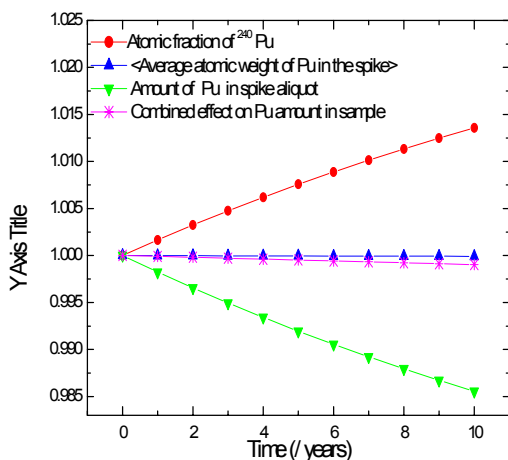


Fig 1: Fractional changes in different parameters as a function of time due to radioactive decay of Pu isotopes in ^{240}Pu spike

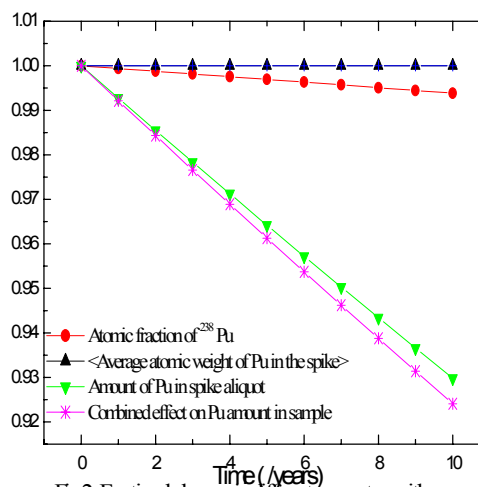


Fig 2: Fractional changes in different parameters with time due to radioactive decay of Pu isotopes in ^{238}Pu spike

Gamma Spectroscopy Applications in D&D Process Development, Inventory Reduction Planning & Shipping, Safety Analysis & Facility Management During the Heavy Element Facility Risk Reduction Program

Mark Mitchell*, Brian Anderson, Leonard Gray, Robert Vellinger, Michael West, Lennox Harris, Reginald Gaylord, Jennifer Larson, Greg Jones, Norris Harward, John Shingleton
*Lawrence Livermore National Laboratory, Livermore CA 94552 USA
UCRL-ABS-218325

This presentation discusses the development of new applications for gamma ray spectroscopy for D&D process development, inventory reduction planning and shipping, safety analysis, and facility management. These applications of gamma spectroscopy were developed and implemented during the Risk Reduction Program (RRP). The RPP successfully downgraded the Heavy Element Facility (B251) from a Category II Nuclear Facility to a Radiological Facility. Gamma spectroscopy is concluded to be an important tool in project management, work planning, and work control (“*expect the unexpected and confirm the expected*”), minimizing worker dose, and resulted in significant safety improvements and operational efficiencies.

Inventory reduction activities utilize gamma spectroscopy to identify and confirm isotopics of legacy inventory, in-growth of daughter products and the presence of process impurities; quantify inventory; prioritize work activities for project management; and supply documentation satisfying shipper/receiver requirements. D&D activities utilize *in-situ* gamma spectroscopy to identify and confirm isotopics of legacy contamination; quantify contamination levels and monitor the progress of decontamination; and determine the point of diminishing returns in decontaminating enclosures and glove boxes containing high specific activity isotopes such as ^{244}Cm and ^{238}Pu . *In-situ* gamma spectroscopy provided quantitative comparisons of several decontamination techniques (e.g. TLC-free Stripcoat, Radiac wash, acid wash, scrubbing) and is used as a part of an iterative process to determine the appropriate level of decontamination and optimal cost to benefit ratio. Radioactive contaminants included: $^{166\text{m}}\text{Ho}$, ^{232}U , ^{233}U , ^{235}U , ^{237}Np , ^{238}Pu , ^{239}Pu , ^{240}Pu , ^{241}Pu , ^{242}Pu , ^{241}Am , $^{242\text{m}}\text{Am}$, ^{243}Am , ^{243}Cm , ^{244}Cm , ^{246}Cm , ^{248}Cm , and ^{249}Cf .

Facility management utilizes gamma spectroscopy, in conjunction with other characterization techniques, process knowledge, and historical records, to provide information for work planning, work prioritization, work control, and safety analyses (e.g. development of stop work points). This approach resulted in B251 successfully achieving Radiological status on schedule. Gamma spectroscopy helps define operational approaches to achieve ALARA, e.g. hold points, appropriate engineering controls, PPE, workstations, and time/distance/shielding. Applications of gamma spectroscopy can improve upon similar activities at other facilities.

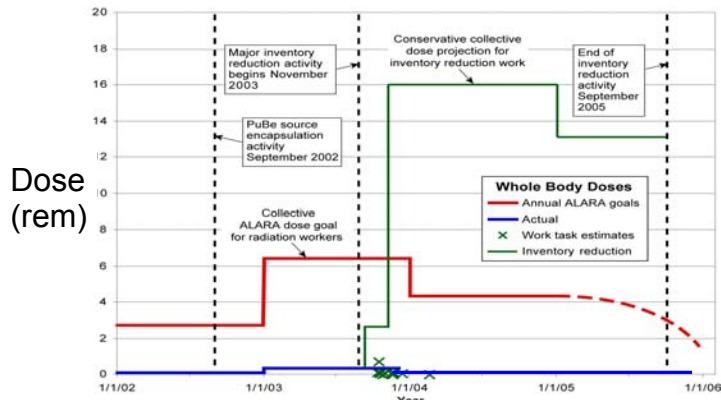


Figure 1. ALARA Comparison of Actual vs. Predicted Dose Demonstrates Success of Work Control Practices

***IN-SITU* GAMMA SPECTROSCOPY SUPPORTED D&D PROCESS DEVELOPMENT**

The D&D Project utilized gamma spectroscopy both as a D&D process development tool and as characterization tool in support of D&D. The RRP monitored the progress of decontamination and compared the effectiveness of several decontamination techniques by using *in-situ* gamma spectroscopy. Gamma spectroscopy resulted in a ground breaking success - no one had decontaminated facilities with this level and variety of high specific activity isotopes (e.g. ^{244}Cm , ^{238}Pu , ^{228}Pa , aged ^{232}U). D&D processes developed using applications of *in-situ* gamma spectroscopy were pivotal to the success of the RRP. The RRP completed D&D of 40 of 49 Enclosures in 1 year; characterized all enclosures (gamma spectroscopy, alpha-swipe tab sampling); processed 37 lower-contaminated gloveboxes through D&D and shipped to RHWM as LLW; and emptied 2 highly-contaminated Blue Cave enclosures with little or no contamination to the room. Special packaging of contaminated equipment included a glovebox transferred as TRU Waste in a Standard Waste Box (SWB) and 2 glove boxes transferred as TRU Waste in a Type A Box. This work generated over 800 waste parcels, 84 TRU drums, and numerous LLW drums.



Figure 2. *In-situ* gamma spectroscopy of contaminated glove boxes and equipment

Reference: Mark Mitchell et al, *New Applications of Gamma Spectroscopy: Characterization Tools for D&D Process Development, Inventory Reduction Planning & Shipping, Safety Analysis & Facility Management During the Heavy Element Facility Risk Reduction Program*, submitted to: 2006 MARC VII Conference

Calculated Neutron Source and Spectra in Plutonium Metal and Compounds

G.Vlaskin

A.A.Bochvar VNIINM (All-Russian Research Institute of Inorganic Materials), Moscow, Russia

METHOD OF EVALUATION

An accurate knowledge of the specific neutron yields and spectra are very important values for plutonium metal and compounds. It appeared evident that the best way of obtaining the yield and spectrum is by calculation, using the differential (α,n) cross sections and decay constants.

NEDIS[1] is a computer code that determines neutron production rates and spectra from (α,n) reactions and spontaneous fission. The code is capable of calculating (α,n) source rates and spectra in four types of problems: homogeneous media(i.a. mixture of α -emitting source material and low-Z target material), where the radius of of α -emitting source material particles (as sphere) may be account for, two–region interface problems (i.a. a thin/thick slab of α -emitting source material in contact with a thick slab of low-Z target material), three-region interface problems(i.e. thin or thick slab of α -emitting source material between of different low-Z target material), and (α,n) reactions induced by a monoenergetic beam of (α,n) particles incident on a thick slab of target material. Spontaneous fission spectra are calculated with evaluated half-life, spontaneous fission branching, and Watt spectrum parameters for 51 actinides.

The (α,n) spectra are calculated using experimental anisotropic angular distribution in the center-of mass system with a library of 23 sets of measured and/or evaluated total cross sections and for each product nuclide level states, and functional α -particle stopping cross sections for $Z \leq 98$. The code outputs the magnitude and spectra of the resultant neutron source. It also provides an analysis of the contributions to that source by each light element in the problem. Fig.1 show comparisons of calculated (α,n) neutron source spectra for the $^{238}\text{PuBe}_{13}$ (1 gr. ^{238}Pu) compound determined by 1-NEDIS, 2-NEDIS using isotropic library JENDL[2], 3-SCALE5(isotropic library LANL[3]).

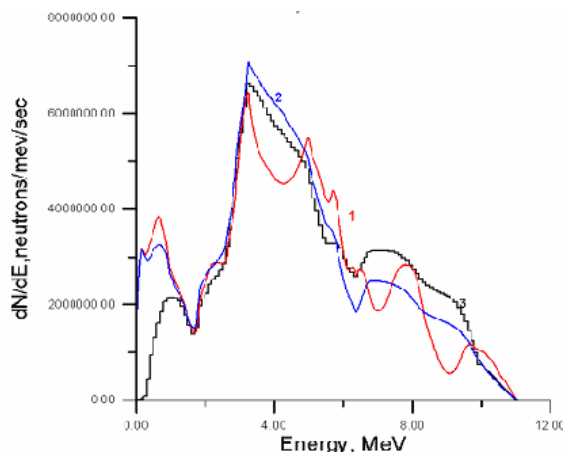


Fig.1 Energy-dependent neutron sources strength in $^{238}\text{PuBe}_{13}$ as calculated by 1)NEDIS,2)NEDIS library JENDL,3)SCALE5

When light element impurities $\leq 1\%$ in plutonium metal the simple formula 1 may be used to calculate neutron yield due to (α,n) reactions.

$$Y = \sum a_{il} C_l M_{Pu} \alpha_i \quad (1)$$

Where

C_l – mass content of light element l (weight percent);

α_i – mass content of isotope i in plutonium (weight percent);

M_{Pu} - mass of plutonium (gram)

a_{il} - coefficients in Table 1 calculated using the NEDIS computer program (per 1 gram Pu).

$$a_{il} = Y_{NEDIS} / (C_l M_{Pu} \alpha_i) \quad (2)$$

Table 1

element	a_{il}			
	²³⁸ Pu	²³⁹ Pu	²⁴⁰ Pu	²⁴² Pu
Li	5.32e+02	1.04e+00	3.91e+00	2.68e-02
Be	1.70e+04	4.96e+01	1.83e+02	2.66e+00
B	4.37e+03	1.34e+01	4.95e+01	7.40e-01
C	2.52e+01	6.54e-02	2.42e-01	3.29e-03
O	1.52e+01	4.28e-02	1.58e-01	2.29e-03
F	1.87e+03	4.78e+00	1.77e+01	2.33e-01
Mg	2.43e+02	5.55e-01	2.06e+00	2.55e-02
Al	1.28e+02	2.38e-01	8.88e-01	9.28e-03
Si	2.20e+01	4.79e-02	1.78e-01	1.87e-03

- 1 G.N.Vlaskin, E.V.Chvankin. Atomnaya energiya.(Rus), v.74, n.2, 1993, p.134-139.
- 2 T. Murata, K. Shibata. Evaluation of The (α ,n) Reaction Nuclear Data for Light Nuclei, J.of Nucl.Sci. &Techn.,Supl,2, Aug.,2002, Proc. Of Int. Conf. Nucl. Data for Sci. &Tech. Tsukuba, Japan, 2001,v.1 p. 76-79.
- 3 ORIGEN-ARP 2.00 Isotope Generation and Depletion Code System - Matrix Exponential Method with GUI and Graphics Capability, RSICC code package C00702PC58600. - May 2002

Determination of long-lived Plutonium isotopes in environmental samples

E. Hrncsek^{*}, R. Jakopič[†], P. Steier[‡], A. Wallner[‡]

^{*} ARC Seibersdorf research GmbH, 2444 Seibersdorf Austria

[†] Jožef Stefan Institute, Ljubljana Slovenia

[‡] Institut für Isotopenforschung und Kernphysik der Universität Wien, VERA Laboratory, Währinger Str. 17, 1090 Wien Austria

A combination of Alpha Spectrometry and Accelerator Mass Spectrometry (AMS) was used for the determination of the isotopic ratios of Plutonium isotopes in environmental reference samples and samples contaminated from nuclear reprocessing.

After adding Pu-236 tracer, Plutonium was separated by ion exchange with AG1-X8 resin from 7.2 M HNO₃. Samples for Alpha Spectrometry were prepared by microprecipitation with NdF₃ using cellulose nitrate membrane filters. The Pu-236 tracer was used to determine the absolute specific activity of Pu-239 and Pu-239+Pu-240 by Alpha Spectrometry.

Sequentially, a part of the filter was used for determination of the isotope ratios of Pu-239, Pu-240, Pu-242 and Pu-244 by AMS at the Vienna Environmental Research Accelerator (VERA) facility. To this end the filter material was reprocessed. Fe was added, Pu was co-precipitated with Fe(OH)₃ and finally solid samples were prepared. The various Pu isotopes were extracted from a sputter ion source and separated by their masses. AMS - being independent on the half-life of a radionuclide - provides isotope ratios directly by counting the radionuclides with a particle detector.

Results for the isotopic ratios of the samples will be shown and the capabilities and detection limits achievable for determination of Pu-242 and Pu-244 will be discussed.

Pu, Np and U Valence States and Type of Molecules Determination by Chemiluminescence Effects and Pulse Laser Spectroscopy Methods

I.N.Izosimov¹, N.G.Gorshkov¹, L.G.Mashirov¹, N.G.Firsin¹

¹ Khlopin Radium Institute, 2nd Murinski ave 28, St. Petersburg 194021, Russia
e-mail: izosimov@atom.nw.ru

Selective and sensitive direct actinide elements trace amounts detection in the different samples presents today major importance for ecology, radwaste handling and control, rehabilitation of contaminated areas and risk assessment. The behavior of actinides in environment is determined by actinides valence states and type of molecules. Information about actinide valence states in trace analysis is essential to fix the actinides emission source and the propagation history. The most sensitive (for example – TRLIF) laser spectroscopy methods with time resolution (TR) use photoluminescence for detection, don't give information about valence states and for some actinides and lanthanides detection in solutions [1,2] have limit of detection (LOD) up to 10^{-13} mol/l(M) (Table 1).

Table 1. LOD by Time Resolved Laser Induced Fluorescence (TRLIF) method.

Element	UO ²⁺	Cm ³⁺	Am ³⁺	Eu ³⁺	Tb ³⁺	Gd ³⁺	Dy ³⁺	Sm ³⁺	Ce ³⁺
LOD(M)	10^{-13}	10^{-13}	10^{-9}	10^{-13}	10^{-9}	10^{-8}	10^{-10}	10^{-10}	10^{-9}

Pu, Np and some valence form of U does not give the photoluminescence in solutions and for it's detection not most sensitive (LOD – 10^{-5} - 10^{-7} M) laser spectroscopy methods are used.

Today the chemiluminescence effects using in biology and medicine [3] for trace amount detection of different substances with LOD up to 10^{-9} - 10^{-13} M and it is possible to determine the elements valence states and type of molecules. In our experiments [4,5] we observed the chemiluminescence of solutions induced by Pu, Np and U after excitation by pulse laser radiation. High sensitive TR methods may be used for this chemiluminescence detection (fig.1).

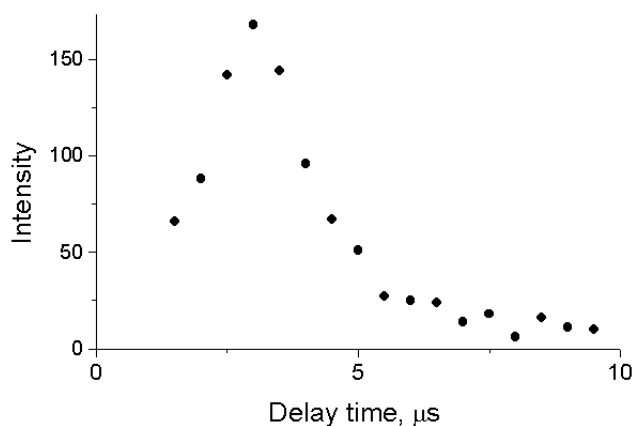


Fig.1: Kinetic curve of luminol chemiluminescence induced by excited plutonyl complexes.

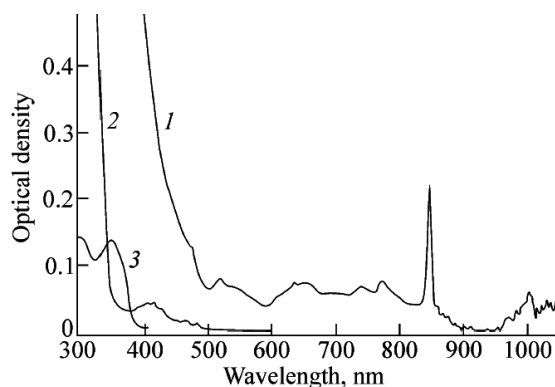


Fig.2: Absorption spectra of (1)-PuO₂²⁺, (2)- UO₂²⁺ and (3)-luminol.

Chemiluminescence is widely used as a base for detection methods in many fields, such as flow injection analysis, chromatography, biology, medicine, etc. [3]. We have observed and study the chemiluminescence effects

in solutions containing U, Pu and Np [4,5]. It's open possibility for chemiluminescence application in *Nuclear Chemistry*.

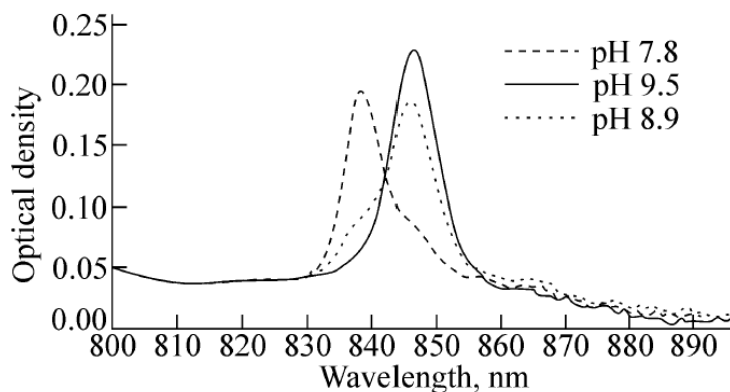


Fig.3: Absorption spectra of plutonyl complexes in 42 % CsF + H₂O solutions at different pH values. Two complexes are in solution: PuO₂F₅³⁻ (band 839nm) and PuO₂F₄OH³⁻ (band 846.5nm).

By proper selection of lasers radiation wavelengths (fig.2, fig.3), one or multi-step actinides complexes excitation scheme and chemiluminogenic label it is possible to induced chemiluminescence only by selective excitation of detectable actinide complexes .

The chemiluminescence effects using allows to essentially spread scope for trace amount detection of actinide in solutions, determination of the actinide valence states in solutions and determination of the molecule type containing actinide. Especially perspective is to use the chemiluminescence effects for detection of actinides and complexes containing actinides in solution in the cases when in such systems actinide does not give direct luminescence but can induce chemiluminescence. Multi step chemiluminescence excitation scheme may be efficiently used for detection selectivity increasing [5].

The sensitivity of the chemiluminescence methods is higher than sensitivity of other methods (LIPAS for example) which are used for non-luminescent actinides and molecules detection now. The combinations of the chemiluminescence effects with high sensitivity and high selectivity laser spectroscopy methods make it possible to carry out an effective detection both of luminescent and *non-luminescent* actinides and molecules containing actinides (especially U, Pu and Np) in different solutions.

- 1 C.Moulin, P.Decambox and P.Mauchien, *Anal.Chem.* **68**,(1996) 3204.
- 2 I.N.Izosimov, *Proc. 4th International Workshop "Laser spectroscopy on beams of radioactive nuclei"*, May 24-27, 1999, Poznan, Poland. . Ed. JINR, Dubna, E15-2000-75, p.169.
- 3 C.Dodeigne, L.Thunus and R.Lejeune, *Talanta* **51**, (2000) 415.
- 4 I.N.Izosimov, N.G.Gorshkov, L.G.Mashirov, N.G.Firsin, A.A.Kazimov, S.V.Kolichev, N.A.Kudryshv and A.A.Rimski-Korsakov, *Proc. 5th International Workshop "Application of lasers in atomic nuclei research"*, Poznan, Poland, 2001. Ed. JINR, Dubna, E15-2002-84, p.153.
- 5 N.G.Gorshkov, I.N.Izosimov, A.A.Kazimov, S.V.Kolichev, N.A.Kudryshv, L.G.Mashirov, A.V.Osokin and N.G.Firsin, *Radiochemistry* **45**, (2003) 28.

Plutonium in Higher Oxidation States in Alkaline Media

I.G. Tananaev, M.V. Nikonov, B.F. Myasoedov

Vernadsky Institute of Geochemistry and Analytical Chemistry Russian Academy of Science,
Moscow 199991 Russia

INTRODUCTION

The discovery and studies of *5f* elements in unknown oxidation states are of a noticeable interest for theoretical inorganic chemistry and enrich the chemistry of transuranium elements. Before our experiments it was well known that the highest oxidation state for Pu was (VII). Hence the electron structure of Pu(VII) as $5f^7$ permits to suppose that this actinide may exist in the oxidation state +8 with the electron configuration of an inert gas. During 40+ years a several attempts to prepare Pu(VIII) have been made. The main aim on these experiments was to oxidize Pu(VII) by different agents in the various media, but all of these attempts were not successful. Seemingly, there is no way to prepare Pu(VIII), indeed. However the discovery of unexpected Pu(VIII) species has a great interest, and we started the experiments in this field.

EXPERIMENTS

The blue-black solution of Pu with the characteristic absorption spectrum (AS) having the main maximums at 607, and 635 nm is prepared by interaction of fine pure 2,9 mM Pu(VI) in 1,5M NaOH with 3,5% vol. O₃/O₂ mixture (gas flow 5-7 dm³/h, 20°C) during 30 min. It was detected that addition of a small (0,05 ml) drops of a non ozonized 1.3 mM Pu(VI) in 1,5M NaOH step by step to the 3 ml portion of ozonized (colored) solution goes to instantly decrease of optical density of the blue-black solution proportionally to the growth of amount of the added initial solution of Pu(VI). It was supposed that the ozonizing of Pu(VI) in 1-3M NaOH leads to formation of a mixture of Pu(VII), and assumed Pu(VIII), who directly in the experiments above interacted with the initial non ozonized Pu(VI) solution by the following scheme: Pu(VI) + Pu(VIII) → 2Pu(VII) (1). Knowing the amount of Pu(VI) in the first aliquote, interacted with Pu, treated with ozone (0,05 ml × 1,3 mM = 6,5•10⁻⁵ mmol) and decrease of an optical density of the mixture at 635 nm (~ 0,18), the probably value of molar extinction coefficient (ε) of Pu(VIII) was estimated as ~2600 ± 400 M⁻¹cm⁻¹. The value of ε^{Pu(VII)} at the 500-550 nm was found as ~100 M⁻¹cm⁻¹. From data above the yield of assumed Pu(VIII) in the experimental solution was estimated to be ~(15±5)%.

Alternative way, the unknown oxidant could produced during Pu(VI) ozonizing in alkaline solution (Pu ozonide, peroxy compound of Pu^{VII}, and so on), which can interacted with initial Pu(VI) in alkaline solution. For specification of the data obtained the complementary experiments have been carried out:

1. The spectrophotometric titration of the product of reaction (1) by H₂O₂ was provided. The addition of H₂O₂ causes well seen changes in the spectra of the testing solution. The stoichiometric ratio of [Pu]:[H₂O₂], determined after the completing of the titration was ~2.2:1. The data obtained can confirm that Pu in the tested solution was in +7 oxidation state.

2. The interaction of 0.2 ml aliquots of the just ozonized 1.8 mM Pu(VI) in 2M LiOH with 1 ml of 5mM Np(VI) in 2M LiOH had been carried out. The considerable changes in the AS of the mixture solution had been observed in the result of titration. Addition of ozonized Pu(VI)

solution to Np(VI) cause the appearance of the band with 620 nm in the spectrum, typical for Np(VII) solutions. Knowing the amount of Pu in the added aliquote and the amount of the formed Np(VII), it was possible to design that the ratio of Np:Pu $\sim 1.2 \pm 0.1$. This fact confirms the initial supposition that ozonization of Pu(VI) in alkaline media leads to the formation of the mixture of Pu(VII) and unknown oxidant, probably Pu(VIII) in the experimental solutions.

3. Two redox-reactions had been studied: (a) interaction of Pu(VI) with Fe(VI) in 1M NaOH solution; and (b) contact of ozonizing Pu(VI) alkaline solution with Fe(III). As a results of these experiments it was found that Pu(VI) solutions are found to be oxidized by ferrate-ions in 1,5M NaOH. On the other hand, the preliminary ozonized Pu solutions oxidize Fe(III) to Fe(VI). These data contradict to the known literature ones about the behavior of Pu ions in the highest oxidation states in alkaline solutions. As ferrate-ions oxidize Pu(VI) ions we conclude that the value of the redox potential of pair Pu(VII)/Pu(VI) is $<0,72$ V (vs NHE).

4. Reducing of assumed Pu(VIII) by different kind reducing agents to direct Pu(VII) were carried out. As the work was based on spectrophotometry, AS of the chosen reductant and the products of their oxidation should not have intensive absorbance bands in visible range at least in the interval of absorbance of Pu(VIII), and (VII). The Cl^- , Br^- , I^- , IO_3^- and $\text{C}_2\text{H}_5\text{OH}$ were tested. Unfortunately, it was found that even small excess of these reagents, added to assumed Pu(VIII) led to fast and irreversible formation of Pu(VI). Contrary, the AS of the product of interaction of a mixture of Pu(VII) and assumed Pu(VIII) with $[\text{NO}_2^-] = 0.1\text{M}$ at $[\text{NaOH}] < 1\text{M}$ had not neither intensive absorbance band at 607, and 635 nm, supposed for the spectrum of Pu(VIII), nor maximums of absorbance at 655, 871 and 1021 nm, known for alkaline solutions of Pu(VI) (fig. 1). The similarity of AS of solutions after interaction of a mixture of Pu(VII) and assumed Pu(VIII) with nitrite-ions, and with Pu(VI) are detected.

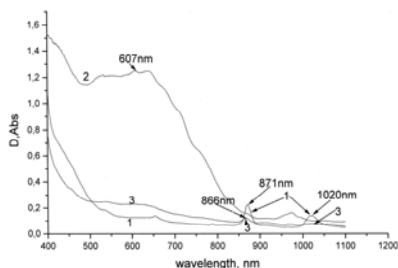


Fig.1. (1) AS of the initial 1,8 mM Pu(VI) in 0,45 M NaOH; (2) AS of the same solution after 1 h ozonization; (3) AS of the ozonized solution (2) after 0.05ml of 2M NaNO₂ was introduced there.

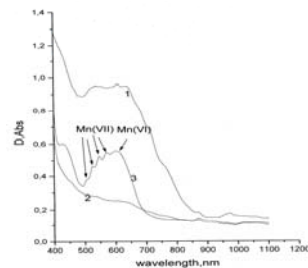


Fig.2. AS of 1 mM Pu(VI) in 0,5M NaOH, after 1 h ozonizing before (1) and after (2) addition of 0,005 mmole NaNO₂, and with the consequent introduction of 0,001mmole of K₂MnO₄.

5. The interaction of the just described solution with manganate ions at $[\text{NaOH}] = 0.5\text{M}$ causes the crimson coloration of the reaction product, and the bands of absorbance of Mn(VII) appeared in the AS (fig. 2). It was shown also in the separate experiment that Mn(VI) did not interact with Pu(VI) stock solution under the same conditions. Thus, it is possible to conclude that Pu in +7 oxidation state is really the product of reducing of an ozonizing colored solution by nitrite-ion in alkaline media. All of the data obtained confirmed that the Pu(VIII) formed during ozonizind of Pu(VI) in the alkaline solution, which has a characteristic AS with the main maximums at 607, 635 nm, that earlier is attributed to absorption of Pu(VII).

The work was supported by the U.S.DOE-OBES, Project RC0-20004-SC14, and RUC2-20012-MO-04.

Optical absorbance spectroscopy of Pu ions in aqueous solution

E. Bauer, S. D. Reilly, M. P. Neu

Los Alamos National Laboratory, Los Alamos NM 87545 USA

INTRODUCTION

There is frequent need to determine the oxidation state and concentration of plutonium ions in aqueous solution for research and development applications. Optical absorbance spectroscopy of plutonium ions in acidic solutions is an efficient and effective way to determine the combination of oxidation states present. The characteristic optical absorbance spectrum for each oxidation state, as seen in Figure 1, together with Beer's Law, is used to determine the concentration of each ion present.

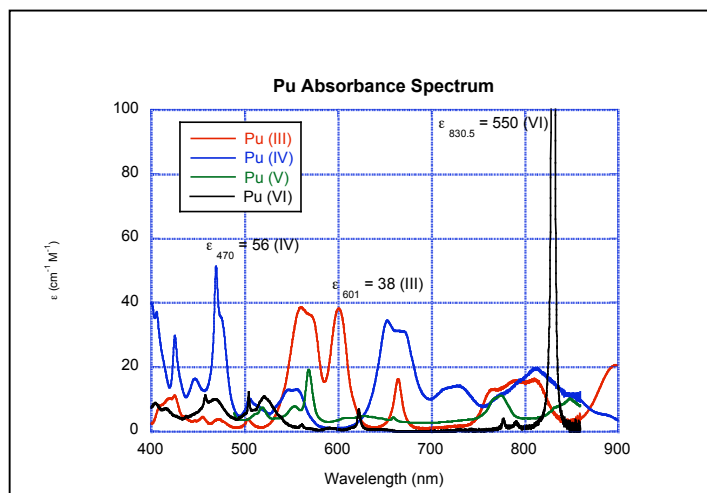


Fig 1: Characteristic optical absorbance spectra of Pu oxidation states in 1 M HClO₄ solution.

The frequently-cited Pu spectra reported by Cohen in 1961¹ were recorded using a Cary Model 14, the first commercial recording spectrophotometer. With the widespread use of optical absorbance spectrophotometers with greater resolution and sensitivity, it would be beneficial to reinvestigate the characteristic spectra and absorptivities of each plutonium ion in commonly used media. For instance, the Cary 6000i UV-vis-NIR spectrometer utilizes an InGaAs detector in the NIR region, which provides better resolving power and is approximately 100 times more sensitive than the traditional PbS detector in older models.² This NIR

region encompasses the narrow, characteristic PuO₂²⁺ 830.5 nm absorbance band.

We will use a Cary 6000i to analyze well-characterized solutions of plutonium in different oxidation states. We will determine and report the characteristic spectra of each oxidation state in common mineral acids, as well as solutions of sodium chloride (0.5, 2 and 5M) and sodium nitrate (1 and 3M).

EXPERIMENTAL

A ²³⁹Pu solution of known concentration and isotopic composition in 1 M HClO₄ was prepared and then analyzed using the Cary 6000i. The spectra for this solution is shown in Figure 2. The solution was oxidized to a pure Pu (VI) solution by saturation with ozone for several days. We varied the spectral band width (SBW) to determine the minimum SBW necessary to resolve the

narrow PuO_2^{2+} 830.5 nm peak (Fig. 3). The optimum SBW will be used to analyze duplicate samples of Pu (VI) solutions and results will be compared to counted samples to determine Pu (VI) concentration in the analyzed solution. From this information epsilon for this peak will be determined using the Beer-Lambert law:

$$A = \epsilon bc \quad (1)$$

In the above equation 1, A is a proportionality constant called the absorptivity and refers to the amount of light absorbed at a given wavelength. The path length (length of the path of light traveling through the sample) is signified by b and is expressed in cm. Concentration is expressed in molarity. Epsilon is a constant that is calculated by comparing absorptivity vs. concentration and is expressed as $\text{cm}^{-1} \text{M}^{-1}$.

A similar analysis will be done for pure oxidation states of III, IV and V in mineral acids as well as sodium chloride and sodium nitrate solutions. Characteristic peaks for each oxidation state will be examined and epsilons calculated and reported.

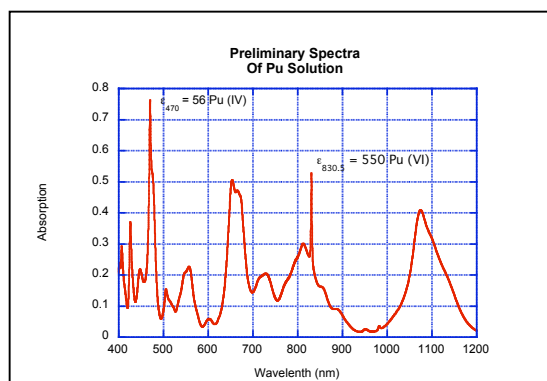


Fig 2: UV-vis/NIR spectrum of Pu in 1 M HClO_4 before oxidation with ozone.

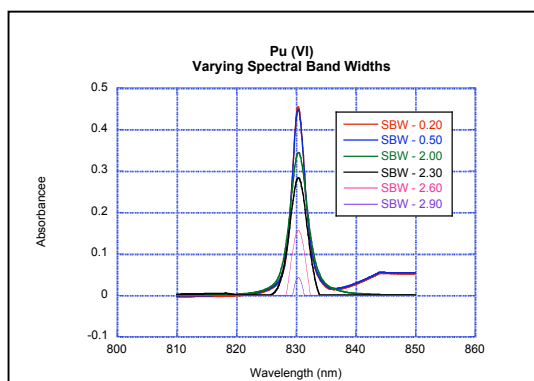


Fig 3: Characteristic 830.5 nm PuO_2^{2+} peak recorded using different spectral band widths.

RESULTS AND DISCUSSION

The preliminary spectrum of the Pu solution to be used in the experiments (Fig 2) indicated that the solution was a mixture of Pu (III, IV and VI). Saturating the solution with ozone resulted in complete oxidation to Pu(VI). The spectrophotometer spectral band width must be set small enough to resolve the narrow Pu absorbance bands such as the one at 830.5 nm (full width half height is approximately 2 nm). The spectrum of the pure Pu(VI) solution recorded using different SBW values is shown in Fig. 3. SBW values larger than 0.20 do not fully resolve the narrow peak.

- 1 D. Cohen, J. Inorg. Nucl. Chem. **18**, 211 (1961).
- 2 J. J. Comerford, Varian Instruments UV-Vis-NIR Application Note No. 88, 2003.

Study on Valence of Pu, Np and Tc in Nitric Acid after Electrolytic Reduction

H. Hoshi*, Y.-Z. Wei*, M. Kumagai*, T. Asakura†, Y. Morita†

*Institute of Research and Innovation, Kashiwa, Chiba 277-0861 Japan

†Research Group for Aqueous Separation Process Chemistry, Nuclear Science and Engineering Directorate, Japan Atomic Energy Agency, Tokai-mura, Ibaraki 319-1195 Japan

INTRODUCTION

For the development of nuclear fuel cycle, it is one of the most important tasks to improve reprocessing process more economically and efficiently¹. Especially, to establish the Fast Breeder Reactor (FBR) cycle system for the future, it is strongly desirable to develop a new reprocessing process which uses more compact equipments and produces less radioactive wastes compared to the present PUREX process. For this purpose, we have proposed a novel aqueous reprocessing system named ERIX Process (The Electrolytic Reduction and Ion Exchange Process for Reprocessing Spent FBR-MOX Fuel) to treat spent FBR-MOX fuels. As shown in Fig. 1, this process consists of (1) Pd removal by selective adsorption using a specific anion exchanger; (2) electrolytic reduction for the valence adjustment of the major actinides including

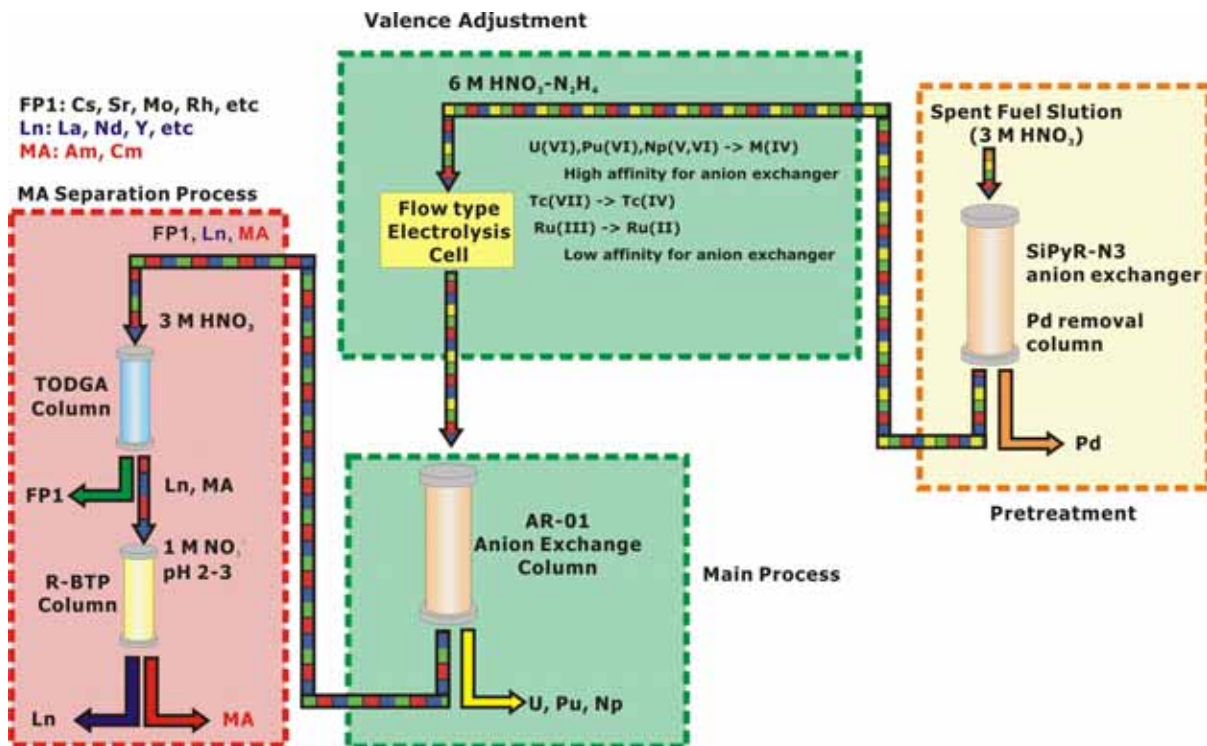


Fig 1: ERIX Process

U, Pu, Np and some fission products (FP) such as Tc and Ru; (3) anion exchange separation for the recovery of U, Pu and Np using a new type of anion exchanger, AR-01; and (4) selective separation of long-lived minor actinides (MA = Am and Cm) by extraction chromatography^{2,3}.

The adjustment of valence of actinides, e.g. U(VI) to U(IV), is one of the most important subject to increase affinity onto anion exchanger for quantitative recovery of U, Pu and Np in this process. For this purpose, nitric acid concentration of spent fuel solution is adjusted to 6 M and it is reduced at -300 mV (vs. Ag/AgCl) through a novel flow-type electrolysis cell. In this work, valence of Pu, Np and Tc in concentrated nitric acid solution after the electroreduction was studied.

ELECTRO REDUCTION

It is well known that Pu and Np take several oxidation states in nitric acid solution. Usually, Pu(IV) is most stable in nitric acid solution. Pu(III) is quickly oxidized to Pu(IV) by nitrous acid, however, Pu(III) exists in nitric acid solution with some reductant, e.g. hydrazine. In this ERIX Process, U(VI) is reduced to U(IV) in 6 M HNO₃ solution at -300 mV (vs. Ag/AgCl) and hydrazine is used as a HNO₂ scavenger.

Electroreduction of 6 M HNO₃ solution containing Pu, Np and Tc through flow-type electrolysis cell was examined. According to the UV-Vis spectra, Pu and Np were reduced to Pu(III) and Np(IV), respectively. Under the modification of hydrazine, Pu stably existed as Pu(III) in 6 M HNO₃ solution after electroreduction. However, Pu(III) was liable to be oxidized to Pu(IV) in case of coexisting with Tc or Ru by their catalytic reaction. Especially, oxidation ratio of Pu(III) to Pu(IV) with Ru was faster than that with Tc. Anion exchanger column separation of the reduced solution was also performed. As the results, it was found that all of the Np was reduced to Np(IV) which was quantitatively recovered from the column by dilute nitric acid solution. Since Pu was eluted together with the Np(IV), it is presumed that the Pu(III) was oxidized to Pu(IV) inside the anion exchanger column.

Tc(VII) is the most stable oxidation state of Tc in spent fuel solution and it is strongly adsorbed onto an anion exchange resin in nitric acid as the form of pertechnetate anion (TcO₄⁻). Therefore, quantitative recovery of Tc from anion exchanger column is one of the important subjects in this process. Owing to the difficulty of evaluation of Tc oxidation state by UV-Vis spectra, above reduced solution was analyzed by anion exchanger column. After electro reduction, because Tc indicated no adsorption onto anion exchanger column, Tc(VII) was considered to be reduced to Tc(IV) or Tc(II)⁴. Tc was separated from U, Pu, and Np, through anion exchanger column after electro reduction.

This paper is the results from “Development of the ERIX Process for Reprocessing Spent FBR-MOX Fuel” entrusted by the Ministry of Education, Culture, Sports, Science and Technology of Japan (MEXT).

- 1 Y.-Z. Wei, et al., , *Proc. of PBNC-2002*, Shenzhen, China, October 21 - 25, 2002.
- 2 H. Hoshi, et al., *J. Alloy. Compd.*, **374**, 451 (2004).
- 3 Y.-Z. Wei, et al., *J. Alloy. Compd.*, **374**, 447 (2004).
- 4 H. Hoshi, et al., *J. Radioanal. Nucl. Chem.*, **262**, 601-605(2004)

Condensation and Fragmentation Reactions of Cationic Uranium Complexes in the Gas Phase

Gary Groenewold^{1*}, Michael Van Stipdonk², Garold Gresham¹, Winnie Chien², Anita Gianotto¹, and Kevin Cossell¹

¹Department of Chemical Sciences, Idaho National Laboratory, Idaho Falls ID, USA

²Department of Chemistry, Wichita State University, Wichita KS, USA

INTRODUCTION

The ultimate disposition of uranium in the environment or in processes related to separations is dependent on aspects of its chemical speciation, including oxidation state, organic complexing ligands, and attached solvent molecules. Ligand preferences and exchange reactions play a key role in dictating how uranium will be partitioned in heterogeneous systems, and hence knowledge of these factors is important for predicting behavior. Useful insight can be gained by examining solvent addition and exchange reactions of gas-phase uranium ions occurring in the gas phase of a trapped-ion mass spectrometer. The appeal of working in this environment is that explicitly-defined species can be isolated and examined for reactivity trends and relative ligand binding preferences.

EXPERIMENTAL METHODS

Examination of reactions uranium cations requires their formation, isolation, which then enables either condensation or fragmentation reactions to be carried out. Ion formation was accomplished using either electrospray, or by primary ion bombardment. Electrospray of uranyl-solvent solutions was performed using a Finnigan LCQ-DECA instrument, which has a quadrupole ion trap for its mass analyzer. Primary ion bombardment of U-containing solid targets was conducted using an ion trap-secondary ion mass spectrometer, that was designed and conducted in-house at the INL. In all experiments, ions of interest were isolated by ejecting competing ions that have different masses from the ion trap. In the condensation experiments, ions were then allowed to react with gaseous neutral molecules, which enables evaluation of reaction pathways and kinetics. In the fragmentation experiments, ionic complexes were excited by application of an external resonant frequency to the end caps of the ion trap, which increased the kinetic energy and produced hyperthermal collisions with the He bath gas.

RESULTS

Initial studies of U(IV), U(V) and U(VI) dioxo cations examined addition of H₂O.¹ The extent of ligation increased with the oxidation state. [UOOH]⁺ (U(IV)) eventually formed [UOOH(H₂O)₃]⁺ (total of 5 ligands), whereas [UO₂OH]⁺ (U(VI)) formed [UO₂(OH)(H₂O)₃]⁺ (6 ligands). The U(V) cation [UO₂]⁺ displayed intermediate behavior.

Acetone (A) is a stronger gas-phase nucleophile than water, and formed complexes in an analogous manner: for example, the U(VI) ion [UO₂OH]⁺ formed [UO₂OH(A)₃]⁺, indicating that A and out-competed water in ligation on the U center. The [UOOH]⁺ cation was the exception to this pattern, ultimately preferring to form the mixed complex [UOOH(A)₃(H₂O)]⁺. Increasing the charge state from +1 to +2 increased the extent of ligation in the U(VI) species: starting from

$[\text{UO}_2]^{2+}$, the penta-ligated $[\text{UO}_2(\text{A})_5]^{2+}$ uranyl complex was formed.² This showed that the extent of ligation in the gas phase was similar if not identical to that in solution.

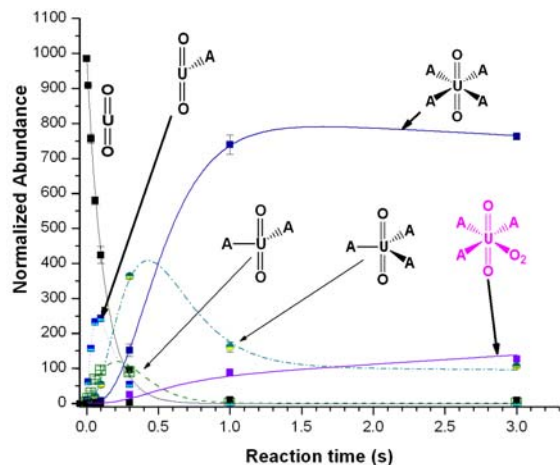


Figure 1. Kinetic profile showing addition of consecutive addition of acetone (A) and O_2 to $[\text{UO}_2]^+$.

The dioxo U(V) complex was best described as a ligated $[\text{UO}_2^{2+}\text{O}_2^-]$ ion pair.

New horizons were also revealed by examining fragmentation reactions of uranyl complexes. Fragmentation of undercoordinated $[\text{UO}_2\text{NO}_3(\text{ROH})_n]^+$ showed elimination of HNO_3 , indicating that in the local environment of the U center, the alcohol was functioning as a stronger acid than was HNO_3 .⁴ In the case where R = isopropyl, the isopropoxy ligands present on the intermediates that were formed by the HNO_3 elimination then underwent U-mediated oxidation, forming both acetone and acetaldehyde and eliminating H_2 at the same time.⁵ Other evidence for U insertion into C-H and C-C bonds has since been observed in amide and phosphoryl complexes.

This research was supported by the U. S. Department of Energy, and by the National Science Foundation.

¹ Gresham, G. L., et al. *J. Phys. Chem. A*, **2003**, *107*, 8530.

² M. J. Van Stipdonk et al., *J. Phys. Chem. A.*, **2004**, *108*, 10448.

³ G. S. Groenewold et al.; *J. Am. Chem. Soc.*, **2006**, Web Release: 2/11/2006; DOI: 10.1021/ja0573209.

⁴ Van Stipdonk, M. J., et al. *J. Am. Soc. Mass Spectrom.*, **2003**, *14*, 1205.

⁵ Van Stipdonk, M. J., et al., *Int. J. Mass Spectrom.*, **2004**, *237*, 175.

Soft X-ray Synchrotron Radiation Investigations of Actinide Materials

D. K. Shuh^{*}, H. J. Nilsson^{*†}, T. Tyliczszak^{*}, R. E. Wilson^{*}, S. M. Butorin[‡], K. Kvashina[‡], J.-H. Guo^{*}, L. Werme^{†‡}, and J. A. Nordgren[‡]

^{*}Lawrence Berkeley National Laboratory, Berkeley, CA 94720 USA

[†]SKB, Box 5864, S-102 40, Stockholm, Sweden

[‡]Dept. of Physics, Uppsala University, Box 530, S-751 21, Uppsala, Sweden

INTRODUCTION

Microspectroscopic and fluorescence-based techniques have been exploited for investigations of actinide materials at sources of soft X-ray synchrotron radiation (SR) because of the capability to perform experiments with small amounts of actinide materials. Soft x-ray SR methods are able to elucidate the roles of the 5f electrons in the chemical bonding of the actinides, characterize the electronic structures of actinide materials, and probe the surface chemistry of actinide materials. Soft x-ray SR techniques generally require optimization and modification of experimental hardware for use with radioactive materials. Results from soft x-ray SR investigations have had and will impact in areas of actinide science related to f-electron bonding, aging, corrosion, gas-solid interactions, actinide transport, and the development of nanoscale actinide materials characterization techniques.

At the Advanced Light Source of Lawrence Berkeley National Laboratory (LBNL), we have been utilizing and developing soft x-ray methods for use with actinide materials. Currently, we have been regularly employing near-edge x-ray absorption fine structure (NEXAFS), x-ray emission spectroscopy (XES), resonant inelastic x-ray scattering (RIXS), and scanning transmission x-ray microscopy (STXM) to investigate a range of fundamental properties in actinide and actinide-relevant materials.

ACTINIDE SCANNING TRANSMISSION X-RAY MICROSCOPY

The ALS Molecular Environmental Science (ALS-MES) STXM has been developed into a characterization tool for actinide particulates and for general soft x-ray actinide science. The ALS-MES STXM permits NEXAFS and imaging with 30 nm spatial resolution. The results from studies of U, Np, and Pu oxides will be presented, demonstrating the capabilities and limitations of soft x-ray STXM spectromicroscopy for investigations of actinide systems^{1,2}. The actinide 4d edges are employed for both imaging and for oxidation state determination. Of particular importance is the capability to directly probe the edges of light elements by NEXAFS, such as the oxygen K-edge, that are integral constituents of many actinide materials. A plutonium elemental map from a particle obtained during precipitation of colloids containing Pu is shown in Figure 1. Representative oxygen K-edge spectra from the AnO₂ were collected, and for UO₂, the spectrum resembles the oxygen K-edge from the bulk material. Actinide sample preparation methods, as well as sample radiation damage considerations, will be described.

ACTINIDE X-RAY EMISSION/RESONANT INELASTIC X-RAY SCATTERING

Soft x-ray XES and RIXS investigations of actinide materials have been performed at the actinide 5d and light element 1s edges at ALS Beamline 7.0.1. Reference spectra have been collected from the dioxides of uranium through plutonium. The chemical reactions of aqueous transuranic species with Fe surfaces have been characterized under the same conditions as in previous studies of U interactions with Fe surfaces³. For Np, the oxidation state of the surface species was Np(V) since the RIXS loss features differed from those of NpO₂. The first Np measurements have been followed by recent studies of PuO₂ and Pu interactions with Fe. The initial XES/RIXS measurements of curium have also been recently performed. Complementing the spectroscopy at the actinide 5d edge have been the measurements of several actinide oxide reference materials at the oxygen K-edge.

In addition to the bonding information gained on fundamental actinide reference materials, the application of NEXAFS/XES/RIXS at both the actinide and light element edges has the potential to fully characterize the nature of bonding in a larger range of actinide materials and complexes.

This work was supported by the Director, Office of Science, Office of Basic Energy Sciences, Division of Chemical Sciences, Geosciences, and Biosciences of the U.S. Department of Energy at the Lawrence Berkeley National Laboratory under Contract No. DE-AC02-05CH11231.

- 1 H. J. Nilsson, T. Tylliszczak, R. E. Wilson, L. Werme, D. K. Shuh, *J. Anal. Bioanal. Chem.* **383**, 41 (2005).
- 2 H. J. Nilsson, T. Tylliszczak, R. E. Wilson, L. Werme, D. K. Shuh, *Proc. Royal Soc. Chem.*, in press, (2006).
- 3 S. M. Butorin, D. K. Shuh, K. Kvashnina, I. Soroka, K. Ollila, J.-H. Guo, K. E. Roberts, L. Werme, J. Nordgren, *Mater. Res. Soc. Symp. Proc.* **807**, 166 (2004).

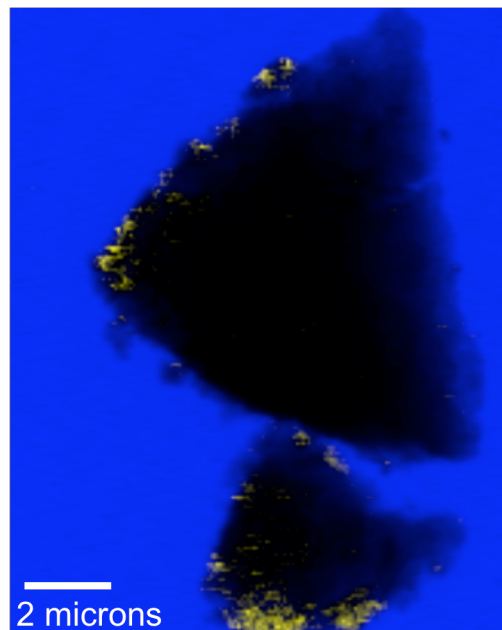


Fig. 1: Elemental map of plutonium (yellow) on silicon dioxide particles collected with the ALS-MES Beamline 11.0.2 STXM.

Electrochemical Studies of Actinide Species in Room Temperature Ionic Liquids

M. E. Stoll^{*}, W. J. Oldham[†], D. A. Costa^{*}

Los Alamos National Laboratory, Los Alamos NM 87545 USA

^{*}Nuclear Materials Technology Division (NMT-15) and [†]Chemistry Division (C-INC)

The use of room temperature ionic liquids (RTIL's) for electrochemical methods is currently receiving a great deal of attention¹. The properties of RTIL's that make them advantageous for electrochemistry include a large electrochemical window (~5 V), relatively high conductivity, negligible vapor pressure, and high thermal stability. Our research efforts have focused on exploring the electrochemical behavior of actinide ions and complexes in RTIL's comprised mainly of the bis(trifluoromethylsulfonyl)imide anion, $^-\text{N}(\text{SO}_2\text{CF}_3)_2$, paired with 1,3-dialkylimidazolium, quaternary ammonium, and pyrrolidinium cations. The electrochemical behavior of actinide complexes in non-aqueous media is an area of research that deserves further attention due to the potential for new processing methods. The inherent properties of RTIL's compared to conventional organic solvent/supporting electrolyte systems and molten salts may make them ideally suited for the processing of nuclear materials. In this regard knowledge concerning the fundamental redox behavior of actinide complexes in RTIL's is needed. Our presentation will focus on our recent results with coordination and organometallic complexes of uranium including some novel imido analogs of the uranyl ion prepared recently by our colleagues at LANL². Another related aspect of our research that will be covered concerns the electrodeposition of electropositive metal ions from RTIL solutions. Pyroprocessing in molten salt media is a powerful method of purification and separation for actinide metals. The ability to perform similar processes at ambient temperature in RTIL's could enable more efficient processes with increased safety. Results on the cathodic electrodeposition of Na, K, Li, and Al ions will be presented along with our efforts to date on the electrodeposition of uranium.

1 P. He, H. Liu, Z. Li, J. Li, *J. Electrochem. Soc.* **152**, E146, (2005) and references therein.

2 T.W. Hayton, J.M. Boncella, B.L. Scott, P.D. Palmer, E.R. Batista, and P.J. Hay, *Science* **310**, 1941 (2005).

Hydrolysis of Plutonium(IV) in 0.5 M HCl/NaCl

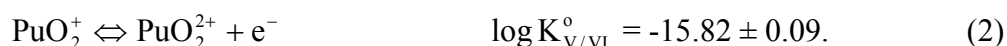
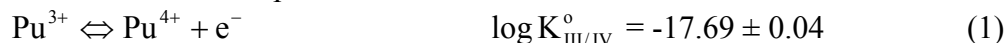
J.-I. Yun^{*}, H.R. Cho^{*}, M. Altmaier^{*}, V. Neck^{*}, A. Seibert[†], C.M. Marquardt^{*}, C. Walther^{*}, Th. Fanghänel^{*}

^{*}Institut für Nukleare Entsorgung, Forschungszentrum Karlsruhe, D-76021 Karlsruhe, Germany

[†]European Commission, JRC, Inst. for Transuranium Elements, D-76125 Karlsruhe, Germany

There have been a number of potentiometric, extraction, solubility, and spectrophotometric studies of the first hydrolysis constant of Pu(IV) as discussed in the NEA-TDB.^{1,2} The values scatter by about 1.5 orders of magnitude primarily because of redox reactions. Reliable hydrolysis constants can be found only when the electrochemical potentials are cautiously controlled, and when the total equilibrium Pu(IV) concentrations in solution are measured. None of the available studies provide reliable thermodynamic data for higher hydrolyzed species of Pu(IV). The extraction study of Metivier and Guillaumont³ was considered as the best available.^{2,4}

A spectrophotometric study of the hydrolysis of Pu(IV) in 0.5 M H/NaCl is performed in the concentration range from 10^{-5} to $3 \cdot 10^{-4}$ mol/l and at pH_c 0.3 – 2.1. The Pu(IV) stock solutions are prepared electrochemically by oxidation of Pu(III) and the oxidation state distribution is confirmed by spectrophotometry (UV/Vis for higher concentrations, 1-m capillary waveguide UV/Vis for lower concentrations). The redox potentials are both measured and calculated from the plutonium oxidation distributions by spectrophotometry using well-known equilibrium constants for the redox reactions of plutonium.^{1,2,4}



Our recent study⁵ demonstrates that the molar absorbance of Pu(IV) at 470 nm remains unaffected by mononuclear hydrolysis and the normalized absorption spectra of the first and the second hydrolyzed species ($\text{Pu}(\text{OH})_n^{4-n}$, $n = 1,2$) do not differ from those of the Pu^{4+} ion. The decrease in the molar absorbance of Pu(IV) is merely ascribed to the formation of polymeric and/or colloidal species. Therefore, the total equilibrium concentration of $\text{Pu(IV)}_{\text{aq}}$ can be determined directly by spectrophotometry. By applying the hydrolysis constants of Pu(IV) selected in the NEA-TDB^{1,2} and using Eq. (3), the equilibrium concentration of the Pu^{4+} ion is calculated:

$$[\text{Pu}^{4+}] = [\text{Pu(IV)}_{\text{aq}}] / (1 + \sum_{y=1}^4 \beta'_{1y} [\text{OH}^{-}]^y). \quad (3)$$

In parallel, the poised Eh values of the plutonium oxidation distributions are measured with Pt and Ag/AgCl reference electrode and corrected versus the SHE ($pe = 16.9 \cdot Eh(\text{V})$ at 25°C) for the purpose of comparison.

As shown in Fig 1 a), the pe values calculated from the plutonium redox couple, Pu(V)/Pu(VI) (○), are consistent with the measured pe values (+). However, the pe values calculated from Pu(III)/Pu(IV) couple (□) deviate. This implies that the formation constants of hydrolyzed Pu(IV) species² are overestimated. Combining Eq. (1) and (3) allows the independent determination of the hydrolysis constants of Pu(IV):

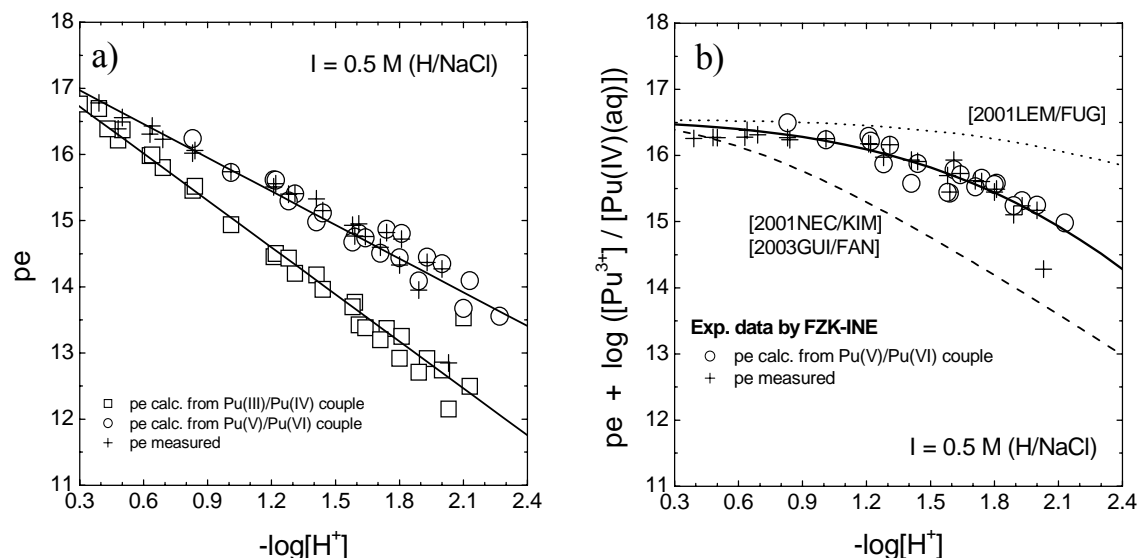


Fig 1: a) Redox potentials calculated from the different plutonium couples, Pu(III)/Pu(IV) (\square) and Pu(V)/Pu(VI) (\circ) by using Eq. (1) and (2) based on the spectrophotometry and measured pe values (+), b) Calculation with Pu(IV) hydrolysis constants of the present work (solid line) in comparison with calculation using previous selections (dotted line¹ and dashed line^{2,4}).

$$pe + \log([Pu^{3+}]/[Pu(IV)_{aq}]) = -\log K'_{III/IV} - \log\left(1 + \sum_{y=1}^4 \beta'_{1y} [OH^-]^y\right). \quad (4)$$

The first, the second, and the third hydrolysis constants for Pu(IV) determined in our study and corrected to $I = 0$ with the SIT are systematically lower than those of Metivier and Guillaumont selected in recent reviews:^{2,4}

$$\begin{aligned} \log \beta_{11}^{\circ} &= 14.0 \pm 0.2 \quad (\log \beta_{11}^{\circ} = 14.6 \pm 0.2^{2,4}) \\ \log \beta_{12}^{\circ} &= 26.8 \pm 0.6 \quad (\log \beta_{12}^{\circ} = 28.6 \pm 0.3^{2,4}) \\ \log \beta_{13}^{\circ} &= 38.9 \pm 0.9 \quad (\log \beta_{13}^{\circ} = 39.7 \pm 0.4^{2,4}). \end{aligned}$$

- 1 R.J. Lemire, *et al.*, (OECD-NEA TDB) Chemical thermodynamics of neptunium and plutonium, Elsevier (2001).
- 2 R. Guillaumont, *et al.*, (OECD-NEA TDB) Update on the chemical thermodynamics of uranium, neptunium, plutonium, americium and technetium, Elsevier, (2003).
- 3 H. Metivier and R. Guillaumont, Radiochem Radioanal Lett **10**, 27 (1972).
- 4 V. Neck and J.I. Kim, Radiochim Acta **86**, 1 (2001).
- 5 C. Walther *et al.*, submitted to: Radiochim Acta (2006).

Anhydrous Photochemical Reduction of Well-defined Uranyl(VI) Complexes

P. Duval*, S. Kannan

*University of Missouri-Columbia, Columbia MO 65211 USA

Abstract

Applications directed toward the remediation and reprocessing of nuclear waste have focused on various redox strategies to immobilize soluble UO_2^{2+} to insoluble U(IV), employing microorganisms (i.e., sulfate-reducing bacteria)¹ or chemical (i.e., citrate, TiO_2 , $\text{Fe}(0)$), electrochemical or photochemical reduction methods.² The photochemical reduction with substrates such as alcohols is considered to proceed through two steps, entailing a one-electron reduction to uranyl(V) followed by the disproportionation of the unstable UO_2^+ intermediate, although mechanistic details remain remarkably sparse.³ While the redox instability of the UO_2^+ ion hampers study of this elusive oxidation state, details are even murkier surrounding the transformation of the dioxo group and the identity of the final uranium(IV) species, as well as the complex interplay of the bimolecular disproportionation reaction. Although these reactions have been evaluated under a variety of experimental conditions, perhaps the most important factor that influences this redox chemistry, *the coordination sphere of the precursor uranyl species*, has largely been ignored.

It is in this context that the photochemical reactivity of *well-defined cationic uranyl(VI)* complexes under *non-aqueous* conditions employing systematic control over variable experimental conditions (i.e., light source, reductant, solvent, etc.) is presented, with a focus on structural and electronic characterization of the products. The results offer mechanistic insight into alternate pathways of dioxo activation during the photochemical reduction of uranyl(VI) that are operable only under anhydrous conditions.

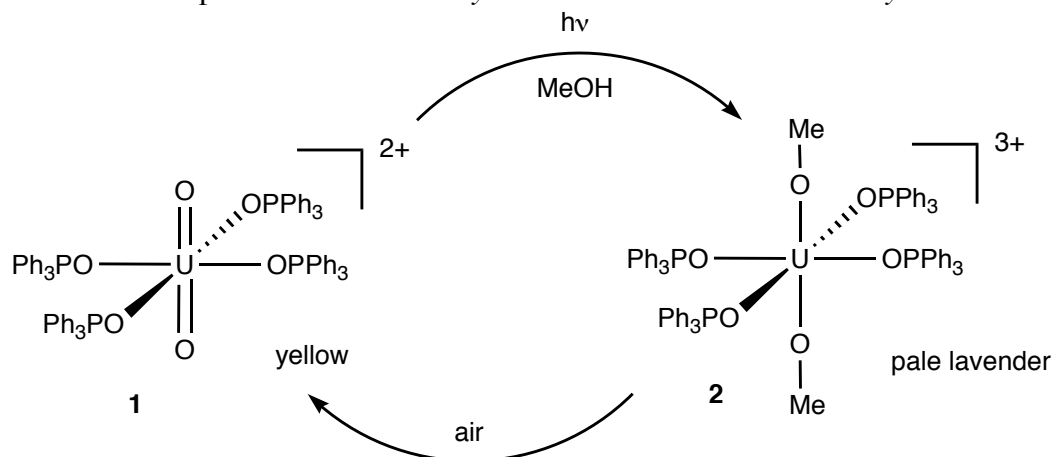


Fig 1: Reversal in the normal trend of uranyl(VI) reactivity: interchanging axial occupancy with an intact equatorial coordination sphere.

One example illustrated in Figure 1 includes an unprecedented reversal of the normal trend in uranyl ligand substitution reactivity, whereby the equatorial coordination sphere *remains intact* while the axial site occupancy cleanly and *reversibly* interchanges between oxo and methoxide ligands. Replacement of the dioxo unit with *trans* methoxide groups occurs during the photochemical reduction of a uranyl(VI) complex in *anhydrous* methanol, yielding a uranium(V) methoxide complex **2** instead of the expected tetravalent oxidation state. Complex **2** quantitatively reverts to the starting uranyl(VI) precursor upon exposure to air.

This work was supported by the American Chemical Society Petroleum Research Fund, the Missouri University Research Reactor, and the University of Missouri Research Board.

- 1 R B Payne, D M Gentry, B J Rapp-Giles et al., Appl. Environ. Microbiol. **68**, 3129 (2002).
- 2 T M McClesky, T M Foreman, E E Hallman et al., Environ. Sci. Technol. **35**, 547 (2001).
- 3 C P Baird and T J Kemp, Prog. React. Kinet. **22**, 87 (1997).

Spectrophotometric Determination of Iron in Plutonium Materials: Qualification and Trace Optimization

K. Garduno*, E. J. Lujan*, L. F. Walker*, and L. Tandon*

*Los Alamos National Laboratory, Los Alamos, NM 87545 USA

ABSTRACT

The Plutonium Assay Team within the Analytical Chemistry Group (C-AAC) at Los Alamos National Laboratory performs a broad range of analyses for the Pit Manufacturing Project including: “Controlled-Potential Coulometric Determination of Plutonium in Sulfuric Acid Electrolyte” (CPC) and “Spectrophotometric Determination of Iron in Plutonium Materials.” The standard spectrophotometric method that is presently used for iron analyses has been used for over fifty years and has not been superseded by any other instrumentation method. Inductively Coupled Plasma by Mass Spectrometry (ICP-MS), Inductively Coupled Plasma by Atomic Emission Spectrometry (ICP-AES), and X-Ray Fluorescence (XRF) are all methods that can be used to determine iron concentrations; however, these methods are quite limiting primarily because the instrumentation is expensive and the analytical results do not meet the accuracy and precision attained by using the spectrophotometric procedure. The iron determination must be performed prior to the CPC determination for total plutonium because iron is quantitatively oxidized during CPC measurement. Iron assay can have a significant impact on the final results of the plutonium assay where each 23 ppm of iron content will contribute to a 0.01% correction to the plutonium value by CPC. Significant experimental work has been performed on the methodology of “Spectrophotometric Determination of Iron in Plutonium Materials” to qualify the method for pit manufacturing. This method was initially developed for the assay of iron in various plutonium materials. The major steps in this procedure are reduction to iron(II) and plutonium(III) oxidation states with hydroxylamine hydrochloride; separation of plutonium by oxalate precipitation; formation of the iron-orthophanthroline complex; and spectrophotometric measurement. When the plutonium metals or oxides have been dissolved, it is recommended that the sample aliquot that will be analysed for iron is an aliquot taken from the same solution that has been dissolved and prepared for the coulometric determination of plutonium. Hydroxylamine is added to the supernate to ensure complete reduction of iron to Fe(II). The Fe(II) o-phenanthroline complex is formed in an acetate-buffered solution at pH 6. Iron is measured as the Fe(II) o-phenanthroline complex at 510 nm. The spectrum is characteristically broad and a spectrophotometer with a broad pass of up to 10 nm is acceptable.

Since the instruments used in many analyses range from the newest state-of-the-art to older, aging equipment, the pit manufacturing program requires that all analytical instruments be qualified before they are used to analyse materials that will eventually be used in the weapons program. To maintain this robust capability, certification of a backup instrument is required in case the currently qualified instrument fails. It is evident that there is value added to the pit manufacturing program because it avoids a single-point failure for plutonium as well as for iron

assay. Since the instrument for iron assay is relatively inexpensive, the qualification of a second instrument as backup is an economically sound investment. The analytical instrument currently used for the spectrophotometric determination of iron in plutonium materials is the Bausch and Lomb Spectronic 100. The experimental data that has been collected will demonstrate the accuracy and precision of the new Secomam Prim Light spectrophotometer against the qualified Spectronic 100.

Outside the qualification program, this basic procedure can be adjusted to meet varying needs. By slightly changing some of the parameters of the procedures, further experiments involving lower detection limits for electro refined plutonium metal have been completed using the same methods and instruments previously mentioned. Through dilution techniques the upper limits for iron determination may extend into the percent range. Using controls for lower detection limits, the iron content can be measured as low as <10 ppm. At the high end the relative precision is 2% and at the low end a precision of 5 ppm absolute can be obtained.

LA-UR-06-1132



Photo A: After reduction to the Pu(III) oxidation state, the oxalic acid is added and the oxalate precipitate appears immediately.



Photo B: After the reduction to Fe(II), the iron-orthophenanthroline complex forms.

Development of a Continuous Crystallization Process for Separating Uranium from Nitric Acid Solution

D. Ford, G. Jarvinen, D. Mullins, M. Mayne, H. Reichert, R. Gonzales

Los Alamos National Laboratory Los Alamos, NM 87545

Crystallization of uranyl nitrate at low temperatures from nitric acid solution has been considered as a potential head-end process for removing most of the uranium from spent light water reactor fuel after the fuel is dissolved in nitric acid. The crystallization process potentially could reduce the cost of LWR fuel partitioning because it provides a selective and compact process for removing most of the uranium. Subsequent separation processes would only need to handle the smaller volume of remaining actinides and the fission products. We have evaluated an approach that uses a continuous adiabatic crystallizer operating near room temperature. The crystallizer vessel chosen is a vertical circulating loop where the solution will be cooled and concentrated by the evaporation of a portion of the nitric acid and water at reduced pressure; uranyl nitrate hexahydrate crystallizes from this supersaturated solution. The distilled acid can be recycled for use in the fuel dissolver, for crystal washing, or for dissolving washed crystals. A detailed process flowsheet was defined and data on crystallization conditions and decontamination factors for various fission product elements has been obtained from small-scale batch tests. Prototype continuous crystallizer units have been built and tested first using non-radioactive solutions and then depleted uranyl nitrate solution. The progress to date on developing this crystallization process will be reviewed.

Self-Diffusion Coefficients and Structure of the Trivalent f-Element Ions, Eu, Gd and Am , Bk, Cf and Es in Aqueous Solution

H. Latrous

Faculté des Sciences de Tunis, 2092 El-Manar, Tunisia

This paper is dedicated to the memory of J. Oliver[†] TLR Oak Ridge, USA and M Chemla[†] Paris VI - France

INTRODUCTION

Self-diffusion coefficients D of the trivalent aquo ions of Eu, Am and Bk have been determined in dilute (pH =2.5) HClO_4 , $\text{Nd}(\text{ClO}_4)_3\text{-HClO}_4$ solutions at 25°C by an open end capillary method (O.E.C.M.). This method measures the transportation time of ions across a fixed distance. The variation of D versus the square root of the concentration of the solution was found to be non-linear in the studied concentration range. The limiting value D_0 for **f-Element trivalent ions, Eu, Gd and Am , Bk, Cf and Es in Aqueous Solution** at zero ionic strength are respectively 6.10 , 5.90 , 6.19 , 5.95 , 5.72 and $5.72 \times 10^{-6} \text{ cm}^2\text{s}^{-1}$. The plot of $D = f(\sqrt{C})$ for the **Am, Cf and Bk** trivalent ions can be compared to those for **Eu, Es and Gd** obtained under the same conditions, tacking into account of electronic configuration,

Moreover, it may be argued that the trivalent ions of **Eu, Gd , Am , Bk, Cf and Es** in aqueous solutions, have the same hydration number, as the $5f$ and $4f$ trivalent ions in the absence of hydrolysis, complexing or ion pairing at pH 2.5 should be the same.

EXPERIMENTAL METHOD

The O.E.C.M has been run at a constant temperature ($T = 25 \pm 0.01^\circ\text{C}$)^[1]. The quartz capillaries of length 1 were filled with an electrolyte solution of concentration C labelled with the radioactive tracer $^{152}\text{Eu}^{3+}$, $^{153}\text{Gd}^{3+}$ and $^{241}\text{Am}^{3+}$, $^{249}\text{Bk}^{3+}$, $^{249}\text{Cf}^{3+}$ and $^{254}\text{Es}^{3+}$. The radioactive solution was kept in contact with an inactive solution of the same composition. We denote by $C_0(x,0)$ the total activity in the capillary at time $t = 0$. After a diffusion time t , the final average activity will be $C(x,t)$. By solving Fick's equation with the proper limiting conditions, the ratio $C(x,t)/C_0(x,0)$ can be related to the self-diffusion coefficient D by the equation:

$$D_i = D_i^0 - \frac{a\sqrt{C}}{(1 + b\sqrt{C})} \quad (1)$$

The radioactivity measurements have been carried out separately for each actinide. For Eu, Gd , Am, and Cf, which are gamma emitters, the measurements were obtained directly on quartz capillary using a hollow NaI crystal detector.

For the alpha emitter Es, the initial and final activities were measured as the specific activities of the inner solutions.

The beta counting of $^{249}\text{Bk}^{3+}$ has been confirmed by alpha radiometry.

RESULTS AND DISCUSSION

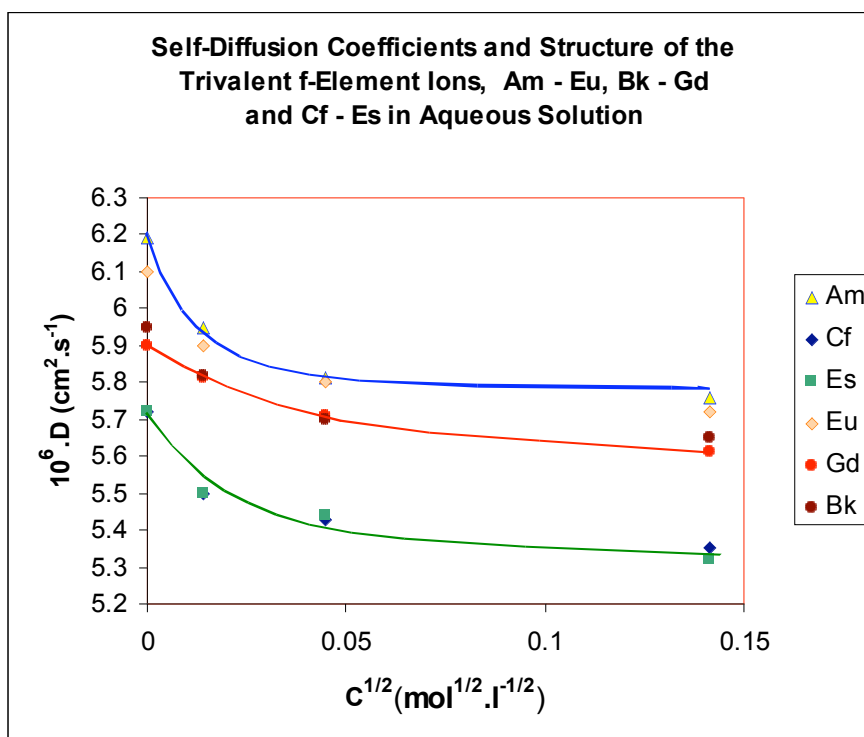
Experimental results of self diffusion coefficients ($10^6 \cdot D \text{ cm}^2 \cdot \text{s}^{-1}$) are shown in table 1^[2,3]

Table 1: Experimental Self Diffusion coefficients Values for 4f and 5f trivalent ions

C	$c^{1/2}$	Am	Cf	Es	Eu	Gd	Bk
0	0	6.19	5.72	5.72	6.1	5.9	5.95
0.0002	0.01414214	5.95	5.5	5.5	5.9	5.81	5.82
0.002	0.04472136	5.81	5.43	5.44	5.8	5.71	5.70
0.02	0.14142136	5.76	5.35	5.32	5.72	5.61	5.65

The plot of $D=f(C^{1/2})$: are shown in figure 1

Figure 1: Self Diffusion coefficients Values for trivalent ions of the selected f-Elements Shown.



The values of hydration numbers of trivalent ions are given in table 2.

Table 2: Hydration number for some 4f and 5f trivalent ions^[5]

Element	Am	Eu	Bk	Gd	Cf	Es
N	9	8.76	(8.8)	8.4	9	8.1

The plot of $D = f(\sqrt{C})$ (Figure 1) for these f-Elements trivalent ions shows the similarity as following :

- **Am** and **Eu** has similar electronic configuration the $4f^7$ et $5f^7$
- **Cf** and **Es** has similar sub shell 5f and successive elements , $5f^{10}7s^2$, $5f^{11}7s^2$
- **Bk** and **Gd** has 5f and 4f sub half-filled configuration $5f^9 7s^2$ and $4f^7 5d^1 6s^2$

The electronic configuration of 4f and 5f-Elements are given by G.T Seaborg

CONCLUSION

We have avoid hydrolysis, complexing and ion pairing by working at $\text{pH} = 2.5$.

- The results of diffusion of **Cf** and **Es** shows us that the **5f** elements whose has similar sub shell 5f half-filled configuration, has the same behavior .
- Results of diffusion of the two couples **Am - Eu** and **Bk - Gd** shows us that **4f and 5f**, similar electronic configuration and sub half-filled configuration ,trivalent ions element has the same behavior ^[4,6].

We can conclude that we can predict the transport properties of 4f elements from 5f elements and reverse.

The observations on plot of $D = f(\sqrt{C})$ for these f-elements trivalent ions make a diagnostic on the other 4f and 5f-Elements .

The variation of D is the same for 4f and 5f-Elements having the same configuration and in the case of filling the second half of shell 4f or 5f. Theses results are confirmed by the same hydration number ~ 8 (water molecules) ^[5].

Acknowledgements: We thank Prof. L.G. Haire(TRL., Oak-Ridge USA) , P.Turq (PARIS VI P.M. Curie), R.Guillaumont, (PARIS XI) J.Barthel (Regensbourg) for helpful discussions and suggestions. We thanks Dr M. Fluss for the invitation to attend **Pu Futures-2006**.

References

1. H. Latrous, Rev. Fac. Sci. Tunis, 1 (1981) 75.
2. H. Latrous, M. Ammar, J. M'Halla, Radiochem. Radioanal.Lett., 53 (1982) 33.
3. H. Latrous, J. Oliver, M. Chemla, Zeitschrift, fur Physikalishce Chemie, Neue Folge, 159(1988)195..
4. H. Latrous & J Oliver Radioanal.Nucl, Chem. Act, 156: 291-296 (1992)
5. F. H. David and B. Fourest, New J. Chem., 1997, 21, n°2, 167-176
6. H. Latrous & J.Oliver J.Mol .Liq, 81 (1999) 115-121

Solubility and Solubility Product of Tetravalent Metal Hydrous Oxides

T. Sasaki*, T. Kobayashi*, K. Fujiwara†, I. Takagi*, H. Moriyama*

*Department of Nuclear Engineering, Kyoto University, Kyoto 606-8501 Japan

†Japan Atomic Energy Agency, Muramatsu, Tokai, Naka-Gun, Ibaraki 319-1194 Japan

INTRODUCTION

The solubility products of actinides and fission products are one of the most important factors to be considered for the safety assessment of radioactive waste disposal since it directly controls their solubility. However, the reported values especially for tetravalent actinides often scatter and there are very large differences of several orders of magnitude between the lowest and the highest values. It has been recognized that such large differences are possibly due to the chemical property of samples, the solubility as low as the detection limit, the long equilibration period, the separation technique, and so on.^{1,2} Careful measurements and analysis are thus needed for the solubility of tetravalent actinides. For comparison, we have measured the solubility of a similar tetravalent metal, zirconium, in our recent study.³ Zirconium was observed to form not only mononuclear species but also polynuclear or colloidal species even in the lower pH region by hydrolysis reaction. In the present study, the results of zirconium are discussed by comparing with those of tetravalent actinides.

SOLUBILITY CURVES

The solubility of Zr at 25°C and a given ionic strength with NaClO₄ was measured by ICP-MS after separating the aqueous phase from the solid phase by the ultrafiltration method (3k Da NMWL membrane). The solid phases used were the amorphous hydrous oxide, Zr(OH)₄(am), and crystal oxide, ZrO₂(cr), for over- and undersaturation methods, respectively. Obtained results are shown in Fig.1. The solubility for Zr(OH)₄(am) decreases with an increase of pH in the acidic condition, and it is not significantly dependent on the ionic strength. On the other hand, much lower solubility for ZrO₂(cr) was obtained from

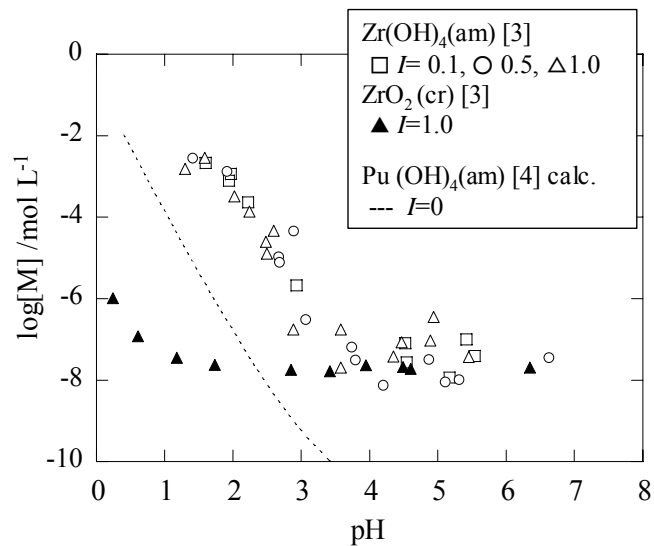


Fig 1: Solubility of tetravalent metal oxides as a function of pH.

undersaturation. It is interesting to note that, in spite of different conditions of the initial solid phase, the two solubility curves agreed with each other at higher pH than 4 as low as 10^{-7} to 10^{-8} mol L⁻¹.

For comparison, the solubility curve for Pu(OH)₄(am), predicted by the improved hard sphere model, is also shown in Fig.1⁴. It is noticed that the predicted curve is almost composed of mononuclear hydrolysis species of Pu(OH)³⁺, Pu(OH)₂²⁺ and Pu(OH)₃⁺ in equilibrium with Pu(OH)₄(am) while the observed solubility curve for Zr(OH)₄(am) may include not only mononuclear species but also polynuclear or colloidal species. A careful analysis is then needed to obtain the solubility product values.

SOLUBILITY PRODUCTS

The solubility product ($\log K_{sp}^{\circ}$) values at ionic strength $I=0$ were obtained from the solubility data by using the SIT corrections. Fig. 2 shows a comparison of the K_{sp}° values of tetravalent metal oxides, in which the values are plotted as a function of the inverse square of the M⁴⁺ ionic radii. Different trends of the K_{sp}° values are clearly observed for tetravalent actinides and for zirconium, which may be explained by considering non-electrostatic interactions of actinides.

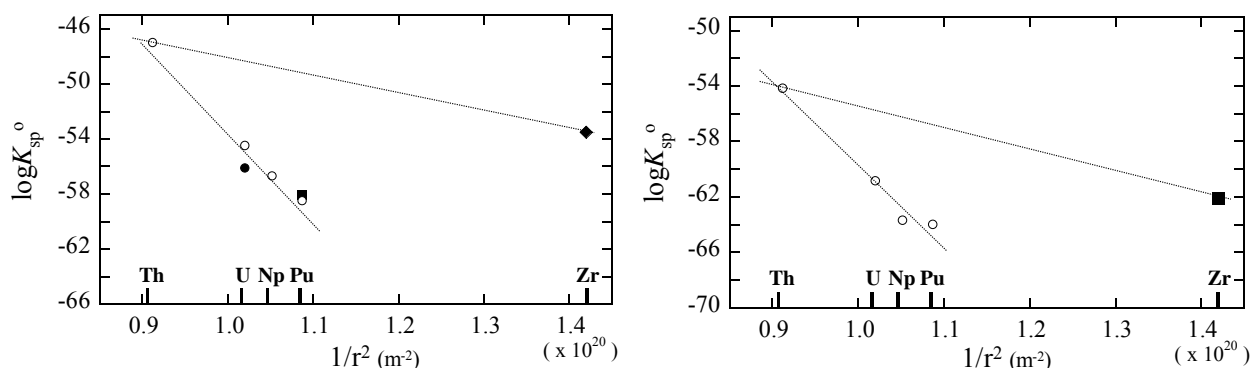


Fig 2. Variation of solubility product values for M(OH)₄(am) (left) and MO₂(cr) (right) of actinides^{1,2} and zirconium³.

- 1 V. Neck and J.I. Kim, Radiochim. Acta, **89** (2001) 1.
- 2 K. Fujiwara, H. Yamana, T. Fujii and H. Moriyama, Radiochim. Acta, **90** (2002) 857.
- 3 T. Kobayashi, *et al.*, submitted to: Radiochim. Acta., (2006).
- 4 H. Moriyama, T. Sasaki, T. Kobayashi and I. Takagi, J. Nucl. Sci. Technol., **42** (2005) 626.

Ternary Complex Formation of Eu(III) and Am(III) with Pyridine-2,6-dicarboxylate in Aquatic Solutions

K.K. Park, T.R. Kwon, Y.J. Park, E.C. Jung, W.H. Kim

Korea Atomic Energy Research Institute, 150 Deokjin-dong, Yuseong, Daejeon, Korea, 305-353

1. INTRODUCTION

Reliable estimates of radionuclide solubilities are needed for the safety assessment of nuclear fuel disposal in an underground vault. Solubility of radionuclides in an aquatic system is controlled mainly by solid-water equilibria and partially by complexation with ligands coexisting in the aquatic system. Many researches on the binary complex formation of radionuclides with carbonate and several organic ligands have been performed. More recently, studies on the ternary complex formation are of interest because organic matters react with binary hydrolyzed- or carbonate- complexes to form a ternary complex, thereby affecting the solubility of radionuclides.

In this work, the hydrolysis and the carbonate complexation of Eu(III) and Am(III) in the presence of pyridine-2,6-dicarboxylate are investigated.

2. EXPERIMENT

Ternary complex formation of M(III)-L-OH and M(III)-L-CO₃ (M=Eu or Am with trace ²⁴¹Am, L= pyridine-2,6-dicarboxylate) was investigated in the pH range of 7 to 10 in 0.1 and 0.01 M NaClO₄ media at 25 °C. For the formation of M-L-OH, NaOH free of CO₂ was added to the metal-ligand solution (M=0.1 mM, L=0 to 0.15 mM) of pH 7 under Ar gas environment. For the formation of M-L-CO₃, HClO₄ was added to the solution containing Na₂CO₃ (0.2 to 10 mM) of pH 10 in air sealed vessel. The precipitate was separated by filtration or by centrifugation. The content of metal in aqueous phase was determined by ICP-AES or ICP-MS (Eu), LSC (²⁴¹Am) and that of ligand was determined by absorption spectrophotometry (in the presence of excess EDTA at pH 8). Finally, the composition of precipitate was calculated.

3. RESULTS AND DISCUSSION

An increase in pH of Eu-ligand solution ([L]/[Eu]=1) caused a precipitation at pH ≥ 7, while the precipitate was not observed in case of [L]/[Eu] ≥ 2. This suggests that another insoluble species is formed together with Eu(OH)₃ in the presence of L. From the measurement of fluorescence spectra for the solution containing dispersed precipitates ([L]/[Eu]=1, pH 8) by the excitation of 277 nm-line (absorption line of L), it was found that the emission peak of Eu at 615 nm due to 'hypersensitive' transition (⁷F₂ → ⁵D₀) was greater than that of Eu at 585 nm due to 'non-hypersensitive' transition (⁷F₀ → ⁵D₀). This spectral feature is found to be essentially the same as in the complexation between Eu³⁺ ion and ligands,¹ indicating that the precipitate has a Eu-L bond to exert intra-molecular energy transfer. These observations can be explained by the formation of ternary complex such as {EuL(OH)}⁰ through the reaction between {EuL}⁺ and OH⁻.

The removal of Eu and L from aqueous phase by precipitation depended on pH as well as the concentrations of L and carbonate. In absence of carbonate and L, the removal of Eu began at

about pH 7.2 and was completed at pH lower than 8. In the presence of L alone, the removal of Eu started at higher pHs, *i.e.* 7.6 when [L]/[Eu]=1.0 and 7.9 when [L]/[Eu]=1.5, and the removal was not completed even at pH 10. Simultaneously, the removal behavior of ligand with respect to pH was observed essentially the same as in that of Eu. This suggests that the formation of soluble species such as $\{\text{EuL}_n\}^{(3-2n)}$ (n=2 or 3) competes with the formation of $\text{Eu}(\text{OH})_3$ and $\text{EuL}(\text{OH})$, and that the formation of $\text{EuL}(\text{OH})$ is favored over that of $\text{Eu}(\text{OH})_3$ in this experiment.

The species distribution calculation based on the stability constants² shows that, with increasing pH, the $\{\text{EuL}\}^+$ species decreases but $\{\text{EuL}_n\}^{(3-2n)}$ (n=2 or 3) species increases, thereby expected that the removal of Eu decreases. In our experiment, however, the removal of Eu did not decrease with an increase in pH. Moreover, the concentration ratio of L to Eu removed by precipitation was calculated and found to be almost constant value of 0.65 at relatively high pH. These mean that $\text{EuL}(\text{OH})$ and $\{\text{EuL}_n\}^{(3-2n)}$ are formed. It is proposed here that the formation of the former is favored over that of the latter at our experimental conditions. The solubility product of $\text{EuL}(\text{OH})$ was calculated and the value of pK_{sp} was 14.

The presence of carbonate caused a decrease in the formation of precipitate, as expected by the formation of soluble carbonate species. The concentration ratio of L to Eu in precipitates was decreased. However, the solubility of Eu was higher than expected by stability of carbonate complex³, indicating that $\{\text{EuL}\}^+$ reacts with CO_3^{2-} to form a soluble species such as $\{\text{EuL}(\text{CO}_3)\}^-$.

The trace ^{241}Am showed exactly the same removal behavior as Eu, indicating that Am(III) also can form ternary complexes of insoluble $\text{AmL}(\text{OH})$ and soluble $\{\text{AmL}(\text{CO}_3)\}^-$ species.

4. CONCLUSION

In the presence of ligand with two carbonate-functional groups, Eu(III) and Am(III) could form an insoluble hydrolyzed ternary complex, $\text{ML}(\text{OH})$ and a soluble carbonate ternary complex, $\{\text{ML}(\text{CO}_3)\}^-$. The solubility product of $\text{EuL}(\text{OH})(\text{L}=\text{pyridine-2,6-dicarboxylate})$ was determined ($\text{pK}_{\text{sp}} = 14$) and could be considered similar to that for Am(III).

Acknowledgements-This study is supported by the Ministry of Science and Technology. We thank for help to Y.B. Kim in ^{241}Am measurement with LSC, and K.S. Choi and Dr. S.H. Han in Eu measurement with ICP-AES and ICP-MS.

REFERENCES

1. Richardson, F. S. Chem. Rev. **82**, 541(1982).
2. A.E. Maetell and R.M. Smith, Critical Stability Constants, Vol. 1, Plenum Press, New York, 1974.
3. A.E. Maetell and R.M. Smith, Critical Stability Constants, Vol. 5, Plenum Press, New York, 1982.

Determining the Electronic Structure of Pu using Unorthodox Spectroscopies

James G. Tobin

*Lawrence Livermore National Laboratory, Livermore CA 94552 USA
Email: Tobin1@LLNL.Gov

DISCUSSION

The standard method to determine the band structure of a condensed phase material is to (1) obtain a single crystal with a well defined surface and (2) map the bands with angle resolved photoelectron spectroscopy (occupied or valence bands) and inverse photoelectron spectroscopy (unoccupied or conduction bands). Unfortunately, in the case of Pu, the single crystals of Pu are either nonexistent, very small and/or having poorly defined surfaces. Furthermore, effects such as electron correlation and a large spin-orbit splitting in the 5f states have further complicated the situation. Thus, we have embarked upon the utilization of unorthodox electron spectroscopies, to circumvent the problems caused by the absence of large single crystals of Pu with well-defined surfaces. The talk will include a discussion of resonant photoelectron spectroscopy [1], x-ray absorption spectroscopy [1,2,3,4], electron energy loss spectroscopy [2,3,4], Fano Effect measurements [5], and bremsstrahlung isochromat spectroscopy [6], including the utilization of micro-focused beams to probe single-crystallite regions of polycrystalline Pu samples. [2,3,6]

This work was performed under the auspices of the U.S. DOE by Univ. of California, Lawrence Livermore National Laboratory under contract W-7405-Eng-48.

REFERENCES

1. J.G. Tobin, B.W. Chung, R. K. Schulze, J. Terry, J. D. Farr, D. K. Shuh, K. Heinzelman, E. Rotenberg, G.D. Waddill, and G. Van der Laan, "Resonant Photoemission in f-electron Systems: Pu and Gd", Phys. Rev. B **68**, 155109 (October 2003).
2. K.T. Moore, M.A. Wall, A.J. Schwartz, B.W. Chung, D.K. Shuh, R.K. Schulze, and J.G. Tobin, "The Failure of Russell-Saunders Coupling in the 5f States of Plutonium", Phys. Rev. Lett. **90**, 196404 (May 2003).
3. G. van der Laan, K.T. Moore, J.G. Tobin, B.W. Chung, M.A. Wall, and A.J. Schwartz, "Applicability of the spin-orbit sum rule for the actinide 5f states," Phys. Rev. Lett. **93**, 097401 (Aug 2004).
4. J.G. Tobin, K.T. Moore, B.W. Chung, M.A. Wall, A.J. Schwartz, G. van der Laan, and A.L. Kutepov, "Competition Between Delocalization and Spin-Orbit Splitting in the Actinide 5f States," Phys. Rev. B **72**, 085109 (2005).
5. J.G. Tobin, S.A. Morton, B.W. Chung, S.W. Yuand G.D. Waddill, "Spin-Resolved Electronic Structure Studies of Non-Magnetic Systems: Possible Observation of the Fano Effect in Polycrystal Ce," Physica B, Proceedings of SCES05, Vienna, Austria, Accepted 2005.
6. J.G. Tobin, M.T. Butterfield, N.E. Teslich Jr., R.A. Bliss, M.A. Wall, A.K. McMahan, B.W. Chung, A.J. Schwartz, "Using Nano-focussed Bremsstrahlung Isochromat Spectroscopy (nBIS) to Determine the Unoccupied Electronic Structure of Pu," Royal Society of Chemistry, Proceedings of the Actinides 2005 Meeting, Manchester, UK, Accepted 2005.

Symmetry reduction of δ -plutonium: an electronic-structure effect

K.T. Moore*, P. Söderlind†, A.J. Schwartz†, D.E. Laughlin†

*Lawrence Livermore National Laboratory, Livermore, CA 94550, USA.

†Materials Science and Engineering, Carnegie Mellon University, Pittsburgh, PA 15213 USA.

Classical crystallography does not incorporate anisotropy of atomic bonds within its framework [1]. Rather, it assumes a spherical atom at each lattice site. While this assumption is justifiable for some elements, it becomes less reliable for those with complicated electronic structures. Nowhere is this more the case than with plutonium, which is the most enigmatic metal in the Period Table [2-8]. Recently, the phonon dispersion curves for single-grain δ -plutonium were recorded using inelastic X-ray scattering [9], confirming other measurements [10,11] that it is the most anisotropic face-centered cubic (fcc) metal known. The shear moduli C_{44} and C' differ by a factor of ~ 7 , which is in strong contrast to aluminum exhibiting a factor of 1.2 [12]. In addition, δ -Pu has a negative coefficient of thermal expansion and has the most crystallographically expanded lattice of all six Pu allotropes (fcc is usually the most densely packed crystal structure). This is evidence that a simple hard-sphere assumption is inappropriate for Pu and that the bonding strengths between the 12 nearest neighbors of the fcc δ -Pu lattice are not equal. In turn, this means that the total symmetry of the metal may not be fcc, but rather a lower symmetry class.

We present a novel use of first-principles calculations, which yields the bond strengths of the 12 nearest neighbors within the δ -Pu crystal. Using these calculated bond strengths, we systematically progress through crystallographic arguments showing that δ -Pu belongs to the monoclinic space group Cm rather than the cubic $Fm\bar{3}m$ space group. Our results provide new insight into why plutonium is the only metal with a monoclinic ground state and why tetragonal, orthorhombic, or monoclinic distortions of δ -Pu are likely. These distortions have considerable ramifications for the behavior of the metal as it ages, accumulating damage via self-irradiation. Finally, we anticipate the use of these calculations and crystallographic arguments in tandem will expand crystallographic determination of complicated materials to incorporate electronic structure, consequently providing a unique way to explain complex properties.

Calculating the energy response (ΔE) of a small ($\sim 2\%$) displacement of an atom along each of the 12 nearest-neighbor directions and scaling this with the displacement magnitude ($u = 0.049\text{\AA}$), an approximate force or strength of the bonds is realized. This is the “bond strength.” These energies are obtained from first-principles electronic-structure calculations within the framework of density-functional theory (DFT). This approach has proven to be accurate for most metals in the Periodic Table, including Pu [13]. The computational details are similar to those in Ref. [13] with the major difference being that here we study a 27-atom supercell of fcc Pu to allow for the above-mentioned atomic displacements. To simplify the calculations, the effect of electron spin is only accounted for by a parallel arrangement and not coupled to the orbital degree of freedom.

We begin with the assumption that the lattice is fcc with $a = b = c$; the motif is the calculated bond strengths for the 12 nearest neighbors. The results of the calculations are shown

in Figure 1. where the change in energy normalized by the displacement length ($\Delta E/u$) are given. Notice how $\Delta E/u$ varies from ~ 3.3 to ~ 5.3 , showing the large degree of variation in bond strength between the 12 nearest neighbors. The twelve nearest neighbors can be separated into six pairs of two where the bond strengths are close in value: blue (3.3), black (3.5-3.7), red (3.7-3.9), pink (3.9-4.1), green (4.5-4.7), and brown (4.7-5.3). In the (001) plane, the $[110]$ bond is roughly equal to the $[\bar{1}\bar{1}0]$ bond (green), and the $[\bar{1}10]$ bond is roughly equal to the $[\bar{1}\bar{1}0]$ bond (black). In the $\{011\}$ planes, we see that $[0\bar{1}\bar{1}] \sim [\bar{1}0\bar{1}]$ (blue), $[0\bar{1}\bar{1}] \sim [\bar{1}0\bar{1}]$ (red), $[0\bar{1}\bar{1}] \sim [\bar{1}0\bar{1}]$ (pink), and $[011] \sim [\bar{1}0\bar{1}]$ (brown). It is important to note that not only the bond strength, but also the repeatability of groupings dictate the choice of sets. In other words, there is a clear separation between the brown and pink sets and the clear separation between the red and blue sets. It is interesting that the bonds in the (001) plane are almost equal directly across the central atom, whereas the bonds in the $\{011\}$ planes are not and have a more complicated arrangement.

When an fcc lattice is joined with the calculated bond strengths as a motif, the resultant structure is *c*-centered monoclinic with the space group *Cm*; there is one mirror plane along (110). In addition, the structure is not centrosymmetric (defined as: $x = -x$; $y = -y$; $z = -z$). The reduced space group for δ -plutonium enlightens why the ground state of the metal is monoclinic, why distortions of the metal are viable, and has considerable implications for the behavior of the material as it ages.

This work was performed under the auspices of U.S. Department of Energy by the University of California, Lawrence Livermore National Laboratory under contract No. W-7405-Eng-48.

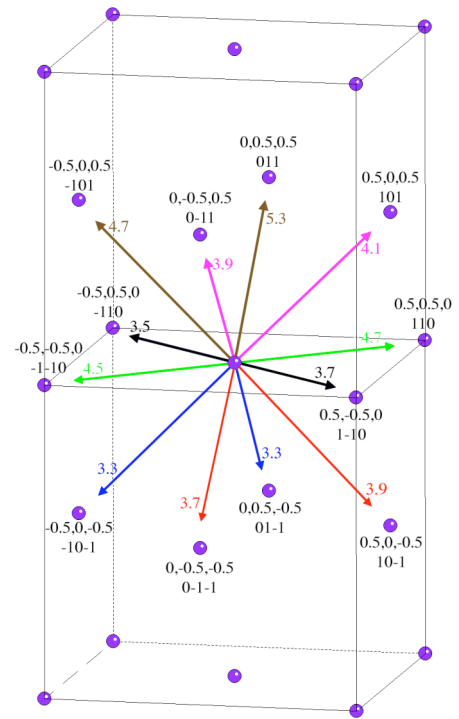


Figure 1. Calculated bond strengths for δ -Pu.

- [1] F.D. Bloss, *Crystallography and Crystal Chemistry* (Holt, Rinehart, and Winston Inc., 1971).
- [2] R.C. Albers, *Nature* **410**, 759 (2001).
- [3] S.S. Hecker, *Metall. Mat. Trans. A* **35**, 2207 (2004).
- [4] H.L. Skriver, O.K. Andersen, B. Johansson, *Phys. Rev. Lett.* **41**, 42 (1978).
- [5] J.L. Smith, E.A. Kmetko, *J Less Comm. Met.* **90**, 83 (1983).
- [6] S.Y. Savrasov, G. Kotliar, E. Abrahams, *Nature* **410**, 793 (2001).
- [7] K.T. Moore *et al.*, *Phys. Rev. Lett* **90**, 196404 (2003).
- [8] G. van der Laan *et al.*, *Phys. Rev. Lett* **93**, 097401 (2004).
- [9] J. Wong *et al.*, *Science* **301**, 1078-1080 (2003).
- [10] H.M. Ledbetter, R.L. Moment, *Acta Metall.* **24**, 891 (1976).
- [11] R. J. McQueeney *et al.*, *Phys. Rev. Lett.* **92**, 146401 (2004).
- [12] R. Stedman, G. Nilsson, *Phys. Rev.* **145**, 492 (1966).
- [13] P. Söderlind, B. Sadigh, *Phys. Rev. Lett* **92**, 185702 (2004).

Effect of Chemical and External Pressure on the Structure of Intermetallic Compound CeNi

A. Mirmelstein*, E. Clementyev*, V. Voronin†, D. Kozlenko§, A. Kutepov*, A. Petrovtsev*, Yu. Zuev*

*Russian Federal Nuclear Center – Institute of Technical Physics, Snezhinsk 456770, Russia

†Institute for Metal Physics, Russian Academy of Sciences, 620041 Ekaterinburg GSP-170, Russia

§Frank Laboratory of Neutron Physics, JINR, Dubna 141980, Russia

INTRODUCTION

The study of mechanisms of the transitions between different structural modifications for the materials with almost empty or almost filled $f_{5/2}$ -electronic configurations may provide a new insight into the origin of their ground-state properties, especially in the case if the structural transitions involve volume discontinuity driven by electron correlation effects. The intermediate-valence compound CeNi exhibits anomalous behavior of many physical properties including the first-order structural phase transition with volume discontinuity^{1,2} and well-defined ground-state coherent effects in the magnetic response function observed by the inelastic neutron scattering technique³. Thus, CeNi is an attractive model system to investigate the influence of the coherent effects on the mechanism of the volume-collapse phase transitions. However, the structure of the high pressure phase remains unknown and the P - T phase diagram is established only at relatively low pressures (< 0.8 GPa) in the limited temperature range below 150 K.

The aim of the present work is to determine the structure of the high-pressure phase of CeNi and to compare the results with the structural modifications resulting from the chemical pressure induced by either La (negative chemical pressure) or Lu (positive chemical pressure) substitutions for Ce in the CrB-type CeNi lattice.

RESULTS AND DISCUSSION

CeNi, $Ce_{1-x}La_xNi$ ($0 \leq x \leq 1$) and $Ce_{1-x}Lu_xNi$ ($0 \leq x \leq 0.4$) samples were prepared by arc melting of high purity elements (~ 99.98) in the argon atmosphere. Obtained compositions were then recrystallized in vacuum and founded in cylindrical ingots of a diameter ~ 10 mm. Ingots were then annealed in dynamical vacuum for 120 h. According to X-ray and neutron powder diffraction measurements, all samples were found to be of single phase with the CrB-type of crystal structure (the $Cmcm$ space group).

In order to study the effect of chemical pressure, neutron powder diffraction patterns for the samples under study were recorder at room temperature using D7A diffractometer (Institute for Metal Physics, Ekaterinburg) with $\lambda=1.5324$ Å. The results are summarized in Table 1 and Fig. 1. La substitutions for Ce expand the crystal lattice in all the main crystallographic directions, while substitutions with Lu lead to the lattice compression. The main structural elements of the CrB structure are the zig-zag chains of Ce and Ni ions propagating along the c crystallographic direction. Respectively, the lattice parameter c varies much less due to chemical pressure than a and b parameters.

While direct high-pressure structural data were absent, there is a strong argument that the topology of the Fermi surface of CeNi does not change across the transition⁴. It means that the primary external pressure effect is to rearrange the atomic coordinates within the primitive cell of CeNi. Such an effect is also essential for chemical doping. Figure 1 demonstrates the variation of

Table 1. The crystal lattice parameters of CeNi as a function of La and Lu substitutions for Ce.

Composition	a (Å)	b (Å)	c (Å)
Ce _{0.8} Lu _{0.2} Ni	3.7457(9)	10.4069(11)	4.3416(10)
CeNi	3.7860(8)	10.5489(10)	4.6335(9)
Ce _{0.9} La _{0.1} Ni	3.8014(9)	10.5716(10)	4.3683(10)
Ce _{0.8} La _{0.2} Ni	3.8191(10)	10.5869(10)	4.3697(10)
LaNi	3.9048(9)	10.7917(9)	4.3900(10)

the atomic coordinate y for Ce/La/Lu and Ni as a function of the unit cell volume ($x = 0$ and $z = 0.25$ for both the rare-earth and Ni positions).

The results of neutron powder diffraction study of structural modifications in CeNi induced by either chemical (negative for Ce_{1-x}La_xNi, $0 < x < 1$, and positive for Ce_{1-x}Lu_xNi, $0 < x < 0.4$) or external pressure up to 5 GPa are used for electronic structure calculations of CeNi in terms of the spin-polarized relativistic density functional theory in generalized gradient approximation.

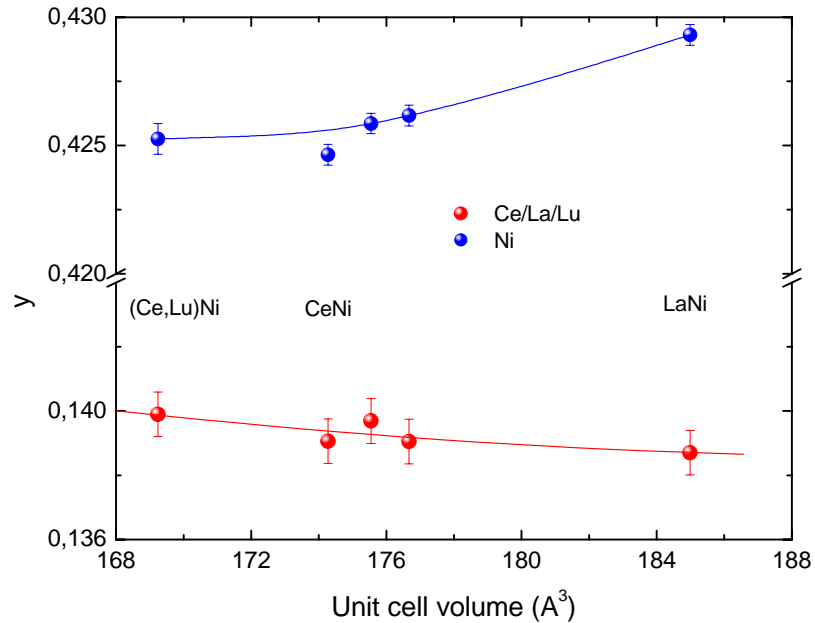


Fig. 1. Atomic coordinate y for Ce/La/Lu and Ni atoms in Ce_{1-x}Ln_xNi (Ln = La, Lu) as a function of the unit cell volume.

This work was performed under auspices of Russian Federal Agency for Atomic Energy (project “Actinides”). Financial support by RFBR (grant # 05-08-33456-a) is gratefully acknowledged.

- 1 D. Gignoux and J. Voiron, Phys. Rev. B **32**,4822 (1985).
- 2 D. Gignoux *et al.*, JMMM **70**, 388 (1987).
- 3 E. Clementyev *et al.*, Phys. Rev. B **61**, 6189 (2000).
- 4 S. Araki, R. Settai, Y. Inada, Y. Onuki, Physica B **281&282**, 736 (2000).

Magnetic Dynamics in Correlated Electron Metals Poised Between Localization and Itinerancy

E. Clementyev^{*,†}, A. Mirmelstein^{*}, and P. Böni[†]

^{*}Russian Federal Nuclear Center - Institute of Technical Physics, 456770 Snezhinsk, Russia

[†]Physics Department E21, Technical University of Munich, 85747 Garching, Germany

INTRODUCTION

Excitation spectra are indispensable experimental data to the understanding of the ground state and the major interactions in plutonium. In particular inelastic neutron scattering (INS) experiments can yield valuable answers with respect to the puzzling question raised over the absence of any evidence of magnetic moments in plutonium¹. Despite of the impressive range of information which has been attained by measurements of physical properties and theoretical studies the investigation of the dynamic properties of plutonium is by no means complete². INS is very limited in the case of plutonium to say it soft and almost nothing is known on the magnetic spectral response in this metal. However a lot of INS data has been collected for other strongly correlated metals and intermetallics with electrons balanced between itinerant and

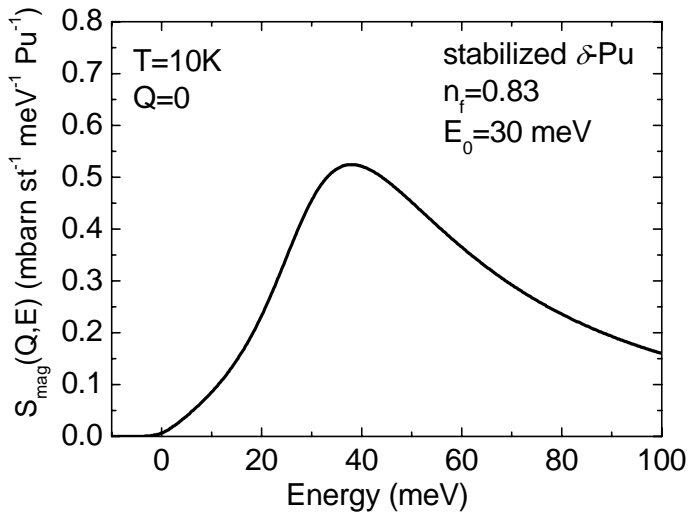


Fig 1: Calculated magnetic spectral response in fcc Pu at $T=10\text{K}$. Parameters of the KMH spectral function: Kondo energy $E_0=30$, fractional occupation of the 5f shell $n_f=0.83$.

RESULTS AND DISCUSSION

The magnetic spectra of Ce-based compounds contain various contributions. In addition to the main spectral feature, namely the broad single-ion-like magnetic response due to spin fluctuations, other peaks are clearly visible in the INS spectra⁴. We discuss coherent magnetic peaks in paramagnetic Ce-based systems, crystal field and intermultiplet transitions,

localized states. Pu is not unique among metallic systems regarding such phenomena as the unit cell volume collapse and the partial delocalization of the f-electrons. Cerium and Ce-based compounds demonstrate many peculiarities of the 4f electron shell similar to the 5f shell in Pu. The concept of shifted homology of Ce and Pu is known for about 30 years³. In the present study we discuss the magnetic spectral response observed in Kondo systems with different characteristic Kondo energy scales. The plausible magnetic excitation spectrum of fcc Pu is calculated on the basis of the INS data collected in Ce-based systems and the analysis of the thermodynamic properties of Pu.

contributions due to dynamic magnetic correlations and soft magnetic modes observed by INS on single crystals and powder samples.

A realistic description of the INS spectra in Kondo systems can be achieved on the basis of the non-crossing approximation solution of the non-interacting Kondo impurities model and using the spectral function derived by Kuramoto and Müller-Hartmann (KMH)⁵. INS spectra, specific heat, magnetic susceptibility in Ce systems are reasonably well described by the single energy scale. According to our analysis of the thermodynamic properties of δ -Pu (Pu fcc phase stabilized at low temperatures by Ga) the characteristic Kondo energy scale in fcc Pu is about 30 meV. This energy scale along with the fractional occupation of the 5f shell $n_f=0.83$ yields the value of the Sommerfeld coefficient $\gamma=64.5$ mJ K⁻² mol⁻¹ and the low temperature magnetic susceptibility $\chi=0.4$ memu mol⁻¹. The plausible INS spectrum of fcc Pu at T=10K is shown in Fig. 1. Due to the single-ion model used in the calculation any possible coherent magnetic excitations are missing in the spectrum. Using the Kramers-Kronig relation of the dynamic and static magnetic susceptibilities and the KMH spectral function (see Ref.6 and references therein) the static bulk susceptibility has been calculated for fcc Pu $\chi(10K)=0.38$ memu mol⁻¹.

To illustrate the unusual dynamics of a pure itinerant system we present new results on the magnetic and electronic excitations in chromium single crystal⁷. Both Cr and α -Pu demonstrate characteristic features of itinerant electrons.

The most interesting energy transfer range to search for the magnetic excitations in fcc Pu is 20 meV < E < 150 meV. Such a range implies relatively high incoming neutron energy, much higher than used in Ref. 1. As far as α -Pu is concerned the range of interest extends up to a few hundred meV. The most promising INS measurements must be done on ²⁴²Pu samples. On the basis of our positive experience with highly absorbing samples (like natural boron based MgB₂ with the neutron absorption cross section of about 1500 barn/f.u. and 10-boron rich TmB₁₂) we discuss the feasibility of the INS experiments using the most common ²³⁹Pu isotope ($\sigma_{\text{abs}}=1017$ barn).

This work was performed under the auspices of the Russian Federal Agency of Atomic Energy (project "Actinides"). Financial support by the RFBR (grant 05-08—33456-a) is gratefully acknowledged.

- 1 J.C. Lashley, *et al.*, Phys. Rev. B **72**, 054416 (2005).
- 2 Los-Alamos Science, ed. By N. Cooper, v. **26** (2000).
- 3 B. Johansen and A. Rosengren, Phys. Rev. B **11**, 1367 (1975).
- 4 E. Clementyev, *et al.*, Phys. Rev. B **61**, 6189 (2000).
- 5 Y. Kuramoto and E. Müller-Hartmann, J. Magn. Magn. Mater. **52**, 122 (1985).
- 6 E. Holland-Moritz and G.H. Lander, in *Handbook on the Phys. and Chem. of Rare Earths*, v. **19**, ed. K.A. Gschneidner, *et al.*, Elsevier (1994).
- 7 E. Clementyev, *et al.*, Physica B **350** (1-3), 67 (2004).

Density-Functional Calculations of α -Pu-Ga (Al) Alloys

A. Landa^{*}, P. Söderlind^{*}, L. Vitos[†]

^{*}Lawrence Livermore National Laboratory, Livermore CA 94552, USA

[†]Royal Institute of Technology, Stockholm, SE-10044, Sweden

At atmospheric pressure plutonium metal exhibits six crystal structures upon heating from room temperature to the melting point. The least dense phase (δ -Pu, fcc) has a 25% larger volume than the ground-state (α -Pu, monoclinic) phase and is thermodynamically stable at temperatures between 593 and 736 K. In order to extend the stability of δ -Pu to ambient temperatures, plutonium is alloyed with a small amount of so-called ' δ -stabilizers', for example, Ga or Al. The α phase has no equilibrium solubility with any of these δ -stabilizers but upon cooling of the δ -Pu-Ga (Al) alloys, under certain conditions, Ga (Al) atoms can be trapped in the α lattice causing an expansion. An expanded monoclinic Pu-Ga (Al) phase is usually called "the α' phase". Hecker *et al.*¹ suggested that the enhanced volume of α' -Pu is solely due to the random distribution of Ga (Al) solutes in the monoclinic lattice and the unexpanded α lattice can be restored if the solute atoms are forced to move into preferred positions, e.g., during annealing. Recently, Sadigh and Wolfer confirmed this hypothesis by performing the plane-wave pseudopotential calculations for a variety of super-cell configurations². However, all these configurations reproduced specific ordering of the solute atoms (Ga) at the selected sites in the α -Pu monoclinic structure, and disordered Pu-Ga alloys could not be considered. This problem is solved in the present calculations.

We employed two complementary techniques: (i) the exact muffin-tin orbital method (EMTO)³ incorporated with the coherent potential approximation (CPA) to treat a compositional disorder and (ii) an all-electron full-potential linear muffin-tin orbital method (FPLMTO)⁴ that accounts for all relativistic effects in Pu. Both methods establish that a random distribution of Ga (Al) atoms in the monoclinic lattice of α -Pu results in a maximum expansion of this lattice. Any kind of ordering of Ga (Al) on the monoclinic lattice results in shrinking of the lattice constant in comparison with complete disorder of the solutes. The ordered α_8 -(Pu-Ga (Al)) configuration possesses the smallest lattice constant which is very close to that of pure α -Pu. In addition, energetics of the ordered and disordered configurations is discussed.

Acknowledgements: This work was performed under the auspices of the U.S. Department of Energy by the University of California Lawrence Livermore National Laboratory under Contract No. W-7405-Eng-48.

1 S.S. Hecker, D.R. Harbur, and T.G. Zocco, Prog. Mater. Sci. **49**, 429 (2004).

2 B. Sadigh and W. G. Wolfer, Phys. Rev. B **72**, 205122 (2005).

3 L. Vitos, in *Recent Research and Development in Physics* (Transworld Research Network Publisher, Trivandrum, 2004), Vol. 5, pp. 103-140.

4 J.M. Wills, O. Eriksson, M. Alouani, and D.L. Price, in *Electronic Structure and Physical Properties of Solids: The Uses of the LMTO Method*, edited by H. Dreysse, Lecture Notes in Physics Vol. 535 (Springer, Berlin, 2000), pp.148-167.

Electronic structure of Pu with ab-initio Gutzwiller method

J.P. Julien^{*}, J. Bouchet[†]

^{*}CNRS-LEPES, BP 166, 38042 Grenoble cedex 9, FRANCE

[†]CEA-DAM, DPTA, 91680 Bruyères-le-Châtel, FRANCE

ABSTRACT

We present an ab-initio, variational, multi-configurational method to study solids with strong local Coulomb interactions. First, we generalize a density matrix approach to multiband Gutzwiller ansatz. The variational (Rayleigh-Ritz) parameters are the probabilities of atomic configurations. As a result, an effective Hamiltonian includes renormalized hoppings as well as an analytic formula for optimized on-site levels. Secondly, this approach is coupled to a first principles DFT-LDA (density functional theory in the local density approximation) LMTO (Linearized Muffin Tin Orbitals) calculation that provides a band Hamiltonian. When the interaction term is added to get the full Hamiltonian we treat in this 'LDA+Gutzwiller' formalism, we avoid the double counting of the LDA interaction by subtracting it from the on-site energies. Our method conciliates the ab-initio, parameter free, realistic description of bands, as well as a strong correlation aspect of the coherent part of the spectrum. It can be considered as an improvement of the 'LDA+U' method having the same starting Hamiltonian but where interactions are calculated beyond a too crude mean field level. Application to Plutonium will be presented, with peculiar attention to the equilibrium volume, electronic specific heat and discrimination between localized and less localized states, giving some new insight in the still controversial electronic structure of this element.

This work was initialized under the auspices of the Commissariat à l'Energie Atomique under Contract No 9M 1898. The authors wish to thank R.C Albers of Los alamos National Laboratory for supporting of the present work and warmfull hospitality. We are also grateful to F. Jollet, A. Pasturel and A. Georges for stimulating discussions.

- 1 J.P. Julien and J. Bouchet, Physica B 359-361, 783 (2005).
- 2 J.P. Julien and J. Bouchet, *accepted to*: Prog. Theor. Chem. Phys. (2006) and arXiv:cond-mat/0509321(2005).

Magnetic state of f electrons in δ -phase of Pu-Ga alloys studied by Ga NMR

S. Verkhovskii*, V. Arkhipov*, Yu. Zouev[†], Yu. Piskunov*, K. Mikhalev*, A. Korolev, S. Lekomtsev[†], I. Svyatov[†], A. Pogudin*, V. Ogloblichev*, and A. Buzlukov*.

*Institute of Metal Physics, Ural Branch of Russian Academy of Sciences, Ekaterinburg, Russian Federation (verkhovskii@imp.uran.ru)

[†]Russian Federal Nuclear Center - Institute of Technical Physics, Snezhinsk, Russian Federation

The rich phase diagram of plutonium¹ presents six polymorphous transitions. The unique structural, transport and magnetic properties are determined by the degree of itinerancy for $5f$ electrons in each of the Pu allotropes. Many efforts are undertaken, at present, to elucidate the ground state of the f -electron system in δ -Pu and in stabilized δ -phase alloys.

In the report on the basis of the ^{69}Ga NMR and static magnetic susceptibility data (Fig.1) the temperature dependence of spin susceptibility is discussed for the $\text{Pu}_{0.95}\text{Ga}_{0.05}$ alloy, stabilized in δ -phase. The static magnetic susceptibility and the ^{69}Ga NMR spectra were measured in the temperature range (10 - 350) K and (10 - 650) K, respectively, at the sample, prepared as a set of electrochemically polished plates $\sim 200\mu\text{m}$ in thickness. Magnetic shift (the Knight shift) of the ^{69}Ga NMR line is controlled by static local magnetic field arisen at nonmagnetic gallium due to the spin polarization transferred from the f electrons shell of the more magnetic neighboring Pu-ions². Thus the Knight shift K , dependent of electron spin, measures local spin susceptibility, $\chi_{s,\text{loc}}$, which can be composed by contributions being different in origin.

At $T > T^* = 235$ K the temperature dependent part of the Knight shift tracks the bulk susceptibility $\chi(T)$, following the Curie-Weiss law $K(T) \sim (T + \theta)^{-1}$ with $\theta = 280(40)$ K. The relation $K(T) \sim \chi(T)$ is violated with decreasing temperature below 200 K. A similar breakdown of the proportionality between $K(T)$ and $\chi(T)$ occurs at low temperature in many metallic compounds with the heavy fermion (HF) behavior, and this phenomenon is considered to occur at the expense of the f electron system.

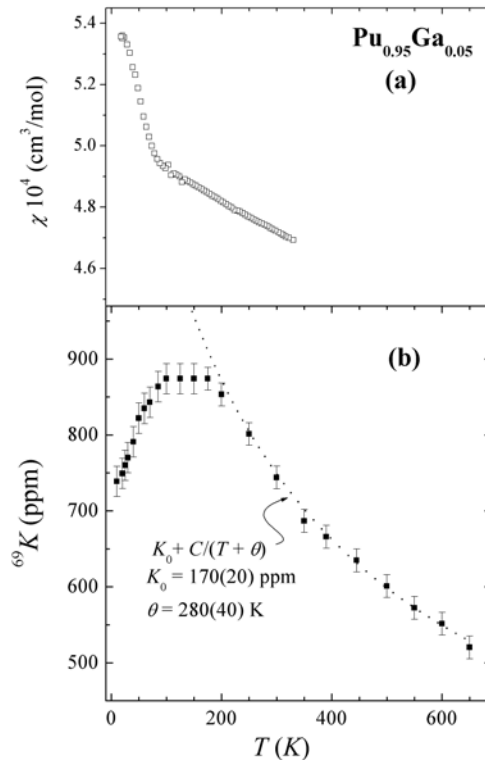


Fig.1. Magnetic susceptibility (a) and Ga NMR shift (b) vs T in $\text{Pu}_{0.95}\text{Ga}_{0.05}$ alloy.

The subsequent joint analysis of the static magnetic susceptibility and the Knight shift data sets obtained in a wide range of temperature has allowed to find out the following peculiarities of the magnetic state of f electrons in the $\text{Pu}_{0.95}\text{Ga}_{0.05}$ alloy³:

- The temperature dependence of spin susceptibility at $T > T^*$ is typical for nonmagnetic Kondo lattice, where the localized electron spins fluctuate independently each other without any macroscopic coherence.

- The spin contribution of the f -electrons $\chi_{s,5f}$ to the total magnetic susceptibility is estimated as $\chi_{s,5f} \sim 0,08(1)\chi$. This estimate correspond to the localized f - electrons with very small value of magnetic moment $\mu_{\text{eff},5f}(g_e=2) = 0,15(5) \mu_B/\text{at.Pu}$. The corresponding filling of the $5f$ shell should resemble the $5f^6$ atomic configuration of Pu with $L = 0, S = 0$, as it was suggested for δ -Pu in Ref.4. This feature leads to suppression of the spin magnetism in δ -Pu. The T-independent orbital term determines the value of the f electron susceptibility of in δ -phase of the alloy.

- The different behavior of $K(T)$ and $\chi(T)$ occurred in alloy below 200K can be described rather well using two-spin fluid description of the HF materials developed in Ref. 5. As shown in Fig.2 the HF component of the Knight shift K_{cf} is increased with temperature decreasing. The tendency for K_{cf} to saturate below 300K can indicate, that, probably, the HF (coherent) spin-fluid component is formed completely. The final conclusion on the magnetic state of the Pu-ions occurred at low temperature can be done after the origin of additional excess in the local spin susceptibility revealed below 70K will be properly clarified.

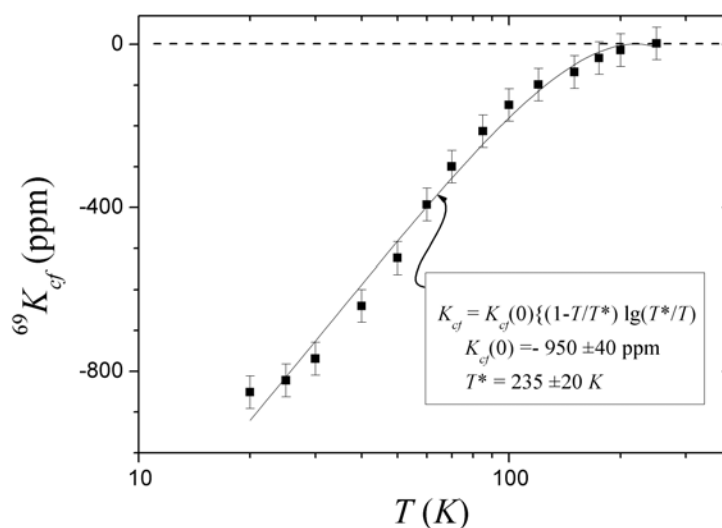


Fig.2. The coherent HF component of the Knight shift vs T in $\text{Pu}_{0.95}\text{Ga}_{0.05}$ alloy. The black curve is a fit with the expression $K_{\text{cf}}(T) = K_{\text{cf}}(0)\{(1 - T/T^*) \lg(T^*/T)\}$ according Ref. 5 at $K_{\text{cf}}(0) = -950(80)$ ppm и $T^* = 235(40)$ K

Acknowledgments

The work was supported by the Russian Grant (RFBR No 06-02-16130).

¹ S.S. Hecker and L.F. Timofeeva, *Los Alamos Sci.* **26**, 244 (2000)

² Yu. Piskunov, et al., *Phys. Rev. B* **71**, 174410 (2005).

³ S.V. Verkhovskii, et al., *JETP Lett.* **82**, 139 (2005).

⁴ A.O. Shorikov, A.V. Lukoyanov, M.A. Korotin, and V.I. Anisimov, *Phys. Rev. B* **82**, 024458 (2005).

⁵ N.J. Curro, B.-L. Young, J. Schmalian, D. Pines, *Phys. Rev. B* **70**, 235117 (2004).

The ground state and localization of 5*f* electrons in α - Pu

H. R. Gong and A. K. Ray

Department of Physics, the University of Texas at Arlington, Arlington, TX 76019

INTRODUCTION

Plutonium (Pu) is arguably the most complex metallic element known to mankind and has attracted extraordinary scientific and technological interests because of its unique properties. For instance, it has, at least, six stable allotropes between room temperature and melting at atmospheric pressure, and undergoes a 25 percent increase in volume when transformed from its α -phase to δ -phase, an effect which is crucial for issues of long-term storage and disposal. It is commonly believed that 5*f* electrons in Pu, which represent the boundary between the delocalized (itinerant) 5*f* electrons in the light actinides and the localized 5*f* electrons in the heavy actinides, are responsible for the unique properties of Pu, but the exact phase of the delocalization-localization transition has not been clearly identified so far. Among the six allotropes, the ambient ground-state α -Pu with a low-symmetry monoclinic structure has been studied by various groups over the years both experimentally and theoretically. It is commonly believed that α -Pu is relatively accurately described by standard density functional theory. However, the ground state of α -Pu continues to be a matter of significant controversy.¹ As a continuation of our research in actinide chemistry and physics,² we report here results on bulk α -Pu at NSP-NSO, NSP-SO, SP-NSO, SP-SO, AFM-NSO, and AFM-SO levels of theory, with two types of anti-ferromagnetic configurations.

COMPUTATIONAL METHOD AND RESULTS

Our computations have been carried out using the full-potential all-electron method with mixed basis APW+lo/LAPW method implemented in the WIEN2k suite of programs.³ The generalized-gradient-approximation to density functional theory (GGA-DFT) with a gradient corrected Perdew-Berke-Ernzerhof (PBE) exchange-correlation functional is used and the Brillouin-zone integrations are conducted by an improved tetrahedron method of Blöchl-Jepsen-Andersen. As far as relativistic effects are concerned, core states are treated fully relativistically in WIEN2k and for valence states, two levels of treatments are implemented: (1) a scalar relativistic scheme that describes the main contraction or expansion of various orbitals due to the mass-velocity correction and the Darwin *s*-shift and (2) a fully relativistic scheme with spin-orbit coupling included in a second-variational treatment using the scalar-relativistic eigenfunctions as basis. For all the calculations, a constant muffin-tin radius (R_{mt}) of 2.30 a.u. is used and the plane-wave cut-off K_{cut} is determined by $R_{\text{mt}} K_{\text{cut}} = 8.0$. The Brillouin zone is sampled on a uniform mesh with 24 irreducible *K*-points and the energy convergence criterion is set to be 0.01 mRy. In the present study, the unit cell of α -Pu is a simple monoclinic structure (P2₁/m) with sixteen atoms. To find the total energy minimum, the atomic volume of α -Pu is varied at each

theoretical level, respectively, while the following parameters are fixed according to experimental values: the atomic positions, the ratios of b/a and c/a , and the angles between the three axes.

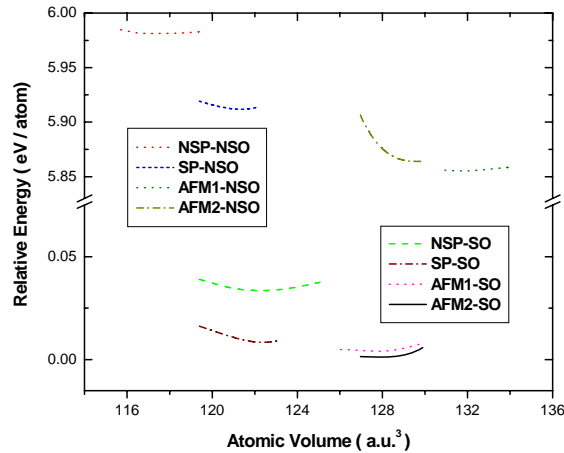


FIG. 1. Calculated total energies of α -Pu at various theoretical levels.

As Fig. 1 indicates, an anti-ferromagnetic state including spin-orbit coupling effects is found to be the ground state of α -Pu with an atomic volume of 128.9 a.u.³ and a bulk modulus of 58.8 GPa, in excellent agreement with experimental results. Density of states studies indicate that the 5f electrons of α -Pu are primarily delocalized as compared to our previous results of δ -Pu where the 5f electrons were found to be mainly localized. Thus the 5f electrons of α -Pu are on the delocalized side of the localization-delocalization transition, while 5f electrons of δ -Pu are on the localized side, signifying that the delocalization-to-localization transition from light actinides to heavy actinides should happen somewhere between α -Pu and δ -Pu. In addition, we find that specific anti-ferromagnetic settings have important roles on the properties of α -Pu and the spins of ferromagnetic α -Pu have a tendency to become anti-ferromagnetic.

This work is supported by the Chemical Sciences, Geosciences and Biosciences Division, Office of Basic Energy Sciences, Office of Science, U. S. Department of Energy (Grant No. DE-FG02-03ER15409) and the Welch Foundation, Houston, Texas (Grant No. Y-1525).

1. A. O. Shorikov, A. V. Lukoyanov, M. A. Korotin, and V. I. Anisimov, Phys. Rev. B **72**, 024458 (2005).
2. X. Wu and A. K. Ray, Phys. Rev. B **72**, 045115 (2005); A. K. Ray and J. C. Boettger, Phys. Rev. B **70**, 085418 (2004); J. C. Boettger and A. K. Ray, Int. J. Quant. Chem., **105**, 564 (2005); M. N. Huda and A. K. Ray, Eur. Phys. J. B **40**, 337 (2004); Physica B **352**, 5 (2004); Eur. Phys. J. B **43**, 131 (2005); Physica B **366**, 95 (2005); Phys. Rev. B **72**, 085101 (2005); Int. J. Quant. Chem. **105**, 280 (2005); H. R. Gong and A. K. Ray, Eur. Phys. J. B, **48**, 409 (2005); H. R. Gong and A. K. Ray, Proc. MRS Fall 2005 Symposium; accepted for publication; Surf. Sci. accepted for publication; D. Gao and A. K. Ray, Eur. Phys. J. B, in press; Proc. MRS Fall 2005 Symposium; accepted for publication; D. Gao and A. K. Ray, submitted for publication; P. Dholabhai and A. K. Ray, submitted for publication.
3. K. Schwarz, P. Blaha, and G. K. H. Madsen, Comp. Phys. Comm. **147**, 71 (2002).

Magnetic Properties of Pu-Ga Alloys

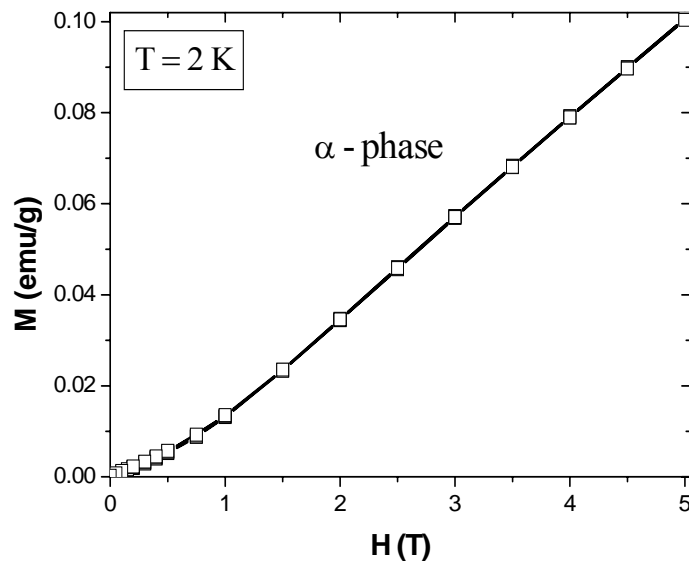
V. Arkhipov*, Yu. Zuev†, F. Kassan-Ogly*, A. Korolev*, I. Svyatov†

*Institute of Metal Physics, Ural Branch of RAS, Ekaterinburg, Russia

†Russian Federal Nuclear Center — Institute of Technical Physics, Snezhinsk, Russia

The results of studies of temperature and field dependences of the magnetization and susceptibility of Pu-Ga alloys with 0.5 and 5.0 at % of Ga are presented. At room temperature the samples were in α and δ phases according to either U.S. or Russian Pu-Ga phase diagram¹. The measurements were performed on a SQUID magnetometer MPMS-5XL (Quantum Design) in the fields up to 5 T and in the temperature range from 2 to 400 K. The samples were put in a Pyrex ampoule filled with gaseous helium under the pressure of 0.5 atm. The figure shows anomalous magnetization dependence on an external magnetic field for a sample with 0.5 at.% Ga (α phase) at $T=2$ K.

As it is seen from the figure the behaviour of magnetization differs from that in pure paramagnet in which case it should be a straight line intersecting the origin. Moreover, as our



measurements showed, the magnetization curves over the cycle $+5\text{T}-0\text{T}-5\text{T}-0\text{T}+5\text{T}$ manifest a hysteresis with a residual magnetization of 0.002 emu/g and coercive force of $\sim 1800-2000$ Oe. Our further measurements showed that the anomaly, discovered at $T=2$ K, disappears at ~ 10 K. A similar anomalous behaviour of $M(T)$ at $T < 10$ K is also observed for the samples with 5 at.% Ga (δ phase). It may be supposed that the observed anomalies of magnetic properties (magnetization and magnetic susceptibility) of Pu-Ga alloys

are related to a possible appearance of the α' phase at low temperatures. To our knowledge such anomalies of $M(T)$ and $\chi(T)$ were not yet reported in available literature references.

This work was supported by the Russian Foundation for Basic Research, Project No. 06-02-16130

Electronic Structure Measurements and Photoemission Band Mapping of α -Uranium

R.K. Schulze, C.P. Opeil, B. Milhaila, M.E. Manley, R. Albers, K.B. Blagoev, and J.L. Smith

Los Alamos National Laboratory, Los Alamos, NM 87545

α -URANIUM SINGLE CRYSTAL

For the first time, relatively large, high quality single crystals of a pure actinide metal, in this case, α -uranium, have become available¹ through electrolytic growth from a molten salt, and we have begun a comprehensive investigation of the electronic structure of this material by photoemission and band mapping measurements. The platelet-like crystals of the orthorhombic α -uranium exhibit the (001) plane as the largest dimension, and it is upon this surface that these measurements have been performed. The surface exhibits sharp LEED patterns upon cleaning and annealing to 480 K, consistent with the bulk orthorhombic structure of the α -uranium and thus indicating that no dramatic surface reconstruction exists. XPS analysis indicates initial cleaned surfaces at the annealing temperature of less than 1% of a monolayer oxygen impurity.

α -URANIUM ELECTRONIC STRUCTURE

We have measured the α -uranium photoemission core level spectra and valence band energy distribution curves in both angle resolved and partially angle integrated modes. In addition, we have made these measurements on high purity polycrystalline α -uranium samples in an attempt to more closely have the measurement reflect a fully angle integrated density of states. These measurements have been done as a function of temperature from 173 to 873K, and yield not previously observed high-resolution features in the ultraviolet photoemission spectroscopy (UPS) data, particularly at low temperatures (figure 1). At higher temperatures the manifold at the Fermi edge is broadened and the peak top location appears to shift in energy. Comparison of the valence band at excitation photon energies of 21.21 and 40.81 eV at a sample temperature of 173K indicates a mix of U5f and U6d density in the initial manifold within 0.5 eV of the Fermi edge. These assignments will be discussed. In addition we have examined the shallow U6p states using soft X-ray photoemission. These states, and in particular the U6p_{3/2} spin-orbit state, show anomalous splitting. The indication here is that the 6p state is no longer core-like and is hybridized in the uranium metal. This is confirmed with comparison to a full Dirac calculation, which shows the correct value in the spin-orbit splitting and indicates the hybridization in the U6p_{3/2} band.

α -URANIUM BAND MAPPING

We have examined the band structure across the principal symmetry directions of the Brillouin zone $\Gamma \rightarrow \Sigma$, $\Gamma \rightarrow Y$, and $\Gamma \rightarrow S$, as well as an examination of the band structure and Fermi distribution as a function of temperature from 173 K to 373 K. First-principles electronic band-structure calculations have been performed using a generalized gradient approximation

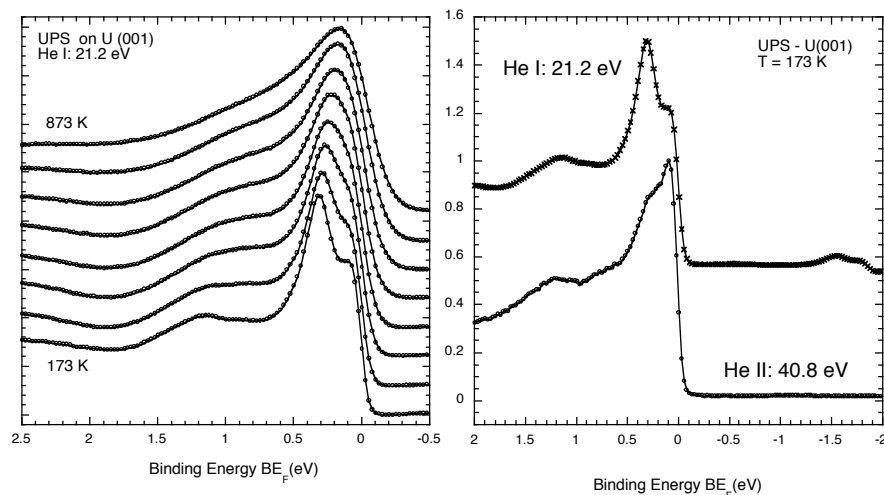


Figure 1. Temperature dependent valence band photoemission (left) of the near Fermi edge DOS of the U(001) surface from 173 to 873K in 100K steps. Comparison of the near Fermi edge photoemission with $h\nu=21.21$ and 40.81 eV at a sample temperature of 173K (right).

coupling in this system to be related to the unusual thermal allotropic phase transformations exhibited in uranium and other actinides including plutonium. The behaviour exhibited in uranium is believed to be a precursor for the full electronic state transition of plutonium in moving through the allotropic phases, and localization of the f-electrons. The details of these measurements and their implications for actinide electronic structure will be discussed.

1 H.F. McFarlane, K.M. Goff, F.S. Felicione, C.C. Dwight and D.B. Barber, *Journal of Metals* **49** (1997) 14.

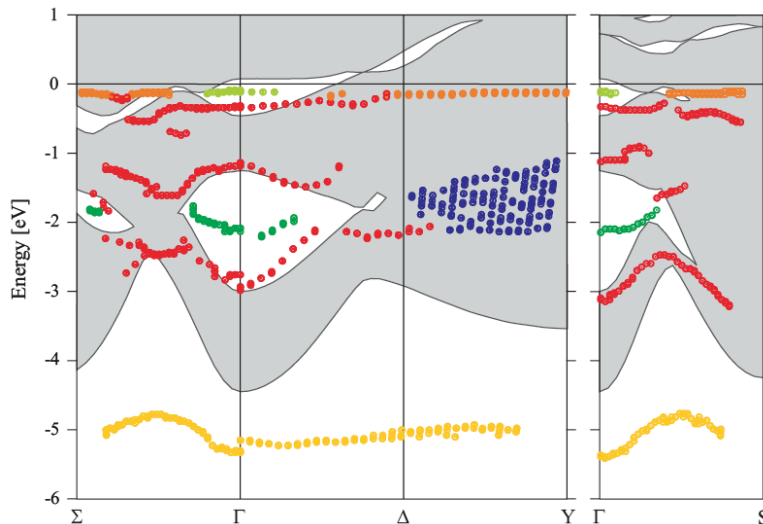


Figure 2. Electronic band map of α -uranium. The coloured data points are band locations in energy and momentum extracted from the experimental data, and the grey background fill the $\Gamma \rightarrow Z$ integrated calculation of the band structure.

(GGA) method in the full-potential linearized-augmented-plane-wave (FLAPW) method, including 6p orbitals to accommodate the shallow U 6p states as interacting. These calculations show partial agreement with the experimental measurements (figure 2). The major differences have been justified by the presence of electronic surface states and the strong suggestion of electron-phonon coupling effects. We believe the electron-phonon

Symmetry considerations on the ground state of NpO_2

S. Di Matteo ^{*}, R. Caciuffo[§]

^{*}European Synchrotron Radiation Facility, B P 220, F-38043 Grenoble CEDEX, France

[§]European Commission, Joint Research Centre, Institute for Transuranium Elements, Postfach 2340, Karlsruhe, D-76125 Germany

INTRODUCTION

The ground-state symmetries of Np ions in the low temperature phase of NpO_2 ($T < T_0 = 25$ K) are discussed with reference to the results of resonant x-ray scattering (RXS) experiments suggesting the occurrence of long-range magnetic octupolar order with an electric quadrupole secondary order parameter¹. Two models have been proposed in the literature: one based on a 4 doublet² (in D_{3d} point group), the other on a 5 (6) singlet³. We show, through a theoretical group analysis, that the 4 doublet is not compatible with the available experimental data. Our analysis supports the hypothesis of a singlet ground state.

Experimental results indicate the absence of structural distortions, either internal or external, and an ordered magnetic dipole moment smaller than $0.01 \mu_B$ (see Ref. 3 for a brief review of the experimental results, and a complete list of references). Quadrupole magnetic moments being excluded, because Np positions are inversion centres, magnetic octupole moments can be considered as possible order parameters, as suggested by Santini and Amoretti². In particular, the components of the octupole moments transforming like 2 (singlet) and 5 (triplet) in octahedral fields can be considered, the 4 triplet being rejected because it would imply the presence of an induced magnetic dipole, as detailed in Ref. 2. The first possibility is maintained in Ref. 2 and appears compatible with a 4 doublet ground-state in D_{3d} . The second type of symmetry for the octupole has been advanced in Ref. 3 and assumes a 5 (6) singlet ground-state.

Here, we analysis of the ground-state symmetry, from the perspective of the D_{3d} local symmetry at Np^{4+} -sites indicated by RXS, and we try to clarify some subtleties related to time-reversal symmetry. This also opens the way to a straightforward identification of the allowed order parameters and a direct classification of the possible ground states. The analysis supports the conclusions reported in Ref. 4, where a singlet ground state was proposed for NpO_2 on the basis of specific heat measurements.

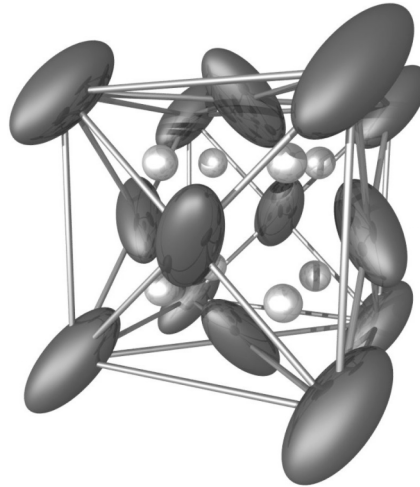


Fig 1: Schematic representation of the triple- k longitudinal ordering of Np electric-quadrupole moments in NpO_2 .

SYMMETRY CONSIDERATIONS

In the high-temperature phase, NpO_2 crystallises in the Fm-3m space group. The (003) reflection in such a group is forbidden by symmetry at all orders, even in resonant conditions. Therefore, its detection at Np M_4 edge in the low-temperature phase shows that the local symmetry of Np^{4+} ions below T_0 is a subgroup of the cubic group m-3m (O_h). The only maximal nonisomorphic subgroup of Fm-3m that is non-symmorphic and simple cubic is Pn-3m, which has the same diffraction pattern as Fm-3m for both Np and O atoms, thus explaining why usual diffraction is not sensitive to any symmetry-lowering below T_0 . The Np ions are accommodated at positions 4b, with reduced local symmetry -3m (D_{3d}). The character table of the D_{3d} (double) group can then be used to derive the ground state symmetry and the allowed octupolar components.

The seven degenerate components of the octupole magnetic moment in spherical symmetry $SO(3)$ split, in D_{3d} symmetry, into two doublets $_3$, two singlets $_2$ and one singlet $_1$, the latter corresponding to the totally symmetric irreducible representation of $L=3$ in D_{3d} . The experimental evidence of the absence of dipolar long-range order forces us to consider only those components of magnetic octupole not belonging to the same representations as the dipole, otherwise this latter would be induced as secondary order parameter. In D_{3d} symmetry only one octupolar component has the desired property, the one belonging to the totally symmetric representation $_1$. This latter can be written in terms of spherical harmonics with quantization axis along the trigonal [111] direction, and the corresponding expression in terms of equivalent angular momentum operators can be easily derived.

The $_8$ ground-state quartet of O_h splits, in D_{3d} , into a doublet $_4$ and a couple of Kramers-related singlets $_5$ and $_6$. Even though they belong to two different representations of the D_{3d} double group, the latter are degenerate in presence of time-reversal symmetry, and their degeneracy splits only when time-reversal is broken. The four states can be written in terms of the basis $||J=9/2, J_z\rangle$, assuming the quantization direction along the three-fold symmetry axis. In presence of a time-reversal symmetry breaking, the double degeneracy of the $_4$ doublet would be lifted giving a lowest-lying component with a net dipolar moment. This is against the experimental evidence. Therefore, we have to assume that the ground state of Np in the low-temperature phase is a $_5$ (or a $_6$) singlet. The structure of the singlet is such that the average value of any component of the magnetic moment J_a ($a=x, y, z$) is zero: only trilinear objects $J_a J_b J_c$, e. g. magnetic octupoles, have expectation values different from zero.

- 1 J.A. Paixao et al., Phys. Rev. Lett. **89**, 187202 (2002)
- 2 P. Santini and G. Amoretti, Phys. Rev. Lett. **85**, 2188 (2000)
- 3 R. Caciuffo et al., J. Phys. Cond. Matt., **15**, S2287 (2003)
- 4 N. Magnani et al., Physica B **359-361**, 1087 (2005)

^{69}Ga NMR in $\text{Pu}_{1-x}\text{Ga}_x$ ($x < 0.01$) alloy

Yu.V. Piskunov^{*}, K.N. Mikhalev^{*}, Yu.N. Zuev[†], S.V. Verkhovskii^{*}, V.E. Arkhipov^{*}, I.L. Svyatov[†], A.E. Shestakov[†], A.V. Pogudin^{*}, V.V. Ogloblichev^{*}, and A.L. Buzlukov^{*}

^{*}Institute of Metal Physics, Ural Branch of Russian Academy of Sciences, Ekaterinburg, Russia (piskunov@imp.uran.ru)

[†]Russian Federal Nuclear Center - Institute of Technical Physics, Snezhinsk, Russia

^{69}Ga NMR spectra measured in the monoclinic α -phase¹ of the $\text{Pu}_{0.995}\text{Ga}_{0.005}$ alloy are presented in this report. The investigated strips of alloy (20x3x0.2 mm) were single phase without detectable macroscopic impurity of other phases in accordance with the optical metallography and x-ray diffraction technique.

The ^{69}Ga NMR spectrum of this alloy in the external magnetic field of 9.4 T consists of central line (transition $-1/2 \leftrightarrow +1/2$) and a broad pedestal of the satellite lines (transitions $\pm 1/2 \leftrightarrow \pm 3/2$). Such a spectrum can be considered as typical for a powder of imperfect cubic crystals, where the local deviations of cubic symmetry of charge distribution around Ga-atom take place. The nucleus of Ga has electric quadrupole moment $eQ=0.17 \cdot 10^{-24} \text{ cm}^2$. Arising electric field gradient (eq_{ii}) causes essential broadening of satellite lines $\Delta\nu_Q \sim e^2Qq_{zz}$. At the same time, the shift (^{69}K) and the linewidth ($\Delta\nu$) of central transition are determined by local fields, which are caused by hyperfine coupling from the nearest surrounding of Pu-atoms.

In initial state of alloy (see Figure 1a), the linewidth of central transition essentially (in 2.5-3 times) larger than its magnitude for the stabilized δ -phase alloys^{2,3}. The growth of ($\Delta\nu$) is determined by the distribution width of the Ga-Pu interatomic distances, which is increased in the mechanically-pressed state of the α -phase of alloy under investigation.

Annealing of the sample at the temperature higher than α - β structural transformation (150° C during 8 h.) causes an essential change in the shape of central line (see Figure 1b). The fine structure of the central line can be represented as a superposition of two lines with different $\Delta\nu$ and ^{69}K . The broad line-2 of relative intensity 0.67(10) demonstrates a shift being approximately independent on temperature,

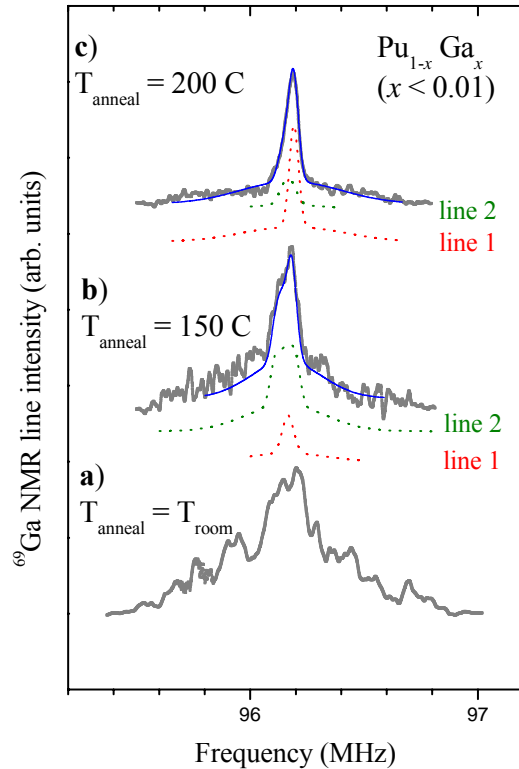


Fig 1: The ^{69}Ga NMR spectra measured at magnetic field of 9.4 T at 20 K in $\text{Pu}_{0.995}\text{Ga}_{0.005}$ alloy. a) the initial α -phase; b) after annealing at $T_{\text{anneal}}=150 \text{ C}$ during 8 h.; c) after annealing at $T_{\text{anneal}}=200 \text{ C}$ during 20 h. The dotted lines are the result of simulation of the experimental spectrum by two lines with different intensities.

as it takes place for static magnetic susceptibility of α -Pu (see Figure 2). While the shift of the more narrow line-1 having the less intensity changes with temperature like $^{69}\text{K}(T)$ -dependence in the stabilized δ -Pu alloy $\text{Pu}_{0.95}\text{Ga}_{0.05}$ ^{2,3}. An additional annealing of the alloy at $T = 200$ C during 20 h. leads to progressive narrowing of the central line at the expense of the line-1, dominating in intensity, as shown in Figure 1c.

It is reasonable to assume that the annealing performed above the α - β structural transformation, should take off only the mechanical strength, persisted in the initial α -phase¹. The x-ray examination of the annealed sample at room temperature results in the absence of any traces of macroscopic areas of δ - phase with characteristic size exceeding 100 nm.

In accordance with the ^{69}Ga NMR and x-ray data one can conclude that in the α -phase of $\text{Pu}_{0.995}\text{Ga}_{0.005}$ the microscopic areas with a size less than 100 nm exist. The local charge and magnetic environment of the solute Ga in these microscopic areas is similar to the observed in the stabilized δ -Pu alloy $\text{Pu}_{0.95}\text{Ga}_{0.05}$ ^{2,3}.

Acknowledgments

The work was supported by the Russian Foundation for Basic Researches (Project No. 06-02-16130). Yu.P. acknowledges the "Russian Science Support Foundation" for a financial support.

¹S.S. Hecker and L.F. Timofeeva. Los Alamos Sci. **26**, 244 (2000)

²Yu. Piskunov, K. Mikhalev, A. Gerashenko, et al., Phys. Rev. B **71**, 174410 (2005).

³S. Verkhovskii, et al., JETP Lett. **82**, 139 (2005).

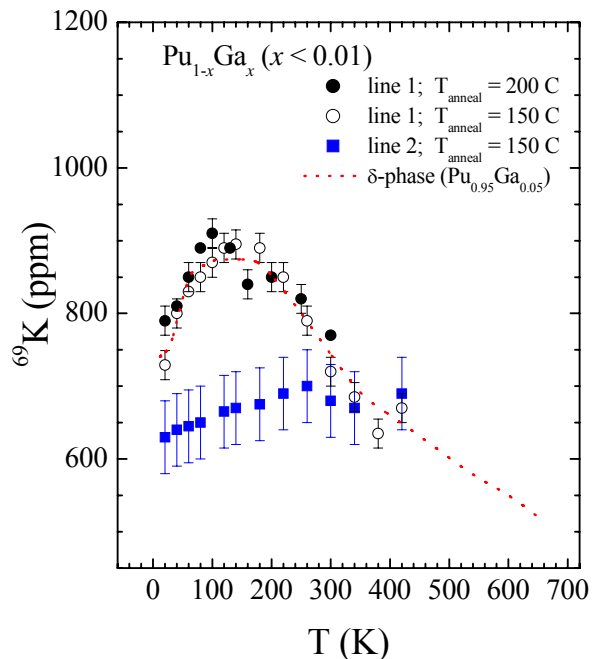


Fig 2: Temperature dependences of the ^{69}Ga NMR shift for the line-1 and line-2 in the $\text{Pu}_{0.995}\text{Ga}_{0.005}$ alloy.

Effect of Composition and Age on the Density of Delta Plutonium Metal

R. Mulford*, W. Brown†

*Los Alamos National Laboratory, Los Alamos, NM 87545 USA

DENSITY CHANGES AND AGING

Measurements on new and aged plutonium metal from a variety of sources indicate some factors which affect the density of the delta-phase metal. The density is observed to vary as a function of age. The rate of variation with age is not uniform, but exhibits three stages: an early stage of about three to ten years, an intermediate stage of up to 35 years, and a late stage. Behavior observed for samples of advanced age may be due to differences in composition as well as age.

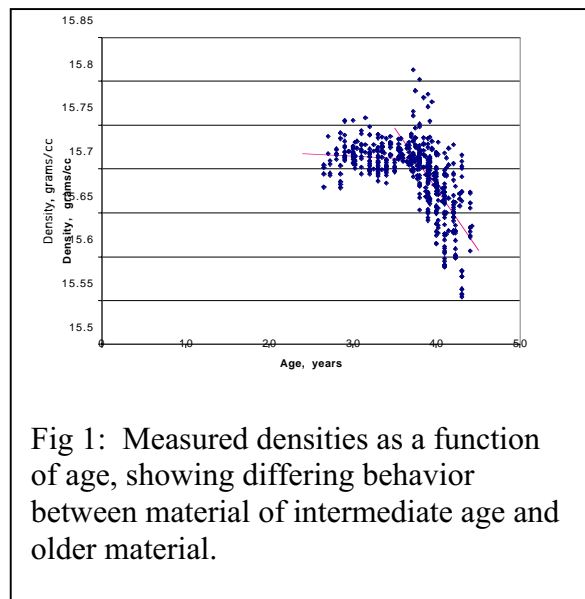
Changes in density are due to several consequences of radioactive decay of the plutonium atoms. Possible causes include helium accretion in the metal lattice, accumulation of americium, ingrowth of uranium, and radiation damage. The relative rates of self-irradiation processes and decay processes in plutonium permit some separation of some of the physical and chemical aging effects in time, and may allow distinct rates for lattice damage and gas accumulation to be inferred.

The oldest plutonium samples available exhibit a wider range of compositions than newer material. Compositional variations may mask possible aging mechanisms, but do allow study of perturbations to density produced by compositional variations.

MEASUREMENTS, ANALYSIS AND RESULTS

Measurements were made by the Archimedes method of immersion, and corrected for temperature expansion of the immersion fluid, FC-43. A posteriori uncertainty varied between 0.0003 and 0.001 g/cc. Daily calibrations yielded information on the behavior of the immersion fluid, and provided statistical information on variations in the measurements. We report the effect of sample mass on measured values of density and on observed a posteriori uncertainties in reported values. The influence of oxidation on measurements is examined. Limitations of the technique are discussed.

Rates are obtained by making linear fits to ensembles of similar samples, by tracking the changes in a single sample over several years, or both. Results indicate a decrease of about 0.003%/annum for samples of intermediate age, in agreements with results of TEM imaging and



measurement of helium bubbles.¹ New material exhibits rates of between 0.016% and 0.02%/annum, somewhat less than rates of 0.06%/annum reported for XRD studies.² Plutonium of advanced age exhibits a rate of 0.06%/annum, both in the behavior of the ensemble and in the change in individual samples.

Corrections for lattice expansion by americium have an effect on the reported rates of change in density. The behavior of americium in the lattice has been reported to depend on the location and thermal history of the americium. Corrections to density and assumptions are discussed.

The possibility of the formation of uranium plutonide as uranium accumulates within the lattice has been examined. In most cases, excess uranium present at casting has been observed in a second phase as U₆Fe. Cases examined here permit study of uranium introduced into the lattice without thermal equilibration with second phase regions, and present a case in which insufficient iron makes consumption of uranium by the formation of U₆Fe stoichiometrically impossible.

Early time behavior of castings has received some study^{2,3} as a case of lattice disorder, and also as a perturbation by chemical changes produced by decay.⁴ Changes in helium accommodation may also play a role.⁵ Density measurements on new and aged castings are compared with data obtained from a variety of sources⁶ in an effort to clarify some of the mechanisms that contribute to the density and structural changes.

SIGNIFICANCE AND RELEVANCE

Changes in the structure of plutonium metal as a function of age are of interest as an example of radiation damage at very low dose rates, relative to the majority of externally irradiated cases available for study. The effects of auto-irradiation have implications for engineering and lifetime prediction in nuclear weapons and devices such as sources.

Density changes must be factored into a wide variety of other physical measurements, such as compressibility, strength, elastic properties, and permittivities, particularly as they apply to samples that may be aging during the course of the study. A general study of density changes may simplify the interpretation of detailed measurements intended to quantify specific mechanisms.

- 1 A.J. Schwartz, M.A. Wall, T.G. Zocco, and W.G. Wolfer, *Phil. Mag.*, **85**(4-7) (2005)
- 2 N.T. Chebotarev and O.N. Utkina, in *Plutonium and Other Actinides*, Eds. JH. Blank and R. Lindner, North-Holland Publishing Company, Amsterdam p. 559-565 (1976)
- 3 R.N. Mulford, Los Alamos National Laboratory report, LA-UR-06-0771 (2006)
- 4 W. Wolfer, Lawrence Livermore National Laboratory, private communication.
- 5 M. Baskes, Los Alamos National Laboratory, unpublished work.
- 6 B. Chung, Lawrence Livermore National Laboratory and L. Morales, Los Alamos National Laboratory, private communications.

Analysis of Density Changes in Plutonium Observed from Accelerated Aging using Pu-238 Enrichment

B. W. Chung, C.K. Saw, S.R. Thompson, T.M. Quick, C.H. Woods, D.J. Hopkins, and B.B. Ebbinghaus

Lawrence Livermore National Laboratory, Livermore CA 94552 USA

INTRODUCTION

Plutonium, because of its radioactive nature, relentlessly undergoes self-irradiation damage through out its volume. Plutonium decays to uranium by α -particle emission. The α -particle takes away most of the energy and eventually comes to rest as a helium atom. While both particles produce displacement damage in the form of Frenkel-type defects, most of the damage results from the uranium recoil nucleus. The defects resulting from the residual lattice damage and helium in-growth results in microstructural and physical property changes. Because these self-irradiation effects would normally require decades to measure, with a fraction (7.5 wt%) of ^{238}Pu is added to the reference plutonium alloy thus accelerating the aging process by approximately 18 times the normal rate. By monitoring the properties of the ^{238}Pu -enriched alloy over a period of about 3.5 years, the properties of plutonium in storage can be projected for periods up to about 60 years. Previously, we reported the observation of density and volume changes due to self-irradiation in enriched alloys¹. In this paper, it will shown that the change in density is a result of the change in lattice parameters, which saturates within approximately three years of aging, and the continued build-up of helium in-growth. This analysis is founded upon microstructural measurements such as X-ray diffraction.

EXPERIMENTAL

The length change was primarily determined by dilatometry measurements. The length change was compared to immersion density measurements and lattice parameters measured from X-ray diffraction.

Dilatometers have been set up to monitor long-term growth resulting from the lattice damage and helium in-growth in (~ 7.5 wt%) ^{238}Pu -enriched alloys. Details of experiments are presented elsewhere¹. Two different lengths of ^{238}Pu -enriched alloy specimens (3 cm and 2 cm) are used to differentiate between surface oxidation and volumetric swelling in the materials. The dilatometer chamber atmosphere is helium backfilled after evacuation with an oil-less vacuum pump. Each dilatometer has three wells: one for a 3 cm long specimen, one for a 2 cm long specimen, and one for a zero-dur reference material.

The immersion densities on the enriched and reference alloys were obtained shortly after the initial fabrication and then subsequently at least every six months. Between measurements, the samples were stored in a helium-filled incubator at 50°C. The equipment closely matches a design used by Bowman *et al.*² and uses about 200 ml of Fluorinert Electronic Liquid FC-43 as the immersion fluid. Prior to a measurement, the system is calibrated using NIST glass (SRM 1827A) and a tantalum specimen as standards. This is generally followed by a measurement on

the plutonium reference alloy and the ^{238}Pu -enriched alloy. To obtain stable measurements and ensure that all surface oxide is removed, multiple measurements are performed.

RESULTS and DISCUSSION

The length change (ΔL) normalized with the initial length (L_0) of each spiked alloys at 35°C is shown in Figure 1. The time is represented as an equivalent time (in year) obtained by multiplying the measurement time by the accelerating factor of 18.59. Each dilatometer contains a pair of long (3cm) and short (2cm) length specimens. The $\Delta a/a_0$ of the sample is from X-ray diffraction where $\Delta a/a_0$ represents the measured lattice constant change (Δa) normalized with the initial lattice constant (a_0). As plotted in Figure 1, the spiked alloys have increased in length significantly. Based on microstructural characterizations, the initial changes in the volume and density are a result of the change in lattice parameters, which saturates within approximately three years of aging. Following the initial transient, the change is mainly caused by continued build-up of helium in-growth.

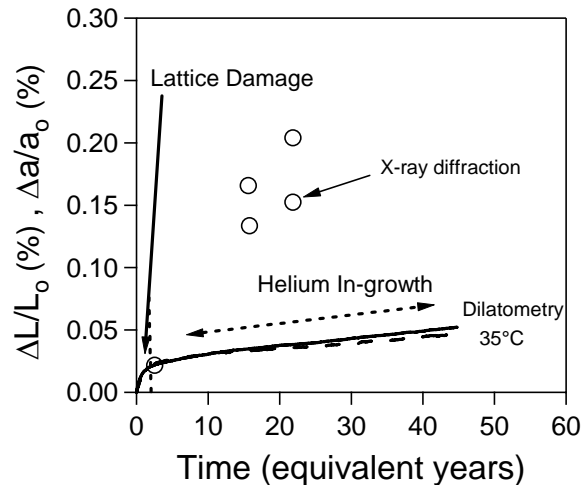


Figure 2. Dilatometry and X-ray diffraction measurements show dimensional expansion with aging.

SUMMARY

We found reasonable agreement in the density change behaviour between enriched and reference alloys from combined dilatometry and immersion density measurements. Based on microstructural analysis, the decrease in plutonium alloy density is a result of the dimensional expansion from the accumulation of residual lattice damage and helium in-growth.

This work was performed under the auspices of the U.S. Department of Energy by the University of California, Lawrence Livermore National Laboratory under Contract No. W-7405-Eng-48.

- 1 B.W. Chung, S.R. Thompson, C.H. Woods, D.J. Hopkins, W.H. Gourdin, and B.B. Ebbinghaus, submitted to: J. Nucl. Mater. (UCRL-JRNL-216611) (2005)
- 2 H.A. Bowman, R.M. Schoonover, and M.W. Jones, J. of Res. Nat. Bur. Stand., 71C, (1967) 179.

Modeling of plutonium alloy swelling by kinetic rate equation

N. Gras-Naulin, P. Julia

CEA – Centre de Valduc, F-21 120 IS-SUR-TILLE, FRANCE

INTRODUCTION

Understanding and predicting all the impact of plutonium alloys aging on the reliability and safety of nuclear stockpile is one of the most challenging aspects of plutonium metallurgy. One of the consequences of plutonium aging is swelling. This phenomenon has several origins: voids or bubbles formation due to vacancies clustering, alpha decay sub products (Am, Np, U, He ...). These defects are created by displacement cascades due to alpha decay of plutonium. Many experiments allow measurement of the total swelling but none of them permit a perfect identification and quantification of each contribution. So we try to use modeling as a tool to evaluate the contribution of the different phenomenon involved in swelling.

Kinetic rate equation modeling allows determination of the concentration in vacancies clusters versus time for each size of cluster¹. From these concentrations we can extract the total change in volume of the material due to void formation, $\Delta V/V$:

$$\Delta V/V = \sum 4/3 \pi r_n^3 C_n$$

with r_n : radius of a cluster containing n vacancies

C_n : concentration in cluster of size n.

The results obtained by this modeling are compared to those measured by optical-fiber Bragg grating sensors. This technique allows continuous measurement of the elongation of the sample². The total swelling of the material is then obtained versus time.

RESULTS

Kinetic rate equation physics is in the input data. Energetic data such as formation and migration energies of vacancy and interstitial, diffusion coefficient of interstitial and vacancy are needed. Molecular dynamic calculations were performed in order to obtain pertinent data in regard with the material we want to model³. Dose rate is an important parameter, but the key data is the freely migrating defects that escape their nascent cascade and are able to induce microstructure evolution. This fraction depends on mobility of defects and can be estimated by simulation using molecular dynamic and Kinetic Monte Carlo models. For the time being, we did not perform this simulation and we use results obtained on aluminium⁴. The production efficiency of freely migrating defect is 15% of the defect production value predicted by NRT model.

Simulation over several years was performed and results are presented on figure 1. Superposition of the curve calculated by kinetic rate equation with the one obtained by dilatometry exhibited a difference of behavior. Contribution of defects induces a saturation of swelling after about 6 months whereas no saturation is observed experimentally.

Contribution of chemical defects is quite important and can explain the continuous rise of swelling. So we add to the results obtained by kinetic rate equation, swelling due to the increase of americium concentration⁵ and helium contribution through out the increase of volume due to formation of helium bubbles⁶. Total swelling is reported on figure 2 and compared to experimental results. Calculated curve is a little bit more conform to the dilatometric measurement but there is still a difference between the two curves.

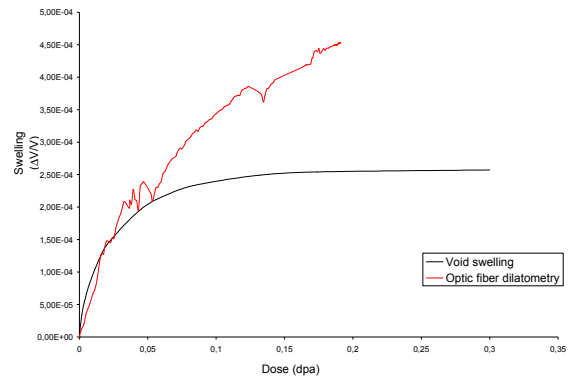


Figure 1: Void swelling versus dose

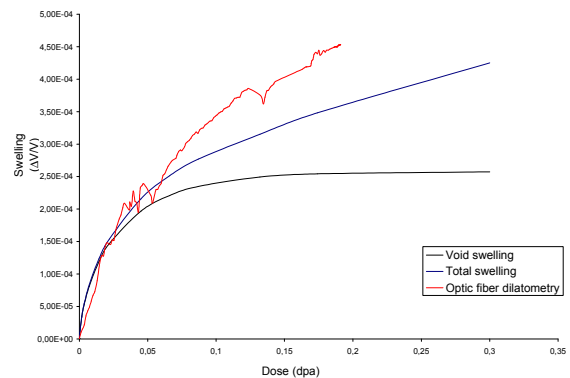


Figure 2: Total swelling versus dose

DISCUSSION

The difference of swelling is probably due to a complementary effect which is neglected in the previous simulation. This neglected phenomenon has an increasing importance and we can not predict long term swelling without understanding it and take it into account. Several guesses are explored; the most favorable is an interaction between vacancies clusters and helium which could exacerbate volume change. Modeling this interaction is a great challenge and is our current subject of interest.

References:

- 1: A. Hardouin Duparc *et al.*, J. Nucl. Mater. 302 (2002) 143
- 2: P. Julia, Plutonium Futures – The Science (2003) 109
- 3: L. Berlu, Technical report CEA/DRMN/SEMP (2006)
- 4: A. Almazouzi *et al.*, Nuclear Instruments and Methods in Physics Research B 153 (1999) 105-115
- 5: F.H. Ellinger *et al.*, J. of Nucl. Mater., 20 (1966) 83-86
- 6: W.G. Wolfer, Los Alamos Science 26 (2000), 277-285

The TTT-diagram of unalloyed plutonium $\alpha \rightarrow \beta$ -transformation.

A.V. Troshev, A.M. Lyasota, S.I. Abramenko, Yu.N. Zuyev, V.N. Kordyukov,
B.G. Levakov, B.V. Litvinov, E.P. Magda, A.A. Snopkov

*Academician E.I. Zababakhin All-Russia Research Institute of Technical Physics,
456770, Snezhinsk, Chelyabinsk region, PO Box 245
Fax: 351-323-51, E-mail: btk@five.ch70.chel.su*

The majority of investigations into kinetics of plutonium $\alpha \rightarrow \beta$ -transformation were performed under quasi- and isothermal conditions using oil baths to maintain constant temperature of the samples. The exception are experiments, performed by M.C. Faiers and R.G. Loasby, on studying kinetics of $\alpha \rightarrow \beta$ -transformation at pulse electric heating (Proceedings of the 3-rd and 5-th International Conferences – Plutonium-1965 and Plutonium-1975).

As a result of this work thermal-kinetic curves were obtained in temperature-time-degree of phase transformation coordinates, the so-called TTT-diagrams (Temperature-Time-Transformation). These diagrams represent one of fundamental properties of plutonium.

But until the present time due to inconsistency and spread in values of temperatures of transformation starting in some intervals of incubation period the known TTT-diagrams can not be combined into a uniform TTT-diagram of plutonium $\alpha \rightarrow \beta$ transformation starting.

The authors of this paper have supplemented the known data with the results of investigations into kinetics of phase transformation during pulse volumetric heating of plutonium samples on pulse nuclear reactors available at VNIITF. The authors propose the version of reasonably completed TTT-diagram of unalloyed plutonium $\alpha \rightarrow \beta$ -transformation, which covers a change in incubation period of starting of isothermal phase transformation within $10^{-5} \dots 10^5$ s (Fig.1).

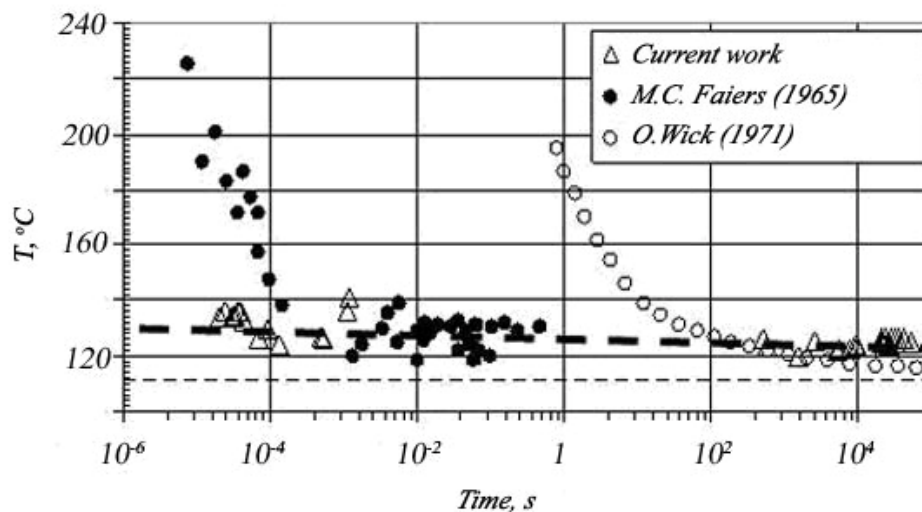


Fig. 1 – Generalized TTT-diagram of plutonium $\alpha \rightarrow \beta$ -transformation starting (dotted line), proposed by authors, and published data.

Helium Bubble Behavior in Plutonium Alloys at the Atomistic Level

S. Valone*, M. Baskes*, R. Hoagland*

*Los Alamos National Laboratory, Los Alamos NM 87545 USA

MODELING RADIATION DAMAGE IN PLUTONIUM

Self-irradiation damage in plutonium metal and alloys generates a series of defect structures that range from point defects to macroscopic density changes. One approach to modeling these defect structures is a reliable atomic level model, which at a minimum accounts for the Pu-Ga-He system. An atomistic model for this system has been previously developed based on the modified embedded atom method (MEAM) [1]. The model was applied to both alloys [2] and He bubbles in those alloys, under constant temperature and volume conditions [3]. Changes in the local structure of the bubbles at various temperatures, gallium concentrations, and helium concentration within a single bubble could be observed. In this study, we use constant hydrostatic pressure boundary conditions. The MEAM potential for the Pu-Ga-He system used here is substantially the same as before [3], except for small changes in the He-He and Pu-He interactions. The He-He interaction was reduced at high pressure by requiring that interaction to exactly reproduce the experimental cold curve at those pressures, as well as exactly matching the *ab initio* curve for the He₂ dimer. The Pu-He interaction was modified to reduce the solubility of the He in the metal. This was done by changing the scaling ratio between the He and Pu density contributions to 0.15 from 0.04. This value was chosen to obtain a 0.75 eV heat of solution for the He. This heat of solution was chosen because it is in the mid-range of accepted values for He in metals when the He is placed in a substitutional site in the metal. Changes in the constant volume results was inconsequential at the He bubble pressures considered, as a result of the small changes in the potential.

HELIUM BUBBLE BEHAVIOR AT CONSTANT HYDROSTATIC PRESSURE

The results of simulations of He bubbles in 5 at-% Ga-stabilized Pu at constant pressure show minimal changes relative to those at constant volume. The volume changes are less than 1%. The interstitial cluster in the cell at 300 K and a 2:1 He-to-vacancy ratio, remains immobile on the timescale of the simulations (50 ps). The distribution of He in the bubble at these conditions is shown in Fig. 1 for both constant volume and pressure boundary conditions.

At both higher temperatures (1000 K) and higher He densities (2.5:1 and 3:1 He:vac), the local structure of the metal lattice in the neighborhood of the He bubble remains close to the structures observed under constant volume conditions. At temperatures close to the melting point, there are indications of greater solubility of He in the metal. At high He densities, the He disturbs the local structure of the metal and some He is injected into the metal (Figs. 2a and 2b).

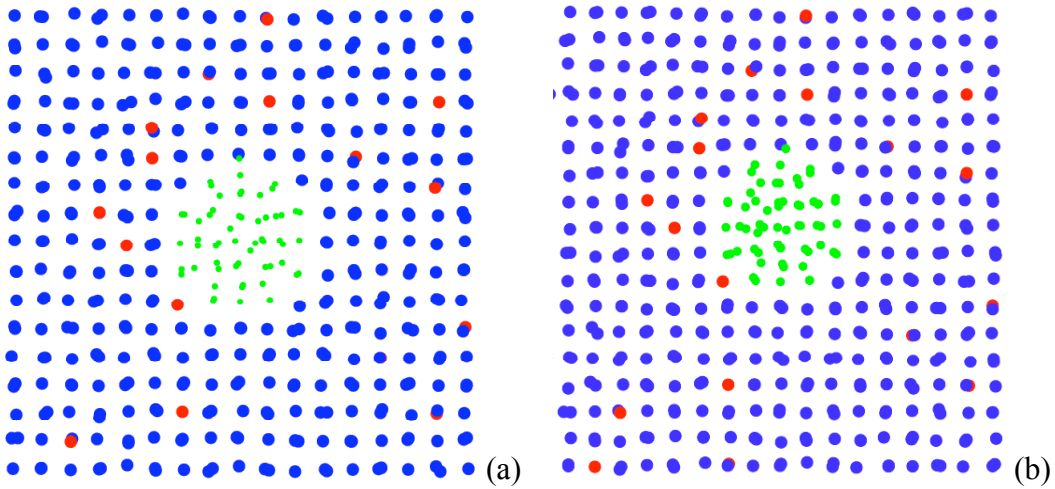


Fig. 1: Cross-sections of He Bubble at 300 K, 5 at-% Ga, 2:1 He:vac ratio, and (a) constant V and (b) constant P = 0.

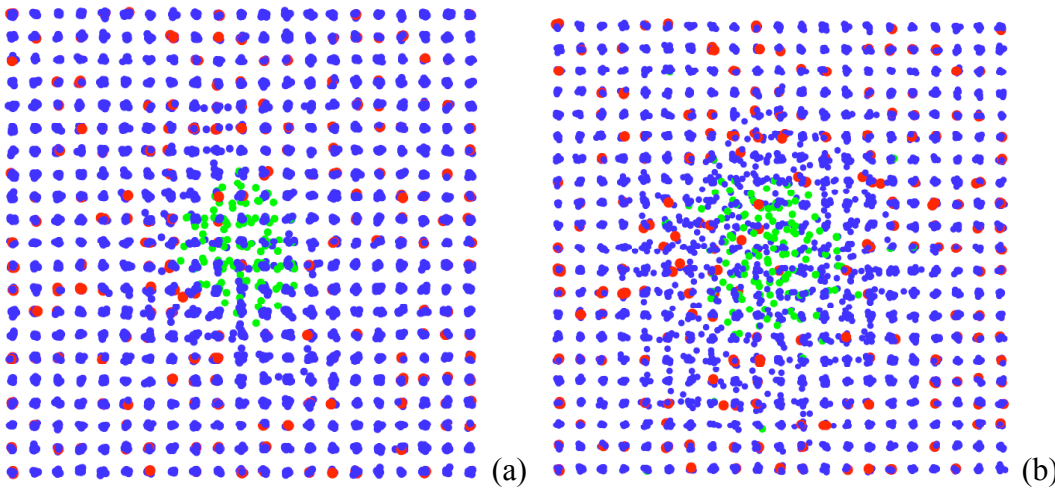


Fig. 2: He bubble at 300 K 5 at-% Ga, constant P, and (a) 2.5:1 and (b) 3:1 He:vac ratio.

This work was performed at Los Alamos National Laboratory under the auspices of the U. S. Department of Energy, under contract No. W-7405-ENG-36.

- [1] M. I. Baskes, Phys. Rev. B 46, 2727 (1992); M. I. Baskes, Phys. Rev. B 62, 15532 (2000); M. I. Baskes, S. P. Chen, and F. J. Cherne, Phys. Rev. B 66, 104 (2002).
- [2] M. I. Baskes, K. Muralidharan, M. Stan, S. M. Valone, and F. J. Cherne, JOM 55, 41 (2003).
- [3] S. M. Valone, M. I. Baskes, and R. L. Martin, Phys. Rev. B, accepted (2006).

Formation and Recovery of Irradiation and Mechanical Damage in Stabilized δ -Plutonium Alloys

F. J. Freibert, D. E. Dooley, D. A. Miller, and A. Migliori

Los Alamos National Laboratory, Los Alamos NM 87545 USA

HISTORICAL PERSPECTIVE

In 1958, Bochvar, et.al. authored a paper in which the binary phase diagram for the Pu-Al system exhibited a stabilized δ -phase field which extended to compositions no greater than 14 atomic percent and to temperatures no lower than 175 °C, at which point the alloy undergoes a eutectoid decomposition into β -Pu and Pu₃Al.¹ This behavior was cited in 1961 by Ellinger, Land and Miner when discussing X-ray diffraction data for stabilized δ -phase Pu-Al alloys, which had been aged at ambient temperatures for 10 years.² In this work, Ellinger, et.al. witnessed a slight lattice expansion (~0.1%) in Pu-Al alloys varying in composition from 11.5 to 12.8 atomic percent and attributed this swelling to lattice defects.² Following on this theme, in 1975 Chebotarev and Utkina reported observing lattice expansion (<0.2%) in δ -phase Pu-Al and Pu-Ga alloys, increasing linearly with alloy concentration, whether the materials had undergone shear or self-irradiation damage.³ Based on this experimental data, Chebotarev, et.al. attributed this lattice expansion to a crystallographic modification, a lattice distortion in the face-centered cubic (FCC) atomic positions. Later work by Inozemtsev, Panteleyev, and Chebotarev showed lattice swelling of similar magnitude in Pu-Al and Pu-Ga alloys exposed to neutron irradiation.⁴ In all reported cases of this behavior, the volumetric expansion was relieved by annealing the alloys at temperatures up to 250 °C.¹⁻⁴

EXPERIMENTAL RECOGNITION OF DAMAGE ACCUMULATION

Interstitial defects in crystalline structures have often been cited as explaining thermo-physical and mechanical changes which result from the accumulation radiation damage. The most stable interstitial atomic configuration of FCC metallic elements is that of the $\langle 100 \rangle$ split-interstitial or $\langle 100 \rangle$ dumbbell interstitial.⁵ These defect structures were first uniquely identified in electron-irradiated Al single crystals via diffuse X-ray scattering as inducing a lattice expansion and having a tetragonal symmetry.⁶ Many studies of radiation damage in FCC alloys has shown that these defect structures can form at substitutional impurity sites as a mixed $\langle 100 \rangle$ dumbbell interstitial consisting of an impurity atom and a host atom being stable to temperatures of 200K or higher.⁷ No matter what atoms combine to form the $\langle 100 \rangle$ dumbbell interstitials in FCC metals, these defect structures not only generate lattice swelling, but also induce unusual changes in the lattice properties such as decreased elastic moduli, large thermal atomic displacements, and decreased Debye-Waller factors.⁷

Based on the results of recent work conducted at Los Alamos National Laboratory^{8,9} it is proposed that Pu-Ga mixed $\langle 100 \rangle$ dumbbell interstitials, caused by self-irradiation processes in naturally and accelerated aged Pu-Ga alloys, induce volumetric swelling and elastic modulus alterations in these alloys as a function of time and Ga concentration. This volumetric swelling, which is in agreement with the historic mechanical and self-irradiation damage data¹⁻⁴, is

similarly removed at temperatures greater than 250 °C and returns on further room temperature aging (see Figure 1). The explanation for the extreme thermal stability of these defect structures can be found in the altered local bonding environment for the interstitial pair and first-nearest neighbors in which the Pu atom, when trapped adjacent to a Ga atom, reduces its size through the on-site localization of a *5f* electron in response to its reduced coordination number. Recent magnetic susceptibility experiments conducted by McCall, indicate that *5f* electron localization accompanies self-irradiation damage.¹⁰ Data from X-ray diffraction¹¹, EXAFS¹², and neutron diffraction¹³ experiments in naturally and accelerated aged Pu-Ga alloys have shown tetragonal lattice distortions, altered Pu-Ga and Pu-Pu bond lengths, lattice micro-strain, and large thermal atomic displacements correlating with similar radiological and thermal histories. The existence of these defect structures in Pu-Ga alloys would also explain the absence of void swelling, which is typical for other FCC metals in similar irradiation environments.

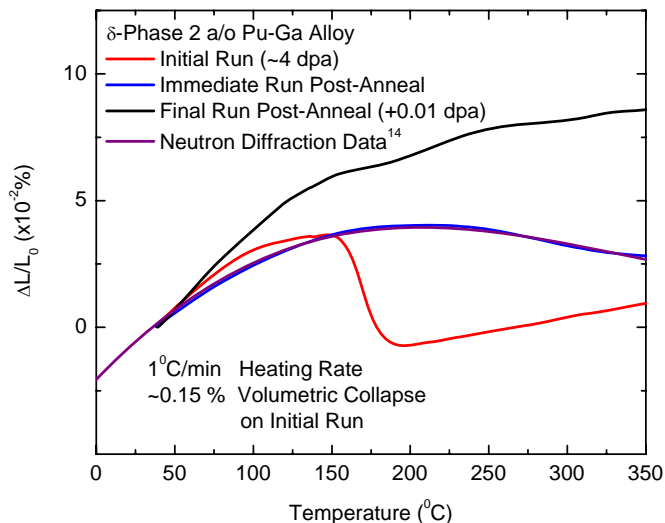


Fig 1: Thermal expansion data for self-irradiated δ -phase Pu-Ga alloy before and after high temperature annealing (>450 °C). Crystallographic data¹⁴ is included to show that annealing removes bulk defects.

This work was conducted under the auspices of the Department of Energy.

- 1 A.A. Bochvar, S.T. Konobeevsky, V.I. Kutaitsev, I.S. Menshikova, and N.T. Chebotarev, Proceedings of the Second United Nations International Conference on the Peaceful Uses of Atomic Energy, **6** 184 (1958).
- 2 F.H. Ellinger, C.C. Land, and W.N. Miner, J. Nucl. Mater. **5**, 165 (1962).
- 3 N.T. Chebotarev and O.N. Utkina, Proceedings of the 5th International Conference on Plutonium and Other Actinides, edited by H. Blank and R. Linder, 559 (1975).
- 4 V.V. Inozemtsev, L.D. Panteleyev, and N.T. Chebotarev, International Conference on Radiation Material Science (22-25 May 1990: Alushta (USSR)).
- 5 R.A. Johnson and E. Brown, Phys Rev **127**, 446 (1962).
- 6 P. Ehrhart and W. Schilling, Phys Rev B **8**, 2604 (1973).
- 7 P.H. Dedrichs, C. Lehmann, H.R. Schober, A. Scholz and R. Zeller, J. Nucl. Mater. **69&70**, 176 (1978).
- 8 F. Freibert, unpublished data (2006).
- 9 A. Migliori, private communication (2006).
- 10 S. McCall, private communication (2006).
- 11 L. A. Morales, A. C. Lawson, S. Conradson, D. P. Moore, E. N. Butler, M. Ramos, and T. Lee, Actinide Workshop, Los Alamos National Laboratory, LAUR-04-3104 (2004).
- 12 S.D. Conradson, L.A. Morales, D.P. Moore, M. Ramos, J. D. Olivias, C. Valot, and A. Ignatov, Los Alamos National Laboratory Report, LAUR-02-6246 (2002).
- 13 A.C. Lawson, et.al., Philosophical Magazine **85**, 2007 (2005).
- 14 A.C. Lawson, et.al., Los Alamos Science **26**, LAUR-00-4100 (2000).

Atomistic Study of Vacancy Clustering and Cluster Dynamics in Pu

BP Uberuaga, RG Hoagland, AF Voter, and SM Valone

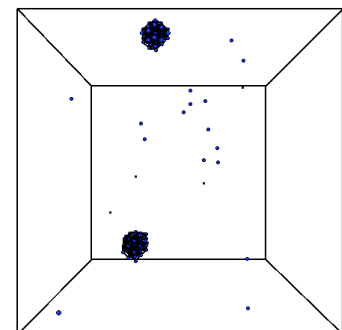
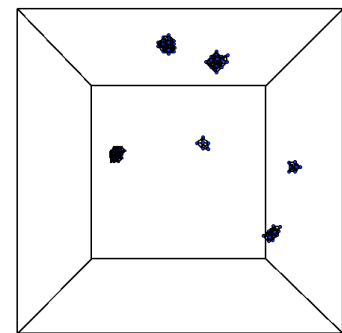
*Los Alamos National Laboratory, Los Alamos NM 87545 USA

Understanding defect mobility and defect-defect interactions is crucial for predicting the long time behaviour of materials. This is especially important for Pu, in which aging phenomena lead to void swelling, the physics of which are determined by interstitial and vacancy point defects. Vacancy clustering will lead to void growth, which will, in turn, give rise to macroscopic swelling. Voids also act as a trap for He gas, giving rise to bubbles that also impact the properties of the material. Thus, understanding the mechanisms by which vacancy voids form and their properties once formed is a key component to understanding Pu aging. While we are generally interested in the full problem of void growth and He incorporation, in this talk we will focus on the properties of the voids themselves.

Using atomistic models, we investigate the clustering behaviour of vacancies in delta-Pu. We study the stability and dynamical properties of clusters containing between 1 and 20 vacancies using the modified embedded atom method¹ (MEAM) to describe the Pu-Pu interaction. The dynamics of these clusters are examined using accelerated molecular dynamics methods², in particular parallel-replica dynamics³.

We find that very small clusters, from size 1 to 5, are mobile, diffusing as objects with identifiable diffusion rates. In particular, di-vacancy clusters diffuse more rapidly than do mono-vacancies. The ramifications of this are explored in a simple kinetic Monte Carlo (KMC) model which ignores higher cluster mobility and which compares the predicted cluster behaviour for two MEAM parameterizations of Pu. In Pu4, an older parameter set, mono-vacancies diffuse faster than di-vacancies. For this model, many small clusters form and diffuse. In PuX, a new model, di-vacancies diffuse faster and the result is that larger, mobile clusters form which sweep up mono-vacancies as they diffuse. See Figure.

For larger clusters, we find surprising behaviour. In simulations of voids containing 20 vacancies using parallel-replica dynamics, we find that, at 400K, the void is essentially very stable on the microsecond timescale. However, after a microsecond has passed, the void spontaneously transforms into a stacking fault tetrahedron (SFT), at which point, the defect exhibits more vacancy motion on its surface than before the transformation. To our knowledge, this is the first time a direct transformation from void to SFT has been observed. In PuX, the SFT is actually significantly higher in energy than the original void, suggesting that this



KMC simulation of vacancy clustering with two MEAM models: Pu4 (top) and PuX (bottom)

transformation is entropically driven. This also illustrates the limitations of the previous KMC model, which assumed that vacancy clusters remain spherical even for large sizes.

We thus examine the stability of larger clusters, containing up to 20 vacancies. We first compare different cluster geometries to determine which is the most stable, energetically, for the various sizes. We compare planar arrangements versus spherical void geometries. We also examine stacking fault tetrahedra. This gives an idea of what structure will be the most stable as a function of size and temperature.

We also performed a similar study in Cu, to both understand the generality of the results obtained for Pu as well as to more thoroughly study a simpler model system. We find very similar behaviour for Cu. In particular, the 20 vacancy void also transforms into an SFT at temperatures of 400K and timescales of microseconds. In the case of Cu, we are better able to examine the details of the transformation from void to SFT and find that it is “catalyzed” by the motion of an extra vacancy on the surface of the void.

Acknowledgements should be placed at the end of the text in italics.

1 *M. I. Baskes Physical Review B* **46**, 2727 (1992).

2 *A. F. Voter, F. Montalenti, and T. C. Germann, Annual Review of Materials Research* **32**, 321 (2002).

3 *A. F. Voter, Physical Review B* **57**, R13985 (1998).

Mesoscale Structure and Collective and Cooperative Phenomena in Delta-Stabilized PuGa

Dylan R. Conradson, Nicolas Bock, Erik K. Holmstrom, Rafael Howell, Steven D. Conradson
Los Alamos National Laboratory, Los Alamos NM 87544 USA

Local structure measurements have demonstrated that below the 3.5 at-% Ga limit where delta-stabilized PuGa is susceptible to the temperature and pressure-induced martensitic transformation to the alpha phase it exhibits nanoscale heterogeneity. Embedded in the delta host, up to 20% of the Pu atoms reside in domains that are depleted of Ga and form a second type of structure called “sigma” that cannot relax to the alpha phase because of the tensile and epitaxial forces exerted on it by its intimate contact with the delta lattice. Although averaging to another cubic structure, sigma Pu is expanded by 6–7% relative to delta so that it must contain interstitial Pu atoms to retain the delta density and it is modulated so that the nearest neighbor shell is actually split around its average distance. It therefore does not resemble any of the known phases of Pu, posing the question of whether it is natural phase analogous to cubic Fe that would be stable under negative pressure or whether its structural properties are dominated by minimizing the strain at the delta-sigma interfaces. The answer is critical in understanding aging mechanisms in this material because defects are most likely stabilized in delta-stabilized PuGa at very high concentrations to form additional types of ordered structures and releasing internal epitaxial strain might explain this observation.

We have addressed this question by 1) using the information available to devise models of the structure of heterogeneous PuGa that duplicate certain aspects of its properties and 2) using band structure calculations to determine their stability. Within the first part of this work we have devised two structures that capture different features of sigma Pu. One of them duplicates both the local and long range average structures by multiplying the fcc unit cell into a 2x2x2 supercell and expanding and contracting the two cubes along one of its diagonals. Inserting interstitials is, however, not possible without creating some physically unrealistic short Pu-Pu distances so the density is too low. An alternative uses a different modulation of the same supercell to match the density, but in doing not all of the 3.5 Å Pu-Pu bonds are split so it fails to meet all of the structural criteria. Band structure calculations on this second structure show that minimizing the energy involves atoms displacements that do not render the structure closer to the experimental results, indicating that the epitaxial energy may be the dominant parameter determining the overall sigma structure. Additional calculations provide further insights into this process as well as helping to identify the preferred locations and structures of defect sites.

This work was supported by the Heavy Element Chemistry Program, Chemical Sciences, Biosciences, and Geosciences Division, Office of Basic Energy Sciences, and the Enhanced Surveillance Campaign, National Nuclear Security Administration, U.S. Department of Energy under contract W-7405. XAFS and XRD were performed at SSRL (Stanford Linear Accelerator Center) and APS (Argonne National Laboratory), which are operated by the US Department of Energy, Office of Basic Energy Sciences. Health Physics operations at SSRL and APS were supported by the Seaborg Institute for Transactinium Science at LANL.

Computation of Irradiation Damage in Alpha-Decay Actinides

I.I. Konovalov

All-Russia Scientific and Research Institute of Inorganic Materials (VNIINM), Rogov st. 5a
Moscow 123060 Russia

INTRODUCTION

Code VACS «Vacancy Activated Condense System» has been developed for calculation of microstructure parameters and properties change in metal nuclear fuel and structural materials producing inert gas atoms under neutron irradiation^{1,2}.

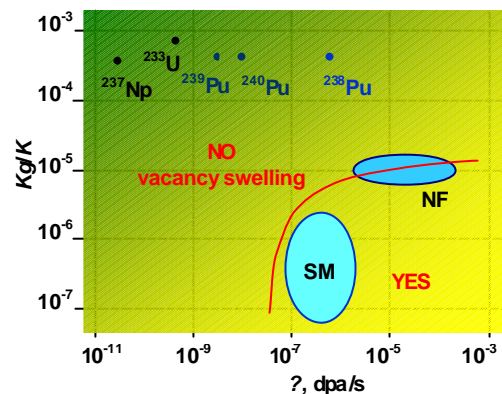
Use of code VACS for self-irradiated metal ^{239}Pu has shown certain conformity of calculated results and experimental data³. The code also has been used for calculation of structure change of alloys in hypothetical system $^{238}\text{Pu} - ^{239}\text{Pu}$ ⁴.

PHISICAL MODEL AND COMPUTAITION RESULTS

Basic thesis of calculation model used in code VACS are given. The kinetics of microstructure irradiation damage: concentration of point defects, density of loop and line dislocations, helium bubble morphology are calculated. The evaluation of influence of microstructure changes on macroproperties of some isotopes U, Np, Pu in metal form under long-life self-irradiation are discussed.

CONCLUSION

In studied field of isotopes physical parameters there are no areas of instable irradiation processes leading to accelerated vacancy swelling. Calculation results of structural changes in self-irradiating metals correspond to basic features of irradiation damage in metal nuclear fuels generating inert gas Xe, Kr and structural materials generating He in reactor core conditions.



The area of vacancy swelling in dependence of damage rate K and rate of inert atoms production Kg . SM – Structural Materials, NF – Nuclear Fuel.

1. I.I. Konovalov “Code VACS. Theory and Swelling Computation of Nuclear Fuel”, Moscow, VNIINM, 2001-3.
2. I.I. Konovalov, Proc. 23 RERTR Int. Meet., ANL/TD/TMDI-12, **135** (2001).
3. V.?. Orlov, I.I. Konovalov, S.A. Kisilev, et al. in Proc. V Int. Workshop “Fundamental Plutonium Properties”, Snezhinsk, Russia, Sept. 12-16 2005, **52** (2005).
4. I.I. Konovalov and V.?. Orlov in Proc. V Int. Workshop “Fundamental Plutonium Properties”, Snezhinsk, Russia, Sept. 12-16 2005, **54** (2005).

Atomistic study of small helium bubbles in plutonium

Bingyun Ao, Xiaolin Wang, Wangyu Hu, Jianyu Yang, Jixing Xia.

China Academy of Engineering Physics, P.O. Box919-71, Mianyang 621900, Sichuan, China

Department of Applied Physics, Hunan University, Changsha 410082, China

Abstract

We have performed a molecular dynamics (MD) technique to calculate the formation energies of small He_nV_m clusters in Pu using the embedded atom method (EAM), the Mores potential and the Lennard-Jones potential for describing the interactions of Pu-Pu, Pu-He and He-He, respectively. The binding energies of an interstitial He atom, an isolated vacancy and a self-interstitial Pu atom to a He_nV_m cluster are also obtained from the calculated formation energies of the clusters. All the binding energies mainly depend on the He-vacancy ratio (n/m) of clusters rather than the clusters size. The binding energies of a He atom and a Pu atom to a He_nV_m cluster decrease with the ratio, but the binding energy of a vacancy to a He_nV_m cluster increases with the ratio. The results indeed show that He atoms can increase the binding energy of a vacancy to a He_nV_m cluster, and decrease the binding energies of a He atom and a Pu atom to the cluster, namely, He atom acts as a catalyst for the formation of He_nV_m cluster

Keywords Plutonium; Helium; Radiation effects; Molecular dynamics

A multi-scale modelling of self-irradiation effects in plutonium

G. Jomard^{*}, L. Berlu[†], B. Oudot^{*}, G. Rosa[†], P. Faure[†], L. Jolly[†], N. Gras Naulin[†], J. Nadal[†], N. Baclet[†] and F. Jollet^{*}

^{*}CEA – Centre de Bruyères le Châtel, F-91680 Bruyères le Châtel, France

[†]CEA – Centre de Valduc, F-21120 Is-sur-Tille, France

^{*}LLNL

INTRODUCTION

Predicting the long term effects of self-irradiation in plutonium based materials is a real challenge for simulation since that imposes to couple models which span a large domain of length and time scales. Indeed, the fundamental process, the α -decay of plutonium nuclei, creates displacement cascades developing in few nanoseconds over few nanometers. But the tracked effects are macroscopic properties changes occurring after many months or years. Among others, the swelling of plutonium based materials which has been experimentally observed might be crucial for the reliability and safety of nuclear stockpile [1-2]. In order to link the emergence of such phenomenon to the radioactive character of plutonium, we must understand all the stages of aging involved : creation of point and/or clustered defects by collision cascades, long-term evolution of these elementary defects (diffusion, eventually aggregation,...). That is why we have initiated a multi-scale modelling approach of self-irradiation effects in plutonium which is presented in the following.

RESULTS AND DISCUSSION

The basic idea of our approach is to couple modelling methods ranging from ab initio and classical molecular dynamics simulation methods to more macroscopic ones such as Mesoscopic Monte Carlo (MMC) and Rate Equations (RE). Obviously, there is a strong interplay between experiments and the theoretical approach in order to parametrize and validate these various models [2].

Classical molecular dynamics has proven to be a powerful technique to simulate the development of collision cascades in materials [3]. But the pertinence of such simulations is hardly dependent on the interatomic potential used. Comparing two widely used models for metals, the EAM and the MEAM ones, we found that the former is too limited to correctly describe the physics of plutonium [4]. So all the simulations reported below have been carried out within the MEAM potential published by M.I. Baskes [5]. Our aim is to obtain the spatial configuration of defects created by cascades in order to use them as input data in the MMC and RE models. This implies to have defect populations that are statistically representative of the self-irradiation phenomena. We have thus achieved a parametric study to quantify the impact of input parameters as PKA (primary Knock-on Atom) direction, PKA energy or temperature on configuration of defects [6]. For the moment we have achieved simulations of various cascades of 2 and 10 keV at T=300K, that is in a temperature range where δ -Pu can only be metastabilized by imposing a volume constraint on the simulation box with the MEAM potential of Baskes. All these computer simulations show the formation of an amorphous zone that is stable for up to many nanoseconds. The complete annealing of the 2 keV cascades thus occurs after 15 ns (cf. Figure 1). It leads mainly isolated vacancies and small interstitial clusters. This result is quite different from what is observed for more classical FCC metals such as copper, lead or gold where the recombination stage of the cascades is achieved after only 15-20 ps and the major part of the vacancies forms big clusters. Like Valone and coworkers, we have attributed this particularity to the multi-phases character of the Baskes's plutonium potential [7]. In order to check the relevance of what we observed, we plan to repeat such a

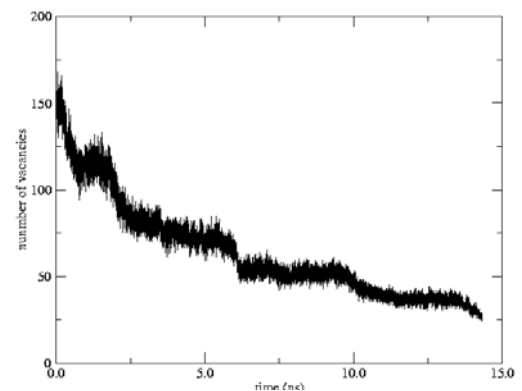


Fig 1: Computed evolution of the number of vacancies for a 2keV cascade in δ -Pu with the MEAM potential [4].

study with MEAM models for both Pu and Ga which will allow us to perform cascades simulations in a more realistic δ -stabilized plutonium crystal.

We have however started to use our predicted defects populations as source term in MMC and RE codes. The various parameters which drive these two models have been either calculated by first-principles or MD methods or set to their experimental values when available (these parameters are mainly the formation and migration energies of various point defects and their clusters). Owing to the limitations of these approaches, this preliminary study does not reach to reproduce the experimentally observed swelling. In particular, for the moment we are not able to take into account the effect of helium or decay elements such as americium. But developments of models are in progress in order to overcome these limitations (cf. communication of N. Gras Naulin et al.).

Concerning the role of helium in the swelling, we have initiated a coupled experimental and theoretical approach based on Positron Annihilation Spectroscopy. The idea is to use first-principles simulations to get a relation between a given defect and the associated positron lifetime in order to help the interpretation of the experiments. We have then implemented the TC-DFT (Two Component Density Functional Theory [8]) in the Abinit code [9].

The lifetimes calculated for bulk δ -Pu, for an isolated vacancy, and for an isolated vacancy containing a helium atom

	τ bulk (ps)	τ vacancy (ps)	τ He filled vacancy (ps)
current work	142	251	197
Sterne and Pask [10]	143	255	170-195

Tab 1 : Calculated positron lifetimes for bulk δ -Pu, in the presence of a vacancy and for a vacancy filled with a helium atom. Our results are compared to those of Sterne and Pask [10].

are in good agreement with previous results presented by Sterne and Pask [10] (cf. Table 1). The comparison between these preliminary results and the experiments seems to indicate that the major part of the vacancies-based defects present in aged plutonium-based materials contains helium. We are currently performing calculations for larger open defects with various helium concentrations to confirm this observation.

- 1 B. Oudot, PhD Thesis, Université de Franche-Comté, Besançon, France (2005).
- 2 N. Baclet, P. Faure, G. Rosa, B. Ravat, L. Jolly, B. Oudot, L. berlu, V. Klosek, J.L. Flament and G. Jomard, Actinides 2005 publishers (Royal Society of Chemistry- 'Advances in Actinide Science')
- 3 K. Nordlund et al., Phys. Rev. B **57**, 7556 (1998).
- 4 G. Jomard and P.M. Anglade, Proceedings of the 3rd International Conference on "Computational Modeling and Simulation of Materials", Part A, 489 (2004).
- 5 M.I. Baskes, Phys. Rev. B **29**, 6643 (2000).
- 6 L. Berlu, G. Rosa, P. Faure, N. Baclet and G. Jomard, MRS Fall Meeting, Boston (2005).
- 7 S. Valone et al., J. Nucl. Mater. **324**, 41 (2004).
- 8 M.J. Puska and R.M. Nieminen, Rev. Mod. Phys. **66**, 841 (1994).
- 9 X. Gonze et al. Comp. Mater. Sci. **25**, 478 (2002).
- 10 P.A. Sterne and J.E. Pask, Plutonium Futures-The science (2003).

Surface Analysis and Reactivity of Plutonium Metal/Oxide Layers

D. Moore^{*}, M. Butterfield[†], T. Durakiewicz^{*}, J. Farr^{*}, J. Joyce^{*}, R. Martin^{*}

^{*}Los Alamos National Laboratory, Los Alamos NM 87545 USA

[†]Lawrence Livermore National Laboratory, Livermore CA 94552 USA

The reactivity of plutonium surfaces is governed by the chemical and physical nature type of surface layers present at the gas-surface interface. These surface layers, under normal conditions, will likely be of a plutonium oxide character and the exact composition of these layers can dramatically influence the ultimate reactivity of the surface to its environment. Therefore, an understanding of the nature of the oxide layer and its formation processes on plutonium metal is important in ultimately understanding its reactivity. In order to more fully understand this complicated situation, we will present surface studies on the plutonium metal/oxide system using a variety of surface analytical techniques including photoemission spectroscopy (PES), x-ray photoelectron spectroscopy (XPS), and Auger electron spectroscopy (AES). In addition to these experimental studies, we will present theoretical calculations of the electronic structure of plutonium oxide layers by means of density functional theory (DFT) methods. Subsequent to the studies on oxide layer formation we will present results on the reactivity of the surfaces to small molecules, e.g. hydrogen. By utilizing a variety of techniques, in connection with theoretical calculations, we will be able to exploit their relative strengths and be able to more fully understand the formation of oxide layers on plutonium metal and their subsequent reactivity to their environment.

PES is an ideal tool for studying the electronic structure of surface oxides. We have performed PES studies of clean plutonium metal surfaces dosed with O₂ under a variety of conditions¹. These studies have revealed clear pictures of the electronic structure of oxide layers formed on clean plutonium metal surfaces under controlled conditions. In Figure 1 we show an example of the PES results for oxide layer formation on plutonium metal via Langmuir (L) level O₂ dosing at 77K. The presence of the Pu sesquioxide (Pu₂O₃) and Pu dioxide (PuO₂) are indicated by the labelled spectral peaks, as is that for Pu metal. We will present complete studies on O₂ dosing of plutonium metal surfaces and the subsequent oxide formation. Additionally, we will discuss the subsequent reactivity of these various surfaces at the gas-surface interface to e.g. H₂.

Recent hybrid DFT calculations have yielded promising results when compared to experimental studies². These calculations predict both actinide oxides to be insulators, with gaps of 2.4 and 2.5 eV for PuO₂ and Pu₂O₃, respectively. The hybrid calculations favorably reproduce the photoemission spectra with peak positions in good agreement with the experiment. For example, for PuO₂ the hybrid calculations show a strong peak at about 2.5 eV with a weaker one near 4.5

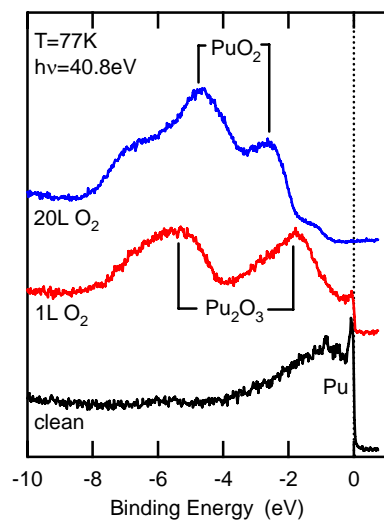


Fig 1: PES data of O₂ dosing on Pu metal showing spectral features of PuO₂, Pu₂O₃, and Pu metal.

eV, in good agreement with the positions from the PES studies shown in Figure 1. We will present results from these recent calculations of Pu oxides as well as recent theoretical results on the reactivity of these surfaces, in particular at the gas-surface interface.

XPS and AES studies will be presented that are complementary to the PES studies of oxide formation and reactivity. Extensive AES studies have been performed on plutonium surfaces and the AES spectra will be used to show the differences between oxide covered surfaces and the underlying plutonium metal. Shown in Figure 2 is an example of AES spectra for a plutonium oxide layer in comparison to the underlying plutonium metal for Pu metal dosed with O₂. Here we show the differentiated spectra for the Pu(OVV) and Pu(OPP) transitions and the Pu(NOV) transition in the left and right panels, respectively. The distinct differences are clearly evident in the differentiated Auger spectra for the oxide and metal surfaces in both cases. For the NOV transition, the peaks for the metal surface are at higher kinetic energies and are sharper than those for the oxide surface. The spectral differences observed between these surfaces are even more dramatic for the (OVV) and (OPP) transitions since these transitions involve the outer valence electrons and are quite sensitive to any changes in the chemical environment. We will in particular present analyses of these lower energy transitions in relation to oxide layer growth and gas-surface reactivity. Finally, similar to the PES studies, subsequent to investigation of the formation or character of the oxide surface we can study its reactivity towards its environment.

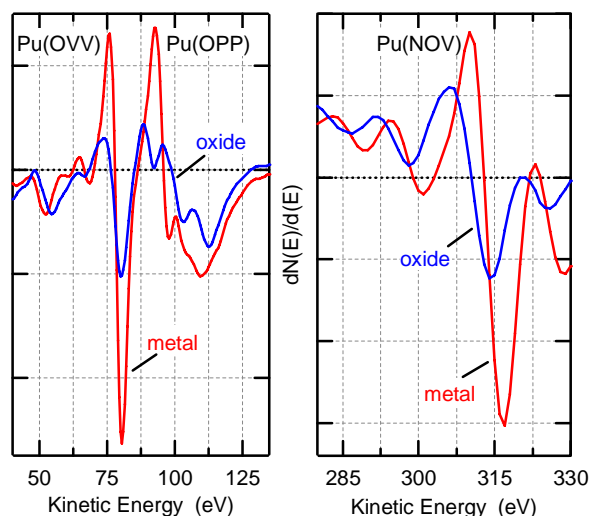


Fig 2: Differentiated AES spectra for O₂ dosing on Pu metal showing the Pu(OVV) and Pu(OPP), left, and Pu(NOV), right, Auger transitions for Pu metal and oxide.

Through the use of a variety of surface analytical techniques we will present results from studies of oxide formation on plutonium surfaces. We will discuss how character and formation of the oxide layers may have subsequent effects on the reactivity of the surface to small molecules, e.g. hydrogen. The experimental results will be complemented by theoretical calculations of the electronic structure of plutonium oxides as well as the reactivity of the gas-surface interface.

LA-UR-06-1267

- 1 M.T. Butterfield, T. Durakiewicz, E. Guziewicz, J.J. Joyce, A.J. Arko, K.S. Graham, D.P. Moore, L.A. Morales, *Surf. Sci.* **571** (2004).
- 2 M. Butterfield, T. Durakiewicz, R. Martin, in "The Actinide Research Quarterly (3rd Quarter 2004), Los Alamos National Laboratory document LALP-04-060, p. 22.

Plutonium oxide transformation kinetics and diffusion coefficient measurement

P Morrall^{*}, S Tull^{*}, J Glascott^{*}, P Roussel^{*}

^{*}AWE, Aldermaston, Reading, Berkshire RG7 4PR, UK

The highly oxophilic nature of plutonium has the consequence that, under ambient conditions, its surface readily develops a tetravalent, PuO_2 , oxide layer. In the absence of O_2 , PuO_2 is thermodynamically unstable on plutonium metal, although the dioxide layer still persists even under the stringent conditions of a high quality inert atmosphere dry box ($\text{O}_2 \sim 1\%$, $\text{H}_2\text{O} < 1$ ppm). However, when plutonium metal samples covered with surface dioxide layers are subjected to ultra high vacuum (UHV) conditions, the dioxide layer undergoes a spontaneous, thermodynamically driven, reduction to the trivalent sesqui-oxide, Pu_2O_3 . Kinetic information about this surface transformation, from PuO_2 to Pu_2O_3 , is gained by following the changing depths of the two oxide layers, using X-ray photoelectron spectroscopy (XPS) as a probe.

A model is proposed for this auto-reaction reaction based on a simple 2D layered structure, where initially a layer of Pu_2O_3 lies between the outer PuO_2 layer, and the Pu metal substrate. When left under UHV conditions the PuO_2 converts, at its interface with the Pu_2O_3 , so that the boundary between the two oxide layers slowly approaches the vacuum interface, and the oxide overlayer is converted to the sesqui-oxide. The rate of this plutonium oxide inter-conversion is controlled by diffusion of oxygen across the steadily expanding Pu_2O_3 layer. Therefore, through investigation of this auto-reduction process, values are obtained for the diffusion coefficient of oxygen through Pu_2O_3 .

© British Crown Copyright 2006/MOD.

PuO₂ Particle Size from Oxidation of Pu Metal in Air at Room Temperature

D. Spearing, B. Bluhm, W. Crooks, D.K. Veirs

Los Alamos National Laboratory, Los Alamos NM 87544 USA

BACKGROUND

Previous studies^{1,2} of PuO₂ particle size and surface area have focused on these properties as a function of sintering temperature. However, little has been done to characterize PuO₂ powder formed from the direct oxidation of Pu metal in air at room temperature. This sort of powder forms on Pu metal parts left exposed to air in non-inert atmosphere gloveboxes, and has been observed on α -Pu buttons shipped to LANL from the Savannah River Site. Of particular concern is the particle size distribution of such powder, and whether or not a significant fraction of the oxide would be at 0.3 μm in diameter, which is the size at which HEPA filter efficiency is at a minimum. According to DOE standard (DOE-STD-3020-97), HEPA filters "...shall exhibit a minimum efficiency of 99.97% when tested at an aerosol of 0.3 micrometers diameter."

EXPERIMENTAL METHOD

A 3.5 kg ingot of high purity α -phase plutonium metal from a previous experiment³ was allowed to oxidize at room temperature in a glovebox with an air atmosphere. Surface area measurements of the oxide were performed using the BET method, and particle size analysis was done using a Beckman Coulter Multisizer in the 2 – 60 μm range.

RESULTS

The surface area was measured to be 7.84 m²/g, which compares well with the value of 6.5 m²/g from a previous experiment⁴. This value also corresponds with the trend observed¹ in PuO₂ of relatively low surface area (≤ 12 m²/g) for oxides calcined at temperatures below 300°C, higher surface areas (30-35 m²/g) for oxides calcined between 300-600°C, and then a drop of in surface area² again at temperatures above 500°C.

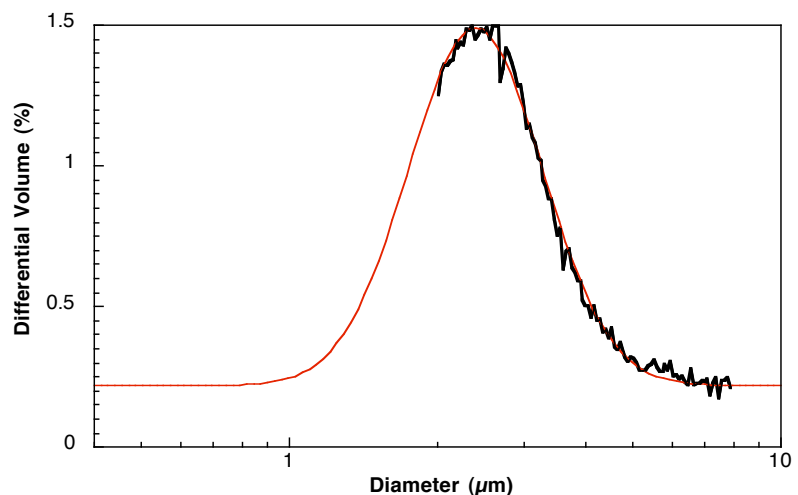


Figure 1 – Differential Volume (%) vs Particle Size (μm). Data are in black, log-normal curve fit is in red.

As mentioned above, particle sizes were measured between 2 – 60 μm . The particle size distribution from 2 – 8 μm is shown in Figure 1. As is evident from Figure 1, there is a significant fraction of particle sizes below 2 μm that we were unable to measure. In order to extrapolate below 2 μm , the observed particle size data were fit to a log-normal distribution⁵, which has been used previously to describe particle size distributions². Based on this fit, the mean particle size diameter was determined to be 2.4 μm with a standard deviation of 1.4 μm .

DISCUSSION

A plot of mean particle size as a function of calcination temperature from a previous study² along with the data point from the current study is shown in Figure 2. Data from the previous study indicate a slight *decrease* in mean particle size as a function of calcination temperature. The mean particle diameter of the plutonium oxide in this study is about one fifth that of the calcined material from previous studies. However, the powder for the calcination studies was synthesized via an oxalate precipitation method in contrast with direct oxidation of metal in air for this study, and thus may not be directly comparable.

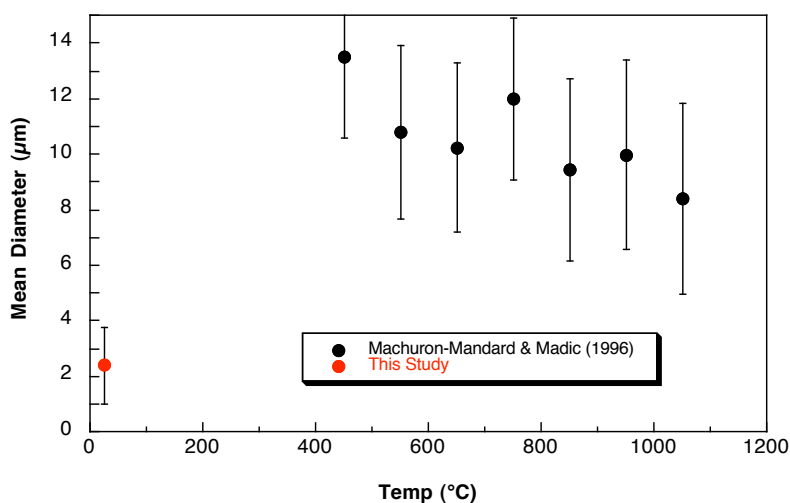


Figure 2 – Mean Particle Size (μm) vs Calcination Temperature ($^{\circ}\text{C}$).

The log-normal fit of the particle size distribution shown in Figure 1 suggests that there is little or no fraction of material below about 0.8 μm . As mentioned above, the HEPA filters are rated to remove 99.97% of all particles at 0.3 μm in diameter. However, a previous study on the gas generation from water adsorbed onto PuO_2 powder⁶ has shown that the particle size distribution of fine powders is not always well fit by a log-normal distribution. In particular, a “tail” was observed on the fine size of the distribution beyond what would be predicted by a log-normal fit. This suggests that there may be a significant fraction of particles at or below the 0.3 μm size. Future studies will focus on determining the particle size distribution below 2 μm and what impact it may have on HEPA filter efficiency.

- 1 O.R.H. Rasmussen, ARH-1153, Atlantic Richfield Hanford Company (1969).
- 2 X. Machuron-Mandard and C. Madic, *J. Alloys and Compds.* **235**, 216 (1996).
- 3 D. Spearing, D.K. Veirs, and F.C. Prenger, *J Nucl Mater.* **299**, 111 (2001).
- 4 J.L. Stakebake and L.M. Steward, *J Colloid Interface Science*, **42**, 328 (1972).
- 5 D.B. Siano, *J Chemical Education*, **49**, 755 (1972).
- 6 D.K. Veirs, LA-UR-05-8853, Los Alamos National Laboratory (2005)

Some physical chemical and radiation properties of plutonium-238 metal prepared from amalgam

V.F. Peretrukhin¹, S.I. Rovny², A.G. Maslennikov¹, V.V. Erchov², V.I. Kapitonov²,
P.P. Chinenov², V.L. Kuvaev²

1-Institute of Physical Chemistry and Electrochemistry, Russian Academy of Sciences, 31
Leninski prospect, Moscow, 119991, Russia

2-Production Association "Mayak", Ozersk, Chelyabinsk region, Russia.

²³⁸Pu metal was prepared from Pu(III) aqueous acetate solution by electrolysis with mercury cathode and by subsequent thermal destruction of plutonium amalgam [1]. This method of ²³⁸Pu metal preparation permits to avoid the neutron irradiation arising from (α,n) reactions with light nuclei, for instance with ¹⁸O. ²³⁸Pu(III) (20 g/l) was reduced to Pu⁰(Hg)_n (n=1-4) and transfer from aqueous solution to amalgam, where (α,n) reaction with mercury is impossible. The mercury was removed from amalgam and from compounds Pu⁰(Hg)_n with argon stream at 300-600°C, plutonium metal was melted in vacuum at 1100°C and cooled. Obtained plutonium ingots were pressed in air atmosphere to prepare the pellets with diameter 6 and height 6-8 mm.

The following properties of ²³⁸Pu metal pellets were measured: density, γ-spectra, specific heat power, specific neutron flux and kinetics of pellets corrosion in air atmosphere at ambient temperature. The pellets density at room temperature depended weakly on the pressure in studied interval 0.45-0.75 kbars and was equal to 16.1-17.1 g·cm⁻³ (81-85% of α-²³⁹Pu X-ray density at the same conditions). Specific heat power was determined by calorimetric measurement as 0.45 Wt/g for all prepared tablets. Gamma spectra of the pellets were registered in energy range from 100 to 3000 KeV to identify the possible impurities of stable light nuclei, which can enter in nuclear reactions (α,α'γ), (α,pγ), (α,nγ). Besides ²³⁸Pu γ-peaks, two γ-peaks with E_γ 1395 and 1982 KeV were observed and associated with the presence of ¹⁸O, entering in the reactions (α,α'γ) and (α,nγ). Analogous γ-measurements of biomedical ²³⁸PuO₂ have shown the number of γ-peaks caused by the presence of light nucleus impurities ¹⁰B, ¹⁸O, ¹⁹F, ²⁸Si. The comparison of ²³⁸Pu metal γ-spectra and that of biomedical ²³⁸PuO₂ demonstrates that electrochemical preparation of ²³⁸Pu metal via amalgam provides more high decontamination from light impurities than the biomedical ²³⁸PuO₂ preparation does.

Rapid neutron flux, emitted by ²³⁸Pu metal pellets, was measured using neutrons coincidence 4π-counter and compared with calculated value, took into account the number of spontaneous fission neutrons of present Pu isotopes and the number of fissions induced in pellet by spontaneous neutrons. Measured specific neutron flux of the tablets (3.4·10³ ns⁻¹g⁻¹) was shown to be higher than calculated one on 300-600 ns⁻¹g⁻¹. This exceeding of experimental neutron flux value to calculated one is explained by the oxidation of ²³⁸Pu metal pellet and by the neutron contribution of the reaction ¹⁸O(α,nγ)²¹Ne.

The kinetics of ²³⁸Pu metal corrosion was studied in air atmosphere at ambient temperature. Two techniques, sample weight gain and continuous neutron flux measurement were used for the determination of corrosion rate and gave the same results. The increase of the ²³⁸Pu mass sample Δm_i/m₀ in time was shown to be proportional to the increase of neutron flux

from the sample $\Delta I_t/I_0$. Three steps of corrosion kinetics have been observed at air atmosphere at ambient temperature: (1) slow latent step (so called "germination period"), (2) high rate corrosion step, ^{238}Pu metal corrosion rate achieved its maximum value $3.1 \cdot 10^{-3} \text{ mg} \cdot \text{cm}^{-2} \cdot \text{h}^{-1}$ and (3) some deceleration of corrosion rate because of PuO_2 layer growth on the metal surface. ^{238}Pu metal corrosion rate maximum value obtained in air atmosphere was the order of magnitude higher than that published for ^{239}Pu in the same experiment conditions. More high temperature and more strong radiation dose rate on the surface of the ^{238}Pu metal than those of ^{239}Pu are the reasons of the increased corrosion rate of ^{238}Pu metal. The mechanism of $^{238}, ^{239}\text{Pu}$ corrosion process is discussed in details in the report.

REFERENCES

- 1 V.F. Peretroukhin, P.P. Chinenov, V.I. Kapitonov, A.G. Maslennikov, V.L. Kuvaev, V.I. Silin. Preparation of plutonium-238 metal and its intermetallic compounds emitting low flux of (α, n) neutrons. International conference GLOBAL-1995, Versailles, France, Sept. 1995. Proceed., vol.2, pp.1716-1724.

CORROSION OF URANIUM ALLOY FUEL IN WATER

V.F. Peretrukhin, A.G. Maslennikov, A.Yu. Tsivadze, C.H. Delegard*,
A.M. Fedosseev, V.P. Shilov, A.B. Yousov, N.Yu. Boudanova, A.A. Bessonov,
K.N. Gedgovd, G.S. Bulatov.

*A.N. Frumkin Institute of Physical Chemistry and Electrochemistry,
Russian Academy of Sciences, 31, Leninsky Prospect, Moscow, 119991, Russia*
* -Pacific Northwest National Laboratory, P.O. Box999, Richland, WA, 99342 USA

Though published data on the corrosion of uranium metal and its alloys are numerous, they are insufficient to accurately predict the corrosion behavior of irradiated uranium during long-term underwater storage. The goals of the present work are to study:

- the corrosion of uranium and its 0.5 and 5 wt% Zr, Nb, Tc, and Ru alloys in water,
- the primary corrosion process,
- the further oxidation of U(IV) hydroxide by dissolved oxygen, and
- U and U-alloys dissolution in water and nitric acid under hydrothermal conditions.

The uranium alloys were prepared from U-Me mixtures by 4-fold repeated arc melting under Ar followed by 24 hours of vacuum annealing at 1230 K. Alloy characterization included electron microscopy, elemental analysis, XRD, microstructure, grain size, and microhardness. The electrochemical corrosion tests were carried out with a rotating disk uranium electrode in anaerobic 0.1 M NaClO₄ (pH 4-9) and 0.1 M Na₂CO₃. Open circuit potentials (OCP) for pure and alloyed uranium at pH 4-9 ranged from -250 to -450 mV vs. the Ag/AgCl electrode and shifted by -100 to -150 mV in 0.1 M Na₂CO₃. The observed OCPs are similar to the standard oxidation potentials of the half reaction



at the studied pH. Closed circuit corrosion potentials (E_{corr}) determined at zero current differed by 20-60 mV from the corresponding OCP. Uranium corrosion rates, determined by chronocoulometry (CC), potential controlled electrolysis (PCE), and chemical element analysis, ranged from 0.00121 to 0.00222 mg cm⁻² h⁻¹ in pH 4-9 0.1 M NaClO₄ at 25°C.

The corrosion mechanism was studied by determining the number of electrons participating in the electrochemical process ($n \sim 1$), the transfer factor ($\alpha \sim 0.5$), and the exchange current density (i_0 from 0.53 to 1.1 μA cm⁻² at pH 4-9). To clarify the role of intermediary U(III) in the corrosion process, the stability of electrochemically prepared U(III) was investigated in neutral solution. Addition of Na₂B₄O₇ or NH₄OH solution to 0.002 M U(III) in 0.05 M HCl to attain pH 7-8 precipitated U(III) hydroxide. The broad UV-Vis bands characteristic of U(III) decreased with time in the U(III) hydroxide suspensions. Spectral analysis of the solution obtained by dissolving 15-min old precipitate in 1.5 M HCl showed that only ~40% of the original U(III) still remained. The rate of U(III) formation during U corrosion in pH 7-8 water and in 0.1 M NaHCO₃ thus is lower than the rate of U(III) hydroxide oxidation by anaerobic pH 7-9 water.

The corrosion rates for uranium alloys with 0.5-5 % Zr or Nb differ by factors of 0.2-5 from that of pure uranium. The addition of 0.5-5% Ru had a greater effect on decreasing the corrosion rate. Determinations of the effect of Tc alloying on the corrosion rate of U in water are in progress.

The oxidation of U(IV) by oxygen in NaHCO₃ solutions proceeds with a rate constant of 5 to 20 liters mol⁻¹ s⁻¹ in 0.01-0.15 M NaHCO₃ at 25°C. This process in pH 3-7 aqueous solution is complicated by the formation of mixed U(IV)-U(VI) colloid suspensions.

The dissolution of U metal in water and in HNO₃ solution has been studied in hydrothermal conditions at 120-160°C. These tests showed that oxidizers (H₂O₂, K₂S₂O₈, I₂) in presence of Pt catalyst dissolved uranium at controllable rates without increased pressurization under sealed tube conditions.

Electrochemical Corrosion Single Crystal Uranium

M.T. Paffett and R. Scott Lillard

Los Alamos National Laboratory, Los Alamos, NM 87545

The long-term stability and electrochemical corrosion characteristics of actinides have historically been examined using techniques and approaches that are macroscopic in nature. Furthermore, the published literature of actinide surface has, to date, been performed exclusively on polycrystalline monolithic samples. Prime examples of these approaches include potentiodynamic polarization of uranium solid samples in aqueous media [1,2]. In this work we approach the localized corrosion of uranium using an in-situ technique, electrochemical scanning tunneling microscopy (ECSTM). This approach has demonstrated great promise in our understanding of localized corrosion at other technologically important metals and alloys. In this presentation we will also compare global electrochemical corrosion characteristics of single crystal uranium to those previously observed for polycrystalline uranium and U-Nb alloys. Results of localized corrosion of single crystal uranium monitored using ECSTM will also be presented and compared with these prior studies. We will attempt to address the role of localized corrosion in observed electrochemical behavior of single and polycrystalline uranium.

1. J.A. Lillard, D.N. Kelly, M.T. Paffett, and R.J. Hanrahan, “**Electrochemically-grown oxides on U-Nb alloys,**” Proceedings - Electrochemical Society (2000), 2000-4(Oxide Films), 100-111.
2. J.W. McWirtter and J.E. Draley, “Aqueous Corrosion of Uranium and Alloys: Survey of Project Literature”, Argonne National Laboratory Report, ANL-4862, May 1952.

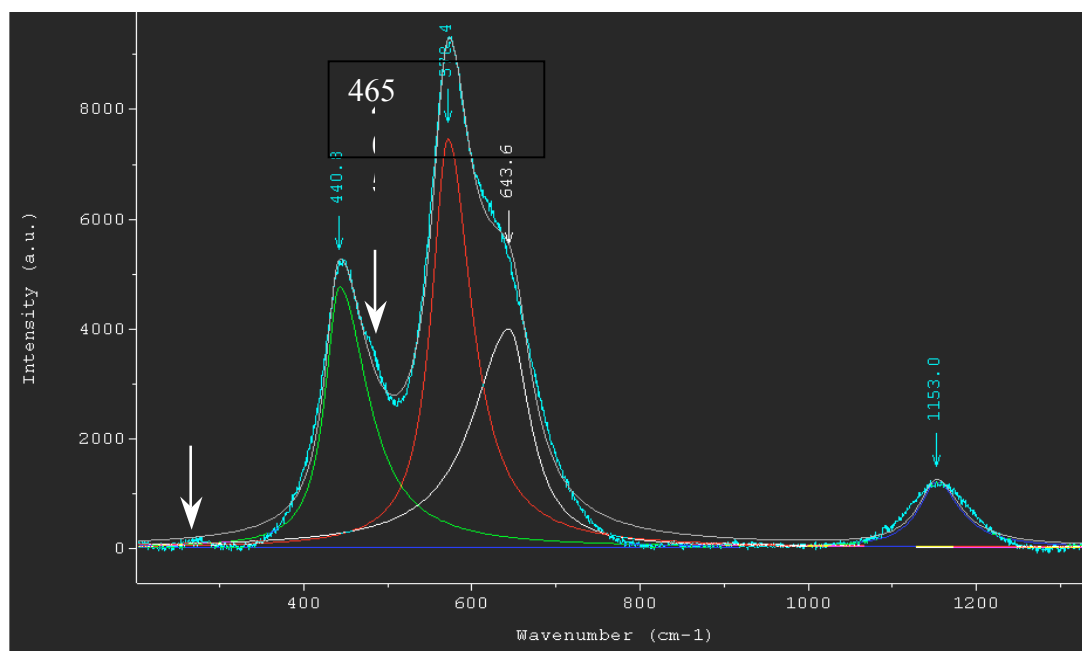
Optical Properties of Actinide Surface Oxides by Ellipsometry and μ -Raman Spectroscopy

W. Siekhaus, T. Trelenberg, M. Wall

Lawrence Livermore National Laboratory, Livermore CA 94552 USA

Uranium

The Raman spectra of epitaxial uranium oxide have recently been observed by μ -Raman spectroscopy¹.



Species	Literature values, cm ⁻¹										
α U ₃ O ₈		235	340	410			475	640	750	805	
U ₄ O ₉	210					465					
UO ₂					446						1150
UO ₂ Kr ion bomb.					446		575				1150
β -U ₃ O ₇	210					465					

Figure 1. Raman spectrum of epitaxial uranium oxide grown in air and comparison with literature values (see literature cited in reference 1).

¹ N. Caculitan, W. Siekhaus, MRS 2005 Fall Symposium Proceedings, in press.

Figure 1 demonstrates that air-grown uranium surface oxide consists of several moieties. The most prominent peak at $\sim 575 \text{ cm}^{-1}$ has been seen in the literature only in UO_2 bombarded with Krypton ions, suggesting that the epitaxial oxide has a highly disordered lattice. Changes in the oxide composition induced by vacuum and exposure to hydrogen were observed in situ by placing the oxidized uranium sample into a small vacuum chamber and monitoring the surface through a fused silica window.

Ellipsometry and Reflectometry have been used to determine the optical constants n and k of the uranium substrate and of the surface oxide grown in air² over a wavelength range from 200 to 1000 nm.

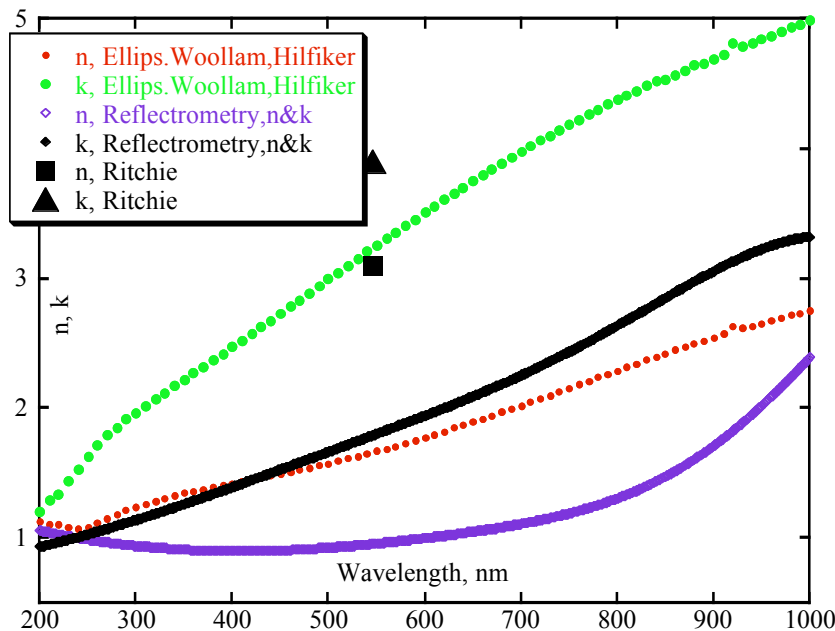


Figure 2. The optical constants n and k of bare uranium as a function of wavelength deduced from ellipsometry and reflectometry, and literature values (Ritchie) of n and k at 546 nm (see literature references in reference 2).

Figure 2 shows that for bare uranium there are substantial disagreements between literature values and values measured by ellipsometry or reflectometry. In both techniques all measurements were done in air while Ritchie's measurements were done on sputtered cleaned

² W. Siekhaus, A. Nelson, MRS 2005 Fall Symposium Proceedings, in press.

Uranium held in an ultrahigh vacuum system. The disagreement is not as pronounced in figure 3, where the n and k values of the oxide measured by ellipsometry and reflectometry are compared with literature values. Both ellipsometry and reflectometry were used to determine the oxide thickness as a function of exposure time to air, and the oxide thickness measurements agree with each other, despite the fact that the optical constants disagree.

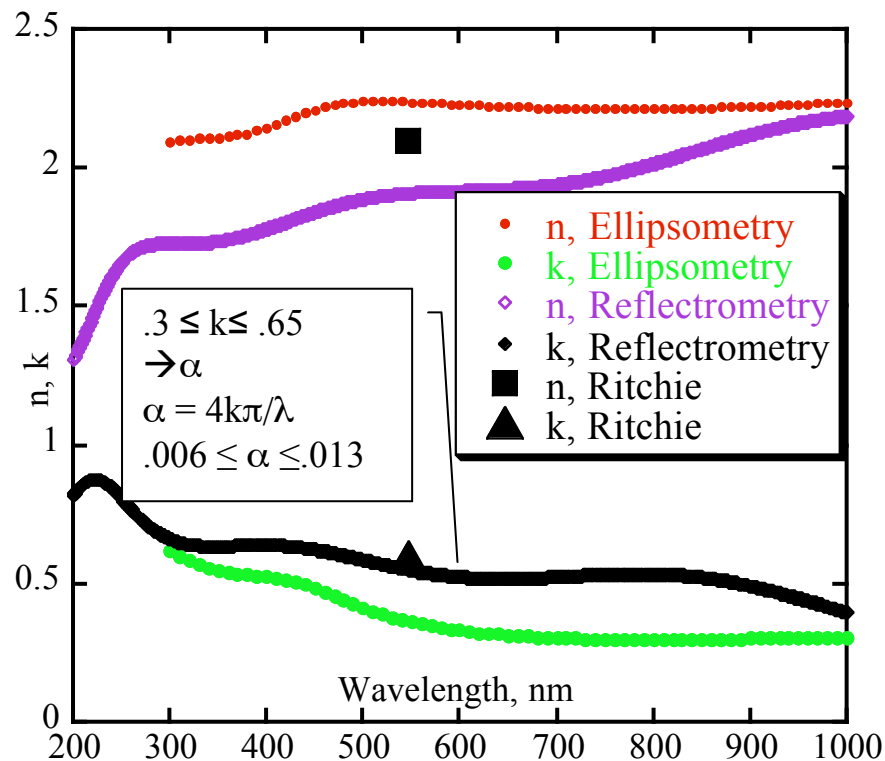


Figure 3. The optical constants n and k of epitaxial uranium oxide as a function of wavelength deduced from ellipsometry and reflectometry, and literature values of n and k at 546 nm.

Plutonium

To perform the same measurements on plutonium a containment cell was designed that holds the small circular plutonium sample (3 mm diameter and .1 mm thick) behind two separated windows. This work is in progress and expected to be completed at the time of the conference.

This work was performed under the auspices of the U. S. Department of Energy by the University of California, Lawrence Livermore National Laboratory under Contract No. W-7405-Eng-48.

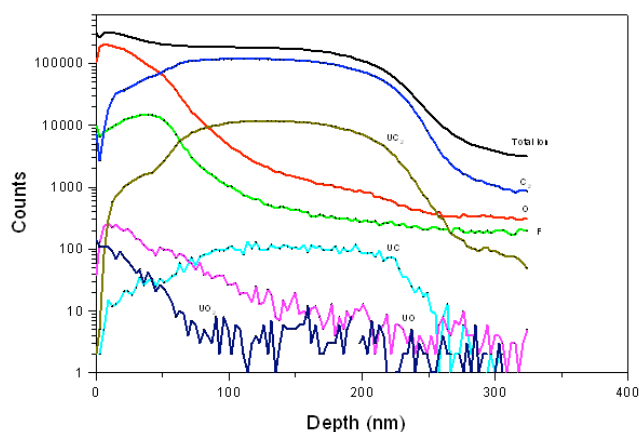
Surface Chemistry of C^+ Implanted Uranium Surfaces for Passivation

A. J. Nelson, T. E. Felter, K. J. Wu, C. Evans, J. L. Ferreira, W. J. Siekhaus, W. McLean

Lawrence Livermore National Laboratory, Livermore CA 94550 USA

ABSTRACT

Preventing the corrosion and oxidation of uranium is important to the continued development of advanced nuclear fuel technologies. Researchers have used N_2^+ and C^+ ion implantation to modify the surface chemistry and structure of uranium to affect the nucleation and growth kinetics of corrosion and to passivate the surface.¹⁻³ These researchers used Auger electron spectroscopy (AES) in conjunction with sputter depth profiling to show that the implanted surfaces had compositional gradients containing nitrides and carbides. Oxygen and molybdenum ion implantation has also been used to affect the hydriding properties and oxidation resistance of uranium.^{4,5} In addition to chemical modification, ion implantation can create special reactive surface species that include defect structures that affect the initial adsorption and dissociation of molecules on the surface. Overall the modified surface layers provide mechanical stability and protection against further air corrosion.



This paper presents the results from an investigation of the surface chemistry, surface morphology and electronic structure of air-exposed C^+ implanted U. Implantation of 33 keV C^+ ions into polycrystalline U^{238} with a dose of $4.3 \times 10^{17} \text{ cm}^{-2}$ produces a physically and chemically modified surface layer that prevents further air oxidation and corrosion. X-ray photoelectron spectroscopy and secondary ion mass spectrometry were used to investigate the surface chemistry and electronic structure of this C^+ ion implanted polycrystalline uranium and a non-implanted region of the sample, both regions exposed to air for more than a year. In addition, scanning electron microscopy was used to examine and compare the surface morphology of the two regions. The U 4f, O 1s and C 1s core-level and valence band spectra clearly indicate carbide formation in the modified surface layer. The time-of-flight secondary ion mass spectrometry depth profiling results shown in the figure reveal an oxy-carbide surface layer over an approximately 200 nm thick UC layer with little or no residual oxidation at the carbide layer/U metal transitional interface.

This work was performed under the auspices of the U.S. Department of Energy by the University of California Lawrence Livermore National Laboratory under Contract No. W-7405-Eng-48.

1. R. Arkush, M.H. Mintz and N. Shamir, *J. Nucl. Mater.* **281**, 182 (2000).
2. R. Arkush, M. Brill, S. Zalkind, M.H. Mintz and N. Shamir, *J. Alloys Comp.* **330-332**, 472 (2002).
3. R.G. Musket, *Materials Research Society Conference Proceedings No. 93*, 49 (1987).
4. E.N. Kaufmann, R.G. Musket, C.A. Colmenares and B.R. Appleton, *Materials Research Society Conference Proceedings No. 27*, 747 (1984).
5. R.G. Musket, G. Robinson-Weis and R.G. Patterson, *Materials Research Society Conference Proceedings No. 27*, 753 (1984).

Surface Chemistry of Plutonium: Properties and Reactivity of the Oxide Carbide Solid Solution

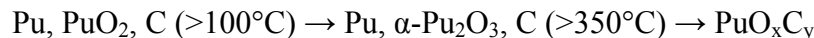
J. M. Haschke*, W. McLean†

*Actinide Science Consulting, Harwood TX 78632 USA

†Lawrence Livermore National Laboratory, Livermore CA 94551 USA

INTRODUCTION

Safe handling and storage of plutonium metal and alloys is contingent on adequate knowledge of surface chemistry and catalytic properties. Recent studies show that violent reaction of metal with air ensues if the surface becomes coated with a catalytically active compound during processing or inert-atmosphere storage.¹ In air at room temperature, Pu is covered by a passive PuO₂ layer that is inherently contaminated with C. When PuO₂-coated metal is heated in the absence of air, the surface layer reacts in a step-wise sequence to form α-Pu₂O₃ and oxide carbide²



The variable-composition oxide carbide solid solution³ is misidentified in early studies⁴ as the monoxide (PuO) and its properties remain largely undefined.

The violent Pu-air reaction cited above is initiated by an α-Pu₂O₃ surface layer that forms during heating or extended storage of the metal in the absence of air.¹ Unlike PuO₂, this oxide is reactive and promotes formation of hydride (PuH₂) by reaction of hydrogen from water, radiolysis or organic materials, and other sources in storage. The resulting Pu₂O₃-PuH₂ double layer initiates reaction of Pu with O₂ and N₂ upon exposure to air at room temperature. High temperatures are generated and metal is transformed into dispersible/respirable products at a rate of 6 cm Pu per hour.

The potential hazard created by formation of α-Pu₂O₃ during storage might be eliminated if the PuO_xC_y product formed above 350°C is passive. In that case, heating of oxide-coated metal in vacuum might be used in preparing Pu for extended storage. Relevant properties of the PuO_xC_y layer formed on the metal have been investigated in order to determine if thermal alteration holds potential for storage applications.

RESULTS

XRD characterization of the surface layer formed by heating PuO₂-coated δ-phase Ga alloy in vacuum at 520°C are consistent with results reported for NaCl-related oxide carbide in equilibrium with Pu.³ The phase formed by a relatively thick (~0.5 μm) PuO₂ layer has a unique composition (PuO_{0.54}C_{0.40}) that coexists only with Pu and Pu₂O₃ and has a₀=5.956 Å. Products obtained with relatively thin (~0.05 μm) PuO₂ layers have larger lattice parameters, but stoichiometry is not defined because a₀ increases as composition changes from PuC_{0.85} (a₀=4.956 Å) to (PuO_{0.30}C_{0.60}) (a₀=4.969 Å) and decreases with increasing x. All compositions are substoichiometric (x+y<1) and density data show anion vacancies.

Crystal chemistry of PuO_xC_y is consistent with hydrolysis studies showing that PuC_y forms CH_4 and lesser amounts of C_2H_6 .⁵ Since XPS data for PuO_xC_y results show that Pu is trivalent and O is present as O^{2-} , charge balance is achieved only if C is multivalent and present in a variable ratio of C^{4+} and C_2^{2-} . The maximum in a_0 coincides with the composition at which the C_2^{2-} concentration goes to zero. Charge balance is attained at high oxygen contents by occupancy of conduction bands with excess electrons. Metallic properties promote catalytic activity and anion vacancies facilitate transport of reactant species through the product layer.

Tests to determine the reactivity of the PuO_xC_y layer show divergent behavior upon exposure to air and to H_2 . XRD analyses are consistent with XPS results² showing that air forms a thin PuO_2 layer. Exposure to H_2 results in rapid reaction at the same rate as observed with a PuH_2 surface¹ and leads to spallation of PuO_xC_y as a hydride forms at the product-metal interface. Therefore, rapid reaction of PuO_xC_y -coated metal with H_2 forms a hydride surface that initiates violent reaction of air.¹

CONCLUSIONS

PuO_xC_y solid-solution layer formed by heating the metal has properties consistent with catalytic behavior. Reactivity studies demonstrate that thermal treatment of Pu does not passivate the surface. Rapid reaction of PuO_xC_y -coated Pu upon exposure to air is not expected. However, if H_2 sources exist in the storage environment, formation of a hydride surface that catalyzes violent reaction upon exposure to air is likely. Therefore caution should be exercised during handling of PuO_xC_y -coated metal.

- 1 J.M. Haschke and T. H. Allen, *J. Alloys Compds.* **320** (2001) 58.
- 2 D.T. Larson and J.M. Haschke, *Inorg. Chem.* **20** (1981) 1945.
- 3 R.N.R. Mulford, E.H. Ellinger and K.A. Johnson, *J. Inorg. Nucl.Mater.* **17** (1965) 327.
- 4 J.M. Cleveland, *The Chemistry of Plutonium*, Gordon and Breach, New York, 1970, p.305-06.
- 5 J.L. Drummond, B.J. McDonald, H.M. Ockenden and G.A. Welch, *J. Chem. Soc.* **1957** (1957) 4785.

Calculations of thermodynamic properties of PuO₂ from first principles

S. MINAMOTO^{*}, K. KONASHI[†], M. KATO[†], A. KUWABARA[†], K. MATSUNAGA[†], I. TANAKA[†]

^{*}Energy & Industrial Systems Dept., CRC Solutions Corp, Tokyo Japan

[†]Institute for Materials Research, Tohoku University, Sendai Japan

[†]Japan Atomic Energy Agency, Ibaraki Japan

[†]Department of Materials Science and Engineering, Kyoto University, Kyoto Japan

Abstract

Plutonium dioxide is non-stoichiometry compound and its thermal property would highly depend on the non-stoichiometry. And due to the lack of experimental data for plutonium dioxide, thermodynamical data were not established.

In recently, the coupling of first-principle calculation and lattice dynamics theory, thermodynamical data could be obtained numerically. In this study, we applied first principle plane-wave calculation to get total energy of plutonium dioxide and applied lattice dynamics theory to get phonon dispersion for both perfect crystal and crystal which contains oxygen defect.

Total energy calculation for perfect crystal reproduced experimental lattice parameter well. And after phonon density calculation for both types of crystal structures of plutonium dioxide, contribution of vibration to thermodynamical data was investigated.

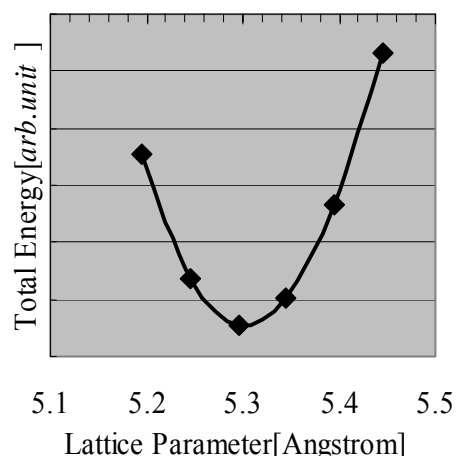


Fig.1 Total energy for perfect crystal

Reference.

1. M. Stan and P. Cristea, "Thermochemistry of Defects and Oxygen Diffusion in PuO₂-x", Trans. Am. Nucl. Soc. 91 (2004)491.
2. G. Kresse and J. Furthmüller, "Efficient iterative schemes for ab initio total-energy calculations using a plane-wave basis set", Phys. Rev. B 54(1996)11169.
3. M. Nolan, S. Grigoleit, D.C. Sayle, S.C. Parker, G.W. Watson, "Density functional theory studies of the structure and electronic structure of pure and defective low index surfaces of ceria", Surface Science 576 (2005)217-29.

A First-Principles Electronic Structure Study of the Adsorption of Carbon Monoxide on (100) Surface of γ -Uranium

Pratik P. Dholabhai and Asok K. Ray

Department of Physics, the University of Texas at Arlington, Arlington, TX 76019

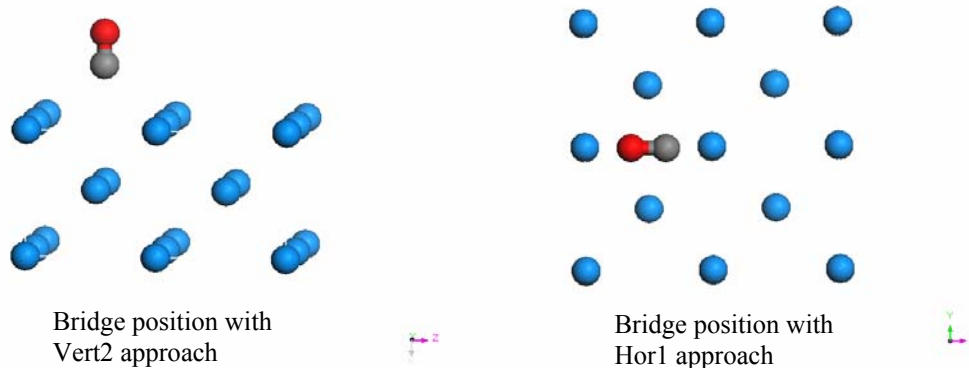
INTRODUCTION

The electronic structures of the actinides are of major scientific and technological interests, partly because of the fascinating and remarkable properties of the $5f$ electrons and partly because of the enormous potentials of the actinides in nuclear applications. Uranium (U), the heaviest naturally occurring actinide element, is largely known due to its use as a nuclear reactor fuel. U occupies a central position in the early actinide series, with only three $5f$ electrons hybridizing with the $6d$ and $7s$ electrons showing itinerant behavior. The uranium-oxygen system is one of the most complex metal oxide systems due to the high reactivity of uranium with oxygen and towards oxygen and carbon containing systems such as H_2O , CO_2 , and CO .¹ Uranium crystallizes in to a rather open structure, the orthorhombic α -phase with four molecules per unit cell at ambient conditions, followed by the body-centered tetragonal β (bct) phase at $940^\circ K$ and then the γ (bcc) phase at $1050^\circ K$ at ambient pressure.² As a continuation of our research in actinide surface chemistry and physics,³ this work has focused on the adsorption of CO on the (100) surface of γ - U.

COMPUTATIONAL METHOD AND RESULTS

Carbon monoxide adsorption on (100) surface of γ -uranium have been studied at the non-spin-polarized level of theory using the generalized gradient approximation of density functional theory (GGA-DFT) with Perdew and Wang (PW) functionals and the DMol3 suite of programs.⁴ Double numerical basis sets with polarization functions (DNP) are used for carbon and oxygen and a real space cut-off of 5.0 \AA was used.. For uranium, the outer 14 electrons ($6s^2 6p^6 5f^3 6d^1 7s^2$) are treated as valence electrons and the remaining 78 electrons are treated as core by a hardness conserving semilocal pseudopotential. To simulate periodic boundary conditions, a vacuum layer of 30 \AA was added to the unit cell of the layers. To study carbon monoxide adsorption, the (100) surface was modelled with three layers of uranium at the experimental lattice constant and the unit cell per layer was chosen to contain four uranium atoms. To simulate periodic boundary conditions, a vacuum layer of 30 \AA was added to the unit cell of the layers. Carbon monoxide molecule, one per unit cell, was allowed to approach the uranium surface along three different symmetrical approaches: i) directly on top of a U atom (*top* position); ii) on the middle of two nearest neighbor U atoms (*bridge* position); iii) in the center of the smallest unit structures of the surfaces (*center* position). The interstitial positions were found not to be bound. For each of these positions, several approaches of chemisorption were considered: 1) CO molecule approaches vertically to the surface with oxygen atom facing the surface (Vert1 approach); 2) CO molecule approaches vertically to the surface with carbon atom facing the surface (Vert2 approach); 3) CO molecule parallel to the surface and parallel to the bcc lattice vectors (Hor1 approach); 4) CO molecule parallel to the surface having an angle of 45° with the

bcc lattice vectors, i.e., parallel to the diagonal of the square lattice (Hor2 approach). Some approach positions are shown below.



For CO adsorption, the bridge position of (100) surface with vert2 approach is found to be most favorable site with a chemisorption energy of 2.932eV for the non-spin-polarized case. The distance of the lower carbon atom from the uranium surface is found to be 1.589Å for non-spin-polarized case. The distance between the carbon and oxygen for this most favorable position is found to be 1.134Å for the non-spin-polarized case. A significant charge transfer from the first layer of the uranium surface to the carbon and oxygen atoms is found to occur, implying that the bonding is partly ionic. A comparison of the density of states (DOS) for the most favorable chemisorbed site with the DOS for bare uranium indicates that the CO 2*p* orbitals hybridize with U 5*f* bands, and a part of the U 5*f* electrons become more localized. Overall pattern of the density of states does not change significantly after the adsorption of CO on uranium layers.

This work is supported by the Chemical Sciences, Geosciences and Biosciences Division, Office of Basic Energy Sciences, Office of Science, U. S. Department of Energy (Grant No. DE-FG02-03ER15409) and the Welch Foundation, Houston, Texas (Grant No. Y-1525).

¹ E. Swissa, J. Bloch, U. Atzmony, and M. H. Mintz. Surf. Sci. **214**, 323 (1989).

² D. A. Young. Phase Diagrams of the Elements (University of California Press, Berkeley, CA, 1991).

³ X. Wu and A. K. Ray, Phys. Rev. B **72**, 045115 (2005); A. K. Ray and J. C. Boettger, Phys. Rev. B **70**, 085418 (2004); J. C. Boettger and A. K. Ray, Int. J. Quant. Chem., **105**, 564 (2005); M. N. Huda and A. K. Ray, Eur. Phys. J. B **40**, 337 (2004); Physica B **352**, 5 (2004); Eur. Phys. J. B **43**, 131 (2005); Physica B **366**, 95 (2005); Phys. Rev. B **72**, 085101 (2005); Int. J. Quant. Chem. **105**, 280 (2005); H. R. Gong and A. K. Ray, Eur. Phys. J. B, **48**, 409 (2005); H. R. Gong and A. K. Ray, Proc. MRS Fall 2005 Symposium; accepted for publication; Surf. Sci. accepted for publication; D. Gao and A. K. Ray, Eur. Phys. J. B, in press; Proc. MRS Fall 2005 Symposium; accepted for publication; D. Gao and A. K. Ray, submitted for publication; P. Dholabhai and A. K. Ray, submitted for publication.

⁴ B. Delley, J. Chem. Phys. **92**, 508 (1990); J. Chem. Phys. **113**, 7756 (2002).